CONTRIBUTION TO THE DEVELOPMENT OF CONSISTENT STABILITY DESIGN RULES FOR STEEL MEMBERS

Dissertation

eingereicht an der
Fakultät für Bauingenieurwissenschaften der
Technischen Universität Graz

Graz University of Technology

Dipl.-Ing. Andreas TARAS

Erstbegutachter: O.Univ.-Prof. Dipl.-Ing. Dr.techn. Richard GREINER
Institut für Stahlbau und Flächentragwerke – TU Graz, Austria

Zweitbegutachter: Univ.-Prof. Dr. Dinar CAMOTIM
Instituto Superior Técnico - Universidade Técnica de Lisboa, Portugal

Graz, im Mai 2010

Abstract

This thesis is concerned with open questions relating to the accuracy and safety of buckling design rules for steel members. It identifies a series of inconsistencies in the current practice of design of these members against instability and comes up with novel solutions to overcome them.

The accuracy of design rules is addressed for the buckling modes of lateral-torsional, torsional-flexural and in-plane beam-column buckling. It is shown that the load-carrying capacity of steel members for these modes can be assessed with great accuracy on the basis of simple, case-specific second order (Ayrton-Perry) equations. Thereby, it is of paramount importance that the proposed design equations are calibrated to accurately reflect the results of materially and geometrically non-linear GMNIA FEM calculations. For the purposes of determining how accurately a formulation reflects the true mechanical behaviour of a certain member in a buckling mode, these GMNIA calculations are inevitably of deterministic nature, but are conveniently carried out on "model members" that inherently reflect a certain,desired safety level through their assumptions regarding imperfections and geometry. By doing so, the same, consistent procedure was finally adopted for the development of design rules for these buckling modes as for the most-studied and best-understood benchmark case of flexural column buckling. Accordingly, also the resulting design formulae are both formally and mechanically consistent with the benchmark case.

Aspects of safety were addressed both implicitly through the above-mentioned development procedure and explicitly by the use of reliability assessments on the basis of Monte Carlo simulations and First Order Reliability Methods. Random number generation and numerical tests were used to answer some questions related to the nexus between fabrication tolerances and specified imperfections for design. Specifically, the impact of changes to the curvature tolerances of compression members was quantified by the use of these methods. Additionally, the possibility was addressed to move away from "semi-deterministic" buckling rules calibrated onto "model member" GMNIA calculations, and to directly base the calibration of buckling rules on "constant reliability curves". Such curves can be obtained from a combination of numerical GMNIA and probabilistic FORM calculations.

Finally, a systematic development procedure for buckling design rules for steel members is proposed, which allows for a consistent expansion of the findings of this thesis to other buckling modes.

Kurzfassung

Diese Dissertation befasst sich mit offenen Fragen zur Genauigkeit und Sicherheit von Bemessungsregeln für stabilitätsgefährdete Stahlbauteile. In ihr werden eine Reihe von Inkonsistenzen in der jetzigen Bemessungspraxis ausgewiesen und mittels innovativer Lösungsansätze behoben.

Die Genauigkeit der Bemessungsregeln wird für die Stabilitätsfälle des Biegedrillknickens, des Drillknickens und des Biegeknickens unter kombinierter Beanspruchung untersucht. Es wird gezeigt, dass die Tragfähigkeit von Stahlbauteilen gegenüber diesen Versagensfällen mit Hilfe einfacher, aus der Theorie II. Ordnung hergeleiteten Formeln erfolgen kann (Ayrton-Perry Formulierungen). Dabei ist es von besonderer Bedeutung, dass die vorgeschlagenen Formeln an die Ergebnisse von materiell und geometrisch nichtlinearen GMNIA Berechnungen kalibriert werden. Diese GMNIA Berechnungen sind zunächst zwangsweise deterministischer Natur, um die Genauigkeit einer Formulierung im Hinblick auf die Vorhersage der Tragfähigkeit eines bestimmten „Modell-Balkens" beurteilen zu können. Sie sind aber vorteilhaft in ihren Imperfektions- und Geometrieannahmen für den mit einem gewünschten Vertrauensniveau abgestimmt. Durch diese Vorgehensweise wird volle Konsistenz mit der Entwicklung des Referenzfalles für alle Stabilitäts-Bemessungsregeln hergestellt, dem Biegeknickfall von Stützen. Infolge dessen wurden in der vorliegenden Arbeit auch die resultierenden Bemessungsregeln sowohl formell als auch mechanisch in vollständiger Konsistenz mit dem Referenzfall formuliert.

Fragen der Sicherheit wurden sowohl implizit durch die obenbeschriebene Vorgehensweise als auch explizit durch die Durchführung von Zuverlässlichkeitsuntersuchungen mit Hilfe von Monte Carlo und „First Order Reliability" Methoden erörtert. Die Generierung von Zufallszahlen und numerische (Monte Carlo) Versuche wurden zur Beantwortung von Fragen der Verknüpfung von Herstellungstoleranzen und Imperfektionen für Tragfähigkeitsberechnungen angewandt; ein Beispiel hierfür ist die Quantifizierung des Effekts der Änderung von Geradheitstoleranzen für Druckglieder. Zudem wurde in dieser Arbeit die Möglichkeit untersucht, in Zukunft die Kalibrierung von Bemessungsregeln nicht mehr auf Basis von "semi-deterministischen" Knickkurven durchzuführen, sondern direkt auf Basis von Kurven konstanter Zuverlässigkeit. Diese können mit Hilfe einer Kombination von GMNIA und FORM Berechnungen ermittelt werden.

Abschließend wird eine systematische Prozedur zur Entwicklung von Bemessungsregeln für stabilitätsgefährdete Stahlbauteile vorgeschlagen, welche eine konsistente Erweiterung der in dieser Arbeit dargestellten Konzepte auch auf andere Stabilitätsfälle ermöglicht.

Table of Contents

PART III – Design Rules for Beam-Columns, Summary & Conlusions

Acknowledgements

This thesis would not have been possible without the support of my supervisors, colleagues, friends and family. I would therefore like to express my deep-felt gratitude to all the individuals who have guided and accompanied me throughout this very intensive and fruitful chapter in my life.

First and foremost, I would like to sincerely thank my supervisor, Prof. Richard Greiner, for his guidance, trust and understanding. For over five years now, his mentorship has been essential to my professional development. He gave me the opportunity to work in a very stimulating research context, driven by his own intellectual curiosity and his dedication as a scientist, engineer and teacher. By entrusting me with a vast scope of research and engineering tasks, and by helping me to pursue my own interests in structural engineering, he ensured that my experience working as his assistant was truly well-rounded.

I would also like to thank Prof. Dinar Camotim for taking over the laborious part of reviewing my thesis and participating in the doctoral examination committee. From the onset of our correspondence, he showed great patience and commitment to his task. He also very kindly invited me to spend some days at the Instituto Superior Técnico in Lisbon to discuss my work. Our conversations there gave me confidence and great motivation, for which I owe Prof. Camotim my deep gratitude.

A heart-felt thank you goes to all my colleagues at the Institute for Steel Structures and Shell Structures, who have always encouraged me and never refused a helping hand. Particular gratitude is expressed to the two colleagues with whom I had the pleasure of sharing an office, Dr. Robert Ofner and Dr. Markus Kettler. They always offered good advice when I felt at a loss and lent me an ear whenever I needed one.

One tends to forget it during the writing of a PhD thesis, but there are other things in life besides structural engineering. I must thank my friends for having reminded me of that whenever possible. Even though I sometimes disappeared off the radar for weeks, they were always there for me when I came back, and helped me put all things into the right perspective.

At this point, I want to thank the people who, through their love and moral support, truly enabled me to pursue my dream of working in research during these years. When Andrea entered my life over two years ago, she gave me the joy and serenity that make everything seem easy. I will never forget how incredibly patient and supportive she has been during the last several months of my PhD endeavour. I am very much looking forward to spending much more time together now.

PART I

Introduction, Background of Buckling Curves & Methodology

1

Introduction

1.1. Motivation and Objectives

Buckling theory and buckling design have accompanied the development and advancement of steel as a building material and of structural steelwork as a construction method since the very beginning. This must be attributed to the specific characteristics of steelwork, for which –due to the high strength of the material- the slenderness of components is of paramount importance. One or the other form of buckling determines the ultimate resistance of practically all of these components whenever compressive stresses are present. It is therefore understandable why the structural engineers working with steelwork have always been interested in determining the *buckling resistance* of a structural component –and of the structure as a whole- as accurately as possible.

The *buckling resistance* of a structural component can be assessed - with varying degrees of accuracy - using a variety of methods. As research tools, *experimental methods* and *numerical methods* -using mostly non-linear Finite Element Methods (FEM)- have been widely used in the past and present to gather information that leads to a better understanding of the main parameters governing a stability problem. In recent times, these two methods are also often combined to obtain so-called *numerical* ("Monte Carlo") *tests*, i.e. numerical calculations with random sets of input parameters. When appropriately employed, they combine the inexpensiveness –in terms of time and money- of a numerical calculation with the safety-relevant "scatter" inherent to a real component.

Theoretically, a future scenario can be envisaged in which exclusively full non-linear numerical FEM calculations are used by practitioners and designers to assess the buckling resistance of steel structures. However, this does not seem to be desirable from today's point of view. The frequent discussions in the scientific community about the safety or representativeness of one or another design rule, based on this or that assumption in a numerical simulation, prove that the application and interpretation of such calculations still pose a series of problems even at the basic scientific level. Thus, at the moment, the stability design of a large structure conducted solely with non-linear numerical methods and (arbitrary) normative imperfection assumptions will be far too prone to questioning of its safety level or misinterpretation of its results to be acceptable as a method for practical structural design. Both the experimental and the numerical methods alone will therefore be of little *direct* help to designers in their task of dimensioning a structure that is fit for its planned

utilization. Thus, simple analytical methods, design charts and tables, and above all formulaic descriptions of *buckling curves* will likely retain a dominant role in the future.

In the semi-probabilistic Eurocode design philosophy laid out in EN 1990, such buckling curves (or rather, the formulaic representation thereof) represent the prime example of a complex, multi-variable "resistance function", see Fig 1-1, of which the *level of reliability* can be assessed using the methodologies presented in that standard. All design rules concerned with member buckling checks currently contained in the Eurocodes, as well as the rules present in the various national predecessor codes for structural design, make use of such *formulaic descriptions of buckling curves and buckling strength*.

Within the framework of a semi-probabilistic structural design philosophy, buckling curves and buckling rules have a *dual function*:

1. *Accuracy:* they must describe the physical behaviour (the strength) of a given, actual component with a high level of precision. Evidence for this precision must generally be provided for a large number of different cases, in order to prove the mechanical soundness of a buckling rule and exclude "chance" as the cause of accuracy for a single given case.

2. *Safety:* when used in design, they must represent a specified (or specifiable) level of safety against buckling failure. In semi-probabilistic design, it is thereby important that this safety level be modifiable by a single, constant *partial safety factor* for a wide spectrum of design checks (e.g. a single factor for all types of stability checks). Design rules furthermore must
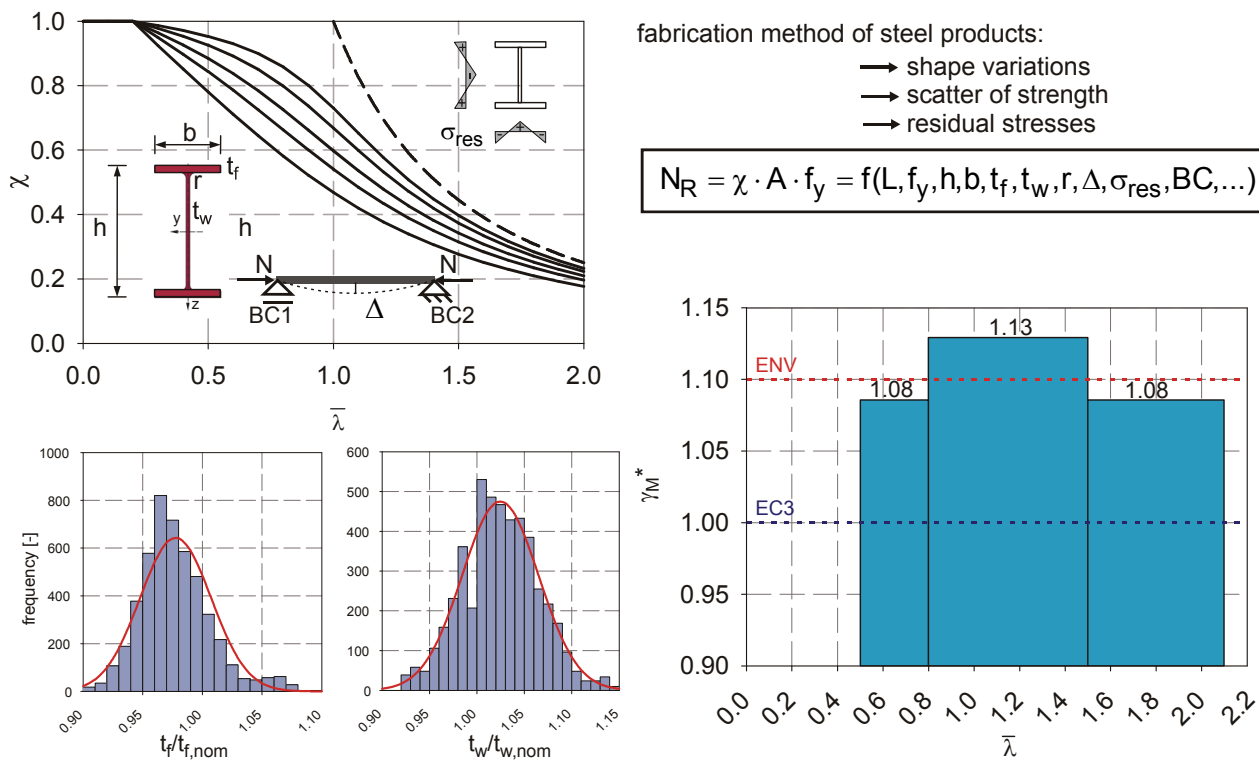
Fig 1-1 *Buckling curves as "resistance functions" in the terminology of EN 1990*

be in line with fabrication tolerances and inspection methods of the structure.

Since fulfilling this double role is not straightforward, it is understandable why both during and after the development of the Eurocode 3 (EN 1993) much effort has been (and is being) put into the development and improvement of these buckling curves and rules. Thereby, the need for an increase of *consistency* of the different buckling curves is a common denominator of all proposals for amendments of the current practice.

In this context, the *following inconsistencies* found in buckling design rules for steel members can be listed in order to explain the need for a reconsideration and renewed study; thereby, chapter numbers are given in brackets at the end of each paragraph to indicate where in this thesis the mentioned aspect –with the relevant background literature- is discussed with more detail:

i.   The mechanical background and the accuracy of the single member stability checks are not consistently the same for the different cases. While the rules for flexural column buckling are based on a very extensive combination of experimental and numerical studies, and on a mechanically coherent derivation of a buckling reduction factor, the rules for lateral-torsional and torsional-flexural buckling are essentially based on the adoption of the column curves, with or without some minor modifications (Chapter 4 through 8).

ii. The inherent reliability level of the single member design checks is not consistent for the different buckling modes and, within a single mode, not equal throughout slenderness ranges (Chapter 4, 5 & 6).

iii. No commonly accepted, standardized procedure is currently available that allows for the assessment of the impact of changes to single production habits and tolerance requirements on the safety of established stability design rules. This poses a series of problems in the context of the introduction of the new European standard EN 1090-2 (2008) for the fabrication and erection of structural steelwork, which contains specifications for the acceptability levels and inspection requirements for geometric imperfections of compression members that markedly differ from previous requirements in many countries (Chapter 5).

iv. Different, methodologically not fully compatible concepts are used for the design of steel members under combined loading (beam-columns). One concept makes use of interaction factors to account for the coupled effects of the single load cases, and another concept uses "overall" buckling reduction factors for the combined load case. While the so-called "overall" concept is formally (but not physically/mechanically) better integrated with the design rules for single load cases -since it uses the same, Ayrton-Perry type of formulation of buckling strength-, the code regulations using the interaction concept are currently based on a much more thorough analytical and numerical background (Chapter 9).

The present thesis is to be seen as an effort to overcome these inconsistencies. It takes on a number of selected, currently discussed problems of member buckling design and aims at finding innovative solutions to them.

The following points were thereby seen as *objectives of this thesis*:

1) Clarifying the foundations of the common methods of representation of buckling strength and of the current design rules from today's perspective, and presenting this background in the form of a cohesive report. The most-studied and best-understood case of column buckling could thereby be identified as the "benchmark case" for the development or improvement of rules for other buckling phenomena.

2) Developing new expressions for the description of buckling curves for the basic cases of lateral-torsional, torsional and torsional-flexural buckling and calibrating them to numerical curves, with the aim of improving both accuracy and safety of member design rules, and of obtaining methodological and mechanical consistency with the benchmark case of column buckling.

3) Formulating a statistical/numerical method that allows to determine the safety level of a given buckling curve, respectively to obtain numerical curves that represent a constant reliability level throughout slenderness ranges.

4) Answering some current questions that stem from the introduction of the European fabrication standard for structural steelwork EN 1090-2 (2008), more specifically with the new geometrical fabrication and erection tolerances given therein, and the implication of these innovations on the currently used, long-established buckling rules. Thereby, the nexus between tolerances, real shape deviations and code imperfections is discussed. This specific task is put in the more general context of answering questions stemming from changes to production habits and their impact on design rules.

5) Describing the two main approaches used for the buckling design of beam-columns under combined loading – the interaction concept and the "generalized slenderness" concept based on overall load cases- and highlighting the respective advantages and disadvantages.

6) On the basis of the in-plane case, finding an analytical form of representation of the beam-column buckling phenomenon that is integrated in "generalized slenderness " concept and, in the context of this derivation, demonstrating the compatibility and equal ranking -in terms of mechanical coherence-, of the two design concepts.

1.2. Scope and limitations

This thesis deals with the buckling behaviour of isolated steel members and with reliability issues concerning these structural elements. The most common rules and methods currently employed to determine the structural safety of steel members are subjected to a thorough re-analysis and are amended where necessary to increase their mechanical consistency and safety requirements. Since

the considered, existing rules are predominantly based on studies of the behaviour of single span columns, beams and beam-columns with double-symmetric cross-section loaded by in-plane transversal loads and axial forces, the same scope is adopted for this thesis, see Fig 1-2. Specifically, the thesis will deal with the behaviour of:

i. Columns, i.e. members loaded purely by axial forces, with double-symmetric I-shaped cross-sections and with or without lateral supports.

ii. Beams, i.e. members loaded by in-plane bending moments, again with double-symmetric I-shaped cross-sections.

iii. Beam-columns, i.e. members loaded by a combination of axial and transversal loads, with double-symmetric, open or closed cross-sections.
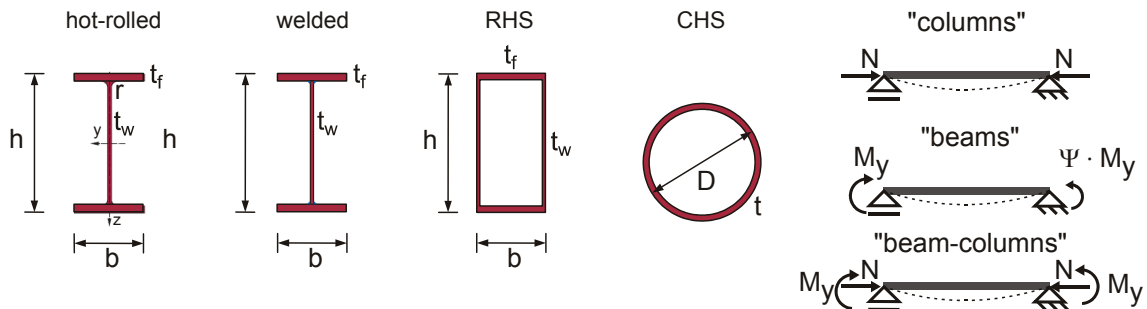
Fig 1-2 *Cross-section types and loading conditions considered in this thesis*

The majority of the numerical calculations in this thesis were carried out with deterministic, "fixed" input parameters in order to study the realistic buckling behaviour of the considered type of members, and used as basis for a calibration of newly developed design rules. Parametric studies were performed where single parameters of the studied case were varied in order to study the parameter's specific influence. Additionally, a large number of numerical calculations were carried out by using random input variables in order to obtain "numerical test results" in the context of Monte Carlo simulations.

From the point of view of reliability, the scope of this thesis is connected with the requirements of the Eurocode – EN 1990 (2002) and the Construction Products Directive (EEC, 1988): all developed rules implicitly assume that products are being used that comply with the "essential requirements with regard to mechanical strength and stability", which specifically entails that they are produced according to harmonized European standards and that the fabricators operate a factory production control system as a tool for controlling production quality (tolerances, material properties, welding procedures, residual stresses).

The limitations of the thesis are of course directly connected with the above-mentioned breadth of the considered field of study: neither the behaviour of unsymmetric sections nor the effects of member continuity and boundary conditions –as present in whole structures- were considered. In spite of these limitations, it is believed that the overall findings derived from this thesis hold a degree of validity that extends beyond the scope detailed above, as the methodological and conceptual aspects of these findings are of a rather general nature.

1.3. Organization of the thesis

In this thesis, the pursuit of the objectives described in section 1.1 is organized in separate *parts*:

- *Part I* focuses on general aspects concerned with the origin, usage and development of member buckling rules. Following this introductory 1st chapter, the original derivations and succeeding expansions and applications of the most common member buckling formulae are described in chapter 2. Chapter 3 deals with methodology, focusing on numerical, analytical and probabilistic tools as they were used in this thesis.

- *Part II* is concerned with basic member buckling cases of columns or beams. In the introductory chapter 4, it discusses the main inconsistencies and sources of current research need associated with all basic member buckling cases, and identifies some common strategies to overcome these inconsistencies. Chapter 5 discusses the "benchmark" case for all member buckling cases, i.e. flexural column buckling. It presents the development of current European column buckling rules from today's perspective. Additionally, this chapter addresses issues of reliability, both in general terms and for a specific, ongoing discussion regarding the impact of changed fabrication tolerances for compression members.
Chapters 6 and 7 treat two additional basic member buckling cases, i.e. lateral torsional buckling and torsional-flexural (column) buckling, respectively. New formulations are developed that increase both accuracy and consistency with the "benchmark" case.
In chapter 8, the design rules resulting from the efforts of chapter 6 and 7, as well as the established rules of chapter 5, are summarized in a common design chart, which shows the obtained consistency of the design rules.

- *Part III* contains a chapter that gives an outlook on specific problems of the development of design rules for beam-columns, as well as the summary and conclusions for the whole thesis. In chapter 9, the two main concepts for the treatment of beam-columns in design are discussed, namely the "interaction concept" and the "generalized slenderness" concept. In order to demonstrate how to integrate the accuracy of the interaction concept design rules with the advantages of the generalized slenderness concept, a new formulation is developed for the in-plane buckling case of beam-columns that is mechanically sound and consistent with the Ayrton-Perry type formulations used in the design rules for the basic member buckling cases. Additionally, chapter 9 contains a discussion of some inconsistencies of the "general method" for the design of members and structures against out-of-plane buckling.
In the 10th and final chapter, a summary of the content of the present thesis is given and the main findings are discussed. The original contributions included in this thesis to engineering knowledge and to the consolidation of existing knowledge are listed. Finally, some general conclusions are drawn based on the main findings of the thesis.

2

Buckling Curves: Definition and Representation

2.1. Scope

In the introduction (chapter 1), it has been argued that buckling formulae and curves presently continue to have significance to the design of steel structures against instability. Additionally, the buckling curves currently found in international design codes will also be of relevance to the development of future, improved stability design rules. Thus, it is important to comment upon the origins, derivations, fields of application and limitations of the most common methods of representation of buckling resistances and buckling curves. Giving a holistic perspective from today's state of knowledge can be assumed to be - if not original-, certainly valuable to the research community. That is the purpose of this chapter.

In order to focus the attention on this specific purpose, the considerations in this chapter will be made with regard to the most-understood and best-documented case of member buckling, i.e. flexural column buckling.

The chapter starts with a definition of buckling curves in general terms. It then proceeds with a discussion of the most significant approaches to the representation of buckling curves, both in terms of mathematical descriptions ("buckling formulae") and in terms of graphical representation.

2.2. Definition and Presentation

In this thesis, a *buckling curve* is defined as any kind of representation of *buckling strength* R_b as a function of *its theoretical limit loads* R_{ult} and R_{cr}:

$$R_b = f(R_{ult}, R_{cr}) \tag{2.1}$$

With

R_b ..... buckling resistance, i.e. the load level at which the peak of a load-deformation (R-u) curve would be measured in tests, see Fig 2-1.

R_{ult} ..... theoretical limit resistance of the component if the effects of the studied buckling case *are omitted*. This can for instance be the plastic or elastic capacity of the cross-section, depending on the studied case and cross-section.
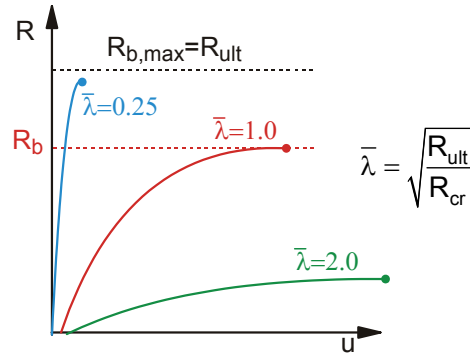
Fig 2-1   Schematic representation of the buckling strength R_b.

R_{cr} ..... theoretical, elastic critical buckling resistance obtained from a buckling bifurcation analysis. In the case of member buckling, this is the so-called "Euler buckling load".

In most cases, the designer will make use of a buckling curve that represents a certain, more-or-less explicitly defined reliability level. In these cases, it is fitting to speak of a *design buckling curve*, representing a characteristic value $R_{b,k}$ or a design value $R_{b,d} = R_{b,k} / \gamma_{M1}$ of the buckling strength.

It is often convenient to define the buckling strength not in absolute terms, but in relative terms to the limit load R_{ult}, using the symbol χ for the ratio. This is mostly done for characteristic values of both resistances:

$$\chi = \frac{R_{b,k}}{R_{ult,k}} \tag{2.2}$$

As the name *buckling curve* implies, the buckling strength plotted over representative parameters has some sort of curvilinear shape. In terms of *representation* of this dependence, two forms have the largest diffusion in the literature. They are plotted in Fig 2-2 for the example of the European column buckling curves, and described in the following. In the example, the buckling strength $R_{b,k}$ is represented by the buckling axial load $N_{b,k}$.

In the first form of representation, shown in Fig 2-2a, the buckling strength (in relative form χ) is plotted over the normalized slenderness, defined in general terms as follows:

$$\bar{\lambda} = \sqrt{\frac{R_{ult,k}}{R_{cr}}} \xrightarrow{\text{column buckling}} \sqrt{\frac{N_{ult,k}}{N_{cr}}} \tag{2.3}$$

In the second form of representation, shown in Fig 2-2b and going back to Merchant (see section 2.4.2), the relative buckling strength χ is plotted over the ratio $R_{b,k}/R_{cr}$. The origin of this form of presentation is further discussed in section 2.4. This form of representation is used with considerable advantage especially to represent shell buckling phenomena (Rotter, 2002). In principle, all analytical and numerical buckling curves, as well as test results, can be plotted using this form of representation, often resulting in a better visualization and understanding of the differences between different buckling phenomena.
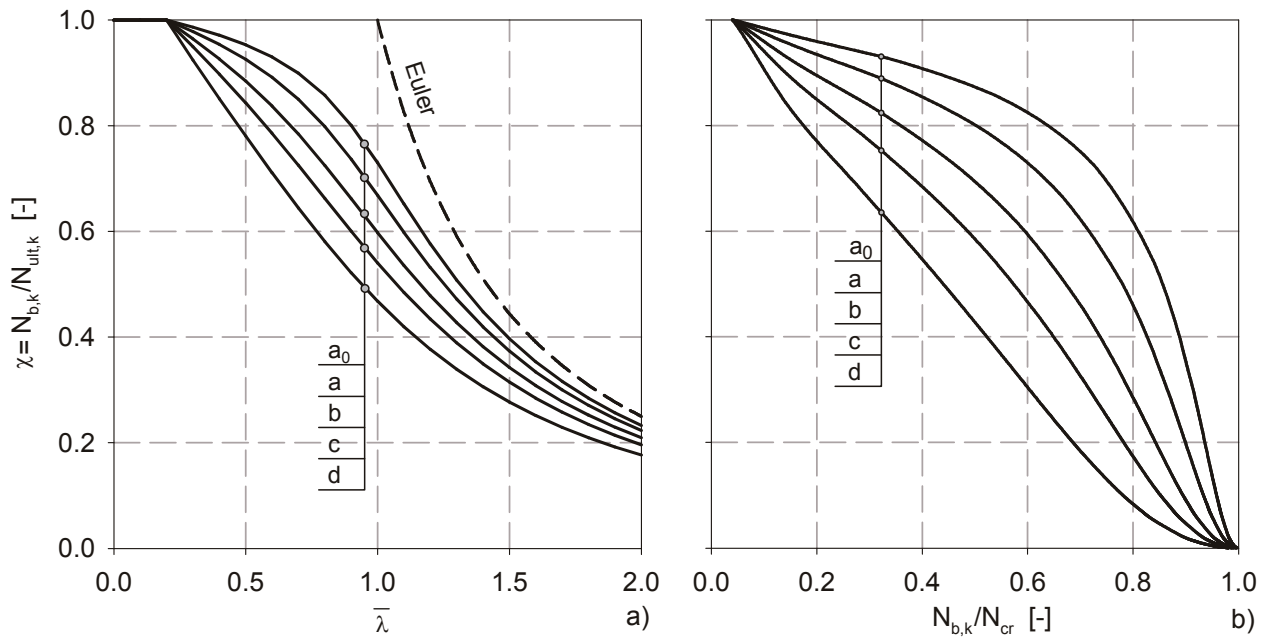
Fig 2-2   Forms of representation: as function of slenderness (a); Merchant-Rankine form (b).

2.3. Early approaches based on theoretical or empirical limits.

In the mid 19th and early 20th century, the first prescriptive rules concerned with the codification of design buckling curves were brought forward. Before this time, at least in Central Europe, the design of columns was carried out according to experience or empirical formulae found in civil engineering manuals (Kurrer, 2008). Early examples of codified buckling curves in Germany are shown in Fig 2-3, plotted as "allowable compressive stresses" over the geometric slenderness λ=L/i. The figure also shows the theoretical and empirical basis of these regulations. Essentially, these are the bifurcation theory of Euler (1759), the empirical-experimental strength lines of Tetmajer (1890), and the tangent-modulus theory as originally developed in Germany by Engesser (1891) and Kárman (1910). Internationally, the latter is better known through its confirmation and expansion by Shanley (1946).

Fig 2-3 illustrates the basic idea behind these early buckling curve regulations: the theoretical or experimental buckling curves were thought to accurately reflect the actual behaviour of near-perfect struts. In order to account for actual deviations from the "perfect" conditions assumed by Euler, Engesser, etc., or present in the small-scale tests of Tetmajer, abundant safety factors were applied to the theoretical load to obtain the "allowable" compressive working stress of columns. Over time, due to positive experience and desire for more slender columns, these safety factors were slowly diminished, going from 5 in 1910 (Prussian building regulation) to 2.5 (DIN 4114).
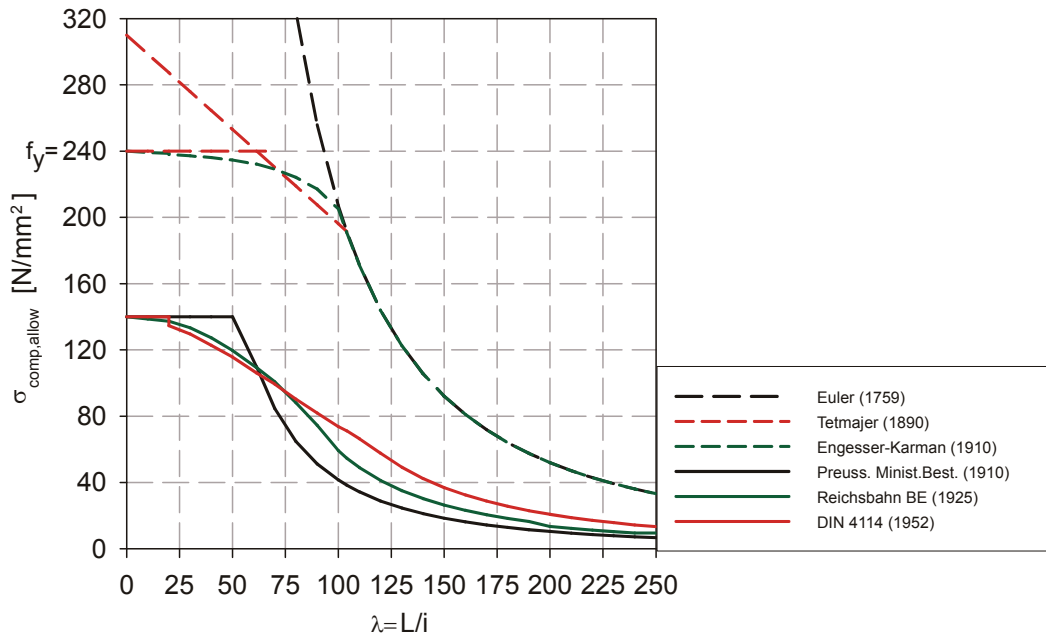
Fig 2-3   Early column buckling curves based on theoretical limit loads.

2.4. The Rankine-Gordon-Merchant approach

While Euler's and Engesser's & Kárman's mathematically consistent theories of column buckling, in combination with tests on near-perfect small-scale specimens, such as those performed by Tetmajer, long represented the only basis for practical column design in Continental Europe, so-called "rational" or "semi-rational" formulae enjoyed early popularity in the Anglophone world. These formulae were developed (mostly by engineering practitioners) by making more-or-less plausible assumptions regarding the deformations of columns and the stresses in critical cross-sections during the buckling process and introducing factors that could be used to fit the resulting mathematical expression to test results.

One well-known example of such a "semi-rational" expression is the *Rankine-Gordon* column formula (Rankine 1866, 1898). Especially the interpretation and representation given to it by Merchant (1954) is still in use today in various fields of stability research and practice.

2.4.1. The original derivation – "Rankine-Gordon formula"

According to Timoshenko (1983, p.209), the formula was originally derived by Tredgold for a column with rectangular cross-section and later calibrated by Gordon to test results documented in the literature. Rankine extended the applicability of the formula to more general cross-sections and published it in his *Manual of Civil Engineering*, greatly increasing its popularity.

Using the variables illustrated in Fig 2-4, the first step in the derivation of the Rankine-Gordon formula consists in establishing that the deflection w of a beam or column is proportional to the square of the length and the maximum bending moment and inversely proportional to the second moment of area I of the cross-section, (2.4).
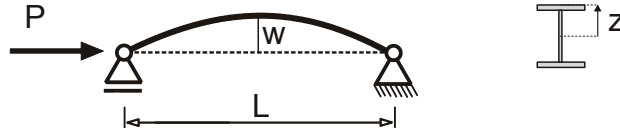
Fig 2-4   Rankine-Gordon derivation, used variables.

$$w = c_1 \cdot \frac{L^2 \cdot M_{max}}{I} \tag{2.4}$$

Thereby, the constant c_1 must have the dimension of length^2/force.

Furthermore, it can be stated that the maximum bending stress σ_M is proportional to M_{max} and the distance z, and inversely proportional to the second moment of area I, (2.5).

$$\sigma_M = c_2 \cdot \frac{M_{max}}{I} \cdot z \tag{2.5}$$

In this case, the constant c_2 is dimensionless. By combining the two expressions, we obtain

$$w = \frac{c_1}{c_2} \cdot \frac{L^2 \cdot \sigma_M}{z} = c_3 \cdot \frac{L^2 \cdot \sigma_M}{z} \tag{2.6}$$

The new constant c_3 is merely a combination of c_1 and c_2 and therefore still has the dimension of length^2/force. Expression (2.6) states that *for a given bending stress*, the deflection w is proportional to L^2/z. The *fundamental assumption* of the Rankine-Gordon derivation is now expressed by (2.7):

$$w = c \cdot \frac{L^2}{z} \tag{2.7}$$

Here, c denotes a dimensionless constant that represents a combination of $c_3 \cdot \sigma_M$, thereby containing the (unknown) bending stress σ_M. The exact, underlying composition of the constant c is however ignored in the rest of the derivation. Since c and c_3 are constants, this is equivalent to assuming that, for a certain pin-ended column with a given cross-section, the bending component of the ultimate stress distribution at failure is also *constant* and *independent of the length*.

The derivation proceeds with the formulation of a maximum stress equation for the deflected column, using $M = P \cdot w$ obtained from simple equilibrium.

$$\sigma_{max} = \frac{P}{A} + \frac{M}{I} \cdot z = \frac{P}{A} + \frac{P \cdot w}{I} \cdot z = \frac{P}{A} + \frac{P \cdot c \cdot L^2}{I} \tag{2.8}$$

By introducing a first-yield failure criterion, using the yield stress f_y as limiting stress, as well as the identity $i^2 = (I/A)$ we obtain expression (2.9).

$$\sigma_{max} = \frac{P}{A} + \frac{P \cdot c \cdot L^2}{A \cdot i^2} = \frac{P}{A} \cdot \left(1 + c \cdot \left(\frac{L}{i} \right)^2 \right) = \frac{P}{A} \cdot \left(1 + c \cdot \lambda^2 \right) = f_y \tag{2.9}$$

The nominal ultimate buckling stress $\sigma_b = P/A$ at failure can therefore be calculated as

$$\sigma_b = \frac{P_b}{A} = \frac{f_y}{\left(1 + c \cdot \lambda^2\right)} \qquad (2.10)$$

Expression (2.10) represents the Rankine-Gordon column formula in its classical form. According to Timoshenko & Lessells (1928), commonly used values for f_y (here not directly comparable to a yield stress) and c for the design of machine components made of steel were f_y=3000 kg/cm² and c=1/7500.
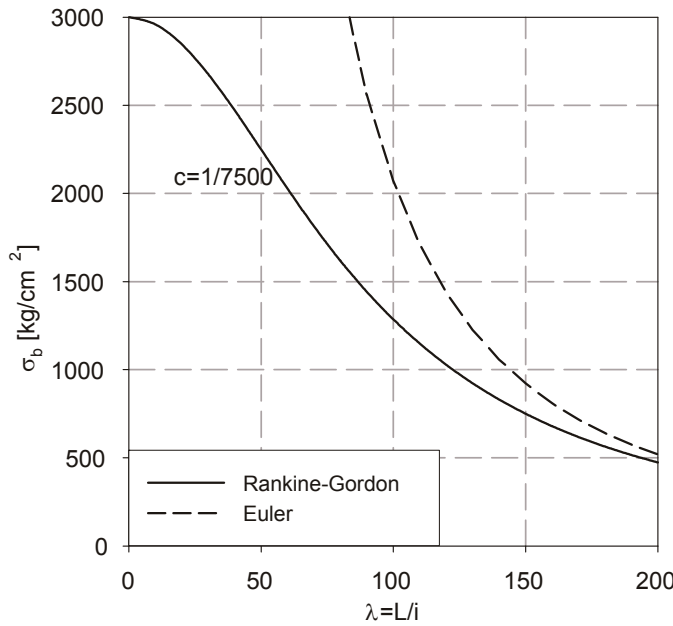
Fig 2-5   Rankine-Gordon buckling stress in [kg/cm²] using a constant of c=1/7500

Fig 2-5 shows the curve representing the buckling stresses that were calculated using these parameters. The Euler-stress σ_{cr} –calculated with a value of E=2100000 kg/cm²- is also plotted in this figure.

Expressed in terms of the common normalized variables χ ($=N_b/N_{ult,k}=\sigma_b/f_y$) and $\bar{\lambda} = \sqrt{N_{ult,k} / N_{cr}} = \lambda / \lambda_1$, (2.10) becomes

$$\chi = \frac{N_b}{A \cdot f_y} = \frac{N_b}{N_{ult,k}} = \frac{1}{\left(1 + k \cdot \bar{\lambda}^2\right)} \qquad (2.11)$$

with

$$k = c \cdot \lambda_1^{\,2} = c \cdot \pi^2 \frac{E}{f_y}$$

The impact of the dimensionless factor k on the position of the Rankine-Gordon buckling curve in the χ-$\bar{\lambda}$ plane is shown in Fig 2-6. One feature of the curves that might be surprising at first sight is the fact that they do not necessarily converge asymptotically towards the Euler hyperbola $1/\bar{\lambda}^2$, actually intersecting the Euler curve when k becomes smaller than unity. A limit value

consideration of equation (2.11) shows that this expression is only asymptotical to the Euler hyperbola if k is equal to 1.0. According to Popov (1952, p. 358), this special case was in use for machine design in North America in the first half of the 20th century and was known as *Ritter's semi-rational formula*.
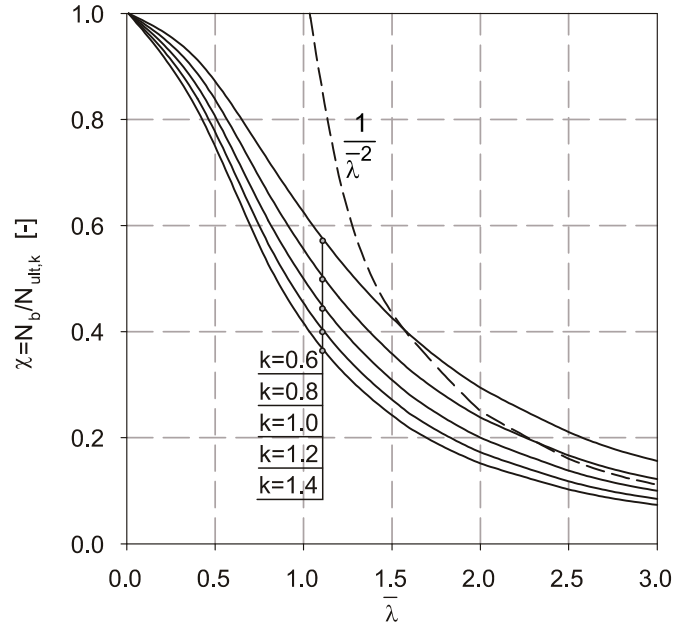
Fig 2-6   Rankine-Gordon formula with varying factors k, compared to Euler buckling criterion

2.4.2. Merchant-Rankine interpretation and visualization

A more modern interpretation and representation of the Rankine-Gordon formula was developed by Merchant (1954). Equation (2.11) can be re-written as follows, using $\bar{\lambda}^2 = N_{ult,k} / N_{cr} \triangleq N_{pl} / N_{cr}$:

$$\chi = \frac{N_b}{N_{pl}} = \frac{1}{\left(1 + k \cdot \dfrac{N_{pl}}{N_{cr}}\right)} \tag{2.12}$$

from which follows:

$$\frac{N_b}{N_{pl}} + k \cdot \frac{N_b}{N_{cr}} = 1 \tag{2.13}$$

N_b/N_{pl} and N_b/N_{cr} are the ratios of the ultimate buckling load N_b to the plastic limit or Euler critical load, respectively. If we regard each of these ratios as abscissa and ordinate variables of a Cartesian coordinate system, we can interpret expression (2.13) geometrically as a straight line that passes through N_b/N_{pl}=1.0, and through N_b/N_{cr}=1/k. This is plotted in Fig 2-7 for various values of k, showing the same lines plotted in Fig 2-6 in what came to be called the *Merchant-Rankine* (MR) form of presentation introduced in Fig 2-2.
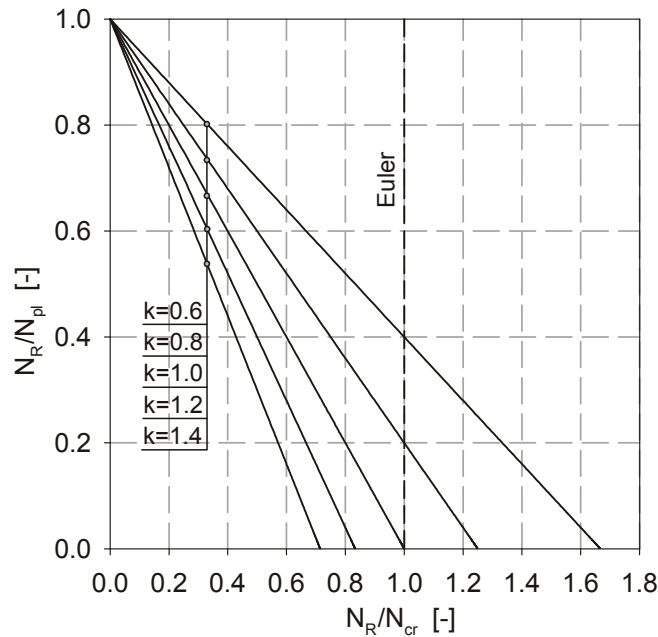
Fig 2-7   Merchant-Rankine representation of the original Rankine-Gordon formula with varying values of k

Horne and Merchant (1965) considered equation (2.13) to be *rational* only for the case of k=1.0, since only in this case the two rational limits of stability design are reached, i.e. the fully plastic limit load without stability effects and the purely elastic critical load without plasticity and material strength effects. Equation (2.13) then becomes:

$$\frac{N_b}{N_{pl}} + \frac{N_b}{N_{cr}} = 1 \qquad (2.14)$$

Merchant suggested an expansion of the use of (2.14) to the design of frames, thereby replacing the plastic limit and elastic critical normal forces N_{pl} and N_{cr} of a column with the global plastic and elastic load amplification factors R_{ult} and R_{cr} of a frame. This method is effectively an early application of an "overall" approach to the stability design of whole structures.

Horne (1963) also gave a somewhat more "modern" theoretical justification to the version of the Rankine equation given by (2.14), using a combination of an elastic-plastic (E-P) analysis with "sudden" development of plastic hinges and a rigid-plastic (R-P) analysis (also see Ligtenberg, 1965; Maquoi&Jaspart, 2001).

It is worthwhile to take a look at this derivation from today's perspective. Thereby, Fig 2-8 is used to exemplify the assumptions made in the derivation and to illustrate the comments to it.

i.   In the elastic-plastic analysis of a pin-ended column with a sinusoidal imperfection of amplitude $\bar{e}_0$, the buckling load N_b is reached when the plastic moment capacity $M_{pl,N\text{-}b}$ – which includes the effect of the normal force N_b on the plastic capacity of the cross section- is reached at mid-span. If the dimensionless variable m is used according to Fig 2-8, the

ratio m_b is reached: $m_{b,1}$ for the shorter column and $m_{b,2}$ for the longer one. This can be expressed as follows, using the elastic amplification factor $1/(1-N/N_{cr})$:

$$\frac{N_b \cdot \bar{e}_0}{1 - \dfrac{N_b}{N_{cr}}} = M_{pl,N-b} = m_b \cdot M_{pl} \tag{2.15}$$
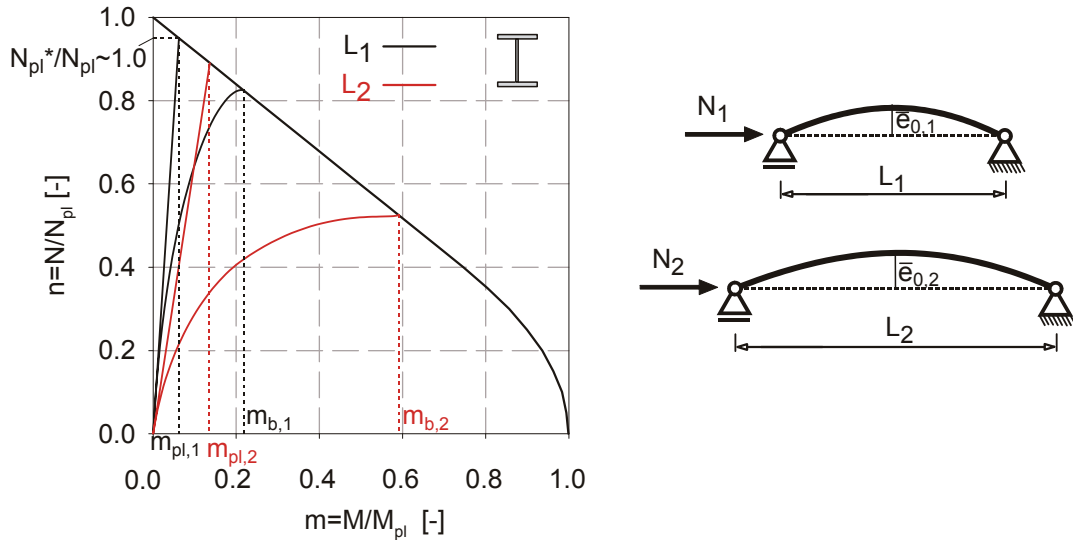
Fig 2-8   M-N cross-sectional interaction line of an IPE section; visualization of the assumptions made in the Horne derivation of the Merchant-Rankine equation.

ii. In the (first order) rigid-plastic analysis of this column, the ultimate (plastic) load N_{pl}^* is achieved when the plastic moment capacity $M_{pl,N-pl}$ is reached at mid-span. Again using the dimensionless variable m, the ratio m_{pl} is reached: $m_{pl,1}$ for the shorter column and $m_{pl,2}$ for the longer one. Since the column is thought to be rigid, the bending moment at mid-span is always equal to $N \cdot \bar{e}_0$, as no additional bending deformations occur. In Fig 2-8, this shows as a straight line in the n-m plane. For most practical columns, $\bar{e}_0$ will be comparatively small both in terms of the fraction of length and (more importantly here) in *absolute* terms. This means that there will be a rather small difference in the rigid analysis between N_{pl}^* and the full plastic capacity $A \cdot f_y = N_{pl}$; this is illustrated for the column of length L_1 in Fig 2-8. If this holds, we can write.

$$N_{pl} * \cdot \bar{e}_0 \approx N_{pl} \cdot \bar{e}_0 = M_{pl,N-pl} = m_{pl} \cdot M_{pl} \tag{2.16}$$

iii. In the derivation of the Merchant-Rankine formula, the *assumption is now made* that m_b *is equal to* m_{pl}. We can therefore set (2.15) and (2.16) equal and obtain:

$$\frac{N_b}{1 - \dfrac{N_b}{N_{cr}}} = N_{pl} \tag{2.17}$$

Equation (2.17) is equal to (2.14). This derivation is – at first glance- more coherent and "advanced" than the original Rankine-Gordon derivation because of the apparent inclusion of

plasticity considerations and the lack of an arbitrary constant. However, a look back to equation (2.6) and (2.7) and the comments made there shows that the *fundamental assumption* of this derivation is exactly the same: that the bending component of the ultimate stress distribution at failure is *constant* and -for any given value of $\overline{e}_0$ - *independent of the length of the member*.

As Fig 2-8 schematically illustrates, these assumptions can only *approximately* be met under very specific circumstances:

- not too slender columns
- with somehow "intermediate" imperfection amplitudes

so that the ratio between m_b and m_{pl} indeed is almost "independent" of length (in this range) and approaches unity. If the column is too slender and stability effects become too dominant, and/or if the load eccentricity or column out-of-straightness is too large, it is obvious that the ratio m_b/m_{pl} will be significantly larger than unity, since m_b will be significantly larger than m_{pl}. If however the initial out-of-straightness $\overline{e}_0$ is too small, again the ratio m_b/m_{pl} will be far larger than 1.0, this time because m_{pl} is too small.
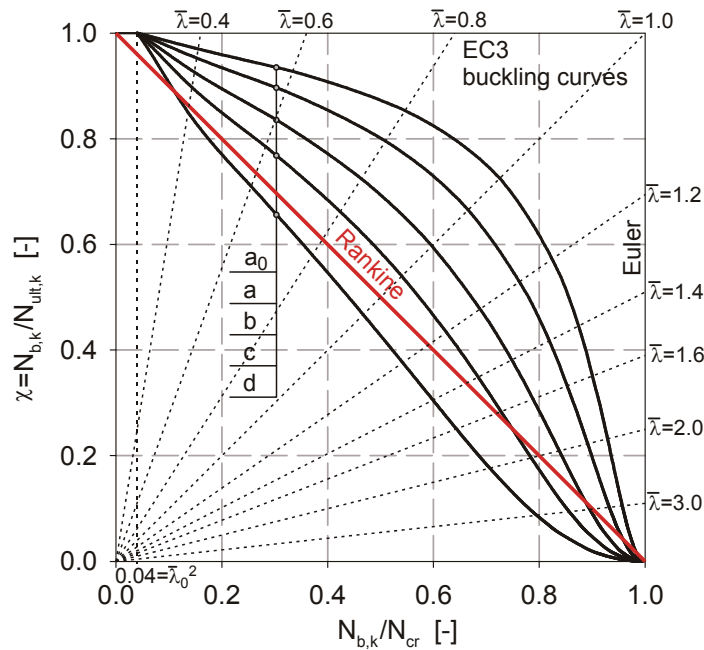
Fig 2-9   Comparison of the Rankine equation with the European column buckling curves using the Merchant-Rankine form of representation

In order to better illustrate these comments, the Rankine equation (2.14) is compared in Fig 2-9 to the ECCS column buckling curves in their current Eurocode 3 version. The Merchant-Rankine form of presentation is used. The figure shows that the Rankine equation (straight line from top left to bottom right) approximates the course of the European column buckling curves "c" and "d" reasonably well for slenderness ratios of $\overline{\lambda} = 0.4$ to 1.4, with line "c" in particular being almost parallel to the Rankine line up to this point. For higher slenderness ratios, the slope of line "c"

clearly diverges from the Rankine line. This matches the comments made above regarding the Horne derivation quite well:

i.   line "c" and "d" represent columns with somewhat larger equivalent imperfections in the range of $\overline{e}_0$ =L/150 in EC3 part 1-1, clause 5.3.2. Lines "a₀" to "b" all represent columns with smaller inherent imperfections.

ii.   for slender columns, the Rankine line doesn't appear to represent a good description of the column behaviour.

From a purely safety-related perspective, it should be noted that for columns with *small initial imperfections*, the Rankine equation describes the actual column strength rather inaccurately, but results in an abundantly safe design; for columns with *large initial imperfections*, on the other hand, the accuracy *and safety* of the equation are lacking.

2.4.3. Modified Merchant-Rankine formula

The plots of the European column buckling curves, as presented in Fig 2-9, illustrate that realistic buckling curves of structural members have a shape that clearly diverges from a straight line in the Merchant-Rankine form of presentation. This was acknowledged over the course of the development of the European column buckling rules. A modified, so-called "generalized" version of equation (2.14) was therefore brought forward in Europe in the 1970s (Unger, 1977; Murzewski, 1977; Lindner, 1978; Allen, 1978) and suggested as a viable means of description of more complex, realistic buckling curves. In the summative Merchant-Rankine form, the "generalized" equation can be written as:

$$\left(\frac{N_b}{N_{pl}}\right)^n + \left(\frac{N_b}{N_{cr}}\right)^n = 1 \tag{2.18}$$

In explicit form and using the dimensionless variables χ and $\overline{\lambda}$, (2.18) becomes:

$$\chi = \frac{N_b}{N_{pl}} = \left(\frac{1}{\left(1 + \overline{\lambda}^{2n}\right)}\right)^{1/n} \tag{2.19}$$

These equations are evaluated for different values of the single parameter n and plotted in Fig 2-10 using both the Merchant-Rankine (MR) and the slenderness-dependent form of representation. While Fig 2-10b shows that this formula again yields column buckling curves that are *plausible* and *rational*, it is in the representation used in Fig 2-10a that the advantage of this generalized expression is better appreciated.
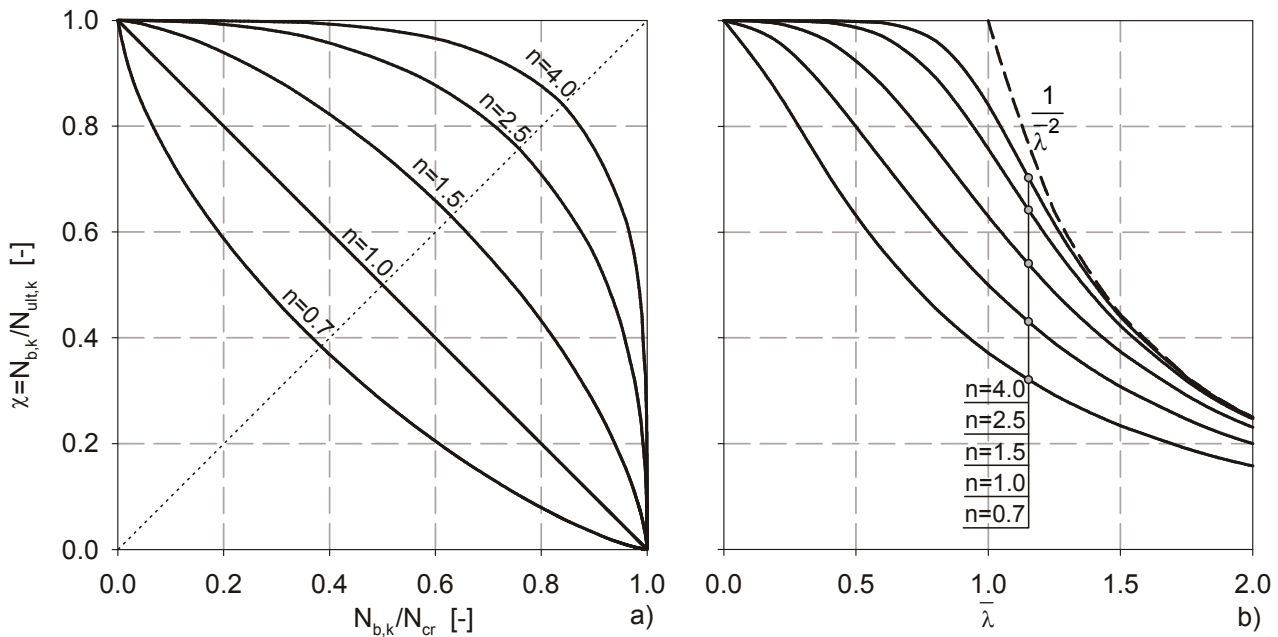
Fig 2-10 Generalized Merchant-Rankine formula plotted using (a) the MR- and (b) the slenderness dependent representation

This figure shows that the *single parameter n* in equation (2.19) allows for a good approximation of the curved shape of realistic column buckling curves, e.g. compare again to Fig 2-9.

Expressions (2.18) and (2.19) have found broad international acceptance in the past:

i. Lindner (1978) calibrated the parameter n to find the best-fit value to describe the (originally only tabulated) ECCS column buckling curves, obtaining results that are comparable to the more complex Ayrton-Perry type formulae used in the Eurocode today.

ii. This same equation was also used for almost two decades in DIN 18800-2 (1990) for the design against lateral-torsional buckling of I- and H-shaped sections, using values of the parameter equal to n=2.5 for rolled and n=2.0 for welded sections.

iii. It has also been used in the Canadian CSA Standard S16.1-94 (Loov, 1995) for curve-fitting of the originally tabulated American SSRC column buckling curves (Galambos, 1998) leading to accurate representations of the original values.

Despite its apparent advantages, it should however not remain unmentioned that equation (2.18) does not have a mechanical justification in the strict sense, having *no known mechanical derivation*, but is much rather simply a compact and practical formula used for curve-fitting.

If the clarity of the used terminology is thought to be important, it can be argued that this formulation should not be called a "generalized" Merchant-Rankine formula, as this term somehow implies a more "general" validity of the expression. The increased representativeness of this formulation is actually only given *in retrospect*, i.e. after the best-fit value of n was determined to better represent a certain buckling phenomenon, and not *a priori*, as would be expected from a mechanically improved "generalized" expression. Although this can of course be shrugged off as a

minor semantic problem, it would clearly be better - in order to avoid misinterpretation- to refer to formula (2.18) as a "modified" or even "calibrated" Merchant-Rankine formulation.

2.4.4. Comments

Concluding and summarizing the findings illustrated in this section regarding the Merchant-Rankine approach, it can be stated that:

i. The original Rankine-Gordon or Merchant-Rankine formula was derived using assumptions that limit the goodness of its description of the actual behaviour of members to very specific cases.

ii. In spite of this, the formula can often be used as a safe estimate of the buckling limit load of members and structures.

iii. A (formally) generalized version of the formula, which uses only one extra parameter, is very well suited to curve-fitting.

iv. The formula has a mathematical form and geometrical interpretation that called for the introduction of a different form of representation of buckling curves, where the buckling reduction factors (or limit stresses) are plotted over the ratio N_b/N_{cr}, rather than over the length or slenderness of the member.

2.5. The Ayrton-Perry-Robertson approach

Another important approach for the determination and presentation of buckling resistance is represented by the Ayrton-Perry formula. It found early application in design practice – again, especially in the Anglophone world-, and is still widely in use today. Indeed, a version of it is the basis of the member buckling design formulae currently found in the Eurocode.

When compared to the Euler or the Merchant-Rankine approach, the Ayrton-Perry method has one outstanding advantage: it explicitly includes the inevitable imperfections of a structural member, and it does so in a generalized form that allows for an inclusion of geometric *and* structural imperfections. Indeed, by using a generalized or "equivalent" imperfection as the calibration factor to bring the analytical prediction in line with test data or more sophisticated numerical results, it greatly aids the understanding of the meaning of the calibration itself, as it corresponds to both common sense and experience that a column's strength is inversely correlated to the amplitude of a given imperfection.
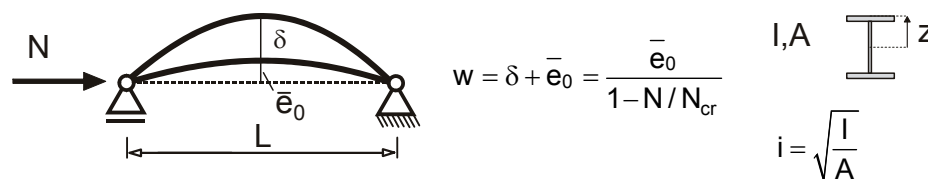
Fig 2-11   Ayrton-Perry derivation, used variables.

2.5.1. Original derivation

The original formula (Ayrton & Perry, 1886) was derived along the lines described in the following, whereby the variables shown in Fig 2-11 are used here instead of the original ones. Ayrton and Perry actually started their considerations by deriving the elastic buckling amplification factor 1/(1-N/N$_{cr}$) for a column with an initial imperfection $\overline{e_0}$. This step is skipped here and the derivation is entered at the point where a maximum stress equation is introduced.

The maximum compression stress in the outermost fibre of the cross-section of a pin-ended column as depicted in Fig 2-11 can be calculated as follows:

$$\sigma_{max} = \frac{N}{A} + \frac{N \cdot w \cdot z}{I} = \frac{N}{A} + \frac{N \cdot \overline{e_0} \cdot z}{I \cdot (1 - N/N_{cr})} = \frac{N}{A} \cdot \left(1 + \frac{\overline{e_0} \cdot z}{i^2} \cdot \frac{1}{(1 - N/N_{cr})}\right) \qquad (2.20)$$

In order to generalize the nature of the initial column imperfection, Ayrton and Perry conveniently *replaced the expression preceding the amplification factor in the parenthesis of equation (2.20) with a new variable m*:

$$\frac{\overline{e_0} \cdot z}{i^2} = \frac{\overline{e_0} \cdot A}{W} = m \qquad (2.21)$$

As they noted, m is "*a term expressing the combination of initial curvature, inaccuracy in application of the load, and want of homogeneity of the material*". If appropriately chosen –i.e. calibrated to test results or other more sophisticated expressions for buckling resistance-, it represents an "equivalent" imperfection which takes into account the above-mentioned effects, including those that do otherwise not enter the purely elastic equation (2.20).

The next step in the derivation consists in introducing a first-yield failure criterion; in this case, at failure the normal force N is equal to N$_b$, and the maximum stress σ_{max} is equal to the yield stress f$_y$. If we write the nominal stress caused by the normal force N$_b$/A at failure as σ_b and the critical elastic buckling stress N$_{cr}$/A as σ_{cr}, the failure condition reads as follows:

$$\sigma_b \cdot \left(1 + \frac{m}{(1 - \sigma_b / \sigma_{cr})}\right) = f_y \qquad (2.22)$$

By multiplying both sides by (σ_b/σ_{cr}-1), re-ordering and bringing all variables to the left side, this equation can also be written as

$$\sigma_b^2 - \sigma_b \cdot (\sigma_{cr} \cdot (1 + m) + f_y) + \sigma_{cr} \cdot f_y = 0 \qquad (2.23)$$

This is a quadratic equation of the form $x^2 + b \cdot x + c = 0$ and can be solved accordingly: $x = 1/2 \cdot \left(-b \pm \sqrt{b^2 - 4c}\right)$. Only the smaller of the two solutions is of interest here. The ultimate buckling stress σ_R=N$_R$/A can thus be calculated using the following formula:

$$\sigma_b = \frac{1}{2} \cdot \left((\sigma_{cr} \cdot (1 + m) + f_y) - \sqrt{(\sigma_{cr} \cdot (1 + m) + f_y)^2 - 4 \cdot \sigma_{cr} \cdot f_y}\right) \qquad (2.24)$$

This is the Ayrton-Perry formula in its original form. Ayrton and Perry were aware of the fact that a realistic expression for m must be determined or specified. In order to achieve this, they proposed to solve equation (2.22) for m, which leads to equation (2.25), and to calculate the "correct" value of m for a number of test results. If a sufficient number of test results are given, it should be possible to find an appropriate expression for m as function of e.g. the length L or the slenderness λ.

$$\left(\frac{f_y}{\sigma_b} - 1\right) \cdot \left(1 - \frac{\sigma_b}{\sigma_{cr}}\right) = m \tag{2.25}$$

Although they observed from tests on small-scale specimens that the value of $\bar{e}_0$ –and hence m- is probably in a slightly hyper-linear functional relationship with the length (or slenderness) of the column, Ayrton and Perry found it convenient to assume that m is a constant fraction of the slenderness λ, i.e $m = \alpha \cdot \lambda$, with α being a certain constant.

Fig 2-12 shows equation (2.24) evaluated for values of f_y and E that Ayrton and Perry stated were valid for wrought iron –f_y=50000 lb/in² and E=29000000 lb/in²- and for various expressions of m. The figure shows that the chosen slenderness-proportional expression for m allows for a *plausible* and rational representation of buckling curves, which asymptotically approach the Euler hyperbola and span a wide range of buckling stresses. The position and shape of the buckling curve in the σ_b-λ plane strongly depends on the value of the proportionality factor α=m/λ. For α=0.0, either the Euler buckling stress or the yield stress of the material represent the upper limits of the buckling stress, which is consistent with the theoretical strength of a "perfect" column.
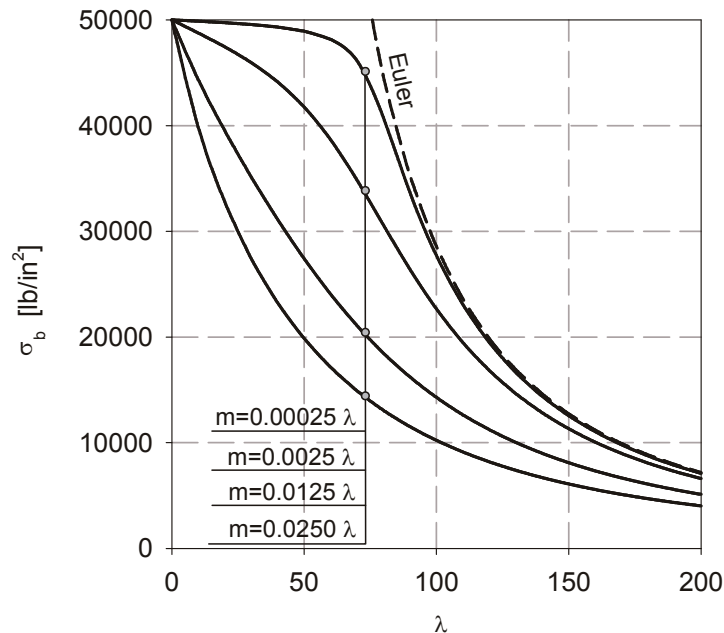
Fig 2-12 Original Ayrton-Perry equation evaluated for different expressions of m and material constants of wrought iron.

2.5.2. Calibration to tests – "Robertson's formula"

Ayrton and Perry provided a formula – equation (2.24)- that allows for a good description of buckling phenomena, *provided that the expression for m is adequate and properly calibrated to test results*. This was first done extensively and with already very good accuracy by Robertson (1925), who performed and collected from various sources a great number of buckling tests on medium-sized specimens (mostly rolled bars of full, circular cross-section).

Robertson used the Ayrton-Perry formula with an expression for the generalised imperfection identical to the one proposed by Ayrton and Perry themselves, however choosing to call it η instead of m:

$$\eta = \alpha \cdot \lambda \qquad (2.26)$$

As is illustrated in the original Fig 2-13 taken from the Robertson publication, he established that for a mild steel with a yield strength of f_y=18.3 to/in² and a Young's Modulus of E=13600 to/in², a value of α=0.001 is a good description of the average of the test results, while a value of α=0.003 yields a curve which forms a good lower bound of these same results. An Ayrton-Perry buckling formula with the latter value of α was used extensively in the UK and in Commonwealth countries, for example still being present in the 1969 version of British Standard BS 449.
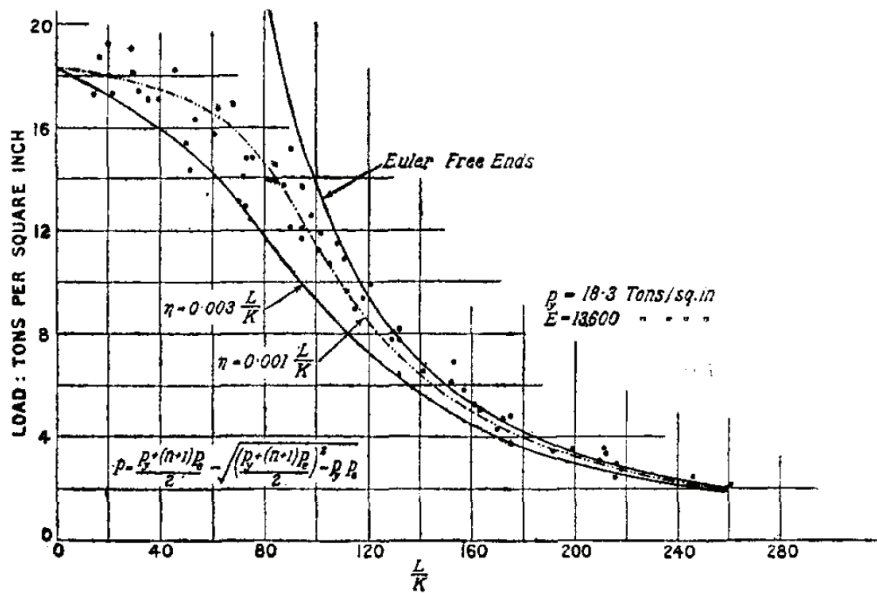
MILD STEEL STRUTS WITH POINTED ENDS (*von Tetmajer*).

Fig 2-13   Tests by Tetmajer (1910) as evaluated by Robertson, showing chosen function for η=m (Robertson, 1925, p.32, Fig.34)

2.5.3. The normalized representation

In order to bring the Ayrton-Perry formula (2.24) into the modern form now found in the Eurocodes, it is necessary to introduce the normalized variables χ and $\bar{\lambda}$, and it is helpful to multiply all stress terms in formula (2.24) with the area, in order to work with forces again. The generalized imperfection factor m of formula (2.24) will be referred to as η from now on, following Robertson's usage. We thus obtain:

$$N_b = \frac{1}{2} \cdot \left((N_{cr} \cdot (1+\eta) + N_{pl}) - \sqrt{(N_{cr} \cdot (1+\eta) + N_{pl})^2 - 4 \cdot N_{cr} \cdot N_{pl}} \right) \qquad (2.27)$$

Using $\bar{\lambda}^2 = N_{pl} / N_{cr}$ we can rewrite the term $(N_{cr} \cdot (1+\eta) + N_{pl})$ as $N_{cr} \cdot (1+\eta+\bar{\lambda}^2)$. It is then convenient to replace the term $(1+\eta+\bar{\lambda}^2)$, which is found both inside and outside of the root, with a new variable; if we call the new variable Φ and set the parenthesis term equal to $2 \cdot \Phi$, we can write (2.27) as:

$$N_b = \frac{1}{2} \cdot \left(2 \cdot N_{cr} \cdot \Phi - \sqrt{4 \cdot N_{cr}^2 \cdot \Phi^2 - 4 \cdot N_{cr} \cdot N_{pl}} \right) = N_{cr} \cdot \left(\Phi - \sqrt{\Phi^2 - \bar{\lambda}^2} \right) \qquad (2.28)$$

By expanding equation (2.28) by $1/N_{pl}$ and using $\chi = N_b / N_{pl}$ and $N_{cr}/N_{pl} = 1/\bar{\lambda}^2$, we obtain:

$$\chi = \frac{1}{\bar{\lambda}^2} \cdot \left(\Phi - \sqrt{\Phi^2 - \bar{\lambda}^2} \right) \qquad (2.29)$$

This equation can now be multiplied with the complement of the bracket term:

$$\chi = \frac{1}{\bar{\lambda}^2} \cdot \left(\Phi - \sqrt{\Phi^2 - \bar{\lambda}^2} \right) \cdot \left[\frac{\Phi + \sqrt{\Phi^2 - \bar{\lambda}^2}}{\Phi + \sqrt{\Phi^2 - \bar{\lambda}^2}} \right] = \frac{1}{\bar{\lambda}^2} \cdot \frac{\bar{\lambda}^2}{\Phi + \sqrt{\Phi^2 - \bar{\lambda}^2}} \qquad (2.30)$$

This finally leads to the form of the Ayrton-Perry formula currently found in the Eurocode:

$$\chi = \frac{1}{\Phi + \sqrt{\Phi^2 - \bar{\lambda}^2}} \qquad (2.31)$$

with

$$\Phi = \frac{1}{2} \cdot \left(1 + \eta + \bar{\lambda}^2 \right) \qquad (2.32)$$

It should be noted that equations (2.31) with (2.32) are not in any way different from expression (2.24), except for the fact that the buckling stress is expressed in normalized terms and referred to the normalized slenderness $\bar{\lambda}$. The position of the buckling curve is still entirely determined by the expression chosen for η and by the value chosen for the imperfection amplitude factor α.

Fig 2-14 attempts to underscore the significance of this statement; it shows buckling curves for different steel grades, determined using formula (2.30) and with $\eta = 0.003 \cdot \lambda$, as Robertson suggested.

Since the current Eurocode formulae result in normalized buckling curves that do not depend on the steel grade, it is perhaps not universally appreciated that the steel grade *does* influence the buckling reduction factor χ if the generalized imperfection η is expressed by a function of λ, instead of $\bar{\lambda}$, as is the case in the current Eurocode formulation.

The current Eurocode expressions for η have the following form:

$$\eta = \alpha \cdot \left(\bar{\lambda} - \bar{\lambda}_0 \right) \tag{2.33}$$

Expression (2.33) was proposed and discussed by Maquoi and Rondal (1978) as one of several possible expressions for η and then established to be the most advantageous formulation in a second paper by the same authors (Rondal & Maquoi, 1979). For column buckling, $\bar{\lambda}_0$ is equal to 0.2; this value is needed to mathematically reproduce the "plateau" of the European column buckling curves as established by ECCS.

The values of α were determined by Maquoi and Rondal to best fit the European column buckling curves, resulting in 5 different values for the 5 ECCS curves. These were presented graphically in Fig 2-2 both in the slenderness-based and the Merchant-Rankine type of representation. An expression for η as function of the *normalized* slenderness $\bar{\lambda}$, instead of λ, of the sort represented by (2.33), results in buckling curves that are independent of the yield strength of the material, which is consistent with the original, tabulated ECCS curves. Some more details on this calibration of the Ayrton-Perry formulation to the ECCS curves will be given in the pertinent chapter 5.
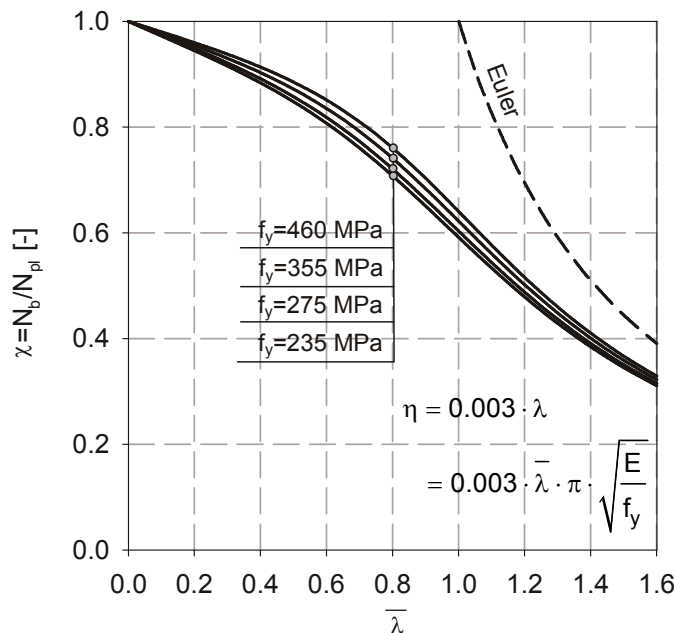
Fig 2-14 Normalized Ayrton-Perry buckling curves evaluated with η as given by Robertson.

2.5.4. "Modified-slenderness" Ayrton-Perry formulations

The classical Ayrton-Perry formulation has sometimes been criticized due to its apparent focus on a "first yield" criterion and due to its not always "perfect" accuracy. In this context, Rotter (1982) proposed an expression that represents a modified version the original Ayrton-Perry formula. He criticized the values of buckling reduction factors resulting from an "unmodified" Ayrton-Perry formulation (again calibrated by Rondal and Maquoi (1979b)) used to describe the North American SSRC column buckling curves, judging them to show excessive deviations from the original values. To improve this situation, he suggested the introduction of a slenderness modification of the following form:

$$\bar{\lambda}_{\mathrm{mod}} = \bar{\lambda} + k \cdot g \qquad (2.34)$$

with k being a constant value that depends on the column curves 1, 2 or 3, and:

$$g = \frac{\bar{\lambda} - 0.15}{\bar{\lambda}^2 - \beta \cdot \bar{\lambda} + \gamma} \qquad (2.35)$$

Multiple regression analysis was used to determine the best-fit values of k, β and γ. By applying this method, the accuracy of the approximation of Rondal and Maquoi's original formulation was increased from a maximum deviation of about 8% in the region of $\bar{\lambda}$=2.0 to ca. half of this value.

This increased accuracy is of course valuable. However, the cost in terms of handiness of this improvement – which mainly affected the practically less-relevant high-slenderness range- seems rather high in this case:

i.   Three additional parameters were introduced; in a code, this requires additional tabulation and leaves more room for error. From the point of view of the application to new buckling design rules for different stability phenomena, these three parameters would have to be laboriously calibrated with all their possible combinations to any new member buckling case.

ii. The slenderness $\bar{\lambda}$ is modified in this approach to obtain a best-fit value of the buckling reduction factor χ; since the slenderness is the most "visual" parameter of a buckling phenomenon, which is well understood and interpreted by the engineer, it is questionable whether it is really recommendable to modify this parameter in order to obtain an improvement of the abscissa variable χ.

Another example of a modified Ayrton-Perry formulation is given by the current "specific case" design formula for LT-buckling, i.e. the formula that is said to apply to bi-symmetric hot-rolled sections. Also in this case, the improvement of the calibration results (to numerical curves, see Greiner et al., 2000) was achieved by an introduction of a "modifier" of the slenderness influence in the formulation, called "β" in this case. This factor was applied in both the formula for χ_{LT} (2.36) and Φ_{LT} (2.37).

$$\chi_{LT} = \frac{1}{\Phi_{LT} + \sqrt{\Phi_{LT}^2 - \beta \cdot \overline{\lambda}_{LT}^2}} \leq \frac{1}{\overline{\lambda}_{LT}^2} \leq 1.0 \qquad (2.36)$$

and

$$\Phi_{LT} = \frac{1}{2}\left[1 + \alpha_{LT}\left(\overline{\lambda}_{LT} - \overline{\lambda}_{LT,0}\right) + \beta \cdot \overline{\lambda}_{LT}^2\right] \qquad (2.37)$$

Since only one additional factor β is introduced, the first one of the above points of "criticism" is mitigated in this case. The second one, however, still holds validity: there's a certain degree of loss of mechanical meaning in this formulation, which is also demonstrated by the fact that this formulation requires an additional "check" of not exceedance of the bifurcation load $1/\overline{\lambda}_{LT}^2$.

2.5.5. Comments

The findings of this section can be summarized and commented upon as follows:

   i.   The Ayrton-Perry formula was derived using a consistent mechanical model based on the second-order theory of a strut with geometrical imperfections.
   ii. As Ayrton and Perry (1886) already recognized, the geometrical imperfection used during the derivation of the buckling formula can conveniently be "generalized" by introducing a function η; this function serves the purpose of including additional imperfections, such as material inhomogeneities and residual stresses, as well as the elasto-plastic cross-sectional capacity at the (buckling) failure load, i.e. effects that can otherwise not easily be included in such a simple mechanical model.
   iii. Robertson (1925), using a generic expression for η that had already been proposed by Ayrton and Perry themselves, was the first to actually calibrate the coefficients of this expression to test results, thereby providing a practical design formula that was extensively used in practice for over half a century.
   iv. Rondal & Maquoi (1978, 1979) provided a calibration to the ECCS column buckling curves, currently found in the Eurocode. Compared to the Robertson formula, the main difference lies in the introduction of a plateau value and in the normalized formulation using $\overline{\lambda}$.
   v.   To improve the accuracy of the Ayrton-Perry formulation for some specific cases, modifications can be thought of. Rotter (1982) presented an early attempt at such a modification. Notionally similar modifications were later introduced to adapt the formulation to buckling cases other than column buckling, namely LT-buckling, also see chapter 6 of this dissertation.

2.6. Pure curve-fitting and empirical approaches

The Merchant-Rankine and the Ayrton-Perry approaches led to the most common formulaic expressions of buckling curves now found in international standards and literature. Both formulations should be best understood as powerful tools for best-fit approximations of more sophisticated numerical or experimental buckling curves, with the added advantage (particularly felt

in the Ayrton-Perry formulation) of having a certain, more or less pronounced degree of underlying mechanical justification. This allows for a satisfactory inclusion of the most important parameters that govern a particular stability problem and accordingly reduces the calibration effort.

However, if the correctness or consistency of the underlying mechanics are not considered to be paramount, but the best possible approximation of a given (usually tabulated or graphical) buckling curve is established as the primary purpose of a buckling formula, then a multitude of other mathematical options are imaginable. Some of these curve-fitting formulae are discussed in the following paragraphs.

2.6.1. Mixed polynomial/hyperbolic formulations

The first of these "pure curve-fitting" formulations uses a summation of *higher order expressions of* $\overline{\lambda}$ for this purpose. Lindner (1978), noting that the shape of the ECCS curves is an apparent mix of parabolic and hyperbolic shapes, suggested a formulation of the type given by (2.38) as one possibility of representing the tabulated ECCS values.

$$\chi = \sum_{i=0}^{4} A_i \cdot \overline{\lambda}^{i} + \sum_{j=1}^{7} \frac{B_j}{\overline{\lambda}^{j}} \qquad (2.38)$$

Eleven constants are needed in this expression to satisfactorily approximate the entire range of the original, tabulated buckling curves (from $\overline{\lambda}$=0.0 to 3.6). The maximum differences between the values given by (2.38) and the original values were smaller than 1.0%; in theory, even this difference could be reduced by introducing even more parameters.

In spite of this discretionary accuracy of the approximation, this formulation has the following problem: a singularity is introduced at $\overline{\lambda}$=0.0 due to the presence of a term with $\overline{\lambda}$ in the denominator. Even if this is ignored by introducing the condition that χ=1.0 at $\overline{\lambda}$=0.0, the range of low slenderness is very sensitive to the actual value of the coefficients A_i and B_j. Even a slight deviation from the actual "best-fit" value in the 4th or 5th decimal figure results in implausible, wrong results.

Fig 2-15 shows the ECCS column buckling curves as approximated by expression (2.38) and using the coefficients A_i and B_j given by Lindner. Although the plots of the resulting curves give very good approximations of the ECCS values at slenderness ratios exceeding $\overline{\lambda}$=0.5, the approximation is very bad at lower slenderness ratios. This is probably due to the mentioned sensitiveness of expression (2.38) at low values of $\overline{\lambda}$; the table containing the coefficients A_i and B_j only mentions a limited number of decimal figures. Since powers spanning +4 and -7 are used, even minor differences in a high decimal figure can dramatically change the resulting shape of the curves at this slenderness range.
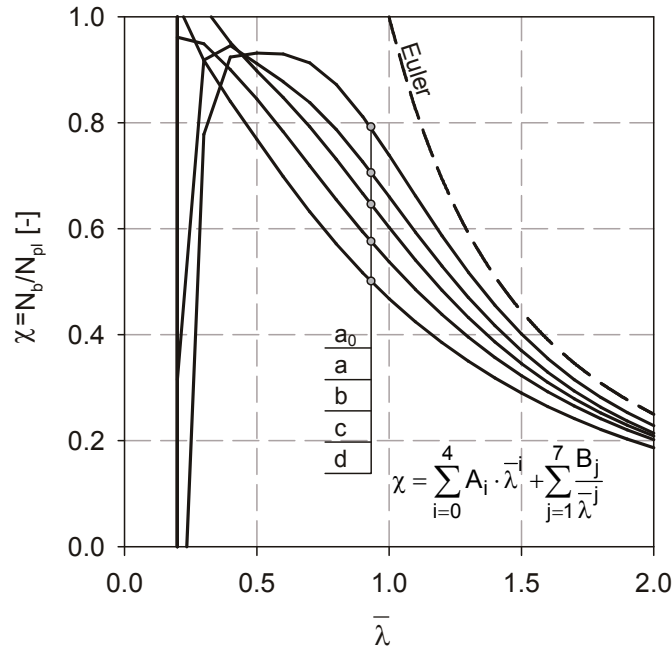
Fig 2-15 Approximation of the ECCS column buckling curves using the curve-fitting expression and coefficients proposed by Lindner (1978)

2.6.2. Polynomials

The above-mentioned problems can of course be circumvented by using a purely *polynomial expression* of the following type to approximate the shape of a buckling curve:

$$\chi = \sum_{i=0}^{n} A_i \cdot \overline{\lambda}^{i} \tag{2.39}$$

In expression (2.39), the value of n can be increased at will in order to augment the accuracy of the approximation. Fig 2-16a shows the approximations of the ECCS column buckling curves resulting from this approach and n=6, while Fig 2-16b plots the resulting error over the normalized slenderness. This figure illustrates that expression (2.39) results in an approximation that is less sensitive and far more accurate at low slenderness ratios. However, since at high slenderness ratios the actual buckling curves approach a hyperbolic function of $\overline{\lambda}$ - the Euler hyperbola -, a purely polynomial expression, centred about the origin of the ordinate axis, inevitably results in a less accurate description of the buckling curve at high values of $\overline{\lambda}$. This clearly shows in Fig 2-16b. Another problem with this expression is represented by the fact that it yields buckling reduction factors χ that (slightly) exceed 1.0 at very low slenderness ratios, and that it does not include the plateau value of $\chi=1.0$ up to $\overline{\lambda}=0.2$ that is actually present in the original ECCS curves.
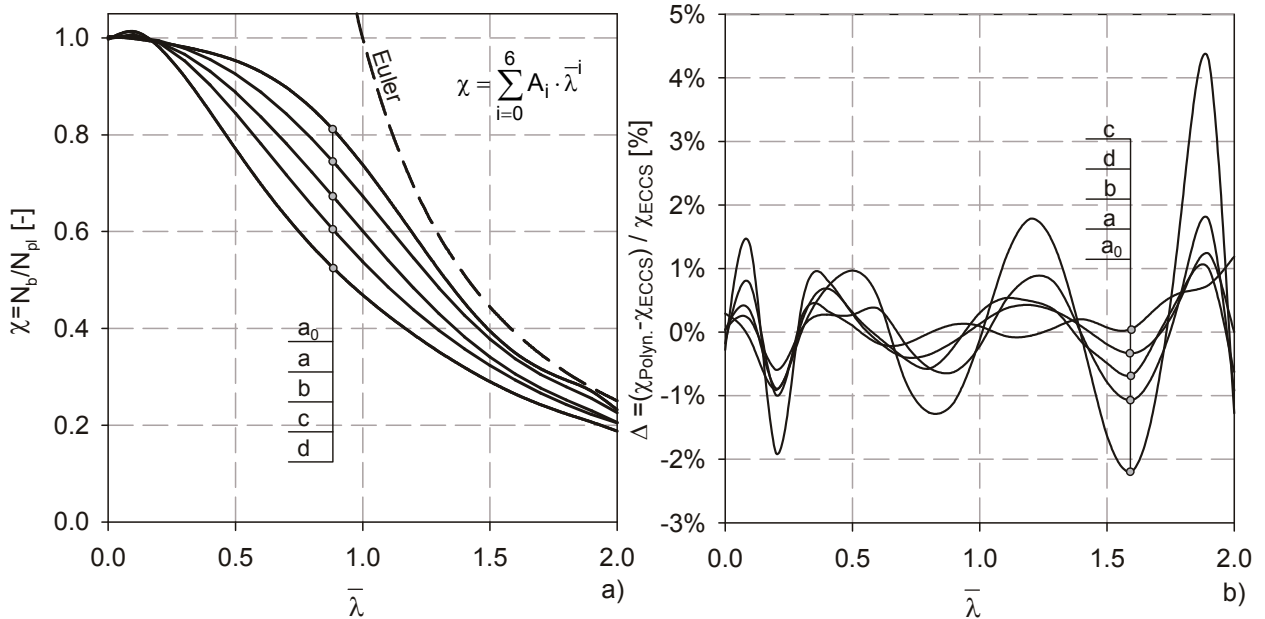
Fig 2-16 a) Polynomial approximation of the ECCS column buckling curves for the case of n=6 and best-fit values of the coefficients A_i ; b) resulting error in the approximation

The problems inherent to expressions (2.38) and (2.39) can be avoided by using a *section-by-section* approximation of a buckling curve, i.e. by dividing the curve that needs to be described analytically into a certain number of segments and determining a polynomial or hyperbolic best-fit equation for this segment. Attention must of course be paid to the continuity of the resulting expression, whereby a zero-order continuity (with the values matching, but the tangents having different slopes) is usually considered to be acceptable.

This approach is used in North America (Galambos, 1998) to describe the SSRC column buckling curves. As an example, the expressions used to approximate the SSRC curve 2P (central curve with average imperfection values) are given in the following, using the familiar normalized variables χ and $\overline{\lambda}$:

$$\text{for } 0.00 \leq \overline{\lambda} \leq 0.15 \qquad \chi = 1.0$$

$$\text{for } 0.15 \leq \overline{\lambda} \leq 1.00 \qquad \chi = (1.03 - 0.158 \cdot \overline{\lambda} - 0.206 \cdot \overline{\lambda}^2)$$

$$\text{for } 1.00 \leq \overline{\lambda} \leq 1.80 \qquad \chi = (-0.193 + 0.803/\overline{\lambda} - 0.056/\overline{\lambda}^2) \qquad (2.40)\text{a-e}$$

$$\text{for } 1.80 \leq \overline{\lambda} \leq 3.20 \qquad \chi = (0.018 + 0.815/\overline{\lambda}^2)$$

$$\text{for } \overline{\lambda} \geq 3.20 \qquad \chi = 1/\overline{\lambda}^2 \text{ (Euler)}$$

The advantage of a segmental, multi-functional approximation is clear: each of the functions can be kept simple, meaning that not that many coefficients are needed for any individual expressions. Since the approximation is performed for different slenderness ranges, it is possible to make the "error" of approximation more homogeneously distributed along these ranges, and not concentrated in either the low or high slenderness range. The disadvantage is of course represented by the

laboriousness and error-proneness given by the correct selection and evaluation of one out of five different equations.

2.6.3. Exponential expressions

Yet another possible way of formulating best-fit equations for buckling curves was developed by Tide (1985; see also Bjorhovde, 1992) and led to the column buckling curve formulation currently found in the North American AISC LRFD specification. It follows a segmental approach, but uses far fewer segments and –more importantly- a very simple *exponential expression* to describe the original SSRC 2P buckling curve in the low-to-intermediate slenderness range:

$$\text{for } 0.00 \leq \bar{\lambda} \leq 1.50 \qquad \chi = e^{-0.419 \cdot \bar{\lambda}^2} = 0.658^{\bar{\lambda}^2}$$

$$\text{for } \bar{\lambda} \geq 1.50 \qquad \chi = 0.877 / \bar{\lambda}^2 \tag{2.41a-b}$$

Fig 2-17a shows a comparison of the segmental and exponential expressions (2.40) and (2.41). The figure illustrates that the much simpler expression (2.41)a is very well able to reproduce the general course of a column's buckling curve. Whether this is the case for other buckling phenomena remains to be seen; as is illustrated in Fig 2-17b, the expression intersects the Euler hyperbola at a relatively steep angle for values of the calibration coefficient k beyond 0.7. This doesn't seem to reflect the stability behaviour of most structural members.
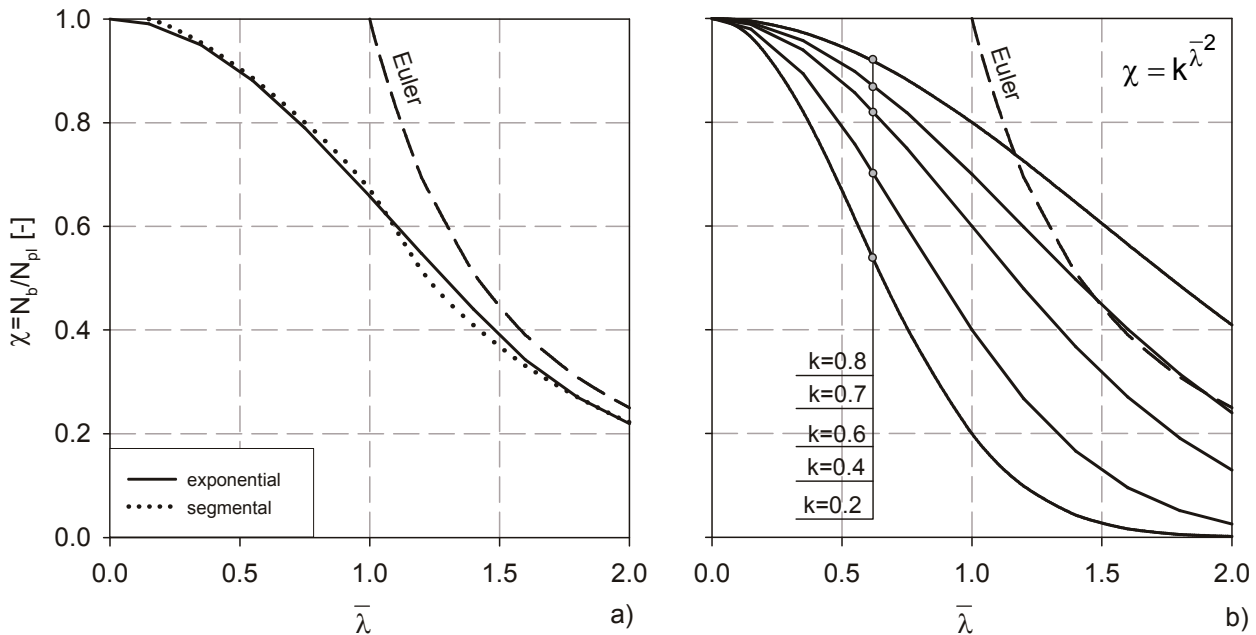
Fig 2-17   a) Comparison of the segmental approach -expr. (2.40)- to the exponential approach – expr. (2.41) found in North American standards; b) potential of the exponential expression for curve-fitting.

2.6.4. Comments

The content of this section can be summarized and commented upon as follows:

  i.   Buckling curves can also effectively be described by purely mathematical expressions, using e.g. polynomials, series of hyperbolic functions, exponential functions or combinations of these.

 ii.   This can be performed either over the entire range of applicability of the buckling curve or segmentally.

iii.   Pure curve-fitting expressions cannot easily be misinterpreted as being anything else but a purely mathematical approximation of an underlying, more sophisticated data pool. Since *all* curve-fitting expressions can actually be interpreted in this way, it can be welcomed if a formula does not mislead the practitioner to believe that it expresses anything much more fundamental than curve-fitting.

2.7. Summary

This chapter discussed the forms of formulaic and graphical representation of design buckling curves for the design of steel members against buckling and presented their most common forms of formulaic and graphical representation. In broad terms, two philosophies were identified for the formulaic description of buckling curves:

  i.   The first philosophy makes use of formulae that are based –to a more or less pronounced level- on mechanical derivations. The most important formulae of this type are the Merchant-Rankine and the Ayrton-Perry ones, used with or without modifications. Original and modified versions of Merchant-Rankine and Ayrton-Perry formulae are practically omnipresent in *European regulations* concerned with member stability.

 ii.   The second philosophy makes use of entirely mathematical curve-fitting equations, with no mechanical background whatsoever. This "pure curve-fitting" approach is the method of choice in *North American regulations* of buckling design checks.

Which one of these two approaches should be recommended depends on the buckling phenomenon at hand. If the variability of buckling curves is not very pronounced, i.e. when the main parameters χ and $\bar{\lambda}$ are able to represent most of the buckling behaviour quite well, nothing can be said against a purely mathematical curve-fitting using polynomials or other similar expressions. This seems to be the case for pure flexural buckling of a column under constant normal force, for example. Also many buckling phenomena in plates and shells tend to yield numerical or experimental buckling curves that are "homogeneous" enough to be approximated by purely mathematical curve-fitting (Rotter, 2002). Member buckling cases, particularly spatial ones, are usually more complex. Therefore, the amount of parameters that actually influence the problem is simply too vast for this approach: no purely mathematical expression of $\chi = f(\bar{\lambda})$ can satisfactorily describe each and every case, unless every single case is separately subjected to curve-fitting. In comparison, formulations

that are based on analytical, mechanical derivations have the advantage of implicitly containing at least some of these additional parameters, greatly reducing the complexity of calibration.

Due to this last point, this thesis will not make use of "pure", mathematical curve-fitting formulae to represent buckling curves and design models of buckling behaviour. Approaches based on simplified mechanical derivations are preferred. Of these, the Ayrton-Perry approach was shown in this chapter to be the best-suited and best-founded one. It is therefore used in this thesis.

Aside from the approaches detailed in this chapter, a variety of other analytical expressions for buckling curves were formulated in the past (see e.g. Osgood, 1946). The origin of some of these formulae can still be traced, while for others these origins have been lost over time and/or are obscure. Since these additional *empirical formulae* can essentially be attributed to one of the two types previously discussed (i.e. either "modified" mechanical formulae or "pure curve-fitting" formulae), an illustration of them would not add much to the topic discussed in this chapter. They are consequently also ignored in the rest of this work.

3

Methodology

3.1. Introduction and Scope

This chapter gives a concise overview of the numerical modelling techniques, the fundamental second-order equations and the statistical tools used in this thesis.

3.2. Numerical Modelling

In this thesis, numerical simulations were used for a variety of purposes:

i.   Determining elastic, critical bifurcation loads in **L**inear **B**uckling **A**nalyses (LBA).
ii.   Calculating the first-order plastic limit loads in **M**aterially **N**on-linear **A**nalyses (MNA)
iii. Obtaining realistic numerical values of the ultimate buckling strength in **G**eometrically and **M**aterially **N**on-linear **A**nalyses with **I**mperfections (GMNIA)

The modelling techniques sketched in Fig 3-1 were used for these three levels of analysis, using the software package ABAQUS (Dassault Systems, 2007). The boundary conditions of the member, as well as the chosen shapes of imperfection and the used finite element mesh, are shown in the figure. As was states in chapter 1, only single-span members with in-plane, out-of-plane and torsional restraints at the supports were considered ("end fork" conditions).

Two different types of elements were used. In many cases treated in this thesis, four-node linear shell elements (S4) with six degrees of freedom per node and finite strain formulation were chosen to model the studied sections. The advantage of these shell element calculations is that they take into account the contribution of shear stresses in plasticity and allow for a more accurate definition of loads and boundary conditions in the case of beams and laterally restrained columns. The mesh density was generally left constant, with 16 elements per flange and web plate generally found to be a sufficient number. For very long (L/h>100) or deep (h/b>3.0) members, the number of nodes in longitudinal direction, respectively in the web, was doubled.

Rigid coupling beams were used to connect the single plates with each other. At the supports, the stiffness terms of these elements were manipulated in order to obtain a stiff load introduction mechanism (allowing to define concentrated loads to simulate moments and axial loads) that nevertheless allowed the cross-section to twist and rotate freely.

In the case of hot-rolled I- & H-sections, the fillets were included in the calculations by adding equivalent beam elements that were placed in the centroids of the flanges. By defining the cross-sections of these beam elements as quadratic hollow sections of variable depth and wall thickness, the total area and –more importantly- torsional stiffness of the modelled member could be calibrated to precisely match the tabulated values given by the production standards for rolled sections. The exact bending capacity was thereby also approximated with minimum error.
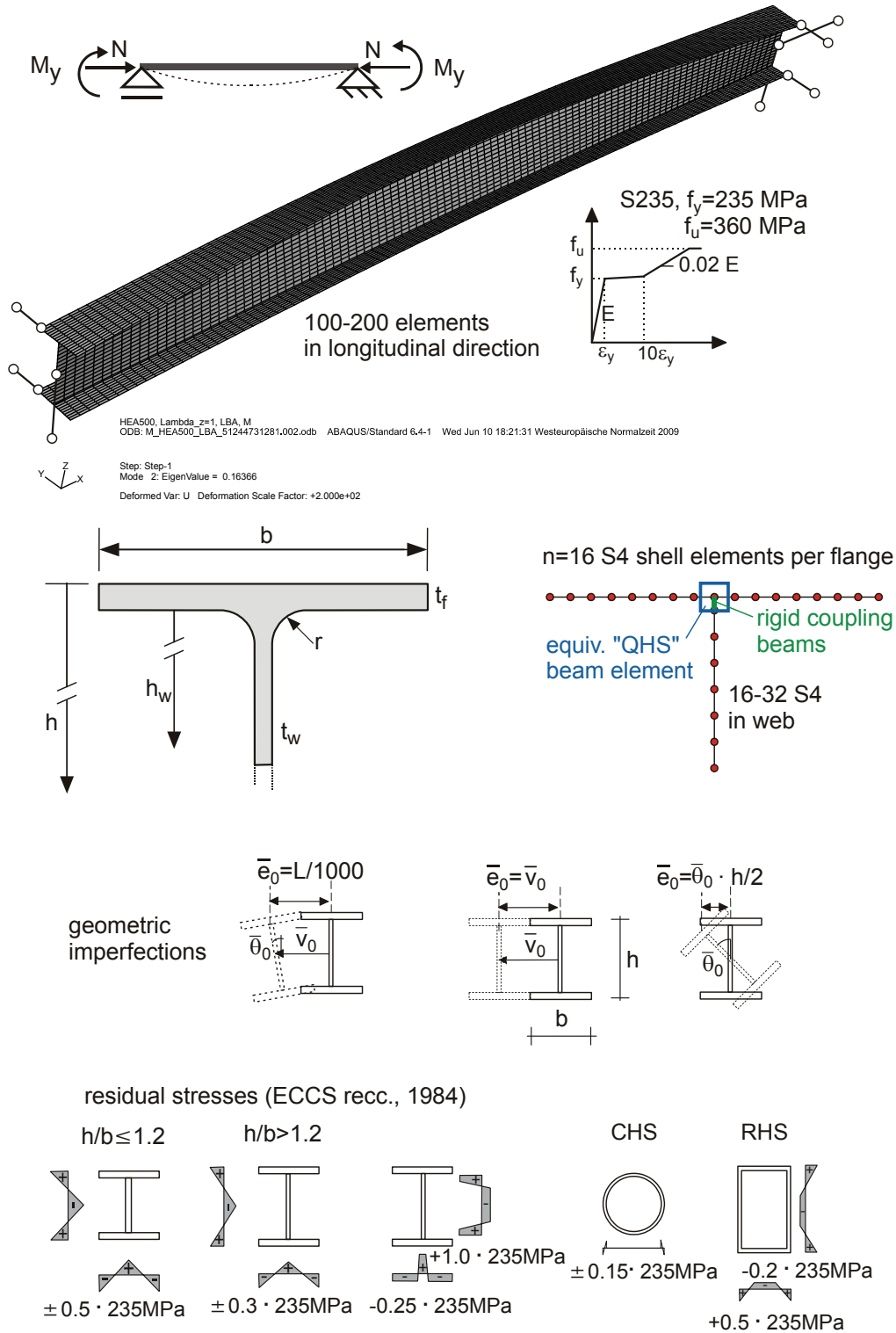
Fig 3-1 Overview of the FEM modelling techniques and assumptions.

In calculations where the buckling mode consisted of flexural buckling in one defined plane, i.e. with no twist of the cross-section appearing in either the first- or second-order deformations, it was found to be justified –and of course far more economic- to use beam elements instead. Calculations using beam elements were also conveniently used whenever cross-sections were studied –mostly for purposes of illustration of some extreme effects- that actually would behave like class 3 or 4 sections due to "premature", local buckling. Beam elements are suited for studying the (theoretical) global buckling behaviour of such cases in the sense that they ignore all local effects. In the used FEM models using beam elements, linear Timoshenko elements (B31 or B31OS) were used. 17 integration points per flange- or web plate were implemented. When required, the effects of the fillet radius were included by adding additional beam elements with equivalent hollow sections, as described above for the shell element models.

As the name implies, imperfections are included in GMNIA calculations, whereby both geometric and structural imperfections (residual stresses) were considered:

i.   The initial geometric imperfections were assumed to follow the shape of the first eigenmode pertaining to the studied buckling case. Depending on the studied case, initial rotations, deflections, or both were thereby considered. The amplitude of these imperfections, as defined in Fig 3-1, was assumed to be equal to $\bar{e}_0$=L/1000 at the compression flange. The assumptions pertaining to the underlying imperfections closely follow the procedure chosen by Beer and Schulz (1970) for the development of the European column buckling curves.

ii. The residual stresses were assumed to vary linearly over the single cross-section components, following the provisions given by ECCS (1984). Accordingly, a distinction was made in the case of hot-rolled I- & H- sections between sections with a depth-to-width ratio of h/b≤1.2 and sections with h/b>1.2. The magnitude of residual stress thus depends on the type of rolled cross-section and is expressed as a fraction of the yield strength f_y of mild steel S235.

When not otherwise indicated, all calculations were conducted for steel grade S235, assuming a yield strength of f_y=235 N/mm² irrespective of plate thickness. Strain hardening was included in the calculations, again following the long-established recommendations of ECCS.

It is customary and good practice to verify numerical models before any systematic numerical study is undertaken. For this purpose, a convincing number of comparative calculations was carried out at the on-set of the studies presented in this thesis. Thereby, a series of benchmark tests were considered, of which only a minimal sample is shown –for illustrative purposes- in Fig 3-2. In very general terms, the employed numerical models were considered to be sound when the following conditions were met:

i.   The bifurcation loads for a variety of basic and combined load cases must lie within a narrow scatter band (+/- 3%) from fully theoretical solutions as reported in the literature.
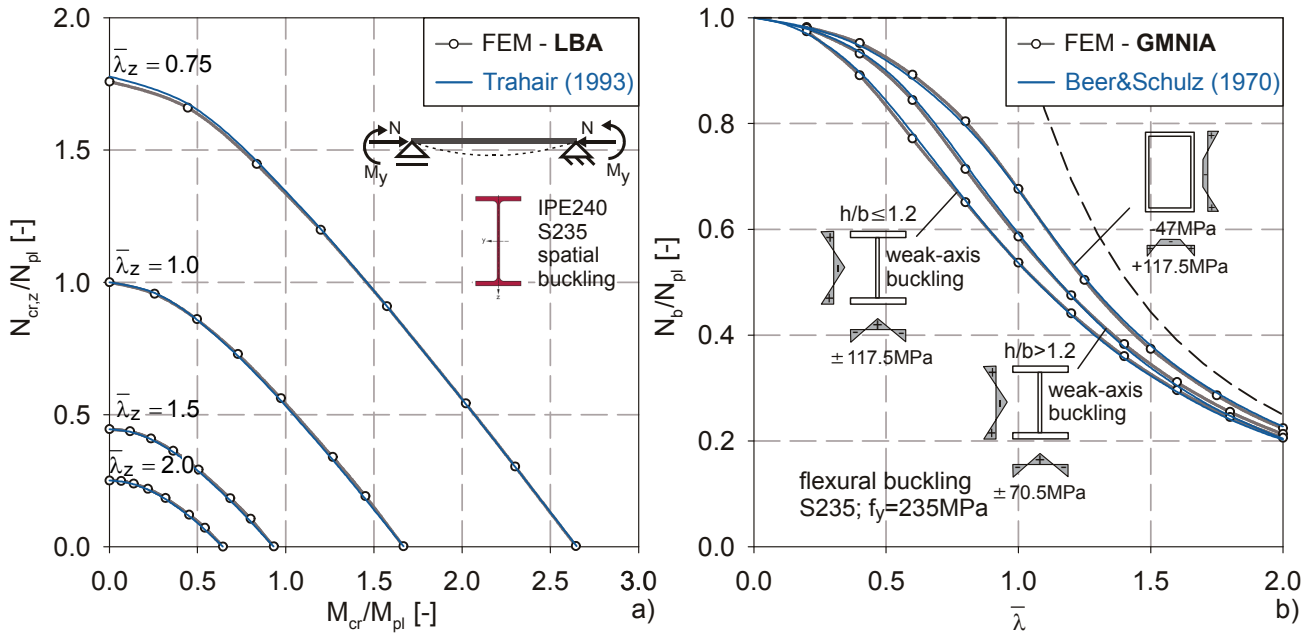
Fig 3-2 Validation of the FEM models: comparison of elastic (bifurcation) buckling loads (a) and of GMNIA calculation results (b) with solutions from the literature.

This is illustrated in Fig 3-2a, which features a normalized representation of lateral-torsional bifurcation loads under N+M for a hot-rolled IPE 240 section. For the basic case of constant values of both axial and bending terms N and M, analytical solutions of the bifurcation load can be found in the literature (e.g. Trahair, 1993). The numerical models used to study these –and all other- buckling phenomena could be shown to yield results with excellent agreement with the theoretical values.

ii.　The ultimate buckling loads as obtained from GMNIA calculations were compared with results published in the literature. A particularly relevant benchmark case for the purposes of this thesis was thereby represented by the (original) ECCS column buckling curves as they were developed and published by Beer & Schulz (1970). These curves were later slightly modified (ECCS 1978) to include an artificial "plateau" up to $\bar{\lambda}$=0.2 that did not show in the numerical calculations, but was seen as practically justified, and then described by a formula (Maquoi & Rondal, 1978) that is still found in the Eurocode 3– EN 1993-1-1. Regardless of these later, minimal changes, the calculations by Beer & Schulz with fixed, statistically calibrated imperfection amplitudes and nominal geometric input data represent the theoretical/numerical foundation of the currently used column buckling curves and –by extension- most other current member buckling rules. It was therefore considered to be of utmost importance in this thesis to use numerical models that were able to reproduce the original curves by Beer & Schulz with high accuracy. The verification of this accuracy is illustrated in Fig 3-2, where the (new) GMNIA results are shown to practically overlap with the curves from 1970, with the error throughout the considered slenderness range being lower than 2%.

3.3. Second-Order Beam Theory – Basic Equations

In part II and III of this thesis, new design formulae are developed for the basic member-buckling cases of lateral-torsional, torsional, torsional-flexural and in-plane beam-column buckling. In all cases, the developed equations are fundamentally based on long-established and well-known second-order equations. The following paragraphs give a short summary of the used equations:

All developed equations are fundamentally based on the following system of differential equations for in- and out-of-plane buckling of a prismatic member under uniform (constant) first order axial forces N and bending moments M_y and M_z, found in equal form in numerous international publications and taken here from Roik (1978), see also Kaim (2004):

$$\begin{bmatrix} EI_z \cdot v^{iv} + N(v^{ii} + v_0^{ii}) \\ 0 \\ M_y(v^{ii} + v_0^{ii}) \end{bmatrix} + \begin{bmatrix} 0 \\ EI_z \cdot w^{iv} + N(w^{ii} + w_0^{ii}) \\ M_z(w^{ii} + w_0^{ii}) \end{bmatrix} + \begin{bmatrix} M_y(\theta^{ii} + \theta_0^{ii}) \\ M_z(\theta^{ii} + \theta_0^{ii}) \\ EI_\omega \theta^{iv} - GI_T \theta^{ii} - N \cdot i_p^2(\theta^{ii} + \theta_0^{ii}) \end{bmatrix} = \begin{bmatrix} 0 \\ 0 \\ 0 \end{bmatrix}$$

(3.1)

whereby v, w and θ are the out-of- and in-plane deflection and the twist, and the index "0" indicates the initial deformations distributed along the length of the member.

This system of differential equations is commonly solved by half sine waves as functions for both the deformation variables and initial imperfection. In general terms, each variables u(x) can be written and differentiated as follows, with $\overline{u}$ being the amplitude of the deformation component.

$$u = \overline{u} \cdot \sin\left(\frac{\pi \cdot x}{L}\right) \qquad u^{ii} = \overline{u} \cdot \frac{\pi^2}{L^2} \cdot \sin\left(\frac{\pi \cdot x}{L}\right) \qquad u^{iv} = \overline{u} \cdot \frac{\pi^4}{L^4} \cdot \sin\left(\frac{\pi \cdot x}{L}\right)$$

(3.2)

The next step consists of entering the terms in (3.2) in (3.1) and introducing the following abbreviations (stemming from the critical bifurcation analysis of the perfect member):

$$N_{cr,z} = EI_z \cdot \frac{\pi^2}{L^2} \qquad N_{cr,y} = EI_y \cdot \frac{\pi^2}{L^2} \qquad M_{cr} = \frac{\pi^2 EI_z}{L^2} \cdot \sqrt{\frac{I_\omega}{I_z} + \frac{L^2 \cdot GI_T}{\pi^2 EI_z}}$$

$$N_{cr,T} = \left(EI_\omega \cdot \frac{\pi^2}{L^2} + GI_T\right) \cdot \frac{1}{i_p^2} = \frac{M_{cr}^2}{N_{cr,z}} \cdot \frac{1}{i_p^2}$$

(3.3)

With these abbreviations, the following linear system of equations is obtained, representing an equilibrium condition at mid-span of the studied member:

$$\left(\begin{bmatrix} N_{cr,z} & 0 & 0 \\ 0 & N_{cr,y} & 0 \\ 0 & 0 & M_{cr}^2 / N_{cr,z} \end{bmatrix} - \begin{bmatrix} N & 0 & M_y \\ 0 & N & M_z \\ M_y & M_z & Ni_p^2 \end{bmatrix}\right) \cdot \begin{bmatrix} \overline{v} \\ \overline{w} \\ \overline{\theta} \end{bmatrix} = \begin{bmatrix} -M_z \\ M_y \\ 0 \end{bmatrix} + \begin{bmatrix} N & 0 & M_y \\ 0 & N & M_z \\ M_y & M_z & Ni_p^2 \end{bmatrix} \cdot \begin{bmatrix} \overline{v_0} \\ \overline{w_0} \\ \overline{\theta_0} \end{bmatrix}$$

(3.4)

The expressions in (3.4) are a stiffness relationship in matrix form, and can be expressed in the following way:

$$\left(\mathbf{K}_{\text{mat}} - \mathbf{K}_{\text{geom}}\right) \cdot \mathbf{u} = \mathbf{F}^{\text{I}} + \mathbf{K}_{\text{geom}} \cdot \mathbf{u}_0 \tag{3.5}$$

with $\mathbf{K}_{\text{mat}}$ ....   (first-order) material stiffness matrix

       $\mathbf{K}_{\text{geom}}$....   geometrical stiffness matrix

       $\mathbf{u}$ ....   vector containing the deformation terms

       $\mathbf{u}_0$........   vector for the initial imperfections

       $\mathbf{F}^{\text{I}}$........   load vector

Simplified, case-specific versions of relationship (3.5) are inverted and solved for the vector **u** in the relevant chapters to obtain deformation amplification factors. These can be used to calculate second-order internal forces, whereby the following simplified relationships were used :

$$M_z = -EI_z \cdot v^{\text{ii}} \qquad M_y = -EI_y \cdot w^{\text{ii}} \qquad M_\omega = -EI_\omega \cdot \theta^{\text{ii}} \tag{3.6}$$

By once-again assuming half-sine waves for the course of the deformations along the member length, the following equations are obtained, valid at mid-span and thus referring to the amplitude of the deformation components:

$$M_z = EI_z \cdot \frac{\pi^2}{L^2} \cdot \bar{v} \qquad M_y = EI_y \cdot \frac{\pi^2}{L^2} \cdot \bar{w} \qquad M_\omega = EI_\omega \cdot \frac{\pi^2}{L^2} \cdot \bar{\theta} \tag{3.7}$$

3.4. Reliability Assessment, Random Number Generation, Monte Carlo Simulations

Reliability aspects have been included in this thesis both within the framework of the statistical evaluation of test results in order to assess the safety level of certain design rules in accordance with the Eurocode (2002) – EN 1990 Annex D, as well as in the context of Monte Carlo simulations to obtain "numerical test results" on the basis of randomly generated input parameters.

3.4.1. Statistical evaluation of test data according to EN 1990

EN 1990 – Annex D contains a standardized procedure –based on First Order Reliability Methods- that allows for the determination of appropriate values (in a semi-probabilistic design concept) of partial safety factors γ_M on the basis of test results. Since the formulae and coefficients of the methodology of EN 1990 are used at different locations in the body of this thesis, a brief summary of the procedure is given in the following.

   i.   EN 1990 – Annex D recognizes the relevance of the accuracy of a design formulation and of its ability to react to variabilities of the input parameters that govern a design problem. The

design formulation therefore takes on an immediate, central part in the statistical evaluation procedure of EN 1990. In the notation of the code, the theoretical value of strength r_t is expressed as a function of its single input parameters.

$$r_t = g_{r_t}(\underline{X})$$ (3.8)

An example for the function g_{rt} is given by a buckling formula that leads to a column strength $r_t = \chi \cdot A\, f_y$, with the vector of the basic variables $\underline{X}$ containing such parameters as the cross-sectional geometry, the yield stress, the column length, etc.

ii. The theoretical strength r_t is compared with the experimental strength r_e in the methodology of Annex D. Thereby, the "actual" values of the basic parameters should be determined for each, single test result $r_{e,i}$. This information about the basic variables is used to calculate the specific strength prediction r_{ti} for a single test result, which can then be plotted as shown in Fig 3-3.
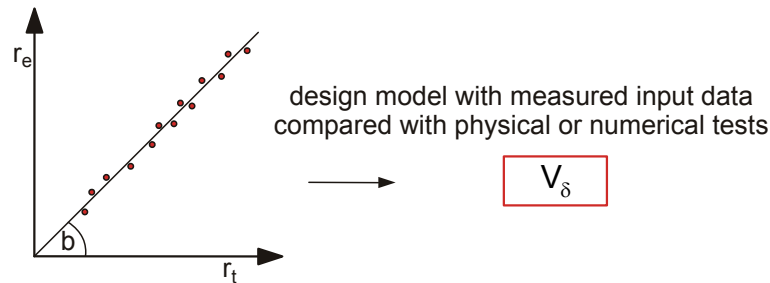
Fig 3-3 Schematical representation of the interpretation of V_δ as variance of the design model.

For a number of n pairs $(r_{e,i}; r_{t,i})$ plotted in the r_t/r_e plane, a regression line through the origin can then be calculated through least-square approximation, using the following formula:

$$b = \frac{\sum_{i=1}^{n} r_{e,i} \cdot r_{t,i}}{\sum_{i=1}^{n} \left(r_{t,i}\right)^2}$$ (3.9)

iii. The coefficient of variation V_δ of the error terms δ_i of the design function is calculated as follows:

$$V_\delta = \sqrt{\exp(s_\Delta^2) - 1}$$ (3.10)

with

$$s_\Delta^2 = \frac{1}{n-1} \sum_{i=1}^{n} \left(\Delta_i - \overline{\Delta}\right)$$ (3.11)

$$\overline{\Delta} = \frac{1}{n} \sum_{i=1}^{n} \Delta_i$$ (3.12)

$$\Delta_i = \ln\left(\frac{r_{e,i}}{b \cdot r_{t,i}}\right) = \ln \delta_i$$ (3.13)

iv.   Up to now, the methodology has only accounted for the differences between a certain pool of test data results (usually in terms of strength) and the prediction of the same strength according to the design function. In the next step, the sensitivity of the design function itself to the variability of the basic input variables must be accounted for, by calculating the error propagation term V_{rt}. In the usual case of a complex, multi-variable design function, V_{rt} is calculated using the following formulae:

$$V_{r,t}^{2} = \frac{VAR\left[g_{r,t}(\underline{X})\right]}{g_{r,t}(\underline{X}_m)^{2}} = \frac{1}{r_{m,t}^{2}} \cdot \sum_{i=1}^{j}\left(\frac{\partial g_{r,t}}{\partial X_i} \cdot \sigma_i\right)^{2}$$ (3.14)

with $\dfrac{\partial g_{r,t}}{\partial X_i} \cdot \sigma_i$: partial derivative with respect to the variable X_i times its standard deviation.

v.   The log-normal variation coefficients can now be calculated as follows:

$$Q_{r,t} = \sqrt{\ln\left(V_{r,t}^{2}+1\right)}$$ (3.15)

$$Q_{\delta} = \sqrt{\ln\left(V_{\delta}^{2}+1\right)}$$ (3.16)

$$Q = \sqrt{\ln\left(V_{r}^{2}+1\right)}$$ (3.17)

with $$V_{r}^{2} = V_{r,t}^{2} + V_{\delta}^{2}$$ (3.18)

vi.   In the next step, the design value of the resistance r_d is calculated:

For n≤100 $$r_d = g_{r_t}\left(\underline{X}_m\right) \cdot \exp(-k_{d,\infty} \cdot \frac{Q_{rt}^{2}}{Q} - k_{d,n} \cdot \frac{Q_{\delta}^{2}}{Q} - 0.5 \cdot Q^{2})$$ (3.19)

For n>100 $$r_d = g_{r_t}\left(\underline{X}_m\right) \cdot \exp(-k_{d,\infty} \cdot Q - 0.5 \cdot Q^{2})$$ (3.20)

with $g_{r_t}\left(\underline{X}_m\right)$ representing the value of the design function evaluated with the mean values of all basic input variables, and $k_{d,n}$ and $k_{d,\infty}$ being the design fractile factors for n and infinite single test results.

vii.   Finally, the required partial safety factor $\gamma_M{}^{*}$, applicable for designs based on nominal input data, can be calculated as follows

$$\gamma_M{}^{*} = \frac{r_{tk}}{r_d}$$ (3.21)

With $r_{tk} = g_{r_t}\left(\underline{X}_{NOM}\right)$, i.e. the design function evaluated with nominal values of the input parameters. This is the quantity usually determined by designers.

3.4.2. Random Numbers – Monte Carlo Simulation

Full scale physical tests of the type that help determine the buckling resistance of steel members are expensive and time-consuming, and furthermore pose many difficulties with respect to load introduction, representation of desired boundary conditions, etc. (see Singer et al., 1998). In order to avoid these difficulties, simulated tests obtained from GMNIA calculations with random input variables ("Monte Carlo simulations") are nowadays increasingly being used instead. This procedure is fully legitimate, provided that the real scatter bands of the single input parameters, as well as the way these parameters correlate, are known. Some very valuable studies (Alpsten, 1972; ECCS, 1978; Melcher, 2004) have already been published that deal with a systematic statistical analysis of the properties of steel products for structural steelwork. Nevertheless, no final consensus seems to have been reached at the present stage as to what set of structural parameters can be regarded as truly representative for the statistical properties of internationally manufactured steel products that are placed onto the European market.

This thesis makes use of Monte Carlo simulations to answer some open questions regarding the safety of compression members, and thereby assumes the above-mentioned, published data-sets to be representative of current production. The numerical values for the single calculations were generated using the standard *inverse transform method* (see e.g. Glassermann, 2004; Ross, 2009) on the basis of cumulative distribution functions (cdf) F for the normal or log-normal distribution, depending on the modelled parameter. A single, randomly generated value X is therefore obtained from F and a randomly generated value U~Unif[0,1]:

$$X = F^{-1}(U), \quad U \sim \text{Unif}[0,1] \tag{3.22}$$

An exemplary illustration of the results of such a generation are shown in Fig 3-4, where the frequency plot for randomly generated variable values for eccentricities is shown to follow the underlying distribution (in form of its probability density function pdf) very well.
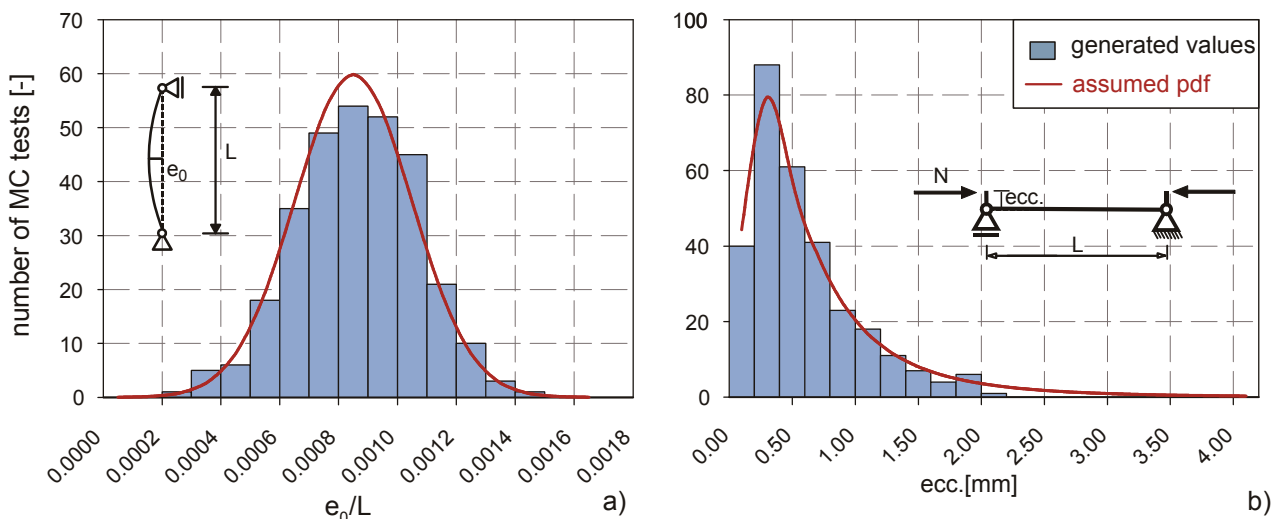
Fig 3-4   Exemplary representation of the generation of random variables on the basis of distribution functions.
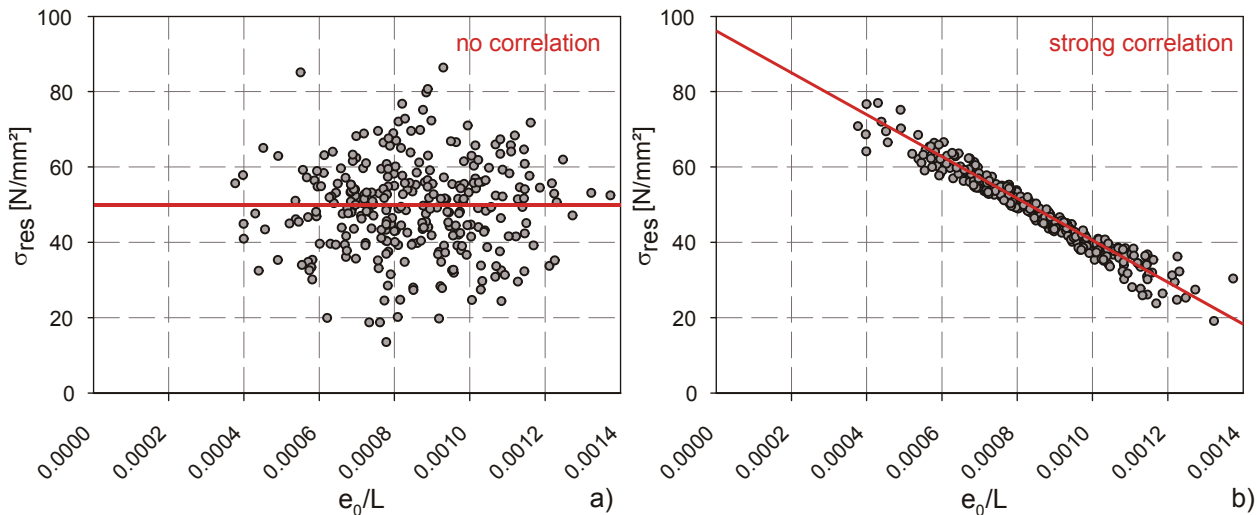
Fig 3-5   Exemplary representation of two variables that (a) do not correlate at all, or (b) strongly correlate.

A controversial issue for the application of the Monte Carlo method is the question of the correlation of the single parameters. This is graphically illustrated in Fig 3-5 for the example of the initial curvature and the residual stresses in a column, generated either without any correlation (a) or with strong correlation. It can be noticed that the maxima and minima of both variables lie close to each other, meaning that when plotted by themselves (like was done in Fig 3-4) would lead to about the same frequencies of occurrence for the whole sample. As a matter of fact, precisely the two parameters plotted in Fig 3-5 are sometimes suspected to be inversely correlated with each other, meaning that smaller residual stresses are systematically present whenever high curvatures are present (Ballio and Mazzolani, 1983 pp. 387). However, for the purposes of this thesis no systematic correlation was considered whenever Monte Carlo simulations were performed. Thereby, the distinction should be kept in mind between correlation of scatter and mean values of the distribution; indeed, for some specific I-sections the fact was taken into account that measurements (Alpsten, 1972) had shown the mean values of the web thickness to be larger than the nominal value while the mean value of the flange thickness was lower than the nominal one. This is, by itself, only proof of a systematic deviation from nominal values, and not for a correlation.

Thus, the disregard of correlation is motivated by the following considerations:

i.   No statistical evaluations exist that would definitively prove such correlations.

ii.   More importantly, the statistical evaluation procedure integrated in the Eurocode – EN 1990 and discussed in section 3.4.1 represents a First Order Reliability Method, based on the assumption that all variables are independent. Since the results of Monte Carlo simulations are intended to be evaluated using this procedure, any information stemming from the inclusion of the correlation would be "overlooked" by the evaluation itself.

PART II

Columns and Beams – Basic Load Cases

4

Member Buckling Cases – Common Issues & Solution Concepts

4.1. Scope

This chapter discusses issues of member buckling design that are common to all basic member buckling cases. It begins with a brief illustration of the current treatment of different buckling cases in design practice. It continues with a discussion of current inconsistencies in member design practice for basic buckling cases. These are mainly identified in the classification of cross-sections according to their geometry, the definition of equivalent, geometrical imperfections, as well as in the level of reliability present over different slenderness ranges. Finally, an outline is given of the general concepts used to overcome some of these inconsistencies in the remainder of part II of this thesis.

4.2. Current treatment of different buckling cases

Different concepts and ideas can be identified in international design codes when it comes to the treatment of different buckling cases, such as flexural buckling versus lateral-torsional buckling versus torsional-flexural buckling, etc. Focusing the attention on past and current practice in Europe and North America, three such concepts are currently of most relevance to designers. They are summarized in Table 4-1 and discussed in the following paragraphs.

    i.   Concept 1 is the traditional treatment given to different buckling cases in many Continental European design codes, such as DIN 18800-2 (1990) and its predecessor codes, as well as most current North American codes (e.g. AISC LRFD - 2004). In this concept, each single buckling case is described (in terms of a buckling curve) by a specific formula. A typical example is the different treatment of *flexural column buckling* and *lateral-torsional buckling* in DIN 18800-2. The former was described by the Ayrton-Perry formulation as it was calibrated by Rondal&Maquoi (1978) to the ECCS column buckling curves – see chapters 2 and 5. The latter was described by a so-called "generalised" Merchant-Rankine formulation. For the sake of "consistency" of design rules, the Eurocode has mostly abandoned this concept. It is therefore not further discussed here.

Concept 1 "n buckling cases – n formulae"	Concept 2 "n buckling cases – 1 formula - n calibrations"	Concept 3 "n buckling cases – 1 formula – 1 imperfection coeff."
$\chi_{z,y} = \dfrac{1}{\Phi + \sqrt{\Phi^2 - \bar{\lambda}_{z,y}^{\,2}}}$ $\chi_{LT} = \left(\dfrac{1}{\left(1 + \bar{\lambda}_{LT}^{\,2n}\right)} \right)^{1/n}$ $\chi_{TF} = \ldots\ldots$	$\chi = \dfrac{1}{\Phi + \sqrt{\Phi^2 - \beta \cdot \bar{\lambda}^2}}$ $\Phi = \dfrac{1}{2} \cdot \left(1 + \eta + \beta \cdot \bar{\lambda}^2\right)$ $\eta = \alpha \cdot \left(\bar{\lambda} - \bar{\lambda}_0\right)$ $\bar{\lambda} = \bar{\lambda}_y, \bar{\lambda}_z, \bar{\lambda}_{LT}, \bar{\lambda}_T, \ldots$ $\boldsymbol{\alpha} = \boldsymbol{\alpha_y, \alpha_z, \alpha_{LT}, \alpha_T, \ldots}$ $\beta = 1.0 \ldots 0.75$ $\bar{\lambda}_{z/y,0} = 0.2 \; ; \; \bar{\lambda}_{LT,0} = 0.2 \ldots 0.4$	$\chi = \dfrac{1}{\Phi + \sqrt{\Phi^2 - \bar{\lambda}^2}}$ $\Phi = \dfrac{1}{2} \cdot \left(1 + \eta + \bar{\lambda}^2\right)$ $\eta = \alpha * \cdot \left(\bar{\lambda} - \bar{\lambda}_0\right)$ $\bar{\lambda} = \bar{\lambda}_y, \bar{\lambda}_z, \bar{\lambda}_{LT}, \bar{\lambda}_T, \ldots$ $\boldsymbol{\alpha* = \alpha_{0,S} \cdot \alpha}$ $\boldsymbol{\alpha = \alpha_z} \; ; \bar{\lambda}_0 = 0.2$

Table 4-1 *Concepts for the treatment of different buckling cases.*

ii. Concept 2 has been built into the existing version of the Eurocode. It defines the buckling reduction factor χ for all buckling cases by means of an Ayrton-Perry formula. The specific load-carrying behaviour of the single buckling cases is reflected, on the one hand, by the use of the specific slenderness of the buckling case. More importantly, a specific categorization is used (h/b ratios, types of section, ...), as well as a specific definition of the generalized imperfection coefficient η. For buckling cases other than the flexural buckling case, this concept is not based on a specific, mechanical derivation, but is simply an adaptation of the formula derived for flexural buckling. More details are given in the specific chapters 5, 6 and 7.

iii. Concept 3 is relatively new. The first steps in this direction were taken by Sedlacek & Müller (2006) and Stangenberg (2006), who proposed this concept as a generalized replacement for *all* current member buckling Eurocode rules, including combined load cases – in this sense, they consider it to be the "general" method for the treatment of member buckling phenomena. It again makes use of an Ayrton-Perry formulation. In this formulation, the imperfection factor η is modified by a new factor (called $\alpha_{0,S}$ in this thesis) that accommodates the result of a more precise second-order elastic formulation for the specific buckling case. This concept therefore *is based on a more accurate mechanical derivation*, at least for basic cases. More details are given in the remaining chapters of part II of this thesis, particularly in chapter 6. What is important to note already is that, in order to be able to "generalize" its use, this method makes use of the *Ayrton-Perry imperfection amplitude factor α_z,* i.e. the value applicable for out-of-plane flexural buckling, for *all* (out-of-plane) member buckling cases.

This means that this concept is *not calibrated* to represent any more sophisticated experimental or numerical buckling curves, but is based on a more or less arbitrary assumption regarding the similitude between different buckling cases. Like concept 2, it also maintains the specific slenderness of the buckling case ($\bar{\lambda}_z, \bar{\lambda}_{LT}, \bar{\lambda}_T$ ...) in the formulation of η. The implications of this latter fact are discussed in section 4.3.2 of this chapter.

4.3. Current inconsistencies

An increase of consistency of the single member buckling design rules is one major concern to the development of improved provisions. While the single points are discussed more thoroughly in the chapters specifically dedicated to the single buckling phenomena, the following three points are worth mentioning in this more general, introductory chapter.

4.3.1. Cross-sectional classification

The first "inconsistency" in the current Eurocode design provisions worth mentioning is the different cross-sectional classification necessary for different member buckling rules. This is schematically summarized in Fig 4-1. Of the three most important member buckling cases treated in this thesis, two (flexural and torsional buckling) are classified using the same geometrical categorization limits h/b, while the LT buckling case uses different limits.
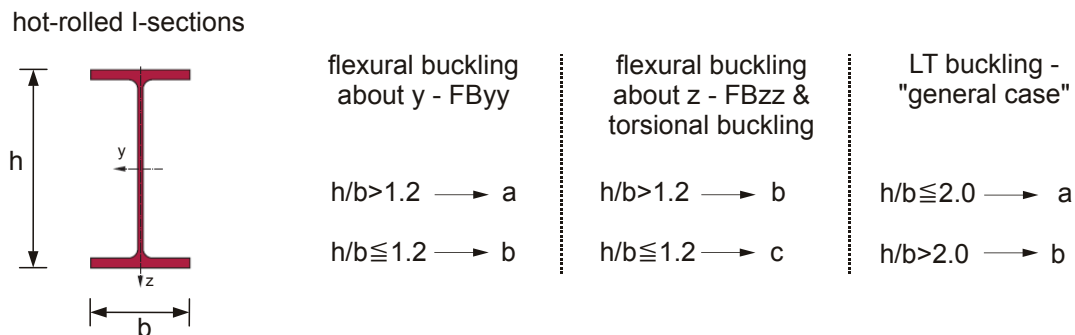
Fig 4-1   *Relationship between buckling curve and cross-sectional geometry according to the Eurocode for different member buckling cases.*

One might think that this is insignificant. From the point of view of practicality of application, it indeed is not much of an issue, especially today when design software is able to automatically take such different classification rules into consideration.

However, these differences in classification are an (indirect) indicator of the fact that the used buckling curves and corresponding formulae do not reflect all specific effects of a buckling phenomenon consistently for all buckling cases. The reasoning behind this statement is the following:

i. The current Eurocode buckling rules for flexural and LT buckling are based on GMNIA calculations carried out for *model columns or beams* with certain, standardized assumptions regarding cross-sectional geometry and geometrical or structural imperfections. The ones used for the development of rules for I- & H-sections are summarized in Fig 4-2. For torsional- and torsional-flexural buckling no specific calculations are known to underlie the present Eurocode rules, see chapter 7; however, it is only reasonable to assume that the same model beam as for flexural and LT buckling would be used for reasons of consistency.
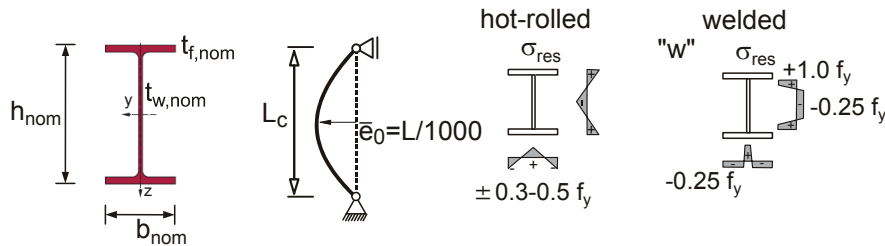
Fig 4-2 *Underlying assumptions for GMNIA calculations as basis of Eurocode member buckling rules.*

ii. As is shown in chapter 5, in the case of flexural buckling there is a direct link between the imperfection assumptions made for these model columns and the resulting buckling curve. The underlying assumptions are thus reflected in the classification of cross-sections with regard to buckling curves. For example, higher residual stresses were assumed in the GMNIA calculations for all hot-rolled I- & H-sections with h/b≤1.2 than for deeper sections. Accordingly, all these sections require the use of a lower buckling curve in design.

iii. In the GMNIA calculations that led to the classification of cross-sections with regard to lateral-torsional buckling, the same imperfection assumptions were made as in the column buckling case, i.e. for example higher residual stresses for hot-rolled sections with h/b≤1.2. The current classification does, however, not show this underlying assumption, as the "jump" of category occurs at h/b=2.0, and not 1.2. This indicates that the used design formula is not fully reflective of the underlying mechanical assumptions.

4.3.2. Length-dependency of geometric imperfections

Both the concept 2 and 3 of Table 4-1 make use of Ayrton-Perry formulations for the description of member buckling curves. As has been shown in chapter 2, and will be further illustrated in chapters 5, 6 and 7, the Ayrton-Perry calibration consists of replacing the term $\overline{e}_0 \cdot W / A$ -resulting from a second-order first-yield limit state equation- by the "generalized imperfection" η.

This simple relationship can of course be inverted to obtain $\overline{e}_0$ as a function of η:

$$\overline{e}_0 = \eta \cdot \frac{W_z}{A} \qquad\qquad (4.1)$$

In the Eurocode 3 and the proposals currently being brought forward to amend it, the generalized imperfection η is always replaced by a relationship of the following type:

$$\eta = \alpha \cdot \left(\overline{\lambda}_S - \overline{\lambda}_0 \right) \tag{4.2}$$

Where α is the generalized imperfection amplitude, $\overline{\lambda}_0$ is a plateau value, and (importantly) $\overline{\lambda}_S$ is the dimensionless slenderness *of the specific buckling case*; that is, $\overline{\lambda}_z$ in the case of out-of-plane flexural buckling, $\overline{\lambda}_{LT}$ in the case of lateral-torsional buckling, $\overline{\lambda}_{TF}$ if we are dealing with torsional-flexural buckling, and so on.

It is interesting to note that this assumption regarding the use of $\overline{\lambda}_S$ in expression (4.2) has some implications on the assumed length-dependency of the underlying imperfection amplitude $\overline{e}_0$, evaluated by using expression (4.1). In Fig 4-3, this is illustrated for an IPE 500 hot-rolled section and for the three basic buckling cases of weak-axis flexural buckling ($\overline{\lambda}_z$), lateral-torsional buckling ($\overline{\lambda}_{LT}$) and torsional buckling ($\overline{\lambda}_T$). Expression (4.2) was evaluated for all cases with a value of α=0.34, as this is the value specified in the Eurocode for all three buckling modes for this specific section.
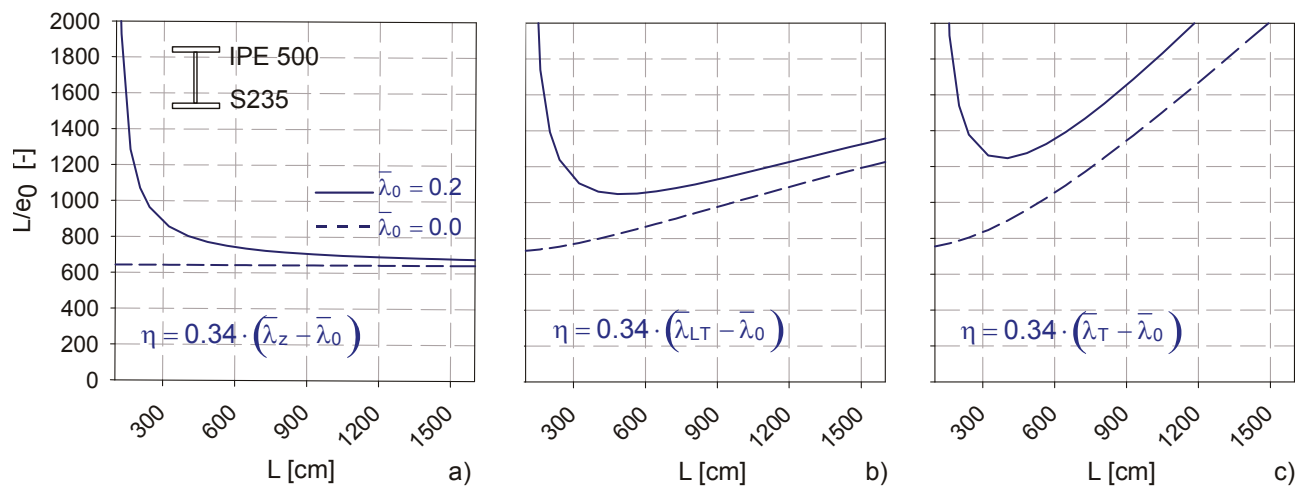
Fig 4-3 *Equivalent geometrical imperfections for an IPE 500 section, plotted as $L/\overline{e}_0$ - weak-axis flexural buckling (a); lateral-torsional buckling (b); torsional buckling (c)*

The figure shows that the equivalent, second order imperfection amplitude $\overline{e}_0$ resulting from these calculations is quite different from case to case, not just in absolute terms, but (more importantly here) in relative terms to the length of the member:

i.   In the case of weak-axis flexural buckling (Fig 4-3a), $\overline{\lambda}_z$ is proportional to the length of the member. Therefore, also η and $\overline{e}_0$ increase linearly with length. Due to the presence of the plateau value $\overline{\lambda}_0$, the imperfection $\overline{e}_0$ has a non-zero value only above the length corresponding to the value of $\overline{\lambda}_0$ (equal to 0.2 in this example); accordingly, the fraction $L/\overline{e}_0$ is not constant, but hyperbolic, approaching infinity at L=0, and the constant value that would result if $\overline{\lambda}_0$ were zero for L=∞.

ii.   In the case of lateral-torsional buckling (Fig 4-3b) and, even more so, in the case of torsional buckling (Fig 4-3c), the dimensionless slenderness ratios $\bar{\lambda}_{LT}$ and $\bar{\lambda}_T$ do *not* increase linearly with the length of the member, but under-proportionally. This leads to the fact that the ratio $L/\bar{e}_0$ increases with length, at least after the "singularity" caused by the introduction of $\bar{\lambda}_0 = 0.2$ is less influential, or in the case of $\bar{\lambda}_0 = 0.0$.

In summary, it can be said that when expression (4.2) is used to define the "generalized imperfection" as the calibration factor in the Ayrton-Perry formulation, this imperfection only increases linearly with length if $\bar{\lambda}_z$ (or $\bar{\lambda}_y$) is used for $\bar{\lambda}_S$. In all other cases, it has a non-linear dependency. This obviously represents a form of inconsistency in the single formulations. The implications of this inconsistency on the accuracy of this calibration are discussed in the specific chapters 5 to 7. It is shown there that the length-dependency is significant to the quality of the calibration, and must be seen in the context of the imperfections used in GMNIA calculations, as well as of real shape deviations.

4.3.3. Reliability issues

The procedures currently used to assess the reliability level of a certain design rule are discussed in chapter 3. The diagrams in Fig 4-4 serve the purpose of illustrating the current situation of the reliability assessment of Eurocode member buckling rules, as it is presented in the literature. Fig 4-4a and b show the results of the evaluation of the ECCS column buckling data for curves b and c, respectively, in terms of the partial safety factor γ_M*. This factor is directly related to the chosen design buckling curve, and expresses the distance between the "design point" that has the desired reliability level and the nominal curve the designer uses to determine a member's "characteristic" buckling strength.

The two diagrams a and b contain single "points" and indicate the result of the evaluation for the single tested (nominal) slenderness ratios (CEC, 1988). They show that, when using the reliability assessment procedure in its (slightly, but not significantly different) 1988 form, values of γ_M* of 1.10-1.14 were determined for the tests pertaining to buckling curve b, and values of 1.02-1.07 for the tests belonging to buckling curve c.

Fig 4-4c and d show the results of the reliability assessment carried out by Müller (2003) on the basis of international test results for weak-axis flexural buckling (lines b and c together) and for LT-buckling of hot-rolled sections, respectively. These evaluations represent the statistical backing of the current Eurocode design rules for these buckling cases. They show that values ranging from 1.08 to 1.13 can be calculated for the pool of available test data in the case of flexural buckling, and values from 0.97 to 1.11 in the case of LT buckling.
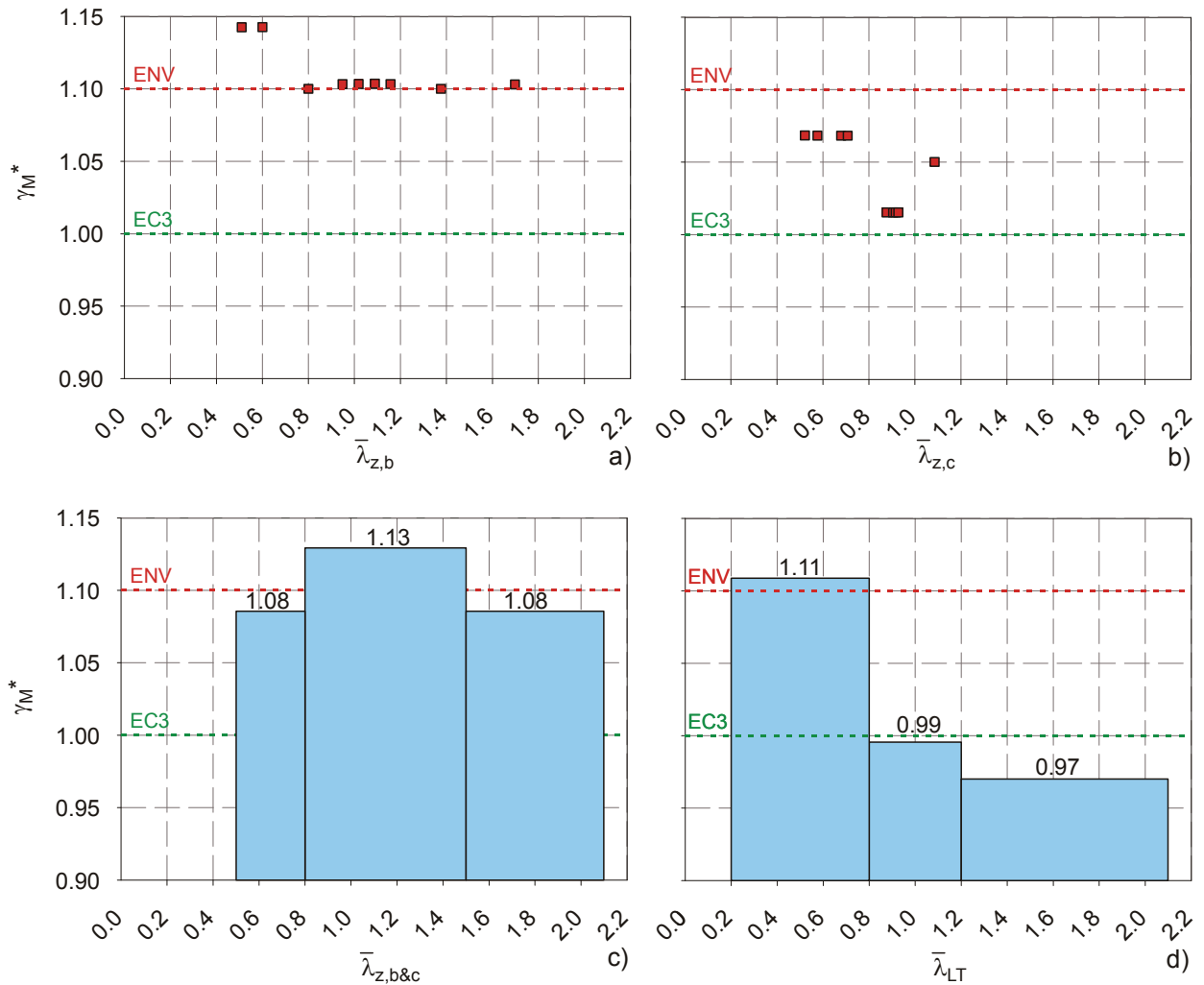
Fig 4-4 *Partial safety factors γ_M^* as indicated in the literature for different buckling cases; weak-axis flexural buckling, line b (a); line c (b); both lines (c); lateral-torsional buckling of hot-rolled beams (d)*

All diagrams also feature two horizontal lines representing the "recommended" values of the codified partial safety factor γ_{M1} according to the ENV version of the Eurocode 3 (1992) and the current provision (2006). The values are 1.10 and 1.00, respectively. While the ENV value of 1.10 is, in an average sense, backed by Fig 4-4, the current EC3 value cannot be justified by the reliability provisions of the Eurocode alone, at least not formally. While no published document is known that fully justifies the adoption of 1.00 for all cases, some sources (e.g. Schleich et alt, 2002; Müller, 2003) state that the weighting factor $\alpha_R=0.8$, which defines the "distance" in standard deviations between the mean, expectation value of the buckling strength and the design value (see chapter 3) on the resistance side, is actually "*too high for steel structures*", and that the "*span for reduction of safety factors lies at about 10%*".

In the paper by Schleich et al., this is demonstrated by calculating the actual value of α_R for three model single-storey frames under dead load, snow and wind, and under the assumption of certain probability densities (mean values, scatter) of both load- and resistance-sided quantities. Due to the

low scatter of resistance quantities in steel structures when compared to the uncertainties on the side of atmospheric loads, in that paper the appropriate value of α_R is calculated to be equal to 0.3, while the load-sided value is α_E=-1.0. Translated back into partial safety factors γ_M applied to nominal strength values, values "below 1.00" could be justified in this particular case.

Of course, it is difficult to argue for or against the adoption of γ_M=1.0 for all member buckling cases based on this single calculation. Generally speaking, the question of the justification of the current Eurocode 3 value of γ_{M1} is (understandably) highly controversial and can only be further discussed at a code committee level; it is therefore not further considered in this work. For the purposes of this dissertation, it is thus more important to assert the following:

i. If the reliability assessment procedure of the Eurocode (EN 1990 – Annex D) is left "untouched", the current member stability rules would actually require non-constant levels of partial safety factors γ_M in order to maintain a constant reliability level over all slenderness ranges.

ii. Due to obvious reasons of practicality in design, it is generally desired to keep the partial safety factor at a constant value for all slenderness ratios. However, one must be aware that doing so with the current design rules means that the reliability level of buckling design checks varies with slenderness.

iii. As was mentioned in section 4.3.1, all current member buckling rules are based on calibrations of (Ayrton-Perry) buckling formulae to GMNIA calculations with deterministic, fixed imperfection amplitudes and geometric assumptions. The non-constant reliability values over the different slenderness ranges are a direct result of this assumption, as is illustrated with much more detail in the following chapter 5. This fact can either be accepted as such, or seen as undesirable. If the latter is the case, new, more sophisticated and consistent concepts must be developed and implemented for the determination of the design buckling strength values, to which then buckling formulae can be calibrated.

4.4. Concepts for increasing consistency

The following section describes the concepts developed in this thesis with the purpose of reducing the inconsistencies outlined in the previous section. This is done in very general terms, with more in-depth procedural aspects left for the specific chapters 5 to 7. This section therefore serves the purpose of presenting the basic ideas as such, and will be referred to in the specific chapters with this intent.

4.4.1. Specific derivations *and* calibrations

In section 4.2, the three most common concepts for the treatment of different member buckling cases in design codes were presented. Of these, concept 2 and 3 were said to be the two currently employed or studied concepts.

In order to overcome the inconsistencies pointed out in sections 4.3.1 and 4.3.2, i.e. the lack of consistency between cross-sectional classification and underlying (GMNIA) imperfection assumptions, as well the length-dependency of the underlying imperfections, this thesis advocates the use of an intermediate position between concepts 2 and 3. This means that it aims at developing formulations for the most relevant member buckling cases that are both specifically calibrated to the buckling case at hand (concept 2), and mechanically better backed (concept 3).

The result of these efforts is an Ayrton-Perry formulation for different member buckling rules of the following form:

$$\chi_S = \frac{1}{\Phi_S + \sqrt{\Phi_S^2 - \overline{\lambda}_S^2}} \leq 1.0 \qquad (4.3)$$

and

$$\Phi_S = \frac{1}{2}\left[1 + \alpha_{0,S} \cdot \alpha_S \cdot \left(\overline{\lambda}_z - \overline{\lambda}_{0,S}\right) + \overline{\lambda}_S^2\right] \qquad (4.4)$$

with

$\overline{\lambda}_S$ ..... dimensionless slenderness for the studied buckling case

$\alpha_{0,S}$ ... specific "load-carrying behaviour" term stemming from a specific second-order Ayrton-Perry derivation

α_S .... generalized imperfection amplitude factor, calibrated for the specific buckling case as best-fit values to GMNIA buckling curves with specified imperfections.

$\overline{\lambda}_z$ normalized slenderness for (weak-axis) flexural buckling, used here to account for the linear length-dependency of the geometric imperfection $\overline{e}_0$.

$\overline{\lambda}_{0,S}$ .... plateau value shown to be justifiable for the specific buckling case

The following Table 4-2 schematically illustrates the pursued goal of these development efforts. It is a table that consistently relates a certain type cross-section and a certain set of assumptions regarding its geometry and imperfections (nominal cross-sectional values, imperfection amplitudes, etc.) to a group of coefficients, which accurately describe the strength of this member when used in expression (4.3) with (4.4).

The final result of these efforts is presented in chapter 8, while the single steps taken to get there are shown in the specific chapters 5 to 7. The main advantages of such a concept are the following:

i. By aiming at an accurate calibration of the factors α and $\overline{\lambda}_{0,S}$ to more sophisticated GMNIA buckling curves, the highest possible correspondence between design rule and the realistic buckling behaviour is obtained. This was already the goal of "concept 2" rules, like the ones currently found in the Eurocode. It is therefore sensible to maintain this goal and to improve its outcome, if possible. The "concept 3" formulations currently being brought forward to some extent renounce this aspect, causing inaccuracies in the description of the physical phenomena that can be significant, as is pointed out in chapter 6.

CROSS-SECTION	IMPERFECTIONS	BUCKLING CASE	$\alpha_{0,S}$	α_S	$\overline{\lambda}_{0,S}$
hot-rolled I-section h/b>1.2	geom. res.stress	FB_z	1	0.34	0.2
		LT	$\left(\dfrac{\overline{\lambda}_{LT}}{\overline{\lambda}_z}\right)^2$	...	...
		...	...	...	...
....	....	....	...	...	...
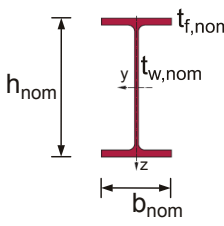
Table 4-2 *Schematic illustration of the desired outcome of newly calibrated member buckling rules.*

ii.   Being able to directly relate buckling curves to a certain set of assumptions regarding cross-sectional geometry and underlying imperfections allows the designer to better assess the sensitivity of a design to changes of these parameters. The imperfection assumptions made for the GMNIA calculations underlying current buckling curves represent (more or less accurately) real effects in members. That is to say that, for example, stockier, hot-rolled sections were shown to indeed have higher residual stresses than sections with higher depth-to-width ratio (Schulz, 1968). In the design concept sketched in Table 4-2, the designer would "feel" this for all member buckling checks.

iii.   The inclusion of a factor $\alpha_{0,S}$ stemming from a specific, second-order derivation, has the advantage of better representing the physical behaviour of a given buckling phenomenon, and mostly so in terms of stiffness effects. As will be shown in the specific chapters, a derivation of a buckling case-specific factor of $\alpha_{0,S}$ is possible when the imperfections are assumed to be affine to the buckling eigenmode.

iv.   By introducing the generalized imperfection coefficient η as a function of $\overline{\lambda}_z$ for *all* buckling cases, the assumption made in the GMNIA calculations of length-proportionality of geometrical imperfections is much better –and consistently- reflected in the buckling curves. In the specific chapters 5 to 7, this is also shown to yield more accurate results than the current use of $\overline{\lambda}_S$ in these expressions.

4.4.2. "Constant reliability curves"

In section 4.3.3, it has been discussed that the current Eurocode member buckling design rules don't actually have a constant reliability level along all slenderness ranges, since they are based on GMNIA calculations that refer to "model beams" with specified, deterministic geometrical input data and imperfection assumptions.

If this situation is deemed to be unsatisfactory, the following ideas can be used to substitute the *deterministic* GMNIA buckling curves by *probabilistic* GMNIA curves. Once these are obtained (for a specified reliability level), the calibration of buckling curves can be carried out accordingly.

The first idea consists of carrying out a sufficient number of physical or numerical (Monte Carlo) tests, which can then be statistically evaluated –with regard to a pre-established buckling formula- according to Annex D. Fig 4-5 exemplifies the results of such an analysis for an IPE 160 section and weak axis flexural buckling, evaluated for Monte Carlo tests and for buckling curve b of EC3. This same calculation will be discussed with more detail in chapter 5, so no details regarding the assumptions for the random variables are given at this point.
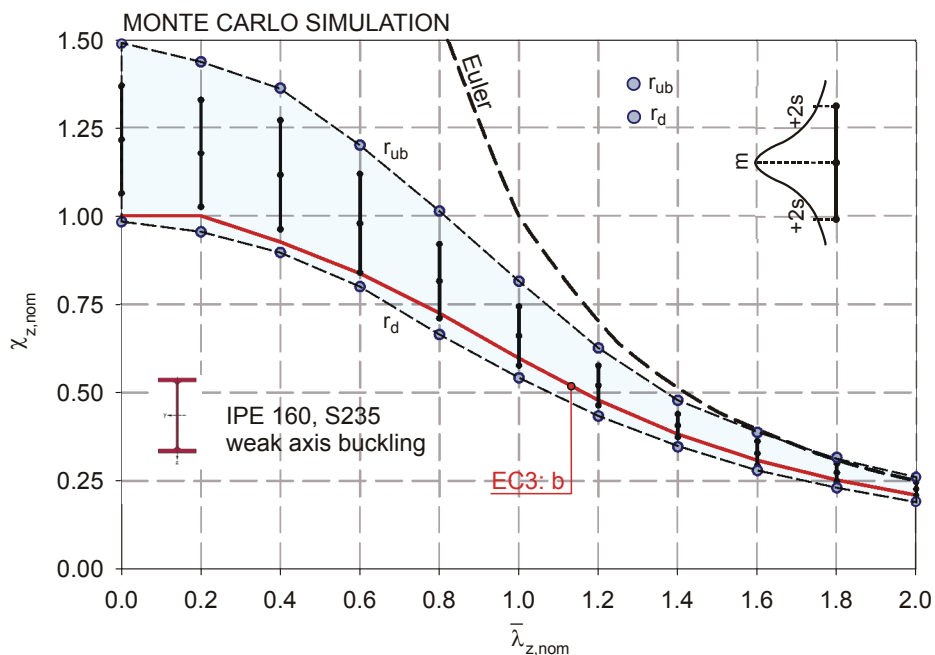
Fig 4-5 *"Constant reliability curves" derived from a Monte Carlo simulation of the weak-axis flexural buckling strength of an IPE 160 section.*

The figure shows the results of the single Monte Carlo tests in a form already used for the development of the ECCS column buckling curves, i.e. it plots mean values and values 2 standard deviations away from the mean, assuming a standard normal distribution.

The results of the "Annex D" reliability assessment are also plotted in Fig 4-5. The design point r_d at a distance of $k_{d,\infty} = 3.04$ log-normal overall standard deviations from the mean, and the upper

bound value r_{ub} at -3.04 log-normal standard deviations, delimit the shaded area. More details about this calculation are also found in chapter 5.

The lower line, representing r_d, can be interpreted as an *estimator* for the buckling curve that, if used in design, would require a constant value of γ_{M1}=1.0 in order to have a constant reliability level over all slenderness ranges. One can see from the figure that the Eurocode column buckling curve b applicable in this case lies above the line r_d, which is compatible with the values γ_M* described in section 4.3.3. The additional uncertainties associated with this line stem from the (unknown, in this case) accuracy of the GMNIA calculations themselves, when compared to tests, and of course from the assumed variability of the independent random basis variables themselves.

The above method is very laborious. It requires random number generation and a lot of numerical "tests" –for every slenderness range- in order to make the evaluation representative. In order to be at least somehow practically applicable, it also requires a pre-established buckling curve formulation to exist, since the evaluation of r_d is then carried out for this formulation. For the purpose at hand, i.e. establishing a better, more "probabilistic" GMNIA buckling curve to be used as basis of a calibration of a buckling formula, this method therefore seems to be *unpractical*.

A *different approach* to the problem can be found by applying the Eurocode EN 1990 Annex D (2002) provisions to the letter, but *for the GMNIA model itself*. This approach is essentially a First Order Reliability Method based on GMNIA calculations, and has the following reasoning:

i. The Annex D procedure is a "First Order Reliability Method" (FORM) used to determine the location of the *design resistance value* r_d for a so-called "resistance function". Normally, one thinks of a formulaic expression (e.g. for a buckling curve) of a component's resistance as being such a resistance function.

ii. Due to the complexity of the phenomenon, in the case of member buckling such formulaic expressions for resistance functions usually must be developed by means of calibration to more sophisticated GMNIA curves in order to obtain high accuracy of representation.
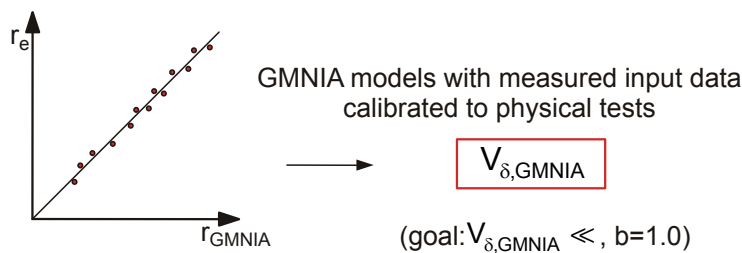
Fig 4-6 *Schematic representation of the scatter of GMNIA calculations compared to physical tests*

iii. It therefore makes sense to regard the GMNIA calculations as some sort of "first step resistance functions", for which the location of the design resistance value $r_{d,GMNIA}$ could be determined using the procedures described in EN 1990.

iv.   These values of $r_{d,GMNIA}$, which *inherently* represent a constant reliability level, can then be used as the basis of calibration of a formulaic expression of buckling curves to be used by designers. If the calibration is accurate and reflects the main parameters well enough, the demand for constant reliability will approximately be satisfied by these formulations as well.

In order to obtain the values of $r_{d,GMNIA}$, the following steps can therefore be envisaged:

1)   *Collect data for the main input parameters ("basis variables") of the studied problem.* These will include the statistical parameters (mean value, standard deviation) of the material (f_y, f_u) and geometrical properties, as well as corresponding information regarding imperfections.

2)   If full-scale physical tests are available beforehand, *calibrate the GMNIA model* in order to obtain as-small-as-possible divergences between tests and numerical calculation results (carried out with the measured input data from the test), see Fig 4-6.

3)   The unavoidable, remaining scatter can then be accounted for by calculating $V_{\delta,GMNIA}$:

$$V_{\delta,GMNIA} = \sqrt{\exp(s_\Delta^2) - 1} \tag{4.5}$$

with

$$s_\Delta^2 = \frac{1}{n-1} \sum_{i=1}^{n} \left(\Delta_i - \overline{\Delta} \right) \tag{4.6}$$

$$\overline{\Delta} = \frac{1}{n} \sum_{i=1}^{n} \Delta_i \tag{4.7}$$

$$\Delta_i = \ln\left(\frac{r_{e,i}}{b \cdot r_{GMNIA,i}} \right) \tag{4.8}$$

$$b = \frac{\sum_{i=1}^{n} r_{e,i} \cdot r_{GMNIA,i}}{\sum_{i=1}^{n} \left(r_{GMNIA,i} \right)^2} \tag{4.9}$$

4)   Calculate the adjusted, *mean value buckling curve* $r_{m,GMNIA}$ resulting from a GMNIA calculation carried out for the mean values of the statistical input data. In consistence with the EN 1990 Annex D terminology, we can define that $g_{r,GMNIA}(\underline{X})$ represents the result of a GMNIA calculation for a row of j different, arbitrary values $\underline{X}$ of the basis variables. If $\underline{X}_m$ is the row of j variables where every value corresponds to its mean, we can write:

$$r_{m,GMNIA} = b \cdot g_{r,GMNIA}(\underline{X}_m) \tag{4.10}$$

This expression includes the linear regression correction factor b, which will be very close to 1.00 if appropriate GMNIA models are used.

5) The key step of the FORM analysis: *calculate the coefficient of variation $V_{r,GMNIA}$ of the GMNIA resistance function:*

$$V_{r,GMNIA}{}^2 = \frac{VAR\left[g_{r,GMNIA}(\underline{X})\right]}{g_{r,GMNIA}(\underline{X}_m)^2} = \frac{1}{r_{m,GMNIA}{}^2} \cdot \sum_{i=1}^{j}\left(\frac{\partial g_{r,GMNIA}}{\partial X_i} \cdot \sigma_i\right)^2 \tag{4.11}$$

Equation (3.14) contains partial derivatives of the GMNIA resistance function. Obviously, these cannot be explicitly calculated, but must be calculated numerically, i.e. by carrying out (at least) one additional GMNIA calculation per variable.

$$\frac{\partial g_{r,GMNIA}}{\partial X_i} \approx \frac{g_{r,GMNIA}(X_{1m},...,X_{im}+\Delta X_i,...,X_{jm})-g_{r,GMNIA}(\underline{X}_m)}{\Delta X_i} \tag{4.12}$$

It should be noted that it is proposed to carry out these partial derivatives at $g_{r,GMNIA}(\underline{X}_m)$, representing the result of a GMNIA calculation with mean values of the basis variables. This somewhat differs from the EN 1990 Annex D procedure, which carries out the partial derivation at the single test data points, thus obtaining (slightly) different values of V_{rt} and of the corresponding design value r_d for every single test. Since, however, the design points r_d are then averaged for a group of data (e.g. all tests of the same nominal slenderness $\bar{\lambda}$) to obtain values $\gamma_M{}^*$, the differences between (4.12) and the Annex D procedure are minimal.

Examples of numerical derivatives, and a discussion of the difficulties and necessary precautions associated with their calculation, will be given later on in this thesis.

6) *Calculate the lognormal variation coefficients* $Q_{r,GMNIA}$, $Q_{\delta,GMNIA}$ and Q:

$$Q_{r,GMNIA} = \sqrt{\ln\left(V_{r,GMNIA}{}^2+1\right)} \tag{4.13}$$

$$Q_{\delta,GMNIA} = \sqrt{\ln\left(V_{\delta,GMNIA}{}^2+1\right)} \tag{4.14}$$

$$Q = \sqrt{\ln\left(V_r{}^2+1\right)} \tag{4.15}$$

with

$$V_r{}^2 = V_{r,GMNIA}{}^2 + V_{\delta,GMNIA}{}^2 \tag{4.16}$$

7) *Calculate the design point $r_{d,GMNIA}$.* If $V_{\delta,GMNIA}$ is calculated on the basis of many tests (n>100) or, more plausibly, if $V_{\delta,GMNIA}$ is thought to be small enough for the realistic GMNIA calculations, r_d can be calculated as follows:

$$r_{d,GMNIA} = r_{m,GMNIA} \cdot \exp(-k_{d,\infty} \cdot Q - 0.5 \cdot Q^2) \tag{4.17}$$

The result of such a series of calculations is shown in Fig 4-7, again for the example of weak-axis flexural buckling of an IPE 160 section. For this calculation, the possible inaccuracies of the GMNIA model itself were ignored, meaning that V_δ was assumed to be zero, and b to be 1.0. These assumptions don't alter the general concept presented here. The assumptions regarding the basis variables (scatter band of material strength, geometry, imperfections) are discussed in chapter 5.
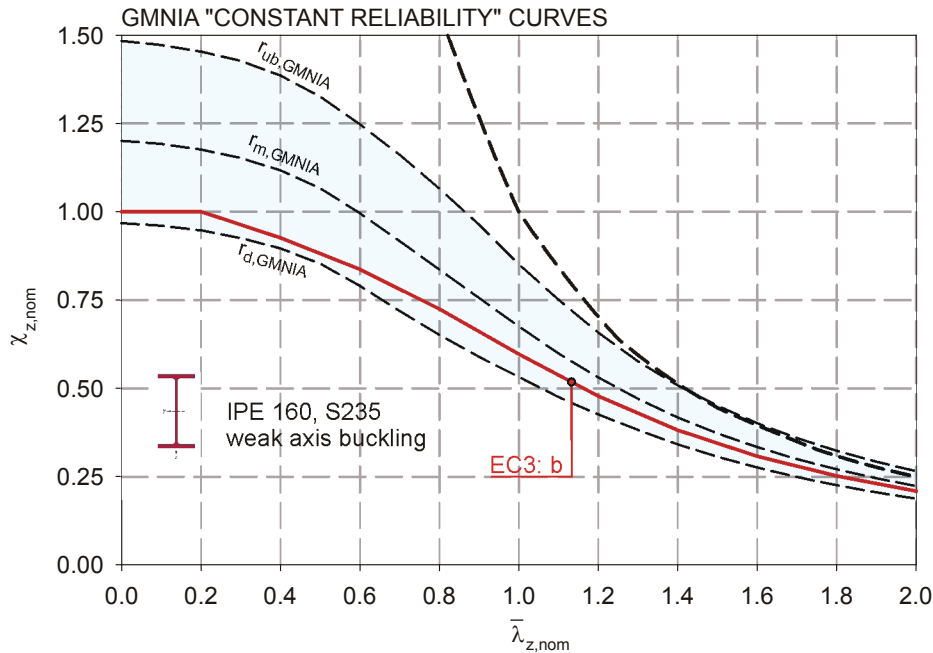
Fig 4-7 *"Constant reliability curves" derived from numerical (GMNIA) calculations for weak-axis flexural buckling of an IPE 160 section.*

The figure also shows the Eurocode buckling curve b, which would apply for this section and buckling case. Again, the non-constant values of γ_M* discussed in section 4.3.3 are reflected in this figure. The line for $r_{d,GMNIA}$ shows where the Eurocode buckling curve *should lie* in order to justify the use of $\gamma_{M1}=1.00$ based on EN 1990 Annex D. If one were interested in knowing where the Eurocode curve should lie to obtain a constant value of γ_{M1} of, for example, 1.05, one would just have to multiply all values of $r_{d,GMNIA}$ by this factor.

When compared to Fig 4-5, the figure in this page shows that the result in terms of the location of the constant reliability, design value buckling curve r_d is practically the same. Of course, this had to be the case due to the fact that Fig 4-5 is based on Monte Carlo simulations that made use of the same basis variables, with the same scatter band, as in the calculations for Fig 4-7. The lines for r_d in both figures, after all, are numerical buckling curves based on certain assumptions regarding the parameter variability. Nevertheless, the *GMNIA constant reliability curves* presented in this section can be considered to be much more practical than the Monte Carlo approach:

i. Contrary to the Monte Carlo concept, this method relies solely on GMNIA calculations, making it a viable tool for the development of new buckling rules.

ii. Instead of simulating dozens of tests with random input variables at each studied nominal slenderness value, the GMNIA constant reliability curves make do with j+1 calculations per value of $\overline{\lambda}_{nom}$, with j being the number of considered basis variables.

iii. For the purposes of this concept, it is often possible to keep this number as low as possible, by identifying the truly important basis variables through a preliminary, deterministic parametric study of the sensibility of the buckling strength for changes of the parameters

within the scatter band. In the above example, these parameters were the yield strength f_y, the flange thickness t_f, the amplitude of the out-of-straightness $\bar{e}_0$ and of the load eccentricity e, as well as the level of the residual stresses σ_{res}.

iv. While the method based on the Monte Carlo simulation requires a certain number of "tests" to become reproducible in terms of values r_d within certain tolerance limits, the presented concept based on partial derivatives is fully reproducible for any given GMNIA model and assumed basis variable variability.

In comparison to the current method, which is based on semi-deterministic GMNIA calculations on "model beams or columns" with specified geometry and imperfection, the probabilistic GMNIA constant amplitude concept is of course still more laborious. In terms of calculation time, it requires j+1 calculations per slenderness range instead of just 1. The significance of this extra computing time is debateable.

Additionally, the developers of buckling rules are faced with new uncertainties in the proposed probabilistic method, since they must gather information regarding basis variables and their scatter band. However, this can't be regarded as a true drawback of the proposed method compared to the current one based on "model beams"; the assumptions for the input data to be used in the "model beam" calculations were calibrated to tests (Beer & Schulz, 1970) and therefore also indirectly based on probabilistic considerations. Thus, the developers of design rules that make use of "model beams" are implicitly making use of these findings. The new concept would not fundamentally change this if, for example, parameters for input data variability were agreed upon on a code committee level, as was the case for the "model beam" assumptions.

It is believed that, in the future, such "constant reliability" curves could play an important role in the development of buckling curves. In this thesis, they will *not* be used as the main concept for the determination of GMNIA buckling curves due to a current lack of consolidated, widely recognized, "state-of-the-art" data pool regarding the variability of material, geometrical and imperfection quantities. They will however be used for comparison reasons, coupled with some plausible assumptions regarding these quantities.

5

Flexural Column Buckling – the Benchmark Case

5.1. Introduction and Scope

This chapter is dedicated to the "benchmark" case for the development of all member buckling rules: the flexural column buckling case. It discusses the development of current European column buckling rules, with the aim of identifying a coherent development procedure for other buckling cases, as well as pointing out the origin of some inconsistencies currently present in design rules.

Additionally, the chapter addresses some open points that have recently arisen in the context of the introduction of a new fabrication standard for constructional steelwork – EN 1090-2 (2009). This standard specifies new, relaxed fabrication and erection tolerances for shape deviations (out-of-straightness) of columns and other compression members. The as-yet unanswered question of whether or not this is "covered" by current design rules is therefore discussed here.

Finally, the chapter addresses the possibility of increasing the homogeneity of the reliability level for all slenderness ranges by introducing *constant reliability curves* as presented in chapter 4.

5.2. The European Column Buckling Curves –

Historical Development from Today's Perspective

The development of the so-called *European column buckling curves* was carried out under the auspices of the European Convention for Constructional Steelwork (ECCS) and by its Technical Committee 8 (TC8), roughly between the mid-1960s and 1978. It comprised a very extensive experimental program, which resulted in the (to date) most complete set of full-scale column buckling test data available internationally, as well as a comprehensive theoretical/numerical study.

The motivation for such an extensive study was (Sfintesco, 1970):

i.   to provide a commonly shared and accepted theoretical and experimental background for a harmonization of the single national column design rules in Europe, and

ii.   to homogenize, as far as possible, the level of safety/reliability throughout all ranges of slenderness of typical steel columns.

Finally, this effort led to the development of five different column buckling curves, termed a_0, a, b, c, d and representing different cross-sectional geometries and their distinct behaviour in buckling. These curves are still found in the Eurocode today.

In this section, the development of the ECCS column buckling curves is subdivided in logically pertinent –but not necessarily chronological- steps, and discussed accordingly. In order to put this discussion in a contemporary context, the single steps are complemented by new, specific numerical (GMNIA) calculations whenever this was thought to be of benefit to the reader.

5.2.1. Step 1: Parameter Identification

The main theoretical background to the development of the ECCS column buckling curves was provided by Beer & Schulz (1969, 1970; Schulz 1968), who carried out extensive numerical studies based on non-linear, large deformation analyses of imperfect columns.

One early motivation behind these calculations was to provide a means of identification of the most relevant parameters governing the buckling phenomenon. This was meant as a supportive activity to the experimental program (see "Step 2"), where these important parameters had to be measured. These parameters are only discussed briefly here, since a more thorough description (with similar conclusions) is given in chapter 6 for the case of LT buckling.

In broad terms, the identified parameters can be split-up in two sub-groups:

i. The first group consists of parameters that have a significant impact in *absolute* terms, but not in terms of *normalized slenderness* $\overline{\lambda}$ *and buckling reduction factors* χ. For example, this is the case for the yield stress (Fig 5-1) and the geometrical shape-deviations of the cross-section (flange thickness, depth, width, etc., see Fig 5-2).
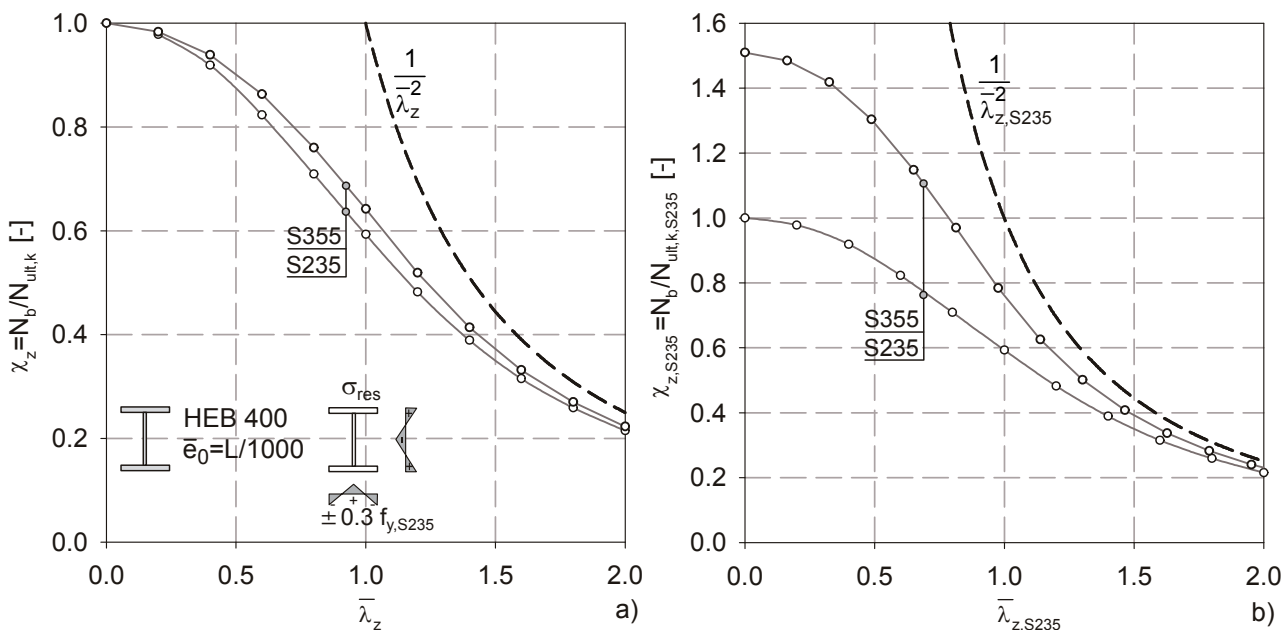
Fig 5-1 *GMNIA calculation, HEB400 section, FB$_{z-z}$: influence of the yield stress on buckling strength in normalized (a) and absolute terms plotted as multiples of $N_b/(A \cdot f_{y,S235})$ (b).*
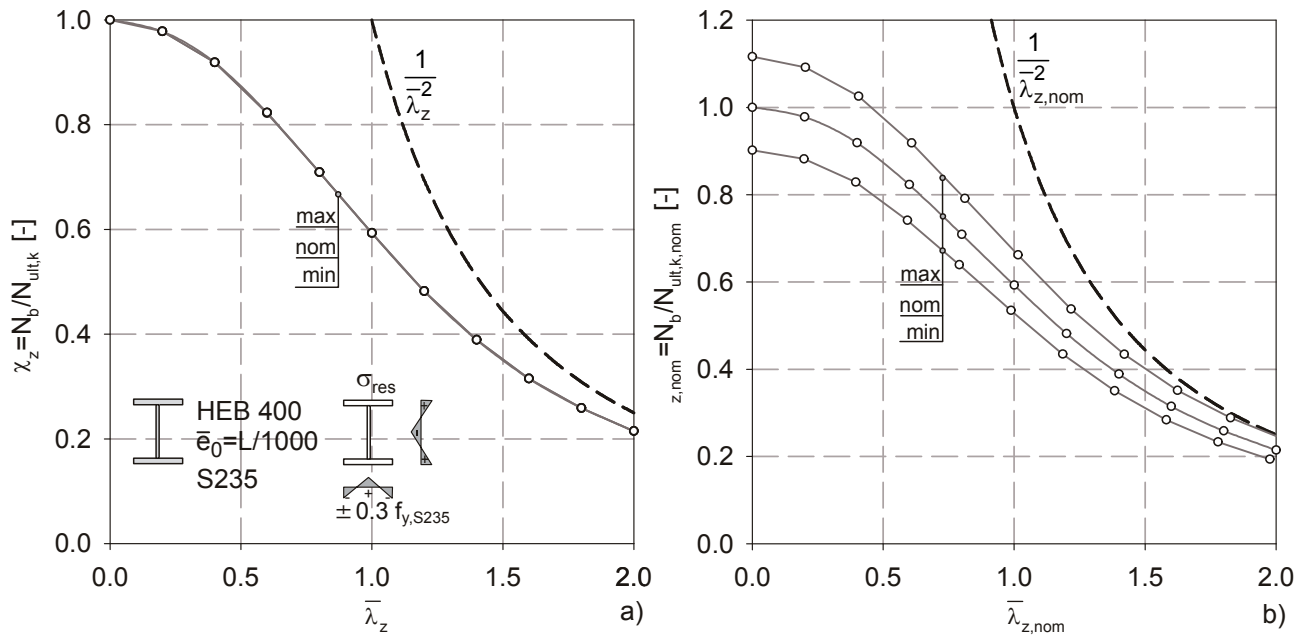
Fig 5-2 *GMNIA calculation, HEB400 section, FB$_{z-z}$: influence of the cross-sectional shape deviations on buckling strength in normalized (a) and absolute terms (b); max, min: maximum and minimum cross-sectional values still in compliance with tolerance limits of EN 10034 (1993).*

The yield stress can be shown to be almost entirely insignificant in *normalized* representation if the residual stresses are assumed to be proportional to it. In absolute terms, its influence strongly diminishes with increasing slenderness.

The shape deviations' influence is quite significant in *absolute terms*, actually increasing with slenderness. In *terms of normalized factors related to the actual cross-sectional capacity*, however, their influence is practically zero. More details on the influence of both parameters on buckling strength is given in chapter 6 in the context of LT buckling.

ii. The second group of parameters is mainly composed of the geometrical imperfections of the member - as opposed to the ones of the cross-section-, as well as the residual stresses (structural imperfections). The impact of these parameters is illustrated for the case of weak-axis flexural buckling of an HEB400 section in Fig 5-3.

These GMNIA calculations show that the three imperfections (out-of-straightness, end eccentricity of the load and residual stresses) all have an influence on the buckling strength that reaches its maximum (in relative terms) at intermediate values of the normalized slenderness $\bar{\lambda}$, between 0.8 and 1.2. In the case of the residual stresses, both amplitude and distribution of these locked-in stresses can be shown to be influential.
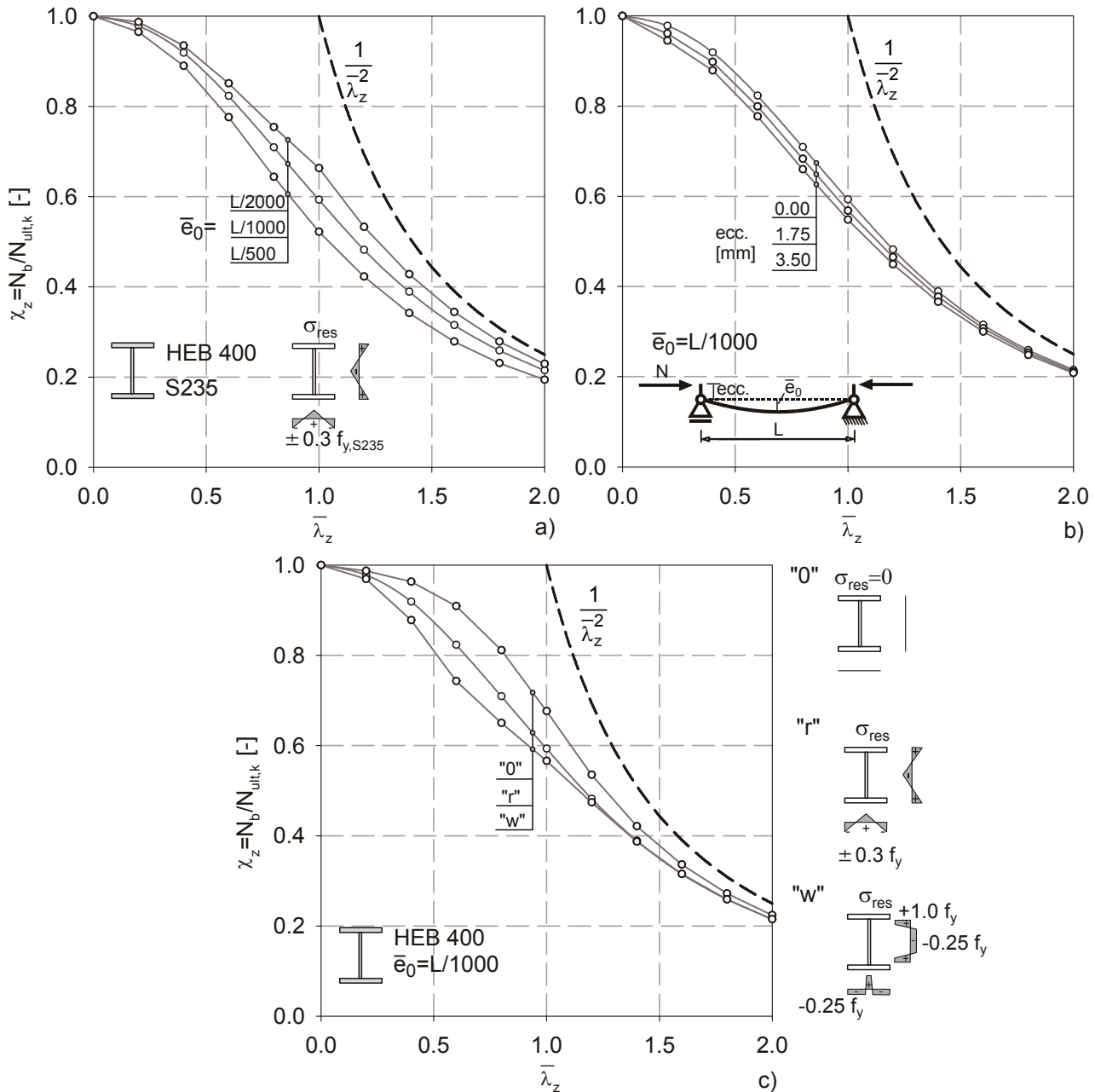
Fig 5-3 *GMNIA calculation, HEB400 section, FB$_{z-z}$: influence of the initial out-of-straightness $\bar{e}_0$ (a), the load eccentricity (b) and the residual stress amplitude and distribution (c)*

5.2.2. Step 2: Experimental Program

The experimental program conducted in the context of the development of the ECCS column buckling curves comprised some 1067 full-scale buckling tests and a correspondingly large number of *complementary tests* to establish the statistical distributions of the main structural parameters presented in Step 1.

The full-scale buckling tests are described in their scope and statistical exploitation by Sfintesco (1970) and Jaquet (1970), as well as Sfintesco & Carpena (1977). Their main findings and use in the context of the finalization of the ECCS buckling curves are discussed under Step 3. In this sub-

section, the *complementary tests* are of more interest. The significant findings for the single parameters are discussed in the following.

Yield Stress

All ECCS full-scale buckling test series were conducted on mild steel comparable to the modern S235 *steel*. In order to check the variability of the strength parameters of the material, the tests were accompanied by stub-column and tensile coupon tests. The results for the IPE 160 series of tests, which comprised sections from four different European countries and from several different production lots, are taken from the paper of Strating & Vos (1972) and plotted in Fig 5-4. The differences in mean value m and standard deviation s between stub column and coupon tests should be noticed. The values stemming from coupon tests are quite comparable with more recent studies found in the literature (Petersen, 1993; Byfield & Nethercot, 1997; ERP, 2003, Melcher et al., 2004) both in terms of mean values and (importantly) scatter. The scatter of the stub-column tests also seems to be in agreement with other sources (Fukumoto, 1983).
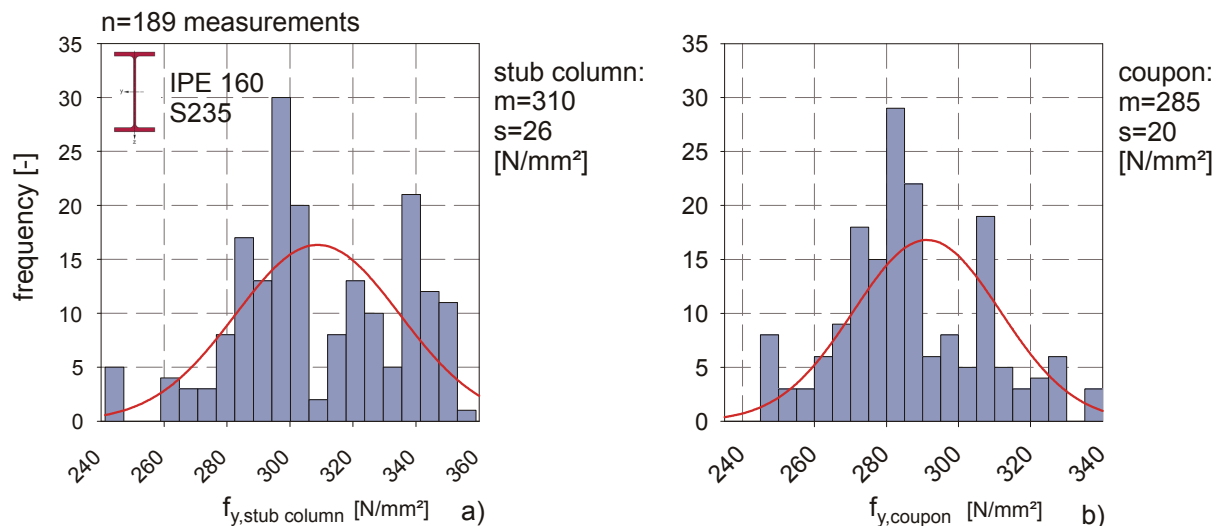
Fig 5-4 *Yield stress measurements for the tested IPE 160 sections; stub-column (a) and tensile coupon tests (b).*

Cross-sectional Geometry

Hot-rolled steel sections, as well as plates and other steelwork manufacturing products, display variations in cross-sectional shape (area, thickness, etc.), ideally with a scatter band that lies within specified *tolerance limits*. In the case of the sections tested over the course of the ECCS program, these variations were primarily checked and recorded in an indirect and "overall" manner by determining the mean area of the sections from a specimens volume, determined by water immersion scales. The results of these measurements for the series of tests on IPE 160 sections is plotted in Fig 5-5. The data was again taken from Strating & Vos (1972). Interestingly, a much more recent study (Melcher, 2004) featured a similar set of statistical parameters for the area of 371 IPE sections (series 160 to 240), with A/A_{nom} having values of m=1.025 and s=0.0325.
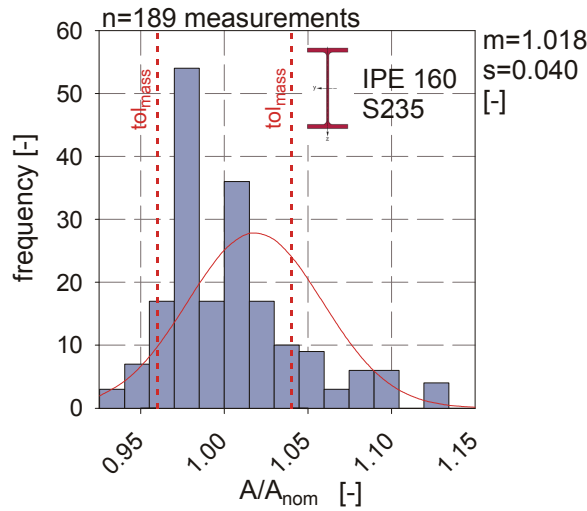
Fig 5-5   *Statistical variation of the cross-sectional area of IPE 160 sections tested by ECCS.*

Additionally and in parallel to the measurements undertaken by ECCS, a major research project was dedicated specifically to the determination of cross-sectional variations of European wide flange sections of the HE series (Alpsten, 1972). The most relevant findings are summarized in Fig 5-6.
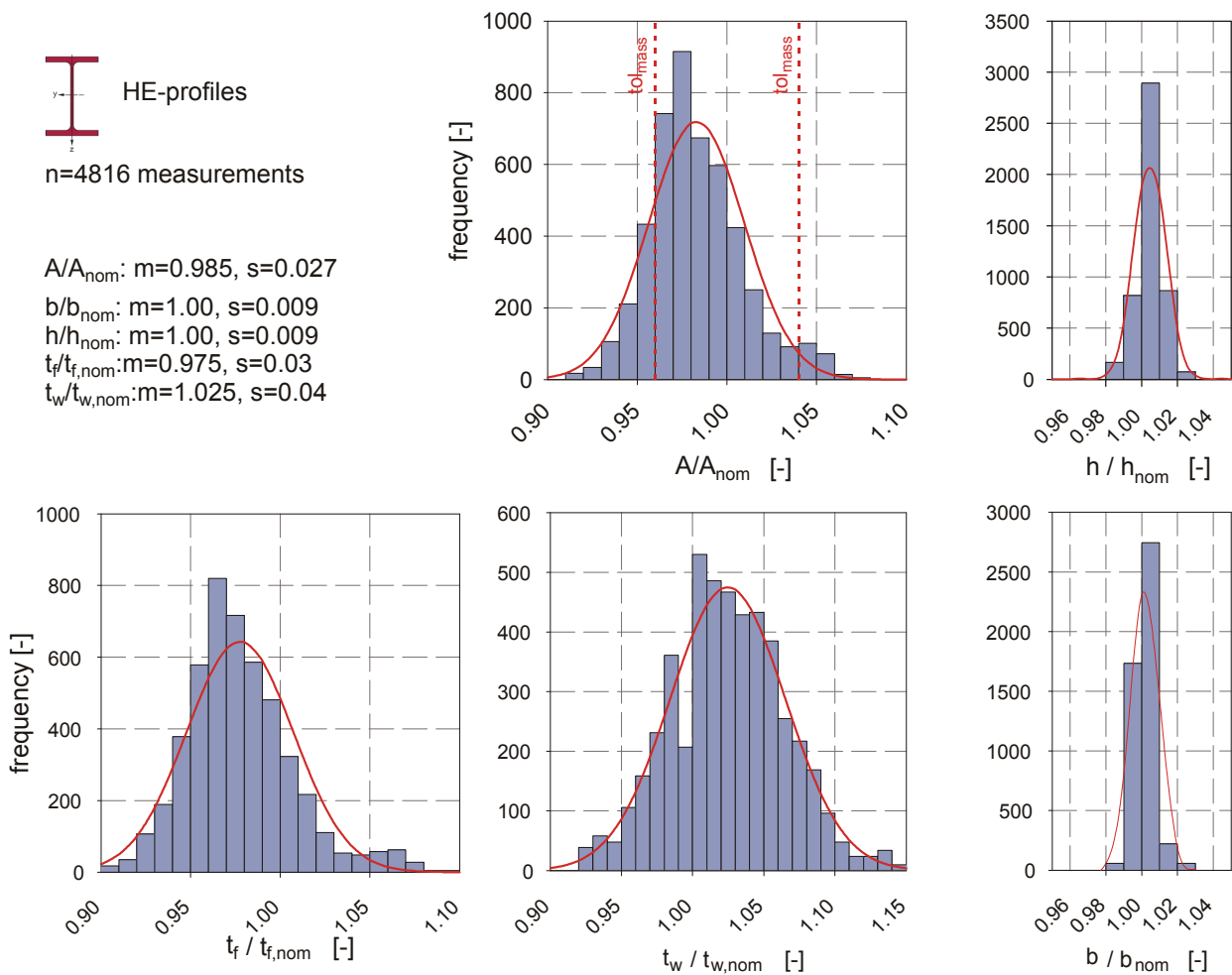
Fig 5-6   *Statistical variation of the cross-sectional geometry of HE sections (data: Alpsten, 1972).*

Alpsten's study represents the most thorough analysis of cross-sectional variations of European HE sections to date, with some 4816 individual sections taken into account. Fig 5-6 shows the data provided by Alpsten and a representation of scaled probability density functions applicable to this data if normal distributions of the parameters are assumed.

A comparison between Fig 5-5 and Fig 5-6 leads to the conclusion that the (much more limited in scope) measurements by ECCS do not entirely fall within the scatter band observed for HE sections. In the case of the IPE 160 sections, the measured shape deviations led to cross-sectional areas that were, on average, slightly larger than the nominal value. In the case of the HE shapes, the area was measured to be on average slightly lower than nominal value. Alpsten (2002) commented on his measurements, noting that it is mainly the flange thickness t_f that is responsible for the tendency of the area to be smaller than the nominal value. The web thickness partially compensates the lower-than-nominal flange thicknesses. This is explicable by an optimization of the rolling process and of the time of changeover of the rolls. Width and depth of the rolled sections were observed to have only a minimal scatter about the nominal value.

It should be noted that the above observations were also generally confirmed in the measurements on HEAA shapes that were recently carried out during a research project at Graz University of Technology (Kettler, 2008).

What is remarkable in both Fig 5-5 and Fig 5-6 is the fact that the tolerance limits of ±4% on *mass*, converted into area tolerances under the (realistic) assumption that the length variation is practically zero and the material density g=7850 kg/m³ is constant, was not generally complied with by the specimens measured by Alpsten and ECCS. In order to understand how this is possible, the minimum and maximum allowable areas, computed from the single plate thickness tolerances of EN 10034, are shown in Fig 5-7 for the HE-A and –B series.
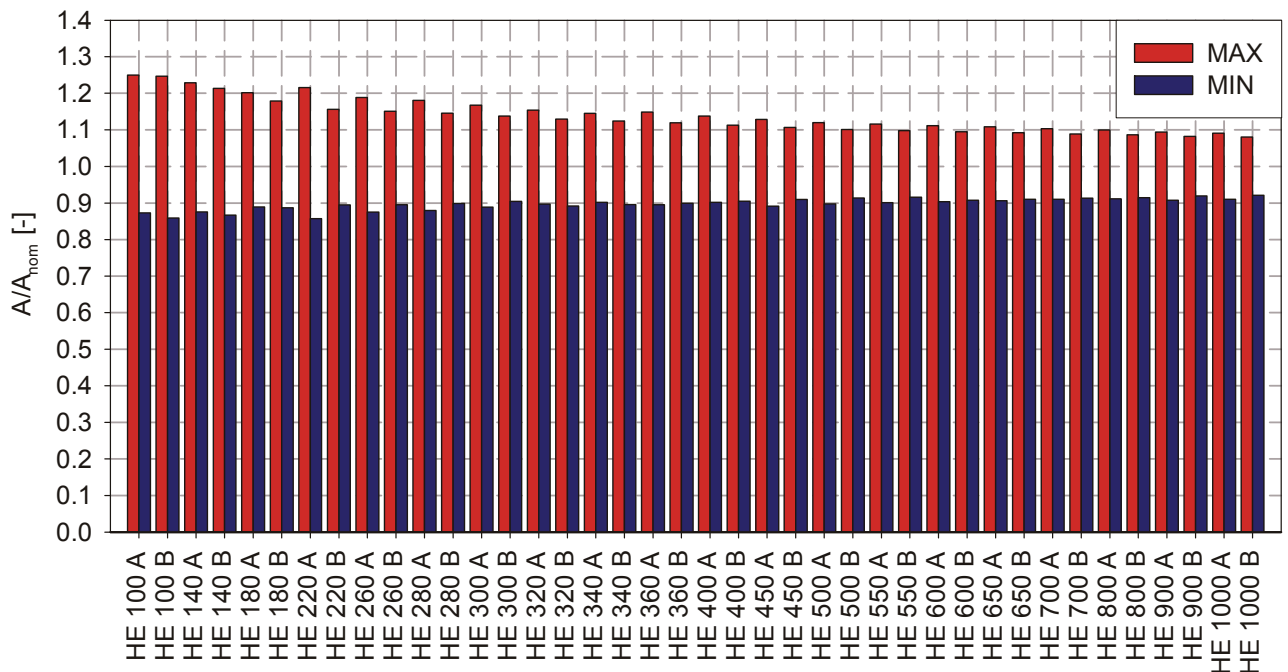
Fig 5-7   *Minimum and maximum allowable area ratio A/A_{nom} for HE-A and –B shapes.*

The figure shows that the area tolerance does not correlate well with the mass tolerance if minimum variations of length and material density are assumed. Cross-sectional areas of less than 90% and more than 120% of the nominal value are explicitly allowed by current mill manufacturing standards. These tolerances are obviously quite significant to the flexural column buckling case under pure axial load. If a value of A/A_{nom} of 90% is accepted as the "actual" minimum value of the area tolerance, the measurements of ECCS and Alpsten appear to confirm that this tolerance is kept at a significant relative "distance" from the actual production scatter band in Europe, lying at ca. 3 standard deviations from the mean.

Initial Out-of-Straightness

Much attention was paid to the initial out-of-straightness (or curvature) of the compression members tested in the ECCS program. In order to test columns thought to be representative of shop conditions, only un-straightened bars that were *straight to the bare eye* ("droite à l'œil" according to Sfintesco, 1970) were used. The curvature was measured by determining the deviation from the straight line connecting the columns' extremities at different points. Ballio and Mazzolani (1983, pp. 132-133) state that many different shapes of curvature were observed, see Fig 5-8. Schulz (1968) and Ersvik & Alpsten (1970) showed that the amplitude of these deflections as fraction of the length is the most significant factor, far out-weighing the importance of the shape itself. Schulz also showed that the first, sinusoidal "wave" amplitude of a Fourier series of an arbitrary initial deflection shape is sufficient to describe the buckling strength of any compression member.
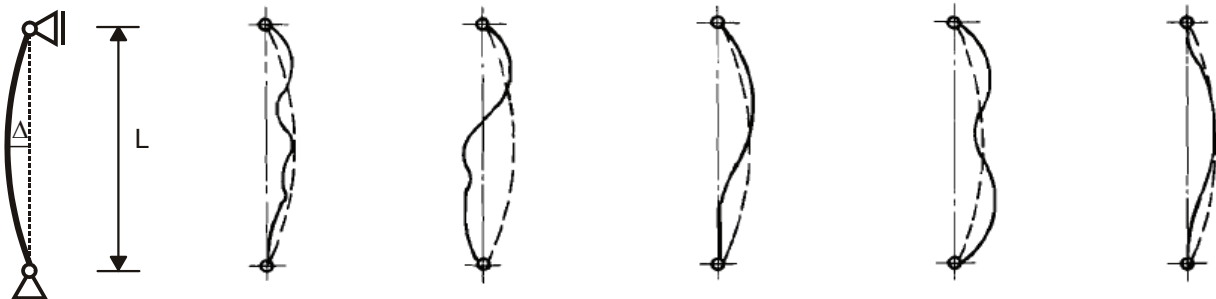
Fig 5-8 *Out-of-straightness Δ: idealized and measured. Figure taken from Schulz (1968).*

The connection between fabrication tolerances and out-of-straightness will be discussed with more detail in section 5.5 of this chapter. At this stage, only the shape deviations actually measured by ECCS will be further described. It shall just be briefly mentioned that the tolerance limit for the initial curvature was set at Δ=L/1000 in the years when the ECCS buckling curves were developed.

Fig 5-9a shows the measured initial curvatures of the tested IPE 160 sections as reported by Strating & Vos (1972). A similar, but not quite identical distribution is also given by Fukumoto (1983). Tebedge et al. (1972) determined values of the initial curvature for heavy HE sections (mostly HEM340 and similar), plotted in Fig 5-9b.
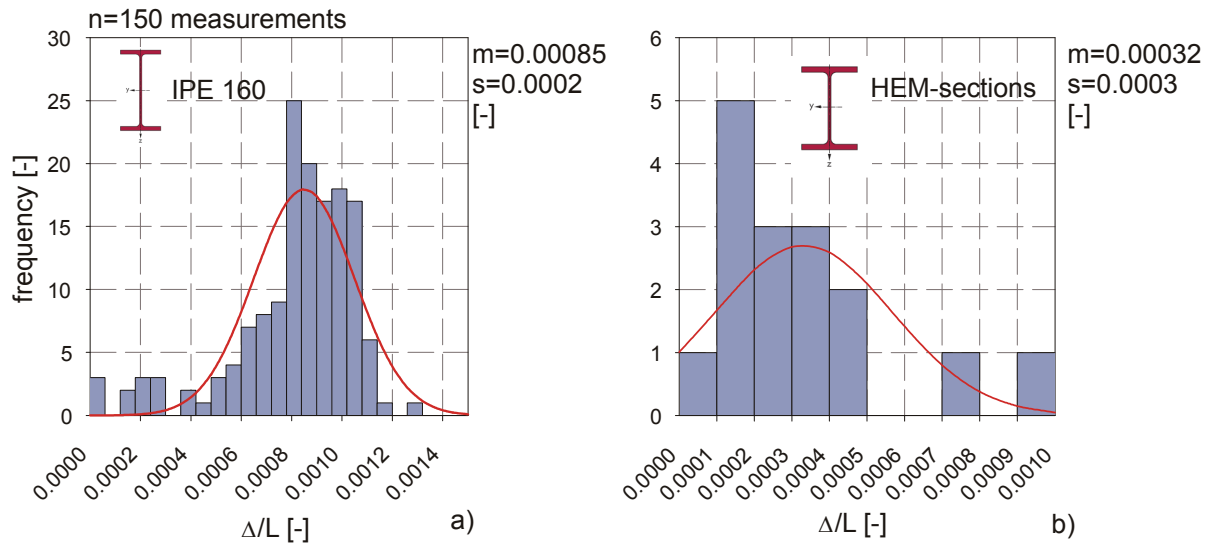
Fig 5-9   *Measured initial curvature Δ as fraction of the column length for some of the ECCS column tests.*

It is interesting to note that the curvatures of deeper, heavy shapes (HE, h>300 mm) were shown to be statistically smaller than the ones observed for cross-sections with smaller depth (IPE, h<200 mm). This is actually in agreement with the *rolling* tolerances of these sections according to EN 10034, see Table 5-1.
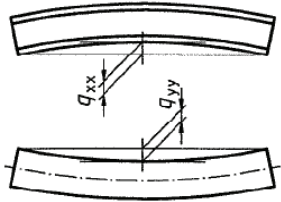
Section depth h [mm]	Curvature tolerance q_{xx}, q_{yy}
80<h≤180	0.30% of L
180<h≤360	0.15% of L
h>360	0.10% of L

Table 5-1   *Initial curvature tolerance according to and using the terminology of EN 10034 (1993).*

Some other probability density functions found in the literature, which are not necessarily directly linked to the ECCS test program but connected to it by the common objective of developing column buckling curves, are shown in Fig 5-10.

The distribution given by Fukumoto (1983) was calculated from a collection of all column test data available internationally in the early 1980s. It is unknown whether this calculation was accompanied by testing of possible correlations and systematic sub-scatters of the single section types. One must suspect that such a larger scatter as the one devised by Fukumoto is not representative for single types of sections.

The distribution given by Bjorhovde (1972) was based on more-or-less plausible assumptions regarding the likelihood of the occurrence of certain values. The probability of having values above the tolerance limit of Δ=L/1000 was assumed to be equal to 2.5%.
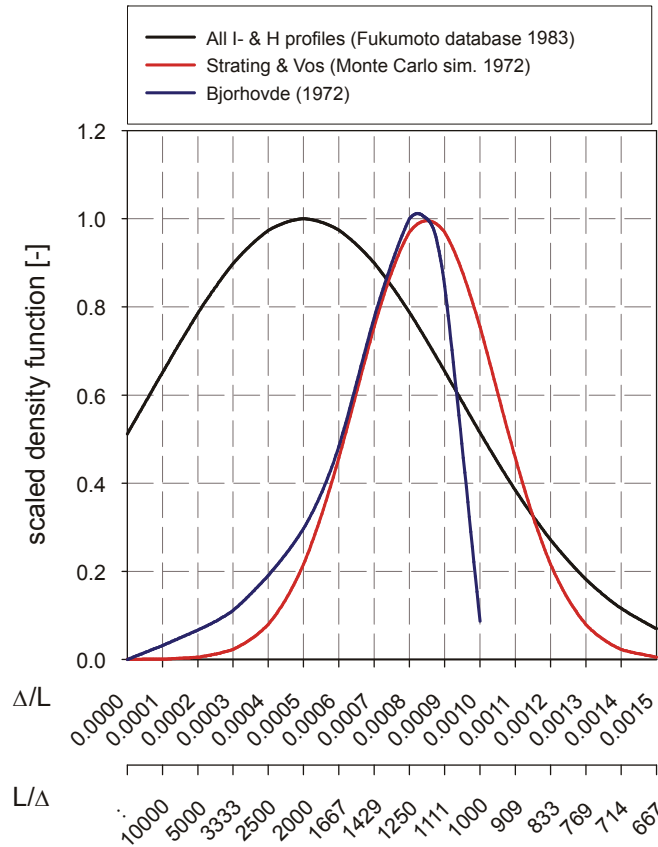
Fig 5-10 *Scaled probability density functions for initial curvature of columns.*

The distribution assumed by Strating & Vos (1972) for their Monte Carlo simulations (see Step 4) was based on the actual ECCS measurements for IPE 160 sections, and can be interpreted as a "tail approximation" of the upper values of the recorded curvatures.

Load Eccentricity

Additionally to the out-of-straightness, load eccentricities at the end of the column can cause second-order bending moments in a column. Fig 5-11 shows the eccentricities measured for the IPE 160 series of ECCS tests. The data is taken from Schulz et al. (1977).

It shall be noted that these eccentricities had a clear definition: for the case of weak-axis buckling , they were equal to the eccentricity of the web with regard to the flange. This definition can be regarded to be correct in light of the fact that the load in the ECCS tests was placed at the centroid of the web. If the web is eccentric with regard to its nominal position, an eccentricity of the load is present.
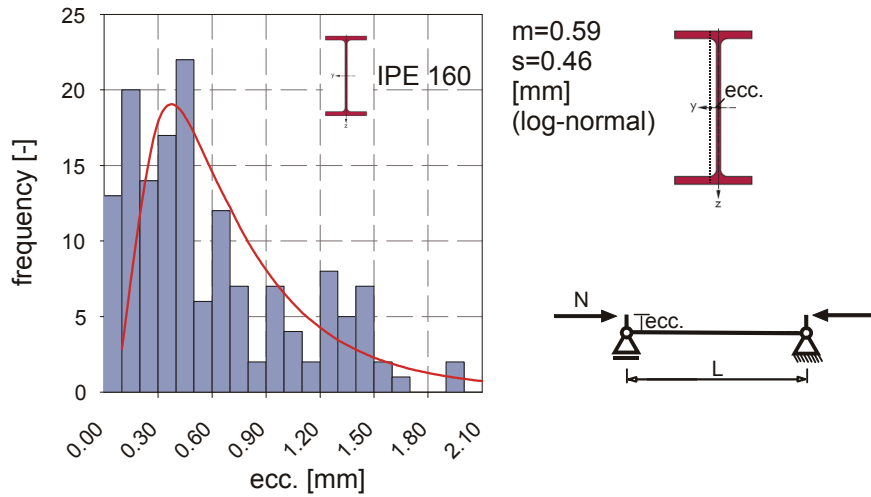
Fig 5-11 *Load eccentricity in the ECCS IPE 160 tests, determined as web eccentricity.*

Residual Stresses

The origin, distribution and amplitude of residual stresses in structural steelwork sections were studied by Alpsten (1967), Young (1971, 1972) in the case of hot-rolled sections, and Brozzetti et al. in the case of welded sections and plated elements. Beer & Schulz (1969) collected some data and discussed the classification of expected residual stresses in hot-rolled sections shown in Fig 5-12a.
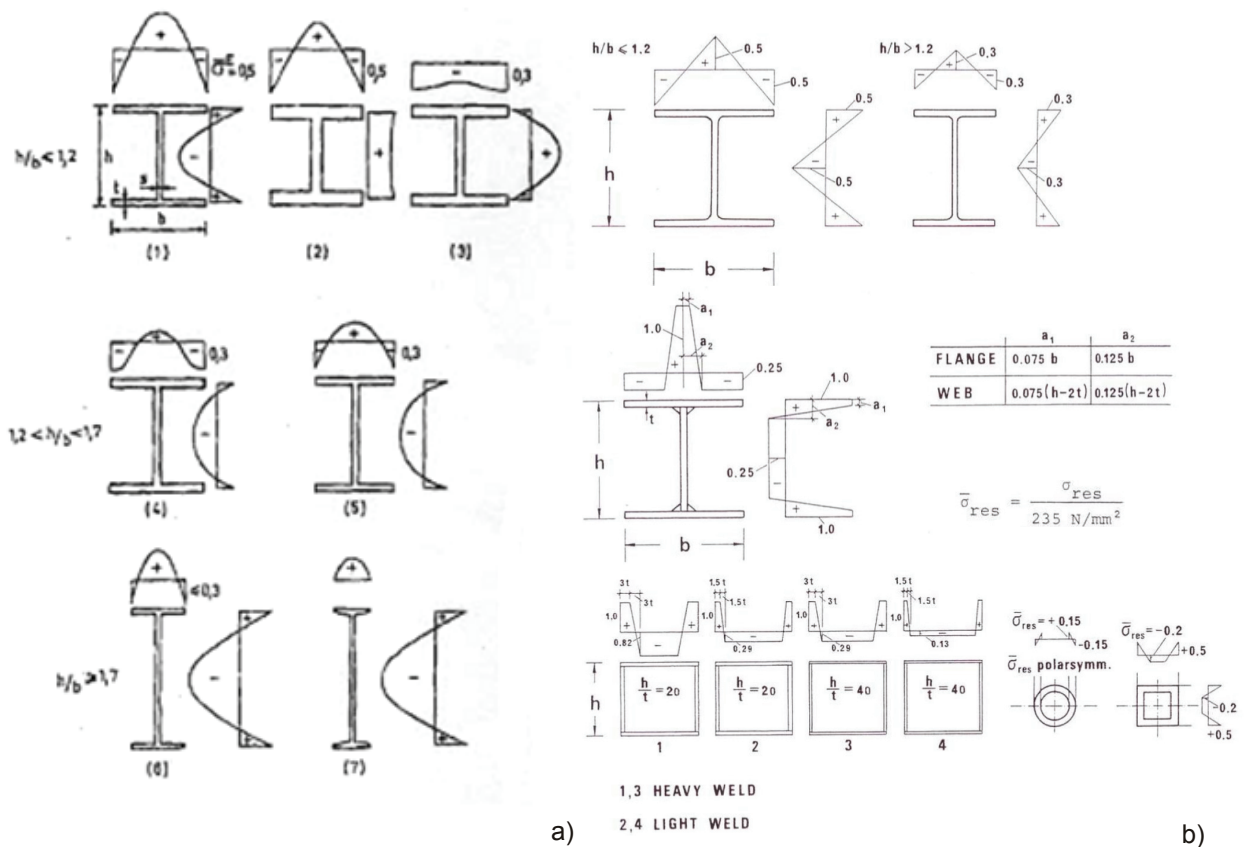
Fig 5-12 *Residual stresses in hot-rolled sections according to (a) Beer&Schulz (1969), and (b) ECCS (1984)*

For comparison reasons, the ECCS recommendations (1984) for modelling residual stress effects in GMNIA calculations are illustrated in Fig 5-12b.

Schulz (1968) mentions the following statistical data regarding residual stresses in hot-rolled sections, Table 5-2:

	t_w/h	$\sigma_{res}/f_{y,nom}$ [N/mm²]	
		MEAN	MAX
h/b≤1.2	<0.05	**0.4**	**0.55**
	<0.075	0.3	0.4
	≥0.075	0.4	0.5
1.2<h/b<1.7	≤0.03	**0.2**	**0.3**
	>0.03	0.3	0.4
h/b≥1.7	-	**0.2**	**0.3**

Table 5-2 *Data collected by Schulz (1968) on residual stresses in hot-rolled I- & H- sections.*

No minimum values are reported by Schulz. The values that are most representative for actual European sections (ratios h/b and t_w/h) are printed in bolted characters. It should be mentioned that Schulz himself was already aware (through the work of Feder & Lee, 1959) that the residual stress in hot-rolled sections is *not proportional to the yield strength, but independent of it*, and that therefore the values in Table 5-2 are *actually only valid for mild steel* (S235). Nevertheless, he accepted this as an extra element of safety for higher-strength steels, which were less well understood at the time.

5.2.3. Step 3: Reliability Level- Justification of the GMNIA Imperfection Assumptions

As was stated in the introduction to this section, one main motivation for the ECCS column buckling research was to develop buckling rules with an homogeneous-as-possible level of reliability throughout slenderness ranges.

According to Sfintesco (1970), the Technical Committee 8 originally intended to achieve this goal purely by experimental means. An early result of this effort is plotted in Fig 5-13, which shows the single, dimensional buckling curve for mild steel (comparable to today's S235) originally published in 1966 by ECCS TC8 (Sfintesco, Carpena et al., 1966). This single curve is based solely on weak-axis buckling tests of I sections and was developed by connecting (with a "spline" curve) the points given by the mean minus two standard deviations (m-2s) of the tests on IPE 160 sections conducted prior to that date. For comparison reasons, the figure also shows the current ECCS / Eurocode 3 column buckling curve b, which applies to IPE 160 sections.
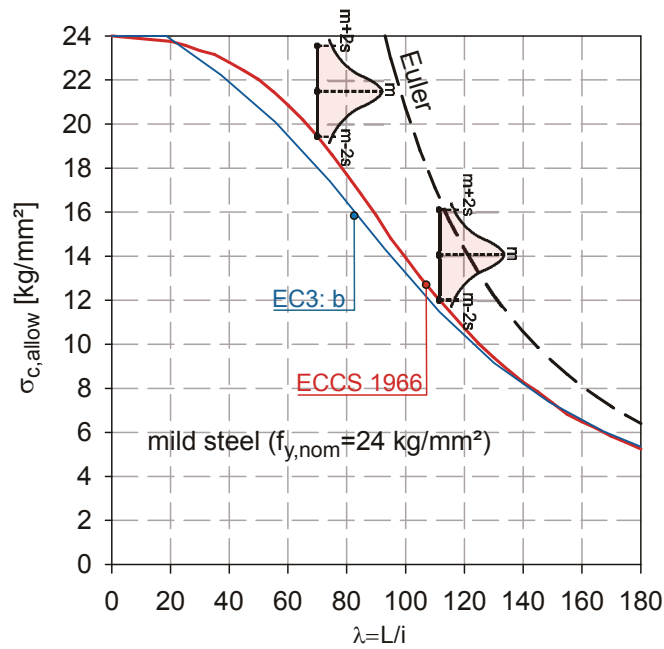
Fig 5-13 *Original, 1966 ECCS column buckling curve based purely on column tests (mostly IPE 160)*

If one omits the question of whether or not "sufficient" tests (in number and representativeness) were conducted to be able to have an acceptable level of confidence in the determined values of m and s, the above-mentioned, purely experimental procedure does indeed lead to a curve that has a constant, specified level of reliability over all slenderness ranges. One might therefore ask why this procedure wasn't fully implemented in the end.

The answer to this question was given by Beer & Schulz (1970):

i. The experimental program alone, while being quite extensive, could not treat all cases of column buckling with sufficient statistical significance. Only weak-axis buckling of relatively "small" sections could be treated in large numbers.

ii. An extrapolation of a design rule from such test results is not acceptable from the point of view of structural safety without the backing of a reproducible, theoretical treatment.

For these reasons, the ECCS column buckling curves were finally developed *primarily by means of numerical (GMNIA) calculations with deterministic, fixed geometry and imperfection parameters*. This allowed for an inclusion of parameters and buckling cases (strong axis buckling, buckling of very heavy sections) which could otherwise not be sufficiently treated even by an experimental program that is as thorough and comprehensive as the one conducted by ECCS TC8. However, in these calculations, the assumptions regarding the (actually stochastically distributed) input parameters were based on a calibration to the ECCS tests, see Fig 5-14. This ensured the necessary feedback to full-scale tests and target reliability levels.
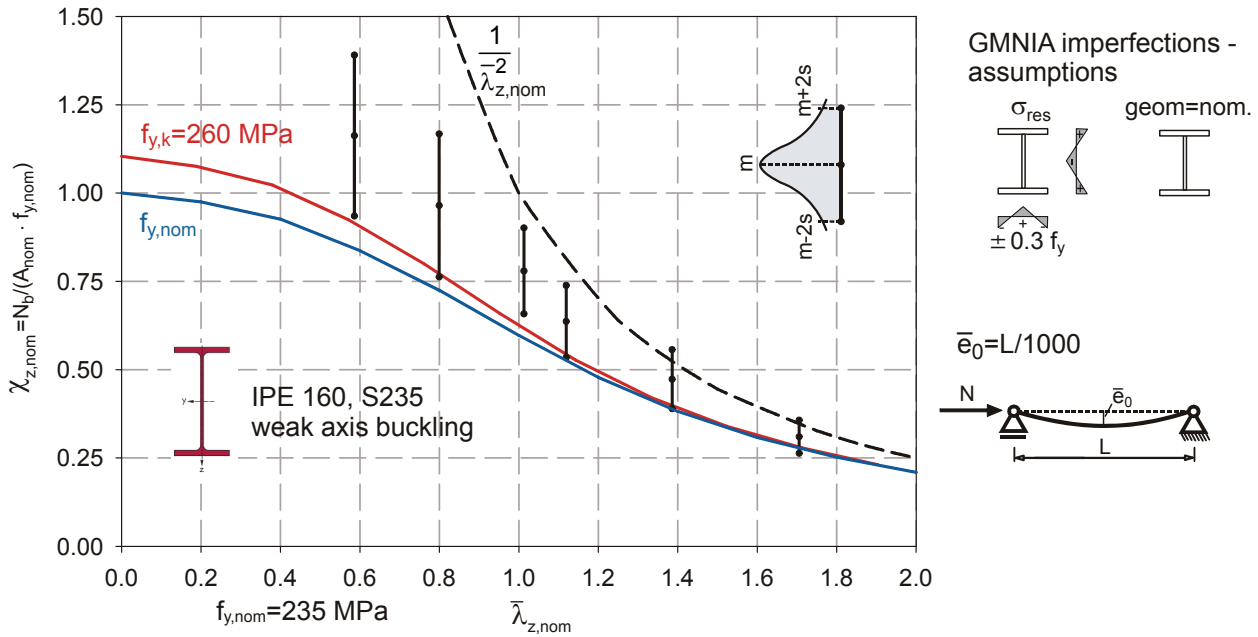
Fig 5-14 *Calibration of the GMNIA imperfection assumptions to the ECCS column buckling tests.*

The figure shows the philosophy and procedure followed by TC8, which can be described as follows:

i. The GMNIA calculations were performed using nominal geometrical input parameters for length and cross-section.

ii. The geometrical and structural imperfections were fixed to *extreme values*: $\bar{e}_0 = \underline{L/1000}$ for the initial curvature, which was equal to the fabrication tolerance Δ_{max}, and the amplitude of σ_{res} equal to the maximum values shown in Table 5-2.

iii. These assumptions were justified by plotting the resulting numerical buckling curves together with the ECCS test results and comparing the position of the curve with the m-2s experimental points.

As is shown in Fig 5-14 (using a "normalized" form, based on a nominal yield stress of $f_{y,nom}$ of 235 N/mm²), an acceptable agreement between numerical curve and experimental points could only be achieved by plotting the curve for a higher yield stress of f_y=260 N/mm²; this was said to be the measured 2.3% fractile (equal to mean minus 2 standard deviations) of the yield stress measurements for the IPE 160 buckling tests, compare with Fig 5-4a.

Sfintesco & Carpena (1977) already pointed out the following, very important point: if design rules are based on GMNIA curves developed with the above assumptions and are then presented in normalized form for all values of f_y, and if –finally- a design code prescribes the use of the *nominal* value of the yield stress $f_{y,nom}$ for buckling design checks, a designer complying with this code will actually make use of the *blue line in Fig 5-14, instead of the (originally intended) red line*; over the entire range of slenderness where yield stress is relevant, such a design curve will therefore be *safer* than intended by the m-2s philosophy.

Due to this observation, Carpena (1971) actually proposed to use a value of the yield stress in column buckling design rules that differs from (i.e., is higher than) the minimum value of the coupon test yield stress specified by steel manufacturing standards such as EN 10025. This proposal was however not followed through, presumably due to the conceptual complications that this would entail; it is indeed not desirable to specify the yield stress to be used in design in function of the design task to be performed.

The implications of this point are discussed with more detail in section 5.4.

5.2.4. Step 4: Monte Carlo Simulations

In 1972, Strating & Vos published a study on the weak-axis buckling strength of IPE 160 sections that made use of statistical input data taken from the "complementary" ECCS tests of section 5.2.2 and applied the Monte Carlo method to simulate full-scale tests. While this study was not *directly* linked to the development of the ECCS curves, it was considered to be an important contribution to it, since it proved that the outcome of the ECCS full-scale tests was fully explicable by purely theoretical means.

The following input data were used by Strating & Vos:

Parameter	m	s	Nominal value
Initial curvature $\overline{e}_0$	0.00085 L	0.0002 L	0.0001L[*]
Area A	2047.33 mm²	81.15 mm²	2010 mm²
Flange thickness t_f	8.1 mm	0.527 mm	7.4 mm
Yield stress f_y	310 N/mm²	26 N/mm²	235 N/mm²
Residual stress σ_{res}[***]	0.20 f_y	0.05 f_y	0.30 f_y[*]
Eccentricity	0.595 mm[**] (ln)	0.461 mm[**] (ln)	0.0 mm
[*] "nominal" values of $\overline{e}_0$ and σ_{res} as used in GMNIA calculations by Beer & Schulz / ECCS			
[**] actually, Strating & Vos used a Gamma-distribution. A log-normal distribution with these parameters was said to be equivalent.			
[***] a parabolic distribution was assumed in the flanges, similar to Fig 5-12a			

Table 5-3 Assumptions of Strating & Vos (1972) for their Monte Carlo simulation of weak-axis column buckling of IPE 160 shapes.

The source of most values in Table 5-3 was already illustrated in section 5.2.2. The results of the Monte Carlo simulation are illustrated in Fig 5-15, again in the normalized form of representation that plots the ratio of buckling strength and *nominal* cross-sectional limit load $A_{nom} \cdot f_{y,nom}$ over the *nominal* value of the normalized slenderness. The original results by Strating & Vos are in good agreement with the ECCS experimental values shown in Fig 5-14, except in the intermediate slenderness range of $\bar{\lambda} \simeq 1.0 - 1.2$, where the Monte Carlo values (m-2s) lie ca. 15% below both test data and the red ECCS curve.
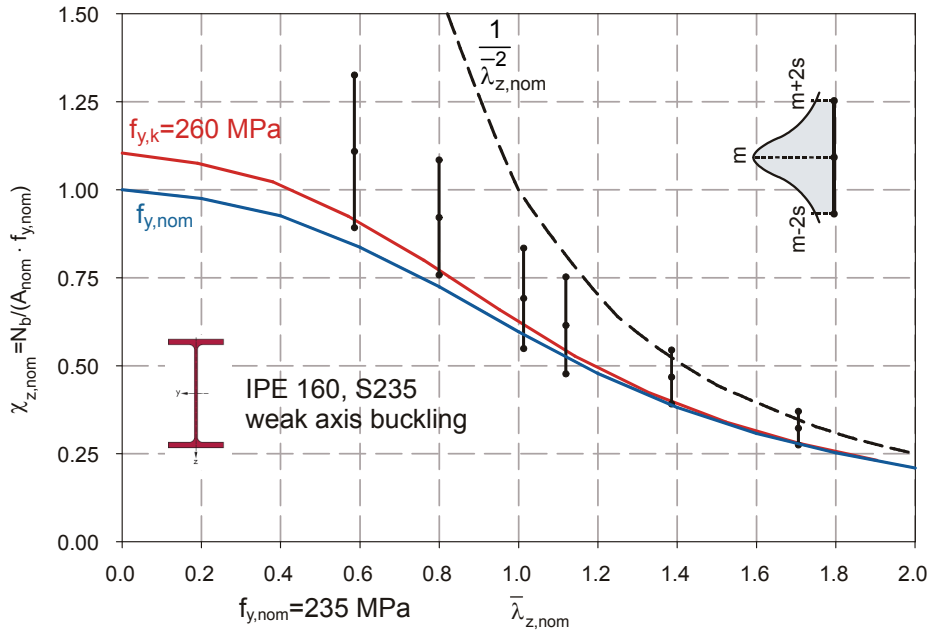
Fig 5-15 *Monte Carlo simulation of Strating & Vos (1972) for weak-axis column buckling of IPE 160 shapes compared to the buckling strength according to the ECCS curve b evaluated for two different values of f_y and plotted as reduction factor of the nominal strength $A \cdot f_{y,S235}$.*

This deviation can be explained in light of the discussion of section 5.2.2 regarding the statistical data from today's point of view. Two points must be mentioned:

i.   The assumed mean value of the flange thickness was significantly larger than the nominal value in these calculations ($t_{f,mean}/t_{f,nom}=1.095$), and the coefficient of variation CoV=0.065 was rather large. This appears to be out of line from what can be justified by actual measurements - see Fig 5-6. That figure, which applies to HE sections, showed values of $t_{f,mean}/t_{f,nom}$ *smaller than 1.0* and (more importantly) a CoV of only 0.03 to be more realistic.

ii.   Strating & Vos assumed the residual stress amplitude σ_{res} to be proportional to the *current yield stress*, i.e. the randomly generated value of the yield stress generated: This implies a strong correlation of residual and yield stress: when the yield stress is far above the nominal value, also the residual stress amplitude is high. As has been stated in section 5.2.2, this is not thought to be conclusive with experimental showings.

Other than these remarks regarding the above assumptions, the idea of Strating & Vos proved to be very advantageous for the purposes of this thesis. Therefore, it is worthwhile to "repeat" Strating's calculation with slightly modified assumptions, and using a Monte Carlo methodology as explained in chapter 3. The new assumptions, summarized in Table 5-4, included a more realistic scatter band for the residual stresses (un-correlated to the yield strength), as well as a separate variation of the single cross-sectional parameters. These were assumed to vary about the mean value, with a CoV of 5% for the flange and web thickness, and CoV=1% for depth and width of the section.

Parameter	m	s	Nominal value
Initial curvature $\overline{e}_0$	0.00085 L	0.0002 L	0.0001L[*]
Yield stress f_y	310 N/mm²	26 N/mm²	235 N/mm²
Eccentricity	0.60 mm (ln)	0.45 mm (ln)	0.0 mm
Residual stress σ_{res}[**]	$0.20 \cdot 235$ N/mm²	$0.05 \cdot 235$ N/mm²	$0.30 \cdot 235$ N/mm²
Flange thickness t_f	7.4 mm	0.37 mm	7.4 mm
Web thickness t_w	5.0 mm	0.25 mm	5.0 mm
Depth h	160 mm	1.6 mm	160 mm
Width b	82 mm	0.82 mm	82 mm
[*] "nominal" values of $\overline{e}_0$ and σ_{res} as used in GMNIA calculations			
[**] a double-linear distribution was assumed, see Fig 5-12b			

Table 5-4 *New assumptions for the Monte Carlo simulation of FBz-z of an IPE 160.*

The outcome of this repetition of Strating's simulation is shown in Fig 5-16. Due to the huge increase of computational power of computers since the calculation of Strating & Vos, many more calculations could easily be obtained in an acceptable amount of time. The simulations were carried out using GMNIA calculations with beam elements. Thirty columns were simulated at ten different nominal slenderness values, from $\overline{\lambda}_{z,nom}$=0.2 to 2.0. For $\overline{\lambda}_{z,nom}$=0.0, the calculations were performed "by hand", i.e. the limit load was calculated from the current value of the area and the yield stress. In order to compare the results directly with the calculation of Strating & Vos (Fig 5-15), as well as with the ECCS experimental data (Fig 5-14), the mean value and standard deviation was computed and plotted in the classical way, assuming standard normal distributions to apply.

The figure clearly illustrates the viability of performing Monte Carlo simulations for member buckling phenomena: results in excellent agreement with the experimental data can be achieved by assuming realistic variations of the main basic variables, and by using appropriate, sophisticated enough GMNIA numerical models.
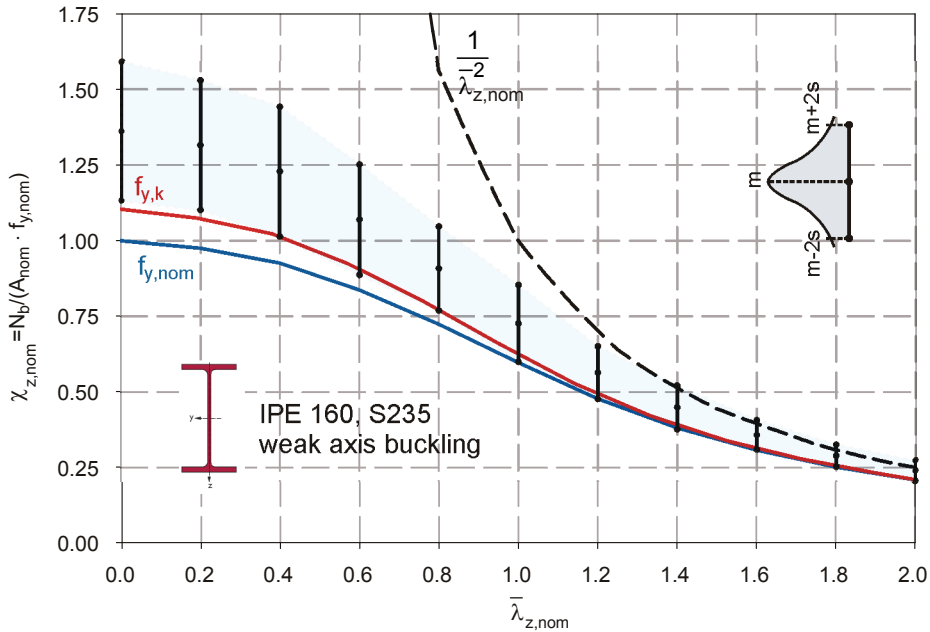
Fig 5-16 *New Monte Carlo simulation for weak-axis column buckling of IPE 160 shapes.*

5.2.5. Step 5: final curves

Finally, after some additional numerical and experimental studies, five separate column buckling curves were published by ECCS in its 1978 "recommendations" (ECCS, 1978). These curves were given as tables, in normalized form – see Fig 5-17. The following points are of interest:

i.   As has been stated above, the curves were essentially based on several series of GMNIA calculations with fixed geometrical and imperfection parameters, whereby the latter were calibrated to the ECCS full-scale buckling tests.

ii. Some modifications were made when finalizing the curves: following the suggestion of researchers at Cambridge University (Young, 1971; Dwight, 1972), a *plateau value at* $\bar{\lambda}=0.2$ was introduced. The rationale behind this choice was to "*include effects of strain-hardening*", which was thought (but not proven) to be responsible for the fact that "*a stocky member can reach its squash load, and may well exceed it*" (Dwight, 1972). The GMNIA calculations by Beer & Schulz did not include strain hardening in the material model; the resulting curves did not show the existence of the plateau, having values of $\chi < 1.0$ at any non-zero slenderness. ECCS TC8 therefore accepted the Cambridge group's line of argumentation (Schulz et al., 1977).

It should be mentioned, however, that more recent studies (e.g. by Wolf, 2006) have proven that the plateau value *cannot be proven by GMNIA calculations with fixed (nominal) geometrical and imperfection parameters even if strain hardening is included in the model*. In the present thesis, this is also confirmed: the GMNIA calculations in section 5.2.1 were performed by modelling strain hardening: *due to the moderate strains at the buckling limit state, no hardening effects were observed even for very stocky columns (*$\bar{\lambda}=0.2$*).*

Fig 5-17 *Original (1978) ECCS column buckling curves, given in diagram form (a) and classification table from Eurocode 3.*

5.3. Putting the curves into an equation

During the development and immediately after the publication of the ECCS column buckling curves in table form, several researchers devoted their time to finding a formulaic description of the tabulated values. Mostly, reasons of practicality were mentioned as motivation for these endeavours. Most of the approaches presented in this context have already been presented in chapter 2. Finally, an Ayrton-Perry formulation emerged as the preferred means of description of the ECCS buckling curves; these are the column buckling formulae we find in the Eurocode today.

5.3.1. Ayrton-Perry formulations

The derivation and form of the Ayrton-Perry formulation has been discussed at length in chapter 2. Their application to the ECCS column buckling curves, and the implications of the specific calibration factors that were eventually chosen, is discussed in the following.

Expression (5.1) represents the starting point: a first-yield buckling condition using second-order internal forces resulting from a sinusoidal pre-deformation. It can be rewritten in normalized form by introducing $\chi = N/(A \cdot f_y)$, $\bar{\lambda}_z = \sqrt{(A \cdot f_y) / N_{cr}}$, and $\eta = A \cdot \bar{e}_0 / W$, leading to (5.2)

$$\frac{N}{A \cdot f_y} + \frac{N \cdot \bar{e}_0}{W \cdot f_y} \cdot \frac{1}{1 - (N / N_{cr})} \leq 1.0 \tag{5.1}$$

$$\chi + \eta \cdot \frac{\chi}{1 - \chi \cdot \bar{\lambda}^2} = 1.0 \tag{5.2}$$

This equation can be shown to be identical to equation (2.30) and can be solved accordingly:

$$\chi = \frac{1}{\Phi + \sqrt{\Phi^2 - \overline{\lambda}^2}} \qquad (5.3)$$

with
$$\Phi = \frac{1}{2} \cdot \left(1 + \eta + \overline{\lambda}^2\right) \qquad (5.4)$$

In the Ayrton-Perry approach, the elastic expression for $\eta = (A \cdot \overline{e}_0 / W)$ is replaced by the "generalized imperfection", i.e. the main calibration function of the formulation, see chapter 2.

Dwight (1972), a British engineer, was quite familiar with the Ayrton-Perry formula; he appears to be the first to have proposed the application of this formula to the ECCS column buckling curves. Recognizing the need for a new calibration of the Ayrton-Perry formula, he suggested the following formulation for η:

$$\eta = \alpha \cdot \left(\frac{L}{i} - S_0\right) \qquad (5.5)$$

with
$$S_0 = \frac{0.2}{\pi \cdot \sqrt{E / f_y}} = \frac{\overline{\lambda}_0}{\overline{\lambda}_1} \qquad (5.6)$$

and α being the generalized imperfection amplitude factor.

The following values of α were proposed by Dwight to describe the ECCS curves a, b and c. They were still in use in UK design codes as recent as the 2000 version of BS5950-1, Annex C:

ECCS curve	α
a	0.0020
b	0.0035
c	0.0055

Table 5-5 *Generalized imperfection amplitude factors α as calibrated by Dwight (1972).*

It is important to appreciate the use of the *geometric* slenderness $\lambda = L/i$, instead of the "normalized" $\overline{\lambda}$ in (5.5). As has been shown in chapter 2, this means that every steel grade (with different yield stress) results in a different position of the buckling curve in the χ-$\overline{\lambda}$ plane, with χ slightly increasing with the yield strength. Dwight argued that this is actually more realistic than a representation where χ is completely independent of the yield stress, especially if the fact is considered that residual stresses are *"largely independent of the yield stress of the steel"*. The calculations that led to Fig 5-1 of this chapter seem to confirm this statement.

It is also interesting to note that, at least for a mild steel of grade S235 with a yield stress of $f_y = 235$ N/mm², the values of Table 5-5 given by Dwight are quite comparable to the ones currently found in the Eurocode for a *normalized slenderness* formulation of η, see Table 5-6:

ECCS curve	Dwight (1972)	Rondal & Maquoi (1979)	EC3 (2006)
a_0		**0.125**	**0.13**
a	$\alpha \cdot \lambda_e = 0.0020 \cdot 93.9 = \mathbf{0.19}$	**0.206**	**0.21**
b	$0.0035 \cdot 93.9 = \mathbf{0.33}$	**0.339**	**0.34**
c	$0.0055 \cdot 93.9 = \mathbf{0.52}$	**0.489**	**0.49**
d	-	**0.756**	**0.76**

Table 5-6 *Comparison between the generalized imperfection amplitude factors α given by Dwight (1972) - valid for steel grade S235-, Rondal & Maquoi (1979) and the Eurocode.*

As has been stated in chapter 2, the current Eurocode expressions for η were determined by Maquoi and Rondal (1978; Rondal & Maquoi, 1979), see (5.7):

$$\eta = \alpha \cdot \left(\overline{\lambda} - \overline{\lambda}_0 \right) \tag{5.7}$$

with α according to Table 5-6, third column. The buckling curves resulting from this formulation are shown in Fig 5-18a as dashed, red lines and compared to the original tabulated values published by ECCS.

In the present study, it is proposed to compare this expression to the values of η_{tab} that would have *precisely* described the tabulated curves. The latter are obtained by solving (5.2) for η:

$$\eta_{tab} = \left(\frac{1}{\chi_{tab}} - 1 \right) \cdot \left(1 - \chi_{tab} \cdot \overline{\lambda}^2 \right) \tag{5.8}$$
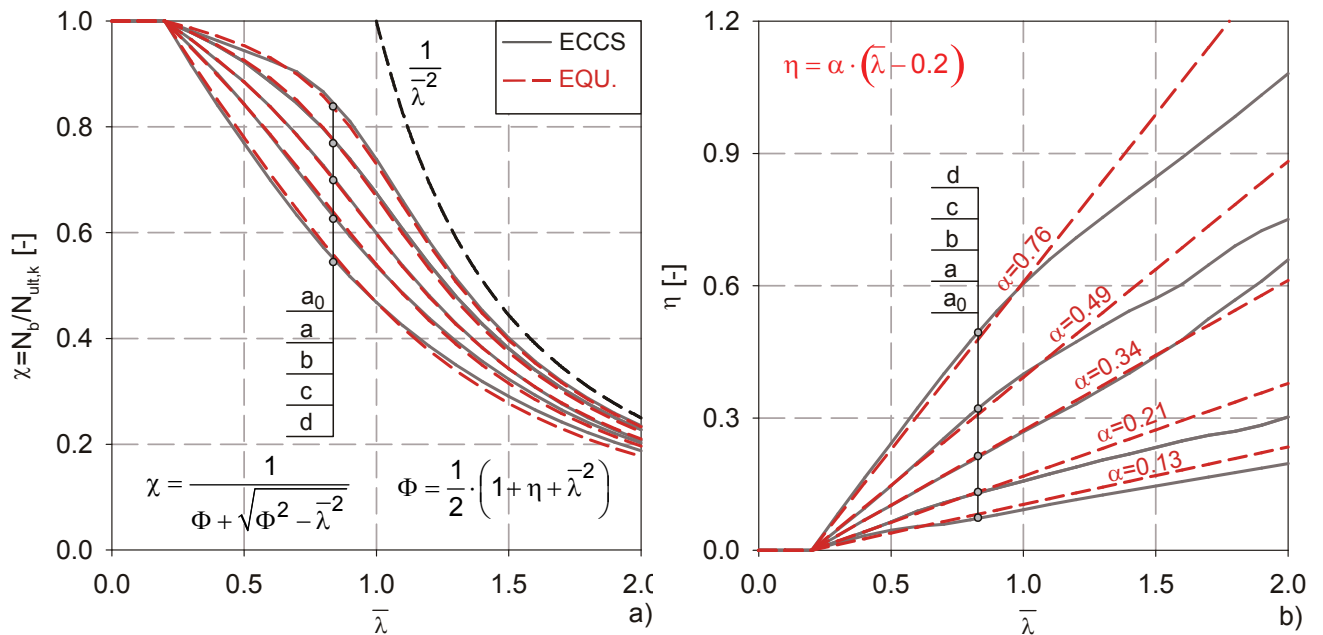
Fig 5-18 *Analytical description of the tabulated (numerical) column buckling curves using an Ayrton-Perry approach; comparison of buckling reduction factors χ (a) and of the generalized imperfection η (b)*

The comparison between expressions (5.7) and (5.8) –solved for the tabulated values of the ECCS buckling curves- is plotted in Fig 5-18b. This representation has the advantage of visually illustrating the significance of an adequate selection of the expression for η. Whenever the value of η_{tab} falls underneath the straight line representing (5.7), the buckling reduction factor given by (5.3) with (2.32) and (5.7) is "safe-sided" in comparison to the numerical value. Hence, the chosen expression (with corresponding coefficients α) for the most part closely follows the numerical values of η_{tab}; at high slenderness ratios and for the "high imperfection" buckling curves c and d, the values of η_{tab} diverge from a straight line, beginning at $\bar{\lambda}=1.0$, reflecting larger deformations than are accounted for in a second-order analysis. However, the significance of accurately describing the value of η_{tab} through (5.7) decreases with increasing slenderness, as the resulting buckling reduction factor χ becomes progressively less sensitive to the underlying bow imperfection at high slendernesses, in comparison to other kinds of imperfections. The tendency of the formulaic, Ayrton-Perry type buckling curves as developed by *Maquoi and Rondal* to (slightly and safe-sidedly) diverge from the numerical curves at high slenderness ratios should nevertheless be kept in mind, since it is shown in chapter 6 to occur in the case of LT buckling as well.

5.3.2. The significance of the imperfection assumption

It is worthwhile, at this point, to elaborate on the significance of the *order of the function* $\eta=f(\bar{\lambda})$ and of the length-dependency of the underlying equivalent imperfection resulting from this order.

In their first (1978) paper, Maquoi and Rondal actually proposed a total of *7 possible expressions for η*, all of which shared the constraint that the expression for η be a function of some order of $\bar{\lambda}$, and that the plateau value of $\bar{\lambda}_0 = 0.2$ be respected. Of those 7 expressions, the three below are considered in the following:

$$\eta_1 = \alpha_1 \cdot \left(\bar{\lambda} - 0.2\right) \tag{5.9}$$

$$\eta_2 = \alpha_2 \cdot \sqrt{\bar{\lambda}^2 - 0.04} = \alpha_2 \cdot \bar{\lambda} \cdot \sqrt{1 - \frac{0.04}{\bar{\lambda}^2}} \tag{5.10}$$

$$\eta_3 = \alpha_3 \cdot \left(\bar{\lambda} - 0.2\right)^2 \tag{5.11}$$

Maquoi and Rondal found that the first two expressions were best suited to represent the European column buckling curves, with discrepancies between the tabulated buckling curve and the formulaic prediction of less than 2%, when the best-fit value of α was used. Of the two, the expression for η_2 was actually found to be *slightly better suited* to describe most of the five ECCS buckling curves in Maquoi and Rondal's original 1978 paper. The third expression –equation (5.11)- on the other hand was the least convenient of all expressions, leading to maximum deviations of more than 10% - and this again when using the best-fit value of α_3. In the following elaborations it will be attempted to explain why this was *inevitably* the case.

By looking back at equations (5.1) and (5.2), it can be appreciated that an equivalent geometric imperfection of amplitude $\bar{e}_0$ can be simply calculated:

$$\bar{e}_0 = \frac{W}{A} \cdot \eta \qquad (5.12)$$

If η is known or given, and the elastic section modulus W_{el} is used in equation (5.12), we obtain the amplitude $\bar{e}_0$ of a sinusoidal initial imperfection which will yield the exact same buckling load N_b as the one given by (5.3), provided that the same value of η and a first yield failure criterion are used. In order to understand the underlying meaning of the three expressions for η (5.9) to (5.11), it is useful to plot this equivalent imperfection for a certain section.
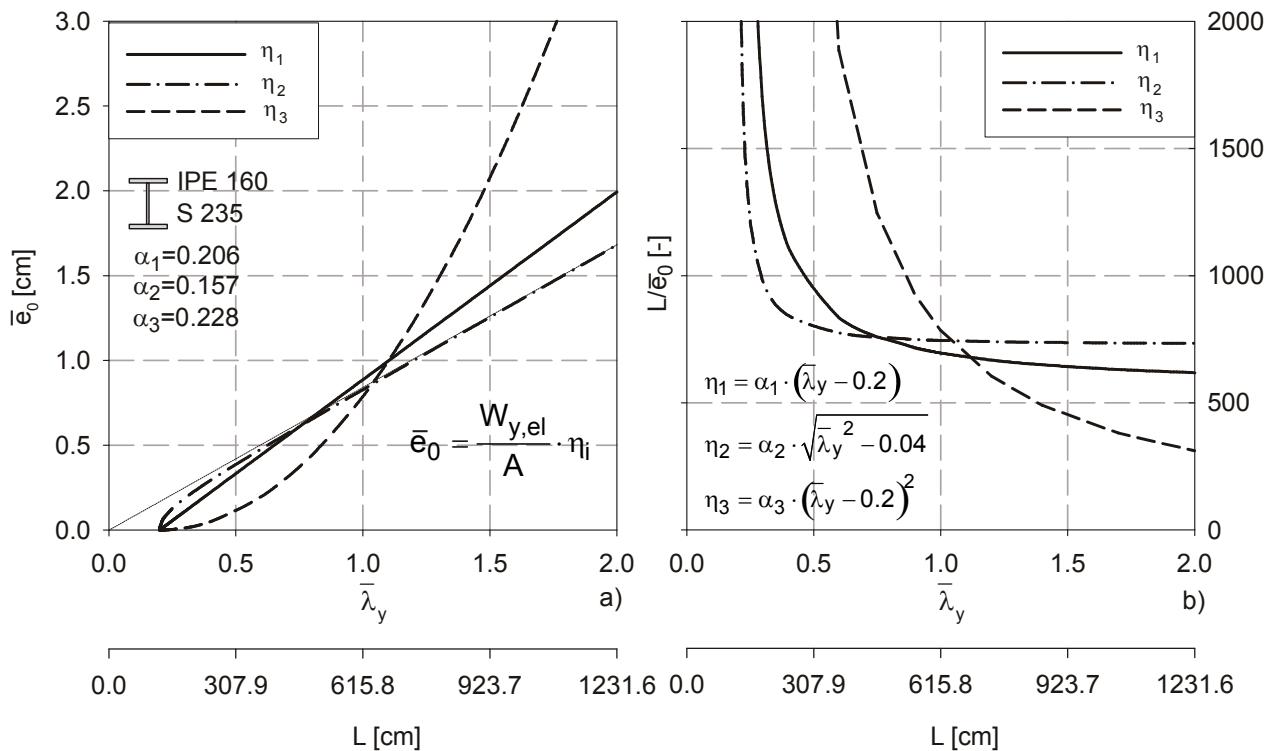
Fig 5-19 *Equivalent imperfection $\bar{e}_0$ in absolute terms and as fraction of length for a first-yield failure criteria for strong-axis buckling of a "welded" IPE 160 section. α_i is the best-fit value for ECCS curve "a".*

Fig 5-19 shows the equivalent elastic imperfection $\bar{e}_0$ for strong axis buckling of a "welded" IPE 160 (without fillet) and the three expressions for η given above. The generalized imperfection amplitude factor α was taken to be equal to the value calibrated by Maquoi & Rondal for the ECCS column buckling curve "a". The chosen section has the geometrical features of an IPE 160, except for the omission of the rolling fillet radius r, having an area of A=19.4 cm^2, a second moment of area about the strong axis of I$_y$=834.1 cm^4 and an elastic section modulus of W$_y$=104.26 cm^3. The normalized slenderness of $\bar{\lambda}_y$=1.0 corresponds to a (buckling) length of L=615.8 cm.

The figure shows that the three underlying equivalent imperfections are quite different from each other for each of the cases:

iv.   the expression η_1 results in a length-proportional imperfection $\overline{e}_0$ that has a value of 0.0 cm at $\overline{\lambda}_y = 0.2$ and then increases linearly at a rate $\overline{e}_0 / \overline{\lambda}_y$ of 1.107 cm/$\overline{\lambda}_y$ or $\overline{e}_0 / L$ of 1/556.2 cm/cm. The latter value directly results from expression (5.9) for η_1 if the plateau value of $\overline{\lambda}_0 = 0.2$ is omitted and the underlying value of $\alpha_1 = 0.206$ is considered:

$$\left(\overline{e}_{0,1} / L \right)_{lim} = \frac{W}{A} \eta_1 \cdot \frac{1}{L} = \frac{W}{A} \cdot \alpha_1 \cdot \frac{\overline{\lambda}_y}{L} = \frac{104.26}{19.4} \cdot 0.206 \cdot \frac{1}{615.8} = 1/556.2 \qquad (5.13)$$

Fig 5-19b, which plots the inverse L/e_0 on the abscissa, illustrates that this constant value of $\overline{e}_0 / L$ is asymptotically approached by the expression for η_1, and this at a rather steady rate.

v.   the expression η_2 results in an equivalent imperfection $\overline{e}_0$ that also has a value of 0.0 cm at $\overline{\lambda}_y = 0.2$ and then rapidly increases to asymptotically approach a rate of $\overline{e}_0 / \overline{\lambda}_y$ of 0.844 cm/$\overline{\lambda}_y$ or $\overline{e}_0 / L$ of 1/729.8 cm/cm. Again, the latter value directly results from expression (5.10) for η_2 if the plateau value of $\overline{\lambda}_0 = 0.2$ is omitted and the underlying value of $\alpha_2 = 0.157$ is considered:

$$\left(\overline{e}_{0,2} / L \right)_{lim} = \frac{W}{A} \eta_1 \cdot \frac{1}{L} = \frac{W}{A} \cdot \alpha_2 \cdot \frac{\sqrt{\overline{\lambda}_y^2}}{L} = \frac{104.26}{19.4} \cdot 0.157 \cdot \frac{1}{615.8} = 1/729.8 \qquad (5.14)$$

In Fig 5-19b, this again shows as a hyperbolic, asymptotic approximation of the limit value of $\overline{e}_0 / L$ resulting from the chosen value of α, this time however at a *much faster rate*.

vi.   the expression η_3 again results in an equivalent imperfection $\overline{e}_0$ that has a value of 0.0 cm at $\overline{\lambda}_y = 0.2$; at higher slenderness ratios, the equivalent imperfection increases parabolically. No limit rate of imperfection increase exists. The imperfections resulting from expression (5.11) are clearly smaller than in the other two cases for slenderness ratios below $1.0 - 1.2$, and increase much faster than the other two beyond this point.

Summarizing these points, it can be ascertained that the expressions for η_1 and η_2 can be equivalently represented by an essentially -if it weren't for the plateau-value of $\overline{\lambda}_0 = 0.2$- length-proportional underlying imperfection $\overline{e}_0$; the expression for η_3, on the other hand, is equivalently represented by an imperfection $\overline{e}_0$ that is proportional to L^2.

The ground has now been laid out for a plausible explanation of why it was *inevitable* that Maquoi and Rondal ended up finding that the best approximations of the European buckling curves are given by expressions (5.9) and (5.10), and the worst by (5.11):

i.   the European column buckling curves that Maquoi and Rondal approximated were determined by means of GMNIA calculations for a length-proportional geometrical imperfection of $\overline{e}_0 = L/1000$ – see section 5.2.3.

ii.   since the additional structural imperfections considered in these GMNIA calculations, i.e. the residual stresses, are constant and independent of length, it is a fair guess to expect that the underlying length-dependency of the assumed geometrical imperfections is still strongly reflected in the resulting buckling curves.

iii.   had a different relationship for the assumed geometrical imperfections been used by Beer & Schulz in their numerical calculations, a different expression than η_1 and η_2 would have yielded the best curve-fitting results.

An example is used to strengthen the case for the last statement above. Using essentially the same numerical methodology employed by Beer and Schulz for the GMNIA calculations of the ECCS research project, two numerical buckling curves are calculated for the strong-axis buckling of the pin-ended, "welded" IPE 160 of Fig 5-19:

i.   *case I*: the buckling curve is calculated using exactly the same assumptions made by Beer&Schulz: the yield strength of the material is f_y=235 MPa, strain-hardening is not considered, the residual stresses have a maximum compressive value of $0.3 \cdot f_y$, and the geometrical imperfection is *proportional to L*, having a value of $\overline{e}_{0,I}$=L/1000.

ii.   *case II*: the buckling curve is calculated using the same assumptions as above, but for a geometrical imperfection that is *proportional to L^2*, instead of L, having a value of $\overline{e}_{0,II}$=L²/615800. The denominator of this expression is chosen so that $\overline{e}_{0,II}$ is equal to $\overline{e}_{0,I}$=L/1000 at the normalized slenderness of $\overline{\lambda}_y$=1.0, i.e. at a length of L=615.8 cm in this case.

The assumptions made for the determination of these two numerical buckling curves are summarized in Fig 5-20.

Since no plateau is to be expected from a numerical calculation that is conducted according to Fig 5-20, the Ayrton-Perry type curve-fitting is performed using modified versions of the expressions (5.9) to (5.11), omitting the plateau value of $\overline{\lambda}_0 = 0.2$. In this case, (5.9) and (5.10) are identical and can be replaced by a single expression. The following expressions are used

$$\eta_I = \alpha \cdot \overline{\lambda}_y \qquad\qquad (5.15)$$

$$\eta_{II} = \alpha \cdot \overline{\lambda}_y^{\,2} \qquad\qquad (5.16)$$

If the claim is correct that the goodness of the Ayrton-Perry approximation mostly depends on the quality of the function η, and if the best-fit value of α is used, η_I can be expected to yield a good approximation for the "case I" assumption of Fig 5-20, while η_{II} should be able to approximate the "case II" assumption well.
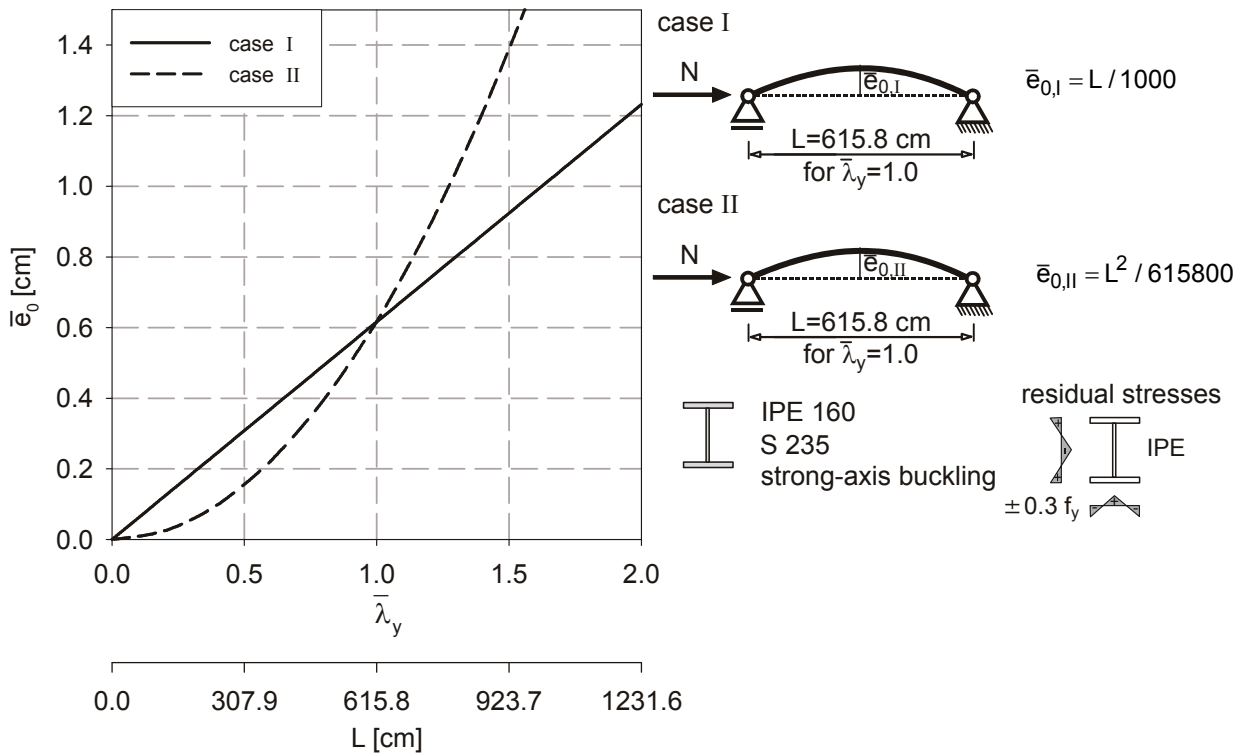
Fig 5-20 *Assumptions made for the illustration example; $\bar{e}_0$: purely geometrical imperfection.*

The results of the example calculations are illustrated in Fig 5-21, using both a length-dependent and a Merchant-Rankine type representation of the resulting numerical and Ayrton-Perry buckling reduction factors χ. The numerical (GMNIA) calculation results are printed in black, while the Ayrton-Perry results are in colour.

Fig 5-21a shows that, due to the fact that the imperfection was chosen so that both imperfections have the same amplitudes for $\bar{\lambda}_y = 1.0$, the numerical curves intersect at this slenderness ratio. In order to be able to better illustrate the impact of the length proportionality of the generalized imperfection function η on the calculation results, the calibration of the factor α was performed for the slenderness ratio of $\bar{\lambda}_y = 1.0$ alone, and not as a least-square approximation of the entire considered slenderness range; doing this leads to identical values of $\alpha=0.156$ for η_I and η_{II}.

Especially the more "spread-out" Merchant-Rankine visualization (Fig 5-21b) clearly shows that expression η_I allows for a close approximation of the "case I" imperfection assumption, while η_{II} does the same for the "case II" assumption.

This example clearly illustrates the significance of a correct, representative choice of the function η when using an Ayrton-Perry type formula to represent a buckling curve. If the Ayrton-Perry type formulation is used for curve-fitting of a numerically determined buckling curve, it is extremely important to choose the expression for η so that it best approximates the imperfection assumptions made in the numerical calculation. An analogous statement can be made about the curve-fitting of experimentally determined buckling curves, where imperfection measurements must be used as guidance.
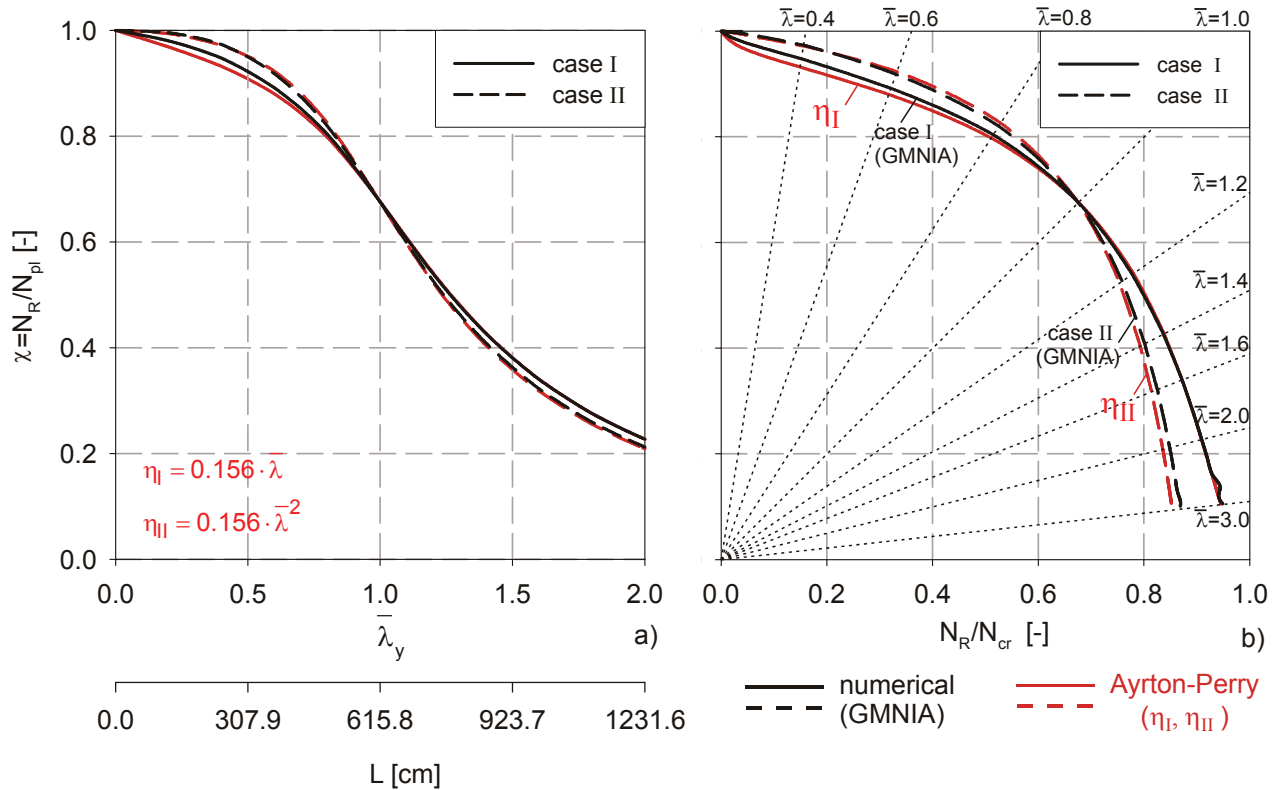
Fig 5-21 *Results of the example calculation with assumptions of Fig 5-20; a) slenderness-dependent plot; b) Merchant-Rankine visualization. Ayrton-Perry versus numerical results.*

5.4. Current reliability level

In chapter 4, section 4.3.3, it was shown that, quite generally, the reliability level inherent in current member buckling rules is not homogeneous throughout all slenderness ranges. For the specific case of flexural column buckling, this is confirmed and plotted in Fig 5-22. This figure again shows the values calculated by Müller (2003) on the basis of the ECCS tests. It also shows (Fig 5-22b) the result of an evaluation of the appropriate partial safety factor γ_M^* according to EN 1990 – Annex D for the new *Monte Carlo simulation* of Fig 5-16.

The evaluation was carried out based on the assumptions of Table 5-7. Since the evaluation procedure assesses the accuracy of the used design formula, only the parameters actually entering (5.3) are needed.

Parameter	m	s	Nominal value
Yield stress f_y	310 N/mm²	26 N/mm²	235 N/mm²
Flange thickness t_f	7.4 mm	0.37 mm	7.4 mm
Web thickness t_w	5.0 mm	0.25 mm	5.0 mm
Depth h	160 mm	1.6 mm	160 mm
Width b	82 mm	0.82 mm	82 mm

Table 5-7 *"Pre-information" used for the statistical evaluation of FBz-z of the Monte Carlo "tests" for weak-axis flexural buckling of an IPE 160 (see Fig 5-16).*
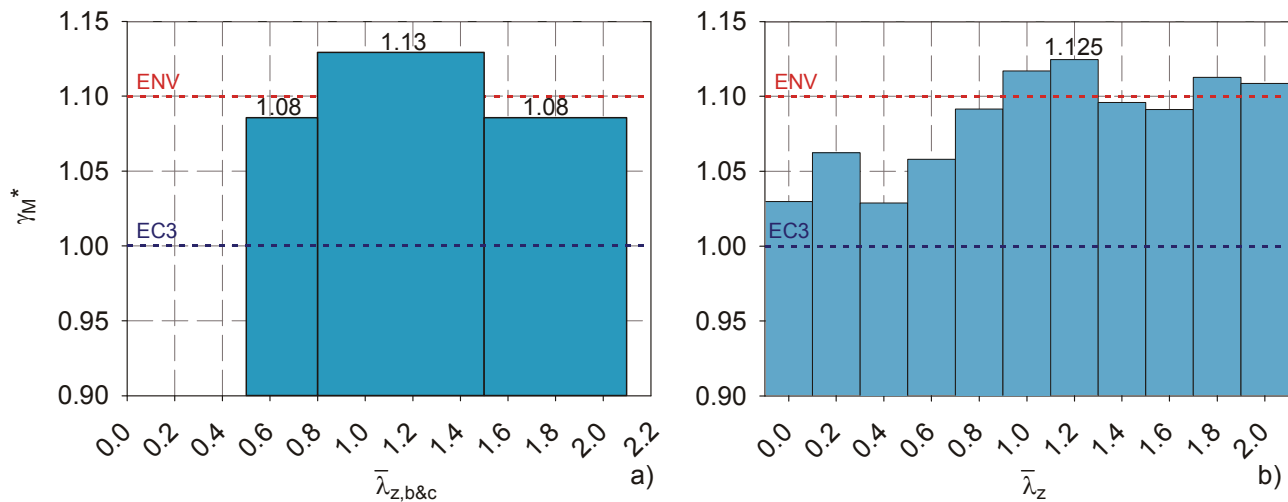
Fig 5-22 *Current reliability level for weak-axis flexural column buckling of IPE sections; according to Müller (a); calculated for the Monte Carlo simulation of Fig 5-16 (b).*

The parameters in Table 5-7 are similar to the ones of Table 5-4, i.e. of the statistical data used for the Monte Carlo simulation itself, but with the exception of the yield stress f_y; since Annex D of EN 1990 mandates the use of "pre-information" about representative statistical values of the single parameters entering the design formula, a value of $f_{y,mean}$=285 N/mm² with CoV=0.06 was chosen instead. These value are in good agreement with the literature (Petersen, 1993; Byfield & Nethercot, 1997) and are well-confirmed by the experimental data, at least by the greatly better documented number of tensile-coupon tests.

As is illustrated in Fig 5-22, the evaluation of the new Monte Carlo tests led to values of γ_M^* that are in excellent agreement with what Müller found to be appropriate for the ECCS tests. Both diagrams (a) and (b) show that the maximum value is reached around a slenderness of $\bar{\lambda}$=1.2, that it lies at about γ_M^*=1.12-1.13, and that it tends to be slightly lower at slenderness values beyond this peak. The Monte Carlo simulation can therefore be assumed to be representative also for the range not covered by tests, i.e. the low slenderness range. Here, a remarkable feature of Fig 5-22 is the spike of the value of γ_M^* at $\bar{\lambda}$=0.2. Although this might surprise at first sight, it is actually entirely logical if one considers that this slenderness range corresponds to the location of the end of the plateau in the ECCS column curves. Since the strength of a member with $\bar{\lambda}$=0.2 must be at least minimally -a few percentage points- lower than the value at an even smaller slenderness, but the plateau ignores this, γ_M^* ends up accounting for it. The relatively steep drop of the buckling curve immediately beyond the plateau's end then explains the drop of γ_M^* between $\bar{\lambda}$=0.2 and 0.4.

Of course, the excellent agreement between Fig 5-22a and b contains some degree of "luck", as both the ECCS and the Monte Carlo buckling strengths, representing a limited number of random test results, do influence the outcome of the above evaluation; in other words, a repetition of the Monte Carlo simulation will not lead to *exactly* the same results as shown in Fig 5-22b.

Nevertheless, the following points can be seen as confirmed by this evaluation:

i.   The ECCS column buckling curves, and, inevitably, the Ayrton-Perry formula calibrated by Maquoi and Rondal to best fit these curves, *does not fulfil its original goal of having a constant reliability level throughout all slenderness ranges.*

ii.   As is illustrated by Fig 5-14, this is due to the fact that the numerical (GMNIA) buckling curves eventually adopted as design curves by ECCS *do not provide such a constant level of reliability* when compared to tests if nominal values of yield stress and geometry are used in combination with high fractile values of the imperfections.

This does not mean that the ECCS buckling curves are not in agreement with the more general original goal, i.e. to develop buckling design curves that had an irrefutable, sufficient level of safety that was acceptable and could be implemented in all European countries. As is also illustrated by Fig 5-14, the desired position (m-2s) of the curve itself is complied with throughout all slenderness ranges; if anything, the final curve is "*safer*" than originally intended at lower slenderness.

In summary, the following can be stated in agreement with the discussion in section 4.3.3:

i.   The current level of reliability of column buckling rules is not directly based on a homogeneous reliability level. Rather, it is based on the intrinsic level of reliability given by a *model member* (referred to as "model column" or "model beam" in the following) with specified characteristics with regard to geometry, material strength and imperfections.

ii.   This is obviously not a *probabilistic* approach in the strict sense of the term. It is, however, in a loose sense *semi-probabilistic*, as it entails the following philosophy: *a column designed to withstand the acting loads under the assumptions inherent to the ECCS curves* (nominal geometry, minimum nominal yield stress, high fractiles of geometric and structural imperfections) *can be assumed to be sufficiently safe, since test results proved these assumptions to be in good agreement with, or safe-sided, in comparison to the desired reliability level.*

5.5. Fabrication tolerances vs. imperfections – effects of changed production habits

This section is dedicated to the treatment of a current, intensely debated topic: the impact of new, relaxed fabrication tolerances on the strength of compression members. The current debate, held at a code commission level (ECCS TC8), was triggered by the introduction of increased tolerances for the out-of-straightness of steel members in the new European standard for the execution of steel structures for constructional steelwork, EN 1090-2 (2008). The question currently being asked is the extent to which these changes are still "covered" by the present design rules. To date, a consistent, logically coherent justification for the acceptance of these changes is still missing.

The study presented in this section is therefore intended as a contribution to this debate. In the broader scientific context, it is intended to serve as an example for the possibility of answering questions regarding *the impact of changes to production tolerances and manufacturing habits on design rules* by means of statistical/reliability methods.

5.5.1. Previous and new regulations

Most codes regulating the execution of steel structures distinguish between *manufacturing* and *erection tolerances*. The former, also called *shop fabrication tolerances*, are concerned with deviations from the nominal dimensions measured in the workshop. They mainly serve as control quantity for the production quality in the shop or factory. The latter are measured on site, after erection. They are a control quantity for the quality of the erection works on site.

Measurement Definition	Standard	Country	Manufacturing Tolerance	Erection Tolerance
 (from EN 1090-2)	AISC Code of Standard Practice (2005)	USA	$\Delta \leqq L/1000$	None ($\Delta \leqq L/1000$)
	BS 5920-2 (2001) & NSSS (2007)	UK	$\Delta \leqq \max(3mm ; L/1000)$	None
	DIN 18800-7 (2002)	DE	Product standards hot-rolled: EN 10034 welded: ISO 13920	None
	ÖN B4300-7 (1994)	AUT	$\Delta \leqq L/1000$	$\Delta \leqq L/1000$
	ENV1993-1-1:1992 / ENV 1090-1:1996	Some EU countries	$\Delta \leqq L/1000$ $\Delta \leqq \max(3mm ; L/1000)$	None
	ECCS Recc. 1978	-	$\Delta \leqq L/1000$	$\Delta \leqq L/667$ & ...
	EN 1090-2:2008	CEN members	$\Delta \leqq L/750$	$\Delta \leqq L/750$
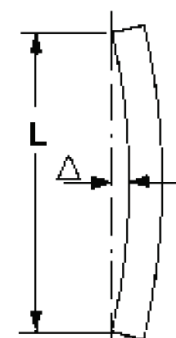
Table 5-8 *Out-of-straightness of compression members (except hollow sections) according to different international standards.*

Table 5-8 summarizes the regulations of the out-of-straightness tolerances for compression members according to different international codes. The following comments can be made:

i.   The *manufacturing* (shop) *tolerances* for out-of-straightness of compression members were fixed at a value of $\Delta \leq L/1000$ in most codes of practice preceding the publication of the new European standard EN 1090-2:2008. It should be mentioned on the side that hollow sections –produced in Europe according to the standard EN 10210-1 (2006)- had and still have a larger tolerance limit of $\Delta \leq L/500$, see Chan & Gardner (2009).

ii. The value of $\Delta \leq L/1000$ is identical to the imperfection assumptions on which the ECCS column buckling curves are based, $\bar{e}_0 = L/1000$, see section 5.2.3. Historically, this tolerance value was actually the *initial motivation* for the adoption of $\bar{e}_0 = L/1000$ in the ECCS GMNIA calculations.

iii. With $\Delta \leq L/750$, EN 1090-2 increases the manufacturing tolerance limit by 1/3.

iv. In previous national European and current international codes, the sections devoted to *erection tolerances* did not generally include provisions regarding the out-of-straightness of compression members. The AISC code only recently added a clarifying drawing where columns are shown to have $\Delta \leq L/1000$ also in the erected configuration, but no comment is given on this – and on how this should be measured- in the text. The same can be stated about the former Austrian Standard ÖN B 4300-7 (1994). Other codes only mention positioning and inclination restrictions for the erection of columns.

v.   The lack of specification of erection tolerances is explicable by the difficulty and cumbersomeness associated with measuring a column's curvature once it is built in. Furthermore, if the curvature is specified as an erection tolerance, it must also be specified how, and with what frequency, this quantity ought to be measured on site – this is not straight-forward and potentially controversial.

acceptance criteria for out-of-straightness
1) single value $\Delta_i \leq L/667$
$m = \sum \Delta_i / n$; $s_n = \sqrt{\sum (\Delta_i - m)^2 / (n-1)}$
2) $m + \alpha \cdot s_n \leq L/667$
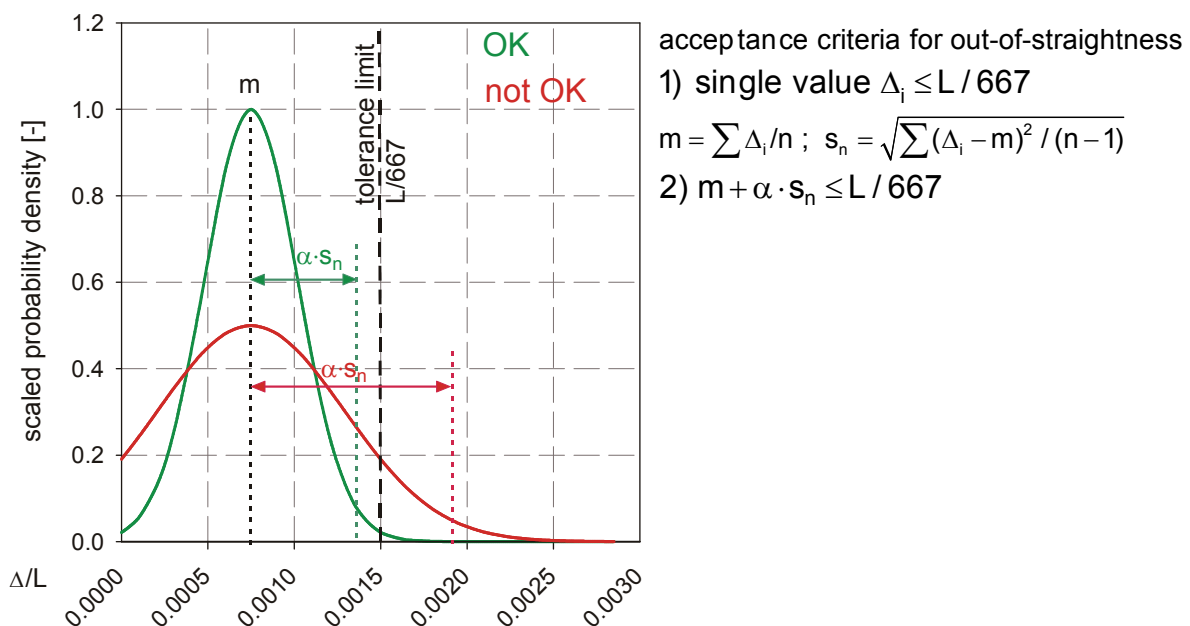
Fig 5-23 *Visualization of the acceptance criteria for column curvature according to ECCS (1978)*

    vi.   The only provision known to specify clear and uncontroversial acceptance criteria for column out-of-straightness *on site* is contained in the ECCS "European Recommendations for Steel Construction" (1978). While this code also uses the value of $\Delta \le L/1000$ for workshop fabrication, it loosens this value to $\Delta \le L/667 = 0.0015\ L$ on site.

   vii.   According to this recommendation, if individual measured values exceed this value, the construction contract's parties are expected to agree upon the subsequent procedure by judging the fitness-for-purpose of the compression element.

  viii.   Additionally to this criterion, the emphasis is placed on the *statistical distribution* of the measured curvature. This is schematically illustrated in Fig 5-23. A series of measurements is accepted as conforming to the requirements when the *mean value plus α times the estimated standard deviation* of measurements lies within the tolerance limit. The value of α decreases with a rising number of measurements n, spanning a range of 3.7 for n=6 to 2.1 for n=100. They are meant to lead to a 90% confidence level regarding the non-exceedance of the tolerance value.

    ix.   EN 1090-2 does specify erection tolerances for the out-of-straightness of compression members. However, no indications are given about how, and how often, these ought to be measured. One must assume that, in theory, *all columns* must be measured and checked against the tolerance criterion if EN 1090-2 applies as part of a construction contract.

5.5.2. Can tolerances be determined from equivalent imperfections?

Some reviews of the current Eurocode design formulae for column buckling have already led (Sedlacek et al., 2008) to argumentations that justify the loosening of the curvature tolerances on the basis of considerations regarding equivalent imperfections for second-order calculations. This line of argumentation uses the following limit state observation for the equivalent *imperfection* $\bar{e}_0$, also see (5.12)

$$\left(\bar{e}_0 / L\right) = \frac{W}{A}\eta \cdot \frac{1}{L} = \frac{W}{A} \cdot \frac{\alpha}{L} \cdot \left(\bar{\lambda} - \bar{\lambda}_0\right) \qquad (5.17)$$

Then, acknowledging the fact that the values of the generalized imperfection coefficient α also have to cover the influence of residual stresses in the Ayrton-Perry formulation, it is argued (*assumption 1*) that, at $\bar{\lambda} = \infty$, this influence of σ_{res} is practically zero. Furthermore, it is –implicitly- assumed (*assumption 2*) that the curve a_0 is representative for a column with practically no locked-in stresses. The following formula can then be derived for strong-axis flexural column buckling FB_{y-y}:

$$\left(\bar{e}_0 / L\right)_{\text{lim,GEOM,FB}_{y-y}} = \frac{2 \cdot I_y}{h \cdot A} \cdot \frac{\alpha_{a0}}{L} \cdot \bar{\lambda} = \frac{2 \cdot i_y^2}{h} \cdot \frac{\alpha_{a0}}{L} \cdot \frac{L}{i_y} \cdot \frac{1}{\pi} \cdot \sqrt{\frac{f_y}{E}} = \frac{2 \cdot i_y}{h} \cdot \frac{\alpha_{a0}}{\pi} \cdot \sqrt{\frac{f_y}{E}} \qquad (5.18)$$

In a third assumption (*assumption 3*), the ratio i_y/h is set to 0.5. With this value, the following was said to be the limit value of the purely geometrical imperfection that is already covered by the current buckling rules, for the most inconvenient case of steel grade S235:

$$\left(\overline{e}_0 / L\right)_{\text{lim,GEOM,FB}_{y-y}} = 2 \cdot 0.5 \cdot \frac{0.13}{\pi} \cdot \sqrt{\frac{235}{210000}} = 1/722 \qquad (5.19)$$

Since $\overline{e}_0 / L = 1/722$ is larger than $\Delta/L = 1/750$, the new tolerance limit was said to be covered by the current design rules.

Plum (2008) has already shown this line of argumentation to be flawed. He pointed out that the assumption regarding i_y/h is not realistic for most commercial I- & H-sections, where this value moves in the range of 0.35-0.42. This simple corrective remark, regarding only one of the three assumptions made above, seems to disprove the above argumentation, since e.g. with $i_y/h = 0.4$, $\left(\overline{e}_0 / L\right)_{\text{lim,GEOM,FBy-y}} = 1/903$, which is *smaller* than $\Delta/L = 1/750$.

Additionally, the following comments can be added:

1) If assumption 2 were true, then in the case of weak-axis flexural buckling FB_{z-z} of typical I- and H-sections, which have ratios of $i_z/b \sim 0.25$, applying (5.18) correspondingly would lead to the conclusion that a tolerance of only $\Delta/L = 1/1444$ is covered by the design rules – an even smaller value than the one that was previously valid at $\Delta/L = 1/1000$.

2) If assumption 2 is dropped, or said not to apply for weak-axis buckling of a member made of S235 steel, the next most plausible buckling curve for this assumption is line b, the "highest" curve for weak-axis buckling of S235 I-sections. In this case, we could calculate the "covered" imperfection as follows:

$$\left(\overline{e}_0 / L\right)_{\text{lim,GEOM,FB}_{z-z}} \cong 2 \cdot 0.25 \cdot \frac{0.34}{\pi} \cdot \sqrt{\frac{235}{210000}} = 1/552 \qquad (5.20)$$

This is larger than both $\Delta/L = 1/1000$ and $\Delta/L = 1/750$, and (importantly) larger than any value ever recorded in the ECCS tests, see Fig 5-9 – it is hard to imagine that this could be covered by the present rules.

These two points confirm that it is not purposeful to attempt to draw any conclusions regarding the permissibility of loosening geometrical shape tolerances *by inference* from considerations stemming from the second-order beam theory and the generalized imperfection amplitude factor α. As this chapter has attempted to show, the current column buckling formulae are essentially based on curve-fitting of a second-order equation onto GMNIA buckling curves. The ("equivalent") second order geometric imperfections were fitted to best match the pre-established buckling reduction factors of the GMNIA curves. Thereby, these "manipulated" second-order equivalent imperfections lost much of their physical meaning, particularly in the *quantitative* sense that is of interest here. Finally, it must be remembered that, from a safety point of view, the values of α must "cover" more than just residual stresses and column curvature: since the structural designer eventually calculates a column's strength with nominal values of cross-sectional geometry and material strength, but in reality these values scatter, the values of α must also account for the scatter of these quantities. This is not acknowledged in the above considerations.

5.5.3. Implications for Buckling Strength - Scenarios for the future

Since all the parameters governing the column buckling phenomenon are random in their nature, and the total level of reliability of the prediction of buckling strength depends on a (random) combination of these random parameters, an assessment of the implications of the new tolerances on the buckling strength can only be carried out by considering the changes to the random distribution of these effects by statistical, probabilistic means.

Ideally, tests could be carried out on columns with geometrical shape deviations representative of the production habits of European steelwork contractors, as they result from the tolerances in EN 1090-2. This is obviously impossible at the present time, as the new code has not yet been implemented by fabricators. For this reason, it was chosen to perform *Monte Carlo simulations with plausible assumptions regarding the future distributions of column shape deviations*. Four different scenarios will be discussed with more detail in the following. They are represented in Fig 5-24.
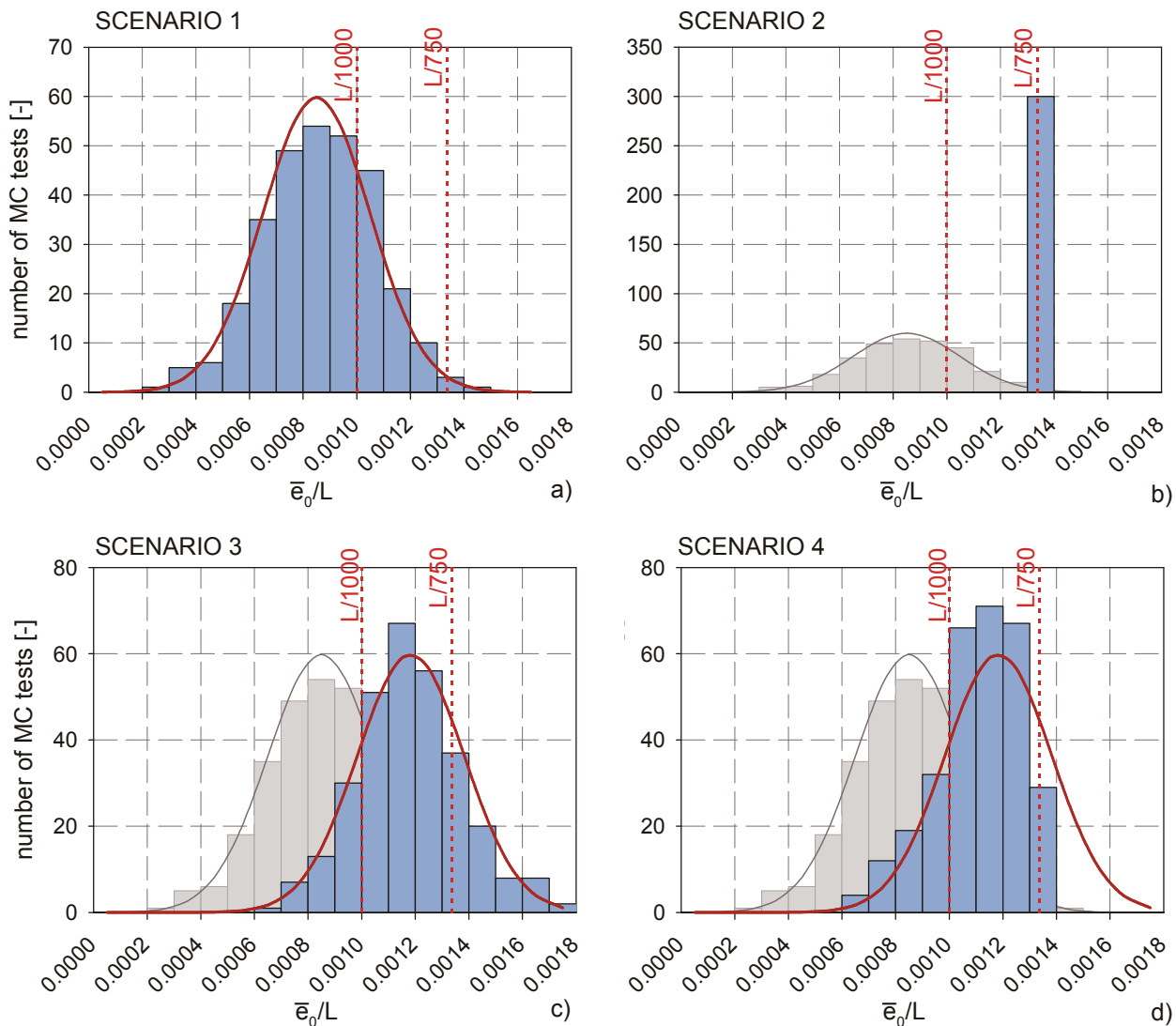
Fig 5-24 *Scenarios for the future development of the scatter band of column curvatures.*

The figure shows the histograms of the values of the initial column curvature (with index $\bar{e}_0$ to indicate that a sinusoidal "equivalent" imperfection shape was assumed in the GMNIA calculations) that were randomly generated for the Monte Carlo simulations. All scenarios are referred to the best-documented (by tests and calculations) case of the weak-axis flexural buckling of IPE 160 sections made of steel grade S235, see section 5.2.2. The scenarios can be described as follows:

- **SCENARIO 1:** the production habits of steelwork fabricators are not altered by the new manufacturing and erection tolerances. The deviations found during the ECCS tests are thought to be representative of real production; thus, the probability density function (pdf) found by Strating & Vos (1972) is assumed to be correct and still valid: m=0.00085 L, s =0.0002 L.

- **SCENARIO 2:** all columns are produced with an initial curvature of $\Delta \cong \bar{e}_0$ =L/750. Although very unrealistic, this scenario is the most unfavourable possibility still allowed by the tolerance limits in EN 1090-2.

- **SCENARIO 3:** steelwork fabricators make use of the new, relaxed tolerances and produce columns that are on average somewhat more curved, i.e. by the the amount L/750 – L/1000. The scatter of the production is otherwise left unmodified. No measurements are undertaken, neither in the shop nor on site, therefore columns with curvatures exceeding the erection tolerance of Δ=L/750 are not effectively prevented from being used in the structure.

- **SCENARIO 4:** identical to 3, but with the addition that all columns are thought to be measured on site. Columns that exceed the erection tolerance value of Δ=L/750 are not allowed; in practical terms, a new random value was generated in this case.

5.5.4. Montecarlo simulations and reliability analysis

The Monte Carlo simulations were carried out using GMNIA calculations and the techniques for random number generation and data control explained in chapter 3, as well as section 5.2.4. Except for the column curvature, the statistical distributions of all other parameters were kept the same in all scenarios, and assumed in accordance with Table 5-9

Parameter	m	s
Initial curvature $\bar{e}_0$	See Fig 5-24	
Yield stress f_y	285 N/mm²	17.1 N/mm²
Eccentricity	0.60 mm (ln)	0.45 mm (ln)
Residual stress σ_{res}	0.20 · 235 N/mm²	0.05 · 235 N/mm²
Flange thickness t_f	7.4 mm	0.37 mm
Web thickness t_w	5.0 mm	0.25 mm
Depth h	160 mm	1.6 mm
Width b	82 mm	0.82 mm

Table 5-9 *Parameter variation for the Monte Carlo simulations – IPE 160 – S235*
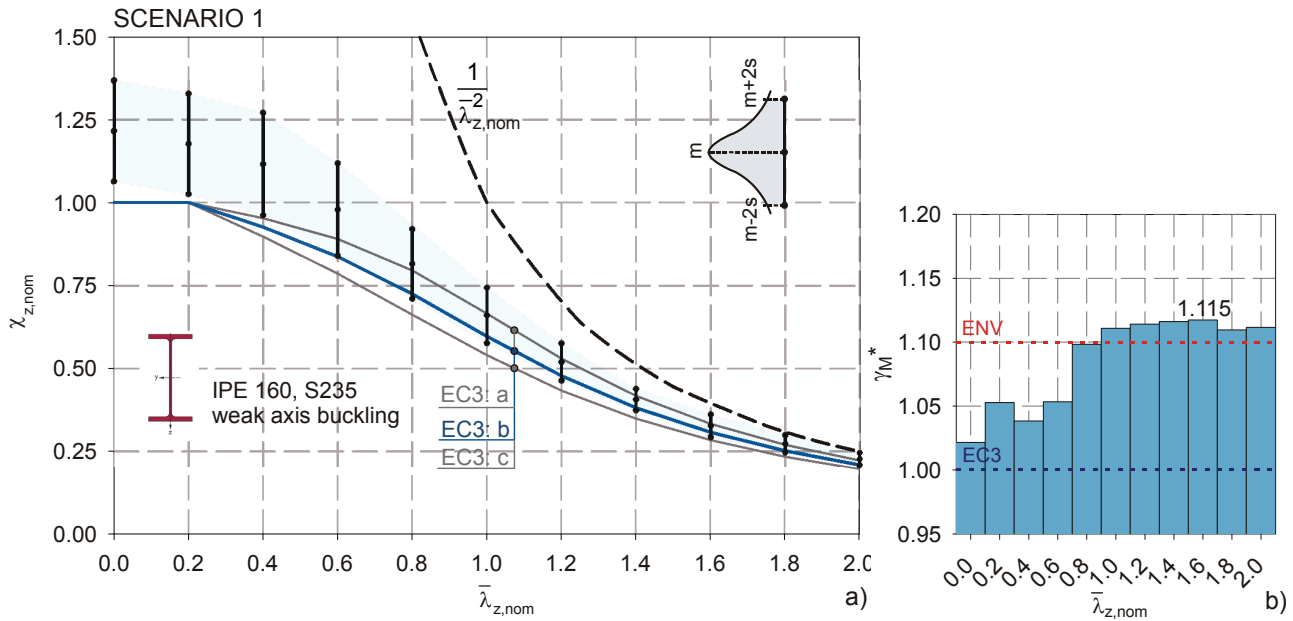
Fig 5-25 *Monte Carlo simulation of FB$_{z\text{-}z}$ of an IPE 160 section – S235: SCENARIO 1; statistical distribution of the simulated tests in a χ-$\bar{\lambda}$ plot (a); reliability analysis acc. to EN 1990.*

The chosen input data is mostly based on the measurements collected by Strating & Vos (1970) and checked and complemented by newer measurement by Melcher et al. (2004), particularly for the flange thickness. The normal or log-normal (ln) distribution was assumed in all cases.

The results of the statistical analysis are shown in Fig 5-25 to Fig 5-28 for the four different scenarios discussed in the previous section. In order to give a more complete und understandable picture of the outcome of these simulations, the χ-$\bar{\lambda}$ form of representation with m-2s bars representing the single "test" results is complemented by a plot showing the result of a reliability assessment in accordance with EN 1990 – Annex D. This assessment was performed using the same input parameters for the statistical data as contained in Table 5-9, and is shown in terms of the required values of the partial safety factor γ_M*. This factor gives a very clear indication of the impact of the single scenarios on the safety level of the column buckling rules, especially when compared to the current reliability level discussed in section 5.4 and in chapter 4.

The figures can be commented upon as follows:

- **SCENARIO 1** - Fig 5-25: the figure shows the position of the "m-2s" points to lie very close to the applicable ECCS column buckling curve b. This would not represent any noticeable change with respect to the current reliability level, see Fig 5-14 and Fig 5-22. The value of γ_M* that was calculated by following the procedure of EN 1990 is very similar to the one calculated by Müller (2003) for the ECCS tests. This is not surprising, since Scenario 1 simulates the case where the initial curvatures are left "untouched" by the changes of tolerance.
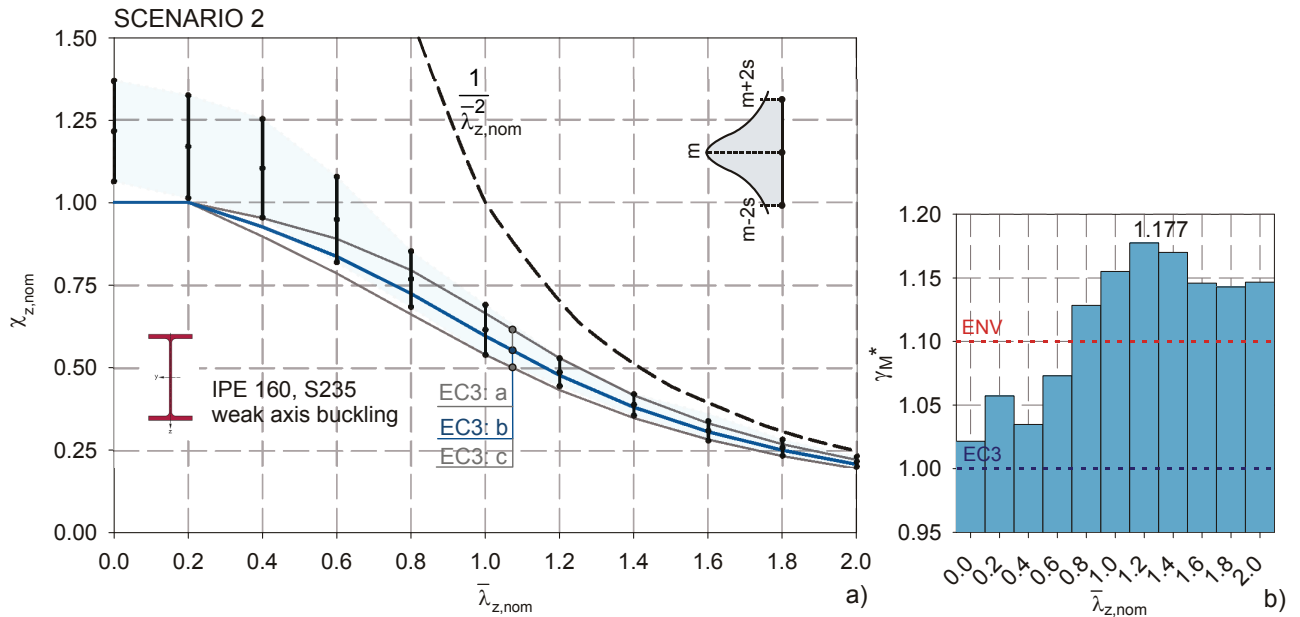
Fig 5-26 *Monte Carlo simulation of $FB_{z\text{-}z}$ of an IPE 160 section – S235: SCENARIO 2.*

- **SCENARIO 2** - Fig 5-26: the figure shows the position of the "m-2s" points to lie noticeably lower than the applicable ECCS column buckling curve b. The difference is most pronounced in the region of intermediate slenderness, around $\bar{\lambda}=1.0$, where the "m-2s "points are very close to the line representing curve c. The maximum value of γ_M* has increased to 1.177 in this scenario.

- **SCENARIO 3** - Fig 5-27: the "m-2s" points start falling significantly below the applicable buckling curve at a slenderness of $\bar{\lambda}=0.8$. In terms of γ_M*, a maximum value of 1.161 is calculated for this scenario.
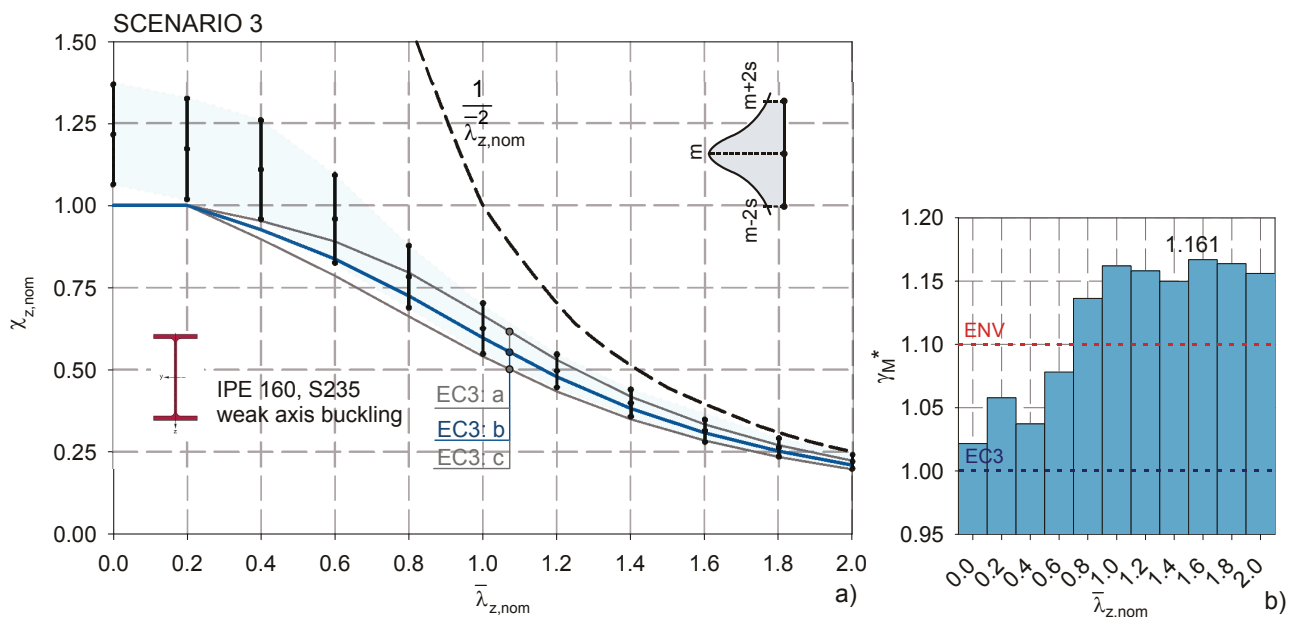
Fig 5-27 *Monte Carlo simulation of $FB_{z\text{-}z}$ of an IPE 160 section – S235: SCENARIO 3.*
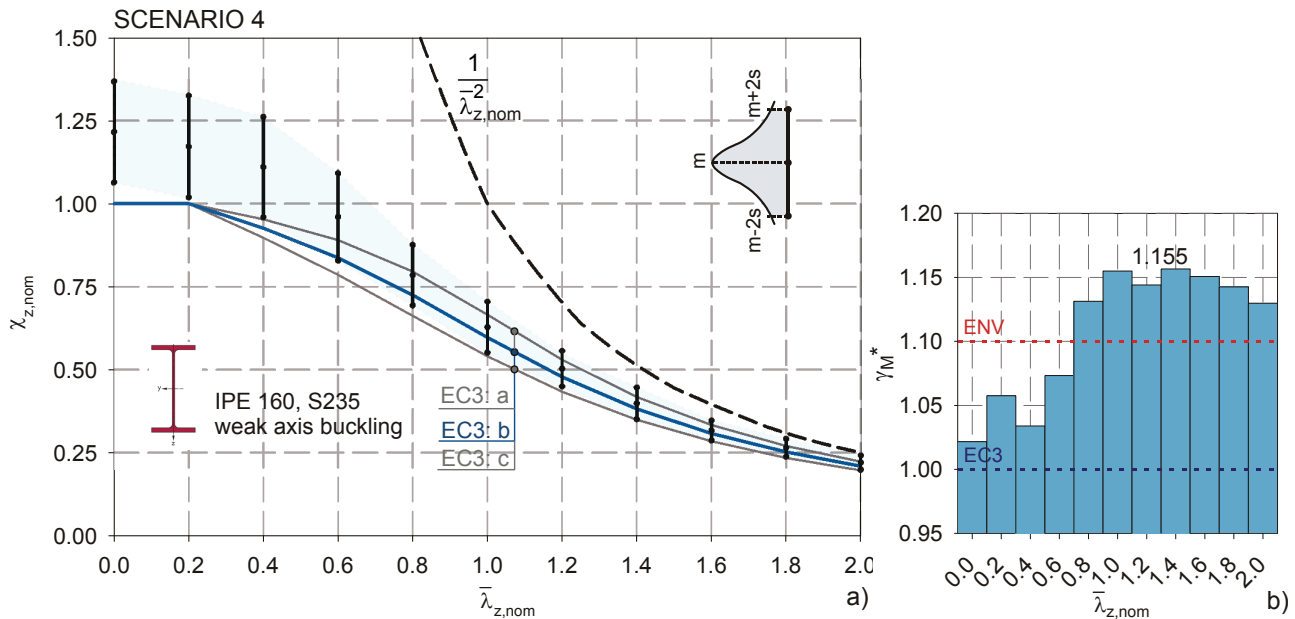
Fig 5-28 *Monte Carlo simulation of FB$_{z\text{-}z}$ of an IPE 160 section – S235: SCENARIO 4.*

- **SCENARIO 4** - Fig 5-28: again, the "m-2s" points start falling significantly below the applicable buckling curve at a slenderness of $\bar{\lambda} = 0.8$. In terms of γ_M^*, a maximum value of 1.155 is calculated for this scenario, only slightly lower than for scenario 3.

5.5.5. Discussion and Conclusion

The outcome of the Monte Carlo simulations shown in Fig 5-25 to Fig 5-28 points out that the reliability level of column buckling *could be affected by the introduction of new tolerance limits*. The scenarios 2 to 4 all treated the possibility that columns produced in the future have –on average- larger initial curvatures than was customary up to now, while all other parameters were left (in terms of scatter band) unmodified. Thus, it is not surprising that the calculations led to an (average) *loss of column strength*, respectively of margin of safety. The magnitude of this loss is in the order of 4 to 6%.

As far as the likelihood of the single scenarios is concerned, it must certainly be admitted that scenario 2 is not plausible, since it cannot be expected that all steelwork fabricators produce columns that have exactly Δ=L/750. However, this extreme scenario is still interesting when compared to the (much more plausible) scenarios 3 and 4: these scenarios treat the possibility that fabricators "relax" their fabrication habits with respect to column curvatures, an outcome that, even if not *necessary*, must certainly be seen as *"desired"* by the new tolerance specifications. The calculations in this section have shown the differences between the "extreme" scenario 2 and the "desired" scenarios 3 and 4 to be rather small. Interestingly, scenario 4 is plausible even if every single column is measured for initial curvature on site and "replaced" if curvatures above Δ=L/750 are detected. Compared to the (similar) scenario 3, where no such measurements are undertaken, the advantage stemming from these measurements is almost zero.

It is important to understand that it is often *not* the purpose of geometric *erection* (on-site) tolerance limits to specify the *extreme upper values* of shape deviations in the erected structure that must not ever be exceeded in order to design a structure safely with a given set of design rules. On the contrary, as the presentation (in section 5.5.1) of the acceptance criteria in the 1978 ECCS recommendation has shown, the philosophy with respect to tolerances on site was that *single values* above $\Delta/L=1/1000$ are acceptable – as long as the *statistical distribution* of these deviations is kept in check, and the production in the shop is confirmed to produce columns within the (shop) limits for Δ. Other, actually implemented international codes implicitly followed a similar philosophy, by assuming that site measurements were entirely unnecessary if $\Delta/L=L/1000$ was checked in the shop, since the statistical distribution of values on site could then be assumed to be acceptable.

Of course, this study only discussed some, possibly "too pessimistic" scenarios. The correlation between tolerance limits and actual deviations is not always quite as clear-cut as has been assumed here. To name one example, Chan & Gardner (2009) have found that the tolerance limits of $\Delta=L/500$ for the initial curvature of cylindrical hollow sections "*may be unduly lax as evidenced by both the observed structural performance and measured imperfections of real columns*". In other words, they observed a poor correlation between actual shape deviations and tolerance limit. They then justified the use of the current buckling rules for such sections, which are also based on GMNIA calculations with $\bar{e}_0/L=1/1000$ and fixed residual stresses, by the actual statistical distribution of the shape deviations. In principle, this is not quite unlike Scenario 1 discussed above: fabrication habits don't "acknowledge" actually laxer fabrication tolerances. Chan & Gardner's conclusion is coherent: they suggest reassessing the tolerance limit towards more realistic, lower levels, "*in preference to adjusting buckling curves to accord with current tolerances*".

Other arguments could be brought in to denounce the scenarios discussed above as too pessimistic: for example, residual stress distributions could be lower now than back in the 1960s and '70s, when the ECCS tests were carried out. Then again, actual column imperfections might be smaller than the deviations measured in the ECCS program. Finally, a beneficial inverse correlation between Δ and σ_{res} (i.e. σ_{res} is systematically lower when Δ is large) is sometimes thought to exist (Ballio & Mazzolani, 1983). These are valid points, but purely speculative at this stage; as Galambos (1998), among others, points out, practically nothing is known about real column curvatures in buildings, and the knowledge and data about residual stresses in mill- or shop-fabricated column sections has also not yet reached a satisfying level in terms of statistical representativeness.

Finally, it can be concluded that the new manufacturing and erection tolerances for compression members, as contained in EN 1090-2, cannot be logically proven to be "covered" by current buckling rules. On the contrary, the *implicit intent* of the new limits, i.e. to allow steelwork fabricators to loosen their fabrication habits with regard to column straightness, has been shown to (plausibly) lead to a drop of the reliability level of column buckling rules by about 5%. Whether this is acceptable or not should be carefully considered by the concerned code committees.

5.6. Constant Reliability Curves

In chapter 4, the possibility of obtaining "constant reliability buckling curves" by means of GMNIA calculations was discussed in general terms. In this section, the feasibility and implications of this approach are presented –in exemplary form- for the case of flexural column buckling.

5.6.1. Input parameters

The basic idea behind the constant reliability curves presented in chapter 4 originates from a reversal of the objectives of the reliability assessment procedure of EN 1990- Annex D; instead of determining (for various slenderness ratios) partial safety factors that lead to a certain, desired level of reliability for a *given buckling curve,* a buckling curve is determined that –from the outset- signifies a desired, possibly constant reliability level.

Of course, doing so requires some basic input data from experimental programs. The data given in Table 5-10 were assumed for the calculations in this sections, based on the complementary tests conducted by ECCS and other research institutions during the development of column buckling rules, see section 5.2.2. Again, all calculations are concerned with hot-rolled I- & H- sections, since the variability of basis variables is best documented for these shapes.

Parameter	HE sections		IPE sections	
	m	s	m	s
Initial curvature $\bar{e}_0$	0.00085 L	0.0002 L	0.00085 L	0.0002 L
Yield stress f_y	285 N/mm²	17.1 N/mm²	285 N/mm²	17.1 N/mm²
Eccentricity[*]	b≤110mm: 0.6 mm (ln) 110mm<b≤325 mm: 0.85 mm (ln)	b≤110mm: 0.45 mm (ln) 110mm<b≤325 mm: 0.6 mm (ln)	b≤110mm: 0.6 mm (ln) 110mm<b≤325 mm: 0.80 mm (ln)	b≤110mm: 0.45 mm (ln) 110mm<b≤325 mm: 0.6 mm (ln)
Residual stress σ_{res}	h/b≤1.2: 0.35 · 235 N/mm² h/b>1.2: 0.20 · 235 N/mm²	h/b≤1.2: 0.075 · 235 N/mm² h/b>1.2: 0.05 · 235 N/mm²	0.20 · 235 N/mm²	0.05 · 235 N/mm²
Flange thickness t_f	0.975 $t_{f,nom}$	0.03 $t_{f,nom}$	$t_{f,nom}$	0.05 $t_{f,nom}$
Web thickness t_w	1.025 $t_{w,nom}$	0.04 $t_{w,nom}$	$t_{w,nom}$	0.05 $t_{w,nom}$
Depth h	h_{nom}	0.01 h_{nom}	h_{nom}	0.01 h_{nom}
Width b	b_{nom}	0.01 b_{nom}	b_{nom}	0.01 b_{nom}

Table 5-10   *Assumptions for the parameter variability for the constant reliability curve calculations.*

Ideally, the proposed procedure would also allow for the calibration of the GMNIA model itself to real tests. This would create some additional confidence in the validity of the constant reliability curves, as it would prove the GMNIA calculations to be accurate, and would allow for a very straightforward consideration of the remaining uncertainties pertaining to the numerical model. This step had to be omitted in this study, due to the fact that no fully documented tests were available or could be carried out. However, it can be argued that the effect of this inaccuracy is fairly small in the case of column buckling, for which the common GMNIA results have been calibrated to tests and used by many other authors. Additionally, the aim of this study is to illustrate the procedure itself, and not to find definitive curves. In this context, this omission is thought to be acceptable.

5.6.2. Partial derivatives

The single steps for the calculation of constant reliability curves were described in chapter four, section 4.4.2, The most important step was the one concerned with the Taylor expansion and linearization, respectively with the calculation of partial derivatives of the GMNIA "resistance function". The following expression was said to be applicable to these derivates:

$$\frac{\partial g_{r,GMNIA}}{\partial X_i} \approx \frac{g_{r,GMNIA}(X_{1m},...,X_{im}+\Delta X_i,...,X_{jm})-g_{r,GMNIA}(\underline{X}_m)}{\Delta X_i} \qquad (5.21)$$
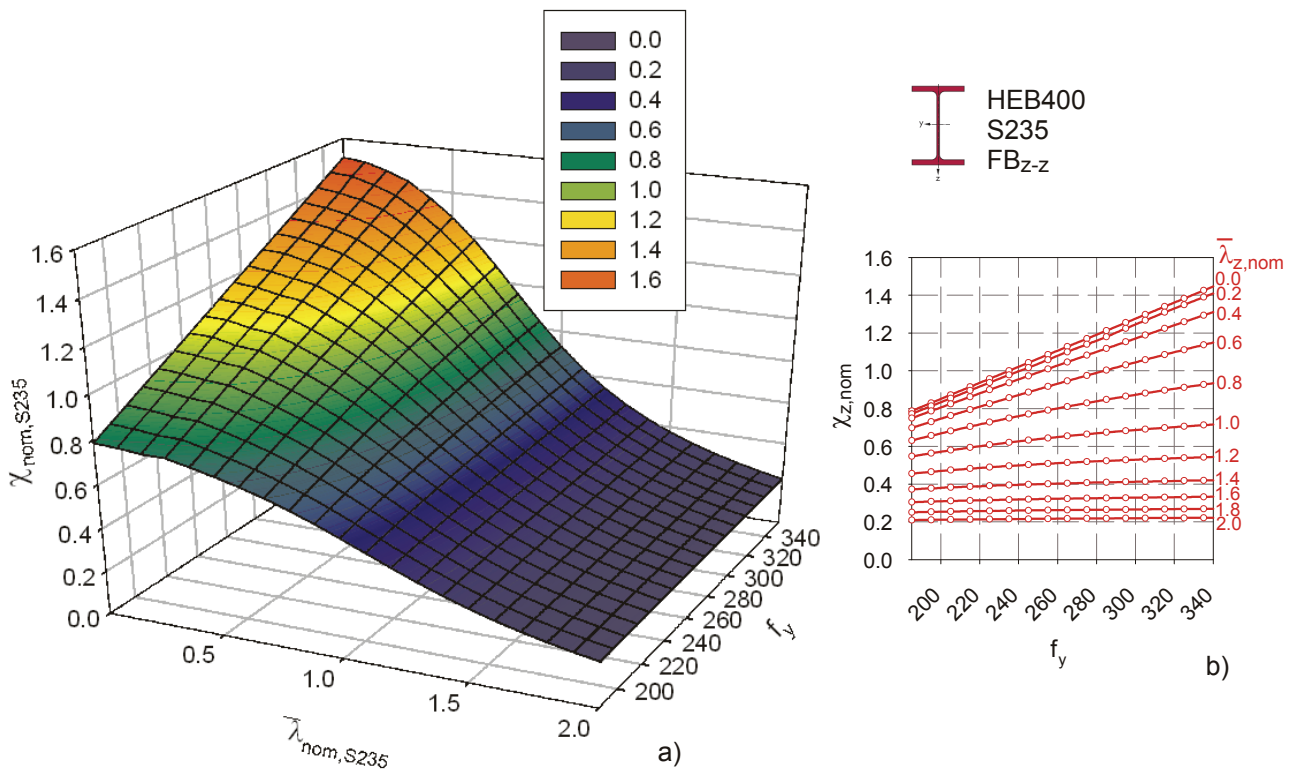
Fig 5-29 *"Resistance function" in terms of χ_{nom} for S235 plotted as function of $\bar{\lambda}$ and f_y for FB$_{z\text{-}z}$ of an HEB 400 section.*

Expression (5.21) represents the equation for an approximate, numerical derivative of the strength function $g_{r,GMNIA}$, which is the function (of all basis variables t_f, t_w, $\bar{e}_0$, σ_{res}, f_y, etc.) describing the (buckling) resistance of the studied member. If this resistance is related to the nominal value of the maximum cross-sectional resistance $R_{ult,k}$, we can replace $g_{r,GMNIA}$ with χ_{nom}. In order to better understand what it means to form numerical derivatives of the numerical quantity χ_{nom}, it is useful to plot it for two variables, e.g. for $\bar{\lambda}_{nom}$ (or the length L) and f_y, with all other variables left constant. This is done Fig 5-29 for the case of weak-axis flexural buckling of an HEB 400 section made of mild steel S235. The figure on the left (a) shows the 3D plot with χ_{nom} on the vertical axis and $\bar{\lambda}_{nom}$ and f_y on the horizontal ones. The figure on the right (b) shows sections through the χ_{nom} surface at different levels of $\bar{\lambda}_{nom}$.

Especially figure Fig 5-29b helps to understand the meaning of the partial derivatives: they represent the slope of the single curves resulting from the sections through the χ_{nom} surface, and are a measure for the impact of the variability of the derived parameter on the χ_{nom} at the studied point. In the case of the yield stress, Fig 5-29 shows that this slope rapidly falls with increasing slenderness/length of the member. At $\bar{\lambda}_{nom}=2.0$, the slope, and thus the influence of the yield stress on the buckling strength, is zero – a known and correct result. The figure also shows why the numerical derivative, calculated using (5.21), is quite insensitive to the chosen interval $\Delta X_i=\Delta f_y$ in the case of the yield stress: for a given point, the sensitivity of the function χ_{nom} to the yield stress appears to be fairly "linear", as is clear when observing the practically straight lines resulting from the sections in Fig 5-29b.
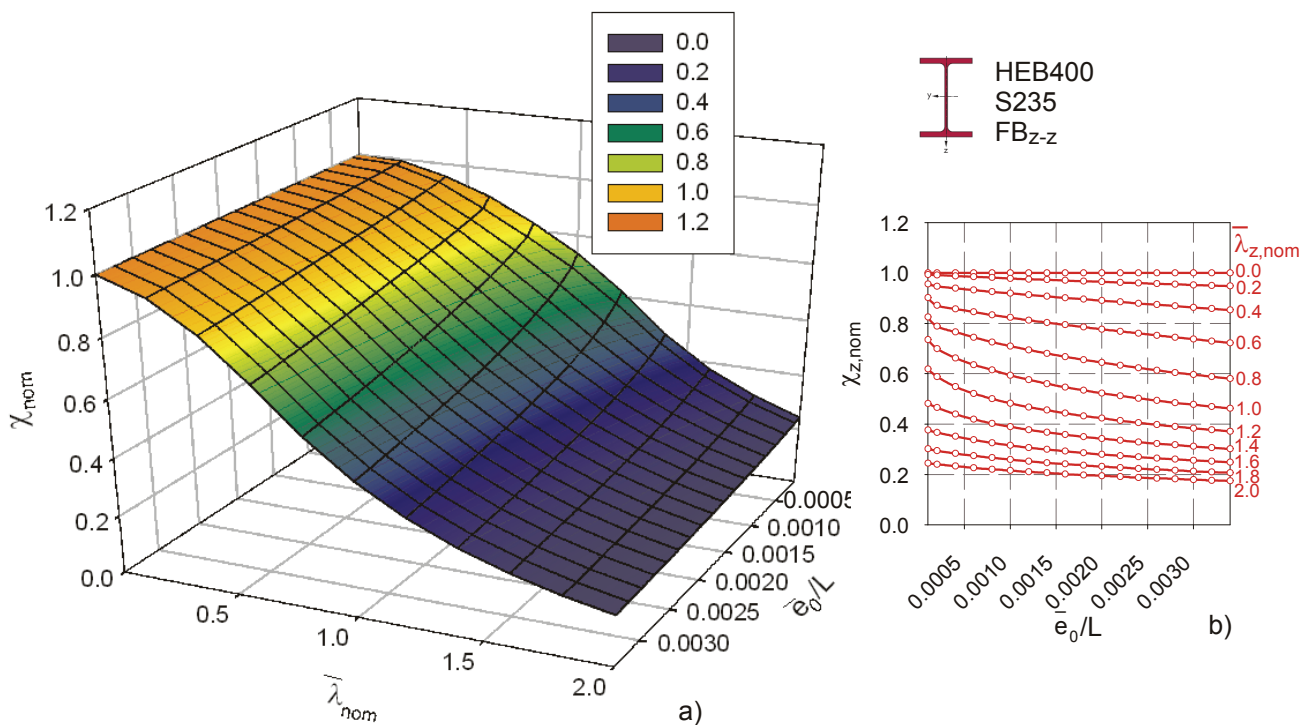
Fig 5-30 *"Resistance function" in terms of χ_{nom} for S235 plotted as function of $\bar{\lambda}$ and $\bar{e}_0 / L$ for FB$_{z-z}$ of an HEB 400 section.*

In order to show that this is not always the case, a second example is illustrated in Fig 5-30. It shows the function χ_{nom} plotted over $\bar{\lambda}_{nom}$ and the geometric imperfection coefficient $\bar{e}_0 / L$. In this case, the influence of the studied parameter $\bar{e}_0 / L$ is strongest at "intermediate" slenderness ranges around $\bar{\lambda}_{nom}$=1.0, as evidenced by the slope of the lines in Fig 5-30b. Furthermore, the slope is higher at low values of $\bar{e}_0 / L$; this means that relatively small modifications of the geometric imperfection have a high impact on χ_{nom} when $\bar{e}_0 / L$ is very small.

One procedural aspect should be mentioned: when carrying out the numerical derivatives, it is important to make sure that the maximum load proportionality factor in the non-linear (Newton Raphson) solution algorithm is reached with "sufficient" accuracy. A certain scatter of this value is inherent to the solution technique, see the schematic representation in Fig 5-31. This scatter is due to the fact that the last converged increment –with a certain tolerance value for the internal force residuals- is accepted as the calculation end result. The initial and maximum increment size and the tolerance value for the residuals must therefore be set to sufficiently low values in order to obtain useable results for the derivative. What constitutes a "sufficiently low" value depends on the sensitivity of the calculation parameter with regards to the parameter for which the derivative is calculated.
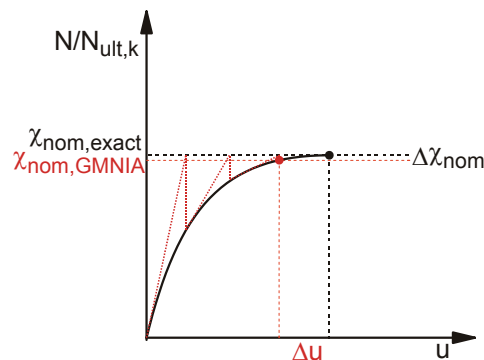
Fig 5-31 *Newton-Raphson solution algorithm –numerical error made during the calculation.*

Finally, some examples of resulting derivatives can be plotted, see Fig 5-32. They show the numerical (GMNIA) derivatives of the function χ_{nom} for the parameters f_y and $\bar{e}_0 / L$ for the weak-axis flexural buckling case of an HEB 400 made of S235. The derivative is calculated at different nominal slenderness ranges $\bar{\lambda}_{nom}$ and *at the mean value points* of the function χ_{nom}, i.e. with all other parameters set equal to the mean values of table Table 5-10.

The figure shows that the partial derivatives are an excellent measure of the sensitiveness of the buckling strength to the studied parameter – the peak of the curve indicates the slenderness where the parameter has the highest impact. Performing these derivatives is therefore also a good tool of a parameter study.
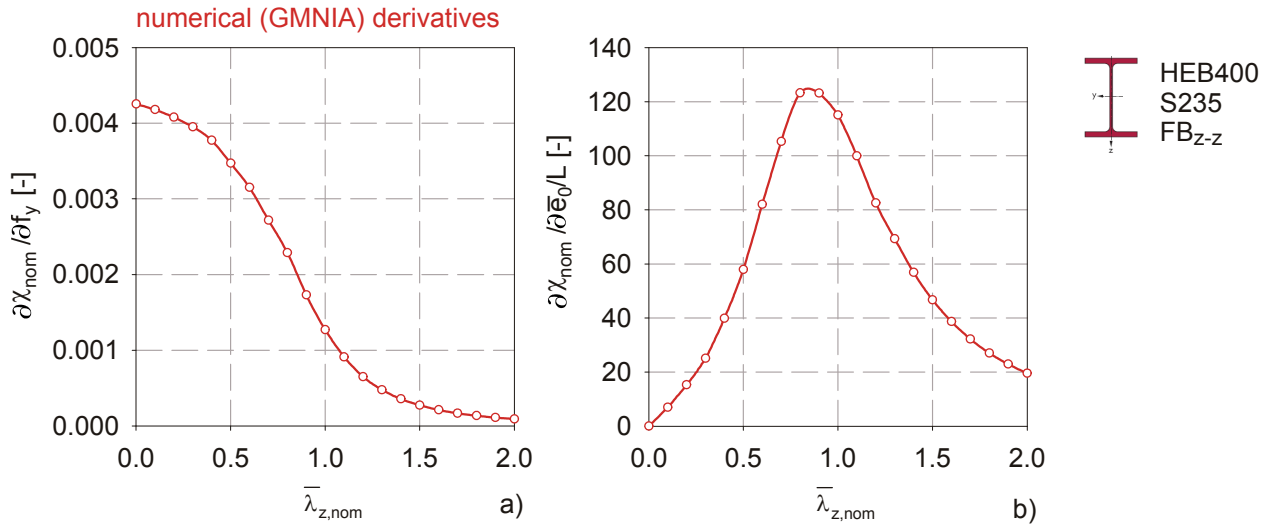
Fig 5-32 *Examples of numerical partial derivatives: for the yield stress (a); for the geometric imperfection coefficient* $\overline{e}_0 / L$ *(b)*

As far as the absolute values of the derivatives themselves are concerned, they depend on the definition of χ_{nom} and of the derived-for parameter. The plausibility of, e.g., the maximum value of the curve in Fig 5-32a, which represents the derivative for the yield stress f_y, can be easily checked: at $\overline{\lambda}_{z,nom}$=0.0 the yield stress enters the buckling strength linearly; thus the derivative must be a constant value regardless of the actual yield stress, and can be calculated to:

$$\partial\chi_{nom} / \partial f_y(\overline{\lambda} = 0.0) = \frac{d\left(A \cdot f_y / (A \cdot f_{y,nom})\right)}{df_y} = \frac{1}{f_{y,nom}} \xrightarrow{S235} 0.004255 \qquad (5.22)$$

This matches the value calculated and plotted in Fig 5-32a.

5.6.3. Exemplary curves

The next pages show some exemplary constant reliability curves calculated following the procedure sketched in chapter 4 and further described in this section. Again, the weak-axis flexural buckling case was treated. Four sections were chosen with the aim of giving a picture of the influence of the different assumptions made in Table 5-10.

Fig 5-33 shows constant reliability buckling curves for FB$_{z-z}$ of an HEB 400 section. This section belongs to the HE group of hot-rolled shapes, and has a depth-to-width ratio h/b>1.2; thus, comparatively low residual stresses were assumed, see Table 5-10. The figure shows reliability levels corresponding to the mean value r_m (50% exceedance), the design value specified by EN 1990 – Annex D for 0.8 times the reliability index β of 3.8, and the "upper bound" line corresponding to the "mirrored" probability of non-exceedance when compared to the design point, i.e. the line at 0.8 times 3.8 standard deviations above the mean line.
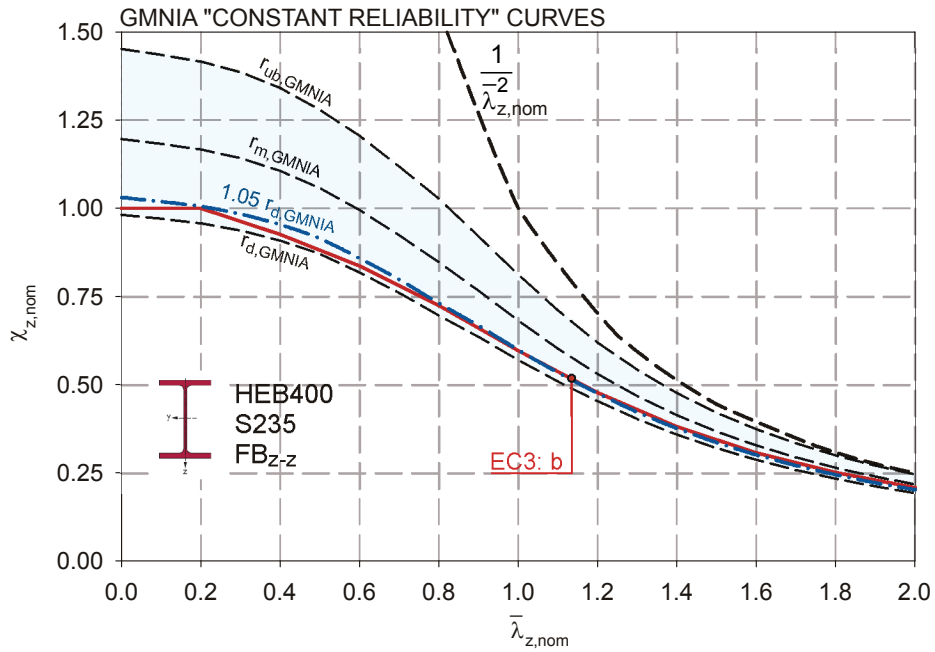
Fig 5-33 *Constant Reliability Buckling Curve (CRC) for a HEB 400 section – S235 – FB$_{z-z}$*

Furthermore, the current Eurocode design buckling curve b is shown, as well as the line at 1.05 times r$_d$. This line represents a buckling curve that, in theory, requires a constant value γ_{M1}=1.05 for all $\bar{\lambda}$ to satisfy the Eurocode reliability requirements.

For the HEB 400 section, this latter line coincides fairly well with the current Eurocode buckling curve b, except at lower slenderness values, where curve b lies below it. This would indicate that buckling curve b would need a factor of not more than γ_{M1}=1.05 to reach the EN 1990 reliability target for this section and buckling case.
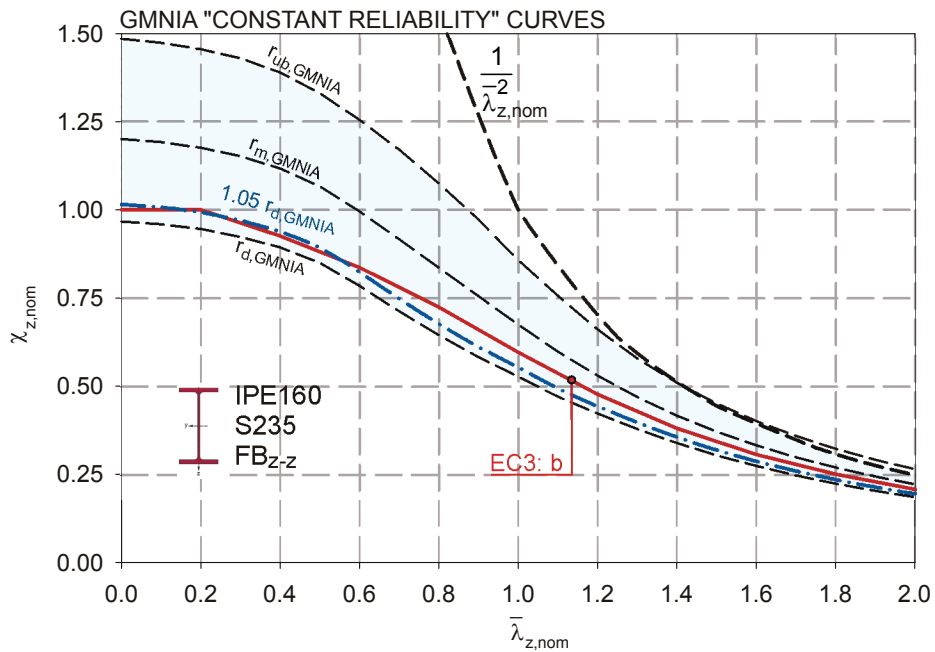
Fig 5-34 *CRC for a IPE 160 section – S235 – FB$_{z-z}$*

Fig 5-34 shows the same calculation for the much-studied (in this chapter) IPE 160 shape. Here both the constant reliability curve for the design point and for 1.05 times r_d fall below the current, applicable buckling curve b. This is absolutely consistent with the reliability studies carried out in 5.4, as well as the calculations done for "scenario 1" in the study concerned with column curvature and tolerances, see Fig 5-25. In that figure, the partial safety factor $\gamma_M{}^*=\gamma_{M1}$ that is required to reach the EN 1990 reliability target was shown to increase with increasing length, and to stabilize beyond $\overline{\lambda}_{z,nom}$=1.1, reaching values of around 1.12. That is the same tendency pointed at by Fig 5-34, where the r_d line and buckling curve b move farther apart beyond $\overline{\lambda}_{z,nom}$=0.4 to then stabilize their relative distance.

It can be shown that a buckling curve corresponding to curve c in the Eurocode would be much closer to the design value r_d – more regarding this follows in the next sub-section.

Two additional examples are shown in Fig 5-35 and Fig 5-36. They treat a HEA 200 and a HEM 320 section, respectively. Both sections have h/b≤1.2; thus, higher average residual stresses, with higher scatter, were assumed. Due to this fact, -and this fact alone-, Beer & Schulz (1970) have classified these sections as belonging to a different buckling curve, namely – for weak-axis flexural buckling- the ECCS curve c shown in the figures.

The two figures show that the buckling curve c indeed lies fairly close (just slightly above) the constant reliability curve at the design point r_d. One can therefore assume that a value of γ_{M1} around 1.05 or lower could be shown to apply for this curve and section type. This is in good agreement with reliability assessment findings for buckling curve c based on real tests, see Fig 4-4. In that figure, values of $\gamma_M{}^*$ calculated for real (ECCS) tests were found to lie between 1.02 and 1.07 for buckling curve c.
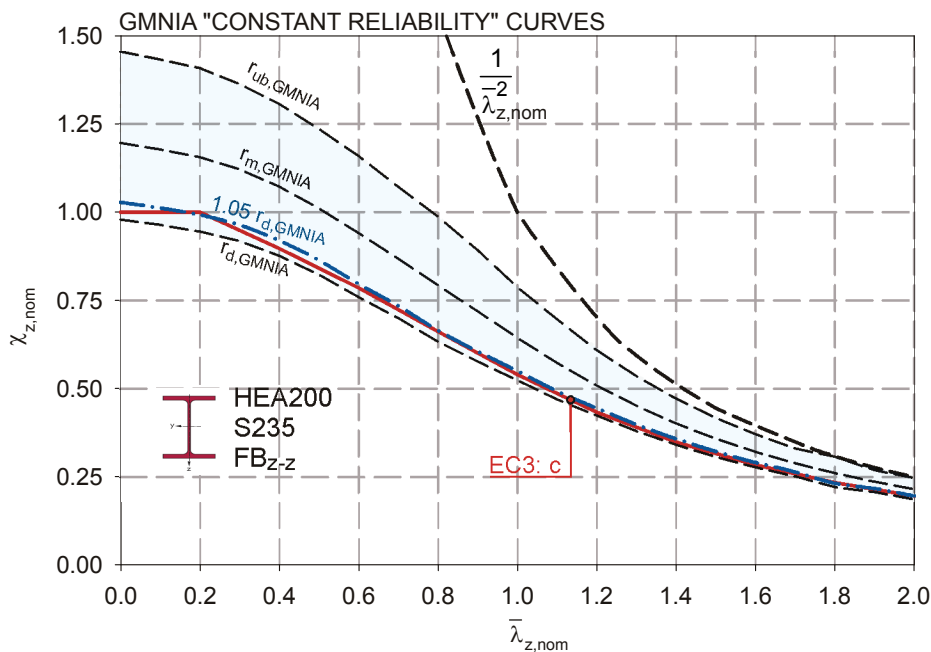
Fig 5-35 *CRC for a HEA 200 section – S235 – FB$_{z-z}$*
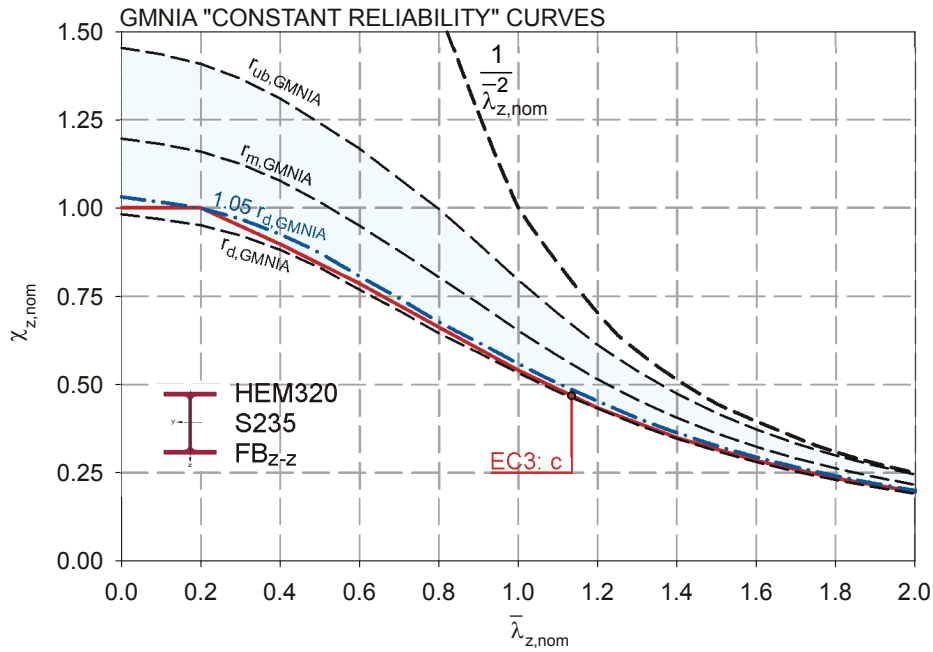
Fig 5-36 *CRC for a HEM 320 section – S235 – FB$_{z-z}$*

5.6.4. Calibration of an Ayrton-Perry formulation

So far, the above figures representing "constant reliability curves" for the design level r$_d$ -Fig 5-33 to Fig 5-36- have only been used to compare the position of the current buckling curves with respect to (an estimation of) the target reliability point. Of course, this is only one use of the proposed concept using constant reliability curves, and not the most important when this concept's potential application for other buckling cases is seen as a goal.

In such a scenario, no pre-existing buckling curves or formulae would be given. Instead, a new calibration of (preferably) an Ayrton-Perry formulation would have to be carried out. This is done exemplarily for the IPE 160 curves of Fig 5-34. That figure shows that the plateau value, or even any value χ=1.0, could not be justified for the r$_{d,GMNIA}$ curve, i.e. with a value of γ$_{M1}$=1.0. Therefore, the calibration is carried out *for the curve representing 1.05 · r$_{d,GMNIA}$*. γ$_{M1}$=1.05 is therefore the "target value" of the partial safety factor and representative of the target reliability level.

In a first step, the "exact" numerical values of η (see section 5.3) are determined by using expression (5.23), which is in principle identical to (5.8). The results are plotted in Fig 5-37a.

$$\eta_{num} = \left(\frac{1}{\chi_{num}} - 1 \right) \cdot \left(1 - \chi_{num} \cdot \overline{\lambda}^2 \right) \qquad (5.23)$$
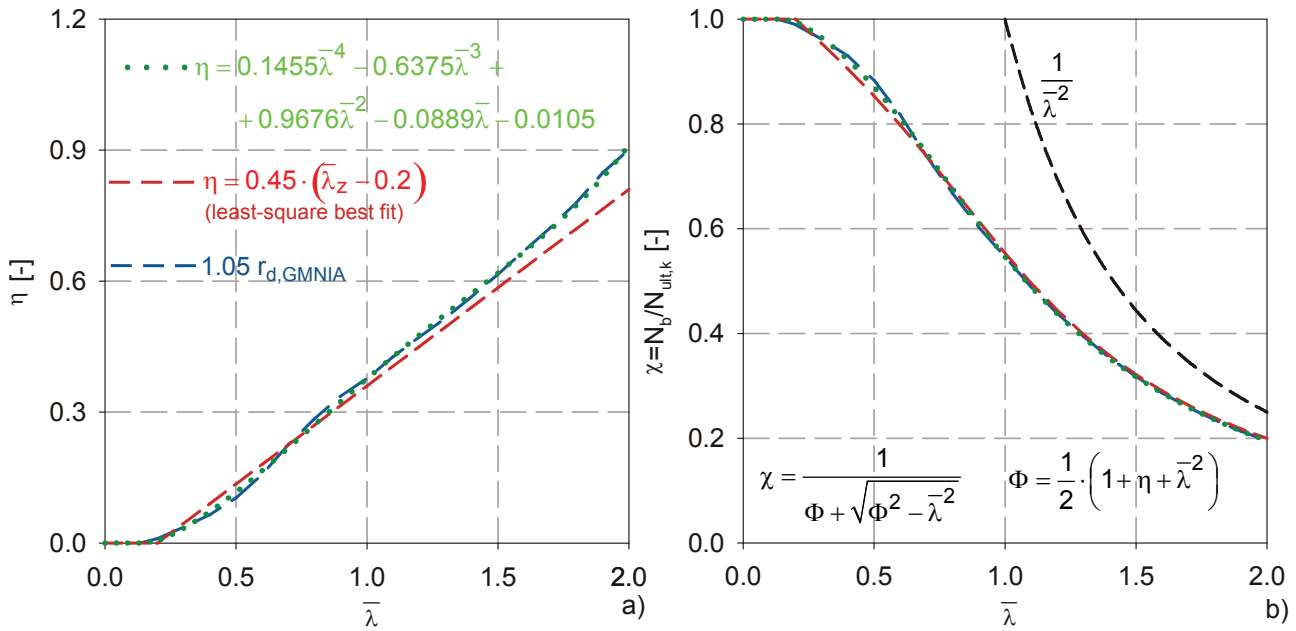
Fig 5-37 *Description of the 1.05·r_d constant reliability curves by an Ayrton-Perry formula; two options for the description of the generalized imperfection η (a); resulting buckling curves (b)*

Then, two strategies will be compared for finding an appropriate formulaic description of the buckling curve:

i. In the first strategy, a formulation of the type $\eta = \alpha \cdot \left(\bar{\lambda} - \bar{\lambda}_0 \right)$ is used, as was done by Rondal & Maquoi (1979). The value of α is calibrated to *best fit the value of* χ over the entire studied slenderness range of $\bar{\lambda}=0.0 - 2.0$. The calibration is done by least square determination. The resulting value of α is equal to 0.45. Thereby, $\bar{\lambda}_0$ was again set to 0.2.

ii. In the second strategy, the obtained (numerical) curve for η_{num}, shown in Fig 5-37a, is described by a fourth-order polynomial.

As can be seen in Fig 5-37a, the polynomial expression is much more accurate in describing η_{num}. This is obvious, not only because a higher order polynomial approximation must inevitably be more accurate than a straight line, but also because the straight line formulation with $\alpha=0.45$ was calibrated to best match χ, not η_{num}. The differences in terms of χ are shown in Fig 5-37b. Also here, the polynomial approximation of the numerical curve is more accurate than the classical "straight line" approach, but only minimally, as can be seen by the fact that all three curves essentially overlap.

The relative differences ("error") between the target line representing 1.05 $r_{d,GMNIA}$ and the Ayrton-Perry approximations using two different expressions for η are shown in Fig 5-38a. The figure shows that the error hardly exceeds 3% (on the "safe side") for the straight line approximation, and is in the range of slightly more than ±1% for the polynomial approximation of η_{num}.
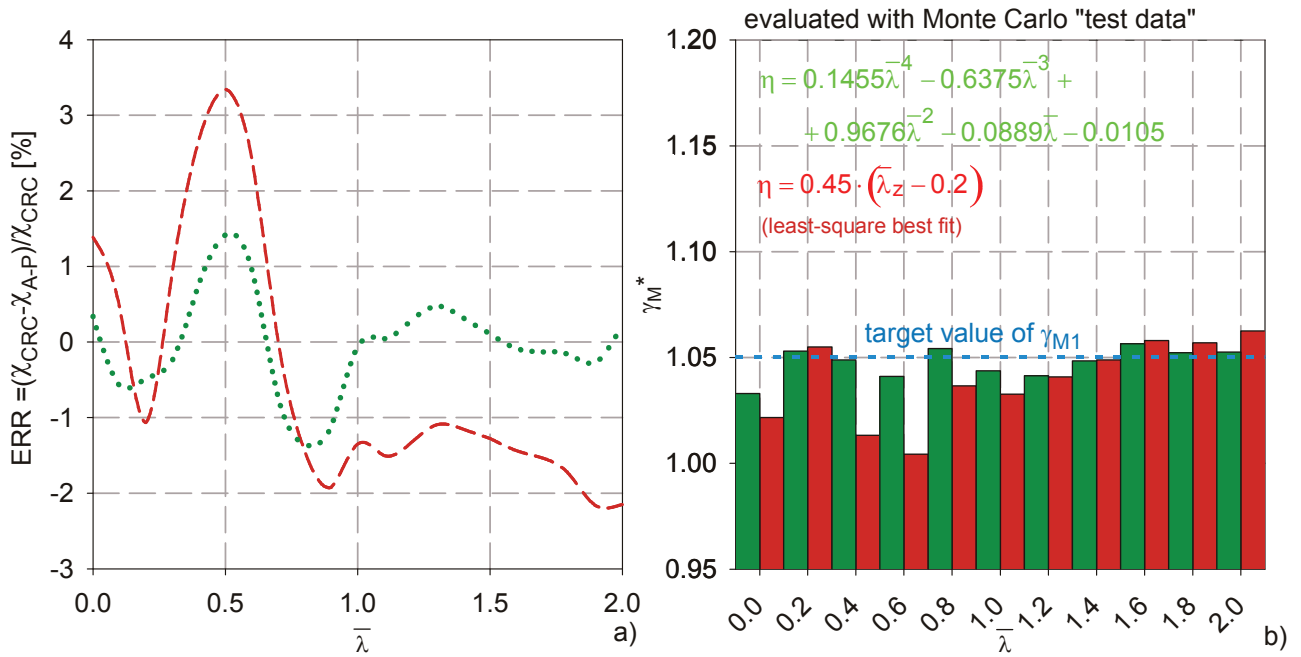
Fig 5-38 *Error of χ-approximation inherent to the two formulations for η (a); Value of $\gamma_M{}^*$ resulting from an evaluation of the Monte Carlo "tests" of Fig 5-25 (b).*

Finally, the results can be assessed with regard to the original goal, i.e. obtaining a buckling curve description that has a (near-) constant reliability level for all slenderness ranges. This was done by evaluating the Monte Carlo "tests" of Fig 5-25 (scenario 1) in accordance with the EN 1990- Annex D procedure and calculate the resulting value of $\gamma_M{}^*$. Those simulated "tests" were shown to result in values of $\gamma_M{}^*$ that are very similar to what Müller (2003) has shown to be applicable to the "real" ECCS tests.

Since the above formulaic description was modelled onto the 1.05 $r_{d,GMNIA}$ constant reliability buckling curve of Fig 5-34, using an Ayrton-Perry formulation of the form of (5.3) with two different options for η, the desired outcome of this calculation should be that $\gamma_M{}^*$ is very close to 1.05 for all values of $\bar{\lambda}$.

The actual outcome is shown in Fig 5-38b. The red bars show the result of the evaluation for the best-fit, straight line formulation for η, while the green bars represent the outcome for the polynomial approximation of η_{num}. The figure should also be compared with Fig 5-25b to appreciate the difference to the current status. It shows that both formulations are able to maintain the scatter of the values of $\gamma_M{}^*$ within a certain, narrow band from a specified "target value". Of the two options for the formulation of η, the polynomial approximation is of course more effective. Compared to the current status of Fig 5-25b, where the target reliability level cannot directly be influenced at all, the straight line formulation for η, which is identical (in form) to the one found in the Eurocode now, is also much more effective. Also for this formulation, values of $\gamma_M{}^*$ within 1.00 and 1.07 were found to apply.

If α=0.45 were therefore used for this section, a nearly constant reliability level would be achieved for this section and buckling case, and a value of γ_{M1} of 1.05 could be accepted as a reasonable, sufficiently safe, constant value for all practical slenderness ratios.

5.6.5. Comments

The application of the *constant reliability buckling curve concept* based on GMNIA calculations and realistic statistical input data for the basis variables, presented in chapter 4, has been applied for the case of weak-axis flexural buckling of some hot-rolled sections. The general feasibility of the concept has been proven by means of examples. Of course, in order to be brought to a level suitable for inclusion in a design code, the following points would have to be considered:

i. The statistical input data for the basis variables is, of course, a potential source of controversy. In order to avoid this controversy, all parties involved in the development and acceptance of buckling rules should, ideally, agree upon a characteristic data pool for the variability of the material, geometry and imperfection values (and their potential correlation) that influence the studied buckling phenomenon.

ii. As the example has shown, the calibration of a formula (e.g. Ayrton-Perry) onto a constant-reliability curve will still lead to some scatter of the resulting value of the partial safety factor γ_M around the specified target value. This is practically inevitable. It would still represent an appreciable increase of consistency of the reliability level, as this scatter can normally be kept small by appropriate calibration.

iii. It must be clearly stated that adopting this procedure would lead, in many cases, to a *different categorization* of different sections with regard to buckling curves (a_0, a, b, ...) than is currently the case in the Eurocode. While the current categorization basically depends on a deterministic, fixed decision with respect to the imperfection amplitudes (especially of the residual stresses), a new categorization would depend on the assumed, probabilistic scatter band of the input parameters, *and* on the sensitivity of the studied member to the variability of these input parameters.

iv. To name an example in order to clarify the previous point, the results presented in this section seem to indicate that, at least if the scatter-band assumptions of Table 5-10 are accepted as valid, a categorization of section for weak-axis flexural column buckling could lead to the conclusion that IPE shapes (all of which have ratios h/b>1.2) are actually to be grouped in the same category as stockier HE sections with h/b≤1.2, while HE sections with h/b>1.2 would pertain to a more convenient, "higher" buckling curve.

6

Lateral-Torsional Buckling of I- & H Sections

6.1. Introduction and Scope

In this chapter, the lateral-torsional buckling mode of prismatic I- & H-sections is treated from different perspectives. First of all, the current design provisions are briefly revisited. Thereby, the inconsistencies between this buckling case and the "benchmark" case of flexural column buckling, particularly for what concerns the categorization of cross-sections, is pointed out. The on-going debate regarding these buckling curves is delineated, and the goal of any further work treating this case is discussed.

Then, a parametric study is carried out in order to identify the most relevant structural parameters that govern this buckling case, and generally to clarify the load carrying behaviour.

In a next step, a large series of GMNIA calculations is carried out for the case of constant bending moment of a single-span member, in order to provide the basis for a new buckling curve formulation based on the now-classical "model beam" with nominal input parameters and fixed imperfection amplitudes, i.e. in analogy to what Beer & Schulz (1970) have done for the column buckling case.

A specific Ayrton-Perry type formulation for the basic case of LT-buckling of members under constant bending moment is then derived and, very importantly, *specifically calibrated*. Thereby, different strategies are followed. At the end, a very accurate formulation could be found, which is able to very well reflect the differences between different assumptions made during the GMNIA calculations.

Since non-uniform bending moment diagrams are omnipresent in practical application of beams, a simplified expansion of the found formulation is also proposed; thereby, it was aimed to combine mechanical rationality with practicality, while at the same time maintaining accuracy. A very accurate formulation was thereby found that requires less additional moment-diagram parameters than current practical formulations in the Eurocode.

The aspects concerned with reliability and safety are mainly treated by the use of Monte Carlo simulations, with the addition of some comparisons with documented test results from the literature. Finally, the applicability of the constant reliability curve concept is also discussed for this buckling case.

6.2. Elastic buckling moment M_{cr} and normalized slenderness for LT buckling

The elastic, critical (bifurcation) buckling moment of prismatic beams has been studied as early as 1910 by Timoshenko. An updated overview of the development of knowledge in the field has been given e.g. by Serna et alt. (2006).

In simple cases such as prismatic beams under constant bending moment, analytical solutions for the critical bifurcation moment M_{cr} can be formulated. In cases where the loading condition is not uniform along the beam's length, approximations have been developed by various authors (see Trahair, 1993). As Andrade and Camotim (2007) have noted, one of the most widely-used formulae for the practical calculation of the critical moment M_{cr} is the so-called *3-factor formula*, which also entered the ENV (1992) version of Eurocode 3:

$$M_{cr} = C_1 \cdot \frac{\pi^2 EI_z}{(k_z \cdot L)^2} \cdot \left[\sqrt{\left(\frac{k_z}{k_\omega}\right)^2 \cdot \frac{I_\omega}{I_z} + \frac{(k_z \cdot L)^2 \cdot GI_T}{\pi^2 EI_z} + \left(C_2 z_g - C_3 z_j\right)^2} - \left(C_2 z_g - C_3 z_j\right) \right] \quad (6.1)$$

where

C_1, C_2, C_3 are modification factors depending on the loading and end restraint conditions

z_g is the distance between shear centre and point of (transversal) load application

z_j $= z_s - 0.5 \int_A (y^2 + z^2) \frac{z}{I_y} dA$

z_s is the coordinate of the shear centre

k_z, k_ω are are effective length factors with respect to in-plane resp out-of-plane buckling

In the case studied in this thesis of beams with double-symmetric cross-sections and end-fork boundary conditions, this equation can be simplified as follows:

$$M_{cr} = C_1 \cdot \frac{\pi^2 EI_z}{L^2} \cdot \left[\sqrt{\frac{I_\omega}{I_z} + \frac{L^2 \cdot GI_T}{\pi^2 EI_z} + \left(C_2 z_g\right)^2} - C_2 z_g \right] \quad (6.2)$$

If the load acts in the shear centre (equal to the centroid in the double-symmetric case), the equation further simplifies:

$$M_{cr} = C_1 \cdot \frac{\pi^2 EI_z}{L^2} \cdot \sqrt{\frac{I_\omega}{I_z} + \frac{L^2 \cdot GI_T}{\pi^2 EI_z}} \quad (6.3)$$

The factor C_1 is defined as the ratio between the critical moment $M_{cr,nu}$ valid for an arbitrary, non-uniform bending moment diagram along the beam's length and the analytically solvable critical moment $M_{cr,u}$ for a uniform bending moment. In the simplest case of a uniform bending moment, the factor C_1 thus per definition assumes a value of 1.0. The analytical solution for $M_{cr,u}$ for a double-symmetric beam is thus given by:

$$M_{cr,u} = \frac{\pi^2 EI_z}{L^2} \cdot \sqrt{\frac{I_\omega}{I_z} + \frac{L^2 \cdot GI_T}{\pi^2 EI_z}}$$ (6.4)

In the following discussion of the design rules for LT buckling, the normalized slenderness $\overline{\lambda}_{LT}$ will be used; it is defined as follows:

$$\overline{\lambda}_{LT} = \sqrt{\frac{M_{pl}}{M_{cr}}}$$ (6.5)

where

M_{pl} is the plastic section capacity $W_{pl} \cdot f_y$ of the cross-section

M_{cr} is calculated using the appropriate formula of (6.1) - (6.4).

Additional details concerning the calculation of M_{cr}, specifically with regard to non-uniform bending moments, are given in section 6.9.

6.3. Design provisions – evolution and current developments

In this section, the current design approaches are briefly discussed. Thereby, details are given only for the basic case of a uniform bending moment diagram. The on-going debate regarding safety and accuracy of the current rules is then discussed.

6.3.1. Existing approaches

The inclusion of specific LT buckling rules in European and North American design codes took place relatively late, in the second half of the 20th century. As Galambos (1998) points out, three approaches have traditionally been employed:

i.   Approach 1: design formulae are used that are purely calibrated to test results, whereby the "rational" limits represented by the pure (plastic) bending capacity M_{pl} and the Euler buckling moment M_{cr} are observed and a straight-line interpolation is carried out between them; this is the approach used in the AISC LRFD (2001) code.

ii.   Approach 2: this approach has been used for quite some time on the European continent, as it already entered the ECCS recommendations of 1978 and the "yellow print" 1981 edition of DIN 18800-2, which eventually led to the first "real" edition (DIN 18800-2, 1990). In its most basic form, it goes back to the work of Unger (1977) and makes use of a modified Merchant-Rankine formula of the following form (using the familiar EC3 notation):

$$\chi_{LT} = \frac{M_R}{M_{pl}} = \left(\frac{1}{\left(1 + \overline{\lambda}_{LT}^{2n} \right)} \right)^{1/n} \tag{6.6}$$

Thereby, n=2.5 is used for hot-rolled sections, whereas n=2.0 is used for welded ones. The formula is evaluated and plotted in Fig 6-1. In spite of its apparent rationality, this approach has been criticized (Fukumoto & Kubo 1977, Fukumoto 1982) for its allegedly insufficient level of safety. Lindner et al (1994) replied to this criticism by providing a statistical justification that made use of a sorted-out data pool that showed that the curves are sufficiently safe, provided a safety factor of γ_{M1}=1.1 is used.
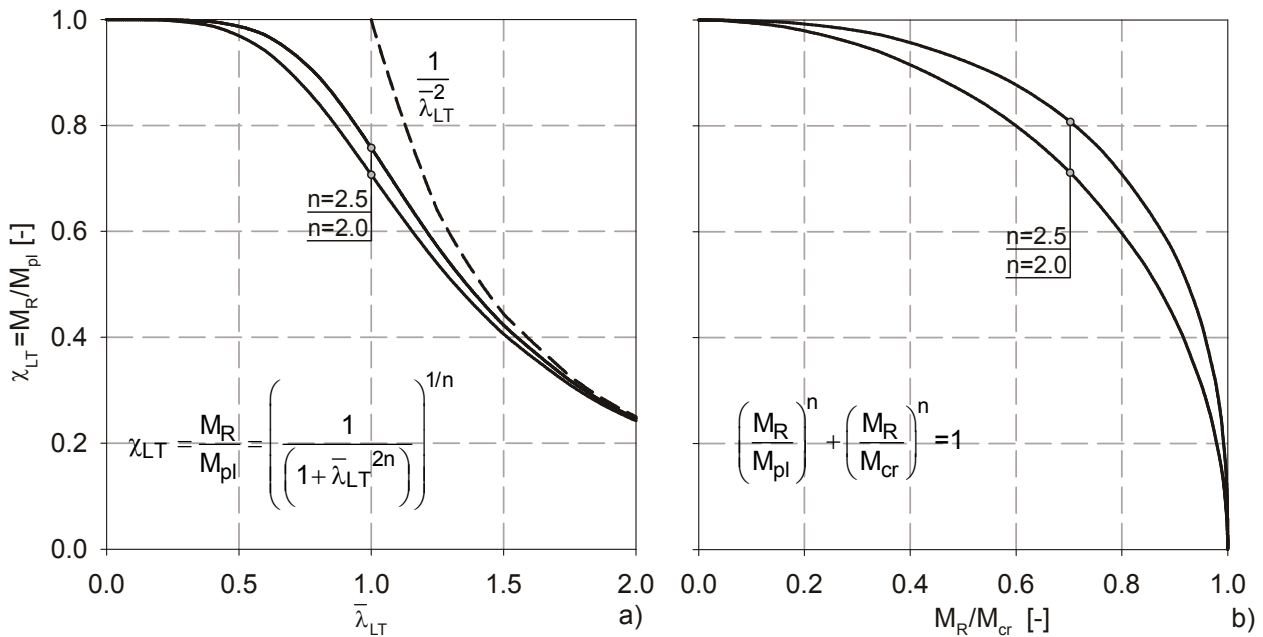
Fig 6-1 *Representation of formula (6.6) in the classic χ_{LT}-$\overline{\lambda}_{LT}$ (a) and in the Merchant-Rankine form (b).*

iii.   Approach 3: this approach assumes that beams and columns "act alike" in terms of stability, meaning that the flexural column buckling curves are (with restrictions and amendments, as will be discussed below) assumed to be accurate for the LT buckling case of beams as well. This approach has been popular in the UK and the Commonwealth countries for some time (see e.g. the last, year 2000 version of BS5950-1), and has been adopted in Eurocode 3 already in the ENV version (1992). In most cases, including the Eurocode, it makes use of the Ayrton-Perry formulation. As this approach is currently in use in Europe, it will be discussed with more detail in the following.

6.3.2. Current design provisions and categorization

According to Eurocode 3 – EN 1993-1-1 (EC3), the design LT buckling resistance $M_{b,Rd}$ of steel members with compact cross-sections is determined by multiplying the plastic cross-sectional moment capacity M_{pl} with a buckling reduction factor χ_{LT}. The reduction factor is determined by using one of two sets of formulae, which are associated with so-called "cases". In the first, "general" case, the following formulae are used:

$$\chi_{LT} = \frac{1}{\Phi_{LT} + \sqrt{\Phi_{LT}^2 - \overline{\lambda}_{LT}^2}} \leq 1.0 \tag{6.7}$$

and

$$\Phi_{LT} = \frac{1}{2}\left[1 + \alpha_{LT}\left(\overline{\lambda}_{LT} - 0.2\right) + \overline{\lambda}_{LT}^2\right] \tag{6.8}$$

where

α_{LT} …. generalized imperfection factor, tabulated according to Table 6-1.

These "general" curves are identical to the column buckling curves, but use a different categorization according to cross-sectional geometry when compared to the column buckling case. For hot-rolled sections, the column buckling curve "a" is used for sections with depth-to-width ratio $h/b \leq 2.0$, while curve "b" applies for more slender sections.

In the "specific" case of hot-rolled sections and equivalent welded sections, the following expressions can be used:

$$\chi_{LT} = \frac{1}{\Phi_{LT} + \sqrt{\Phi_{LT}^2 - \beta \cdot \overline{\lambda}_{LT}^2}} \leq \frac{1}{\overline{\lambda}_{LT}^2} \leq 1.0 \tag{6.9}$$

and

$$\Phi_{LT} = \frac{1}{2}\left[1 + \alpha_{LT}\left(\overline{\lambda}_{LT} - \overline{\lambda}_{LT,0}\right) + \beta \cdot \overline{\lambda}_{LT}^2\right] \tag{6.10}$$

whereby

$\overline{\lambda}_{LT,0}$ …. extended plateau value for LT buckling (recommended value of 0.4).

β …. curve shape modification factor (recommended value of 0.75).

α_{LT} …. generalized imperfection factor for the specific case, see Table 6-1.

This "specific" formulation is based on extensive experimental (Byfield & Nethercot, 1998) and statistical work according to Annex D of EN 1990 for the low-slenderness range around the desired plateau of $\overline{\lambda}_{LT,0} = 0.4$ (King, 2000), as well as on comprehensive numerical studies (Greiner et al. 2000), which were used to develop the design resistance model. The experimental and statistical work justified the introduction of a plateau value of $\overline{\lambda}_{LT,0} = 0.4$, which did not appear in this extent in the numerical studies.
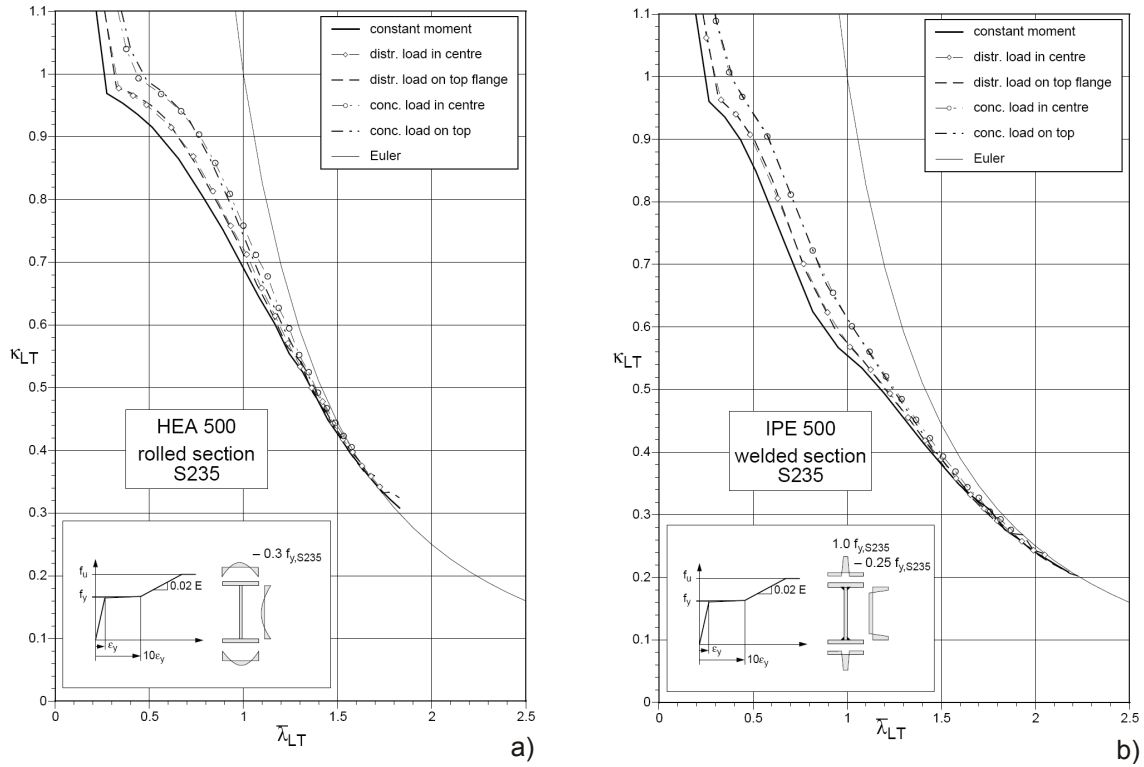
Fig 6-2 *Examples for numerical buckling curves obtained by Greiner & Salzgeber (2000) for the development of the current EC3 "specific" LT buckling curves.*

The numerical studies served the purpose of obtaining a comprehensive set of numerical buckling curves for a great variety of hot-rolled and equivalent welded sections, different load cases and steel grades; they were conducted as geometrically and materially non-linear FEM calculations (GMNIA) with residual stresses and geometrical imperfections in the shape of sinusoidal, *purely lateral* bow imperfections. Two examples for the obtained curves are shown in Fig 6-2. Importantly, it was also shown that the numerical curves very well matched the lower bound of a test data pool found in the literature (see section 6.10.1).

In a final step, the resulting numerical curves were approximated using the above expressions (6.9) with (2.37), whereby the experimentally founded plateau of $\overline{\lambda}_{LT,0} = 0.4$ was introduced as a constraint for the calibration.

Both the expressions (6.7) with (6.8) and (6.9) with (2.37) represent Ayrton-Perry type formulae that were calibrated for the LT buckling phenomenon using the so-called "generalized imperfection coefficient" α as calibration factor. They were, however, not coherently *derived* for the specific case at hand (LT buckling), but rather adapted (and, in the "specific" case, modified) from the column buckling case; by contrast, for the column buckling case the formulation is mechanically coherent, as was shown in chapter 5.

hot-rolled I&H sections		
h/b	General Case	Specific Case
≤ 2.0	$\alpha_{LT}=0.21$(a)	$\alpha_{LT}=0.34$(b)
>2.0	$\alpha_{LT}=0.34$(b)	$\alpha_{LT}=0.49$(c)

Table 6-1 *Generalized imperfection coefficients α_{LT} for LT buckling acc. to Eurocode 3.*

6.3.3. Open questions and current developments

The code provisions of Eurocode 3 – EN 1993-1-1 for the design of steel members against lateral-torsional buckling have lately come under renewed scrutiny from different sides. Whenever these provisions were critically reviewed, the criticism mainly focused on either one of the following aspects:

i. Numerical buckling curves, determined using geometrically and materially non-linear (GMNIA) finite element calculations, were compared to the buckling curves found in the code (Rebelo et al. 2008; Snijder et al. 2008). Depending on the studied section and load case, more or less large discrepancies between the numerical and the code curve were thereby found to exist. This is exemplified by the buckling curves shown in Fig 6-3, where GMNIA buckling curves obtained for the "model beam" and eigenmode-conform geometric imperfections are compared to the applicable "general case" and "specific case" EC3 curves.

ii. The discrepancies between numerical and code buckling curves were sometimes found to lie on the "unconservative" side, see Fig 6-3a, resulting in numerically determined buckling reduction factors that are lower than the code value. This was more frequently found to be the case for the "specific case" (SC) than for the "general case" (GC) curves of EC3. While it is not correct to regard this as a safety issue, it nevertheless led to an on-going debate about the appropriate partial safety factor to be adopted for each of the cases (Rebelo et al. 2008).
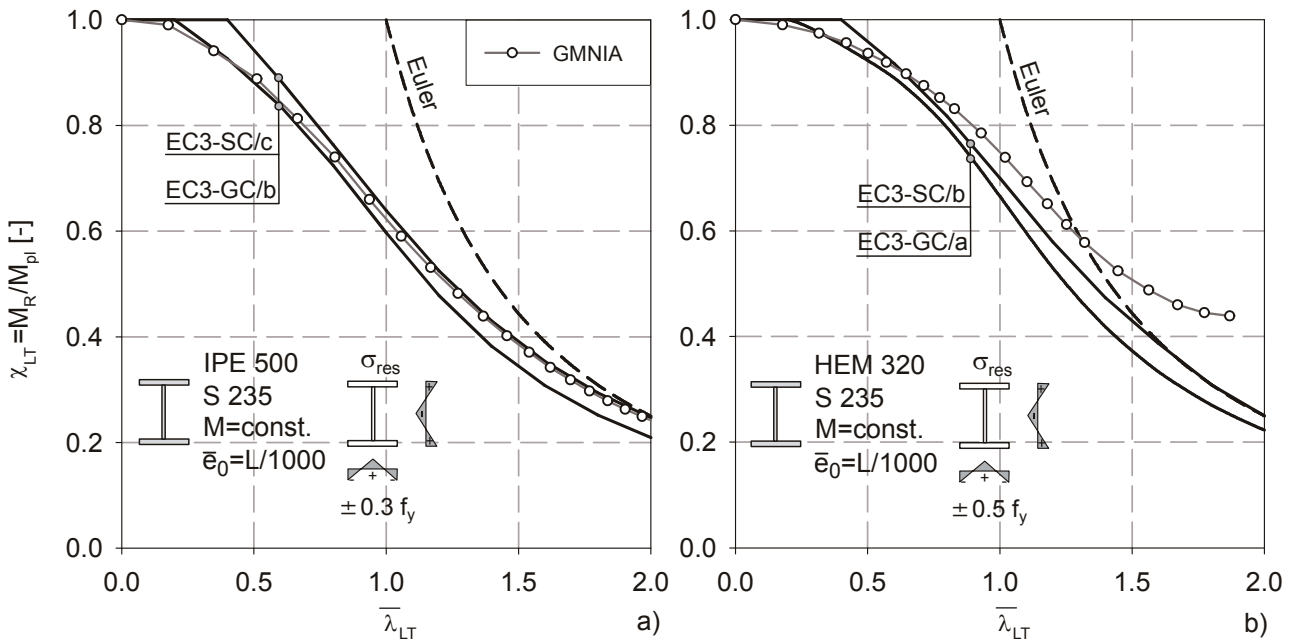
Fig 6-3 *Numerical buckling curves for an IPE 500 (a) and HEM320 (b) section compared to EC3 curves.*

iii. The plot of the numerical buckling curve in Fig 6-3b explains another point that has been raised: the grouping of the properties of the sections is based purely on the depth-to-width ratio h/b, which is but a proxy representation of a variety of effects (torsional stiffness, behavior in plasticity). This grouping often fails to represent the actual behaviour of a certain section in a satisfactory way. In the case of the HEM320 section in Fig 6-3b, even the "less safe-sided" specific case curve of EC3 fails to accurately represent the high resistance of such a stocky section. Quite generally, a very large scatter of the position of the numerical buckling curves in the χ-$\bar{\lambda}$ plane can be observed.

iv. As is also illustrated in Fig 6-3b, the numerical calculations show a post-critical capacity of stocky sections that, albeit being present only for lengths that exceed the practical range, is interesting from a theoretical point of view, see 6.5.3, as well as (Taras & Greiner, 2008b).

v. Some recent studies have focused their criticism of current LT buckling design rules on the perceived lack of consistency with other member buckling cases (columns) and have envisaged the development of a common "family" of buckling curves for all buckling phenomena (Sedlacek & Müller, 2006). In this context, much effort is currently being placed on the development of a "general method" for the stability design of members and whole structures (Stangenberg 2007; Naumes et al. 2008), whereby a "general" slenderness is used and the stability check of a structure is carried out through the application of a single buckling reduction factor χ. In this design philosophy, the LT buckling case merely represents a very special case, albeit a very important one.

In addressing the issues raised in the first four points, the study presented in this chapter acknowledges the need for increased consistency in the design rules for different member buckling cases and makes use of some ideas that were suggested for the "general method", although a different design philosophy is advocated here in the last resort. This philosophy is traditionally based on a careful design against stability of single elements and members, rather than on an all-inclusive, single check of entire structural systems.

In order to achieve these objectives, the steps of a "consistent" development of buckling rules presented in chapter 3 must be followed, whereby special attention is paid to keeping consistency with the "benchmark" case of column buckling. Accordingly, the next step must consist in an identification of the parameters dominating the studied buckling phenomenon, which is carried out using numerical tools.

6.4. Numerical studies – general remarks

The numerical studies have been carried out using the methodology described in chapter 3 for shell element models. Beyond the general assumptions and modelling techniques described in that section, the following assumptions were made in all numerical calculations of this chapter, see Fig 3-1:

i. Only single-span members with in-plane, out-of-plane and torsional restraints at the supports ("end fork") were considered.

ii. In most calculations, and if not stated otherwise, the basic load case with constant bending moment over the member's length was considered. A specific subsection is dedicated to the expansion of the findings for this basic load case to other load cases. The loads are applied as end moments or point loads, whereby the modelling techniques for the load introduction follow what is stated in chapter 3.

iii. If not stated otherwise, all calculations are carried out for steel grade S235. In order to compare the findings to a different steel grade that is as "different" as possible from S235, yet still just within the range of applicability of slender beams, some calculations were carried out for S460. Strain hardening was considered, using the material model as shown in Fig 6-4.

iv. The geometric imperfections were generally assumed to be proportional to the *buckling eigenmode of the studied case*, unless it is specifically stated that other imperfection shapes were assumed; in the latter case, purely lateral or purely torsional imperfections were studied.

residual stress distributions
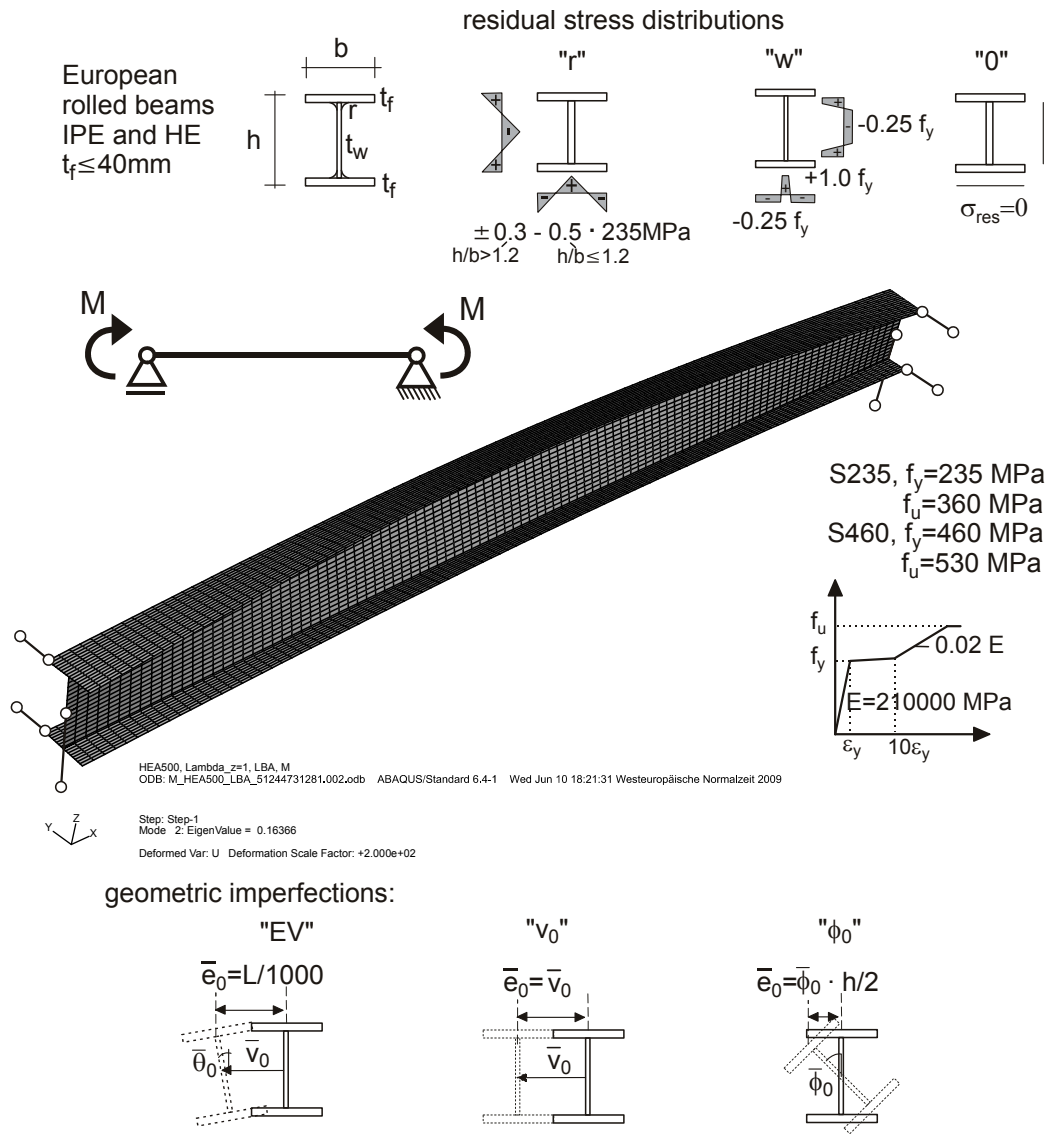
Fig 6-4   Overview of the FEM modelling techniques and assumptions.

v.   The residual stresses were assumed to vary linearly over the single cross-sectional components. Both in the case of hot-rolled and welded members, the common assumptions as recommended in the ECCS recommendations (1984) were followed.

6.5. Preliminary Parametric Study

In this section, the influence of certain, specific structural parameters is studied by means of numerical GMNIA calculations in order to identify their impact on the LT buckling resistance of a section both in terms of absolute strength and in terms of the shape of a buckling curve.

6.5.1. Geometrical imperfections: shape and amplitude

As for other buckling phenomena, the shape and amplitude of initial geometrical imperfections is relevant to the ultimate LT buckling resistance of a member. Fig 6-5 shows numerical buckling curves for the case of a single span IPE 240 section under constant bending moment. Thereby, Fig

6-5a shows the influence of the chosen imperfection amplitude in the case of an imperfection shape that is affine to the first LT buckling eigenmode. Three curves are shown for length-proportional amplitudes $\overline{e}_0$ equal to L/2000, L/1000 and L/500. The largest differences in absolute buckling strength (as percentage of the plastic moment resistance of the section) is present in the region of intermediate slenderness (around $\overline{\lambda}_{LT}=1.0$); at this slenderness, the numerical buckling reduction factors are χ_{LT}=0.697, 0.660, 0.616, respectively.
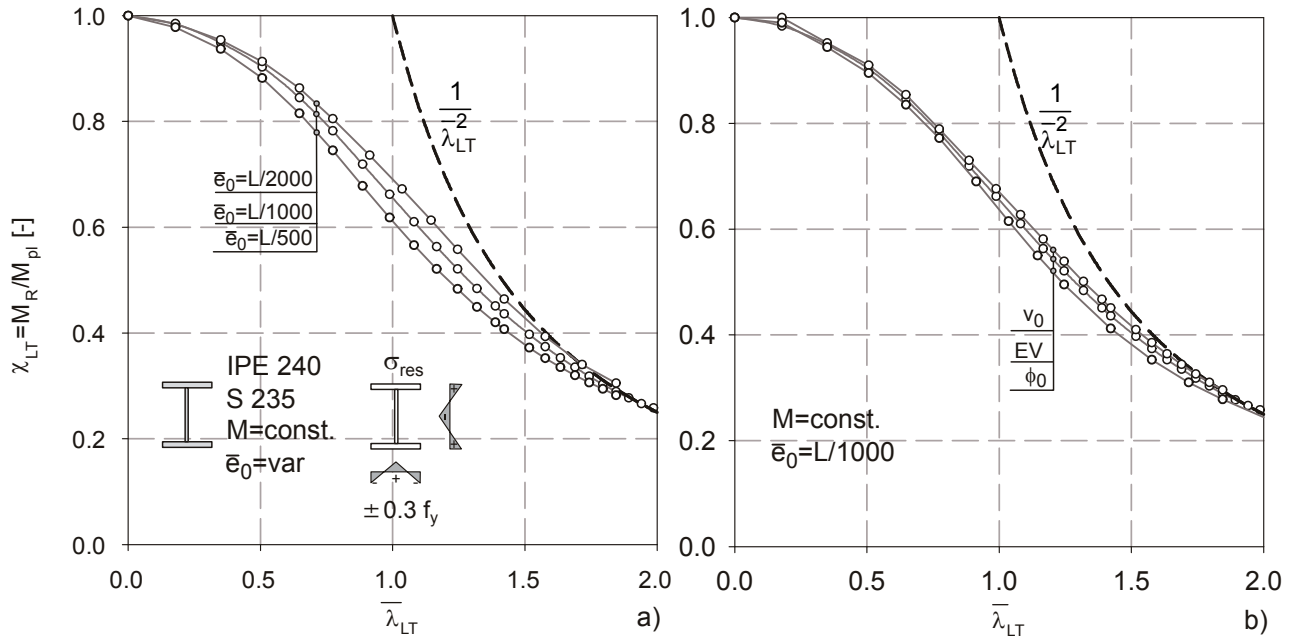
Fig 6-5 *Influence of the imperfection amplitude (a) and shape (b) on numerical LT-buckling curves.*

The largest relative differences (in terms of percentage points) between the three buckling curves are reached at a somewhat higher slenderness range of around $\overline{\lambda}_{LT}=1.2$. The difference between the central line for $\overline{e}_0$=L/1000 and the other two lines just exceeds 8% as a maximum value of discrepancy.

Fig 6-5b shows numerical buckling curves resulting from different assumptions regarding the shape of the initial imperfection. Again for a single span IPE 240 under constant bending moment, 3 different shapes (with constant amplitude $\overline{e}_0$=L/1000) are considered: "v_0" with a sinusoidal lateral deformation equal to the weak-axis flexural buckling eigenmode; "EV" affine to the first LT buckling eigenmode; and "ϕ_0" equal to a merely rotational initial deformation, equal to the first eigenmode for torsional buckling, with no out-of-straightness of the section's centroid. As the figure shows, the influence of the shape is not very pronounced in the given load case; the purely lateral shape of imperfection, leading to the highest values of buckling resistance, lies less than 3% above the line corresponding to an eigenmode-conform imperfection up to $\overline{\lambda}_{LT}=1.5$, and 7% above the lowest line corresponding to a purely rotational imperfection.
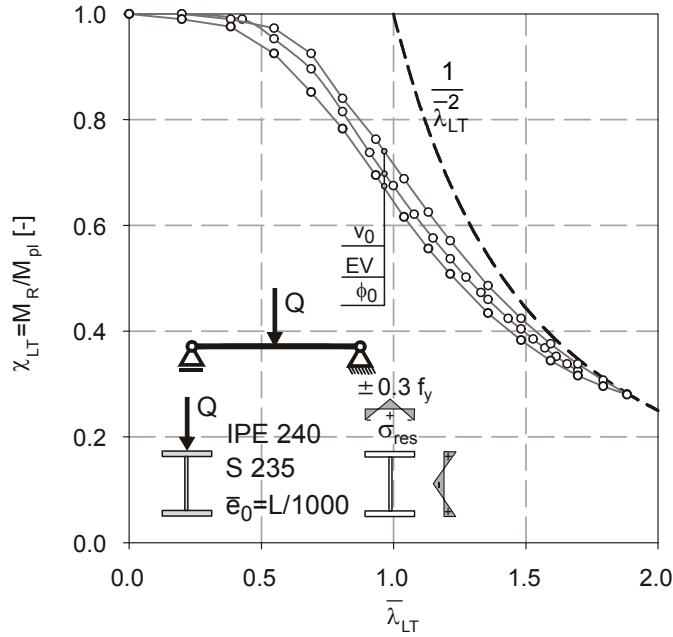
Fig 6-6 *Influence of the imperfection shape – load case "Q", concentrated load at mid-span, top flange*

This explains why relatively little importance was given to the actual shape of the imperfection assumed for numerical calculations that led to the current Eurocode 3 LT buckling curves for the "specific case" of hot-rolled I- & H sections (Greiner et al 2000). For those calculations, a purely lateral out-of-straightness was chosen.

An additional figure, Fig 6-6, points out that the above statements regarding the low influence of the shape of buckling curve do not entirely hold their validity when other load cases are looked at. This figure again shows numerical buckling curves for the three different shapes of imperfection described above, but for a different load case: the case of a concentrated load "Q" at mid-span of an IPE 240 section, and acting on the upper flange. As is illustrated in the figure, the difference between the resulting buckling reduction factors χ_{LT} is larger in this case, being quantitatively comparable to the differences discussed for Fig 6-5a. This is explicable in light of the higher "driving" force of the torsional deformation for this load case, since in the case of the "EV" and "ϕ_0" imperfections a first-order torsional moment is present due to the eccentricity of the load with respect to the shear centre in the imperfect configuration.

6.5.2. Residual stresses: amplitude and distribution

The influence of the amplitude and distribution of residual stresses has been studied extensively for the case of flexural buckling. In these studies, the amplitudes and distributions of residual stresses found to be typical for welded I- & H-sections were shown to lead to significantly lower buckling coefficients χ_{LT} than e.g. the case of hot-rolled beams. Similar effects can be observed when analyzing the LT buckling case; this is illustrated in Fig 6-7 and discussed thereafter.
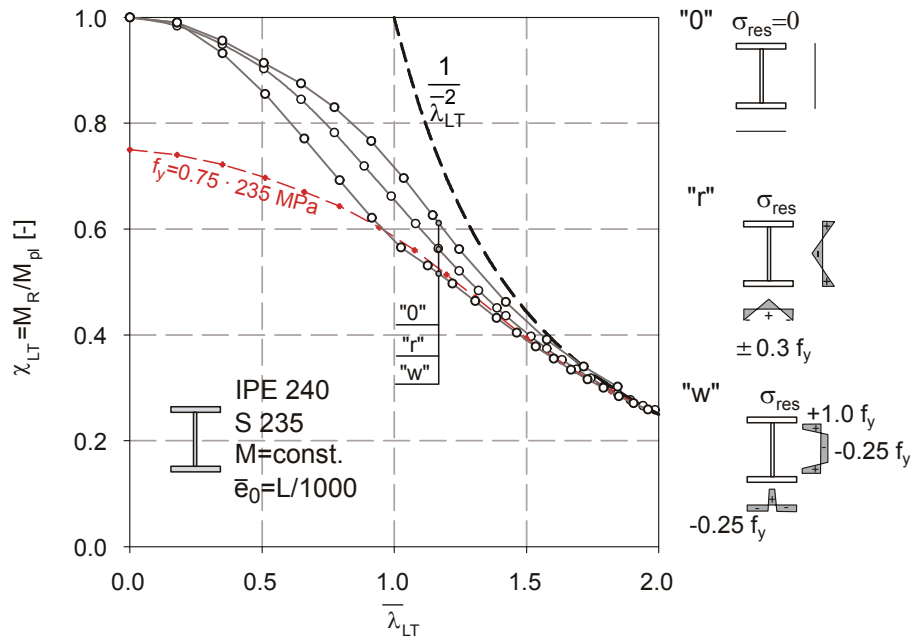
Fig 6-7   *Numerical buckling curves resulting from different assumption reg. residual stresses.*

The figure shows three different numerical buckling curves, calculated for the same IPE 240 section for the M=constant load case and the same, eigenmode-conform imperfection shape and amplitude. The difference between the three lines is represented by the assumptions regarding the residual stresses, whereby "0" denotes the curve for no residual stress at all, "r" for the pattern considered to be typical for hot-rolled beams of this series, and "w" for the distribution of residual stresses typically assumed for welded sections in accordance with the ECCS (1984) recommendation. The figure shows that the assumed residual stresses result in marked differences in the position of the buckling curves of more than 15% between the upper and lower lines in the region of maximum discrepancy, around $\bar{\lambda}_{LT}$ =1.0.

A remarkable feature of the numerical buckling curve for welded sections has already been discussed in the ECCS TC8 report that presents the background to the "specific case" LT buckling curves of Eurocode 3 (Greiner et al 2000): the curve's marked bend at approximately $\bar{\lambda}_{LT}$ =1.0, which is a unique feature of the residual stress distribution assumed to result from welding. In this report, it was pointed out that, after the bend at $\bar{\lambda}_{LT}$ =1.0, the curve matches very well with the one resulting from a calculation for an IPE240 with a yield stress of f_y=0.75 · $f_{y,nom,S235}$= 176.25 MPa and no residual stresses, and plotted over the values of $\bar{\lambda}_{LT}$ and χ_{LT} that relate to the plastic moment capacity of a S235 section. The drop in yield stress of 0.25 times the nominal value $f_{y,nom}$ is equal to the almost constant compressive residual stress assumed to be present in the flanges. The fact that the red line for f_y=0.75 · 235 MPa matches the "w" line at high slenderness indicates that the assumed, almost constant distribution of residual stresses in the "w" case is quite disadvantageous at slenderness ranges around $\bar{\lambda}_{LT}$ =1.0, since it appears to be *equivalent to a drop of the yield strength by 25%.* This is vastly more severe than the bi-linear distribution usually

assumed for hot-rolled sections, even though the amplitude of the maximum compressive stress at the flange's exterior edge is larger in this case.

In reality (see already Brozzetti et alt., 1971), the stress distribution in welded sections depends on a variety of different parameters, among them the fabrication / cutting method for the flange plate itself (rolled plate vs. oxyflame-cut...). Many common welding and cutting processes can cause residual stress distributions in flange plates that are far more beneficial than the one assumed in Fig 6-7, case "w". Considering the wide range of parameters that influence the amplitude and distribution of residual stresses around welded joints, it would therefore certainly be worthwhile to re-assess the representativeness of this distribution.

6.5.3. Section series

The fact that the section series, or more generally the cross-sectional geometry, influences the shape of the LT buckling curve has already been discussed in section 6.3 and will be at the centre of the considerations made in the remainder of this chapter. Fig 6-8 shall therefore merely serve as additional, exemplary evidence of the influence of cross-sectional geometry on LT buckling curves.
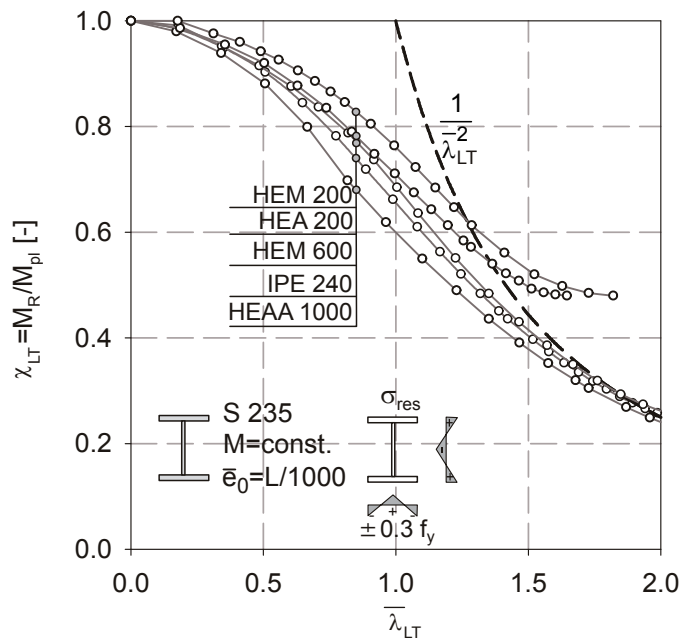
Fig 6-8 *Numerical LT buckling curves for different hot-rolled beams.*

What should be particularly appreciated already at this point is the relatively poor representativeness of the current classification of sections with regard to depth-to-width ratios h/b. The figure shows two sections with widely different h/b ratios, an HEA 200 (h/b=0.95) and an HEM 600 (h/b=2.03), to lead to very similar buckling reduction factors χ_{LT} at least up to $\overline{\lambda}_{LT}$ =1.0, which corresponds to lengths close to the limit of practical application for both these sections. Conversely, two sections with almost identical h/b ratio (again the HEM 600 and IPE 240 with h/b=2.0) have buckling curves that, albeit being close, are farther apart than the HEA 200 and HEM

600 curves, with the section with the (slightly) lower value of h/b actually having a lower-lying buckling curve. Only very deep sections such as the HEAA 1000 (h/b=3.23) clearly show a tendency towards lower buckling curves. The relatively poor describing quality of the depth-to-width ratio has recently also been criticized by Beier-Tertel (2009), who proposed to use the parameter I_y/I_T instead of h/b, arguing that this factor is better able to reflect the significance of a section's torsional stiffness.

Another interesting aspect of the buckling curves in Fig 6-8 is represented by the tendency of the stockier sections to exceed the Euler critical buckling moment M_{cr} (indicated by the hyperbola $1/\overline{\lambda}_{LT}^2$) at high slenderness. In order to understand this "post-critical" load-carrying mechanism, it is necessary to take a look at the load-deformation plots, see Fig 6-9.
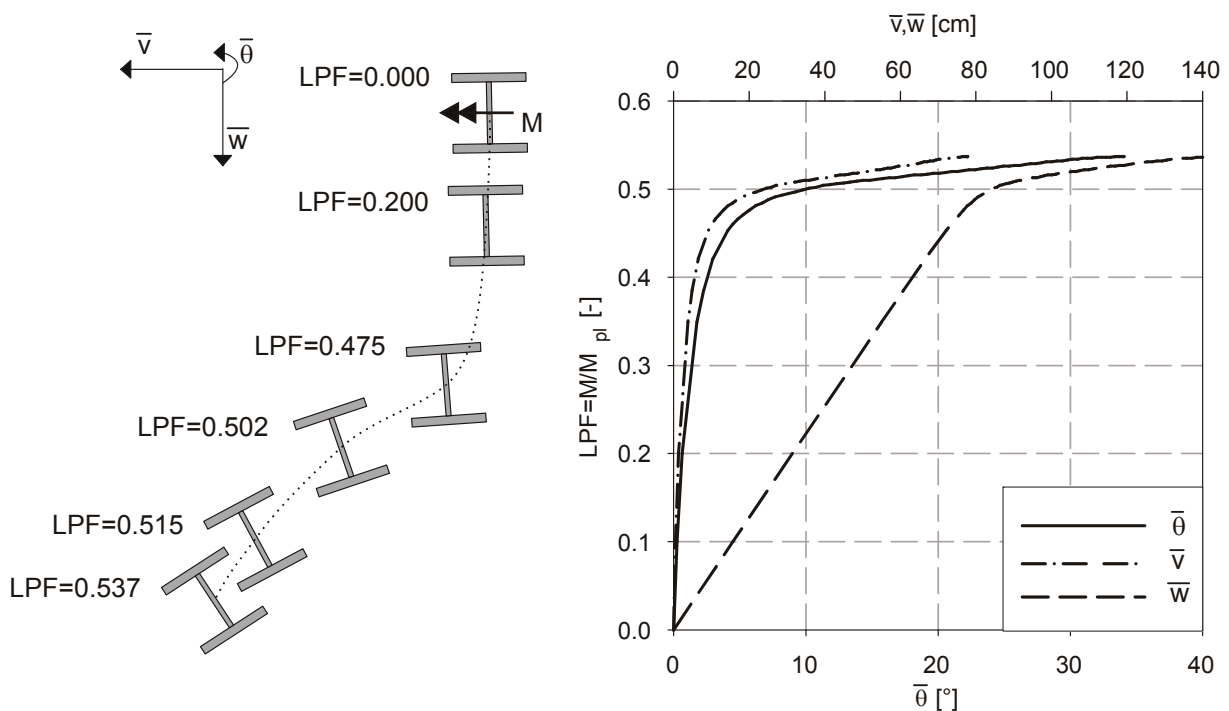
Fig 6-9 *Load-deformation paths for an HEM section with $\overline{\lambda}_z = 6.60$, L=32.68 [m].*

The right-hand plot in Fig 6-9 shows the lateral and vertical deformations $\overline{v}$ and $\overline{w}$ at mid-span, as well as the cross-sectional rotation $\overline{\theta}$ at this position, plotted over the load proportionality factor LPF=M/M$_{pl}$, for a member with $\overline{\lambda}_z$=6.60 and a physical length of 32.68 m. The left-hand side of the figure shows the calculated path of deformation, plotted with a deformation scale factor of 1.0. The usual geometrical imperfections were assumed, which follow the shape of the eigenmode and have an amplitude of $\overline{e}_0$=L/1000. The figure illustrates that, for a member of this extreme length and with the given compact cross-section, very large deformations occur before the ultimate load is reached. Special attention should be paid to the calculated cross-sectional rotation at the ultimate load: this rotation reaches a value of 34°. At this stage of deformation, the cross-sectional strength for bending about the weak axis becomes relevant. With increasing length of the member, the ultimate cross-sectional rotation increases even further: eventually, the cross-section at mid-span

rotates so much that the external bending moment – which, at the end supports, is still applied about the strong axis- acts about the weak axis on this cross-section. Therefore, it can be shown that the numerical GMNIA buckling curve for this specific case asymptotically approaches the ratio $M_{pl,z}/M_{pl,y}$, which for this profile is calculated to 0.478.

This behaviour is only explicable by the large-deformations theory and can therefore not be included in the analytical, second-order formulation proposed in section 6.7. This should however not be considered as a limitation of the practical applicability of the equations presented in that section, as members of such extreme slenderness are not of any practical relevance.

6.5.4. Steel grade

The influence of the steel grade on the buckling strength and buckling reduction factor for the case of flexural column buckling has already been treated by Schulz (1968) and has more recently been subjected to renewed scrutiny by Wolf (2006). In terms of buckling reduction factors χ, numerical curves for two different steel grades were shown to be (practically) identical if two conditions are fulfilled: (a) the residual stresses have the same distribution and are proportional to the yield strength (this includes the case were they are zero), and (b) the amplitude of the geometrical imperfection is assumed to be proportional to the dimensionless slenderness $\bar{\lambda}$, instead of length or the geometrical slenderness λ. Wolf showed that the latter factor has a relatively small influence, leading to values of χ for S355 lying not more than 3% above the values for S235. Whether or not the residual stresses are proportional to the yield stress, on the other hand, was shown to have a larger impact (above 10% for S355/S235 around $\bar{\lambda}=1.0$) in the flexural buckling case.
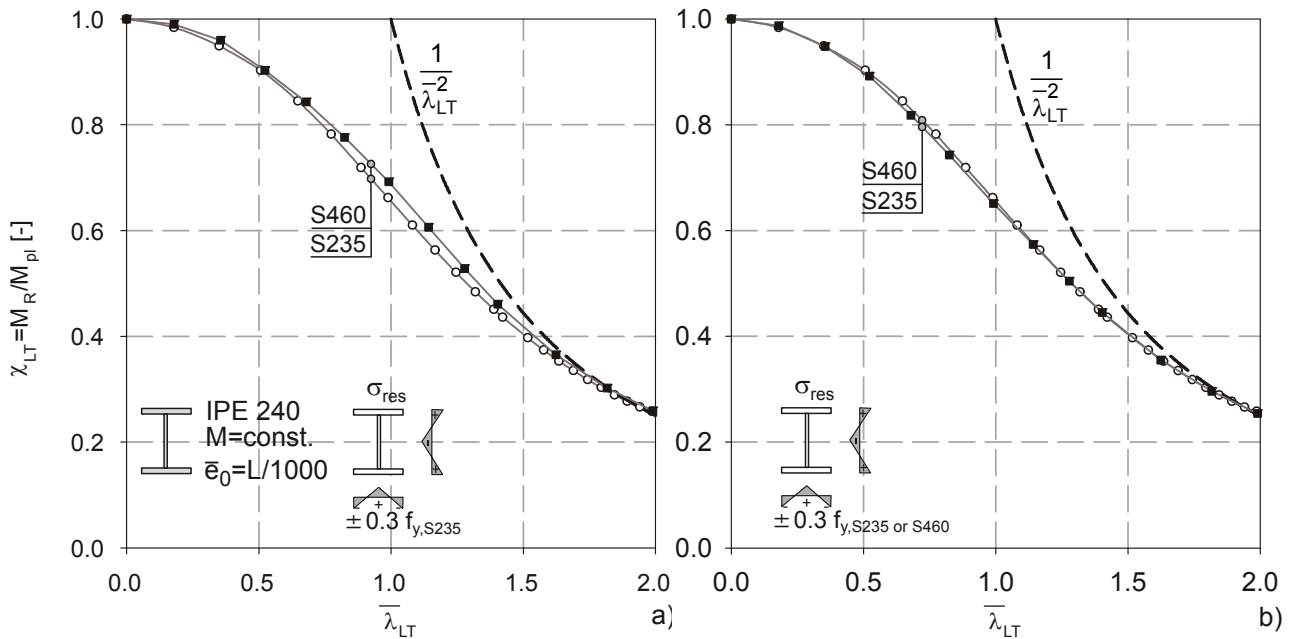
Fig 6-10 *Numerical LT buckling curves – influence of steel grade; with fixed residual stress amplitude (a) and with residual stress proportional to the yield stress (b)*

Fig 6-10 shows the influence of the assumed proportionality of the residual stresses on the buckling curves for two different steel grades for the LT buckling case under constant amplitude, again for an IPE 240. The curves in Fig 6-10a were calculated considering a fixed maximum amplitude of the residual stresses of 0.3 times 235 MPa, while the curves in Fig 6-10b are based on the assumption that the residual stress amplitude is proportional to the yield stress. The figures illustrate that the influence of the yield stress on the resulting factor χ_{LT} is relatively small, being practically non-existent in the proportional residual stress case, and nowhere larger than 6% in the case of fixed residual stresses. As for other structural parameters, the maximum influence is observed around $\overline{\lambda}_{LT} = 1.0$.

The following figure, Fig 6-11, serves the purpose of bringing to attention an aspect that is of particular interest in the context of statistical evaluations of test data and reliability analyses: the decreasing influence of the yield stress on the buckling strength with increasing member length.
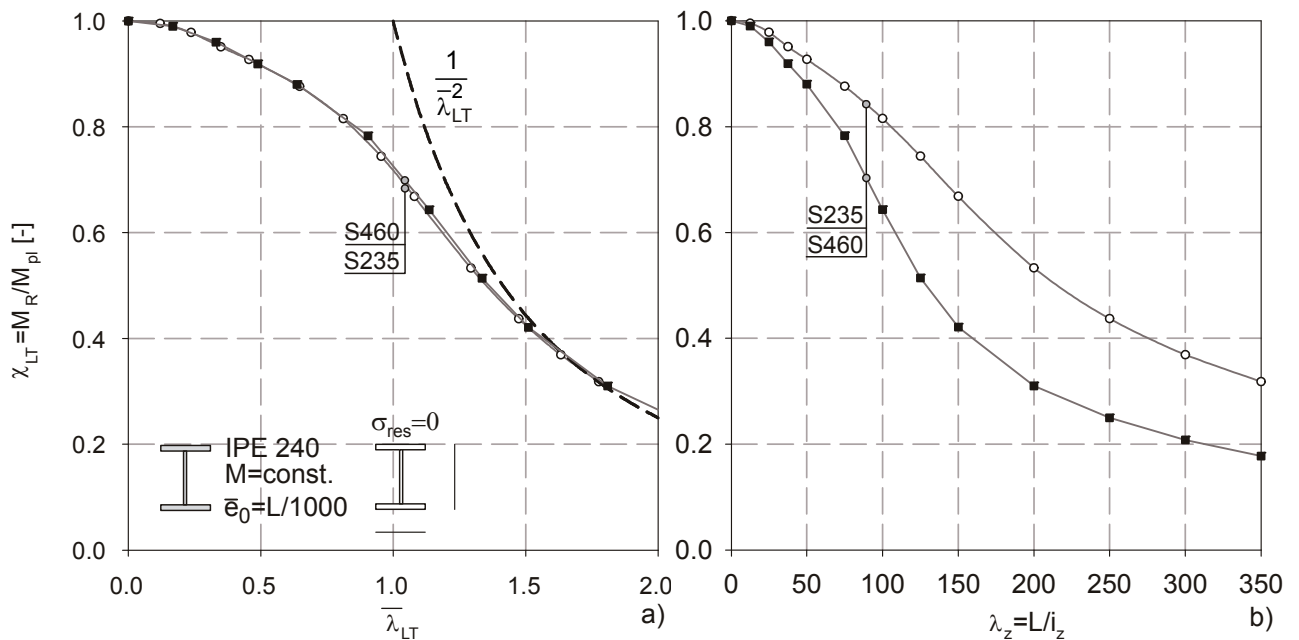
Fig 6-11 *Influence of steel grade without residual stresses – plotted over $\overline{\lambda}_{LT}$ (a) and λ_z (b)*

Thereby, the diagram in Fig 6-11a again shows that the yield strength per se has almost no influence on the position of a buckling curve in terms of χ_{LT}, shown here for the case of an IPE 240 with no residual stresses. Fig 6-11b, on the other hand, plots χ_{LT} over the geometrical slenderness λ_z; this quantity is of course proportional to the physical length of the member, and each value represents a certain member length independently of the the steel grade - while $\overline{\lambda}_{LT}$ does not. While this is trivial and might appear to be irrelevant, it is relevant to the determination of which parameters can be considered to be "independent" - and which ones cannot- for the purposes of a statistical reliability analysis. King (2009) pointed out that the ultimate LT buckling strength M_R of a beam is a function of f_y^{α}, whereby α is an exponent ranging from 1 at very low slenderness to 0 at very high slenderness.

If we acknowledge that χ_{LT}, as function of $\overline{\lambda}_{LT}$, is independent of the steel grade, and if we know the buckling strength $M_{R,S235}$ for the (arbitrarily chosen) steel grade S235, we can write M_{R,f_y} for any other steel grade with a yield strength f_y as follows:

$$M_{R,f_y} = M_{R,S235} \cdot \left(\frac{f_y}{f_{y,S235}} \right)^{\alpha} \tag{6.11}$$

With $M_{R,S235} = \chi_{LT,S235}(L) \cdot W_{pl} \cdot f_{y,S235}$

For a fixed set of geometrical and structural imperfections, and a certain load case, the independent variables of the problem are thus:

i. the member length L – contained in $\chi_{LT,S235}$, which is of a function of L.
ii. the cross-sectional geometry – contained both in $\chi_{LT,S235}$ for the reference steel grade and in W_{pl} (see section 6.5.5).
iii. the steel grade, represented by its yield stress f_y.

The dimensionless buckling reduction factor χ_{LT} for a discretionary steel grade is thus, by itself, *not an independent variable*, as it depends on all of the above variables; it is therefore *not possible* to separate the scatter of χ_{LT} from the scatter of any of the above variables (compare Rebelo et al., 2009). By solving equation (6.11) for α, we obtain equation (6.12).

$$\alpha = \frac{\ln \left(M_{R,f_y} / M_{R,S235} \right)}{\ln \left(f_y / f_{y,S235} \right)} \tag{6.12}$$

In Fig 6-12, the factor α for the example given above is plotted on the right-side axis, along with the resistance M_R for the two steel grades shown in Fig 6-11, but normalized in both cases to the plastic moment capacity of a S235 section (plotted on the vertical axis on the left). This representation is much better suited than the one given in Fig 6-11 to illustrate the swift decrease of influence of the yield stress on buckling strength with increasing member length.

It should be noted that this behaviour attains particular relevance not as much due to the difference in yield stress between two different steel grades, but much rather due to the wide scatter of the yield stress *within* a certain (nominal) steel grade: while this scatter dominates the total scatter of the buckling strength at low slenderness ratios, it does not influence the total scatter at all at a very high slenderness. This is visually very well expressed by the course of the curve representing α in Fig 6-12.
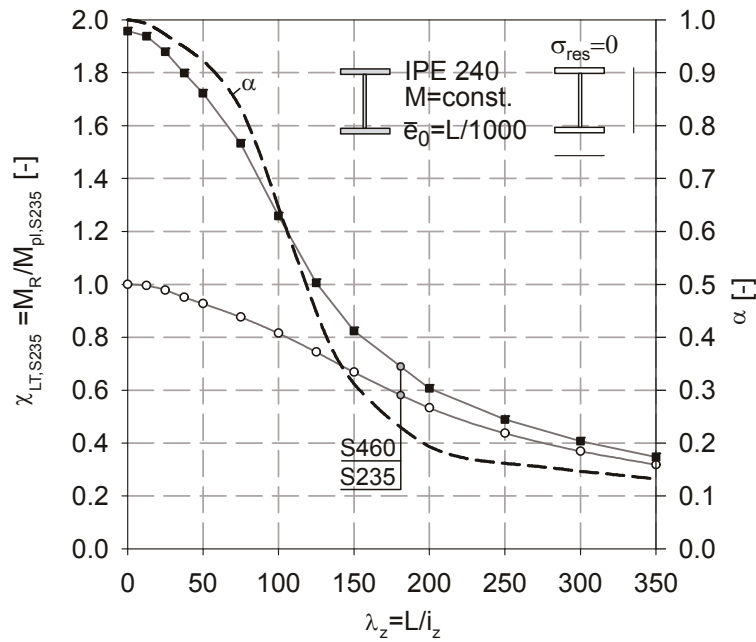
Fig 6-12 *LT buckling strength for S460 and S235 as fraction of the sectional moment capacity for S235 (left axis); Exponent α (right axis).*

6.5.5. Cross-sectional shape tolerances

The manufacturing process of steel members –whether they are rolled, welded or otherwise assembled- must allow for certain geometrical tolerances, i.e. deviations of the actual shape of the cross-section from the nominal one. For the IPE 240 studied in all the examples so far, the allowable deviations of depth, width and thickness are given in EN 10034 (1993) and reported in the following table:

	nominal value [mm]	tolerance max/min [mm]
section depth h	240	+4.0 / -2.0
section width b	120	+4.0 / -2.0
flange thickness	9.8	+2.0 / -1.0
web thickness	6.2	± 0.7

Table 6-2 *Nominal value and maximum permissible shape deviations for an IPE 240 section according to EN 10034 (1993)*

Due to the manufacturing process of hot-rolled I-section, the fillet radius itself is basically constant in all cases, thus no tolerance is specified in the code. Other tolerances refer to total weight and the out-of-straightness of the both cross-section; these are not taken into further consideration in the following.
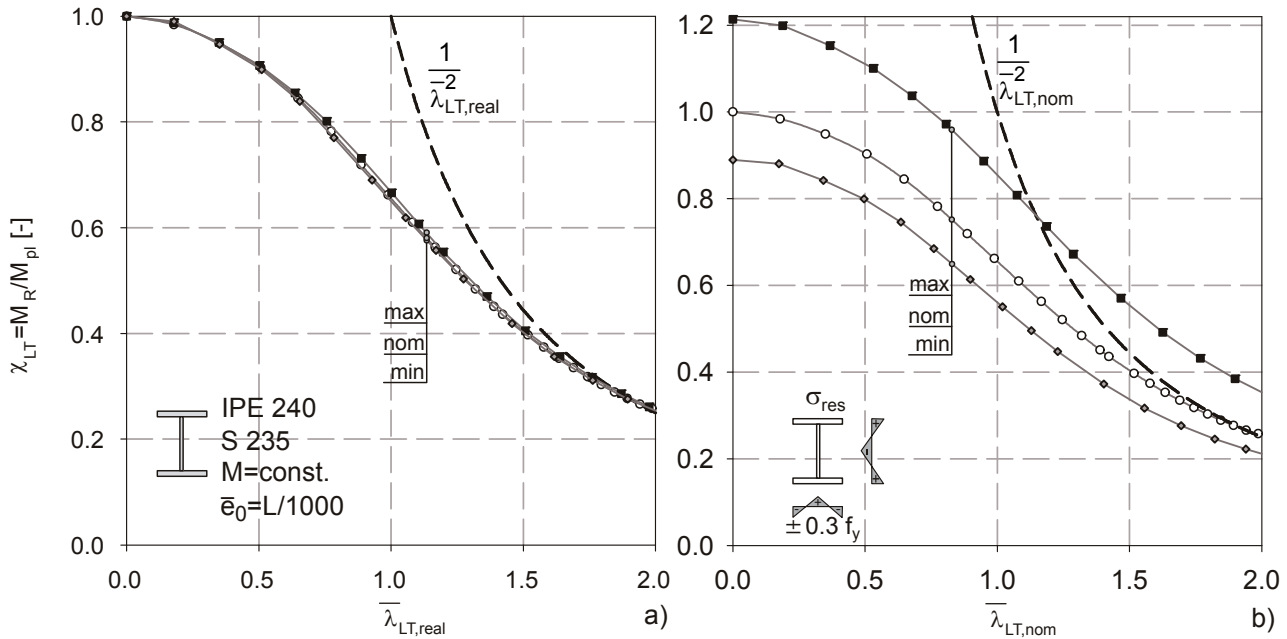
Fig 6-13 *Influence of the cross-sectional shape deviations on the LT buckling strength in relative (a) and absolute terms (b).*

The above figure, Fig 6-13, illustrates the impact that the tolerances have on the shape of the buckling curve. Thereby, plot (a) shows the value of the buckling reduction factor χ_{LT} related to the "real" moment capacity, and plotted over the "real" value of $\overline{\lambda}_{LT}$, both calculated with the "maximum", "nominal" and "minimum" cross-sectional dimensions; the "maximum" cross-section has a depth of 244 mm, a width of 124 mm, a flange thickness of 11.8 mm and a web thickness of 6.9 mm, and the "minimum" cross-section is determined accordingly. As the figure shows, the deviations from the nominal size represented by the cross-sectional tolerances are not large enough to significantly alter the shape of this "real" buckling curve; a comparison with Fig 6-8 thereby helps explaining why there is any difference between the curves at all.

What is perhaps more interesting to notice is the buckling strength in absolute terms, shown in figure Fig 6-13b in terms of χ_{LT} as reduction factor of the nominal section moment capacity, plotted over the nominal value of $\overline{\lambda}_{LT}$. The figure gives a clear indication of the large scatter of buckling stress (for any given length, respectively value of $\overline{\lambda}_{LT,nom}$) that can be caused by deviations of the cross-sectional geometry. As a matter of fact, the influence of the geometry, while slightly decreasing with increasing slenderness (length) in terms of $\chi_{LT,nom}$, actually increases with slenderness in relative terms. For example, at $\overline{\lambda}_{LT,nom} = 0.0$ an IPE 240 section made of S235, with the "maximum" cross-section geometrical parameters within tolerance, has a moment capacity approximately 21% higher than a "nominal" section; at $\overline{\lambda}_{LT,nom} = 2.0$, this ratio reaches 40%, and the difference between the LT buckling moment capacity of the "minimum" and "maximum" section exceeds 80%. It is clear that –especially in the high slenderness range, where the yield stress's scatter was shown to be of secondary importance- the cross-sectional geometry will be paramount to the total scatter of the buckling strength.

6.5.6. Fillet radius

A question often raised in the context of the determination of numerical buckling curves is whether or not a curve for a certain hot-rolled beam is correctly determined even if the fillet radius is omitted. This question is of practical relevance, rather than theoretical, because modelling the fillet with beam- or shell elements is not entirely straight-forward – see chapter 3. In the numerical calculations that underpin the current Eurocode LT and combined N+M buckling provisions, the fillet radius was generally omitted. This has sometimes been criticized. A justification by means of an example calculation has already been given by Kaim (2004). Here, a similar example –but for a different section- is shown, see Fig 6-14. The plot shows that the difference in terms of buckling curves between an IPE240 with the nominal fillet radius (r=15mm) and without (r=0 mm) is indeed small – provided of course that χ_{LT}, M_{pl} and $\overline{\lambda}_{LT}$ are calculated for the corresponding cross-section. However, if the goal of a calculation is to determine the LT buckling strength in terms of M_R, the fillet must be included, as it has a significant impact in this case. For an IPE 240, the cross-sectional plastic moment capacity M_{pl} is ca. 6% higher with fillet radius than without. The M=const. LT-buckling strength M_R of an IPE 240 beam of 3500 mm of length is ca. 10% higher with fillet when compared to the case with r=0. However, the slenderness $\overline{\lambda}_{LT}$ for these two cases is also different, being slightly higher in the case of r=0; in order to have the same value of $\overline{\lambda}_{LT}$, two beams with or without fillet must have different length. As the figure shows, this results in differences in terms of χ_{LT} as low as 2.5% in the given case.

In summary, it can be said that the omission of the fillet radius is justified if only the shape of the buckling curve is studied, while it is obviously not justified if the buckling strength in absolute terms is of interest. The criticism sometimes directed at the omission of the fillet in numerical calculations thus seems to stem more from a misunderstanding of the aims of a certain calculation, rather than an actual questioning of the simple mechanical relationships discussed in this section.
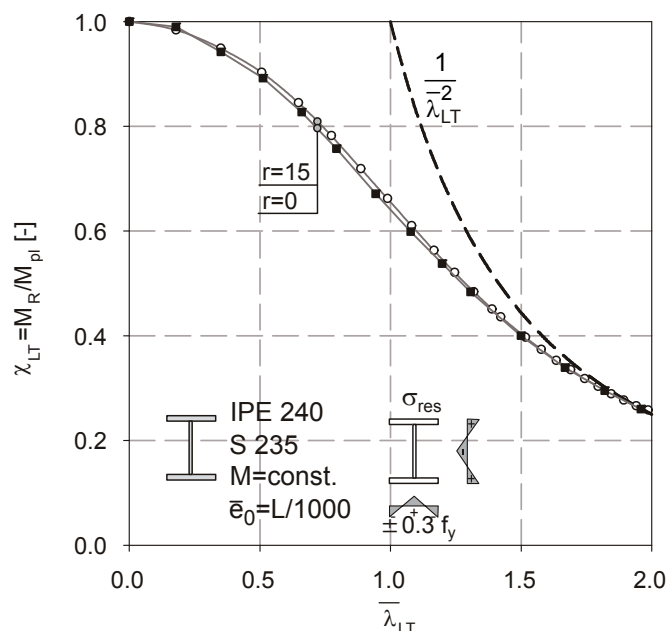
Fig 6-14 *Influence of the omission of the fillet on the shape of the buckling curve.*

6.6. Numerical buckling curves with nominal input parameters

In order to obtain buckling rules that are consistent with and comparable to the ones for the "benchmark case" of flexural column buckling for LT buckling, the procedure during the development of the column buckling curves must be followed. In practical terms, the first step thus consists in the determination of numerical (GMNIA) buckling curves that are based on the "model beam" assumptions of Beer & Schulz / ECCS: nominal geometric and material input parameters, and "fixed" imperfection amplitude coefficients.

The residual stresses were assumed to vary linearly over the single cross-section components, following the provisions given in the ECCS recommendation (1984). Accordingly, a distinction was made between hot-rolled beams with a depth-to-width ratio of h/b≤1.2 and sections with h/b>1.2, see Fig 3-1. The magnitude of residual stress thus depends on the type of rolled cross-section and is expressed as a fraction of the yield strength f_y of mild steel S235. Strain hardening was included in the calculations, also in accordance with the ECCS recommendation. All calculations were conducted for steel grade S235, assuming a yield strength of f_y=235 N/mm².
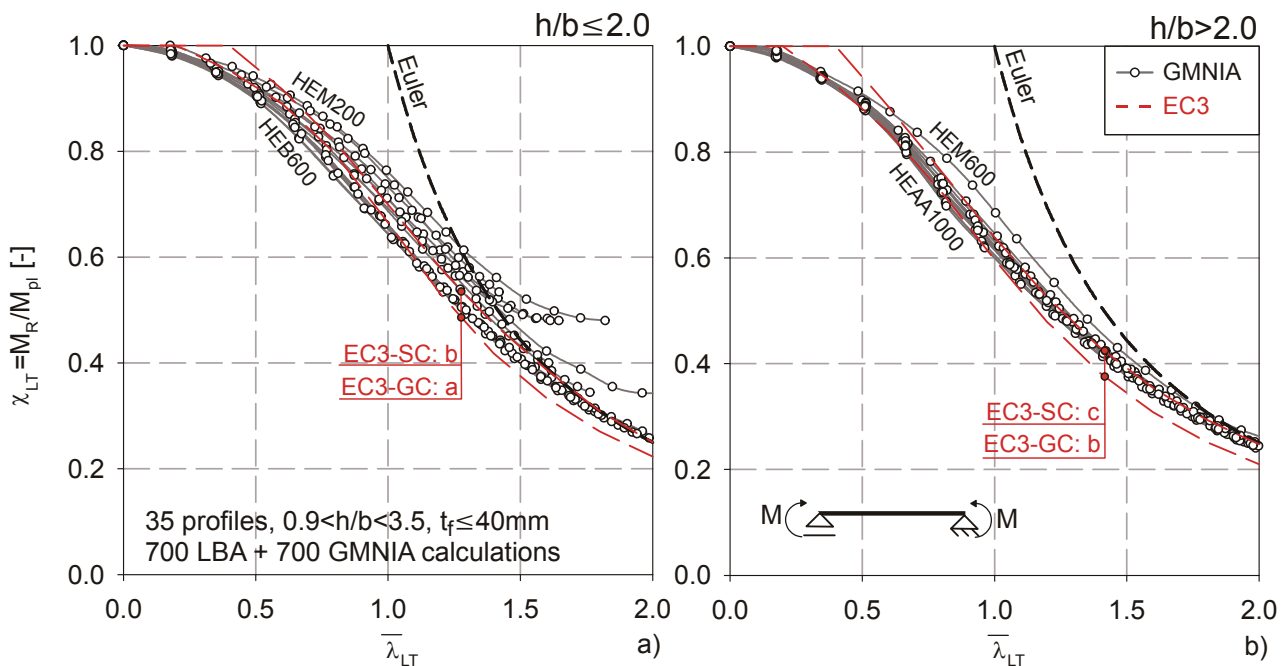
Fig 6-15 *Numerical LT buckling curves for hot-rolled sections of steel grade S235, compared with Eurocode 3 "general" and "special case" curves; h/b≤2.0 (a); h/b>2.0 (b).*

The results of these calculations for hot-rolled sections are shown in Fig 6-15 and compared to the current Eurocode design curves. The figure illustrates what has been stated in the introduction, i.e. that the rather coarse grouping of the properties of the sections according to the depth-to-width ratio h/b can only accurately describe but a few of the sections by one single buckling curve.

Fig 6-16 shows numerical buckling curves valid for welded cross-sections, whereby cross-section geometries almost equal to rolled sections (from HEA 200 to HEA 1000), but without fillet radius, were studied. For these sections, the lack of a "general" accuracy (for all section geometries) of the current design provisions seems to be even more severe.
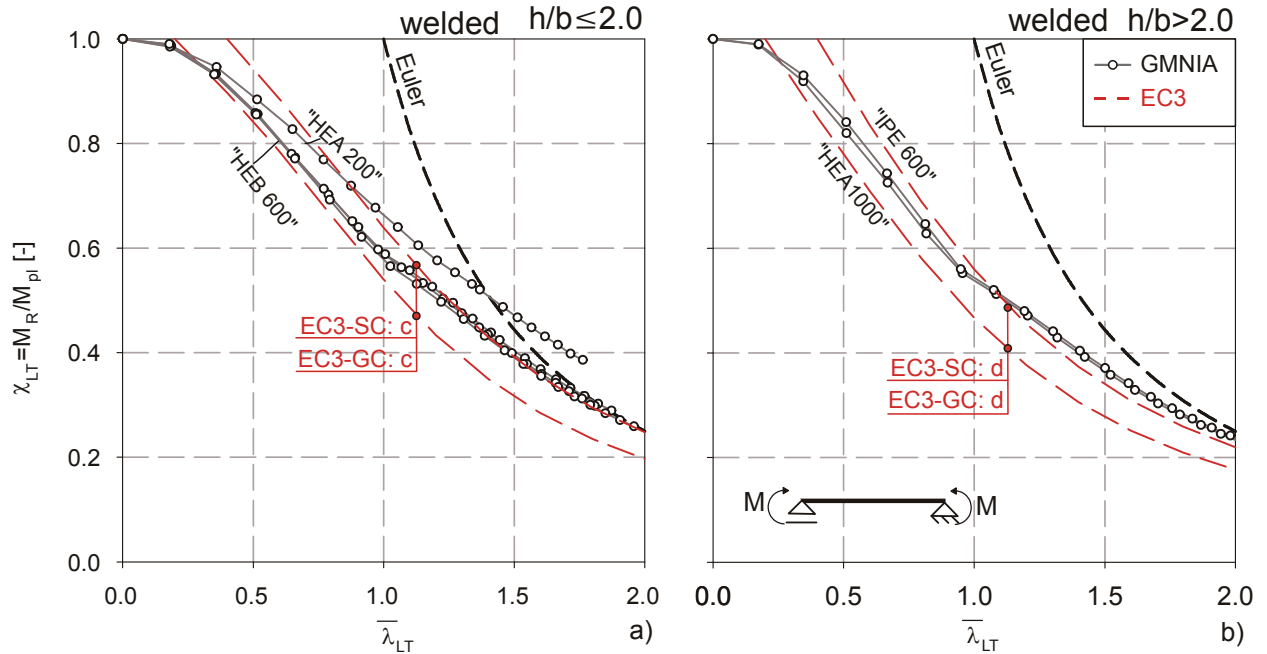
Fig 6-16 *Numerical LT buckling curves for welded sections of steel grade S235, compared with Eurocode 3 "general" and "special case" curves; h/b≤2.0 (a); h/b>2.0 (b).*

6.7. Ayrton-Perry formulation

In this section, case-specific analytical formulae are derived along the lines of the Ayrton-Perry formulation: using second-order internal forces and a first-yield criterion for the definition of an ultimate buckling load. For a single-span member with double-symmetric cross-section and constant bending moment, the assumption of initial lateral and torsional imperfections v_0 and θ_0 of sinusoidal shape lead to the following second-order equilibrium equations:

$$N_{cr,z} \cdot \overline{v} - M_y \cdot \overline{\theta} = M_y \cdot \overline{\theta}_0 \tag{6.13}$$

$$-M_y \cdot \overline{v} + \frac{M_{cr}^{\;2}}{N_{cr,z}} \cdot \overline{\theta} = M_y \cdot \overline{v}_0 \tag{6.14}$$

with: $M_{cr}, N_{cr,z}$ elastic critical buckling loads for lateral-torsional and flexural buckling.

Of all possible combinations of v_0 and θ_0, three special cases can be considered: one case with only lateral imperfections v_0, one case with only torsional imperfections θ_0 and one case with a distribution of θ_0 and v_0 corresponding to the shape of the first buckling eigenmode of the system. The latter approach was e.g. also used by Stangenberg (2006); it implies a coupling of the two degrees of freedom of the problem according to (6.15).

$$\overline{v}_0 = \frac{M_{cr}}{N_{cr,z}} \cdot \overline{\theta}_0 \tag{6.15}$$

By using equation (6.15) in (6.14) and combining (6.14) and (6.13), the following relationships between the deformation amplitudes v and θ and the initial torsional imperfection θ_0 are found:

$$\overline{\theta} = \overline{\theta}_0 \cdot \frac{M_y}{M_{cr} - M_y} \tag{6.16}$$

$$\overline{v} = \overline{\theta}_0 \cdot \frac{M_{cr}}{N_{cr,z}} \cdot \frac{M_y}{M_{cr} - M_y} \tag{6.17}$$

The following expressions can be used to determine the second order internal forces (out-of-plane bending moment M_z and warping moment M_ω) as a function of the occurring deformations:

$$M_z = EI_z \cdot \frac{\pi^2}{L^2} \cdot \overline{v} \tag{6.18}$$

$$M_\omega = EI_\omega \cdot \frac{\pi^2}{L^2} \cdot \overline{\theta} \tag{6.19}$$

By using (6.16) and (6.17) in (3.7) and (6.19), we obtain:

$$M_z = \overline{\theta}_0 \cdot \frac{M_y}{1 - \dfrac{M_y}{M_{cr}}} \tag{6.20}$$

$$M_\omega = EI_\omega \cdot \frac{\pi^2}{L^2} \cdot \overline{\theta}_0 \cdot \frac{M_y}{M_{cr} - M_y} = \frac{N_{cr,z}}{M_{cr}} \cdot \left(\frac{I_\omega}{I_z} \right) \cdot \overline{\theta}_0 \cdot \frac{M_y}{1 - \dfrac{M_y}{M_{cr}}} \tag{6.21}$$

M_z and M_ω can also be expressed in terms of the imperfection amplitude $\overline{e}_0$ by considering the following geometrical relationship:

$$\overline{\theta}_0 = \frac{\overline{e}_0}{M_{cr} / N_{cr,z} + h / 2} \tag{6.22}$$

The maximum stress equation can now be written for the outermost fibre of the compressed flange and set equal to the yield stress in a first-yield failure criterion:

$$\frac{M_y}{W_y} + \frac{M_z}{W_z} + \frac{M_\omega}{I_\omega} \cdot \omega_{max} = \frac{M_y}{W_y} + \frac{M_y}{1 - \dfrac{M_y}{M_{cr}}} \cdot \frac{\overline{e}_0}{M_{cr} / N_{cr,z} + h / 2} \cdot \left[\frac{1}{W_z} + \frac{N_{cr,z}}{M_{cr}} \cdot \frac{I_\omega}{I_z} \cdot \frac{\omega_{max}}{I_\omega} \right] = f_y \tag{6.23}$$

In the present case of a double-symmetric I cross-section, the following relationships hold:

$$W_z = \frac{I_z}{b / 2} \quad ; \quad \omega_{max} = \frac{h \cdot b}{4} \tag{6.24}$$

resulting in the following simplified form of equation (6.23):

$$\frac{M_y}{W_y} + \frac{M_y}{W_z} \cdot \frac{1}{1 - \dfrac{M_y}{M_{cr}}} \cdot \frac{\overline{e}_0}{M_{cr}/N_{cr,z} + h/2} \cdot \left[1 + \frac{N_{cr,z}}{M_{cr}} \cdot h/2\right] = f_y \qquad (6.25)$$

In order to obtain a dimensionless equation, expression (6.25) must be divided by the yield stress f_y. Furthermore, the second term on the left side can be expanded with W_y/W_y and A/A:

$$\frac{M_y}{W_y \cdot f_y} + \frac{M_y}{W_y \cdot f_y} \cdot \frac{1}{1 - \dfrac{M_y}{M_{cr}}} \cdot \frac{A \cdot \overline{e}_0}{W_z} \cdot \frac{W_y}{A \cdot (M_{cr}/N_{cr,z} + h/2)} \cdot \left[1 + \frac{N_{cr,z}}{M_{cr}} \cdot h/2\right] = 1.0 \qquad (6.26)$$

The dimensionless slendernesses and buckling reduction factors can now be introduced:

$$\chi_{LT} = \frac{M_y}{W_y \cdot f_y} \; ; \; \overline{\lambda}_z = \sqrt{\frac{A \cdot f_y}{N_{cr,z}}} \; ; \; \overline{\lambda}_{LT} = \sqrt{\frac{W_y \cdot f_y}{M_{cr}}} \qquad (6.27)$$

Using the expressions (6.27) in (6.26) and simplifying finally leads to the following equation:

$$\chi_{LT} + \frac{A \cdot \overline{e}_0}{W_z} \cdot \frac{\overline{\lambda}_{LT}^2}{\overline{\lambda}_z^2} \cdot \frac{\chi_{LT}}{1 - \chi_{LT} \cdot \overline{\lambda}_{LT}^2} = 1.0 \qquad (6.28)$$

By substituting:
$$\eta^* = \frac{A \cdot \overline{e}_0}{W_z} \cdot \frac{\overline{\lambda}_{LT}^2}{\overline{\lambda}_z^2} \qquad (6.29)$$

we obtain an equation that is identical to the Ayrton-Perry formula (5.2) of chapter 5 and can be solved accordingly:

$$\chi_{LT} = \frac{1}{\Phi_{LT} + \sqrt{\Phi_{LT}^2 - \overline{\lambda}_{LT}^2}} \leq 1.0 \qquad (6.30)$$

and
$$\Phi_{LT} = \frac{1}{2} \cdot \left(1 + \eta^* + \overline{\lambda}_{LT}^2\right) \qquad (6.31)$$

The result of the (elastic second-order) derivation given up to this point is identical to the one given by *Stangenberg* (2006). Equation (6.28) is evaluated for three cross-sections using the elastic values of A and W_z and an amplitude of the initial, sinusoidal geometric imperfection of $\overline{e}_0 = L/1000$ (of EV-conform shape) and plotted in Fig 6-17. The resulting buckling curves show that the torsional rigidity of the sections is quite distinctly taken into account by the proposed analytical formulation. The fact that stocky sections like an HEB400 and HEM200 have a higher resistance against LT buckling when compared to a slender HEAA1000 is thereby (qualitatively) correctly predicted. However, the curves illustrated in Fig 6-17 just represent the outcome of an elastic second order calculation and do therefore not realistically (quantitatively) reflect the actual characteristic resistance against LT buckling.
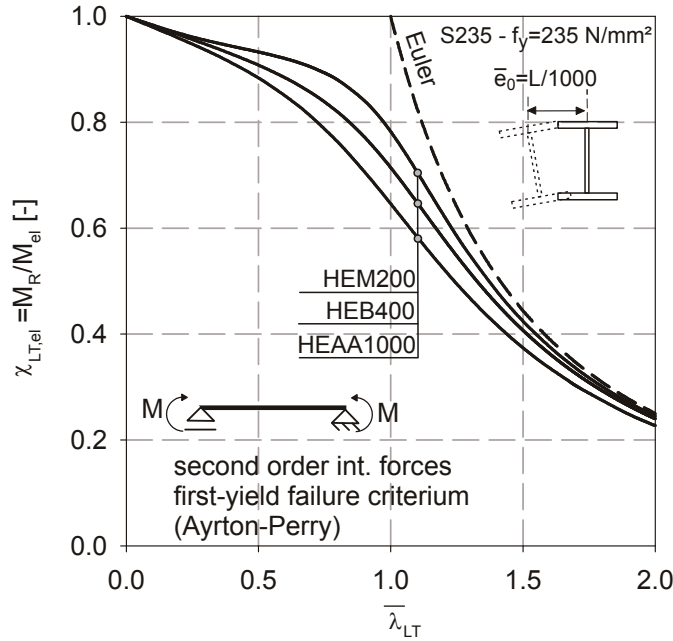
Fig 6-17 Analytical buckling curves according to the purely elastic, second order derivation.

The above derivation has been carried out using the assumption that the initial geometric imperfection is affine to the first eigenmode; this assumption led to a design equation that has the shape of the Ayrton-Perry formula. It is interesting to study how the derivation is affected if a different assumption regarding the initial imperfections is made.

Two cases can be considered: the case where the initial deformation is purely lateral – v_0; and one case where the initial deformation is purely torsional - ϕ_0. Following the same steps that led from equations (6.13) and (6.14) to (6.28), the following relationships are established
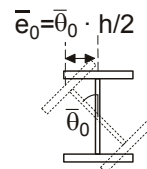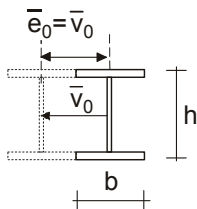
$$\overline{v} = \overline{v}_0 \cdot \frac{M_y^2}{M_{cr}^2 - M_y^2}$$

$$\overline{v} = \overline{v}_0 \cdot \frac{M_{cr}^2}{M_y \cdot N_{cr,z}} \cdot \frac{M_y^2}{M_{cr}^2 - M_y^2} \qquad (6.32)$$

$$\overline{\theta} = \overline{v}_0 \cdot \frac{N_{cr,z}}{M_y} \cdot \frac{M_y^2}{M_{cr}^2 - M_y^2}$$

$$\overline{\theta} = \overline{\theta}_0 \cdot \frac{M_y^2}{M_{cr}^2 - M_y^2} \qquad (6.33)$$

....

....

$$\chi_{LT} + \frac{A \cdot \overline{e}_0}{W_z} \cdot \frac{\overline{\lambda}_{LT}^2}{\overline{\lambda}_z^2} \cdot \left(1 + \frac{N_{cr,z} \cdot h / 2}{M_{cr} \cdot \overline{\lambda}_{LT}^2 \cdot \chi_{LT}}\right) \cdot \dots$$

$$\chi_{LT} + \frac{A \cdot \overline{e}_0}{W_z} \cdot \frac{\overline{\lambda}_{LT}^2}{\overline{\lambda}_z^2} \cdot \left(1 + \frac{M_{cr}}{N_{cr,z} \cdot \dfrac{h}{2} \cdot \overline{\lambda}_{LT}^2 \cdot \chi_{LT}}\right) \cdot \dots$$

$$\cdot \frac{\chi_{LT}^2 \cdot \overline{\lambda}_{LT}^2}{1 - \chi_{LT}^2 \cdot \overline{\lambda}_{LT}^4} = 1,0$$

$$\cdot \frac{\chi_{LT}^2 \cdot \overline{\lambda}_{LT}^2}{1 - \chi_{LT}^2 \cdot \overline{\lambda}_{LT}^4} = 1,0 \qquad (6.34)$$

In the above representation, only the most important results of the derivation have been reported, as the other points (internal forces, stress-based limit state formulation, introduction of dimensionless variables) are identical to the steps taken in equations (3.7), (6.19), (6.24), (6.25) and (6.27). The main difference between the eigenmode-conform and the above derivations lies in the different appearance of the deformation amplification factor, compare e.g. (6.16) and (6.32); in the latter case, this amplification factor is quadratic. This follows through till the final dimensionless limit state equations (6.34).

Contrary to (6.28), which is an Ayrton-Perry equation that can be solved for χ_{LT} accordingly, equations (6.34) cannot explicitly be solved for χ_{LT}. However, iterative root-finding methods can be employed to find values of χ_{LT} that fulfill (6.34). The following figure, Fig 6-18, shows the result of such an analysis for two sections and the two initial imperfection shapes "v_0" and "ϕ_0", as well as the eigenmode-conform imperfection shape.
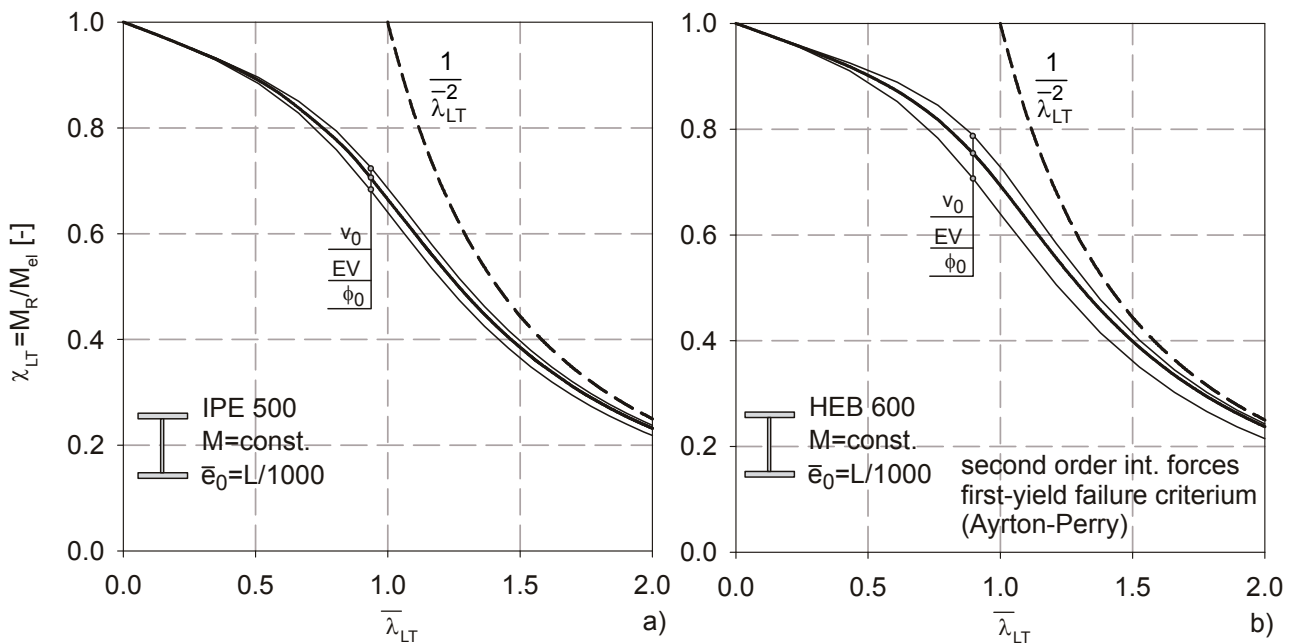
Fig 6-18 *Impact of the imperfection shape on the position of a purely elastic, second-order LT buckling curve.*

As in Fig 6-17, the elastic values of A and W_z and an amplitude of the initial, sinusoidal geometric imperfection of $\bar{e}_0 = L/1000$ were assumed for this calculation. The same remarks regarding the quantitative interpretation of this plot apply as for Fig 6-17.

The two key points illustrated by Fig 6-18 are discussed in the following. For one, the effect of the imperfection shape on the LT buckling strength discussed in section 6.5.1 is also reflected in the analytical derivations. The purely lateral deflection is shown in the figure to result in higher values of χ_{LT} than the the other two imperfection shapes, with the purely torsional being the most detrimental. Additionally, it should be noted that the difference between the three lines depends rather strongly on the studied section, whereby this is especially the case for the purely torsional

imperfection. If we look at equation (6.34) for this case, we can see that the term $M_{cr}/(N_{cr,z} \cdot h/2)$ is present in the term in parenthesis, in the numerator - and not in the denominator as is the case for the purely lateral imperfection. This term is larger for stockier sections than for rather slender ones, and increases with member length and slenderness. This explains why the curve for the purely torsional imperfection appears not to converge towards the curve for the purely lateral and eigenmode-affine imperfection.

Finally, Fig 6-19 illustrates the impact of both imperfection shape and amplitude on the buckling curves obtained from equations (6.28) or (6.34). It is thereby interesting to note that the difference between the curves pertaining to a certain shape strongly increase with raising imperfection amplitude.
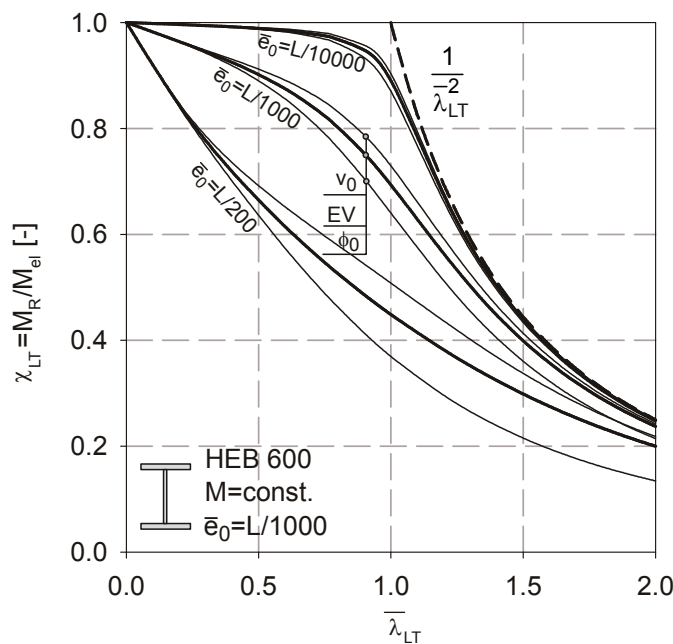
Fig 6-19 *Influence of shape and amplitude on the results of the analytical LT buckling curves.*

The curves for the eigenmode-affine and purely lateral imperfection are clearly "rational" in the sense discussed in chapter 2, since they converge towards the Euler hyperbola both with decreasing imperfection and increasing slenderness. The curve for the purely torsional imperfection also approaches the Euler hyperbola with decreasing imperfection, but has a much slower convergence rate towards the hyperbola at high slenderness.

6.8. Calibration

The analytical, Ayrton-Perry type buckling curve formulation presented in the preceding section and given by expressions (6.30) and (6.31) is specific for the studied case of LT buckling. In the next step, this formulation must be calibrated to the representative numerical buckling curves that were produced in section 6.6. That is done in this section, whereby existing approaches are discussed and new ones are presented. Since the objective of the section is to show the methodology, all considerations are made solely for hot-rolled, commercial European I- & H sections. However, at the end of the section the results are expanded to welded sections.

6.8.1. Representation of existing rules

The existing Eurocode 3 approach, see section 6.3, can be interpreted as a calibration of the factor η^* in equation (6.31) to best represent the numerical/experimental buckling data by analytical curves. Similarly to the assumptions made in the column buckling case, the Eurocode 3 calibration expression for η^* is expressed represented by a linear function of the slenderness $\bar{\lambda}_{LT}$.

$$\eta^* = \alpha_{LT} \cdot \left(\bar{\lambda}_{LT} - \bar{\lambda}_{LT,0} \right) \tag{6.35}$$

with $\bar{\lambda}_{LT,0}$ …. plateau value, equal to 0.2 for the EC3 "general case".

As has been discussed in chapter 5, it is convenient –in order to get a "feel" of the quality of the approximation function for η respectively η^*- to compare the proposed calibration expression – here, (6.35)- to the values of η^*_{num} that *precisely* describe the numerical values.

The latter are obtained by solving (6.28) with (6.29) for η^*:

$$\eta^*_{num} = \left(\frac{1}{\chi_{LT,num}} - 1 \right) \cdot \left(1 - \chi_{LT,num} \cdot \bar{\lambda}_{LT}^2 \right) \tag{6.36}$$

with χ_{num}... value of the buckling reduction factor as obtained from a numerical (GMNIA) calculation, see section 6.6.

Fig 6-20 shows the comparison of the values of η^* that match the numerical buckling curves for hot-rolled I- & H sections presented in section 6.6 –obtained using equation (6.36)- with a buckling curve that results from equation (6.30) with expression (6.35) and using the values for α_{LT} and $\bar{\lambda}_{LT,0}$ of the "general case" of Eurocode 3, see section 6.3. Two aspects can be pointed out:

i. The numerical values η^*_{num} are rather coarsely described by the expressions for η^* found in EC3, (6.35). The lack of accuracy of the current rules was already discussed in the introduction. The representation in Fig 6-20, however, aids the understanding of why this is the case; it also shows that the description is less accurate for stockier sections (with $h/b \leq 2.0$) than for more slender ones.
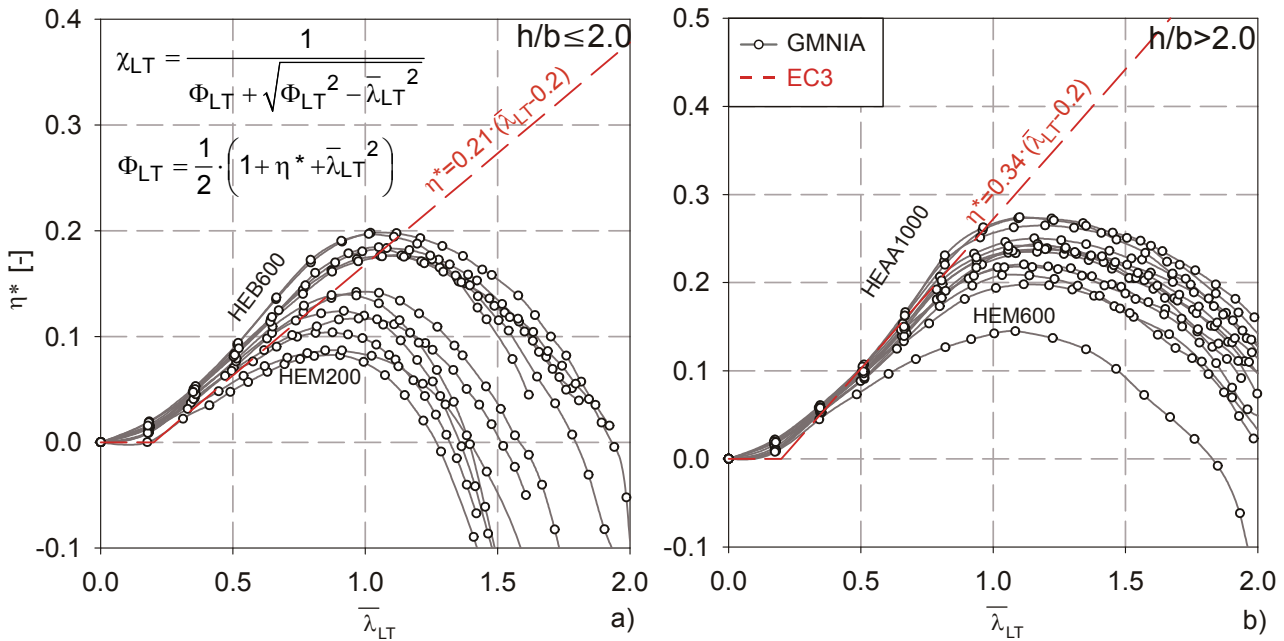
Fig 6-20 *Comparison of the factor* η^* *-see equation - found in EC3 with the numerical values.*

ii. Quite generally, the numerical values of η^*_{num}, when plotted over $\overline{\lambda}_{LT}$, are not well represented by a straight line, having a distinctly non-linear course when $\overline{\lambda}_{LT} > 1.0$. Some of these curves actually fall below a value of $\eta^*_{num}=0.0$. Expression (6.30) degenerates into the Euler hyperbola $1/\overline{\lambda}_{LT}^{2}$ for the case of $\eta^*=0.0$, and values of η^* lower than zero indicate that the Euler hyperbola has been exceeded; indeed this is what was observed in the numerical buckling curves for stocky sections in the high slenderness range.

6.8.2. Generalized imperfection η and equivalent geometrical imperfection e_0

As is discussed in the previous section and in the introductory section 6.3, the current Eurocode 3 formulation is neither very accurate, nor consistent with the physical behavior. Bearing in mind the second-order, Ayrton-Perry type derivation in section 6.7, this can be explained. If we look at the elastic expression for η^* (6.29), we see that this term differs from the term for η used in the column buckling case by the additional coefficient $\left(\overline{\lambda}_{LT}/\overline{\lambda}_{z}\right)^{2}$, which represents a stiffness and strength modification factor that is peculiar to the LT buckling case. By using expression (6.35) to generalize η^* and calibrate it to the numerical values, this term is "blurred" in the calibration and its potential is thereby lost. It therefore makes sense to include this parameter in a description of η^* and to write:

$$\eta^* = \eta \cdot \frac{\overline{\lambda}_{LT}^{2}}{\overline{\lambda}_{z}^{2}} \tag{6.37}$$

The factor η thereby replaces the elastic terms $A \cdot e_0/W_z$. This is exactly the term that was replaced by a generalized expression in the column buckling case by $\alpha \cdot \left(\overline{\lambda}-\overline{\lambda}_0\right)$, see chapter 4.

Again, a calibration function with appropriate calibration factors is needed that is as accurate and simple as possible. Two different expressions for η are discussed here:

$$\eta_I = \alpha \cdot \left(\overline{\lambda}_z - 0.2 \right) \qquad (6.38)$$

$$\eta_{II} = \alpha \cdot \left(\overline{\lambda}_{LT} - 0.2 \right) \qquad (6.39)$$

Expression (6.38) represents a generalized imperfection η that increases linearly with the dimensionless slenderness for weak-axis buckling $\overline{\lambda}_z$, and therefore *with the length of the member*, analogously to the column buckling case. Expression (6.39) represents a factor η that is proportional to $\overline{\lambda}_{LT}$, as is currently commonplace in the EC3 rules for LT buckling. Since $\overline{\lambda}_{LT}$ is *not length-proportional*, the generalized imperfection does not increase linearly with length if (6.39) is used.

It is worthwhile to elaborate on this point, which was already mentioned in broader terms in chapter 4; the generalized imperfection η can more tangibly be expressed by an "equivalent" geometrical imperfection, which is easily calculated by solving equation (6.29) for $\overline{e}_0$:

$$\overline{e}_0 = \eta \cdot \frac{W_z}{A} \qquad (6.40)$$

This equation is also used –in a slightly modified form– in EC3, see clause (5.10), to calculate the equivalent geometrical imperfection amplitudes of frames to be used in second-order design calculations.

Equation (6.40) is evaluated for both expressions (6.38) and (6.39) and plotted over the length in Fig 6-21. Thereby, the elastic section modulus W_z and the area A of an HEM600 section were chosen, as this stocky section series lends itself to a good representation of the studied effects. The imperfection factor α was set to be equal to 0.34 in both cases; this is equal –for this specific section- to both the factor α_{FBz} for weak axis flexural buckling and to α_{LT} for the general case LT buckling case according to EC3. For completeness, it should be stated that, for the calculation of $\overline{\lambda}_z$ and $\overline{\lambda}_{LT}$, once more the yield strength of steel grade S235 and the basic cases of single-span members with constant normal force or bending moment were considered.

Two representations of $\overline{e}_0$ are chosen. In Fig 6-21a, the ratio of length to imperfection $L / \overline{e}_0$ is plotted, while figure Fig 6-21b shows the imperfection itself plotted over the length. The latter figure illustrates that the equivalent geometrical imperfection indeed increases linearly with length when equation (6.38) is used, while (6.39) results in an imperfection that is clearly under-proportional with regard to length. Due to the plateau, both lines do not start at L=0, but at the length corresponding to $\overline{\lambda}_z = 0.2$ and $\overline{\lambda}_{LT} = 0.2$, respectively. Fig 6-21a, on the other hand, shows that –due to the inclusion of the plateau value $\overline{\lambda}_0 = 0.2$, not even equation (6.38) corresponds to a geometrical imperfection that is a *constant fraction of length*. It does however *approach* a constant fraction, as is illustrated by the comparison with the imperfection resulting from $\eta = \alpha \cdot \overline{\lambda}_z$ without

the plateau. Equation (6.38) does therefore qualitatively reflect the assumptions made during the calculation of numerical buckling curves for column buckling (chapter 5) and LT buckling (section 6.6), where the geometrical imperfections were assumed to have an amplitude proportional to the member length.

It should be noticed again that also fabrication tolerances for the out-of-straightness of members are generally defined by constant fractions of length. Equation (6.39), in comparison, represents an equivalent geometrical imperfection that –as a fraction of length- is far from constant. The implications of these findings are discussed in the following sub-section.
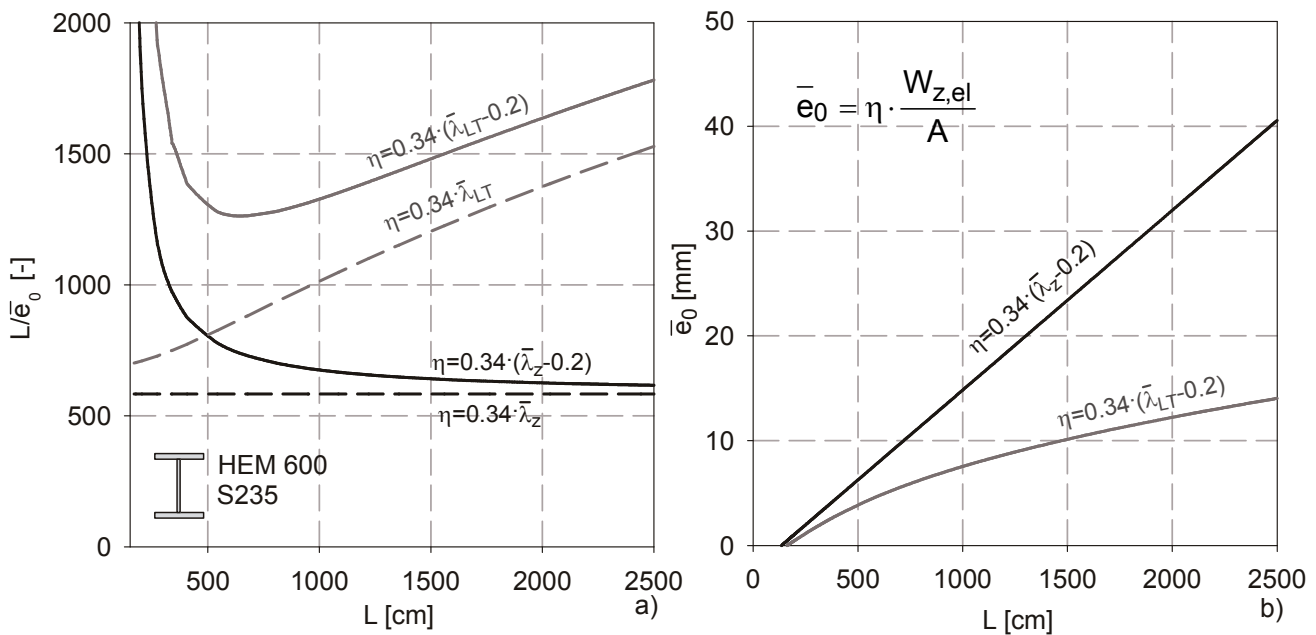
Fig 6-21 *Equivalent geometrical imperfections for a HEM600 section, plotted as $L/\bar{e}_0$ (a) and $\bar{e}_0$ (b) over the member length.*

6.8.3. Calibration of the Ayrton-Perry "generalized imperfection" η

In the preceding paragraphs, it was already pointed out that only a generalized imperfection η expressed by equation (6.38) preserved the basic assumption regarding the geometrical imperfections made during the development of the numerical buckling curves. The implications of this fact on the *calibration* of the specific Ayrton-Perry formulation of section 6.7 to the numerical curves are discussed in the following.

For the purpose of selecting the expression among (6.38) and (6.39) that is best suited for calibration, the "best-fit" value of α for both expressions is determined and the results are compared.

Additionally, a third proposal is examined, which is being brought forward in different publications (Sedlacek/Müller 2006, Naumes 2008) as the expression for the "new European member buckling curves"; in this proposal, it is suggested to use an expression similar to (6.39) and the *same factor*

for α_{LT} that is valid for weak axis flexural buckling, i.e. α_{FBz}, which leads to the following form in the LT buckling case:

$$\eta = \alpha_{FBz} \cdot \left(\overline{\lambda}_{LT} - 0.2 \right) \tag{6.41}$$

This proposal is included in the considerations made in the following paragraphs in order to check its validity for LT buckling.
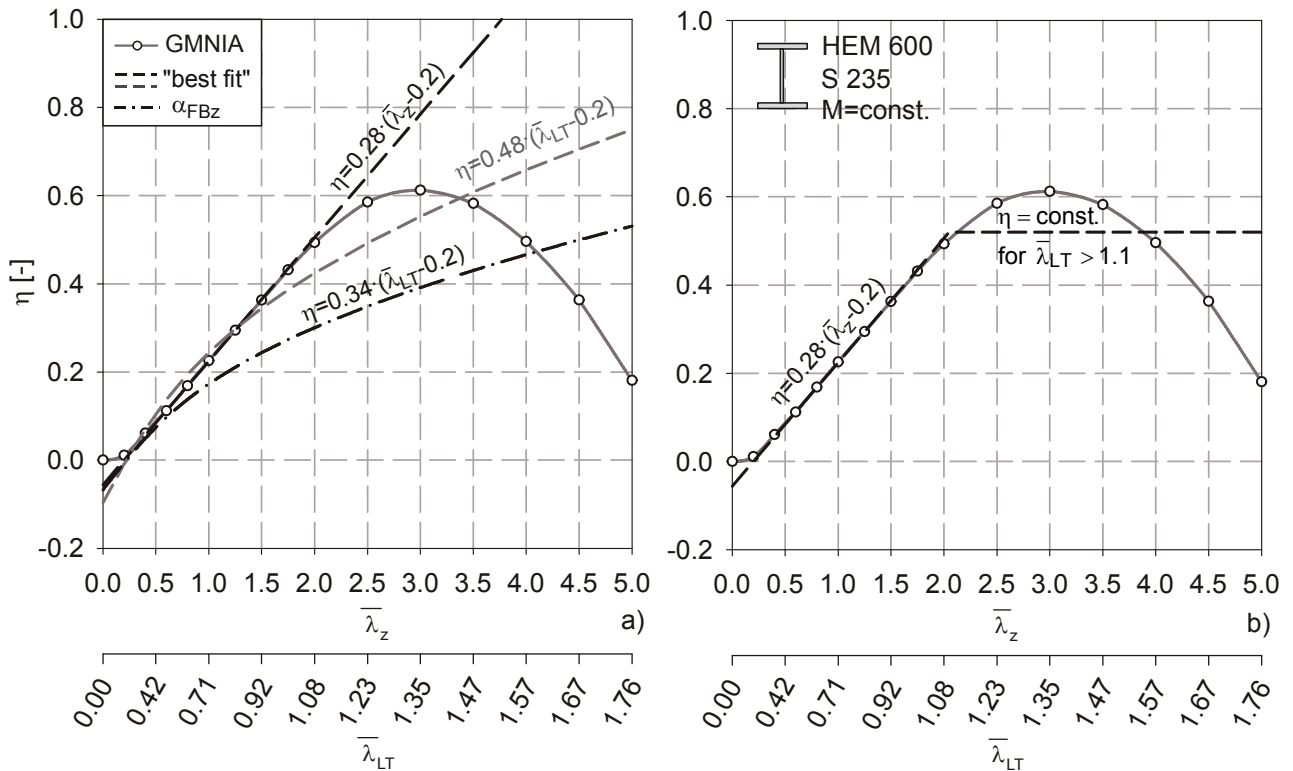
Fig 6-22 *Comparison of the numerical value of the Ayrton-Perry generalized imperfection η with the three approximations given by the three expressions (6.38), (6.39) and (6.41).*

An example is conveniently used to compare the three expressions (6.38), (6.39) and (6.41) for the generalized imperfection. In a first step, the expression for η itself is compared to numerical values obtained by evaluating the following equation – compare with (6.36).

$$\eta_{num} = \left(\frac{\overline{\lambda}_z}{\overline{\lambda}_{LT}} \right)^2 \cdot \left(\frac{1}{\chi_{LT,num}} - 1 \right) \cdot \left(1 - \chi_{LT,num} \cdot \overline{\lambda}_{LT}^{-2} \right) \tag{6.42}$$

Fig 6-22 shows values of η that match the numerical buckling curve for LT buckling of an HEM600 section, plotted over $\overline{\lambda}_z$ (Fig 6-22a). In the figure, these values are compared to the expressions (6.38) and (6.39) with the respective "best-fit" values of α_{LT}, as well as to expression (6.41) with the value of $\alpha_{Fbz}=0.34$ taken from tables 6.1 and 6.2 in Eurocode 3 (2006).

In these calculations, the "best-fit" value of α_{LT} was defined as being the value resulting in the smallest "error" according to a least-square-fitting of the resulting reduction factor χ_{LT} for values of

η_{num} from zero up to the peak in the $\eta = f(\overline{\lambda})$ curve. They are equal to 0.28 for expression (6.38) and 0.48 for (6.39). The following observations can be made:

i. When plotted over $\overline{\lambda}_z$, the numerical values of η_{num} have a clearly linear course up to a value of $\overline{\lambda}_z$ that corresponds to approximately $\overline{\lambda}_{LT} = 1.0$ (see Fig 6-22b). Beyond this point, the slope of the numerical curve quickly changes and the values of η_{num} peak at a value of $\overline{\lambda}_z$ of approximately 3.0, *decreasing* beyond this point.

ii. This is explicable by a change of the dominant imperfection and strength component. The linear segment of the curve reflects the assumptions made for the numerical LT buckling curves in section 6.6, with length-proportional geometrical imperfections. The linear segment of η_{num} thus indicates that geometrical imperfections are dominant here, whereas - for higher $\overline{\lambda}$- residual stresses and large deformations become more relevant.

iii. The function for η given by (6.41) is far removed from the numerical values both in shape and position. At high slenderness ratios (around $\overline{\lambda}_{LT} = 1.6$) it does intersect the numerical curve, but this does not seem to reflect any mechanical behaviour. Since most of the numerical line lies *above* the values of η given by (6.41), the analytical buckling curve resulting from this expression will yield reduction factors χ_{LT} on the "unsafe" side compared to the numerical buckling curve.

In light of these results it can be concluded that expression (6.38), representing a generalized imperfection that is proportional to $\overline{\lambda}_z$ and therefore to the member's length, is the suitable one to approximate the numerical curve, at least in the linear segment of the η_{num} curve.

Contrary to (6.38), expression (6.39) represents imperfection amplitudes deviating from the length proportional ones, which causes problems of fitting the function for η_{num} and may lead to "unsafe-sided" results.

The last points are confirmed in Fig 6-23, which shows the analytical buckling curves given by the evaluation of equation (6.30) with (6.31) and (6.37) for expressions (6.38), (6.39) and (6.41) and compares these curves with the numerical curve for the HEM600 section discussed above. If (6.41) is used to describe η, the value of α_{FBz} is equal to 0.34 for the HEM600 according to EC3 tables 6.1 and 6.2. Two forms of representation are used, the classical representation with the buckling reduction factors χ_{LT} plotted over $\overline{\lambda}_{LT}$ (a), and the *Merchant-Rankine* representation where χ_{LT} is plotted over the ratio of the ultimate buckling load M_R to the Euler critical load M_{cr} (b). The latter form of representation has the advantage of better showing the differences between each curve.

The figure shows that the analytical curves given by expression (6.38) –with the best-fit value of $\alpha_{LT} = 0.28$- practically overlaps with the numerical curves up to a slenderness of $\overline{\lambda}_{LT} = 1.0$, while the "best-fit" curve given by expression (6.39) -$\alpha_{LT} = 0.48$-slightly diverges from the numerical one. The curve given by (6.41), on the other hand, lies significantly above the numerical curve over a wide range of slenderness. A comparison with Fig 6-22a shows this to be consistent with that plot, where

the values of η for expression (6.41) were shown to lie significantly below the numerical values η_{num} over a wide slenderness range.

It has already been stated that also the analytical curve resulting from expression (6.38) diverges from the numerical curve towards the "safe side" beginning at $\bar{\lambda}_{LT} = 1.0$. It is interesting to point out that this divergence almost precisely occurs at a length corresponding to the practical limit of applicability for the given section and load case; lengths exceeding the ratio of L/h=25 (corresponding to L=15.5m for the HEM600) represent a realistic estimate for an upper limit of practical application for the given loading condition, since at a service load level (assumed to be 70% of the ultimate load level) a deformation limit of L/200 is exceeded here. It can therefore be ascertained that a very small error results from the description using expression (6.38) and the best-fit value of α_{LT} *for all practical member lengths.* This was found to be the case for all studied sections.
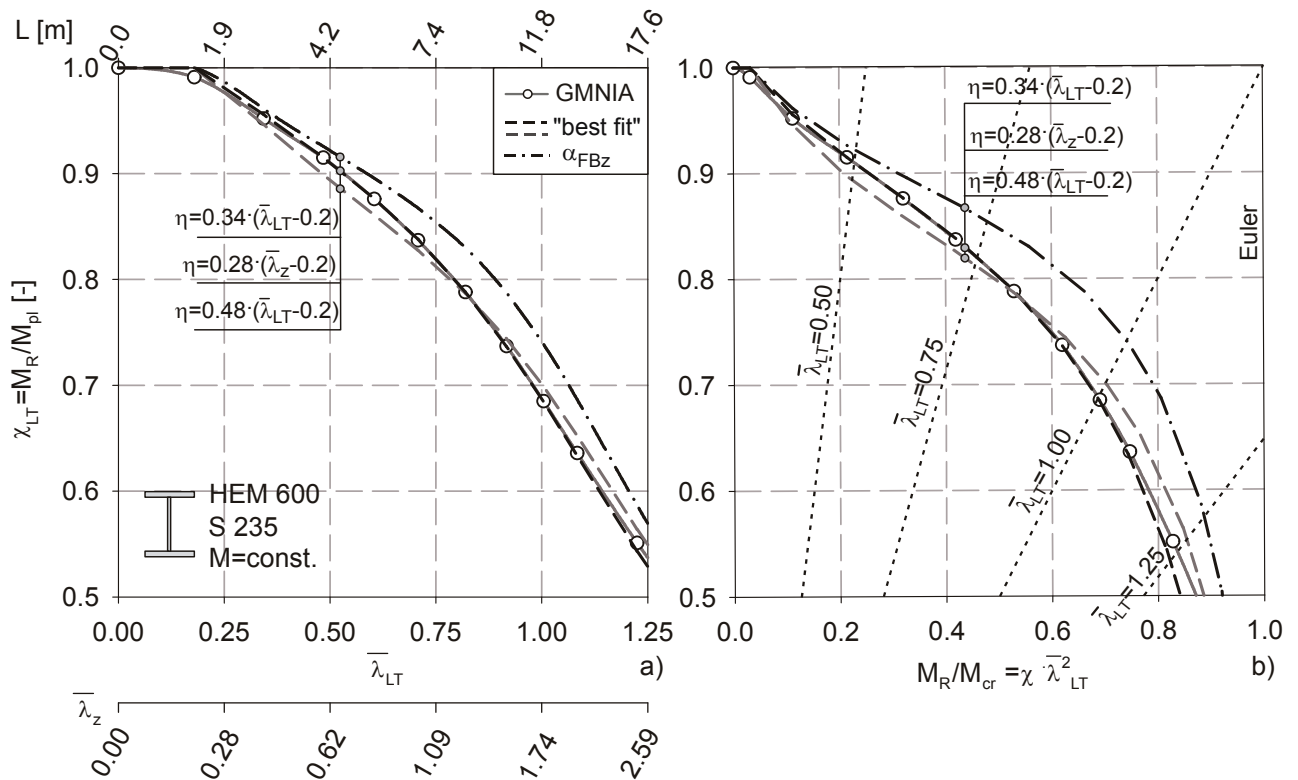
Fig 6-23 *Comparison of numerical and best-fit analytical buckling curves for a HEM600; χ-$\bar{\lambda}$ representation (a); Merchant-Rankine plot (b)*

The maximum error inherent to expression (6.39) with the best-fit value of $\alpha_{LT}=0.48$ is slightly larger, and reaches its maximum on the "unsafe" side for the studied section. This is not necessarily the case for all sections; as a matter of fact, due to the under-proportionality of η with regard to length resulting from (6.39), this expression can in some cases even yield more accurate results in the high slenderness range than expression (6.38) – provided again that the section-specific best-fit value of α_{LT} is used.

The inaccuracy of expression (6.41) is inherent to its core assumption regarding the value of the "generalized imperfection coefficient" α. The values of α_{FBz} given in EC3 for weak axis flexural buckling are larger for hot-rolled beams with $h/b \leq 1.2$ than for deeper sections, which is coherent with the higher residual stresses in stockier sections. The adoption of these values in an equation like (6.41) for LT buckling, however, appears to be going against the actual trend observed in the numerical calculations, where sections with larger h/b require a higher value of α than stockier ones. Thus, using expression (6.41) will result in "un-safe sided" buckling curves for most sections with h/b larger than approx. 1.8, and very "safe sided" curves for sections with $h/b \leq 1.2$.

This last statement is further confirmed by two additional examples, plotted in Fig 6-24. The figures show GMNIA curves for an HEA 200 and an HEAA1000 section, it is hot-rolled, class 1 sections that are at the two extremes of the h/b spectrum of commercial sections. These numerical GMNIA curves, calculated using the common *model beam* geometry and imperfection assumptions, are compared to the result of the Ayrton-Perry formula (6.30) with η^* according to (6.37) and η taken to follow the function (6.41), i.e. the linear function in $\overline{\lambda}_{LT}$, with the generalized imperfection amplitude α equal to the value that is valid for weak-axis flexural buckling, α_{FBz} according to the Eurocode.

The figure again shows the built-in inaccuracies of this formulation. As has been expected, the stocky HEA 200 section is clearly penalized by this formulation of η, since the value of $\alpha_{FBz} = 0.49$, applicable in the weak-axis flexural buckling case for this section, is too "conservative" for LT buckling. The opposite is true for the slender HEAA 1000 section, where the value of $\alpha_{FBz} = 0.34$, applicable for flexural buckling, is not high enough, yielding results that don't reflect the behaviour observed in GMNIA calculations.
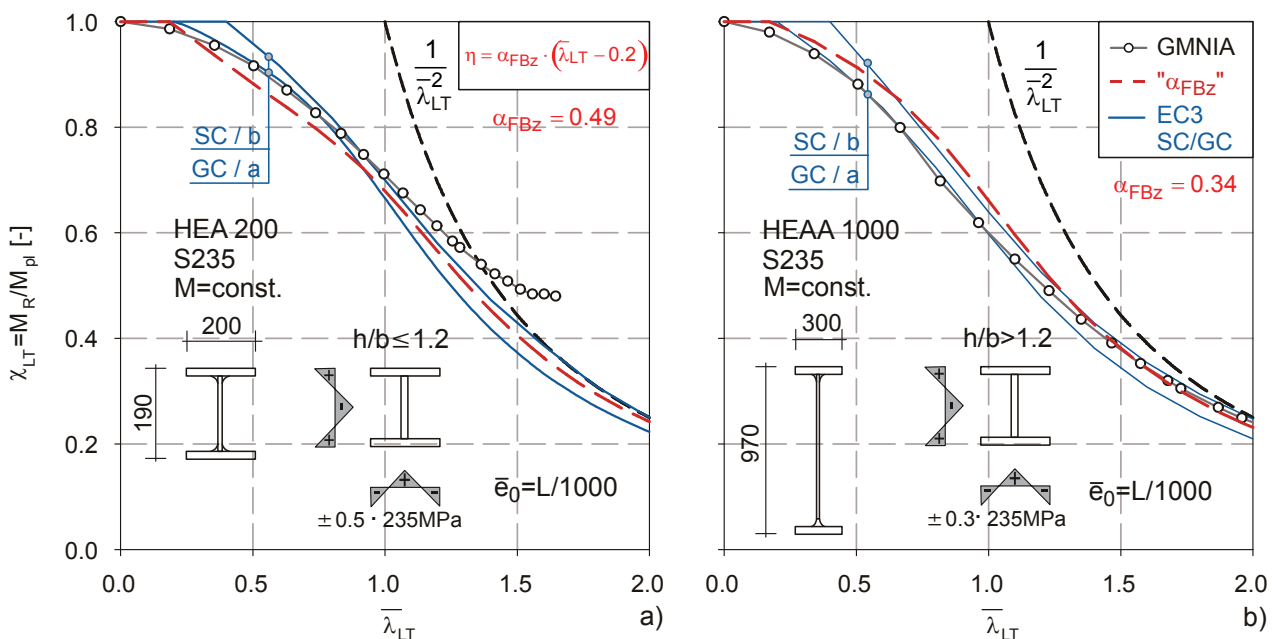
Fig 6-24 *Comparison between GMNIA curves for an HEA 200 (a) and HEAA 1000 (b) section with the results of the analytical formulation (6.30) and η according to (6.41).*

Whether or not the observed discrepancies in Fig 6-24 are acceptable from the point of safety would have to be decided at a code committee level; in spite of margins of error of more than 10% to the "unsafe" side, one could still argue that the discrepancies are in the range of the current design rules. It is however clear that the proposed "new European member buckling curves" (Sedlacek & Müller, 2006), which use expression (6.41) and are intended to be employed for all imaginable combinations of cross-sections and loading conditions, is actually not able to consistently and accurately describe the LT buckling behaviour of the simple, prismatic *model beams,* on which the benchmark case for member buckling design -column buckling- is also based. Considering that the "second simplest" (after column buckling) basic member stability case is being treated here, the above observation cannot but make one sceptical regarding the introduction of the "general method" with the "new European member buckling curves" as a codified design procedure, at least not without considerable additional numerical studies. Due to the apparent lack of accuracy and consistency for LT buckling observed for curves resulting from expression (6.41) in the above–and many other- studied cases, *this expression will not be further considered in this chapter.*

If we now return our attention solely to expressions (6.38) or (6.39) and on the task of their calibration to the developed numerical LT buckling curves, it can be stated that the differences between buckling curves that were calculated using either one of the two expressions do not appear to be dramatic. Provided that the "best-fit" value of α_{LT} is used in both expressions, the curve resulting from expression (6.38) was shown in Fig 6-23 to be only slightly more accurate –in absolute more than in relative terms- than the curve resulting from (6.39).
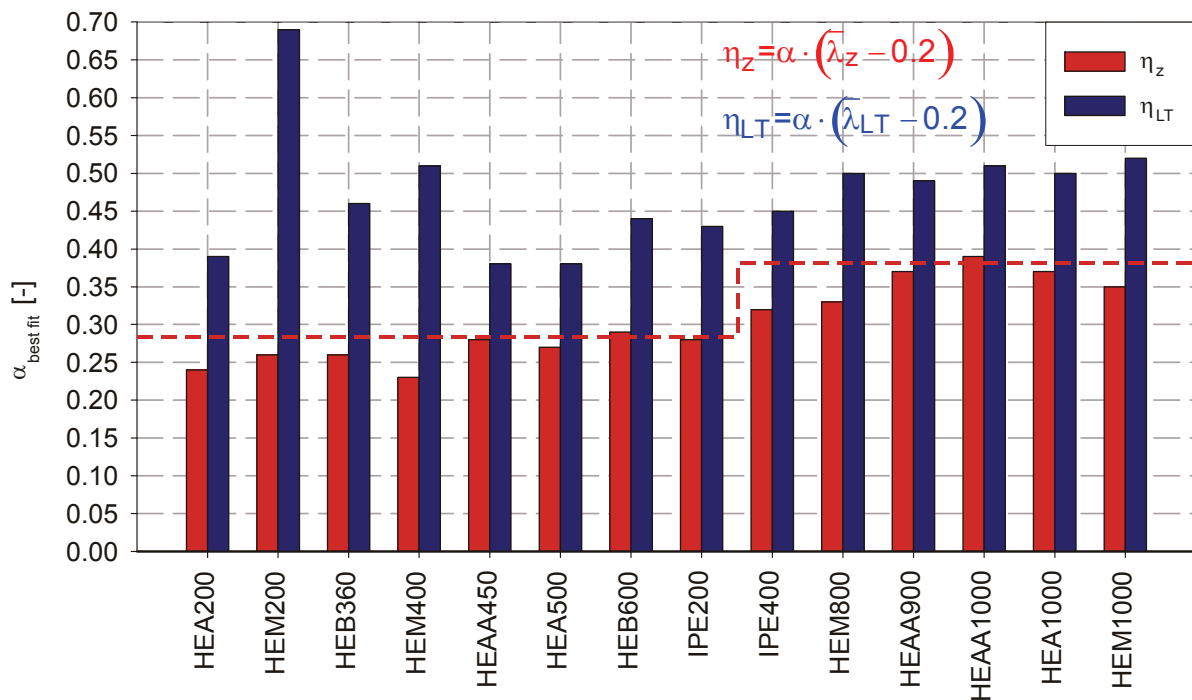
Fig 6-25 *"Best-fit" values of the generalized imperfection amplitude coefficient α.*

Nevertheless, the adoption of expression (6.38) is recommended. This is desirable from a theoretical point of view because it (better) reflects the underlying assumptions regarding geometrical imperfections made during the calculation of the numerical buckling curves. More importantly, it is far better suited for the "grouping" of sections with regard to their geometrical properties (h/b). This is shown in Fig 6-25 through a comparison of "best-fit" values of α_{LT} for some representative sections and expressions (6.38) and (6.39). The sections are ordered with ascending h/b ratio. Up to IPE200, all sections have values of h/b≤2.0, the classification limit for the LT buckling rules in EC3.

Fig 6-25 shows that, if the parameter h/b with a classification limit at 2.0 were to be maintained, only expression (6.38) allows for a satisfactory representation of the actual behaviour. For this formulation, a tendency to an increase of the best-fit value of α_{LT} with increasing h/b is (at least qualitatively) noticeable. For formulation (6.39), no such tendency was observed, showing a remarkable scatter depending on the rolling series (HEAA, IPE, HEM), especially for sections with h/b≤2.0.

Thus, maintaining the classification limit at h/b=2.0, values of α_{LT} according to Table 6-3 are proposed. This proposal is shown in Fig 6-25 as a dashed horizontal line. In Fig 6-26, it is compared to numerical values of η plotted over $\overline{\lambda}_z$.

h/b	hot-rolled I & H
≤2.0	$\alpha_{LT}=0.28$
>2.0	$\alpha_{LT}=0.38$

Table 6-3   *Proposed categorization according to h/b for the approach of section 6.8.3.*

When compared to Fig 6-20, the improved accuracy of this proposal in contrast to the current Eurocode provisions is probably not immediately appreciable. This is better shown in Fig 6-27, which compares the new analytical curve calculated using Table 6-3 with the numerical curve in terms of the buckling reduction factor χ_{LT}; thereby, the sections with the *largest observed discrepancies* between the numerical value η_{num} and η according to Table 6-3 were chosen. Again, both the classical χ-$\overline{\lambda}$ and the Merchant-Rankine representation are used.

Even for these four sections, the error in the prediction of χ_{LT} is small within the practically relevant lengths with L/h≤25. If discrepancies beyond a few percentage points are observed, they are consistently "safesided" and occur only at the upper limit of applicability of the respective section. As the comparison of the lines for the HEM200 section in Fig 6-27 shows, the proposed analytical formulation does not allow for a representation of the post-critical behaviour that was observed for very stocky sections; this is however of no practical relevance, since this behaviour only occurs at unrealistically large lengths.
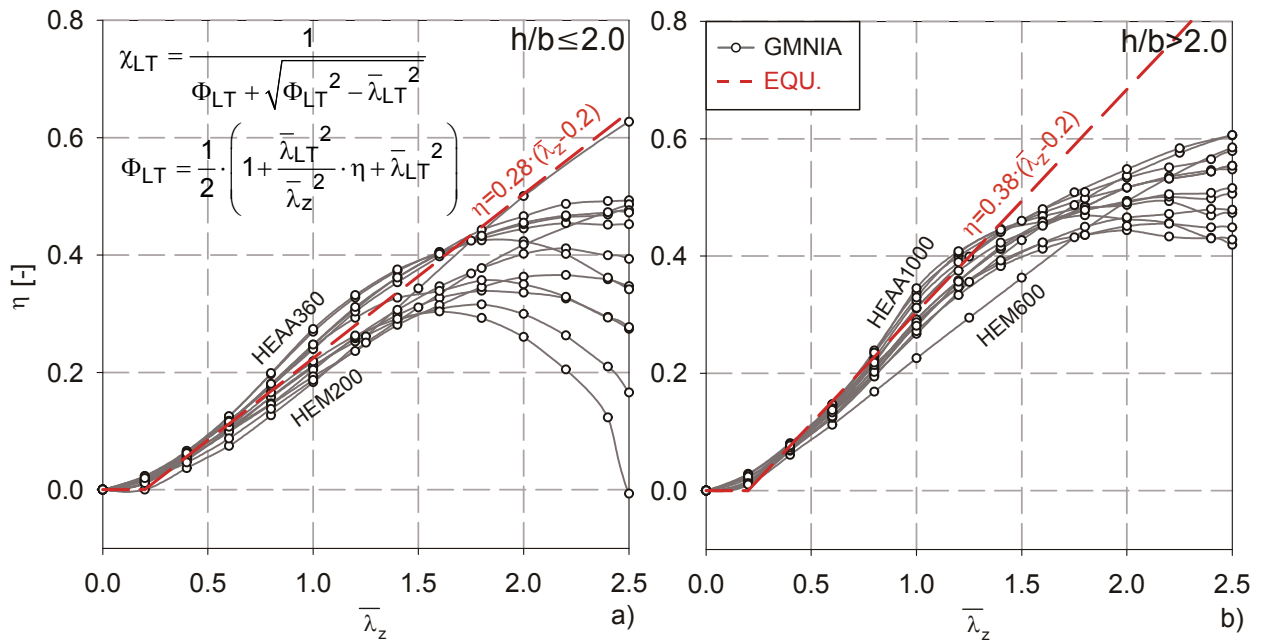
Fig 6-26 *Generalized imperfection η for all numerical buckling curves and proposed approximation.*

The formulation proposed in this sub-section is therefore able to represent the numerical LT buckling curves with good accuracy, whereby the geometrical classification limits of h/b in EC3 are maintained. When compared to the current EC3 curves, the proposal is much more accurate (compare Fig 6-27 with Fig 6-15) especially because the new factor $(\overline{\lambda}_{LT} / \overline{\lambda}_z)^2$ accounts for the most relevant characteristics of each beam.
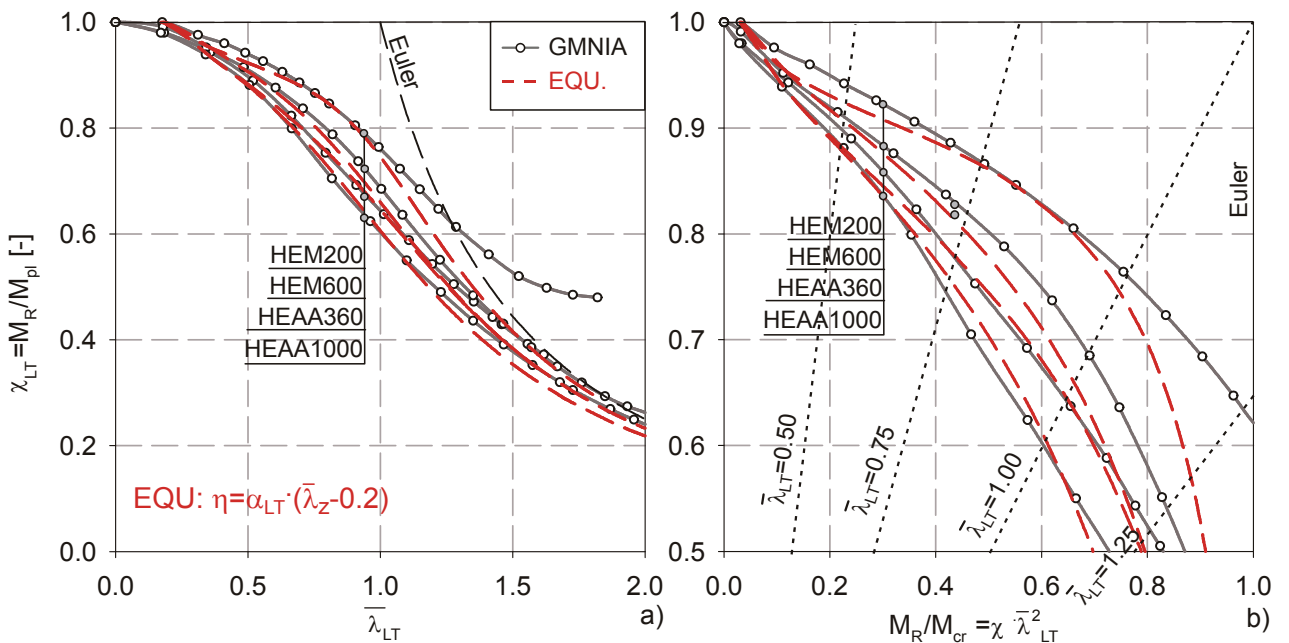
Fig 6-27 *Comparison of the numerical and proposed analytical curves; "worst-fit" sections.*

6.8.4. Introduction of an additional "cross-sectional" factor

While the approach presented in the preceding section is already sufficiently accurate and simple for a code regulation, it still has one major disadvantage from the point of view of mechanical coherence: it doesn't directly reflect the change of residual stresses that –in consistence with the derivation of the column buckling curves- was assumed to occur at the depth-to-width ratio of h/b=1.2. As a matter of fact, α_{LT} in Table 6-1 and 2 is *higher* for sections with lower residual stresses, which is neither logical nor consistent with the column buckling case.

Therefore, an additional factor must be included, while at the same time simplicity must be retained. By observing the best-fit values of α_{LT} for expression (6.38) –see Fig 6-25-, it was found that the increase of this value is approximately proportional to $(h/b)^{0.5}$ or, with far greater accuracy, to the square root of the ratio of the two elastic section moduli $W_{y,el}/W_{z,el}$. By dividing η by this new factor, Fig 6-28 is obtained. Thereby, the numerical values of η are conveniently separated for sections with h/b>1.2 (a) and h/b≤1.2 (b). When compared to Fig 6-26, the introduction of the new factor $(W_{y,el}/W_{z,el})^{0.5}$ results in a remarkable reduction of the scatter of the numerical lines. What is even more remarkable, the slope of the η_{num} curves is now consistent with the change of residual stresses at h/b=1.2.

A proposal can therefore be made: the buckling reduction factor can be calculated using equation (6.30) and the value of Φ_{LT} expressed by (6.43).

$$\Phi_{LT} = \frac{1}{2}\left[1 + \eta \cdot \frac{\bar{\lambda}_{LT}^2}{\bar{\lambda}_z^2} + \bar{\lambda}_{LT}^2\right] = \frac{1}{2}\left[1 + \alpha_{LT} \cdot \left(\bar{\lambda}_z - 0.2\right) \cdot \frac{\bar{\lambda}_{LT}^2}{\bar{\lambda}_z^2} + \bar{\lambda}_{LT}^2\right] \tag{6.43}$$

The value of α_{LT} can be taken from Table 6-4. The red, dashed lines in Fig 6-28a and b show the resulting function for the generalized imperfection η.
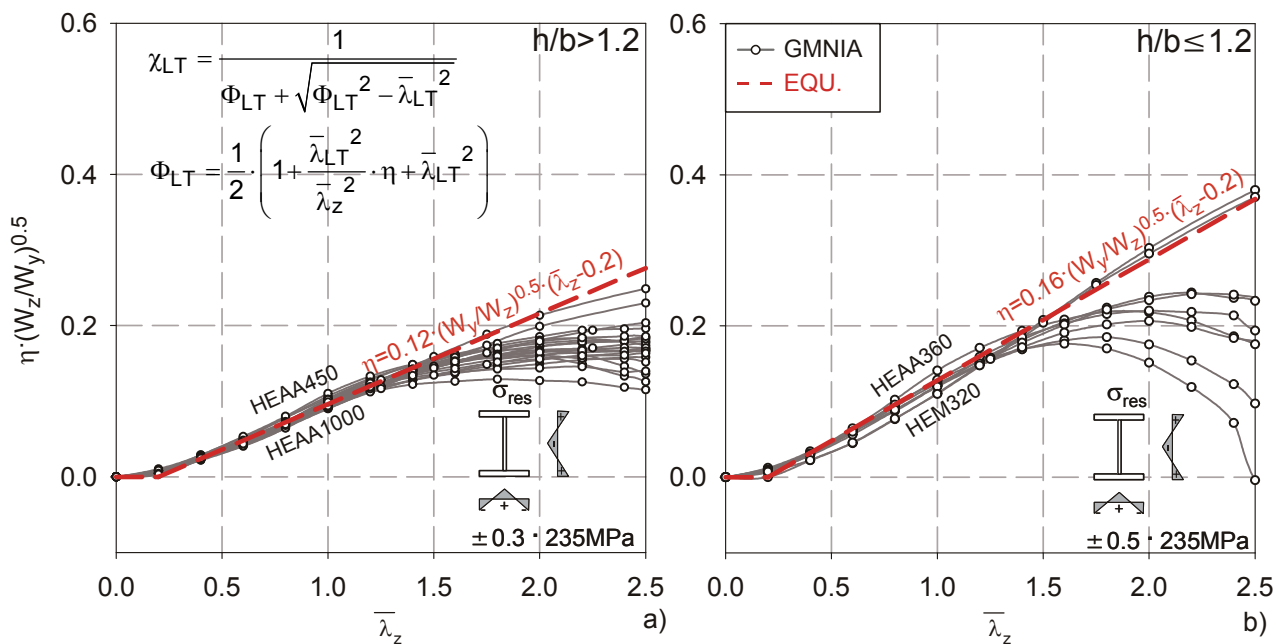
Fig 6-28 *Reduction of scatter by introduction of an additional factor.*

h/b	hot-rolled I&H
≤ 1.2	$\alpha_{LT} = 0.16 \cdot \sqrt{W_{y,el} / W_{z,el}}$
> 1.2	$\alpha_{LT} = 0.12 \cdot \sqrt{W_{y,el} / W_{z,el}}$

Table 6-4   *Generalized imperfection amplitude coefficients for the proposed formulation.*

Finally, the analytical buckling curves $\chi_{LT} = f(\overline{\lambda}_{LT})$ resulting from the proposal made in this sub-section can be compared to the numerical curves, see figure Fig 6-29a. The comparison is carried out for four representative sections, illustrating the remarkable degree of accuracy that is achieved by the proposed formulation. For all considered sections, the error in the prediction of χ_{LT} is extremely small in absolute and in percentage terms, with the exception of members with large $\overline{\lambda}_{LT}$, where a small, safe-sided divergence is present.

If the accuracy in the region of large slenderness is deemed to be insufficient, it can easily be increased by introducing a limit value of η; for example, if η is set to be constant for values of $\overline{\lambda}_{LT}$ >1.1, we obtain analytical curves of the shape shown in Fig 6-29b. For the sections shown in that figure, the maximum error on both the "safe" and "unsafe" becomes negligibly small for all member within the realm of practicality. A comparison between Fig 6-22a and b –where the proposed "cut-off" is signified by the horizontal line beginning at $\overline{\lambda}_{LT}$ =1.1- helps explaining this: beginning at $\overline{\lambda}_{LT}$ =1.0, η_{num} diverges from a straight line; by introducing a "cut-off" limit of η, this is somehow acknowledged.

Thereby, it helps that the precision of η rapidly loses relevance with increasing slenderness; thus, even this very coarse approximation of the "non-linear" segment of the η_{num} curve already results in an appreciably higher accuracy in terms of χ_{LT}. Of course, whether or not the cut-off limit discussed in this paragraph is worthwhile of inclusion in a design provision should be considered in light of the overall safety requirements of the proposal.

In this respect, the Montecarlo simulations carried out in section 6.10 point out that the numerical buckling curves obtained from nominal material and cross-sectional values and "fixed" amplitudes for geometric imperfections ($\overline{e}_0$ =L/1000) and residual stresses do *not have the same level of reliability throughout the slenderness ranges.* While such curves were shown to be clearly "safe-sided" at low slenderness, and in good agreement with the target reliability for "characteristic" values in the most common practical range of slenderness, the curves tended to fall above the values representing this "target" level of reliability at high slenderness. The reason is that imperfection types become relevant, from a probabilistic point of view, that are not necessarily sufficiently covered by the fixed imperfection assumptions made during the numerical GMNIA calculations.
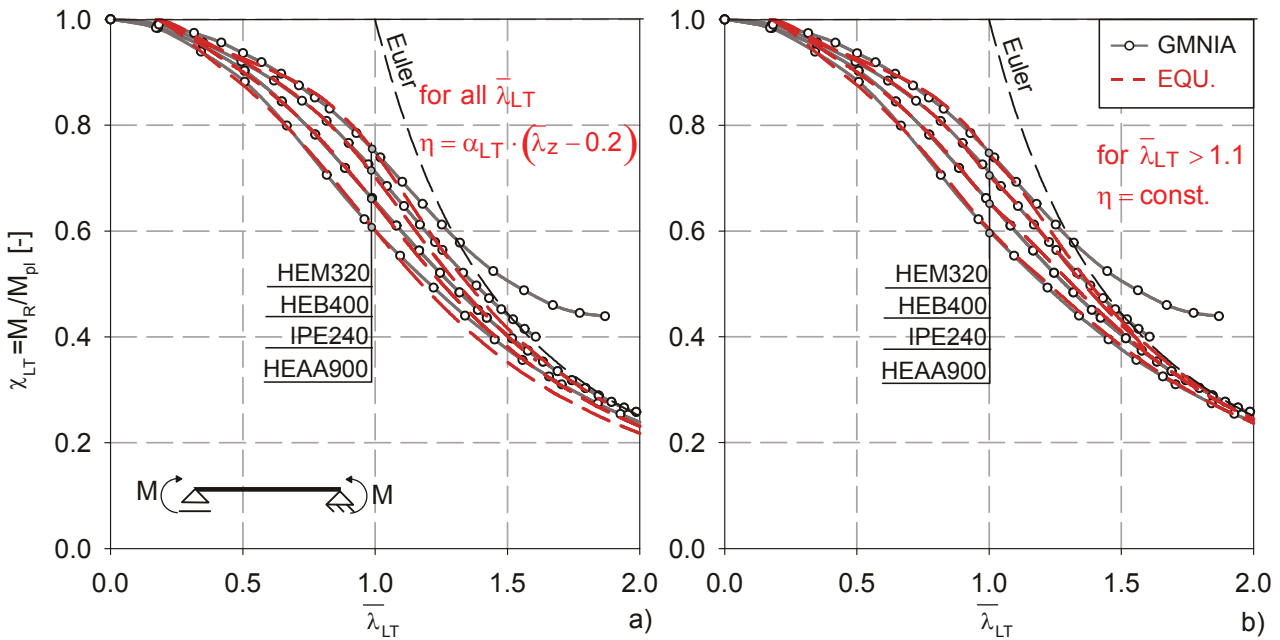
Fig 6-29 *Numerical vs. analytical curves - proposal of section 6.8.4 (a); introduction of a cut-off limit of η (b).*

This is exemplified by the plots in Fig 6-30. They show the results of the Montecarlo simulation of section 6.10 for an HEB 400 section, with mean values and m +/− 2s values marked by the dots in the vertical lines, as well as a numerical buckling curve for this section – calculated according to the criteria mentioned in section 6.6- and the analytical curve that results from (6.30) and the value of Φ_{LT} expressed by (6.43).
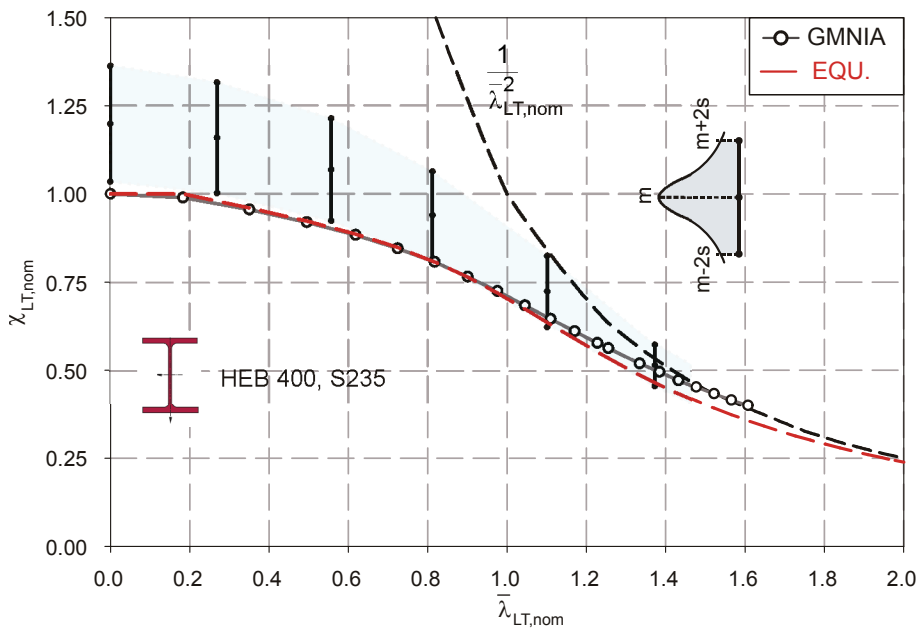
Fig 6-30 *Results of a Montecarlo simulation for a HEB 400 compared to a numerical buckling curve and the analytical formulation of section 6.8.4.*

In section 6.10, it is discussed with more detail that the numerical curve with "fixed" imperfection amplitudes changes from a very low fractile to one that falls within the interval $m-2s \leq \chi_{LT} \leq m$ with raising slenderness. Fig 6-30 shows that the tendency of the analytical curve to fall below the numerical curve at a slenderness exceeding $\overline{\lambda}_{LT}=1.0$ actually has the welcome effect of compensating this effect. In light of this, it makes sense to maintain (6.43) in its proposed form, at least for hot-rolled sections.

6.8.5. Welded sections and other residual stress distributions

In order to encompass the scope of the current "specific case" LT buckling formulae found in EC3, the description of LT buckling curves presented in the previous section 6.8.4 must be expanded to include welded sections that are geometrically "comparable" to the commercial hot-rolled sections. This has been done and is illustrated in Fig 6-31. The figure shows that the parameters discussed in the previous section again allow for a description of the slope of the numerical values of η in the practical, intermediate slenderness range. A "best-fit", least-square calibration of α_{LT} to the numerical χ_{LT} values for all studied sections led to a value of $\alpha_{LT}=0.21 \cdot \sqrt{W_{y,el} / W_{z,el}}$ in the case of welded sections in the studied h/b range of 1.0 to 3.3.

The distinctive bend around $\overline{\lambda}_{LT}=1.0$, discussed in section 6.5.2, is very noticeable both in terms of the generalized imperfection coefficient η and in terms of χ_{LT}. Again, the accuracy of the description could be improved by introducing a "cut-off" limit for η, but this is not followed through here. More pressingly, it is the assumptions regarding residual stresses in welded sections themselves that would be worthwhile of a deeper reconsideration, see section 6.5.2.
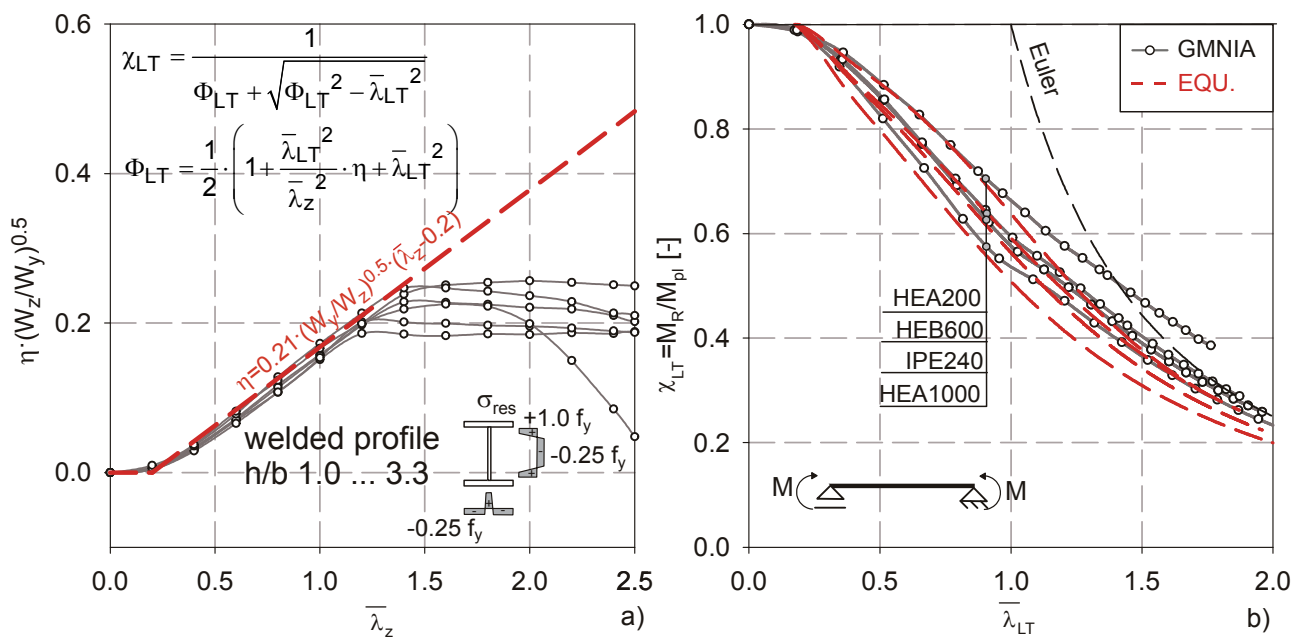
Fig 6-31 *Generalized imperfection coefficient for welded sections (a); buckling reduction factors for four selected sections (b).*

From a theoretical point of view, the most interesting finding is the fact that –again- the assumptions regarding residual stresses are reflected by the best-fit value of α_{LT}. In this context, it's worthwhile to add another "extreme case" to the considerations made herein, i.e. the case in which no residual stresses at all are considered. Fig 6-32 shows the results of numerical calculations for both in terms of the factor η and χ_{LT}, as well as the results of the analytical formulation (6.43) with a best fit value of $\alpha_{LT}=0.08\cdot\sqrt{W_{y,el}/W_{z,el}}$.

Again, the agreement of numerical and analytical curves is excellent in the slenderness range up to $\overline{\lambda}_{LT}=1.0$, although the curves seem to separate slightly before this slenderness in this case.

It can be concluded that the proposed formulation (6.30) with (6.43) is very well suited to represent the LT buckling strength of I- & H-beams for any range of geometrical properties (h/b, W_y, W_z …) and given set of assumptions regarding residual stress distribution and amplitude – the latter, however, requires a specific calibration, resulting in different values of α_{LT} for different underlying residual stress distributions. This is fully consistent with the flexural buckling case.

The following potential for further improvement is given by the proposed equation: it can be asserted that a better knowledge of the *actual* residual stress amplitudes and distributions found in hot-rolled and –even more importantly- welded I- & H-beams would make it worthwhile to develop an expression for α_{LT} that is a *function of the residual stress amplitude and distribution*, hence allowing for an inclusion of the (expected) residual stresses in the design function; this would allow for a consideration of such effects as stress relief heat treatment ("$\alpha_{LT}\simeq 0.08\cdot\sqrt{W_{y,el}/W_{z,el}}$") or improved welding procedures with low heat input ("$\alpha_{LT}<0.21\cdot\sqrt{W_{y,el}/W_{z,el}}$").
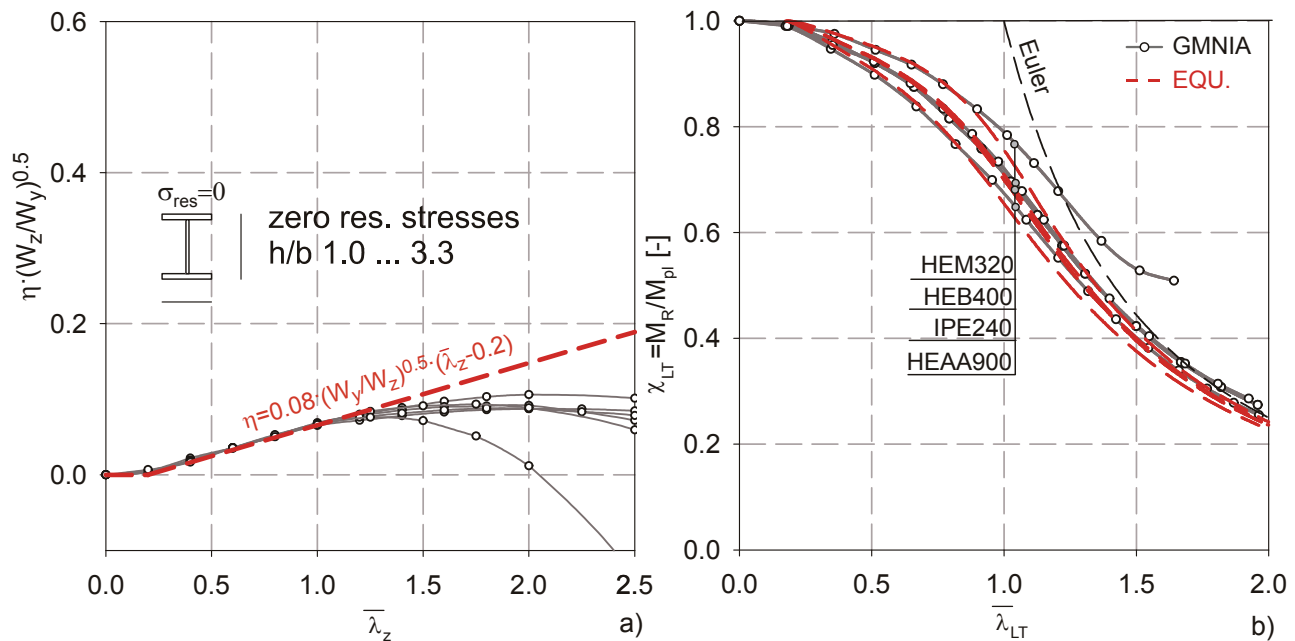
Fig 6-32 *Generalized imperfection coefficient for sections without any residual stresses (a); buckling reduction factors for four selected sections (b).*

6.8.6. Cross-sections with "extreme" geometry – limit values of α_{LT}

All calculations up to this point dealt with commercial, hot-rolled sections of the European IPE or HE series, as well as with "equivalent" (that is similar) welded sections. The cross-sectional factor $\sqrt{W_{y,el} / W_{z,el}}$ was shown to be an accurate descriptor of the behaviour of these sections; however, the factor does not asymptotically approach any constant finite with increasing ratio $W_{y,el}/W_{z,el}$, meaning that for very deep sections, or any sections with "extreme" ratio $W_{y,el}/W_{z,el}$, the generalized imperfection becomes increasingly, excessively large. In other words, it can be expected that this approximate classification factor will not be accurate enough to describe the behavior of at least some, extreme cross-sections. A limiting value of α_{LT} might be necessary, whereby the most straightforward –and desirable- such value is given by α_Z, the generalized imperfection amplitude valid for out-of-plane flexural buckling. The reasoning behind the last statement is that the flange of a very deep section with (comparatively) low torsional rigidity should behave similarly to a column in weak-axis buckling.

In order to check the validity of this reasoning, the sections shown in Fig 6-33 were added to the pool of studied sections. These sections include three (fictitious, non-commercial) hot-rolled sections, one with a very wide flange (ratio h/b=0.75) and a thin web, one very slender rolled section with h/b=6.6, and one section with h/b=4, but with very thick web and flanges, making this a torsionally very rigid section in spite of the high h/b ratio. Two welded sections were also studied, one with a very high h/b ratio of 10, and one with h/b=1.0 and thick plates. The residual stresses were assumed as shown in the figure, which means that no distinction between h/b ratios was made in the case of hot-rolled sections. The geometrical imperfections were assumed to have a shape affine to the eigenmode and to have an amplitude of $\overline{e}_0 = L / 1000$. The single sections are identified in the figure by "R" for rolled and "W" for welded sections. The exact geometrical input data is contained in Table 6-5.

This table also contains the values of α_{LT} that are obtained by applying the formulae in Table 6-4, as well as the value of $0.21 \cdot \sqrt{W_{y,el} / W_{z,el}}$ shown to apply for welded sections in 6.8.5. It also contains the value $\alpha_{LT,max} = \alpha_Z$, which is assumed to be the limiting value of the generalized imperfection.
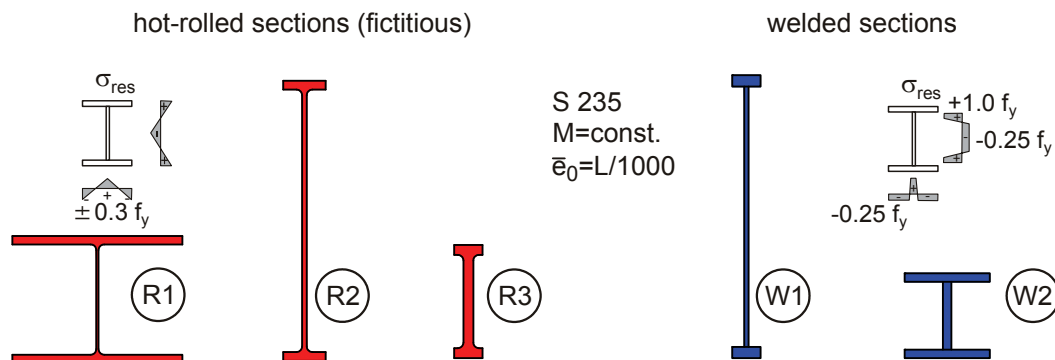
Fig 6-33 *Studied "extreme" geometries; "hot-rolled" (fictitious) and welded sections.*

	R1	R2	R3	W1	W2
h [mm]	450	990	400	1000	300
b [mm]	600	150	100	100	300
t_f [mm]	30	31	35	40	30
t_w [mm]	8	16.5	35	15	30
r [mm]	20	30	35	-	-
I_T [cm^4]	1076.8	524.5	1384.1	530.2	756.1
α_{LT}*	0.171	0.642	0.412	1.339	0.343
$\alpha_{LT,max} = \alpha_z$**	0.34			0.64	

* $0.12 \cdot (W_{y,el}/W_{z,el})^{0.5}$ for all hot-rolled sections, all (h/b); $0.20 \cdot (W_{y,el}/W_{z,el})^{0.5}$ for welded sections

** 0.34 for hot-rolled, 0.64 for welded sections (0.21/0.16 · 0.49=0.64)

Table 6-5 *Studied "extreme" geometries and underlying imperfection amplitudes α_{LT}*

One might notice that the value of $\alpha_{LT,max}$ for welded sections (0.64) is higher than the value for α_z found in the Eurocode for these sections; this stems from the fact –not discussed in full detail here– that the value of α_z for welded sections is not fully compatible with the now-common residual stress assumptions for welded sections; as a matter of fact, Young & Schulz (1977) clearly state that the theoretical/numerical calculations that led to the establishment of buckling curve c for weak-axis buckling FBzz of stocky hot-rolled and welded columns were *all based on the same assumption regarding residual stresses,* and that is the one used for stocky rolled sections.

As a consequence, it can be shown that the imperfection factor α_z should be somewhat higher to accurately describe (column) buckling curves calculated with the "welded" residual stresses of Fig 6-33. This also was reflected in the value of $\alpha_{LT}=0.21\cdot\sqrt{W_{y,el}/W_{z,el}}$ shown to apply for welded sections in LT buckling. This factor is 31% higher than the one that applies for stocky rolled sections ($0.16\cdot\sqrt{W_{y,el}/W_{z,el}}$). Therefore, the upper limiting value of $\alpha_{LT,max}$ is also assumed to lie 31% above the value of $\alpha_z=0.49$; Thus $\alpha_{LT,max}$ is set to 0.64 for welded sections.

Having concluded these introductory considerations, it is now possible to study the behaviour of the sections in Fig 6-33 by means of numerical GMNIA calculations, and to compare these results with the results of the new design formulation of section 6.7 and 6.8 for the different values of α_{LT}, as well as to the current Eurocode rules.

For hot-rolled sections, this is done in Fig 6-34. Figure a shows the behaviour of the very stocky "R1" section. For this section and the given imperfections, for which the formula of Table 6-4 for h/b>1.2 is applicable in spite of the actual ratio, a value of $\alpha_{LT}=0.171$ is calculated. This value is much smaller than the applicable $\alpha_z=0.34$, hence leading to a very high buckling curve. The question was whether or not this behaviour corresponds to the realistic, GMNIA behaviour.
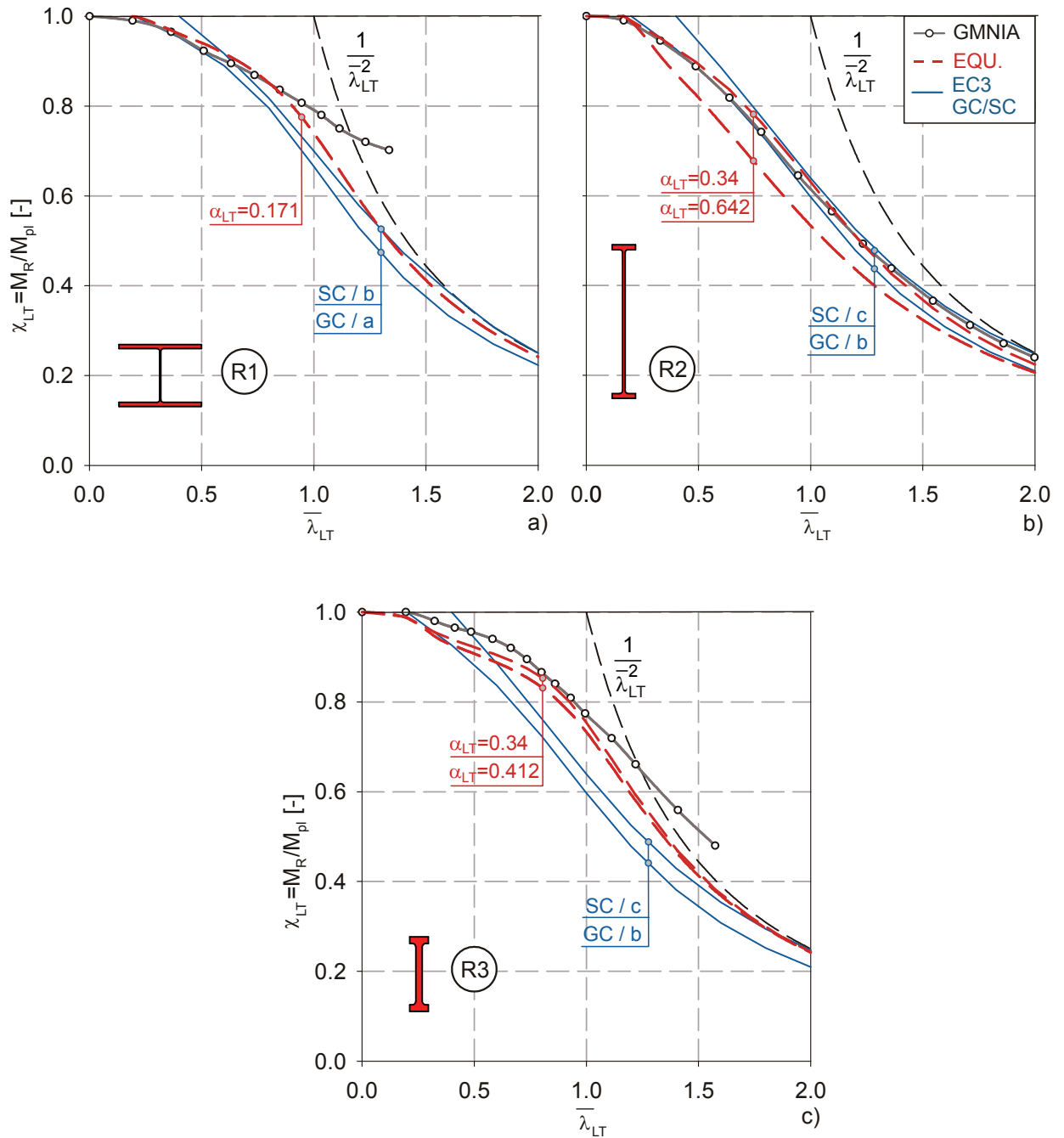
Fig 6-34 *GMNIA buckling curves for fictitious hot-rolled sections with "extreme" geometry; comparison with EC3 rules and with the new design formula.*

The main concern regarding such an unusually stocky section, with wide flanges and a thin web, is that the formulation yields too high values, which would be the case if the two flanges acted "independently", as a two-point cross-section. However, as Fig 6-34a shows, the "EQU" curve representing the new formula and the GMNIA curve almost overlap up to a slenderness of $\overline{\lambda}_{LT}$ of ca. 0.8; at this point, the analytical curve safe-sidedly diverges from the numerical one. It should be mentioned that, once again, this divergence only occurs at very high, non-practical lengths: a slenderness of $\overline{\lambda}_{LT}$ =0.8 corresponds to a length of 17.55 m for this section, i.e. to a L/h ratio of 39. The formulation for α_{LT} therefore seems to be able to accurately describe the behaviour of even

very stocky hot-rolled sections, at least within the practical ranges of length. The advantages in accuracy of the new formulation in comparison to the EC3 rules are also clearly felt for such a section.

Fig 6-34b shows the GMNIA buckling curves for the deep, slender R2 section and the resulting curves according to the new formulation, evaluated for the values of α_{LT} obtained from $\alpha_{LT} = 0.12 \cdot \sqrt{W_{y,el} / W_{z,el}} = 0.642$ and for $\alpha_{LT,max} = 0.34$. As the figure shows, the curve for $\alpha_{LT} = 0.642$ lies much too low for this section, which is what was expected in the first paragraph of this sub-section; the correction factor $\sqrt{W_{y,el} / W_{z,el}}$ is not accurate anymore for sections of this shape. Indeed, the postulated limiting value of $\alpha_{LT,max} = \alpha_z = 0.34$ is much better suited to describe sections of this type, as is clearly illustrated in the figure.

A partly similar, partly opposite tendency is observed in Fig 6-34c for the R3 section; this deep and narrow, yet very thick and torsionally stiff section features a GMNIA buckling curve that lies well above both Eurocode curves. It also lies well above the curve calculated with $\alpha_{LT} = 0.12 \cdot \sqrt{W_{y,el} / W_{z,el}} = 0.412$, and is most accurately described by the curve calculated with the limiting value $\alpha_{LT,max} = \alpha_z = 0.34$. The proposed formulation, combined with the limiting value of $\alpha_{LT} = \alpha_z$, thus seems to satisfactorily describe all studied hot-rolled sections.

The studies conducted for the two welded sections W1 and W2 are illustrated in Fig 6-35. For the slender, deep section W1, the expression $\alpha_{LT} = 0.21 \cdot \sqrt{W_{y,el} / W_{z,el}} = 1.339$ is again shown in Fig 6-35a to lead to a buckling curve that lies significantly below the numerical curve; by introducing the "limiting value" of $\alpha_{LT} = 0.64$ discussed above, the description becomes very accurate.
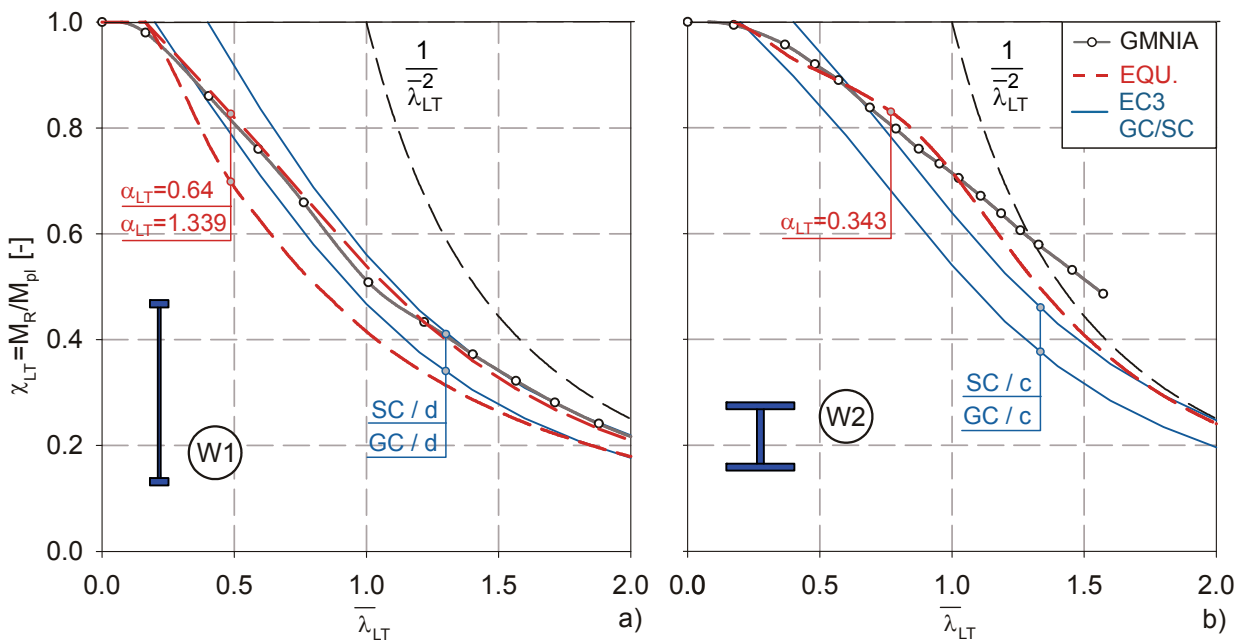
Fig 6-35 *GMNIA buckling curves for welded sections with "extreme" geometry; comparison with EC3 rules and with the new design formula.*

For the very stocky section in Fig 6-35b, the expression $\alpha_{LT} = 0.21 \cdot \sqrt{W_{y,el} / W_{z,el}} = 0.343$ is shown to be very accurate within the practical ranges of length.

In summary, it can be said that the general formulation $\alpha_{LT} = a_{LT} \cdot \sqrt{W_{y,el} / W_{z,el}}$, with a_{LT} being a constant, should be amended by a limiting value corresponding to α_z for hot-rolled sections, and a modification of α_z for welded sections. While this limiting value hardly becomes effective with the common geometries of commercial hot-rolled members, its introduction allows for an accurate and safe description of even some rather unusual sections.

Additionally, the limiting value has the advantage of making the inherent, equivalent imperfections – to be used e.g. in a second-order calculation- more consistent with the weak-axis flexural column buckling case. These can be calculated quite simply from (6.44), also see (6.40):

$$\overline{e}_0 = \eta \cdot \frac{W_z}{A} = MIN\left\{a_{LT} \cdot \left(\overline{\lambda}_z - 0.2\right); \alpha_z\right\} \cdot \frac{W_z}{A} \tag{6.44}$$

With the inclusion of the limiting value, a beam designed against LT buckling using a second-order calculation and a stress-based limit state will require an equivalent geometric imperfection that is *lower or equal* to the one that applies for weak-axis flexural buckling. This is theoretically desirable and particularly advantageous when one thinks of an application with combined loading N + M.

Finally, the following Table 6-6 is proposed for the calculation of the generalized imperfection amplitude α_{LT} for the design of hot-rolled and welded I- & H-sections.

h/b	hot-rolled I & H	Welded I & H
≤1.2	$\alpha_{LT} = 0.16 \cdot \sqrt{W_{y,el} / W_{z,el}} \leq 0.49$	$\alpha_{LT} = 0.21 \cdot \sqrt{W_{y,el} / W_{z,el}} \leq 0.64$
>1.2	$\alpha_{LT} = 0.12 \cdot \sqrt{W_{y,el} / W_{z,el}} \leq 0.34$	

Table 6-6 *Generalized imperfection amplitude α_{LT} and its limit values; final table.*

6.9. Treatment of non-uniform bending moments

In this section, an expansion of the proposed, new formulation for the buckling reduction factor χ_{LT} is presented that allows for a simple and accurate inclusion of the effects of non-uniform bending moment diagrams on the LT buckling strength of I- & H-sections. Since this formulation depends on a correct calculation of the normalized slenderness $\overline{\lambda}_{LT}$ and hence of the elastic, critical bending moment M_{cr} for the non-uniform moment case, this aspect is discussed first in the following.

6.9.1. Euler critical buckling moment

The formulae for the calculation of the elastic critical bending moment were given in section 6.2. It was pointed out that, in the widely used, so-called 3-factor formula (equation (6.1) respectively the subsequent simplification), the factor C_1 serves as the correction factor that modifies the critical moment $M_{cr,u}$ for uniform bending moment to obtain the applicable value for non-uniform moments $M_{cr,nu}$:

$$M_{cr,nu} = C_1 \cdot M_{cr,u} \tag{6.45}$$

Similarly, and bearing in mind that the critical bending moment is used primarily to calculate the normalized slenderness $\overline{\lambda}_{LT}$, it is also common to see the use of a modification factor k_c to be applied to the slenderness:

$$\overline{\lambda}_{LT,nu} = k_c \cdot \overline{\lambda}_{LT,nu} \tag{6.46}$$

Due to the definition of $\overline{\lambda}_{LT} = \sqrt{M_{pl} / M_{cr}}$ and the fact that M_{pl} is constant for prismatic members, C_1 and k_c stand in the following relationship:

$$k_c = \frac{1}{\sqrt{C_1}} \tag{6.47}$$

Many solutions for either C_1 or k_c are found in the literature for a variety of load cases. The ENV (1992) version of Eurocode 3 part 1-1 contains values of C_1 in form of a table; selected values of C_1, as well as the corresponding values of k_c calculated using (6.47), are given in Table 6-7.

Specifically for the case of a linear bending moment diagram, several slightly different formulae for C_1 or k_c are found in the literature. Trahair (1993) mentions the following two, whereby the first one is originally taken from Salvadory (1955):

$$C_1 = 1.75 - 1.05 \cdot \Psi + 0.3 \cdot \Psi^2 \le 2.5 \tag{6.48}$$

$$C_1 = \frac{1}{0.6 + 0.4 \cdot \Psi} \le 2.5 \tag{6.49}$$

Additionally to, and slightly diverging from the values in Table 6-7, ENV 1993-1-1 contains the following formula:

$$C_1 = 1.88 - 1.40 \cdot \Psi + 0.52 \cdot \Psi^2 \le 2.7 \tag{6.50}$$

Moment diagram	C_1 [-]	k_c [-]
	1.00	1.00
	1.132	0.94
	1.285	0.88
	1.365	0.86
	1.565	0.80
M ———— $\psi \cdot M$	Ψ=+0.5; C_1=1.323 Ψ=+0.0; C_1=1.879 Ψ=-0.5; C_1=2.704 Ψ=-1.0; C_1=2.752	0.87 0.73 0.61 0.60

Table 6-7   *Values of C_1 according to ENV 1993-1-1 (1992), and cooresponding values of k_c, valid for double-symmetric beams and end-fork conditions, load acting in the centroid*

Finally, EC3– EN 1993-1-1 clause 6.3.2.3 gives the following formula (6.51) for k_c for the beam under constant moment gradient. All four formulae are evaluated and illustrated in Fig 6-36.

$$k_c = \frac{1}{1.33 - 0.33 \cdot \Psi}$$

(6.51)
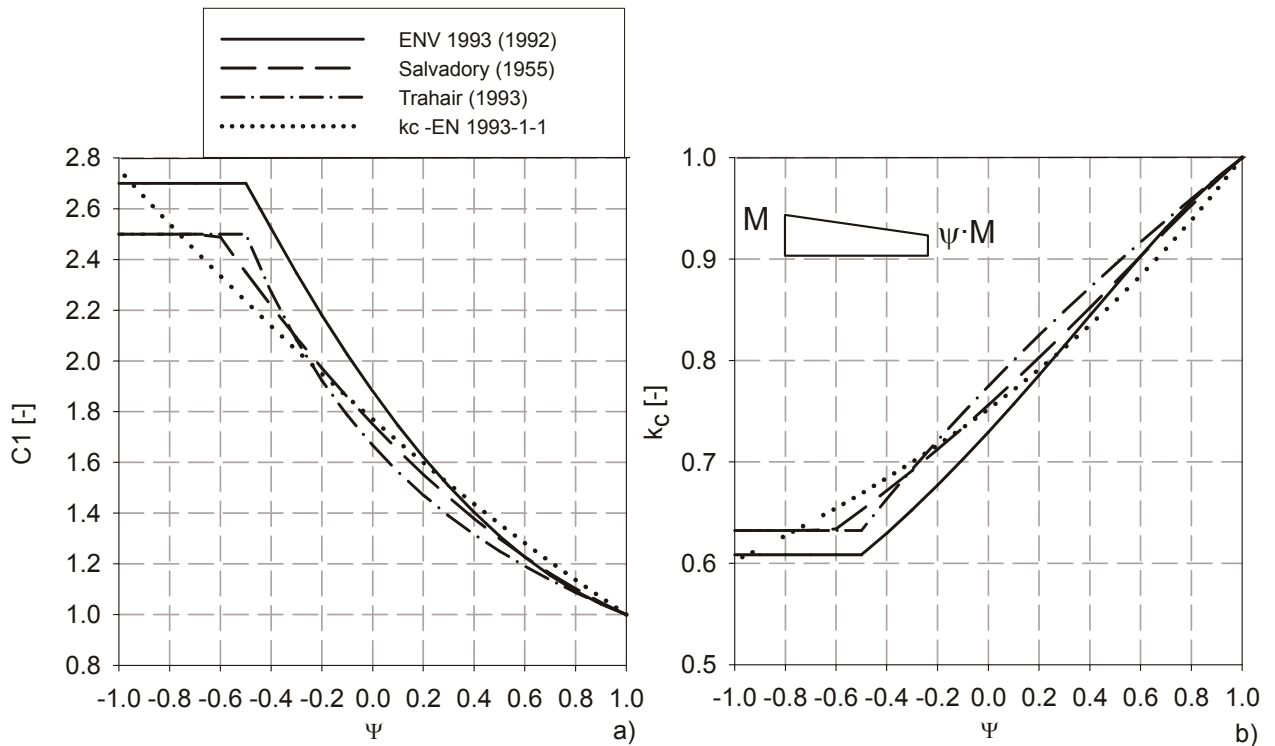
Fig 6-36 *Values of C_1 and k_c for constant moment gradients.*

6.9.2. Elasto-plastic behaviour (GMNIA)

Throughout this chapter, it was shown that the buckling reduction factor χ_{LT} is greatly variable when plotted over $\bar{\lambda}_{LT}$, with the resulting buckling curve's position and shape depending on a variety of factors that are not sufficiently taken into account by $\bar{\lambda}_{LT}$ alone. This is again true for the case of non-uniform bending moment diagrams, as is shown in Fig 6-37. The figure illustrates numerical, GMNIA buckling curves for a hot-rolled IPE 500 section and a variety of bending moment diagrams. The numerical values of χ_{LT} were obtained for geometrical imperfections corresponding to the first (LT) eigenmode shape and with *amplitudes of $e_0 = L/1000$.*

While the reduction factors χ_{LT} in the figure all refer to the same value of M_{pl}, it shall be noted that the value of $\bar{\lambda}_{LT}$ was consequentially calculated with the *correct value of M_{cr}*, using the results of numerical bifurcation analyses and validating them by comparison with the values of C_1 discussed in the previous sub-section. Therefore, the studied IPE 500 section will have different lengths, depending on the moment diagram, for a given value of $\bar{\lambda}_{LT}$.

The figure clearly illustrates that, due to reasons that are discussed with more detail farther below, the buckling curves are greatly influenced by the moment diagram when plotted over $\bar{\lambda}_{LT}$. Specifically the "plateau" value of the curves is clearly very heavily influenced by the moment diagram. Indeed, the differences are so large that ignoring them will necessarily lead to an uneconomical design. This is better illustrated in Fig 6-38. In this figure, GMNIA results are plotted for an IPE 500 section and a linear bending moment diagram with M=0 at one end of the beam.
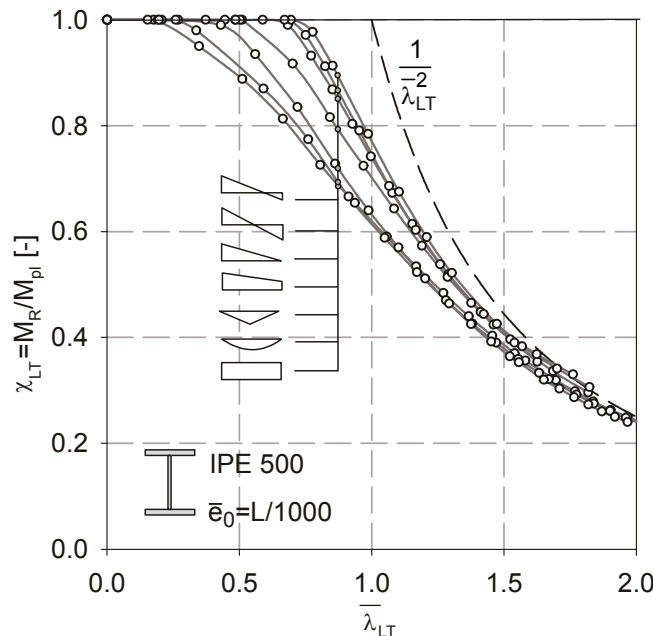
Fig 6-37 *Numerical (GMNIA) values of χ_{LT} for an IPE 500 section and different bending moment diagrams; steel grade S 235, residual stresses according to Fig 3-1.*

The results are compared to the two different codified LT buckling curves for this section according to the Eurocode, as well as to the (unmodified) formulation developed in section 6.7 and calibrated

in section 6.8.4. Again, $\overline{\lambda}_{LT}$ is calculated using the correct value of M_{cr} for all cases. The figure shows that, without modification, neither the Eurocode formulae nor the new formulation are accurate in any but the very large slenderness range. The largest differences occur at low slenderness, which especially for the particular load case studied in Fig 6-38 is the practically most relevant range.

EQU.:

$$\chi_{LT} = \frac{1}{\Phi_{LT} + \sqrt{\Phi_{LT}^2 - \overline{\lambda}_{LT}^2}}$$

$$\Phi_{LT} = \frac{1}{2} \cdot \left(1 + \frac{\overline{\lambda}_{LT}^2}{\overline{\lambda}_z^2} \cdot \eta + \overline{\lambda}_{LT}^2 \right)$$

$$\eta = 0.12 \cdot (W_y/W_z)^{0.5} \cdot (\overline{\lambda}_z - 0.2)$$
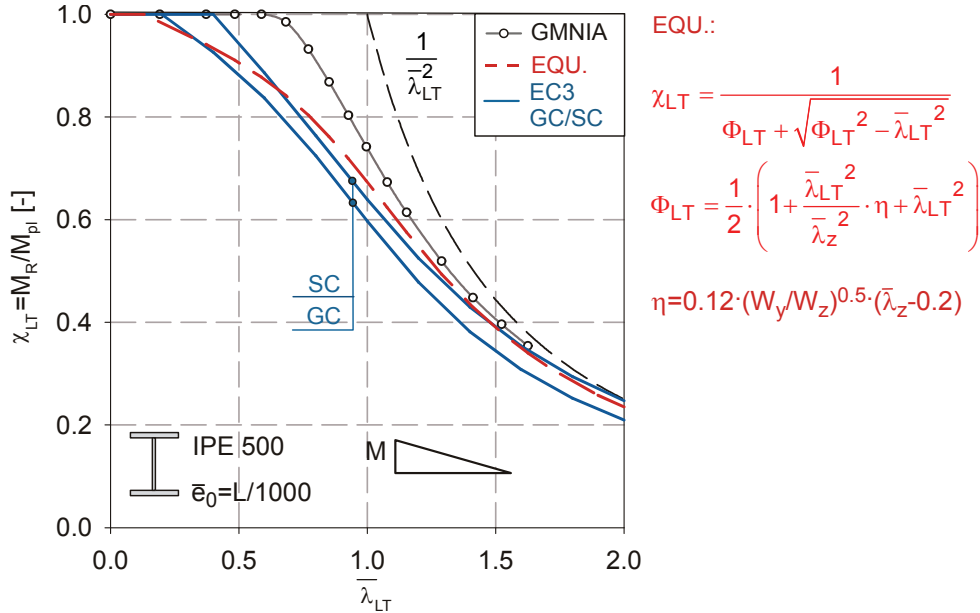
Fig 6-38 *Comparison of unmodified LT buckling formulations with GMNIA results for moment gradient.*

Thus, the buckling reduction factors must be modified if accuracy ought to be improved. Before this is done for the new formulation proposed in this thesis, the current rules in the Eurocode 3 are briefly discussed.

6.9.3. Treatment of non-uniform bending moments in Eurocode 3

In the Eurocode 3, the impact of the bending moment diagram on the buckling reduction factor χ_{LT} is only explicitly addressed in the so-called "specific case" discussed in clause 6.3.2.3 of the code, which was specifically calibrated to double-symmetric hot-rolled (or equivalent welded) sections. In this case, the reduction factor χ_{LT} valid for the "specific case" (SC) is modified by a factor f as follows:

$$\chi_{LT,mod} = \frac{\chi_{LT}}{f} \quad \begin{array}{l} \leq 1.0 \\ \leq 1/\overline{\lambda}_{LT}^2 \end{array} \tag{6.52}$$

$$f = 1 - 0.5 \cdot (1 - k_c) \left[1 - 2.0 \cdot \left(\overline{\lambda}_{LT} - 0.8 \right)^2 \right] \leq 1.0 \tag{6.53}$$

This formulation was proposed by Lindner (2000) and based on curve-fitting of an extensive series of GMNIA numerical calculations (Greiner et al., 2000). Specifically, the factor f was calibrated to give best-fit results when applied to the "specific case" formulations valid for the constant moment

load case. It was found to be convenient to make use of the factor k_c, which was discussed in section 6.9.1, to include the influence of a variable moment diagram by using the information contained in this factor concerned with elastic bifurcation.
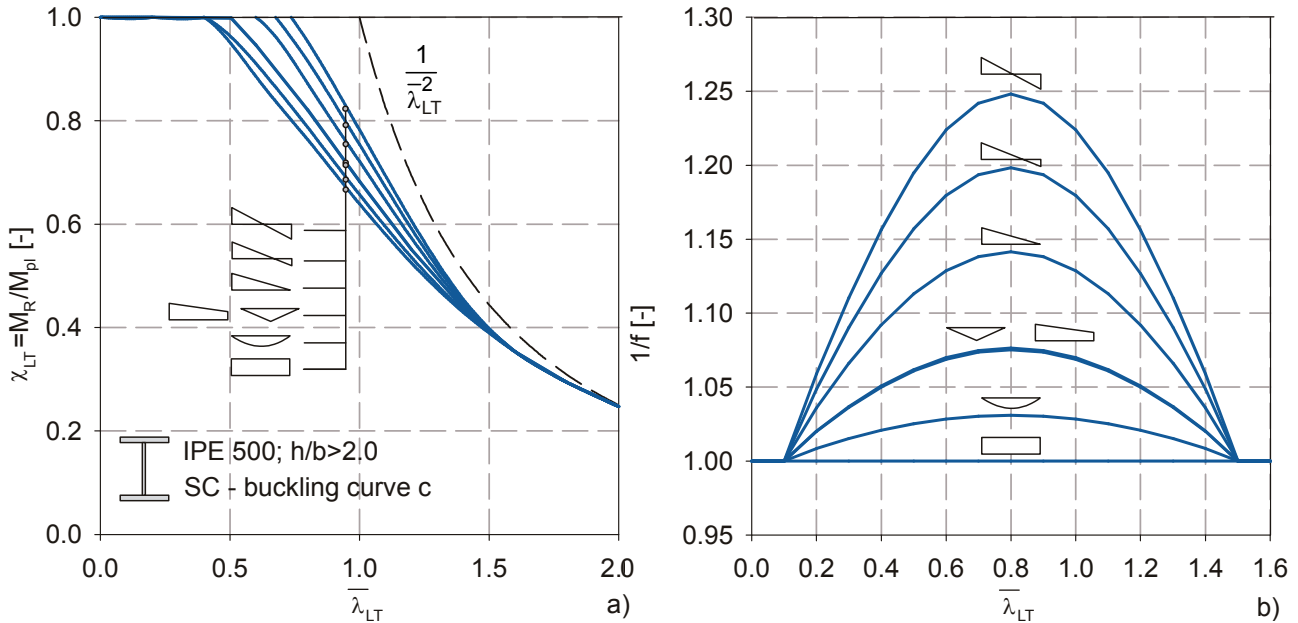
Fig 6-39 *"Specific case" buckling curves for different bending moment diagrams according to the Eurocode (a); modification factor 1/f (b).*

The resulting factor $\chi_{LT,mod}$ and the factor 1/f are plotted in Fig 6-39. The figure shows that the factor 1/f, which indicates the increase of the buckling factor χ_{LT} when compared to its un-modified version, was formulated so that it has a parabolic shape when plotted over $\overline{\lambda}_{LT}$ and reaches its maximum at $\overline{\lambda}_{LT}$ =0.8, with a value of $2/(k_c+1)$. This was observed to be in good agreement with the numerical results. At a value of $\overline{\lambda}_{LT}$ =1.5, the un-modified value of χ_{LT} is again valid for all load cases.

The presented treatment of non-uniform bending moments using the factor f has the advantage of being fairly straightforward and often quite accurate when compared with FEM calculations. It does, however, present the following disadvantages:

i.   The factor f was fitted to be accurate when used in combination with the "specific case" LT buckling curves of EC3. Since the formulation $\chi_{LT,SC}$ itself must be correctly seen as curve-fitting to FEM calculations amended by the statistically justified plateau value, the accuracy of the factor $\chi_{LT,mod}$ depends heavily on the accuracy of $\chi_{LT,SC}$; the latter was shown to be high only for some sections, see Fig 6-15.

ii. Since the factor f has no mechanical justification, other than resulting in a good fit of numerical curves when used in combination with the Eurocode "specific case" factors for χ_{LT}, it has been questioned whether or not it can be used in combination with other LT buckling curves, e.g. with the "general case" curves of the same code. Through a "loop-

hole", this possibility is not entirely excluded by the code, which leaves the option open for so-called "nationally determined parameters". From a "safety" point of view, one can also show that the factor would actually always be "conservative" when used in combination with the (generally lower) general-case curves. Nevertheless, it is clear that this use was not *intended* by the developers of the factor f, and is mechanically entirely unfounded.

6.9.4. Proposal for an adaptation of the new formulation

The development of a new, specific formulation for χ_{LT} in section 6.7 and the calibration of section 6.8 proved to be very accurate and effective for the case of uniform bending moments. However, in Fig 6-38 it was shown that not even this new, specific formulation (referred to as "new formulation" in the following) is able to accurately describe the course of a numerical buckling curve for cases with non-uniform bending moment diagrams. This is of course not surprising and explicable by the fact that the formulation was derived only for the basic case of constant bending moments.

It is therefore clear that the newly developed formula of section 6.7 and 6.8 must be modified in order to obtain an accurate formulaic description of the realistic buckling behaviour of members under non-uniform bending moments. Thereby, existing modifications, specifically the factor f of the Eurocode 3, cannot directly be applied due to the reasons given in the previous section, where it was shown that f can correctly only be used in conjunction with the "specific case" buckling curves of the code. If the factor were applied to the new formulation, it would also often be "unsafe", since the new formulation yields values of χ_{LT} that can lie above the specific-case curves.

A different, new type of modification is therefore introduced in the following, which is based on realistic assumptions and approximations regarding the ultimate LT buckling behaviour.
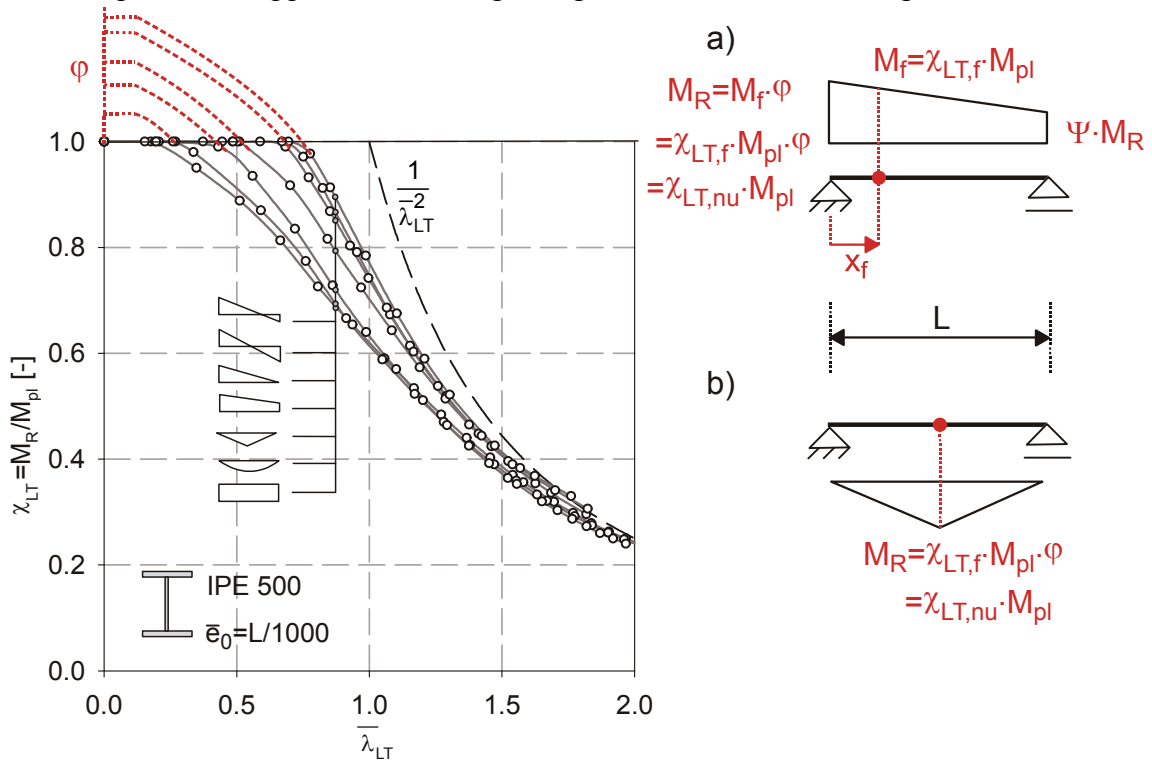
Fig 6-40 *Basic idea: introduction of an "over-strength" factor φ.*

The result is a factor $\chi_{LT,nu}$, i.e. a modified version of the "new formulation" for χ_{LT} introduced in section 6.7, which takes into account the non-uniform bending moments. The basic idea behind the development of this formulation is shown in Fig 6-40.

The plot on the left of Fig 6-40 shows a qualitative, plausible extension of the GMNIA buckling curves presented in section 6.9.2. This fictitious extension can be interpreted as follows:

i. In the case of bending moment diagrams with constant moment gradient, the main effect leading to the observed shifting of the plateau value of the numerical buckling curves towards higher values of slenderness is given by the fact that the location of the maximum (first-order) bending moment in the beam at failure does *not* correspond to the location of failure x_f; the former is at the beam's extremity, while the latter is at a certain location within the beam's free span. By observing the shape of the (extended) curves, one can see that this has a quite similar effect to the one given by an "over-strength" of the material, confront with Fig 6-12; the influence is largest at very low slenderness, and vanishes at very high slenderness. This "over-strength" φ is of course actually not related to the cross-section capacity itself, but to the moment that *would need to be applied at the beam's extremity in order to reach M_{pl} at the location of failure*. This end moment is also the one to which M_R, M_{cr} and χ_{LT} refer. If we assume that, in the case of constant moment gradients, φ indeed only depends on the difference between the location of maximum moment and failure x_f, it can be calculated as follows:

$$\varphi = \frac{1}{\Psi + (1 - \Psi) \cdot (1 - x_f / L)} \tag{6.54}$$

The difficulty of evaluating (6.54) is of course entirely given by the identification of the failure location x_f. In principle, this location can only be determined by a non-linear calculation, which defeats the purpose of developing a buckling design formula in the first place. However, it can be shown that –in the simple, yet practically most relevant cases- the failure cross-section is fairly stably located at certain fractions of the total beam length. Some examples are given in Fig 6-41a for an IPE 500 section with eigenmode-conform imperfections of amplitude $\bar{e}_0 = L/1000$. In this figure, the failure location was identified by the location of the maximum (plastic) strains in the compression flange at failure.

ii. In the case of variable moment distributions with a clearly identifiable failure location, i.e. for example failure at mid-span for a concentrated load at the same location, the beneficial effect in terms of χ_{LT} is less pronounced, see again Fig 6-40. However, in principle the same "over-strength" behaviour is observable. As is indicated in the figure, in this case this cannot be attributed to a mismatch of failure and maximum load position, as these are the same.
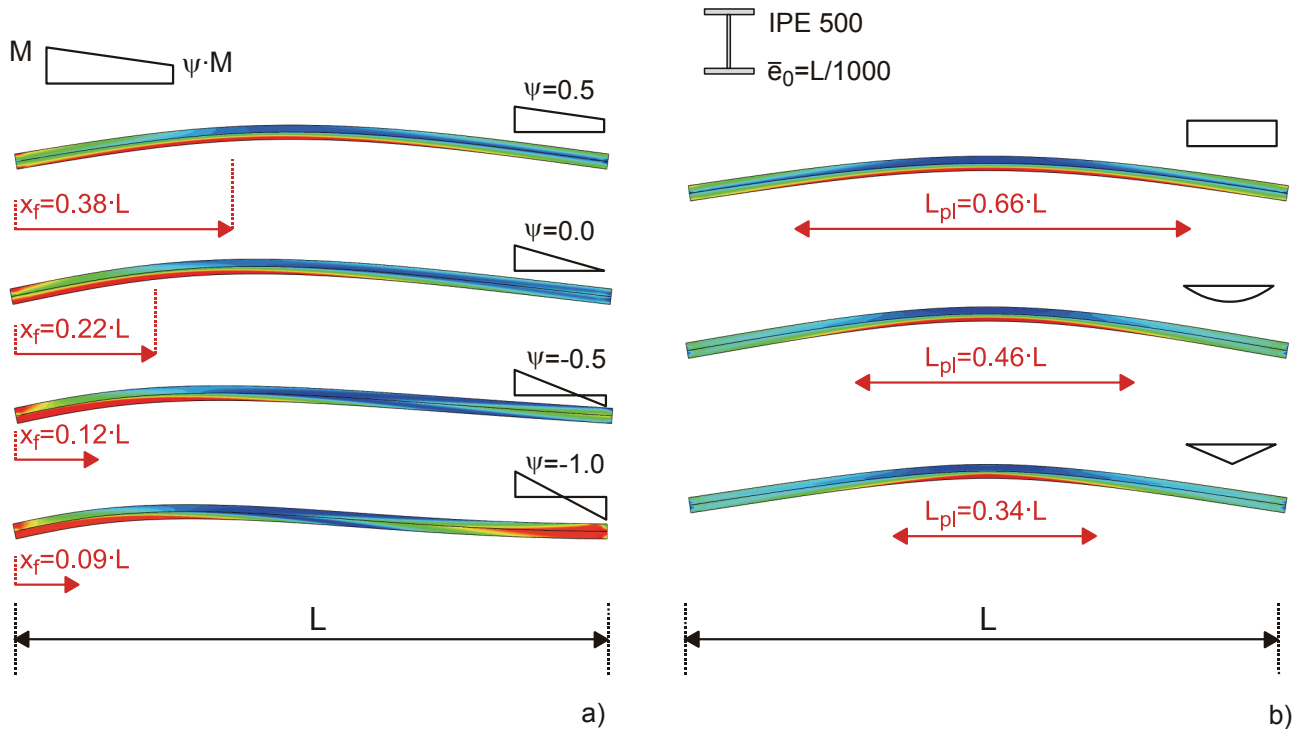
Fig 6-41 *Results of GMNIA calculations for an IPE 500 section of S235, $\bar{\lambda}_z = 2.0$; contour plot of Mises stresses in the compression flange at failure.*

As was pointed out by Greiner et alt. (2000), this must much rather be attributed to a difference in the size of the plastic zone surrounding the exact failure location/cross-section. In Fig 6-41b, the length of the plastic zone at failure, defined as the distance between the outermost locations where the yield strain has been exceeded, is compared for three typical moment diagrams. While the higher "supporting" action cannot be directly quantified from these figures, they do point out the general tendency.

In summary, it can be stated that the observations made regarding the influence of the moment diagram in the GMNIA calculations of Fig 6-40 can primarily be interpreted as the effect of an "over-strength" factor φ with respect to the maximum moment in the beam at buckling. In order to incorporate this "over-strength" in the design formula for χ_{LT} developed in section 6.7, the terms containing "M_{pl}" must be replaced with "$M_{pl} \cdot \varphi$". This results in the following modification to the limit-state formulation:

$$\frac{\chi_{LT}}{\varphi} + \eta \cdot \varphi \cdot \frac{\bar{\lambda}_{LT}^2}{\bar{\lambda}_z^2} \cdot \frac{\frac{\chi_{LT}}{\varphi}}{1 - \frac{\chi_{LT}}{\varphi} \cdot \varphi \cdot \bar{\lambda}_{LT}^2} = 1.0 \tag{6.55}$$

with:
$$\eta = \alpha_{LT} \cdot \left(\bar{\lambda}_z - 0.2 \right) \tag{6.56}$$

and α_{LT} taken from Table 6-4.

Equation (6.55) can again be solved as follows:

$$\chi_{LT} = \frac{\varphi}{\Phi_{LT} + \sqrt{\Phi_{LT}^2 - \varphi \cdot \overline{\lambda}_{LT}^2}} \leq 1.0 \tag{6.57}$$

with

$$\Phi_{LT} = \frac{1}{2} \cdot \left(1 + \varphi \cdot \left(\eta \cdot \frac{\overline{\lambda}_{LT}^2}{\overline{\lambda}_z^2} + \overline{\lambda}_{LT}^2 \right) \right) \tag{6.58}$$

The value of χ_{LT} is limited by 1.0 in this formulation in order to cover all cases where the failure criteria is given by the cross-sectional capacity at the location of the (reference) maximum moment alone.

It must be clearly stated that the above formulation is a *simplificaton* of the actual behaviour. The following assumptions are thereby made:

i.   The second-order buckling amplification factor $1/\left(1 - \chi_{LT} \cdot \overline{\lambda}_{LT}^2\right)$, shown in section 6.7 to be applicable to the LT buckling case under constant bending moment *if eigenmode-conform imperfections are considered*, is applied without modification; in reality, non-uniform bending moment diagrams would require a (moderate) modification of this factor to be fully accurate, as is the case for amplification factors applied to columns with variable shapes of initial imperfection and/or lateral load.

ii. The generalized imperfection amplitude η, calibrated in section 6.8, is taken to be valid in this formulation. This is justified by the fact that the same geometrical and material imperfection amplitudes are applied in the GMNIA calculations, with the only difference being the *shape* of the imperfection.

In practical terms, these simplifications do not necessarily affect the accuracy of the resulting formulation. As a matter of fact, the newly introduced "over-strength" factor is conveniently used to also cover the inaccuracies stemming from the above simplifications, additionally to the actual physical effects that it is intended to take into account (i.e. the distance between failure and loading point, respectively the influence of the size of the plastic zone).

For practical applications, a table (Table 6-8) is proposed containing values of φ for some typical bending moment diagrams, to be used in (6.57) and (6.58). As the following section shows, these values give very satisfying result in terms of accuracy. They were obtained through a series of 96 GMNIA calculations (8 sections, 12 load cases).

The proposal spans values of φ ranging from 1.00 to a maximum of 1.267 at $\Psi=-1/3$ in the case of a constant moment gradient. In the case of non-uniform moments with maximum sagging moment at mid-span, values of 1.05 and 1.11 were found to apply for parabolic and triangular diagrams, respectively. Interestingly, the shape of the curve between the two values at the extremities seems to be the predominant factor in these cases.
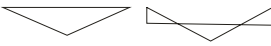
Moment diagram	φ [-]
	1.00
	1.05
	1.11
M $\psi \cdot$M	$1.25 - 0.1 \cdot \psi - 0.15 \cdot \psi^2$

Table 6-8   *Proposed values of φ for hot-rolled and welded I- & H-sections.*

Fig 6-42 shows the results of some of these GMNIA calculations in terms of φ, calculated by identifying the failure location in the numerical calculation and applying equation (6.54) for a series of hot-rolled I-sections with values of h/b spanning from 1.0 to 3.30, and loaded by a constant gradient bending moment. The failure location was thereby identified as the position of the cross-section where the maximum strains occurred.

Additionally, the figure shows a formulaic approximation of the GMNIA results, obtained from a polynomial regression analysis.

The scatter indicates that any formulation of this type can only be an approximation, as the exact failure location is dependent on the section type itself. Nevertheless, the general tendency of the values of φ can be described fairly well by a parabolic approximation.
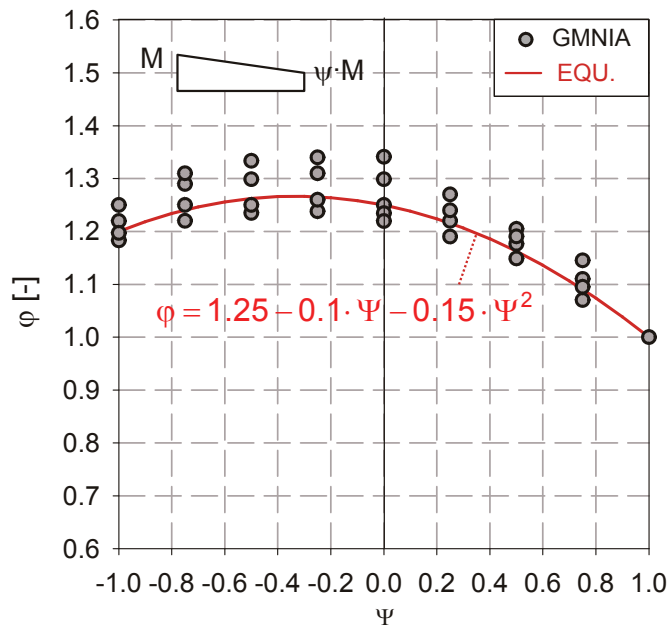
Fig 6-42 *GMNIA results in terms of φ for contant moment gradients and hot-rolled I- & H-sections.*

6.9.5. Accuracy of the new formulation

The accuracy of the proposed expansion of the new formulation to a number of cases with non-uniform bending moment is demonstrated in this section by comparing the results of GMNIA calculations with an evaluation of (6.57) with values for φ taken from Table 6-8. Thereby, results for two typical hot-rolled beam sections are included, i.e. an IPE 500 and an HEB 400 section. These are representative of slender and stocky sections, respectively. All calculations were carried out for steel grade S235, and for eigenmode-affine initial imperfections with amplitude $\overline{e}_0 = L/1000$. The results of these calculations are shown in the following figures (Fig 6-43 - Fig 6-45). The accuracy of the proposed formulation is apparent. In order to be able to better appreciate gains in comparison to the current Eurocode design practice, the applicable formulae (general case and specific case modified by the factor f) are included as well.
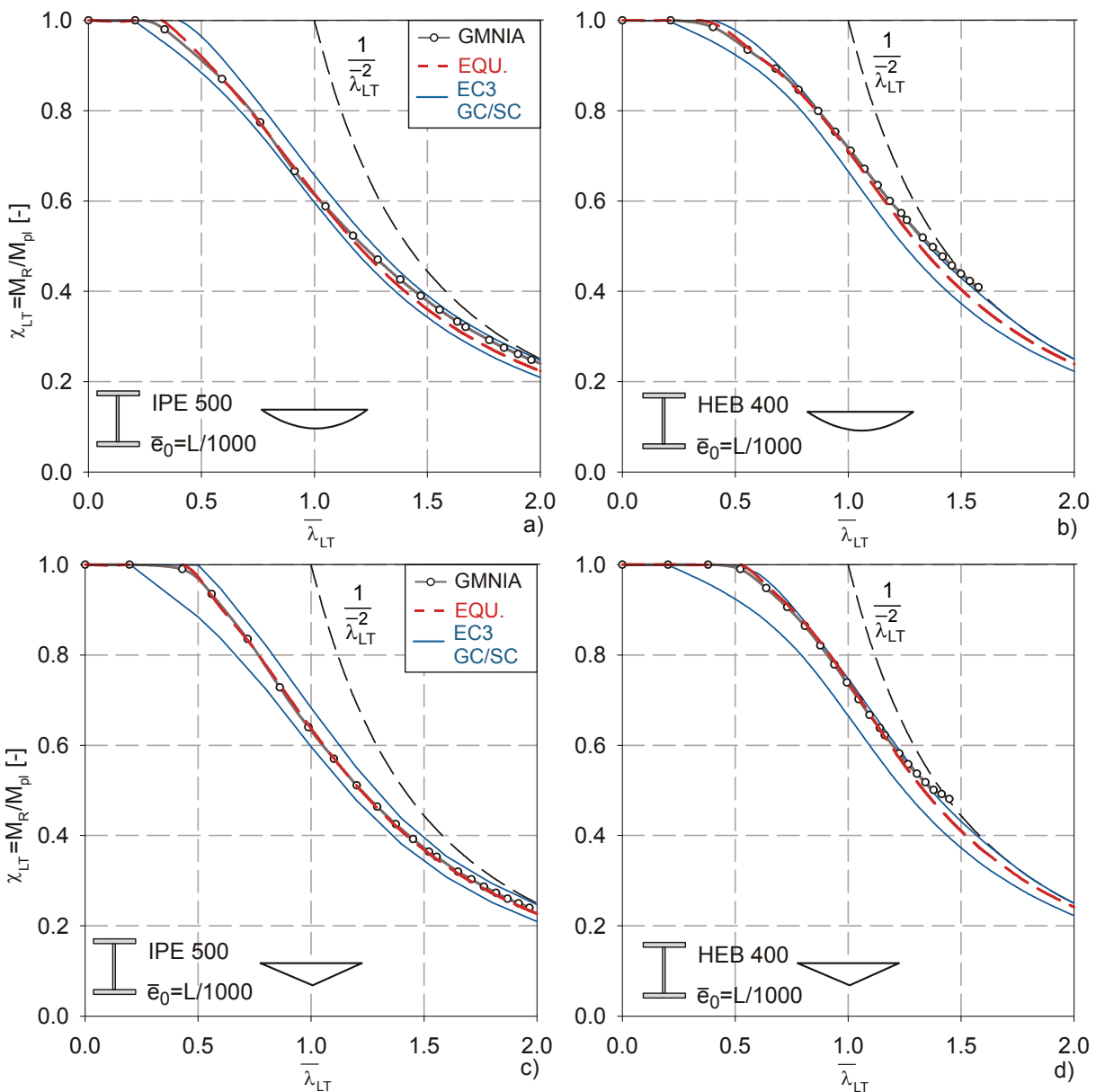
Fig 6-43 *Accuracy for parabolic and triangular moment diagrams with maximum at mid-span.*
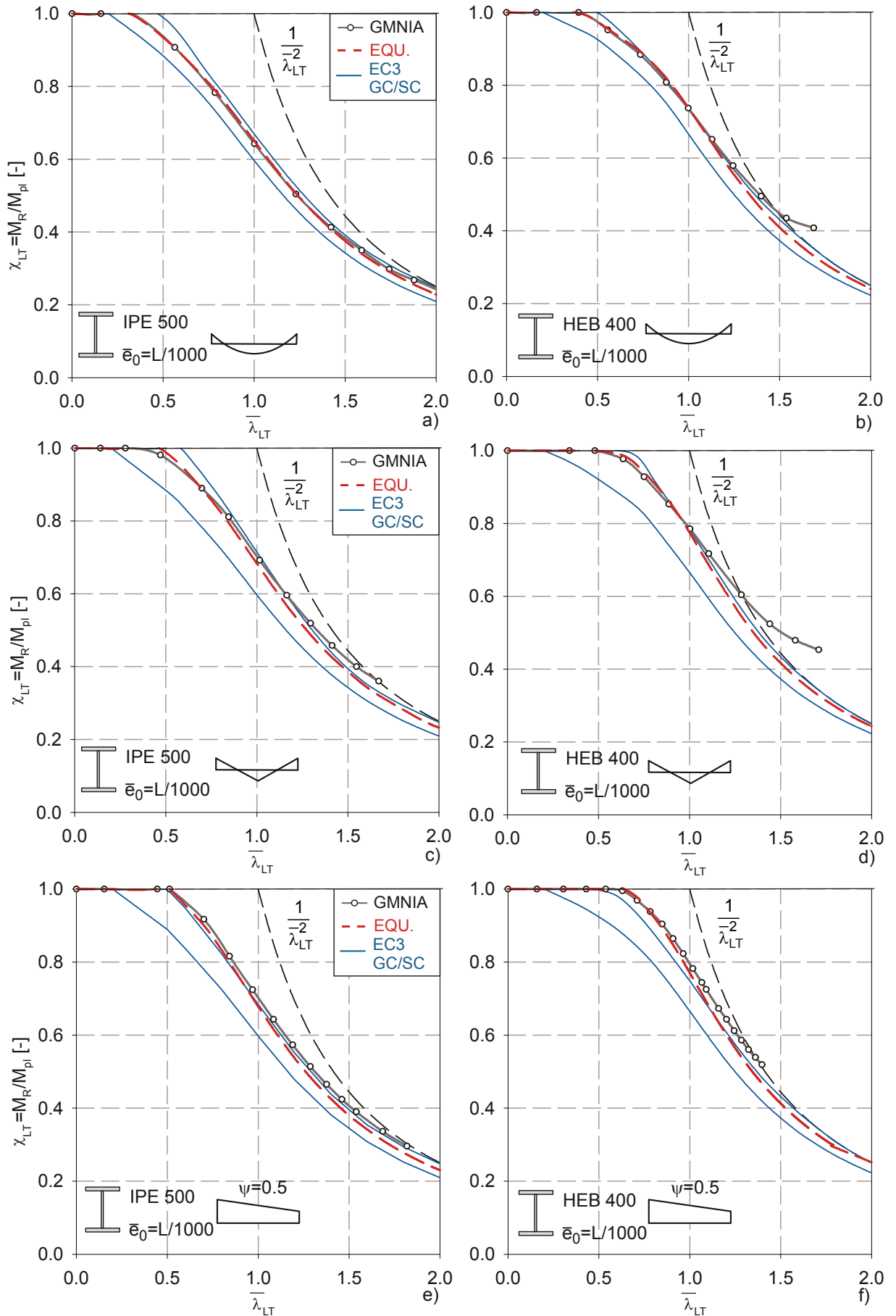
Fig 6-44 *Accuracy for various non-uniform bending moment diagrams.*
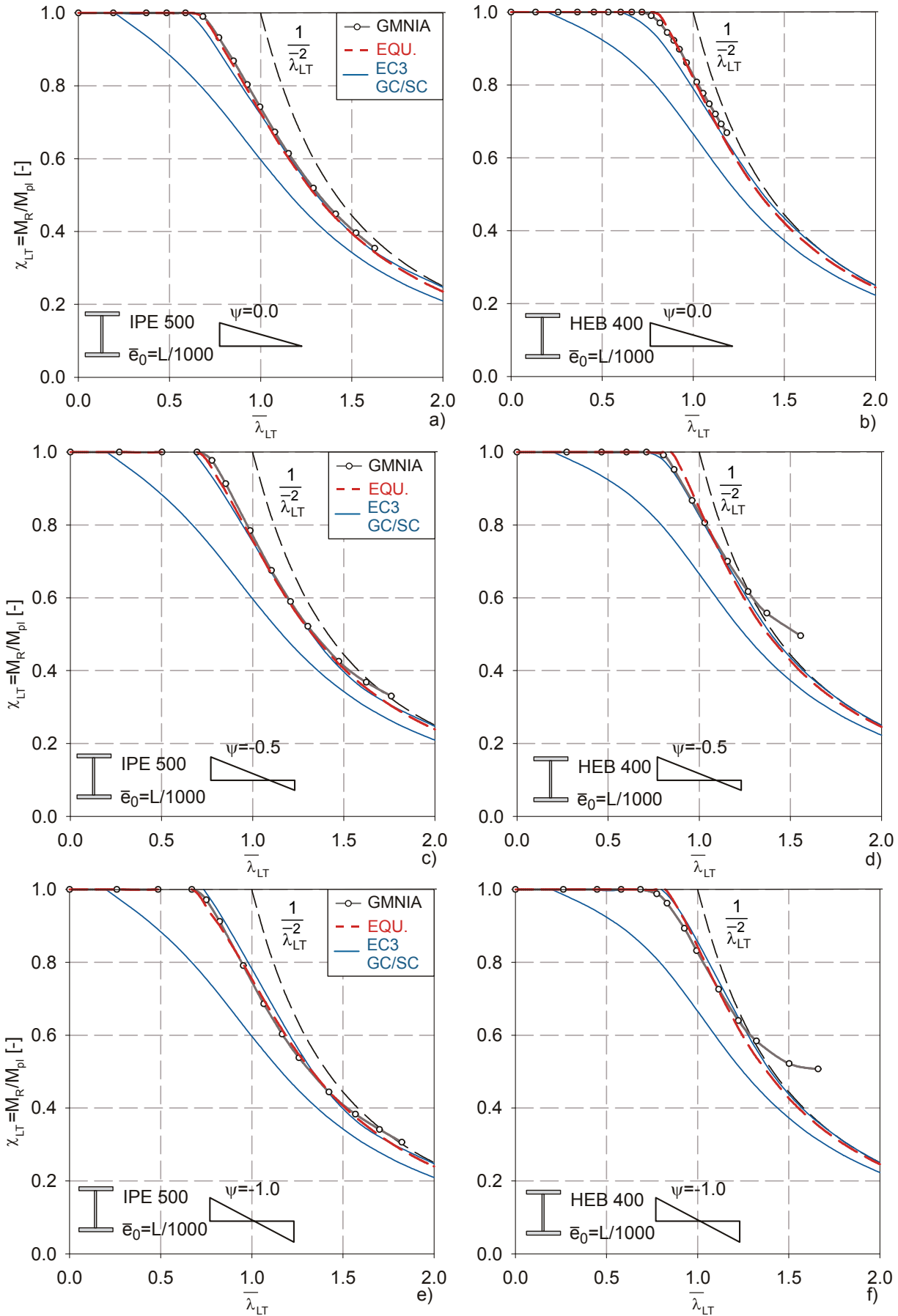
Fig 6-45 *Accuracy for constant gradient bending moment diagrams*

Fig 6-43 to Fig 6-45 show that the proposed, new formulation is able to describe the behaviour of the GMNIA model beams better than the current Eurocode 3 formulations. However, it shall not remained unmentioned that the "specific case" formulation, when modified by the factor f, is also often quite accurate. This should come as no surprise, since this formulation was also specifically calibrated to describe quite similar GMNIA calculations for hot-rolled sections. Again, the main advantage of the new formulation is a combination of accuracy and mechanical soundness. The greater mechanical soundness is, for example, clearly felt by the fact that equation (6.57) requires no additional check against the exceeding of the Euler load $M_R=M_{cr}$, naturally converging against this upper limit for very high slenderness or if α_{LT} is set equal to zero, while the "specific formulation" (6.52) does require such a check.

Additional calculations for different sections (hot-rolled and "equivalent welded") have shown the accuracy resulting from the new formulation to be comparable to what is shown in the following figures, with the largest (conservative) deviations in the practical range of beam length occurring in the case of welded sections, and being smaller than 7%.

The proposal made in this section is by no means exhaustive, as many other bending moment diagrams would need to be analysed even to be considered complete for the simple case of simply-supported beams with uniform cross-section. Nevertheless, it is believed that the proposed procedure could fairly easily be expanded to other cases by obtaining suitable values of φ for these cases, thus providing a methodology that can be replicated in order to obtain accurate design formulae that are based on simple, yet consistent engineering models.

6.10. Reliability Level & Monte Carlo Simulations

All considerations up to this point in this chapter were concerned with the "deterministic" description of the behaviour of a "model beam" with certain, specified structural parameters. The expected reliability level of the newly developed formulae in terms of the Eurocode semi-probabilistic design philosophy is treated in this section. Thereby, reference is made to both real, physical tests published in the literature and to Monte Carlo simulations.

6.10.1. Statistical evaluation based on physical tests

The source of the recommended values of the partial safety factor γ_{M1} for LT buckling in the ENV and EN versions of the Eurocode has already been discussed in chapter 4, Fig. 4-4d, and is re-plotted here in Fig 6-46. In this most recent work dealing with the statistical evaluation of physical test results for LT buckling, Müller (2003) considered tests on I- & H- sections (144 hot-rolled; 71 welded) that were carried out internationally and collected e.g. in the CEC (1988) background document to Eurocode 3, or later by Greiner & Kaim (2001). He evaluated these tests for the so-called "general case" LT buckling rule of EC3 and thereby grouped together a variety of different load cases.
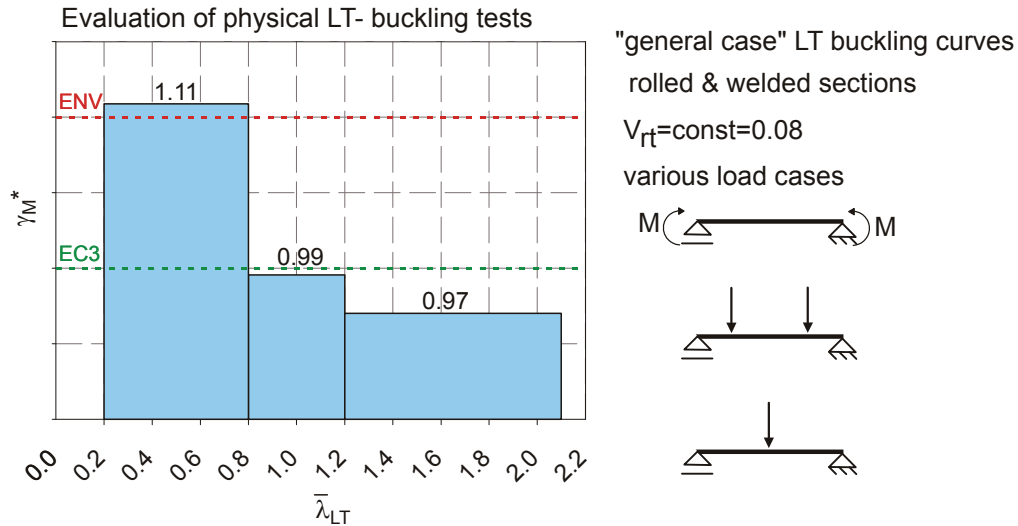
Fig 6-46 *Background of the recommendations for γ_{M1} for LT buckling in the ENV and current (EN) version of EC3.*

The results of this evaluation in terms of γ_M^* led to the conclusion that the "general case" LT buckling curves require a safety factor of $\gamma_{M1}=1.1$, whereby this becomes conservative with increasing slenderness.

In the following, the above conclusions drawn from physical test results are verified and expanded to include the new design formula proposed in this chapter, as well as the "specific case" curves. In order to eliminate the possibility of influencing the statistical evaluation by the grouping of too many different effects, only tests concerned with *a single section series* and *the constant bending moment* load case are considered.

Of the more than 140 tests on hot-rolled sections reported in the CEC (1988) Eurocode background document, the vast majority were carried out in Japan, using Japanese H sections. Of these, 46 tests were carried by Suzuki, Fukumoto and Wakabaya with constant bending moment diagrams between lateral supports and using a **H 200x100x5,5x8** section with a steel grade equivalent to a S235.

These tests are plotted in Fig 6-47 and compared to the current Eurocode regulations and the new design equation (EQU) proposed in this chapter. The GMNIA calculations on which the latter proposal is based are also shown in order to again demonstrate the accuracy of the proposal in describing the behaviour of the deterministic "model beam".

In Fig 6-47a, the results are presented in terms of the nominal buckling reduction factor $\chi_{LT,nom}$ based on the nominal plastic moment capacity $M_{pl,nom}=48.2$ kNm of the studied section, and plotted over the nominal normalized slenderness. In Fig 6-47b, the results (theoretically) refer to the "actual" measured values of M_{pl}, whereby this fact needs some more discussion in the following paragraph. Both plots make use of values of χ and $\bar{\lambda}$ taken from the report by Greiner & Kaim (2001), with only a minor modification of the nominal values, which are made to refer to a nominal yield strength of $f_{y,nom}=235$ N/mm² instead of the original 240 N/mm².
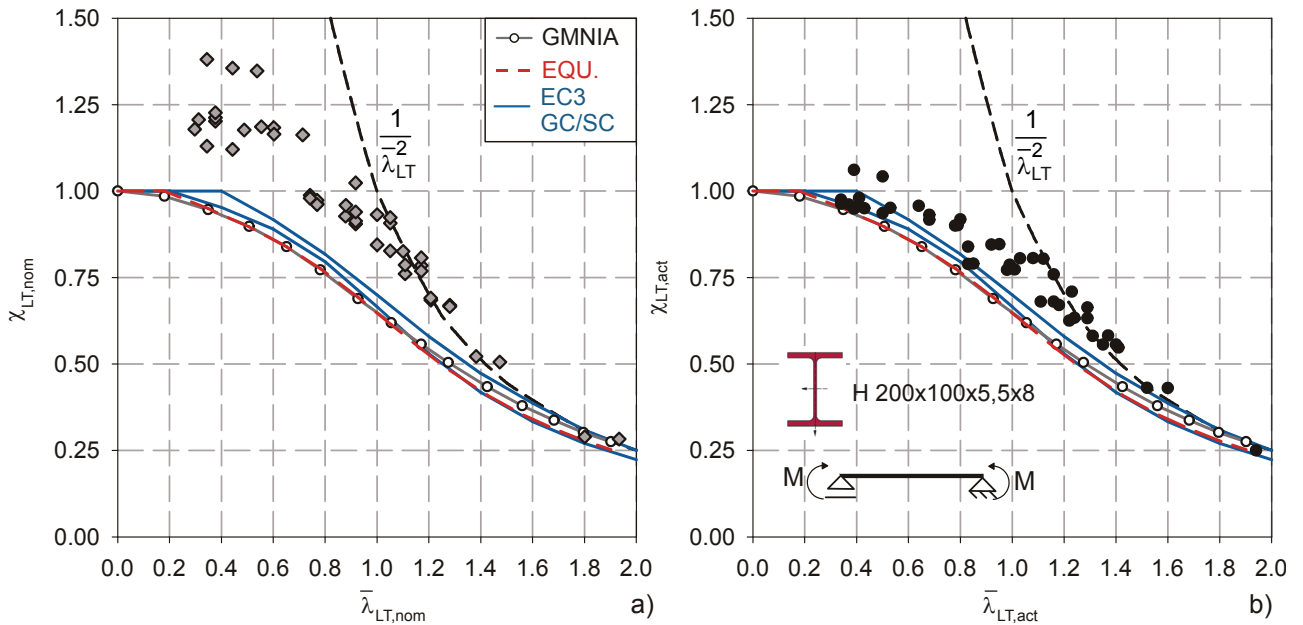
Fig 6-47 *Test results for Japanese H200x100x5,5x8 sections under constant bending moment, plotted over the nominal (a) and actual (b) slenderness; comparison with EC3 rules and the proposal of sections 6.7 & 6.8.*

While Fig 6-47a gives an overview of the "safety level" of the current and proposed rules for this section with regard to actual tests, Fig 6-47b should give an overview of the accuracy of the formulations. Fig 6-47b features somewhat surprising results. For one, it is remarkable that the value of $\chi_{LT,act}$=1.00 is exceeded, even though the "measured" value of M_{pl} is used as the basis of the calculation of the reduction factor. The fact that the three design curves do not match the plotted results is not in itself surprising, as these curves were already intended (through the choice of imperfections in the GMNIA calculations) to represent a lower bound of the actual behaviour. It is however surprising that the scatter of the results appears to be rather large. This is understandable at "intermediate" slenderness ranges, where the imperfections dominate the problem, i.e. parameters that don't enter neither M_{pl} nor M_{cr}. It is anyhow not really understandable at low and high slenderness, where cross-sectional geometry, modulus of elasticity, the yield stress (only at low slenderness), but not the imperfection amplitudes, govern the problem. Since these parameters do all enter M_{pl} or M_{cr}, an exact knowledge of them would certainly mean a rather low scatter of the test results when plotted over $\overline{\lambda}_{LT,act}$. Both these observations give rise to the suspicion that the values of $\chi_{LT,act}$ and $\overline{\lambda}_{LT,act}$ do actually not contain all measured values that concur to the calculation of these parameters.

This is confirmed by a representative excerpt of the data-pool plotted inFig 6-47, given here in Table 6-9. In the table, the data given in the CEC (1988) background document and in the report by Greiner & Kaim (2001) are combined, using the numbering of the CEC document. The CEC document contains "measured" values of the ultimate load ($M_{R,e}$), yield strength ($f_{y,e}$) and of the

plastic moment capacity ($M_{pl,e}$). In order to prove the conjecture made above, the "measured" plastic section modulus $W_{pl,e}$ is calculated from $M_{pl,e}$ and $f_{y,e}$.

H 200x100x5,5x8	h_{nom}	200	mm
	b_{nom}	100	mm

$t_{f,nom}$	8	mm
$t_{w,nom}$	5.5	mm
r_{nom}	8	mm

$f_{y,nom}$	235	N/mm²
$W_{pl,nom}$	205.1	cm³
$W_{pl,nom,r=0}$	200.2	cm³

#	Source	$M_{R,e}$ [kNm]	$f_{y,e}$ [N/mm²]	$M_{pl,e}$ [kNm]	"$W_{pl,e}$" [cm³]	$M_{pl,nom}$ [kNm]	$\overline{\lambda}_{LT,act,e}$ [-]	$\chi_{LT,act,e}$ [-]	$\overline{\lambda}_{LT,nom,e}$ [-]	$\chi_{LT,nom,e}$ [-]
722	Suzuki	58.0	297.2	59.5	200.2	48.2	0.34	0.975	0.313	1.206
719	Wakabaya	65.3	312.9	62.6	200.2	48.2	0.5	1.042	0.443	1.355
752	Suzuki	56.9	305.1	61.1	200.2	48.2	0.68	0.931	0.602	1.184
721	Wakabaya	55.9	304.1	60.9	200.2	48.2	0.8	0.918	0.713	1.162
759	Suzuki	45.2	292.3	58.5	200.2	48.2	1.01	0.773	0.917	0.940
761	Suzuki	49.2	305.1	61.1	200.2	48.2	1.03	0.805	0.917	1.023
1177	Fukumoto	39.7	306.3	63.5	207.3	48.2	1.22	0.625	1.100	0.825

Table 6-9 *Excerpt from the considered test data pool*

The resulting values of $W_{pl,e}$, contained in Table 6-9 show that, in the case of the Suzuki and Wakabaya tests, all values are identical and are equal to the *nominal section modulus* $W_{pl,nom,r=0}$ valid if the *fillet radius is not considered.* Only in the case of the Fukumoto tests, a different value is retrieved. It is therefore safe to assume that the majority of the results plotted in Fig 6-47b are, in reality, not "actual" values of slenderness and of the buckling reduction factor. In all likelihood, only the (coupon) yield stress was measured in many of the LT buckling tests that underpin the current Eurocode safety factors, while the cross-sectional geometry was assumed to be equal to the nominal values. This observation is important due to the following reasons:

i. The lack of information regarding the "actual" values of some base variables (specifically here, the cross-sectional geometry), and the resulting inaccuracies in the calculation of strength according to the design formula for χ, result in discrepancies and –more importantly- a scatter of the discrepancies between the prediction of the design function r_t and the observed test results r_e that are larger than they would be if all values had been measured. This increases the value of the coefficient of variation V_δ of the error of the design function and thus leads to a lower design value r_d.

ii. Additionally to the unknown variability of the cross-sectional geometry in the LT buckling tests, the measured yield stress in all of these tests was significantly higher than the nominal value for a steel grade of S235. In the EN 1990 – Annex D procedure, such cases are specifically addressed and it is recommended to take pre-information of base variable scatter into account when computing the value of the coefficient of variation of the design function V_{rt}. In order to include some degree of pre-information, the statistical evaluation carried out by Müller (2003), which underpins the current Eurocode recommendations, made use of a constant value of $V_{rt}=0.08$. Thereby, the total impact of the variability of the yield stress and

cross-sectional geometry was considered to be constant for all slenderness ranges. This is of course a strong simplification.

The scatter of the test results, when compared to the value predicted by design formulae, is further illustrated in Fig 6-48. The test results of Fig 6-47are plotted in terms of the nominal buckling reduction factor $\chi_{LT,nom}$ and compared to the prediction given by three design formulae. Thereby, a distinction is made between tests with values of $\overline{\lambda}_{LT,nom}$ smaller and larger than 0.8. The calculated values of the regression correction factor b and of V_δ are also included in the plot. Due to the mentioned lack of information regarding what are really the "actual" values of the base variables that enter $\chi_{LT,nom,t}$, the calculated values of V_δ must be assumed to be significantly too high.
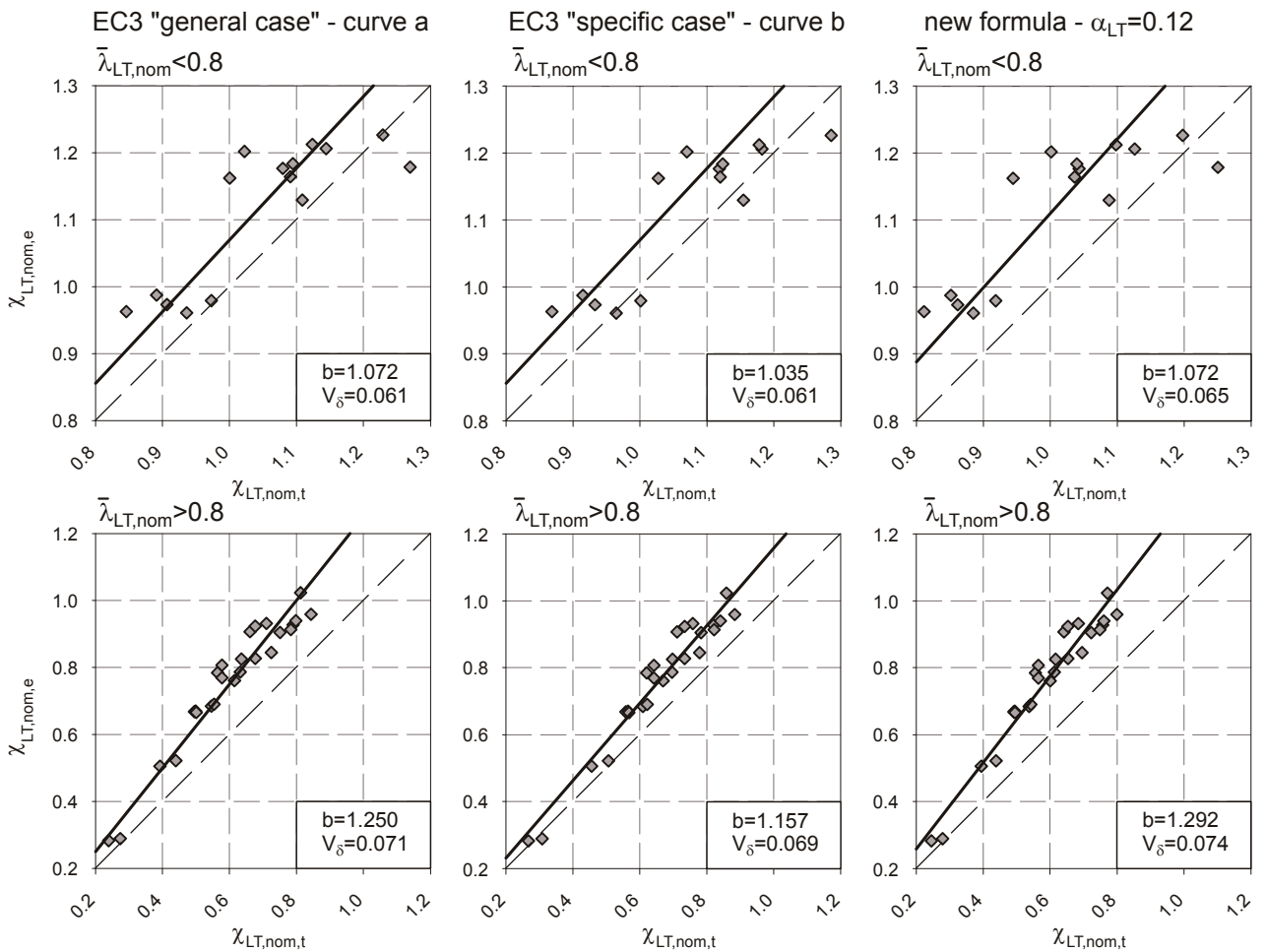
Fig 6-48 *Accuracy of the three different formulations in describing the tests.*

The results of the statistical evaluation of the examined physical test results on H200x100x5,5x8 sections in terms of $\gamma_M{}^*$ is shown in Fig 6-49. The values of $\gamma_M{}^*$ were thereby again calculated using the assumption that $V_{rt}=0.08$. For the factor $k_{d,n}$, D.8.2.2.5.(4) of EN 1990 Annex D was considered, which allows to use the total number of considered test results (n=46) even though smaller sub-groups were analyzed. Therefore, $k_{d,n}=3.04$ was used. A so-called "tail approximation" was also performed in order to eliminate the potentially negative effects of excessively "safe sided" test results from the data pool; this meant the exclusion of three test results.
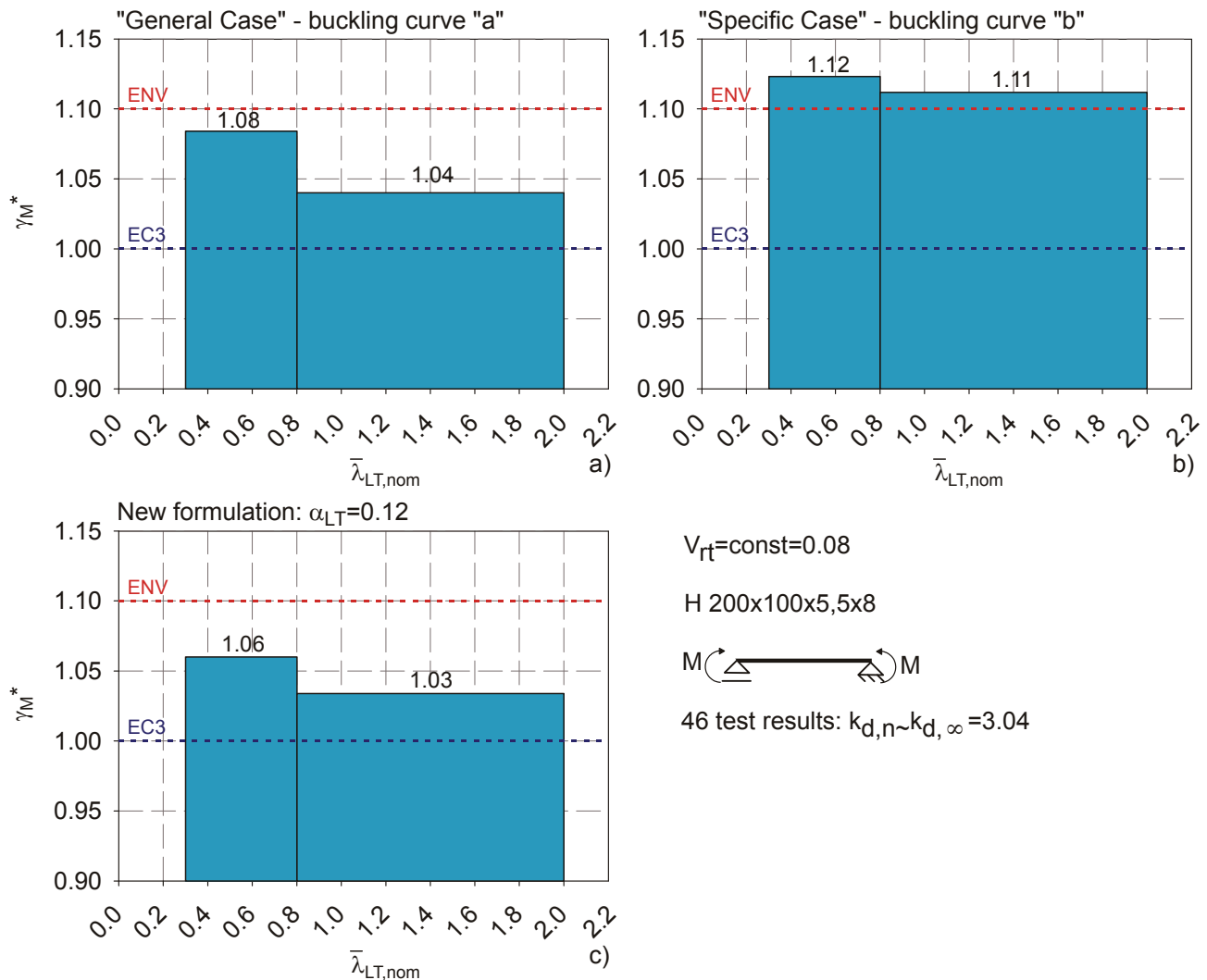
Fig 6-49 *Results in terms of γ_M^* of a statistical evaluation of the tests in Fig 6-47 for the three formulations*

Fig 6-49 can be commented upon as follows:

i.   When compared to Fig 6-46, the evaluation for the "general case" in Fig 6-49a curves shows somewhat lower values of γ_M^* at low slenderness, and higher ones at higher slenderness. Even though the exact same assumptions were used in both figures, one should note that only a portion of the data pool considered for Fig 6-46 was also considered for Fig 6-49a. This alone is a source of discrepancy. The fact that tests with variable bending moment were also included in Fig 6-46 further explains the differences, particularly in the higher slenderness range; since the "general case" curves do not take the (positive) effects of variable bending moments into account, the evaluation must lead to a lower value of γ_M^* if such tests are included, particularly for higher slenderness ratios. The "un-safe" effects of this common grouping are irrelevant to practice in this case, as they only affect one

slenderness range and do not modify the maximum value of γ_M^*. Nevertheless, this is an example of the need for caution when different test populations are grouped together.

ii.   The evaluation for the "specific case" buckling curve leads to values that are fairly constant and just above $\gamma_M^*=1.1$. Since the change from $\gamma_{M1}=1.1$ to 1.0 between ENV end EN versions of the Eurocode was justified independently of the test results (see comments in chapter 4), this result would be in accordance with the desired outcome at the time of the development of the "specific case" curves. King (2008) carried out a separate evaluation of LT buckling tests according to EN 1990 for the "specific case", whereby he also included adequate pre-information regarding the variability of the base variables and, thus, of V_{rt}. This led to the conclusion that values of $\gamma_{M1}=1.0$ could be justified by the tests alone, with calculated values of γ_M^* lying in the range of 1.00-1.05 for tests up to $\bar{\lambda}_{LT,nom}=1.5$.

iii.   The evaluation for the new formulation yields results that are very similar to the ones given by the "general case". This is not surprising, considering that the curves themselves are almost overlapping for this one section, see Fig 6-47.

Finally, some comments can be made concerning the general representativeness of the LT buckling tests documented in the literature when seen in the context of the Eurocode and of the newly proposed LT buckling curves:

i.   The CEC (1988) Eurocode background document only contains 8 tests with hot-rolled sections with a depth-to-width ratio of h/b>2.0. This means that such sections are severely under-represented in the test population underpinning the Eurocode rules, making it somewhat questionable whether or not the statistical evaluation of Fig 6-46 is significant for this type of section.

ii.   More than 50% of all the test results for hot-rolled sections were carried out with sections that had a depth-to-width ratio of exactly h/b=2.0. As was seen in section 6.3.2, this is exactly the "switching point" between different buckling curves, with sections with this ratio still falling in the higher curve (e.g. curve "a" for hot-rolled sections in the "general case"). At least in theory, this situation is always safe-sided for "stockier" sections with h/b≤2.0, since sections with smaller h/b than 2.0 should generally have a "higher resistance" in the normalized sense of χ_{LT}, and this is not accounted for by the "general" and "specific case" curves. It is however accounted for by the new formulation, indicating that the results of Fig 6-49 can no longer be accepted as being generally accurate, or "safe sided", for the new, section-specific formulation.

In summary, the current partial safety factors γ_{M1} for LT buckling in the Eurocode are based on an extensive, yet not entirely satisfactory and comprehensive test population. The fact that a majority of the main structural base variables influencing the buckling problem were not measured during these tests has a negative influence on the outcome of the statistical evaluation, leaving the door open for interpretation, as is proven by the different outcomes of the evaluations done by Müller

(2003) and King (2008). Additionally, the tested section geometries lead to more open questions regarding the actual reliability level for a range of un-tested sections.

In order to address the shortcomings of the data pool and be able to better estimate the influence of the "missing" parameters (h/b ratios, section geometry, more representative yield stress etc.) on the outcome of the statistical evaluation, Monte Carlo simulations are performer in the following sub-section for some exemplary cases.

6.10.2. Monte Carlo simulations and evaluation

The following sub-section documents some selected results of Monte Carlo simulations for LT buckling of hot-rolled sections under constant bending moment. In the absence of any more specific information concerned with the single base variables, the data collected during the development of the ECCS column buckling curves, as well as the data published by Alpsten (1972, 2002), will be used for reference, see chapter 5.

Three sections are studied: the Japanese H200x100x5,5x8 section already treated above, an IPE 500 section representing "slender" beams, and a stockier HEB 400 section. All beams are again assumed to be made of steel grade S235, with a nominal yield stress of f_y=235 N/mm². The assumptions made for the random input data generation in the Monte Carlo simulations are summarized in Table 5-4. Compared to the column buckling case treated in chapter 5, the main difference is represented by the inclusion of the amplitude of the initial rotation $\bar{\theta}_0$ of the section at mid-span. This inclusion became necessary due to its larger significance in the LT buckling case. Since no measured data has been published pertaining to this quantity, a simplified assumption was made for the purposes of this study: it was assumed that one of the flanges has an initial out-of-straightness that conforms to the measurements of the ECCS column buckling tests (i.e. with an average value of $\bar{e}_0$=0.00085 L and a standard deviation of 0.0002 L), while the second flange of the I-section is on average only half as crooked. The standard deviation was chosen so that having a beam with both flanges equally deflected in the same direction and having a beam with one flange perfectly straight have the same probability of occurrence, with both being at one standard deviation from the assumed mean value.

Of course, due to the fact that all the parameters governing the random data generation in Table 5-4 contain a certain degree of assumption and conjecture, the results presented in this section are to be seen as an indication of general tendencies, rather than absolute representations of the real physical and statistical behaviour. Nevertheless, it is believed that important information can be retrieved from these calculations, as these calculations are not hampered by the above-mentioned shortcomings of the experimental program.

section	Parameter	m	s	Nominal value
H200x100x5,5x8	Initial curvature $\overline{e}_0$ *	0.00085 L	0.0002 L	-
	Initial rotation $\overline{\theta}_0$ **	0.00085 L /(2h)	0.0002 L /(4h)	-
	Yield stress f_y	285 N/mm²	17 N/mm²	235 N/mm²
	Residual stress σ_{res}	0.20 . 235 N/mm²	0.05 . 235 N/mm²	0.30 . 235 N/mm²
	Flange thickness t_f	8.0 mm	0.40 mm	8.0 mm
	Web thickness t_w	5.5 mm	0.28 mm	5.5 mm
	Depth h	200 mm	2.0 mm	200 mm
	Width b	100 mm	1.0 mm	100 mm
IPE 500	Initial curvature $\overline{e}_0$ *	0.00085 L	0.0002 L	-
	Initial rotation $\overline{\theta}_0$ **	0.00085 L /(2h)	0.0002 L /(4h)	-
	Yield stress f_y	285 N/mm²	17 N/mm²	235 N/mm²
	Residual stress σ_{res}	0.20 . 235 N/mm²	0.05 . 235 N/mm²	0.30 . 235 N/mm²
	Flange thickness t_f	16.0 mm	0.8 mm	16.0 mm
	Web thickness t_w	10.2 mm	0.51 mm	10.2 mm
	Depth h	500 mm	5.0 mm	500 mm
	Width b	200 mm	2.0 mm	200 mm
HEB 400	Initial curvature $\overline{e}_0$ *	0.00085 L	0.0002 L	-
	Initial rotation $\overline{\theta}_0$ **	0.00085 L /(2h)	0.0002 L /(4h)	-
	Yield stress f_y	285 N/mm²	17 N/mm²	235 N/mm²
	Residual stress σ_{res}	0.20 . 235 N/mm²	0.05 . 235 N/mm²	0.30 . 235 N/mm²
	Flange thickness t_f	23.4 mm	0.72 mm	24.0 mm
	Web thickness t_w	14.3 mm	0.54 mm	13.5 mm
	Depth h	400 mm	4.0 mm	400 mm
	Width b	300 mm	3.0 mm	300 mm

*   refers to one of the flanges, assumed to have a sinusoidal shape

**   on average, one flange has half the initial curvature of the other.

Table 6-10   *Base variables: assumptions for the Monte Carlo simulations.*

In a first step, a Monte Carlo simulation is carried out for the H200x100x5,5x8 section studied in section 6.10.1. The plots in Fig 6-50 show the results of this calculation in a form already used in Fig 6-47 to present the results of the physical LT buckling tests on this same section. Accordingly, Fig 6-50a shows the results in terms of the achieved nominal buckling reduction factor, thus being a representation of the absolute buckling strength, normalized with the nominal plastic moment capacity of the section. Fig 6-50b shows the results in terms of the "actual" values of χ_{LT} and $\overline{\lambda}_{LT}$, meaning that the "actual", randomly generated values of the base variables of Table 5-4 were used in the calculation of M_{pl}, M_{cr}, χ_{LT} and $\overline{\lambda}_{LT}$.
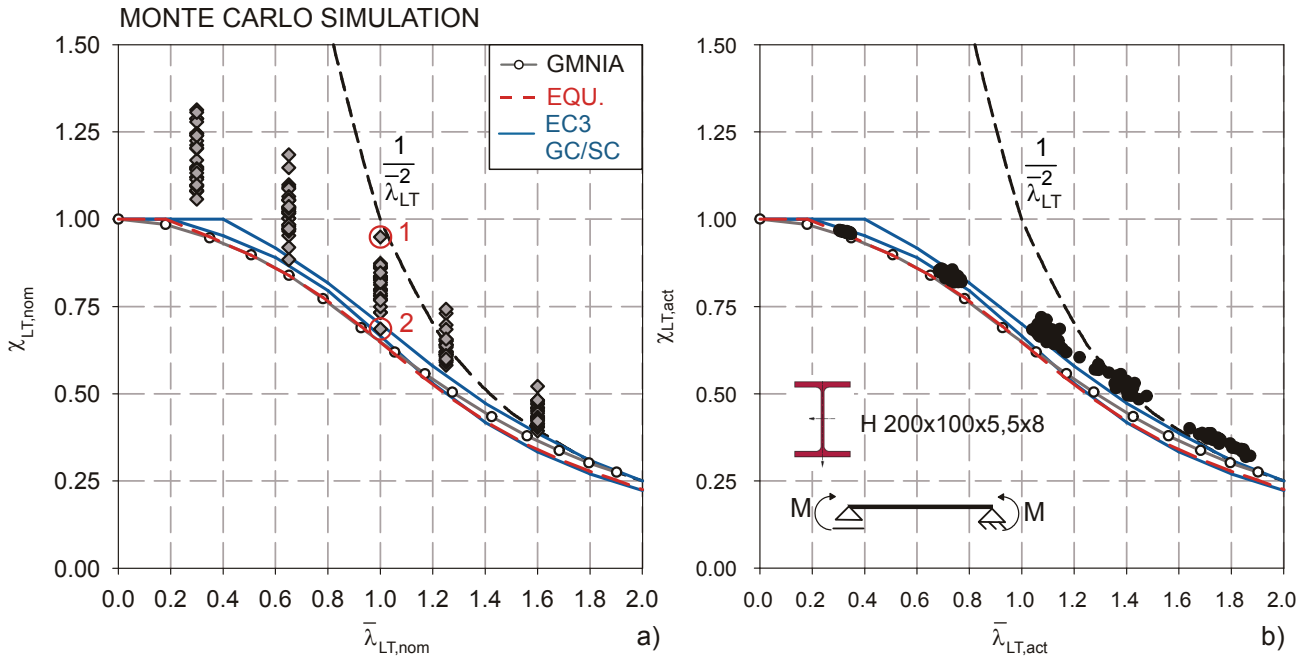
Fig 6-50 *Monte Carlo simulation results, plotted over the nominal (a) and actual (b) slenderness.*

Comparing Fig 6-50 and Fig 6-47, the following differences are apparent:

i. A "lower bound curve" connecting the lowest values of the test results would lie significantly lower in Fig 6-50a when compared to Fig 6-47a. On the other hand, a curve connecting the upper values of the test results in the two figures would be very similar in both. In order to explain this, the base variables leading to two Monte Carlo test results (marked with "1" and "2" in Fig 6-50a) at a nominal slenderness of $\overline{\lambda}_{LT}=1.0$, corresponding to a length of L=2922mm, are looked at in detail in the following Table 6-11:

Base variable	MC test "1"	MC test "2"
Initial curvature $\overline{e}_0$ *	L/954	L/1078
Initial rotation $\overline{\theta}_0$ **	2.67 mrad	6.21 mrad
Yield stress f_y	**309.9 N/mm²**	**253.3 N/mm²**
Residual stress σ_{res}	41.5 N/mm²	62.9 N/mm²
Flange thickness t_f	8.87 mm	7.19 mm
Web thickness t_w	5.69 mm	6.01 mm
Depth h	199.6 mm	200.0 mm
Width b	100.4 mm	100.2 mm

Table 6-11 *Monte Carlo tests "1" and "2" of Fig 6-50; generated input data.*

The comparison of the values contained in the table shows that the main differences between the highest ("1") and lowest ("2") test results are to be found in the initial rotation, the residual stresses and, most importantly, the flange thickness and the *yield stress*.

In order to explain the differences between Fig 6-50a and the physical tests in Fig 6-47a, it is important to recall (by looking at Table 6-9) that the *yield stress in the physical tests was also rather high,* never falling below 280 N/mm² in any of the tests included in Fig 6-47, and often lying above 300 N/mm². Since no values are included in Fig 6-47a with yield stresses as low as the one generated for the Monte Carlo test "2", it is clear that the lowest Monte Carlo tests had to be lower in terms of $\chi_{LT,nom}$.

ii.   A comparison between the Monte Carlo and the physical test results in Fig 6-50b and Fig 6-47b, plotted in terms of $\chi_{LT,act}$ over $\overline{\lambda}_{LT,act}$, at first sight gives some confirmation to the points made in section 6.10.1, i.e. that the scatter of the physical test results in Fig 6-47b is high and caused by a lack of information regarding the base variables. In the Monte Carlo tests, all input data is (inevitably) known, leading to the narrow scatter band in Fig 6-50b.

It is interesting to discuss this figure with some more detail, as it is perhaps not readily understood why even in the case of the Monte Carlo tests, where all input data is known, the test results in terms of $\chi_{LT,act}$ lie at a more or less noticeable distance from the (Eurocode or new) design buckling curves. As a matter of fact, judging from Fig 6-50b, for this specific section the newly proposed design curve appears to be the most *inaccurate* of all three included curves. This seems to be in contrast with what has been demonstrated in section 6.8, where the new formulation was shown to be far more accurate in describing the behaviour of any given section.

Of course, the reason for this apparent inconsistency lies in the fact that the accuracy of the new formulation is referred to the deterministic "model beam" alone; the GMNIA results for this beam with nominal yield stress and cross-sectional geometry, eigenmode-affine geometric imperfections and fixed, high imperfection amplitudes is also included in Fig 6-50b and is shown to also lie significantly below the Monte Carlo test results in terms of $\chi_{LT,act}$. Furthermore, this doesn't necessarily mean that the curve is "inaccurate" for the purposes of reliability, since the assessment of the accuracy of a given formulation (i.e. the calculation of V_δ) is only performed after the linear regression correction factor b is calculated:

$$b = \frac{\sum_{i=1}^{n} r_{e,i} \cdot r_{t,i}}{\sum_{i=1}^{n} \left(r_{t,i} \right)^2} = \frac{\sum_{i=1}^{n} \chi_{LT,nom,e,i} \cdot \chi_{LT,nom,t,i}}{\sum_{i=1}^{n} \left(\chi_{LT,nom,t,i} \right)^2} \qquad (6.59)$$

The factor b can also be thought of as an in-built safety factor in a given design rule. A value of b=1.0 would mean that the design curve describes the *mean values of the test results*, in terms of $\chi_{LT,act}$, while values higher than 1.0 would indicate that the design curve already describes a lower fractile. Neither one of these scenarios affects the "accuracy" of a design rule for the purposes of a reliability analysis.
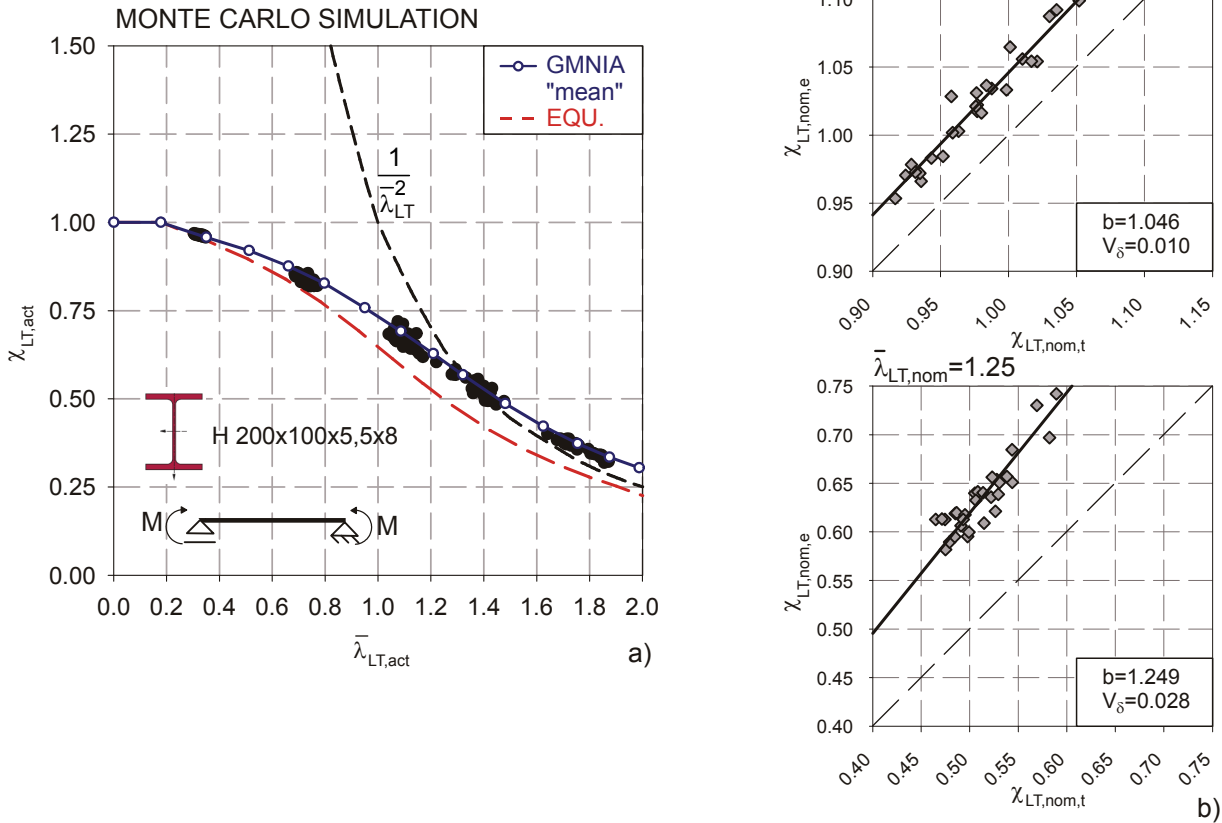
Fig 6-51 *GMNIA curve calculated with the mean values of the input parameters and compared to the newly-developed Ayrton-Perry formula evaluated with (6.43).*

This is further discussed in Fig 6-51. The figure on the left is similar to Fig 6-50b, but omits the current Eurocode curves and only includes the new LT buckling design curve (in red). Additionally, it includes a new GMNIA buckling curve; contrary to the numerical curve that was used for the calibration of the new design rule, this GMNIA curve was calculated using the *mean values m of Table 5-4 as input variables*. Even in terms of $\chi_{LT,act}$, this curve is higher than the new design formula based on the "model beam". The reason for this primarily lies in the beneficial combination of higher yield strength and lower residual stresses, as well as somewhat smaller initial imperfections and a slightly more convenient shape of the imperfection when compared to the eigenmode-affine shape used for the "model beam". Since this curve passes in the middle of the scatter band of the Monte Carlo test results, Fig 6-51a proves that a buckling curve representing the mean values of the base variables would be far better suited to describe the (average) position of test results in terms of $\chi_{LT,act}$ over $\overline{\lambda}_{LT,act}$. Such a curve would, however, require far larger safety factors than one based on a low fractile in order to cover the rare low fractile combination cases that define the design points.

The "accuracy" in terms of V_δ of the new formulation is not affected by these considerations, since the linear regression, and thus the factor b, is very well able to lead to a very accurate description of the tests, see Fig 6-51b. When compared to Fig 6-48, this plot shows the values of V_δ to be significantly smaller in the case of the Monte Carlo tests. The figure contains the results for two values of $\overline{\lambda}_{LT,nom}$; interestingly, if all considered slenderness values are looked at, a tendency can be observed for the factor V_δ to be very low at low slenderness, somewhat larger at values of $\overline{\lambda}_{LT,nom}$ around 1.0, and then decrease again. This is in keeping with the fact that the imperfections are mostly felt in the intermediate slenderness range, and are not included in the buckling design formulae. This means that even though the imperfection amplitudes are known in the case of the Monte Carlo tests, their value is irrelevant to the result of the formula and leads to a larger value of V_δ if the imperfections are relevant.The attention can now be turned to the results in terms of the safety factor γ_M^* of the statistical evaluation according to EN 1990 Annex D for the three sections of Table 5-4. This is done by calculating the values of γ_M^* for all three considered buckling design curves ("general case", "specific case" and "new formulation"). For a better visualization and interpretation of the results, the results of the Monte Carlo simulation are also plotted as m +/- 2s lines in a $\chi_{LT,nom}/\overline{\lambda}_{LT,nom}$ plot and compared to the position of the design buckling curves in this space. In all plots, the "specific case" curve is the higher one of the two Eurocode 3 curves.

Fig 6-52 shows the results of this evaluation for the H200x100x5,5x8 section. The plot on the left essentially contains the same information given by Fig 6-50a, with the difference that the m+/-2s lines already contain some statistical information. It can be seen again that the new formulation yields the lowest design curve for this specific section up to the higher slenderness values, where it basically overlaps with the "general case" curve for this section.
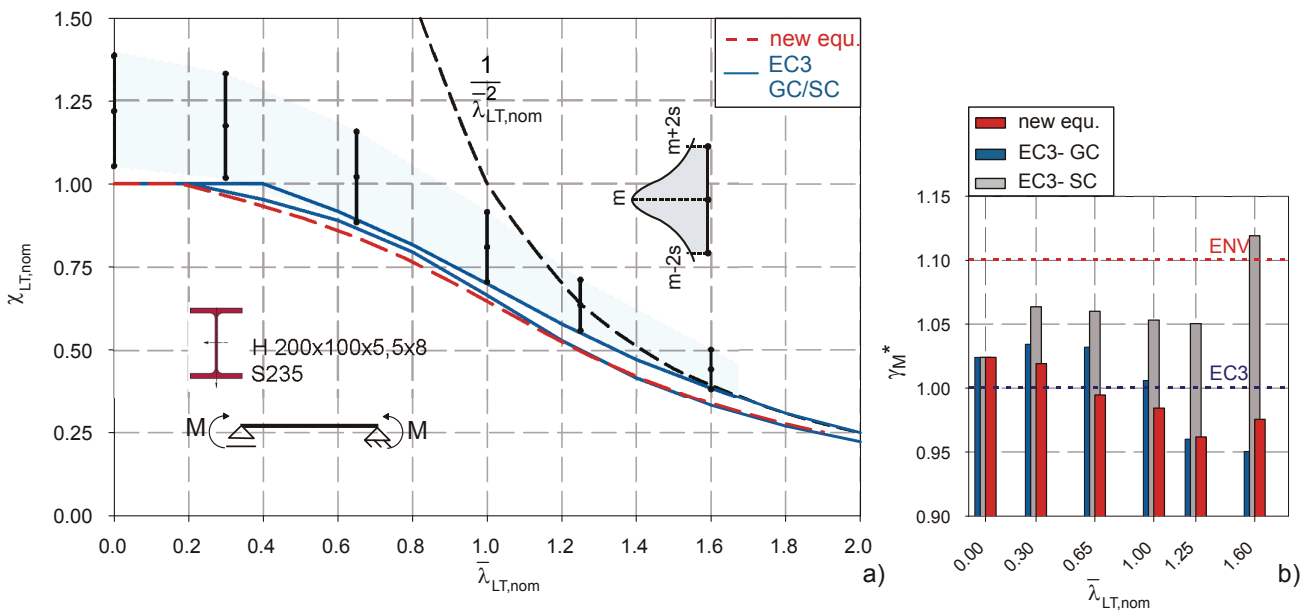
Fig 6-52 *Monte Carlo simulation and statistical evaluation: H200x100x5,5x8 section, S235.*

Fig 6-52b shows the the results of the statistical evaluation in terms of γ_M^* for the H200x100x5,5x8 section. The results are best discussed in combination with Fig 6-49, where the values of γ_M^* were calculated for the physical tests performed with the same section. The values calculated for the Monte Carlo tests are generally lower than the ones calculated for the physical tests, which is in keeping with the comments made about the origin of rather large values of V_δ in the case of the physical tests.

In relative terms, the results in the two figures generally confirm the same tendencies for the values of γ_M^*; both for the "general case" and the new formulation, the obtained values of γ_M^* are (slightly) higher at low slenderness. The new formulation seems to be best suited at maintaining the required value of γ_M^* fairly constant, as the obtained values range between 1.025 and 0.965 with no sudden changes.

The "specific case" evaluation shows a behaviour similar to Fig 6-49b, with the values being slightly higher than for the other two curves, and remaining fairly constant throughout the slenderness ranges. The exception in this case is represented by the results for the nominal slenderness value of $\overline{\lambda}_{LT,nom}=1.6$, where γ_M^* shows a "peak". As Fig 6-52a shows, at this slenderness the "specific case" buckling curve is coincident with the Euler hyperbola. A look at Fig 6-47a reveals that only very few physical tests were carried out at high slenderness $\overline{\lambda}_{LT,nom}\sim1.6$, and these tests were grouped together with tests with lower slenderness beginning with $\overline{\lambda}_{LT,nom}=0.8$ in Fig 6-49b. In the Monte Carlo simulation, 30 tests were simulated at $\overline{\lambda}_{LT,nom}=1.6$, meaning that enough data points for this specific slenderness are contained in the evaluation. Thus, it can be assumed that the representation in Fig 6-49b "missed" a peak in the required value of γ_M^*.

The following two figures (Fig 6-53 and Fig 6-54) show the results of identical statistical evaluations for the IPE 500 and HEB 400 sections, respectively.
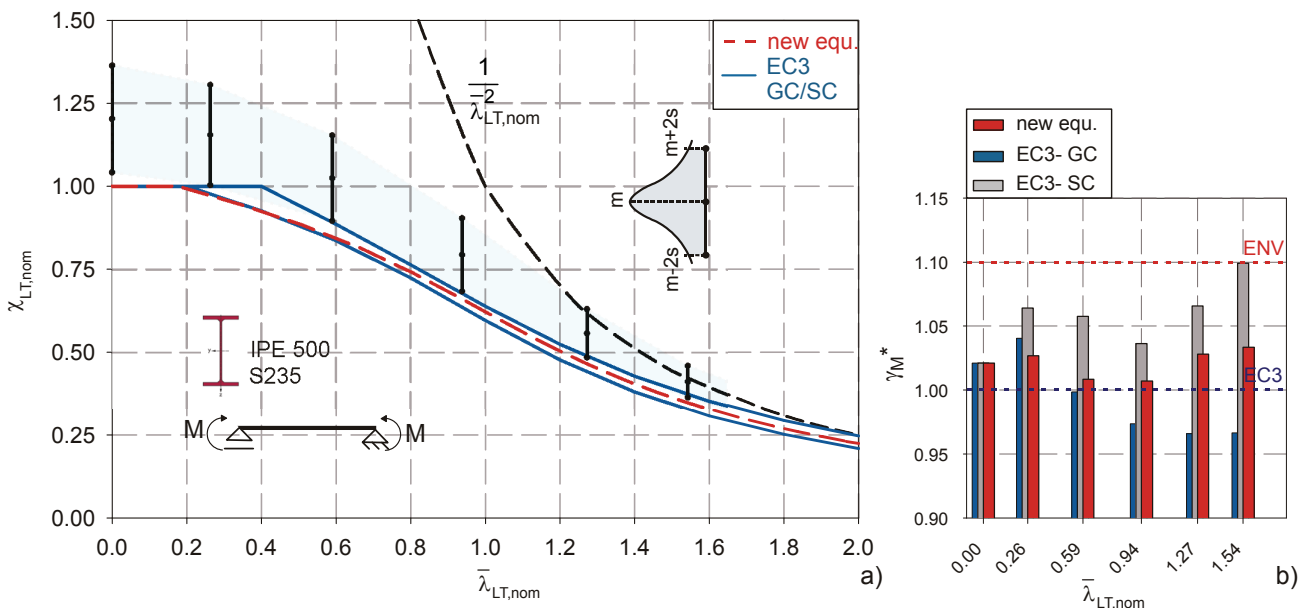
Fig 6-53 *Monte Carlo simulation and statistical evaluation: IPE 500 section, S235.*
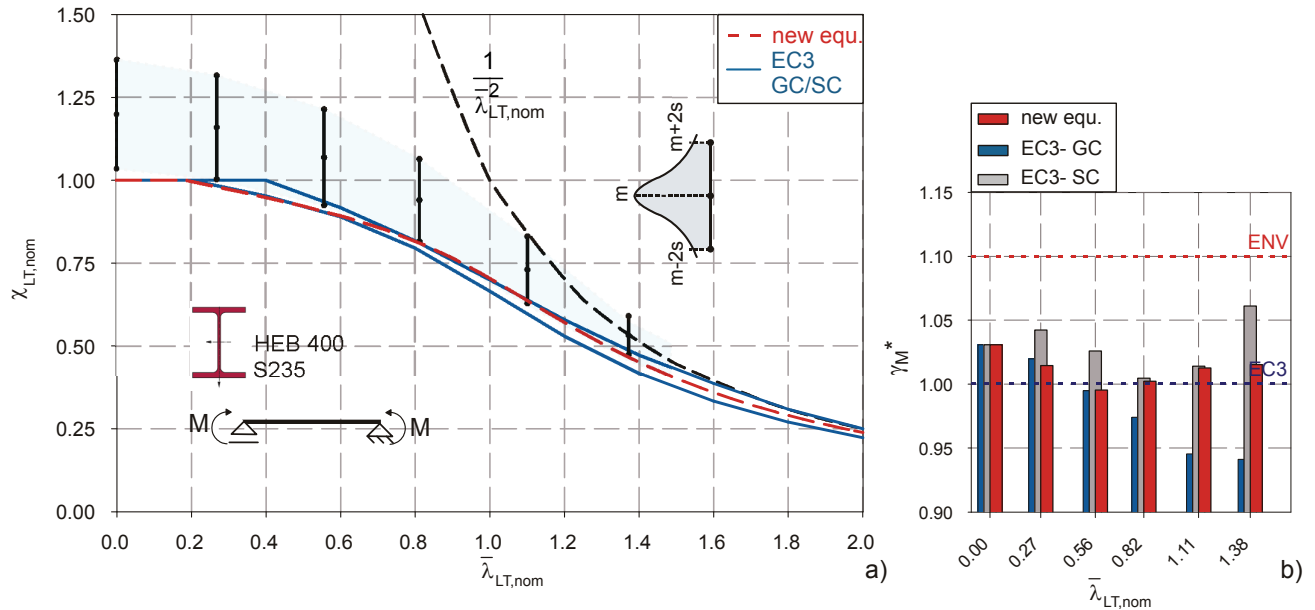
Fig 6-54 *Monte Carlo simulation and statistical evaluation: HEB 400 section, S235.*

The figures on the left show the new formulation (dashed red line) to be specific to the section, while the existing Eurocode formulations are fixed in their position in the $\chi_{LT,nom}/\overline{\lambda}_{LT,nom}$ plane for a certain categorization of h/b. The advantages of the section-specific new formulation become apparent for these two cases: the calculated values of γ_M^* become far more homogeneous in this specific formulation when compared to both the "general case " and "specific case" curves of the Eurocode. The new formulation yields values of γ_M^* that fluctuate around values at or just above 1.0. The "general case" seems to have the general tendency of becoming "more conservative", i.e. requiring lower values of γ_M^*, with increasing slenderness, while the opposite tendency seems to be true for the "specific case" curves.

In summary, the Monte Carlo simulations presented in this section helped to clarify some points concerned with the reliability level of current and proposed LT buckling curves:

  i. The advantages of actually knowing the measured values of all relevant base variables were emphasized.

 ii. The difference in accuracy between a curve that describes a beam with average values of input variables and one with lower fractile values was described, and the implications of these differences on a reliability analysis were discussed.

iii. The possibility of "missing" peaks or sudden increases in the demand for γ_M^* by grouping together tests pertaining to a rather broad range of slenderness was demonstrated and, in one example, shown to be risky in the case of the "specific case" curves.

 iv. One advantage of the newly proposed buckling curve formulation was shown to lie in the fact that the curve is specific for any given section, meaning that the reliability level is intrinsically more homogeneous for different sections than the Eurocode curves with their coarse categorization in accordance to h/b≤ or > 2.0.

6.11. Constant Reliability Curves

In this section, the potential for an applicability of "constant reliability curves" to the development of probabilistically calibrated and categorized LT buckling rules is investigated and briefly presented. Thereby, the basic principles presented in chapter 4 and applied to the column buckling case in chapter 5, section 5.6, are adopted. The main purpose of this presentation is to demonstrate the viability and the difficulties of this sort of calibration.

The same three sections studied in 6.10 (H200x100x5,5x8, IPE 500, HEB 400, all of steel grade S235) are treated again. The method requires probabilistic input data; the values of Table 5-4 are therefore adopted. The numerical partial derivatives for each of the eight base variables, essential to the development of the constant reliability curves, are performed using the same methodology already discusses in chapter 5, section 5.6.

The results of this first order reliability analysis (FORM) are shown in the following figures (Fig 6-55 to Fig 6-57) for the three studied sections. The diagrams can be described as follows:

i. In the figures on the left, the curves r_m, r_d and r_{ub} are plotted, representing the mean curve, the "design value" curve that would (theoretically) require a partial safety factor of exactly $\gamma_M{}^*=1.0$, and the "upper bound" curve representing values that are at the same "distance" (in terms of probability) from the mean value as the design value. All these plots are presented in terms of $\chi_{LT,nom}$ over $\overline{\lambda}_{LT,nom}$.

ii. Additionally, the figure on the left features the design curve resulting from the new formulation proposed in this chapter (red dashed line), a line representing a FORM constant reliability curve that would require exactly a value of $\gamma_M{}^*=1.05$ (1.05 r_d - blue dashed-dotted line), and a *best-fit approximation of 1.05 r_d* (green dashed line).

iii. It was chosen to approximate the 1.05 r_d line with a best-fit description, and not the r_d line, because the r_d curve inevitably drops below $\chi_{LT,nom}= 1.0$ at very low slenderness. This is due to the fact that the cross-sectional capacity itself actually requires a partial safety factor slightly larger than 1.00, at least if the assumptions regarding the statistical distributions of the base variables in Table 5-4 are taken to be valid. This is particularly felt at the end of the plateau of the new design curve $(\overline{\lambda}_{z,nom} = 0.2)$, where values of $\gamma_M{}^*$ of ca. 1.04 ... 1.05 are needed for all three studied sections. The same tendency was also observed in the column buckling case.

iv. The best-fit description was carried out using the same technique employed in section 6.8, particularly using the final formula (6.43) of sub-section 6.8.4, leaving the generalized imperfection amplitude η, or rather the generalized imperfection amplitude factor α_{LT}, up for calibration:

$$\eta = \alpha_{LT} \cdot \left(\overline{\lambda}_{z,nom} - 0.2\right) \tag{6.60}$$

And $\alpha_{LT} = a_{LT} \cdot \sqrt{W_{y,el} / W_{z,el}}$, with a_{LT} being a constant.
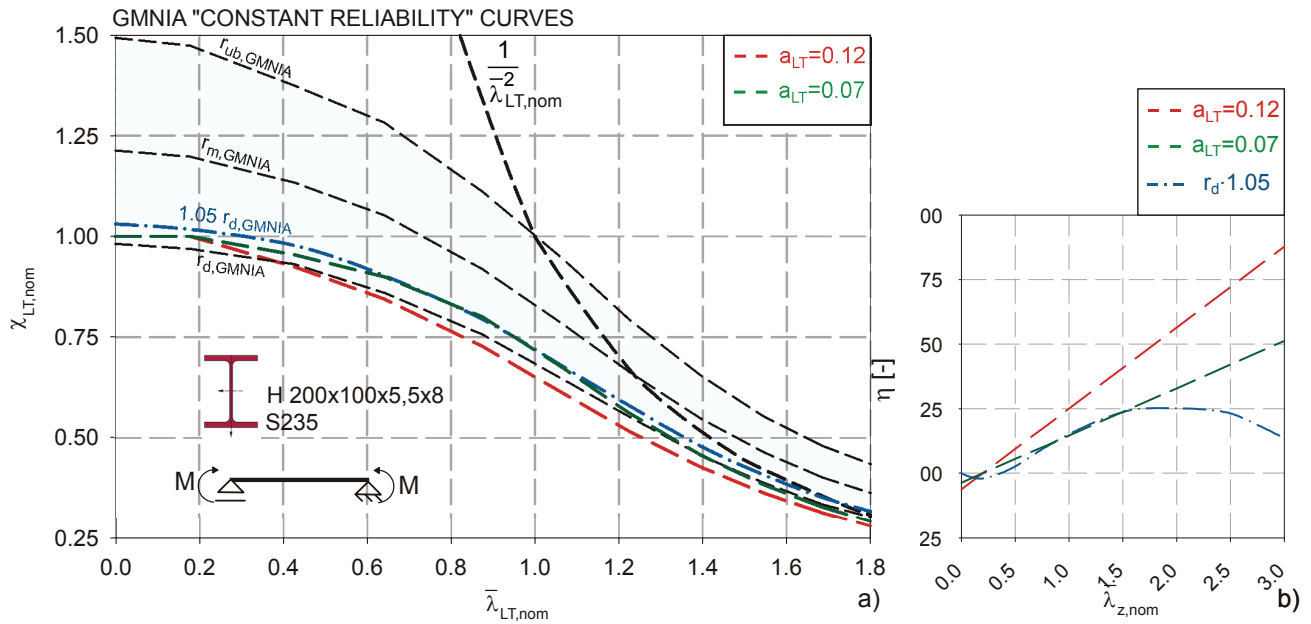
Fig 6-55 *Constant Reliability Curves for a H200x100x5,5x8 section, steel grade S235.*

The figure b), on the right in Fig 6-55 to Fig 6-57, shows the functions of η over $\overline{\lambda}_{z,nom}$ that result from the proposal of Table 6-4 (a_{LT}=0.12, $\alpha_{LT}=a_{LT} \cdot \sqrt{W_{y,el} / W_{z,el}}$,, based on the "model beam" calibration), the "numerical values" of η that were calculated using equation (6.42), and the best-fit function.

The following observations can be made regarding Fig 6-55 to Fig 6-57:

i.   When the lines for r_d and for the new proposal based on the "model beam" (α_{LT}=0.12) are compared, the near-equivalence of the evidence conveyed by the constant reliability curves and by the Monte Carlo simulations of section 6.10.2 becomes evident. This is particularly true of the calculated values of $\gamma_M{}^*$ in Fig 6-52b to Fig 6-54b are looked at. The value of $\gamma_M{}^*$ is directly comparable to the relative distance of the red dashed line for a_{LT}=0.12 and the r_d line in Fig 6-55 to Fig 6-57. For the IPE 500 and the HEB 400 section, the two lines are very close beginning at intermediate slenderness ($\overline{\lambda}_{LT,nom}$~0.4). In the case of the IPE 500, the distance between the two lines r_d and a_{LT}=0.12 is actually the smallest at $\overline{\lambda}_{LT,nom}$~0.6 and then again after $\overline{\lambda}_{LT,nom}$~1.0. These are the points were $\gamma_M{}^*$ is closest to 1.0 in Fig 6-53b. In the case of the H200x100x5,5x8 section, the calculated value of $\gamma_M{}^*$ decreases with increasing slenderness, see Fig 6-52b. This is reflected in Fig 6-55 by an increasing difference between the a_{LT}=0.12 and the r_d line. This difference again becomes somewhat smaller at $\overline{\lambda}_{LT,nom}$~1.5, which is also reflected in the increase of $\gamma_M{}^*$ in Fig 6-52b.
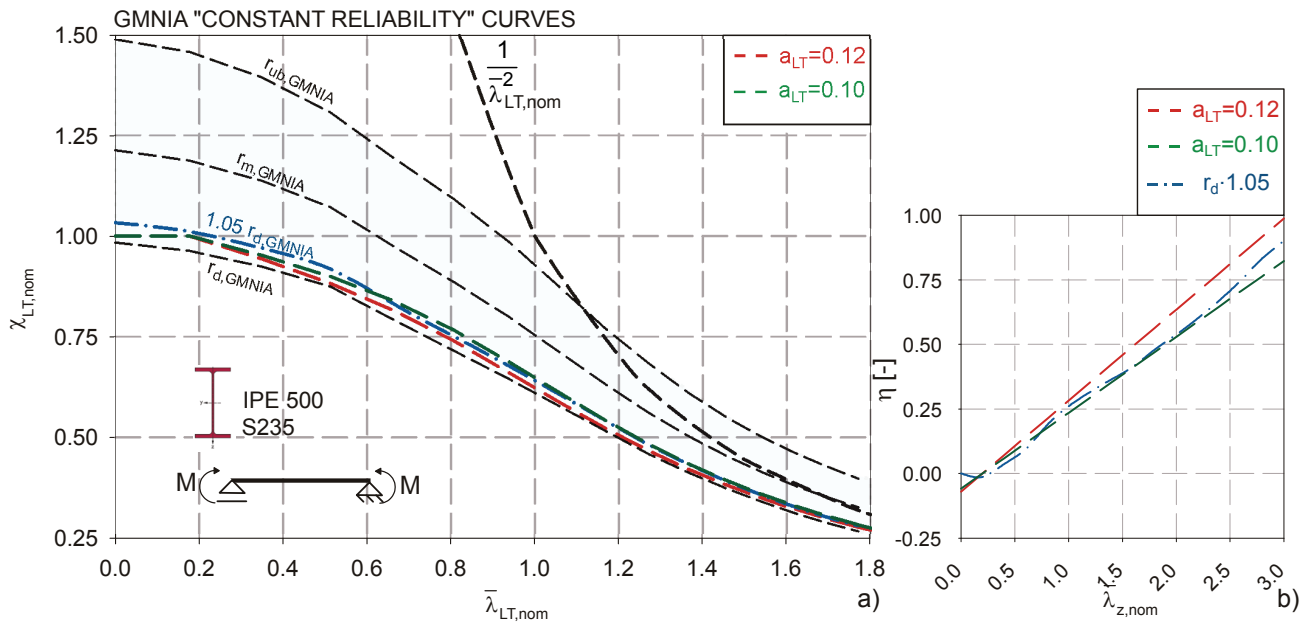
Fig 6-56 *Constant Reliability Curves for an IPE 500 section, steel grade S235.*

ii.   The "best-fit" calibration of the new formulaic expression to the 1.05 r_d line highlights an interesting aspect of a probabilistic calibration: it shows that the type of categorization currently present in EN 1993-1-1 (Tables 6.4 and 6.5 of the code), and also proposed in section 6.8, i.e. an essentially deterministic categorization based on the assumptions made in the GMNIA calculations to which a certain formula is calibrated, is not necessarily able to reflect the differences between different sections in a probabilistic sense.

This is seen in the figures by comparing the determined values of α_{LT} that best fit the 1.05 r_d curves. In the case of the HEB 400 and of the IPE 500 section, values of $a_{LT}=0.09$ and 0.10 were determined to yield the best-fit values in terms of $\chi_{LT,nom}$ over all considered slenderness ratios. In the case of the H200x100x5,5x8 section, the best-fit value was found to be $a_{LT}=0.07$.

Whether or not this already constitutes a sufficient difference to justify a different categorization cannot be decided at this point, for one because the calculations presented in this section are only partly based on actually measured statistical distributions of structural base parameters, and also because such a limited number of sections was considered. It should however be kept in mind that a probabilistic categorization of sections, while desirable from the reliability point of view, will probably require a finer distinction between different types of sections. This is reflective of the different sensitivity to certain parameters: e.g. deep sections will react differently to a variability of flange thickness, or overall depth, than stocky sections.
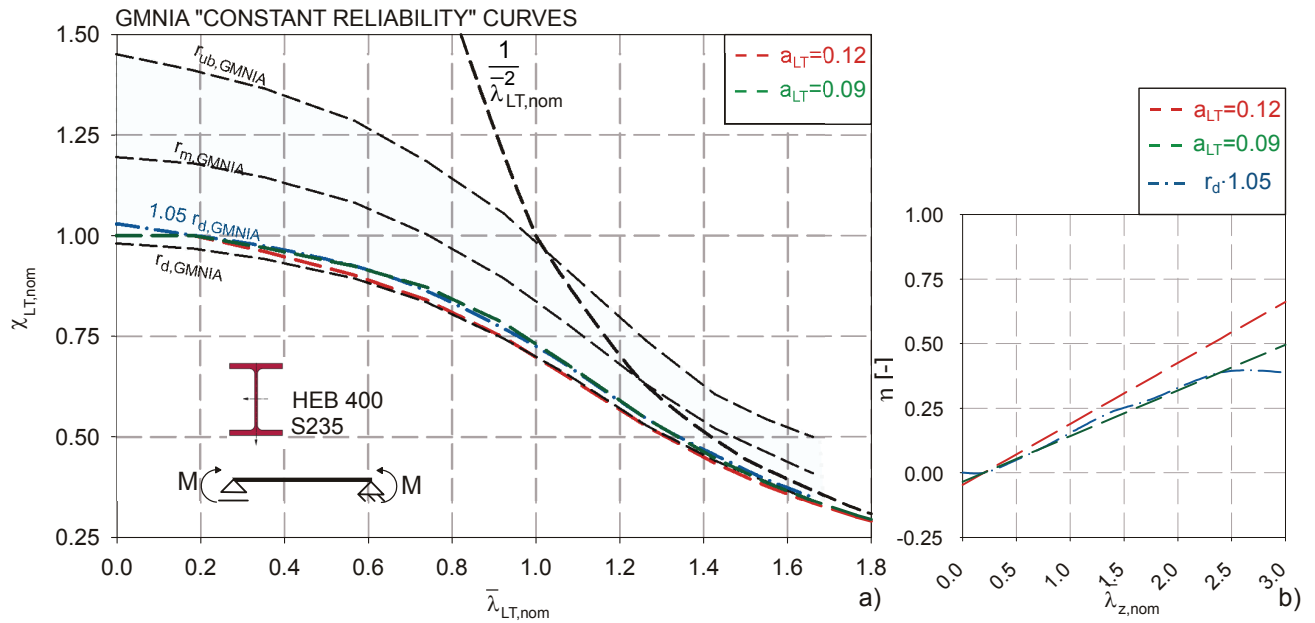
Fig 6-57 *Constant Reliability Curves for a HEB 400 section, steel grade S235.*

Summarizing this section, it can be said that the "constant reliability method" using a numerical FORM analysis with numerical GMNIA derivatives seems to be applicable to the LT buckling case, since it could be shown to be fully compatible with the results of (far more cumbersome) Monte Carlo simulations.

The comments given in section 5.6.5 of chapter five, where the same method was applied to column buckling, hold their validity here. It is believed that an application of the proposed method as a basis for a probabilistically better-founded calibration of a design formulation could be very advantageous, provided that sufficient information is gathered regarding the statistical distribution of the base variables, and widely accepted as sound.

7

Torsional & Torsional-Flexural Buckling of I- & H Sections

7.1. Introduction and Scope

Columns in the shape of I- or H-profiles are frequently restrained in lateral direction; examples for such supports are side rails supporting a cladding system, liner trays, trapezoidal sheeting, sandwich panels, etc. In either case, these elements of the building envelope can usually be thought of as a continuous restraint for the purely lateral deflection of the column, effectively preventing the pure weak-axis buckling mode. In these cases, the buckling failure mode is described by a rotation of the cross-section about the axis of lateral restraint. Depending on the location of the restraints, the column may react by a mere torsional deformation (when the lateral support is in line with the column's centroid), or by a combined torsional and flexural deformation (when the lateral support is eccentric, as is usually the case in the case of cladding). The global ultimate limit (buckling) load is thereby usually reached when one of the flanges reaches its plastic limit load.

The problem of the ultimate strength and buckling behaviour of laterally supported columns and beam-columns is well known; fundamental research work on the topic has already been published by Horne & Ajmani (1971). These early studies mainly focused on the determination of maximum slendernesses (or minimum support spacing and stiffness) for a fully plastic design of beam-columns under combined axial compression and in-plane bending moment using the plastic hinge theory. They constitute the theoretical background for the so-called "stable length" method found in Annex BB.3 of Eurocode 3-1-1 (2006), see also King (2005).

Nevertheless, the basic case of torsional (T) and torsional-flexural (TF) buckling–seen as a member instability phenomenon comparable to flexural or lateral torsional buckling and expressible in the general form of a buckling curve $\chi = N/(A \cdot f_y) = f(\overline{\lambda})$ - is treated with a certain degree of neglect in most international design codes. In the Eurocode 3, torsional and torsional-flexural buckling is considered to behave somewhat similarly to out-of-plane flexural buckling, with the $\overline{\lambda}$-dependent reduction factor χ being equal to the one for out-of-plane flexural buckling.

This chapter is therefore aimed at developing and representing specific buckling curves of members with double-symmetric I- and H-sections with lateral restraints under pure axial compression, which tend to fail in torsional or torsional-flexural buckling. Thereby, single span members are considered

and the lateral restraints are assumed to be applied continuously along the span, see Fig 7-1. The possible contribution of the lateral support to the torsional rigidity of the column-cladding system, as would be given in practice whenever the lateral support runs continuously (rigid node) across the studied column, is ignored in the present study; for many conventional cladding systems, this effect will be comparatively small.

Numerical simulations are carried out on the basis of geometrically and materially nonlinear analyses with imperfections (GMNIA). The results of the GMNIA calculations are illustrated in the form of buckling curves for different cross-section shapes and different positions of the lateral restraints in relation to the centroid of the sections.

Following the procedure applied in chapter 6 for the LT buckling case, a specific, second-order formulation is then developed for the torsional buckling phenomenon. Again, a generalized imperfection is defined in the typical form of the Ayrton-Perry formulation, allowing for a subsequent calibration to pre-established numerical curves.

In a final step the numerically obtained buckling curves are described by a possibly encompassing, calibrated definition of the generalized imperfection. Finally, the newly developed curves are compared to both the numerical curves and the rules given in Eurocode 3-1-1, illustrating the advantage in accuracy provided by the new formulation.

7.2. Elastic critical buckling loads

7.2.1. General relationships

Before the ultimate strength of members subjected to torsional or torsional-flexural buckling can be represented in the familiar form of buckling curves, it is necessary to determine the critical Euler buckling loads N_{cr} for these cases of member instability. The normalized slenderness $\overline{\lambda}_T$ or $\overline{\lambda}_{TF}$ for torsional or torsional-flexural buckling can then be calculated as the square root of the ratio $N_{pl} / N_{cr} = A \cdot f_y / N_{cr}$ as costumary.

The critical Euler buckling loads $N_{cr,T}$ or $N_{cr,TF}$ for torsional and torsional-flexural buckling of members with double-symmetric sections and enforced axis of rotation are well known -see e.g. Timoshenko (1964) or Bleich (1954)- and can be expressed by the following set of equations:

$$N_{cr,TF} = N_{cr,z} \cdot \frac{c^2 + d^2}{i_p^2 + d^2} \tag{7.1}$$

Where

$$N_{cr,z} = \pi^2 \frac{EI}{L^2} \tag{7.2}$$

$$i_p = \sqrt{(I_y + I_z) / A} \tag{7.3}$$

$$c = \sqrt{\frac{I_w}{I_z} + \frac{GI_T}{N_{cr,z}}} \tag{7.4}$$

and d is the distance of the lateral restraint from the centre of gravity, see Fig 7-1.

For practical use in design, the relationship between the buckling loads $N_{cr,T}$ and $N_{cr,z}$ can be expressed equivalently to the procedure used in BS 5950-1 (2000) - Annex G, by referring to the slenderness coefficients $\overline{\lambda}_{TF}$ and $\overline{\lambda}_z$ and combining them through a factor k_T :

$$\overline{\lambda}_{TF} = k_T \cdot \overline{\lambda}_z \tag{7.5}$$

where k_T is a factor accounting for the influence of the torsional rigidity of the section.

In a paper by Greiner et alt. (1999), k_T was evaluated for different cross section shapes and represented in form of diagrams. The diagram in Fig 7-1 was thereby developed under the geometric assumption that the thickness of the web is half the thickness of the flanges. This assumption was necessary in order to eliminate the otherwise free parameter of web thickness from the chosen form of representation. By comparing the results of the calculations carried out under these assumptions with results of calculations for actual rolled beam sections (IPE500 and HEB300), it could be shown that the parameter which best reproduces the beneficial effect of torsional rigidity on the critical buckling behaviour of double symmetric I- and H-sections is the ratio h/t_f of section depth to flange thickness. The assumption concerning the web thickness was shown to yield slightly higher values of slenderness than the ones calculated for actual rolled beam sections and is therefore somewhat on the safe side. Hence, the application of the procedure illustrated in Fig 7-1 allows for a simple and safe evaluation of critical torsional buckling loads over the more accessible buckling loads for out-of-plane flexural buckling.
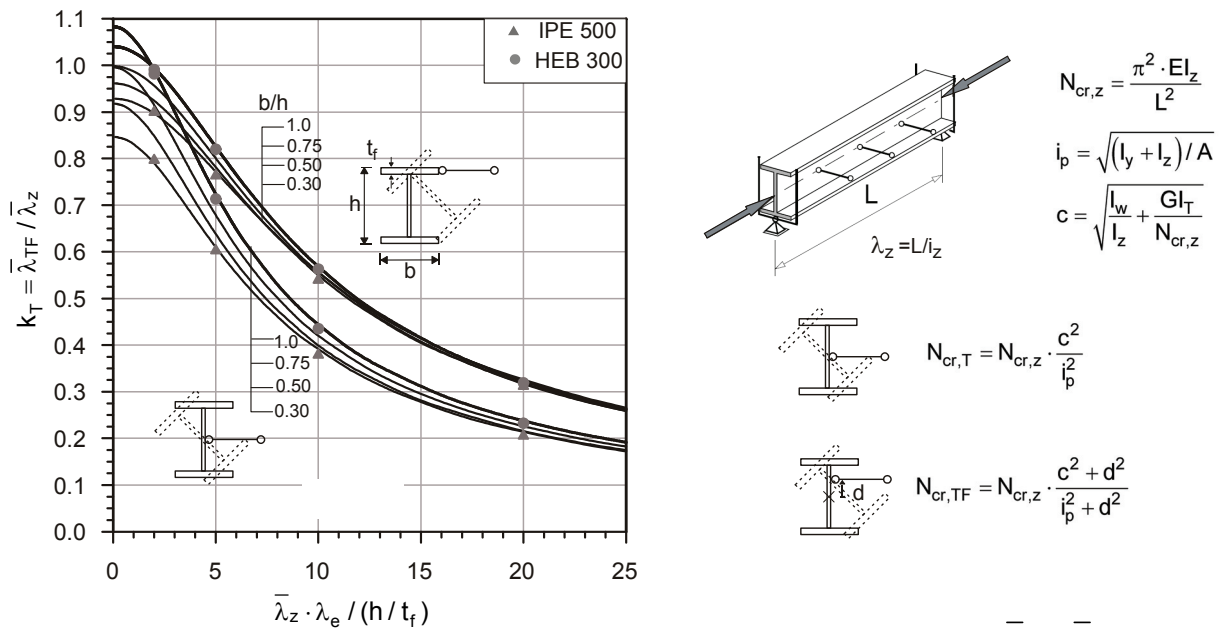
Fig 7-1   *Ratio kt of weak-axis flexural and torsional-flexural slenderness* $k_T = \overline{\lambda}_{TF} / \overline{\lambda}_z$

7.2.2. Comparison with in- & out-of-plane buckling and "limit slenderness"

In order to appreciate the significance of the studied buckling phenomenon, it is first useful to take a look at the critical buckling loads for torsional and torsional-flexural buckling (TB & TFB) and compare them to the other main global buckling modes associated to column buckling, i.e. strong- and weak axis flexural buckling (FByy & FBzz, respectively). This is done for three different sections in Fig 7-2 and Fig 7-3, representative for relatively slender (IPE500), indermediate (IPE240) and stocky sections (HEM 400) as far as their torsional rigidity is concerned. In these figures, the normalized critical (bifurcation) buckling loads N_{cr}/N_{pl} for the different modes is plotted over the length of the section; in all calculations, the fillet radius was included in the calculation of area, torsional rigidity I_T and second moment of area I_y. The boundary conditions are shown in Fig 7-1.
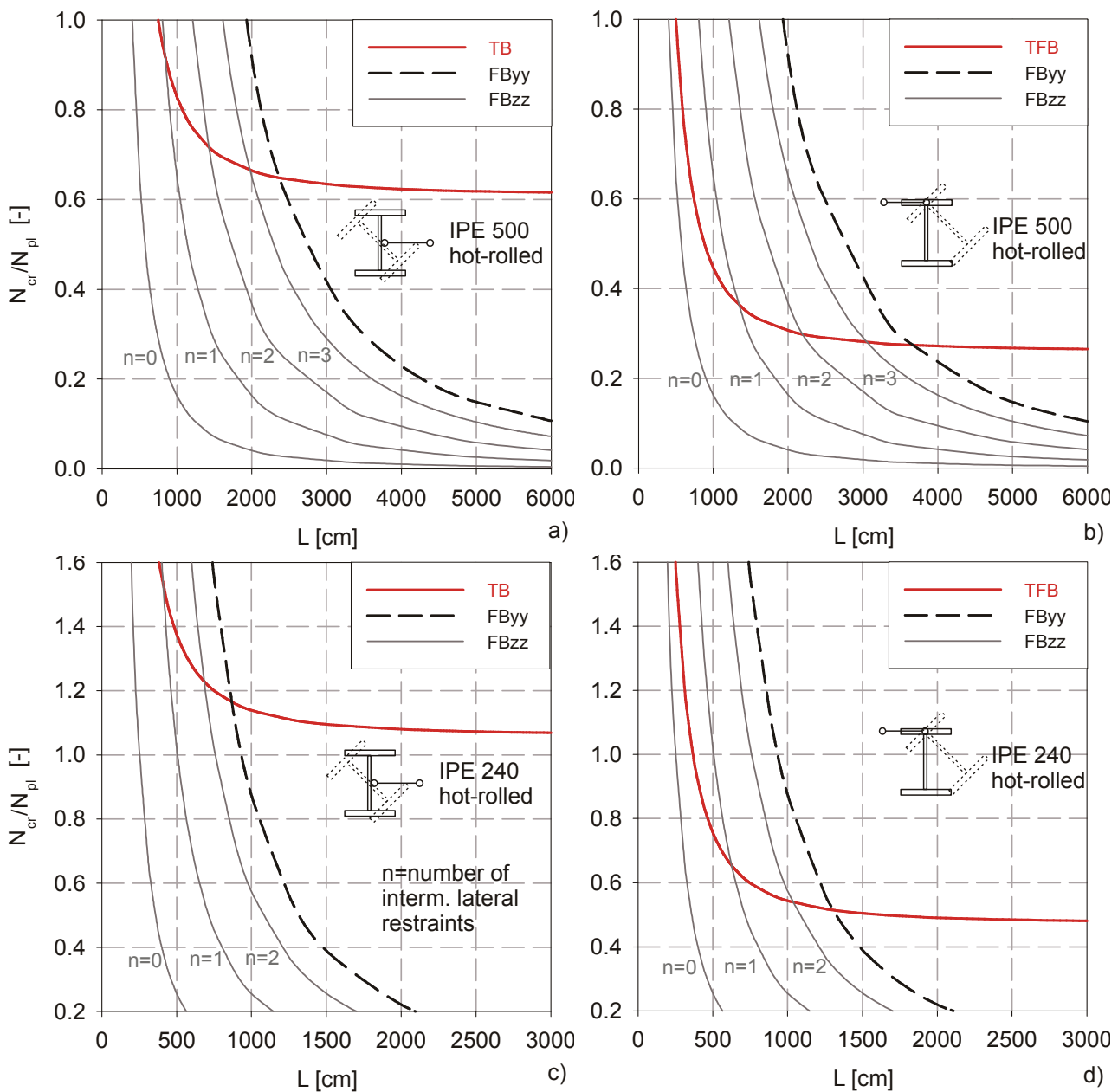
Fig 7-2 *Comparison of critical buckling loads and modes for an IPE 500 and IPE 240 section.*
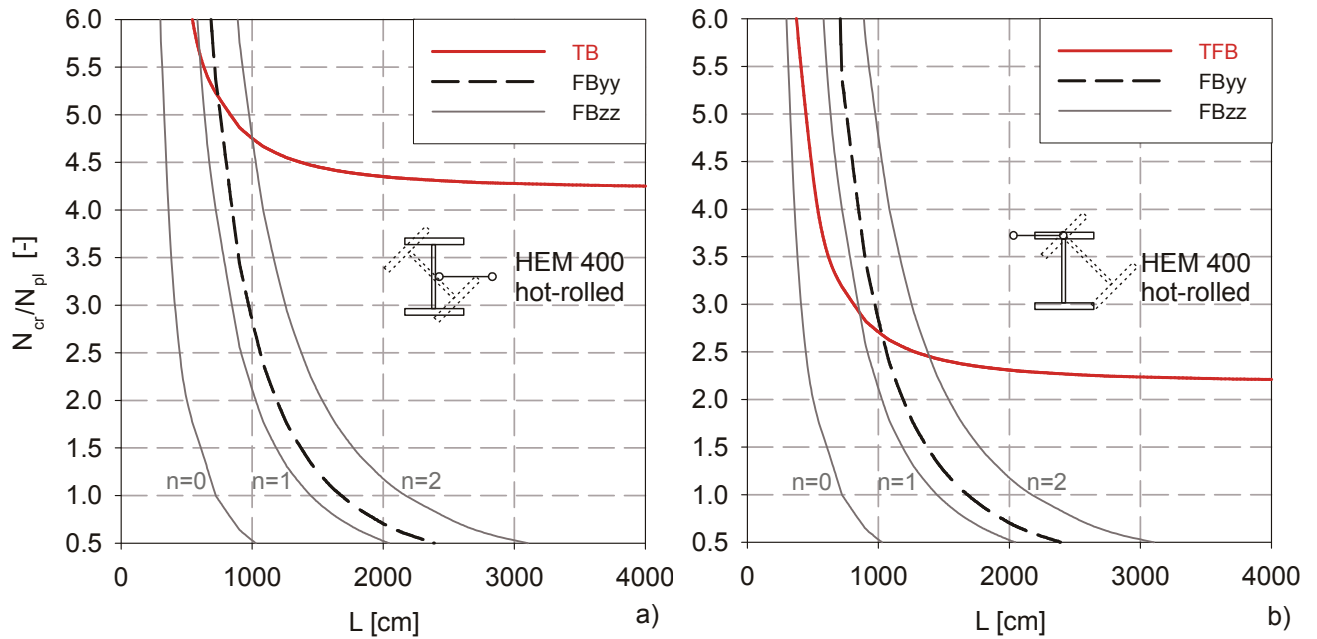
Fig 7-3 *Comparison of critical buckling loads and modes for an HEM 400 section.*

In Fig 7-2a, c and Fig 7-3a TB is compared to FByy and FBzz with a number of intermediate lateral restraints, with n=0 representing a member free of lateral restraints within its span. The figure shows that it takes a varying, section-dependent number of intermediate restraint points in order to have a lower critical buckling load for FByy than FBzz; this number is n=4 in the case of the IPE 500, n=3 for the IPE240, and only n=2 for the HEM 400. More interestingly, in all studied cases a single intermediate lateral restraint is sufficient to push the FBzz critical buckling load beyond the TB bifurcation load in the "lower" range of member length; this "lower" range of length is shown to lie in a very relevant domain of practical applications, with the change of mode lying at ca. 4 to 8 m, and L/h~14 to 18, depending on the section. With increasing number of intermediate restraint points n, the transition from the TB to the FBzz mode is of course pushed even farther towards greater member lengths. Thus, in many practical cases the question of whether or not the lateral restraints represent a "continuous" support will make little difference in design; this is especially true if one considers the current Eurocode rules, where the buckling reduction factors χ_z and χ_{TB} are to be calculated with the exact same buckling curves and with the value of $\bar{\lambda}$ corresponding to the lower value of $N_{cr,z}$ or $N_{cr,T}$, see also the explanations given in section 7.3.

If one considers the case where n is large enough to make the strong-axis buckling case FByy more relevant than the purely flexural FBzz case in terms of N_{cr}, the practical significance of the TB case becomes even more evident from Fig 7-2a, c and Fig 7-3a. The change of mode between TB and FByy occurs at lengths corresponding to ratios L/h of ca. 36 and 47 in the case of the IPE 240 and 500 sections, respectively, making TFB clearly relevant in practice for these sections.

The considerations made up to this point are only further accentuated if the lateral restraints are placed eccentrically with regard to the section's centroid line, i.e. in the case of torsional-flexural buckling TFB. This is shown in Fig 7-2b, d and Fig 7-3b for the three studied sections and a

position of the lateral support that is aligned with the centroid of one of the two flanges of the symmetric I-section. A positioning of the (continuous) lateral support at this location, or rather slightly farther "outside", is quite typical for the effect of cladding in building envelopes. The figures show that the eccentricity d of the support line leads to a significant drop of $N_{cr,TF}$. In the case of the more slender IPE sections, boundary conditions of this type will cause the TFB case to be the only relevant global bifurcation mode in all ranges of practical application, particularly for single-span members.

It has thus been shown that the normalized column slenderness $\bar{\lambda} = \sqrt{N_{pl}/N_{cr}}$ will indeed be governed by $N_{cr,T}$ or $N_{cr,TF}$ in many cases of practical application. One additional, possibly surprising fact resulting from the calculation in Fig 7-2 and Fig 7-3 must however be pointed out: all diagrams in these figures illustrate that, while the critical buckling load $N_{cr,z}$ and $N_{cr,y}$ for flexural buckling approach values of zero for infinite member length, the $N_{cr,T}$ and $N_{cr,TF}$ curves approach a non-zero value. Indeed, a limit value of $N_{cr,TF}$ (which includes $N_{cr,T}$ as a special case) for L equal to infinity can be calculated from equation (7.1):

$$N_{cr,TF,\infty} = \lim_{L \to \infty} N_{cr,TF} = \frac{GI_T}{i_p^2 + d^2} \qquad (7.6)$$

This is, of course, always a non-zero value. As the term itself implies, while the warping resistance's I_ω contribution to the load-carrying behaviour approaches zero with increasing length the torsional rigidity GI_T maintains a non-zero stiffness contribution even at infinite length, causing there to be an almost-constant value of $N_{cr,TF}$ at higher lengths.

This characteristic of TB and TFB has another remarkable effect: it causes all buckling curves $\chi(\bar{\lambda}_{TF})$ to stop at a certain value of the normalized slenderness. This is quite untypical for buckling curves, which generally tend towards infinite values of slenderness. By using (7.6) in the column slenderness definition, we can calculate the limit slenderness as follows:

$$\bar{\lambda}_{TF,lim} = \sqrt{\frac{N_{pl}}{N_{cr,TF,\infty}}} = \sqrt{\frac{A \cdot f_y \cdot \left(i_p^2 + d^2\right)}{GI_T}} \qquad (7.7)$$

As will be shown in the following section, the existence of the limit slenderness means that –as far as the TB and TFB mode itself is concerned- all buckling curves for TB and TFB will *stop* at $\bar{\lambda}_{TF,lim}$ for the simple reason that there is no value of $\bar{\lambda}_{TF}$ beyond this point. How this affects the shape of (numerical) buckling curves will be shown in the following section.

7.3. Numerical (GMNIA) buckling curves and comparison with Eurocode rules

7.3.1. General remarks

In this section, the general behaviour of columns failing in the torsional- and torsional-flexural buckling mode are studied by means of numerical GMNIA calculations and compared to the current Eurocode design regulations.

Again, only single-span members with end fork boundary conditions and intermediate lateral supports were considered, i.e. members with in-plane (parallel to web), out-of-plane (lateral) and torsional restraints at the ends and solely lateral restraints along the free span.

The numerical methodology followed the general indications given in chapter 3. Both beam and shell element models were used, whereby the shell models were mostly used to confirm the beam model's accuracy. The initial geometric imperfections were assumed to be distributed in a sinusoidal shape along the length of the member, having their maximum value at mid-span. The possibility that the imposition of the restraints will influence the initial shape of the member was ignored for the purposes of this study. Both initial rotations and (in the torsional-flexural case) lateral deflections were considered. The amplitude of these imperfections was assumed to be equal to $\bar{e}_0 = L/1000$. Only global imperfections were considered, i.e. no imperfections involving cross-section distortion were taken into consideration. All calculations were conducted for steel grade S235, with $f_y = 235$ N/mm².

The differences between cross-sectional classes (1 to 4) were neglected for the purposes of this study. This means that some sections are treated *as if* they were compact class 1 or 2 sections even when they are actually slender class 4 sections under pure compression. This was done in order to be able to better separate the single buckling effects and focus on the studied case alone.

7.3.2. The Eurocode buckling rules for torsional and torsional-flexural buckling

According to Eurocode 3 – EN 1993-1-1 (EC3), clause 6.3.1.4, the design buckling resistance $N_{b,Rd}$ against torsional or torsional-flexural buckling is calculated by multiplying the plastic resistance $A \cdot f_y = N_{pl}$ with the buckling reduction factor χ_{TF}; thereby, the torsional-flexural mode includes the purely torsional mode as a special case. The reduction factor is calculated from the following Ayrton-Perry formula and – in the case of hot-rolled sections studied in this chapter- the generalized imperfection factor α_{TF} according to Table 6-4.

$$\chi_{TF} = \frac{1}{\Phi_{TF} + \sqrt{\Phi_{TF}^2 - \bar{\lambda}_{TF}^2}} \le 1.0 \qquad (7.8)$$

and
$$\Phi_{TF} = \frac{1}{2}\left[1 + \alpha_{TF}\left(\bar{\lambda}_{TF} - 0.2\right) + \bar{\lambda}_{TF}^2\right] \qquad (7.9)$$

h/b	hot-rolled I (buckling curve)
≤ 1.2	$\alpha_{TF}=0.49$ (c)
>1.2	$\alpha_{TF}=0.34$ (b)

Table 7-1 *Generalized imperfection amplitude according to the Eurocode.*

The generalized imperfection amplitude factor α_{TF} is identical to the one applicable for the weak-axis flexural buckling mode, α_z. The generalized imperfection term $\eta=\alpha_{TF}\left(\bar{\lambda}_{TF}-0.2\right)$ is a linear function of $\bar{\lambda}_{TF}$; as was pointed out in chapter 4, section 4.3.2, this means that the underlying equivalent imperfection amplitude $\bar{e}_0$ is *not* a linear function of the member length, since $\bar{\lambda}_{TF}$ is not proportional to length.

7.3.3. Comparison of GMNIA and Eurocode buckling curves for different sections

The general behaviour of I-sections in torsional or torsional-flexural buckling is illustrated for four different sections and four locations of the lateral restraint in Fig 7-4. The four chosen sections represent a fairly broad band of geometrical proportions, ranging from a stocky HEM 400 to a very slender HEAA 1000, and including two increasingly slender IPE sections (IPE 240 & 500). Nevertheless, all sections have an h/b ratio larger than 1.2, leading to a common assumption for the residual stresses in all cases. This common categorization with h/b>1.2 also leads to the fact that all sections are designed against TB/TFB with the exact same buckling curve b according to the Eurocode, as this is the curve that would also apply for weak-axis flexural buckling.

Fig 7-4a illustrates the buckling strength of the four studied sections for the purely torsional buckling case TB. In this case, the imperfection shape doesn't contain any movement of the section's centroid, as the imperfections are mainly associated to the two flanges, where each of them is pre-deflected by an amount of $\bar{e}_0=L/1000$. The centroid also doesn't deflect during the buckling phenomenon, which is therefore entirely associated with a (circular) rotation of the cross-section, having its maximum at mid-span. The differences between the behaviour (in terms of shape of the numerical buckling curve) of the single sections is clearly visible in the figure: while the behaviour of the slender HEAA 1000 section results in a buckling curve that has a typical, sharp drop of the buckling strength with increasing slenderness, the stocky HEM 400 section is entirely unaffected by buckling in this case. The two IPE sections have a behaviour that is somewhat intermediate between the two previously discussed extreme cases. All numerical GMNIA curves have in common that they lie relatively far above the Eurocode design curve (meaning that the Eurocode curve is "very conservative" for this case), and that they *stop* at (or don't exceed) the limit value of the slenderness $\bar{\lambda}_{T,lim}$ calculated using (7.7) for d=0. This theoretical limit value is indicated with short, vertical dashed lines in the figures.
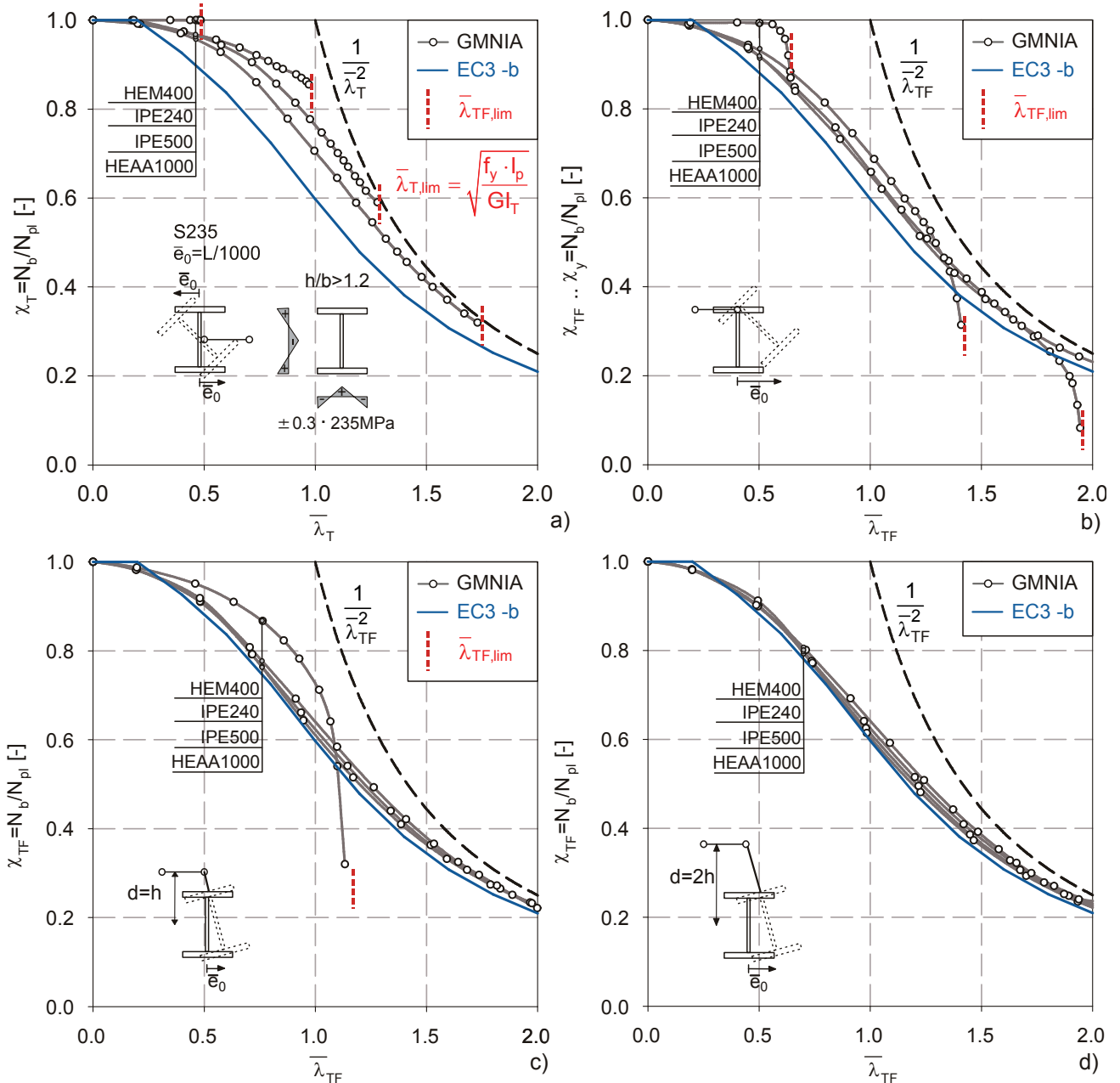
Fig 7-4 *Numerical (GMNIA) TB and TFB curves compared with the Eurocode curve.*

Fig 7-4b-d illustrate cases of torsional-flexural buckling for the same sections, with increasing values of the eccentricity d of the lateral support. The first thing that catches the eye in these three figures is that the numerical GMNIA curves progressively get closer to the Eurocode design curve; the latter is always the same for all cases of TB and TFB.

In the case of lateral supports at the height of the centroid of one of the flanges (Fig 7-4b), the differences between the single sections are still significant, but decreasing when compared to the TB case. The limit slenderness $\overline{\lambda}_{TF,lim}$ is pushed towards higher values and disappears from the plotted graph for the HEAA 1000 section. The HEM 400 reaches its full plastic capacity up to a slenderness value of ca. $\overline{\lambda}_{TF}=0.5$, and then suddenly begins to drop almost vertically; the last plotted point in the curve thereby only indicates the last plotted calculation, not the physical stop of

the curve. The same behaviour is observed for the other three sections as well as they approach their respective value of $\overline{\lambda}_{TF,lim}$.

When d=h (Fig 7-4c), with h being the section depth, the IPE and HEAA sections are very close to each other and increasingly closer to the Eurocode curve. The values of $\overline{\lambda}_{TF,lim}$ lie beyond the plotted range limit of 2.0 for these three sections. Only the HEM 400 section has a behaviour that clearly diverges from the behaviour of the other sections. As the –otherwise rather high- buckling curve approaches the calculated value of $\overline{\lambda}_{TF,lim}$, the buckling curve again drops dramatically.

At a value of d=2h (Fig 7-4d) the buckling curves resulting from the GMNIA calculations are very close to the EC3 design curve (also valid for weak-axis flexural buckling), with only minor differences remaining between the single sections.

The shape of the buckling curves of the four sections shown in Fig 7-4 can be further commented upon and explained as follows:

i.   The fact that the curves' shape is quite distinctly influenced by the section series in the case of TB is –in retrospect- not very surprising. As the name of the torsional buckling mode implies, torsional rigidities and deformations are dominant in this case. Since the torsional rigidity –and its relative contribution when compared to the warping stiffness- is very different for each section, the differences in the shape of the buckling curve are understandable. The reason why the Eurocode does not at all reflect these differences is to be found purely in the scarcity of specific numerical studies of this phenomenon found in the literature, which clearly led the code developers to adopt a cautious lower-bound approach.

ii.   The fact that the Eurocode provision –which is valid for TB *and* TFB- is a lower limit is confirmed by the tendency to approach the Eurocode (weak-axis flexural buckling) curve with increasing section slenderness and –importantly- support eccentricity d. In the limit case of d=∞, buckling curves must inevitably converge towards the Eurocode curve, as this case *is identical to* the weak-axis flexural buckling case, with $\overline{\lambda}_{TF,lim}=\infty$ and $\overline{\lambda}_{TF} = \overline{\lambda}_z$.

iii. The observed, sharp drop of the buckling curves as they reach the limit value of $\overline{\lambda}_{TF,lim}$ in the torsional-flexural buckling case, but not in the purely torsional case, is best explained by representing the results shown in Fig 7-4 in a different form, that is by plotting them over the *length* and the *strong-axis flexural buckling slenderness* $\overline{\lambda}_y$. This is done in Fig 7-5 for the IPE 240 section and the cases d=0 and d=h_s/2, with h_s being the distance between the centroids of the flanges. Additionally to the GMNIA and Eurocode TFB curves for the single cases, these plots include the Eurocode buckling curve for strong axis flexural buckling FByy, as well as the critical (Euler) buckling loads N_{cr} for TFB and FByy. The purpose of this representation is to show that the observed quasi-vertical drop of the buckling curves in the $\chi_{TF}/\overline{\lambda}_{TF}$ space stems from a mode switch between TFB and FByy.
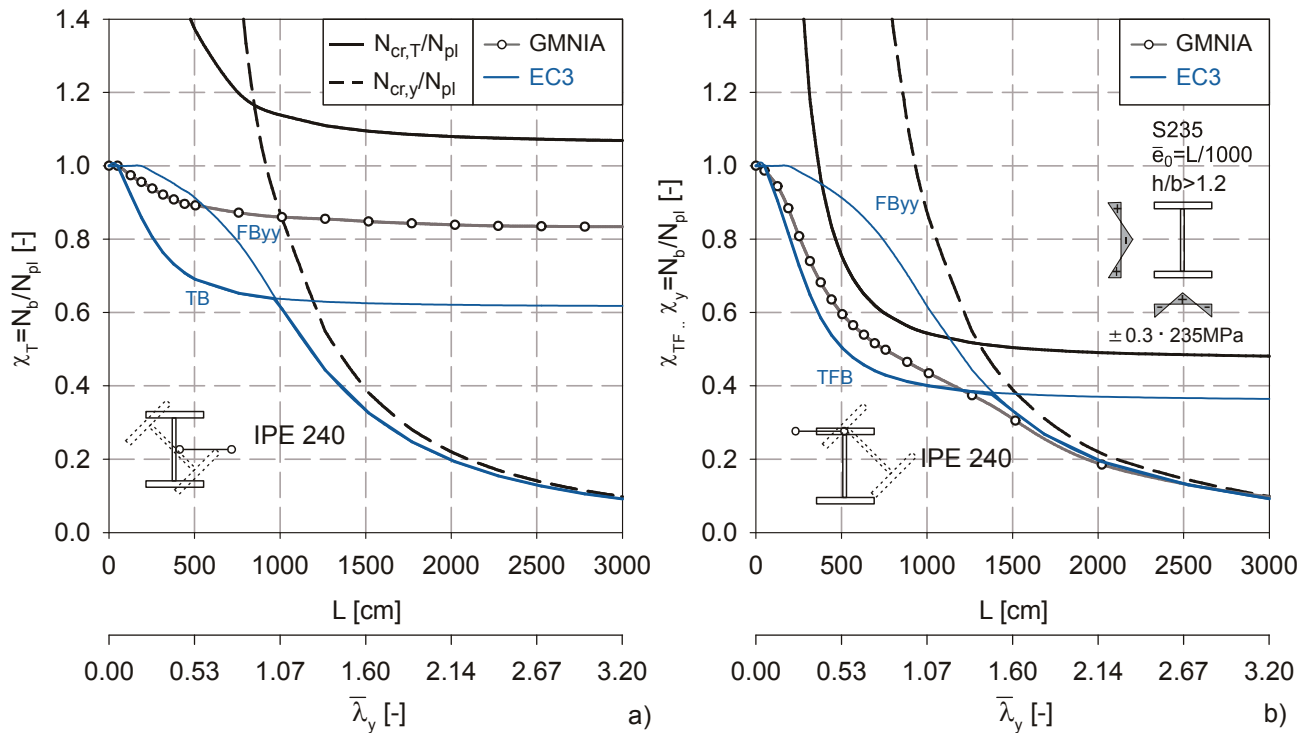
Fig 7-5 *TFB and FByy buckling curves for an IPE 240 section; d=0 (a) and d=h_s/2 (b)*

When the two plots of the numerical results in Fig 7-5a and b are compared, a fact that comes to one's attention is that the GMNIA curve appears to approach a horizontal asymptote in the case of purely torsional buckling (a), which is consistent with the behaviour of the critical TB load $N_{cr,T}$. Contrary to this, the GMNIA curve in the case of torsional-flexural buckling does not approach a horizontal asymptote, but rather approaches the Euler critical buckling load for strong-axis buckling $N_{cr,y}$ with increasing length.

By comparing the results with the Eurocode rules, it becomes clear that the GMNIA TB curve not only lies significantly above the Eurocode values for torsional buckling, but also "misses" the transition to the FByy buckling load predicted by the EC3 rules for this mode. In the studied TFB case, the GMNIA curve still lies well above the Eurocode values in the range that appears to be dominated purely by TFB, then (between L=1000 and 1500 cm) features a smooth transition to $N_{cr,y}$, thereby trespassing the EC3 curve for FByy. Over a relatively small range of length, this "transition" line lies slightly *below* both the Eurocode TFB and FByy buckling curves, meaning that the code regulations are actually somewhat "unconservative" in this range.

It is fairly easy to answer the question of where the differences in behaviour between the studied TB and TFB cases in Fig 7-5a and b stem from: these are to be found in the shape of the imperfection for both cases, particularly in the position of the centroid of the section in the imperfect configuration and with respect to the section's strong axis. While in the TB case the centroid does not move at all throughout the loading process, in the TFB case the imperfection itself has a (very small, but present) component in the direction parallel to the web in perfect configuration, given by the circular shape of the deformation path.
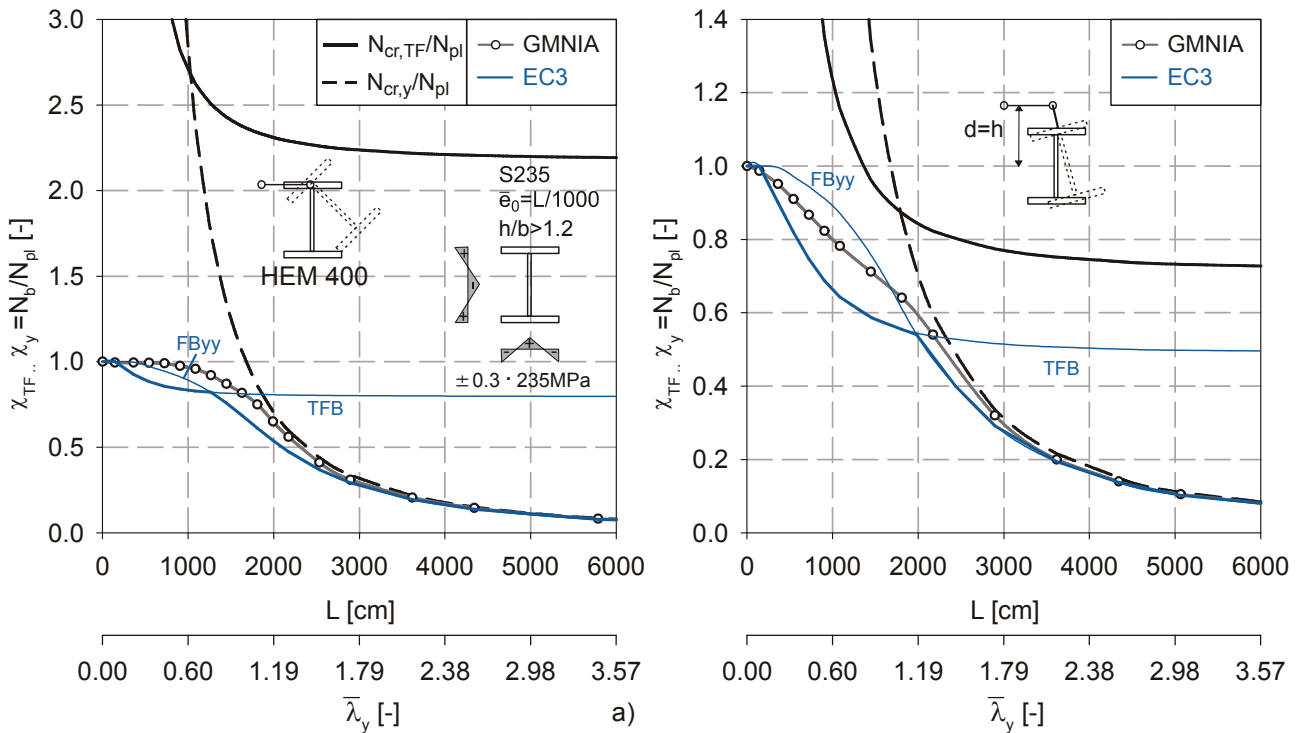
Fig 7-6 *TFB and FByy buckling curves for an HEM 400 section; d=h$_s$/2 (a) and d=h (b)*

Thus, in the TFB case, at a certain length the non-linear load-deformation path enters the strong-axis flexural-buckling path. Since the initial imperfection in this direction is rather small, and certainly smaller than the value of $\bar{e}_0$=L/1000 assumed by Beer & Schulz (1970) when they established the ECCS curve that now became the EC3 column buckling curve a for FByy, the GMNIA curves at very high member length ends up being closer to the critical load $N_{cr,y}$ than the Eurocode design curve for FByy. Of course, this could only happen because no (additional) imperfection in the direction of the web was included in the calculations, as only the effect of TFB and coupled rotational-lateral imperfections is intended to be studied. The same (intentional) lack of imperfection with curvature about the strong axis is also responsible for the "missing" of the bifurcation at $N_{cr,y}$ in the GMNIA calculations for the torsional buckling case in Fig 7-5a.

The transitional behaviour between TFB and FByy is illustrated a bit better when looking at the HEM 400 section, see Fig 7-6. For this section, the classical χ_{TF}=f($\bar{\lambda}_{TF}$) type of representation features rather sudden drops of the buckling load as the limit slenderness value of $\bar{\lambda}_{TF,lim}$ is approached in Fig 7-4a-c. The GMNIA results from Fig 7-4b (d=h$_s$/2) and c (d=h) are looked at again in Fig 7-6, since they are the most interesting. As Fig 7-6a shows, the Eurocode would actually predict a lower TF buckling load than the one given by the applicable FByy curve up to lengths of over 12m for this section and d=h$_s$/2. This is not reflected by the GMNIA curve, which shows a behaviour typical of pure strong-axis buckling, albeit with a smaller imperfection than $\bar{e}_0$=L/1000. Accordingly, the numerical curve stays at χ=1.0 up to a relatively high length, and then smoothly descends towards $N_{cr,y}$. In the case of d=h (Fig 7-6b), the TF buckling mode appears to have a stronger impact on the buckling load at lower member length, albeit not sufficient to make

the current rules for TFB in the Eurocode any less than very "conservative" throughout the length-range where this mode is dominant.

An additional example is illustrated in Fig 7-7, where the GMNIA buckling curves for TB/TFB and variable support eccentricities d are plotted for an IPE 500 section and compared to the applicable Eurocode design curves.
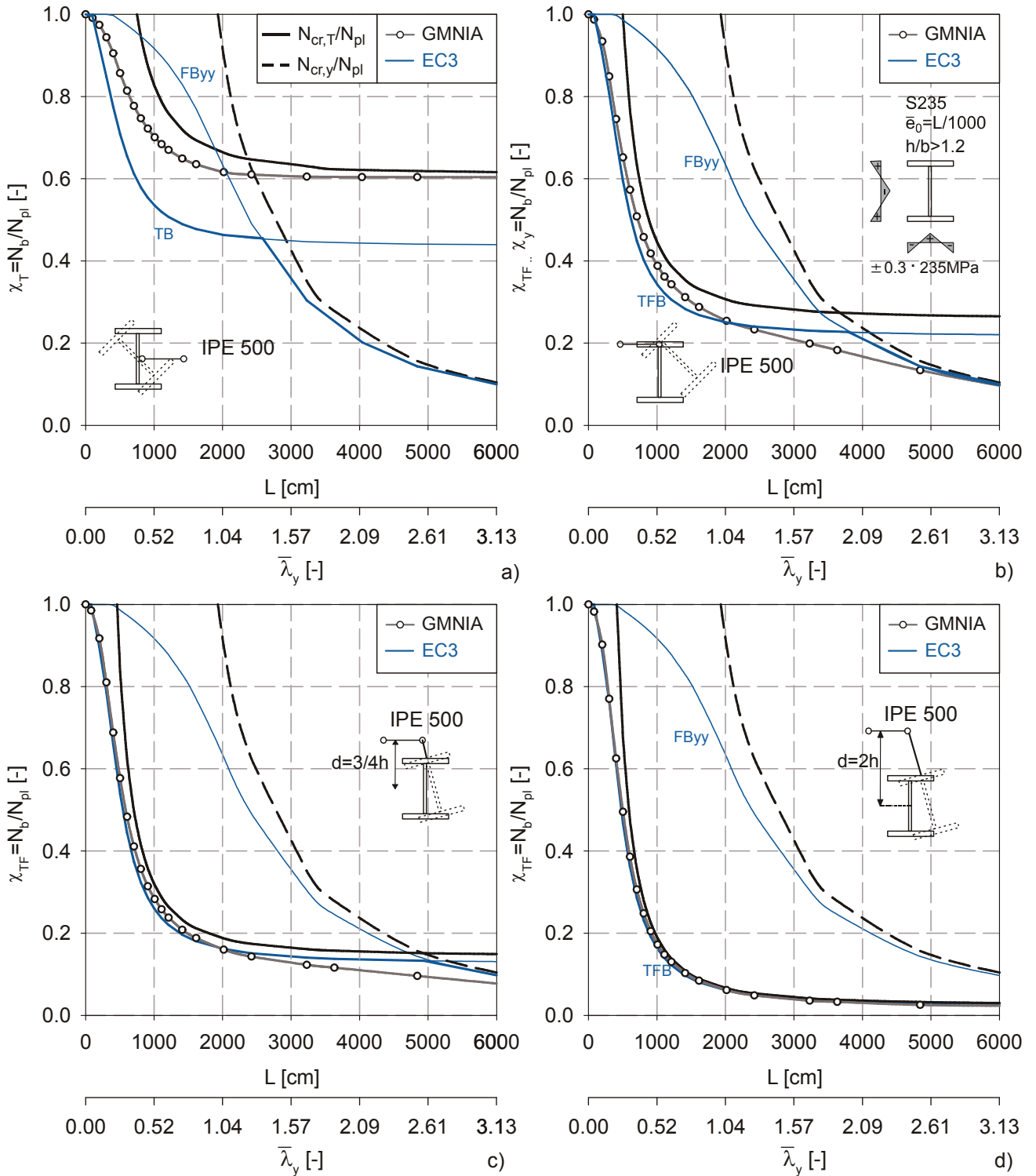
Fig 7-7   *TFB and FByy buckling curves for an IPE 500 section; d=variable.*

Again, the transitional behaviour from TFB to FByy is clearly visible in Fig 7-7b and c. The "unsafe" discrepancies in the length range where both the EC3 design curves lie above the GMNIA curve are most pronounced for the case where the lateral support is at a flange centroid (Fig 7-7b). With further increasing eccentricity, the behaviour becomes increasingly dominated by the TFB mode alone, until finally at d=2h the Eurocode TFB curve appears to describe the GMNIA curve almost perfectly throughout all studied lengths.

In summary, it can be said that the current Eurocode rules describing the torsional- and torsional-flexural buckling mode are rather "conservative" in many cases. This is particularly true in the case of the pure torsional buckling case, where the torsional rigidity of practically all compact (class 1 and 2) hot-rolled and welded I- & H-sections would actually award a much higher TB resistance than is currently granted by the code. In the case of eccentric lateral supports (TFB), the rotational (circular) nature of the deformation path and the associated presence of (small) deflection components parallel to the section's web cause the sections to "switch failure mode" beyond a certain length and to approach a behaviour that is increasingly dominated by the strong-axis buckling mode. Due to the fact that the Eurocode rules do not know "smooth" transitions between the effects of the singly global member buckling cases, this observed transitional behaviour can show some ranges of application where even the (otherwise "conservative") Eurocode rules are "unconservative". The danger of the occurrence of this transitional zone of "unconservatism" is also strongly coupled with the actual position of the lateral support. It can be shown that the studied position at $d=h_s/2$ is in the worst area for this transitional behaviour; for smaller values of d, the component of the imperfection/deformation parallel to the section's web quickly becomes very small, while for larger values of d (outside the section), the "real" TFB buckling behaviour quickly becomes entirely dominant throughout all practical ranges of length.

7.3.4. TFB with one fully restrained flange

In all the above calculations concerned with torsional-flexural buckling, the studied columns were assumed to be continuously supported only in a lateral direction, which corresponds to the configuration most likely to be found in practical applications. These boundary conditions were shown to be due to a transition (beginning at a certain, usually high length) from the TFB mode to the strong-axis buckling mode FByy, due to the presence of deformation components parallel to the web and the free deformability in this direction. This behaviour would clearly be suppressed if one of the flanges were entirely restrained, in directions parallel and perpendicular to the web. In practice, this *bi-directionally restrained* condition of an I-shaped column is possibly not very frequent; applications can be imagined in certain steel sheet pile constructions, where the support in the direction of the web is given (at least in one direction) by the ground. A similar configuration can be imagined to exist for longitudinal stiffeners of large tanks and silos, especially when these are filled and thus very stiff in radial direction. The following pages will treat the behaviour of such columns under pure compression and lateral imperfections of the unrestrained flange.

The comparison between the behaviour of a mono- and bi-directionally restrained flange is shown in Fig 7-8 for an IPE 500 section; thereby, the GMNIA buckling curves for both cases are plotted in the $\chi_{TF}/\overline{\lambda}_{TF}$ space (a), as well as over the member length (b). The differences between the two curves are very large; the bi-directionally restrained column has a significantly higher buckling resistance, which also exceeds the bifurcation load for TFB at a relatively low length of ca. 6m.
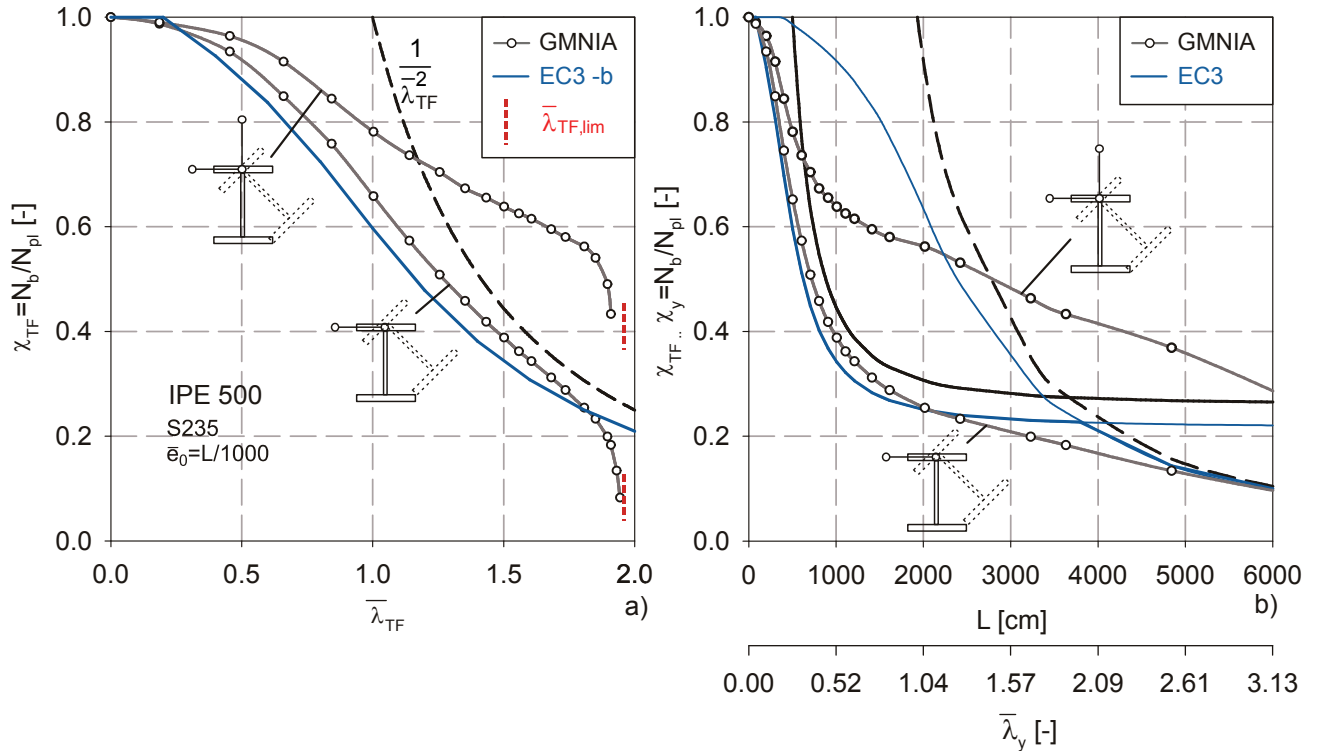
Fig 7-8 *Differences in TF buckling strength between the mono-directionally (laterally) and bi-directionally restrained flange for an IPE 500 section, plotted over $\overline{\lambda}_{TF}$ (a) and L(b).*

Again, the explanation for this behaviour can be found in the geometrically non-linear, "circular" deformation path of the buckling phenomenon: the prevented deformation of the restrained flange in a direction parallel to the web allows the mid-span section to deflect (rotate) much farther and to exploit much more of the cross-section's plastic capacity before the peak of the load-deformation path is reached.

This is illustrated in Fig 7-9, where load/lateral deformation paths for the unrestrained flange are plotted for both studied boundary conditions. The studied section is again an IPE 500, with a length of L=8070 mm corresponding to a weak-axis normalized slenderness of $\overline{\lambda}_z$=2.0. The plotted deformations and stresses are calculated at mid-span. As in all the GMNIA calculations in this chapter, an eigenmode-conform imperfection was assumed in both cases, with an amplitude of $\overline{e}_0$=L/1000=8.07mm. The figure shows that the load/deformation paths for both boundary conditions practically overlap up to a normalized load N/N_{pl} of ca. 0.4. This load factor corresponds to the appearance of the first yield stresses at the right-sided (in the figure) external edge of the upper, unrestrained flange.
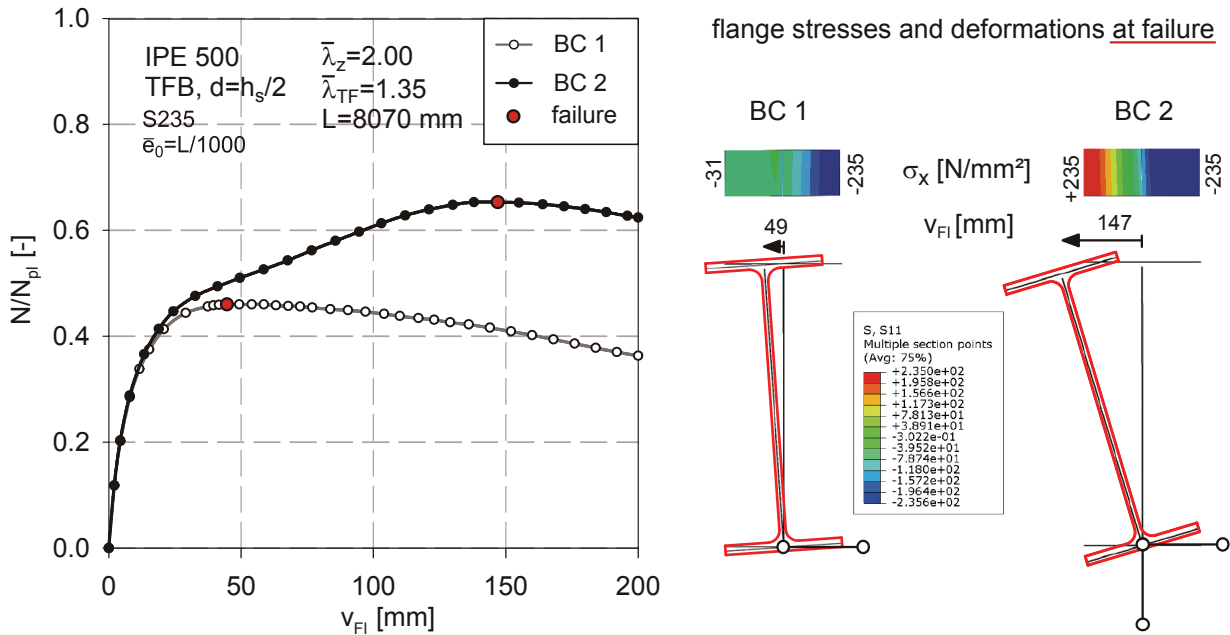
Fig 7-9 *Load-deformation paths for an IPE 500 section in TFB for two boundary conditions.*

Beyond this point, the mono-directionally restrained column (boundary condition BC1) features a drop of stiffness, which culminates in the reaching of the maximum (buckling) load at a load factor of $N/N_{pl}=\chi_{TF}=0.46$. Beyond this point, the column with BC1 displays a typical post-buckling behaviour with a drawn-out, "flat" load-deformation curve.

In the case of the bi-directionally restrained column (BC2), the occurrence of yield at $N/N_{pl}=0.4$ produces a much more gradual decrease of stiffness, which is more typical of failure mechanisms that involve the approach of a plastic mechanism. Indeed, the stiffness appears to "stabilize" in the range beyond $N/N_{pl}=0.5$ up to ca. 0.62, where another gradual decrease occurs that leads to the maximum load factor of $N/N_{pl}="\chi_{TF}"=0.66$. The quotes are intended to indicate that it is up to debate whether or not this maximum load can be classified as a TF buckling load in the strict sense.

The stresses in the unrestrained flange at the maximum (failure) load are also significantly different, depending on the boundary condition. In the case of BC1, about one fifth of the unrestrained flange has reached the assumed yield (compressive) stress of $f_y=235$ N/mm². The rest of the flange is also entirely subject to compressive stresses. The comparatively small deterioration of rigidity against further lateral deformation, caused by the zone of yielding, makes any further increase of deformation impossible. In the case of BC2, the flange stresses at the maximum load feature a significant bending component, emphasized by the fact that the yield stress is reached at both edges of the flange, on one side as compressive, and on the other side as tensile stresses. The compressive area with $\sigma_x=-f_y$ stretches across the entire right side of the flange, while the tensile yield zone takes up a width of approximately $b/5$; this leaves little space for a resulting axial force in the flange.

Interestingly, the achieved maximum load factor of $N/N_{pl}=0.66$ compares fairly well with the section capacity of the IPE 500 section with one flange "missing"; $N_{pl-1flange}/N_{pl}=(A_w+A_{fl})/A_{tot}$ $=79.7/116=0.687$. Indeed, the stress distribution at failure for the whole section can be shown to be a condition very close to full yielding in every fibre, i.e. a primarily global cross-sectional failure.

For practical application, one might ask whether or not this significant over-strength afforded by the bi-directionality of the flange support is practically exploitable, due to the large deformations that appear to occur. As is shown in Fig 7-9, the lateral flange deformation at failure for BC1 is 49mm, equal to ca. b/4 of the section width. The deformation at the maximum load for BC2 is exactly three times as large, reaching 147mm. At least for the studied section, this value appears to be too high for practical acceptance; possibly, a design criterion based on deformations –rather than maximum strength- would have to be defined in practice for the BC2 case, plausibly making the differences between the two cases negligible.

In summary, it can be said that the additional support of the column in a direction parallel to the web would cause a significant increase in ultimate strength of a column subjected to torsional-flexural buckling. Generally, this case will be rare in design and only given in certain, specific types of structures. Furthermore, maximum deformation design criteria might need to be introduced, which would render the differences between the mono- and bi-directionally supported column irrelevant. Due to these reasons, the bi-directionally supported case is not further considered in the remainder of this chapter.

7.3.5. Additional effects: h/b ratio, fillet radius, residual stresses.

Up to now, the study of the realistic, GMNIA buckling behaviour in this section focused on four "real", commercial shapes. Of the four studied sections, the IPE240, IPE 500 and HEAA 1000 could a priori be expected to be sensitive to torsional and torsional-flexural buckling, merely from "engineering judgment", due to their perceived –and real- slenderness for these buckling cases.

The general perception is that the values of h/b, which are usually seen as the main indicator of whether a section is "stocky" or "slender", are –plausibly- also a good indicator of the position ("low" or "high") of a TB and TFB buckling curve in the $\chi_{TF}/\bar{\lambda}_{TF}$ space. This perception was also confirmed by the GMNIA plots in Fig 7-4, where a higher value of h/b clearly correlated with a lower position of the buckling curve. The results obtained and plotted in Fig 7-10 will therefore likely come as a surprise at first sight. In this figure, the previously obtained TB buckling curve for the hot-rolled IPE 500 section is compared with two fictitious, modified "IPE 500" sections with $b=0.5 \cdot b_{nom}=100$ mm and $b=h_{nom}=500$mm, resulting in h/b ratios of 5 and 1, respectively. All other parameters were left entirely unaltered, i.e. the section's flange and web thickness, the fillet radius, and of course the depth h=500mm. Since beam elements were used in these GMNIA calculations, the fact that the b=500 flange is actually vastly in class 4 range could easily be ignored for this academic illustration example.
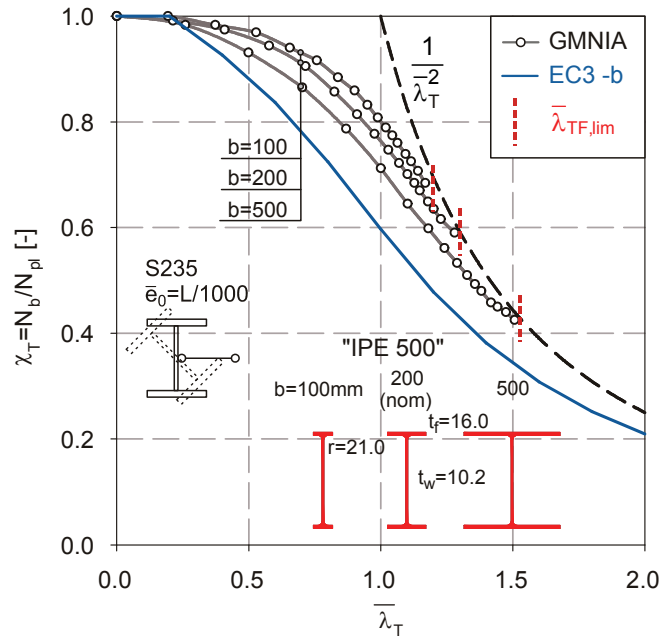
Fig 7-10 *GMNIA buckling curves for modified (b=var.) IPE 500 sections.*

The above-mentioned "engineering judgment" will likely lead one to think that the "slender" section with h/b=5 (b=100mm) will lead to a GMNIA buckling curve that lies significantly lower than the one obtained for the section with h/b=1 (b=500mm). As a matter of fact, an "extrapolation" of the observations made in Fig 7-4, where a section with h/b=1.4 (HEM 400) did not at all react to torsional buckling, could lead to the assumption that the b=500 section will not react to this mode either.

In reality, exactly the opposite is true: as the GMNIA plots in Fig 7-10 show, the putatively "stocky" section is actually quite slender in terms of torsional buckling, and the "slender" section is actually the least prone to this buckling mode. The explanation for this lies in the calculation of the torsional rigidity $I_T \cong 1/3 \cdot \sum a \cdot t^3$, which is most vigorously affected by the single plate thicknesses (as well as the fillet radius), i.e. all quantities that are identical for all three sections studied in Fig 7-10. The width of the flange affects the area A and particularly the polar moment of inertia I_p much more, which –considering that both quantities enter the numerator under the square root in (7.7)- also explains why the limit slenderness is highest in the case of what was thought to be the "stocky" h/b=1 section. It therefore appears that the h/b ratio is a fairly bad instrument for judging the proneness towards torsional buckling of a section.

Another effect that is often controversial when numerical buckling curves are obtained or compared is represented by the fillet radius; more precisely, the controversy arises from the question of whether or not its inclusion is necessary in order to obtain accurate buckling *curves*, provided that the correct/corresponding values of N_{pl}, N_{cr}, $\overline{\lambda}_{TF}$ are used for reference.
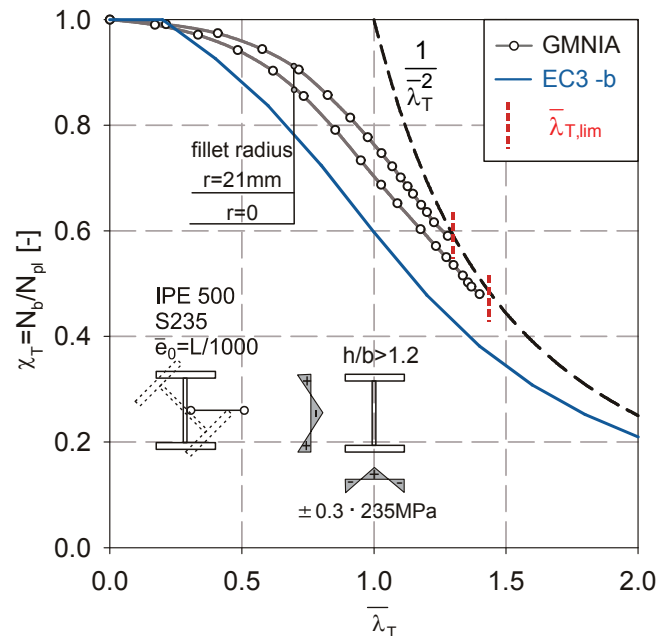
Fig 7-11 *Influence of the fillet radius on the shape of the resulting buckling curve*

In chapter 6, section 6.5.6, the influence of the fillet was shown to be negligible for the LT buckling case, at least as far as the obtained shape and position of the numerical buckling curve is concerned. Correspondingly, Fig 7-11 shows a study of the influence of the fillet radius for the torsional buckling case. The figure illustrates two GMNIA TB buckling curves for an IPE 500 section, both calculated with the same assumptions regarding imperfections, and with the only difference lying in the inclusion or omission of the fillet. It is illustrated in the figure that, contrary to what was observed in the LT buckling case, the fillet radius has a rather significant impact on the resulting shape and position of the TB buckling curve. This is again due to the very high influence of the torsional rigidity on the buckling phenomenon, exemplified among other things in the resulting value of the limit slenderness $\overline{\lambda}_{TF,lim}$. Of course, the purely torsional buckling case is the one most affected by this phenomenon. It can be shown that, in the TFB case, the significance of the fillet on the *shape* of the buckling curve decreases with increasing eccentricity d, and vanishes as the TFB case approaches the behaviour of weak-axis flexural buckling.

A final effect that must be briefly addressed is the influence of the residual stresses. All sections studied so far were assumed to have residual stresses with amplitudes of $\sigma_{res}=0.3\ f_{y,nom,S235}$, which is the value commonly assumed for hot-rolled sections with h/b>1.2. In Fig 7-12, one of the most slender (for TB) possible sections with h/b<1.2, an HEA 360, is studied, using as basis of the GMNIA calculations the applicable, higher amplitudes of the residual stresses of $0.5 \cdot f_{y,nom,S235}=117.5$ N/mm². Additionally to confirming the general tendencies pointed out in this section (limit slenderness values, drop of χ_{TF} at high slenderness, poor representativeness of h/b), the effects of the higher residual stresses also become visible in this figure: with increasing values of d, the numerical curves again approach the Eurocode weak-axis design buckling curve, but this time the lower curve c, applicable for these sections with higher residual stresses.
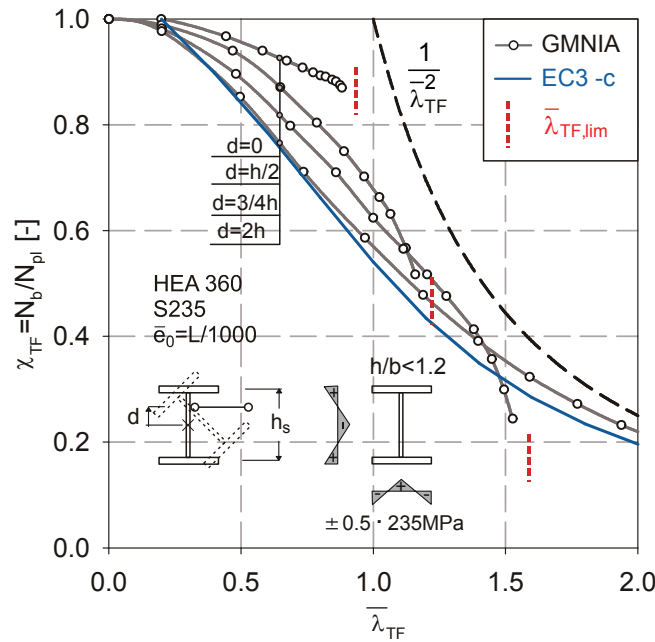
Fig 7-12 *TB and TFB buckling behaviour of a section with h/b<1.2 and correspondingly higher residual stress amplitudes.*

7.4. Ayrton-Perry Formulation

In this section, case-specific analytical Ayrton Perry formulae are derived for the torsional-flexural buckling case of single-span members under constant axial force. The same principles are applied as in chapter 6, section 6.7 for the LT buckling case. The special case of purely torsional buckling (TB), where the eccentricity of the lateral support d is equal to zero, is thereby consistently included in the following derivation as a special case.

7.4.1. Derivation

For a simply-supported column with double-symmetric cross-section and constant axial force N, the assumption of initial lateral and torsional imperfections v_0 and θ_0 (with amplitudes $\overline{v}_0$ and $\overline{\theta}_0$) of sinusoidal shape leads to the following two de-coupled second-order equilibrium equations:

$$N_{cr,z} \cdot \overline{v} - N \cdot \overline{v} = N \cdot \overline{v}_0 \qquad (7.10)$$

$$N_{cr,z} \cdot \left(\frac{I_\omega}{I_z} + \frac{GI_T}{N_{cr,z}} \right) \cdot \overline{\theta} - N \cdot i_p^2 \cdot \overline{\theta} = N \cdot i_p^2 \cdot \overline{\theta}_0 \qquad (7.11)$$

By using (7.4) in (7.11), the latter is written as follows:

$$N_{cr,z} \cdot c^2 \cdot \overline{\theta} - N \cdot i_p^2 \cdot \overline{\theta} = N \cdot i_p^2 \cdot \overline{\theta}_0 \qquad (7.12)$$

The two equations (6.13) and (7.12) are not couple, representing the behaviour of a free column, i.e. one that is not laterally supported between end supports. In the TF buckling case, $\overline{v}$ and $\overline{\theta}$ are geometrically coupled as follows, see Fig 7-1 and Fig 7-4 for geometrical reference:

$$\overline{v} = d \cdot \overline{\theta} \quad \text{and} \quad \overline{v}_0 = d \cdot \overline{\theta}_0 \tag{7.13}$$

The relationships in (7.13) can be used in (6.13); By multiplying the resulting equation by d and summing the resulting term to (7.12), the TFB equilibrium equation in terms of the warping moment about the location of the lateral support is obtained:

$$N_{cr,z} \cdot \left(c^2 + d^2\right) \cdot \overline{\theta} - N \cdot \left(i_p^2 + d^2\right) \cdot \overline{\theta} = N \cdot \left(i_p^2 + d^2\right) \cdot \overline{\theta}_0 \tag{7.14}$$

or, through division by $(i_p{}^2 + d^2)$

$$N_{cr,z} \cdot \frac{\left(c^2 + d^2\right)}{\left(i_p^2 + d^2\right)} \cdot \overline{\theta} - N \cdot \overline{\theta} = N \cdot \overline{\theta}_0 \tag{7.15}$$

The first term in equation (7.15) is identical to the TFB bifurcation load $N_{cr,TF}$, see (7.1). Thus, we obtain the following simple expression for the rotation amplitude $\overline{\theta}$, which contains the second-order amplification deformation amplification factor:

$$\overline{\theta} = \overline{\theta}_0 \cdot \frac{N}{N_{cr,TF} - N} \tag{7.16}$$

This is conceptually identical to the relationship (6.16) in chapter 6, valid for LT buckling. Accordingly, the following expressions can again be used to determine the second order internal forces (out-of-plane bending moment M_z and warping moment M_ω) as a function of the occurring deformations:

$$M_z = EI_z \cdot \frac{\pi^2}{L^2} \cdot \overline{v} \tag{7.17}$$

$$M_\omega = EI_\omega \cdot \frac{\pi^2}{L^2} \cdot \overline{\theta} \tag{7.18}$$

By using (7.16) and (7.13) in (3.7) and (7.18)we obtain:

$$M_z = N_{cr,z} \cdot \overline{\theta}_0 \cdot d \cdot \frac{N}{N_{cr,TF} - N} \tag{7.19}$$

$$M_\omega = N_{cr,z} \cdot \frac{I_\omega}{I_z} \cdot \overline{\theta}_0 \cdot \frac{N}{N_{cr,TF} - N} \tag{7.20}$$

M_z and M_ω can also be expressed in terms of the imperfection amplitude $\overline{e}_0$ by considering the following geometrical relationship:

$$\overline{\theta}_0 = \frac{\overline{e}_0}{d + h/2} \tag{7.21}$$

The maximum stress equation can now be written for the outermost fibre of the compressed flange and set equal to the yield stress in a first-yield failure criterion:

$$\frac{N}{A} + \frac{M_z}{W_z} + \frac{M_\omega}{I_\omega} \cdot \omega_{max} = \frac{N}{A} + N_{cr,z} \cdot \frac{\overline{e}_0}{d + h/2} \cdot \left[\frac{d}{W_z} + \frac{\omega_{max}}{\cancel{I_\omega}} \cdot \frac{\cancel{I_\omega}}{I_z} \right] \cdot \frac{N}{N_{cr,TF} - N} = f_y \tag{7.22}$$

In the present case of a double-symmetric I cross-section, the following relationships hold:

$$W_z = \frac{I_z}{b/2} \quad ; \quad \omega_{max} = \frac{h \cdot b}{4} = (b/2) \cdot (h/2) \tag{7.23}$$

Resulting in the following stress equation:

$$\frac{N}{A} + N_{cr,z} \cdot \frac{\overline{e}_0}{W_z} \cdot \frac{\cancel{d + h/2}}{\cancel{d + h/2}} \cdot \frac{N}{N_{cr,TF} - N} = f_y \tag{7.24}$$

In order to obtain a dimensionless equation, expression (7.24) must be divided by the yield stress f_y. Furthermore, the second term on the left side can be expanded with A/A:

$$\frac{N}{A \cdot f_y} + \frac{N_{cr,z}}{A \cdot f_y} \cdot \frac{A \cdot \overline{e}_0}{W_z} \cdot \frac{N}{N_{cr,TF} - N} = 1.0 \tag{7.25}$$

The dimensionless slendernesses and buckling reduction factors can now be introduced:

$$\chi_{TF} = \frac{N}{A \cdot f_y} \quad ; \quad \overline{\lambda}_z = \sqrt{\frac{A \cdot f_y}{N_{cr,z}}} \quad ; \quad \overline{\lambda}_{TF} = \sqrt{\frac{A \cdot f_y}{N_{cr,TF}}} \tag{7.26}$$

Using the expressions (7.26) in (7.25) and simplifying finally leads to the following equation:

$$\chi_{TF} + \frac{A \cdot \overline{e}_0}{W_z} \cdot \frac{\overline{\lambda}_{TF}^2}{\overline{\lambda}_z^2} \cdot \frac{\chi_{TF}}{1 - \chi_{TF} \cdot \overline{\lambda}_{TF}^2} = 1.0 \tag{7.27}$$

With the exception of the index of the buckling reduction factor χ and the slenderness $\overline{\lambda}$, this equation is identical to equation (6.28) of the LT buckling case. Accordingly, by substituting

$$\eta^* = \frac{A \cdot \overline{e}_0}{W_z} \cdot \frac{\overline{\lambda}_{TF}^2}{\overline{\lambda}_z^2} \tag{7.28}$$

we obtain

$$\chi_{TF} + \eta^* \cdot \frac{\chi_{TF}}{1 - \chi_{TF} \cdot \overline{\lambda}_{TF}^2} = 1.0 \tag{7.29}$$

This equation is identical to the Ayrton-Perry formula (5.2) of chapter 5 and can be solved accordingly:

$$\chi_{TF} = \frac{1}{\Phi_{TF} + \sqrt{\Phi_{TF}^2 - \overline{\lambda}_{TF}^2}} \leq 1.0 \tag{7.30}$$

with

$$\Phi_{TF} = \frac{1}{2} \cdot \left(1 + \eta * + \overline{\lambda}_{TF}^2\right) \tag{7.31}$$

As a remark concluding the derivation, it can be stated that it again was shown to be possible to develop a specific Ayrton-Perry buckling formulation for the studied global member buckling case. The resulting formulation is –remarkably- qualitatively identical to the one developed for LT buckling: again the term $A \cdot \overline{e}_0 / W_z$ is present, as well as a stiffness-related modifier of the form $\overline{\lambda}_S^2 / \overline{\lambda}_z^2$, with the "case specific" slenderness $\overline{\lambda}_S$ being equal to $\overline{\lambda}_{TF}$ in the TFB case.

7.4.2. Representation

Prior to the calibration the newly-developed formulation to realistic GMNIA buckling curves, it is interesting to study the shape of the elastic buckling curves, i.e. the curves that result from equation (6.30) with (6.31) and $\eta *$ calculated as given by (7.28), using the elastic values of A and W_z and an amplitude of the initial, sinusoidal geometric imperfection of $\overline{e}_0 = L/1000$. This is done for the four sections that were already studied in Fig 7-4, i.e. the HEM 400, IPE 240, IPE 500 and HEAA 1000 section. The resulting analytical, elastic Ayrton-Perry buckling curves (A-P_elast) are plotted in Fig 7-13.
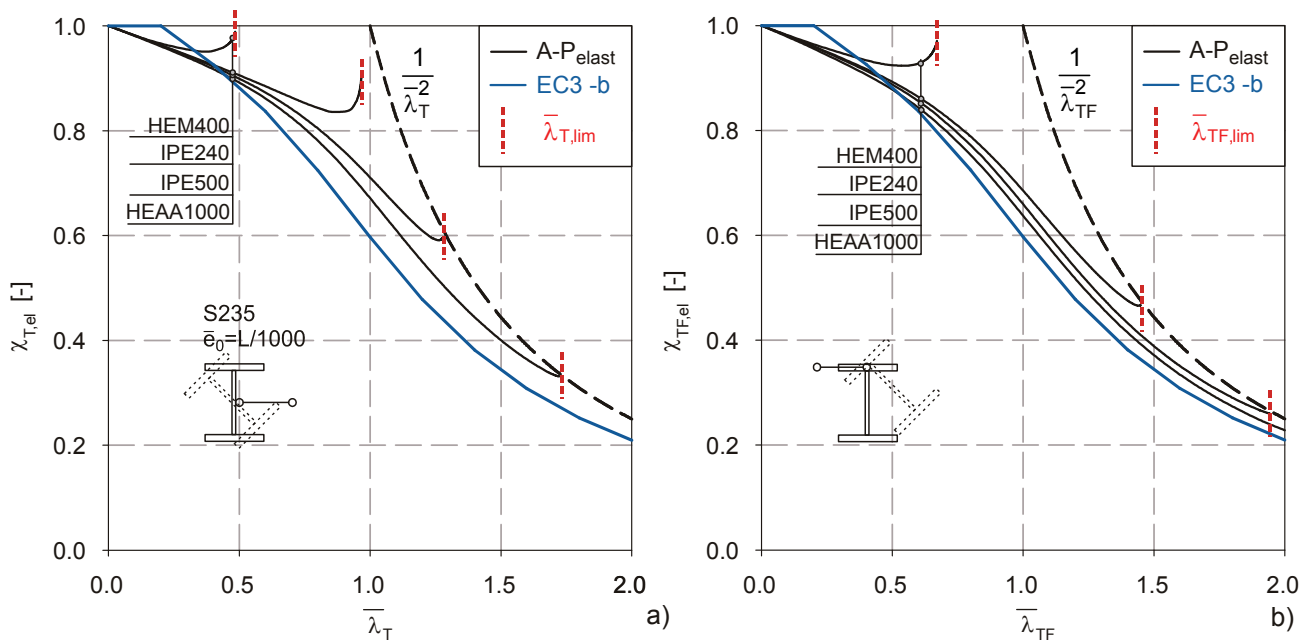
Fig 7-13 *Analytical buckling curves according to the purely elastic, second order derivation.*

Quite generally, the figure illustrates that the resulting, elastic buckling curves already lie significantly higher than the Eurocode buckling curve that would apply for these sections, with the exception of the low slenderness range, where the missing plateau in the purely elastic formulation leads to an immediate drop in the predicted load carrying capacity. Then, it is clear that the torsional rigidity of the single cross-sections is (qualitatively) well represented by the formulation, which distinguishes between different sections primarily due to the very different ratio $\bar{\lambda}_{TF}^2 / \bar{\lambda}_z^2$ for every section: the torsionally stiff HEM 400 "automatically" has a higher buckling reduction curve than the more slender IPE and HEAA sections. As far as the influence of the lateral support eccentricity d is concerned, the differences between Fig 7-13a and b indicate that the drop in load-carrying capacity associated with a larger value of d is also well represented by the developed formulation.

Furthermore, the formulation features the characteristic "limit slenderness" $\bar{\lambda}_{TF,lim}$. As a matter of fact, the perhaps most surprising aspect of the developed buckling formulation is the fact that the curves have a tendency of pointing *upwards* after a certain value of $\bar{\lambda}_{TF}$ is passed, see especially the lines for IPE 240 and HEM 400 in Fig 7-13a and b. The lines in the plot are not entirely drawn out, but can be shown to converge to 1.0 at $\bar{\lambda}_{TF,lim}$ when the limit slenderness is smaller than 1.0, and to the Euler buckling load corresponding to $1/\bar{\lambda}_{TF,lim}^2$ if the limit slenderness is larger than 1.0. Mathematically, this is caused by the term $\bar{\lambda}_{TF}^2 / \bar{\lambda}_z^2$, which tends towards zero at infinite length due to the finite value of $\bar{\lambda}_{TF}^2$ at infinite length. Thus, at infinite length equation (7.28) is zero, making the buckling reduction factor χ_{TF} according to (6.30) reach the solution that is valid for a perfect column ($\bar{e}_0 = 0$).

While this tendency is clearly illogical, one has to bear in mind that the parameter $\bar{\lambda}_{TF}$ is by no means linearly proportional to the length of the member; indeed, it can be shown that the point at which the buckling lines start pointing upward corresponds to extreme, unrealistic lengths of the member. This is absolutely confirmed in the comparisons shown in section 7.6.

7.5. Calibration

Having successfully determined a specific Ayrton-Perry formulation for the studied global member buckling case, we can now proceed to the all-important task of calibrating the imperfection definition to accurately describe the behaviour of the *model beam* with nominal geometry and fixed imperfection amplitudes, as has been done by Maquoi and Rondal (1978, 1979) for the column buckling curves and correspondingly in chapter 6 of this thesis for LT buckling.

Thereby, and as done in chapter 6, the first step is again to re-plot the results of numerical GMNIA buckling curves in terms of the "un-modified" generalized Ayrton-Perry imperfection η* that – when used in the Ayrton-Perry formula-, would *exactly* match the obtained numerical results. This numerical value of η^*_{num} can be calculated from the numerically obtained values of $\chi_{TF,num}$ as follows, also see chapter 5 and 6.

$$\eta*_{num} = \left(\frac{1}{\chi_{TF,num}} - 1 \right) \cdot \left(1 - \chi_{TF,num} \cdot \bar{\lambda}_{TF}^{2} \right) \tag{7.32}$$

In Fig 7-14, this equation is evaluated for some numerical TB buckling curves for hot-rolled I-sections with h/b>1.2, and compared to the current Eurocode rule, where $\eta*$ is expressed by term $\eta* = \alpha_T \cdot (\bar{\lambda}_T - 0.2)$ and $\alpha_T = \alpha_z = 0.34$.
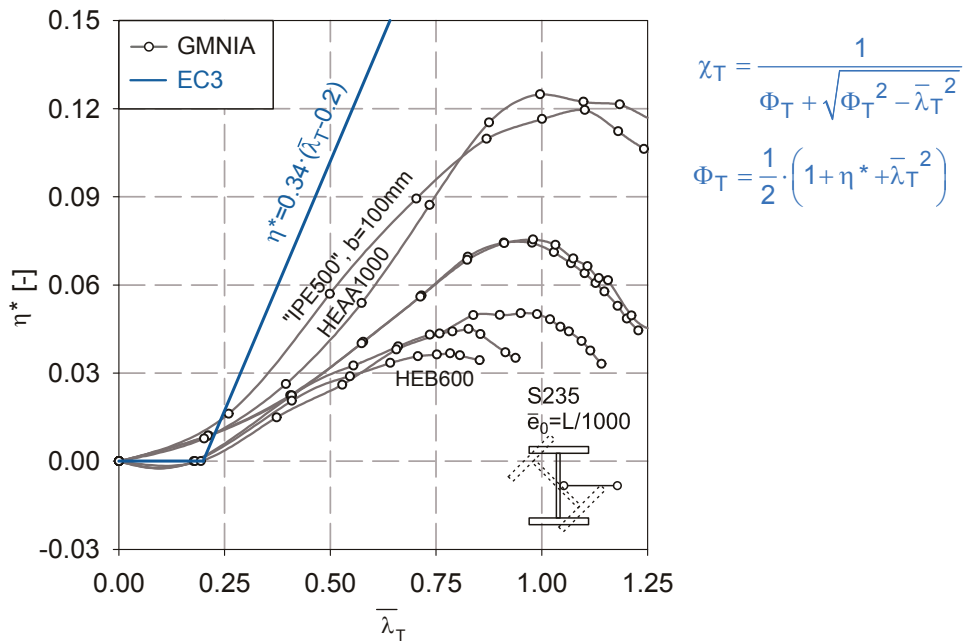
Fig 7-14 *Numerical values of $\eta*$ for a representative selection of cross-sections and the torsional buckling case TB; comparison with the current Eurocode 3 formulation for $\eta*$.*

Two aspects are illustrated in the plot in Fig 7-14:

-   The Eurocode rule is always "conservative" for TB of hot-rolled sections; in the chosen representation, a rule is safe when the numerical GMNIA curves lie below the chosen design formulation.
-   The numerical curves appear to diverge widely, i.e. to depend heavily on the section shape both as far as slope and deviation from a straight line is concerned. Quite generally, the non-linear relationship between $\bar{\lambda}_T$ and the member length appears to cause the numerical curves to bend upwards in the all-important (for accuracy) low slenderness range. This makes a linear function of $\bar{\lambda}_T$ a rather bad descriptor of the behaviour of many sections.

As was done in chapter 5 for flexural and 6 for LT buckling, it can again be shown that the (geometrical) imperfection assumption underlying the numerical curves, i.e. a length-proportional imperfection amplitude of $\bar{e}_0 = L/1000$, is also very dominant in the equivalent, correct generalized imperfection η of the Ayrton-Perry formulation, i.e. the term that comes to replace the purely-elastic expression $A \cdot \bar{e}_0 / W_z$ in the specific Ayrton-Perry derivation. The equivalent numerical value

of η that would exactly describe the GMNIA curves can be calculated by the following amended form of (7.32):

$$\eta_{num} = \frac{\bar{\lambda}_z^2}{\bar{\lambda}_{TF}^2} \cdot \eta*_{num} = \frac{\bar{\lambda}_z^2}{\bar{\lambda}_{TF}^2} \cdot \left(\frac{1}{\chi_{TF,num}} - 1 \right) \cdot \left(1 - \chi_{TF,num} \cdot \bar{\lambda}_{TF}^2 \right) \tag{7.33}$$

Value of η_{num} for different sections and positions of the lateral restraints are plotted over the weak-axis flexural buckling (FBzz) slenderness $\bar{\lambda}_z$ in Fig 7-15, and compared to the value of $\eta = 0.34 \cdot (\bar{\lambda}_z - 0.2)$ that is used by the Eurocode for FBzz.
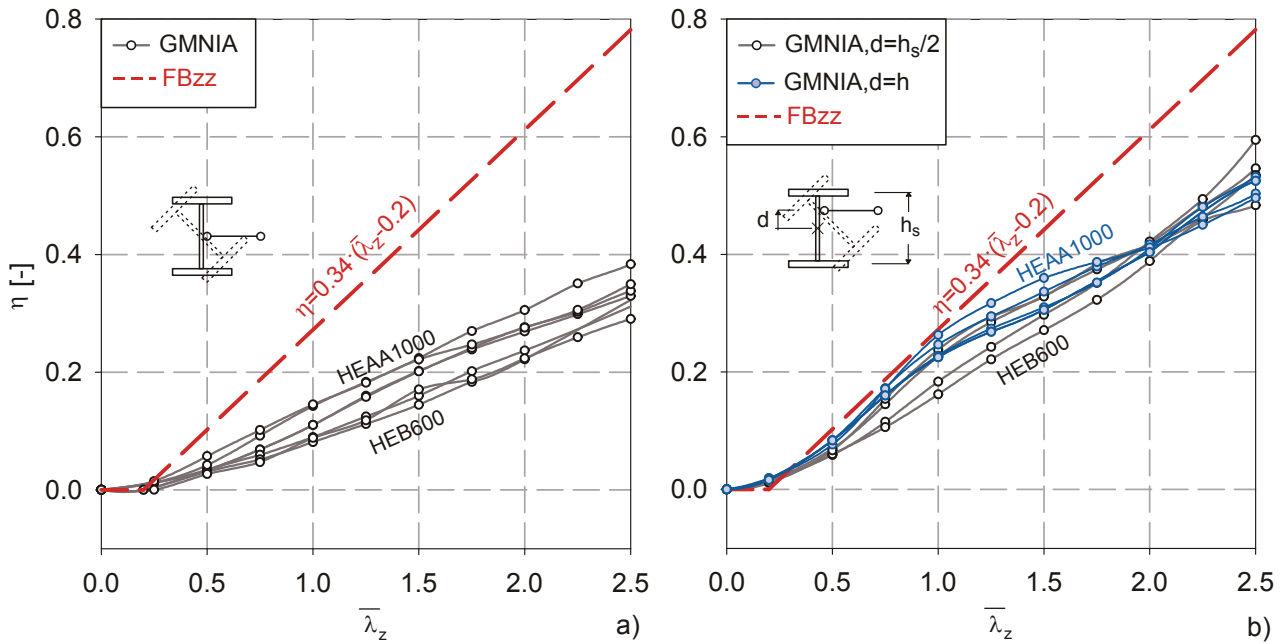
Fig 7-15 *Numerical values of η for different support eccentricities d, comparison with the weak-axis flexural buckling case.*

The figure shows that the imperfections η_{num} that would perfectly describe the GMNIA buckling curves for TB indeed increase almost linearly when plotted over $\bar{\lambda}_z$; this is also true for TFB cases with $d=h_s/2$ and –at least in the low slenderness range- for $d=h$. More importantly, the divergence from a straight line occurs at higher slenderness, where the significance of the imperfection amplitude decreases, and present themselves as a bend downward, i.e. towards safer results. Therefore, it appears safe to say that a calibration formulation for the generalized imperfection that is a linear function of $\bar{\lambda}_z$, i.e. an expression of the type $\eta = \alpha_{TF} \cdot (\bar{\lambda}_z - \bar{\lambda}_0)$, will again yield good results, *provided that the value of the generalized imperfection amplitude α_{TF} is correctly calibrated.* As is shown in Fig 7-15, there are clearly effects in the realistic, large-displacement GMNIA calculation with residual stresses and plasticity that are not sufficiently well covered by the Ayrton-Perry formulation itself; otherwise, the GMNIA curves for η_{num} would all be in the same scatter-band without further modification. The TB case, for example, appears to require much lower

values of η than the TFB cases with higher values of d. This must be included in the calibration of α_{TF} to obtain accurate results.

Considering the slopes of the GMNIA curves in Fig 7-15, as well as the general behaviour of columns failing in TB and TFB described in section 7.3, it appears that an encompassing and rational calibration of α_{TF} must fulfil the following conditions:

- It must account for the fact that torsional-flexural buckling approaches the behaviour of weak-axis flexural buckling when the eccentricity of the lateral supports becomes very large.
- It must also take into account the differences between the single sections, including the differences in residual stresses assumed to exist between sections with h/b≤1.2 and >1.2, without the need for many additional cross-sectional classification criteria.

The first point requires the factor α_{TF} to be formulated in a way that approaches (but does not exceed) the constant value that applies for FBzz, that is e.g. 0.34 for hot-rolled I-sections sections with h/b>1.2. The second point requires the selection of a sensible classification parameter, which best describes the differences between one section and the other.

As has been shown in Fig 7-10, the h/b ratio clearly is not an encompassing classification criterion, since sections with small h/b are not necessarily "stocky" in the context of TFB. A much better parameter is found in the most characteristic feature of the TFB mode: the limit value of the slenderness $\bar{\lambda}_{TF,lim}$, see equation (7.7). This quantity very well reflects the torsional properties of a section, and is clearly correlated with the shape of a buckling curve, since it expresses its maximum extent in the $\chi_{TF}/\bar{\lambda}_{TF}$ space.

Based on the above considerations, and to a calibration to the obtained GMNIA TFB curves, the following formulation for the generalized imperfection η and its amplitude α_{TF} is proposed:

$$\eta = \alpha_{TF} \cdot \left(\bar{\lambda}_z - 0.2 \right) \tag{7.34}$$

and
$$\alpha_{TF} = \alpha_z \cdot \sin\left(\arctan(\bar{\lambda}_{TF,lim} / 2) \right) \tag{7.35}$$

Expression (7.35) is plotted in Fig 7-16b. The characteristic asymptotic shape of the sin(arctan(α)) function is recognizable in the figure. The function is designed to converge towards the coefficient α_z applicable for weak-axis flexural buckling with increasing values of $\bar{\lambda}_{TF,lim}$, and to satisfactorily describe the numerical values of η_{num} for all studied sections and lateral support configurations.

The latter point is illustrated in Fig 7-16a, where numerical values of η_{num} (calculated by applying (7.33) to the GMNIA results obtained for 6 different sections and 5 locations of the lateral support) are "normalized" by a multiplication with the term $1/\sin\left(\arctan(\bar{\lambda}_{TF,lim} / 2) \right)$, and compared to the weak-axis FBzz function for $\eta = \alpha_z \cdot \left(\bar{\lambda}_z - 0.2 \right)$, with $\alpha_z = 0.34$ for the studied sections according to the Eurocode. When compared to Fig 7-15a and b, this representation illustrates that the chosen

function for α_{TF} is well able to "bring together" the different GMNIA curves for η_{num}. The essentially empirical, "rational" selection of the cross-sectional categorization factor $\sin\left(\arctan(\bar{\lambda}_{TF,lim}/2)\right)$ obviously cannot take all the effects into account that cause the differences between a simple first-yield second-order failure formulation and a large-displacement, elasto-plastic GMNIA calculation, so some differences between the function (7.35) and the GMNIA values remain. However, as will be shown in the next section, these differences in terms of η do not cause major discrepancies in terms of χ_T - χ_{TF}.
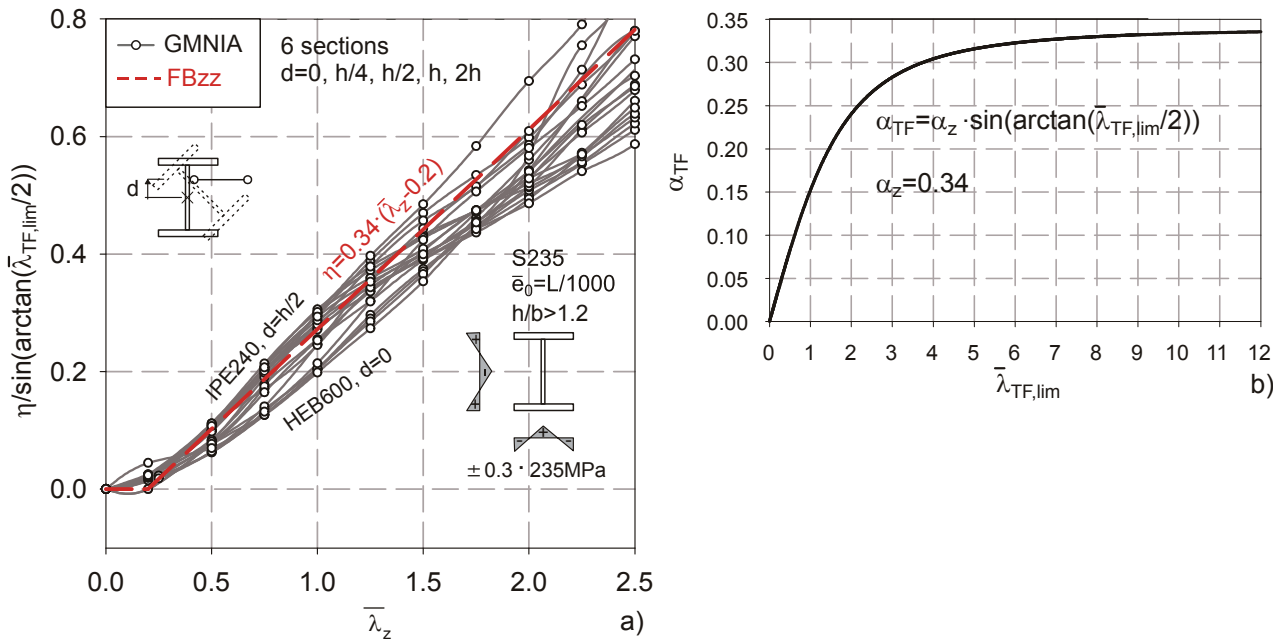
Fig 7-16 *Comparison of (7.35) with the GMNIA values of η_{num} for different sections and support conditions (a); representation of (7.35) for sections with h/b>1.2 (b).*

7.6. Comparison of Analytical and GMNIA curves

In this section, the analytical buckling curve expression developed in section 7.5, and calibrated in section 7.6, is compared to the numerical (GMNIA) TB and TFB buckling curves of section 7.3. This is done in order to illustrate the increase in accuracy afforded by the new formulation, as well as to discuss the implications for design that would follow from the application of the new formulation.

The comparison is first done for the same four hot-rolled sections that were already treated in Fig 7-4. In Fig 7-17, the GMNIA buckling curves for an HEM 400, IPE240, IPE 500 and HEAA 1000 section are compared to the new formulation (EQU) and to the applicable Eurocode 3 buckling curve b. The eccentricity of the lateral support is progressively increased from Fig 7-17a to Fig 7-17d, ranging from the purely torsion TB case (a) to a case with d=2h (d).

The figure shows that the differences between the analytical (EQU) and GMNIA buckling curves are rather small for all studied cases and over most ranges of slenderness $\overline{\lambda}_{TF}$. The proposed analytical formulation appears to be well able to account for the different shapes of the buckling curves, depending on section series and support eccentricity. Larger discrepancies appear only at slenderness values that approach the limit slenderness $\overline{\lambda}_{TF,lim}$. At these higher slenderness ratios, the tendency of the analytical curve to point upward to either the value of 1.0 (if $\overline{\lambda}_{TF,lim} < 1.0$) or to the bifurcation load $1/\overline{\lambda}_{TF,lim}^2$ was already pointed in section 7.4.2; the opposite tendency of the GMNIA for TFB ($d \neq 0$) curves to fall towards the FByy bifurcation load was also already emphasized.
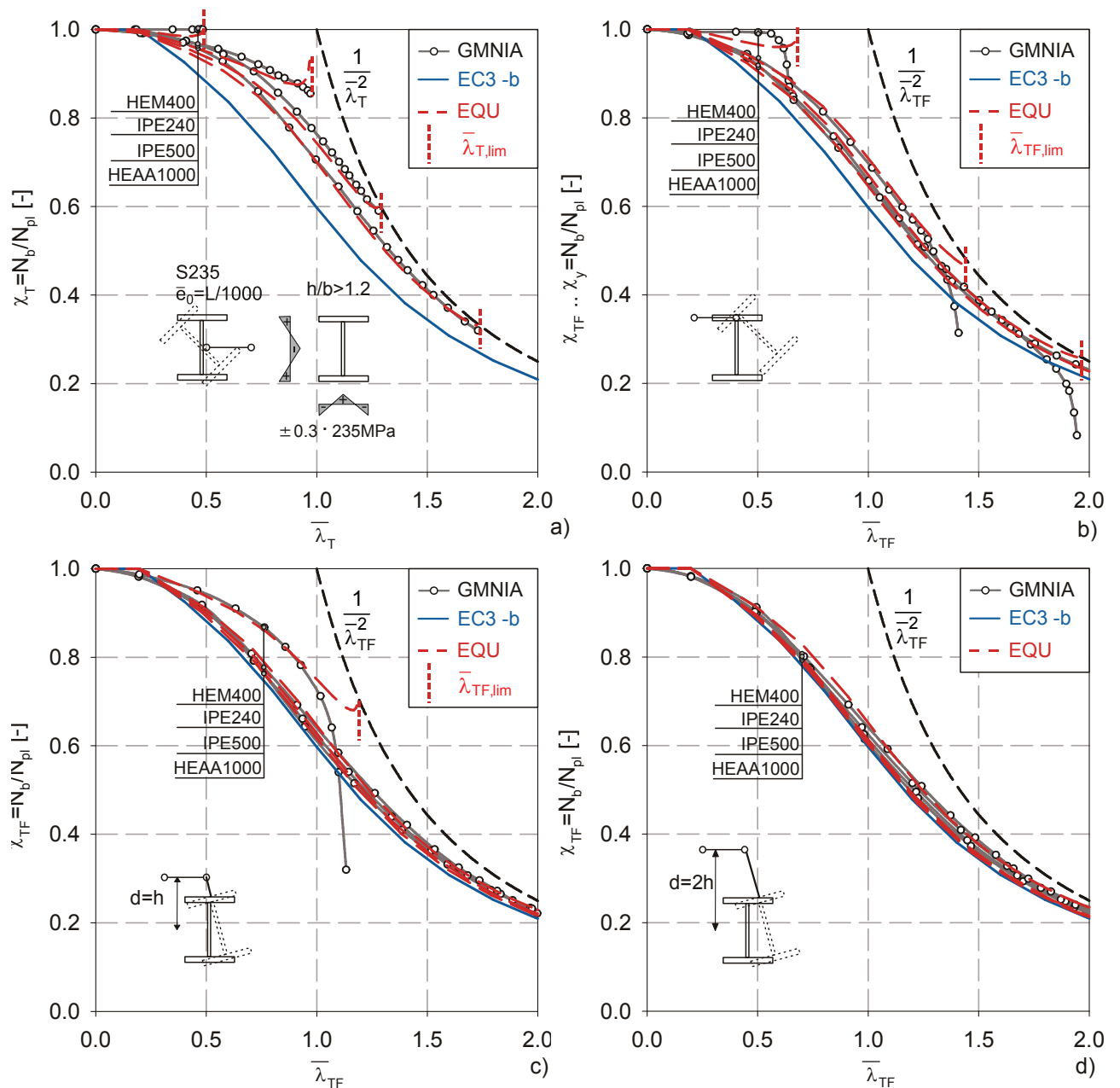
Fig 7-17 Analytical (EQU) TB and TFB curves compared with the Eurocode and numerical (GMNIA) curves.

Since the slenderness for $\bar{\lambda}_{TF}$ stands in a highly non-linear relationship to the member length, it is again helpful to plot the results of Fig 7-17 over the member length (and the strong-axis slenderness $\bar{\lambda}_y$). This is done in Fig 7-18 for the IPE 500 and IPE 240 sections. In these figures, the "EQU" lines representing the analytical buckling curve formulations also include the Eurocode buckling curve for strong-axis flexural buckling FByy, in order to indicate at what length or slenderness the FByy will become the most critical buckling mode in the proposed design procedure.
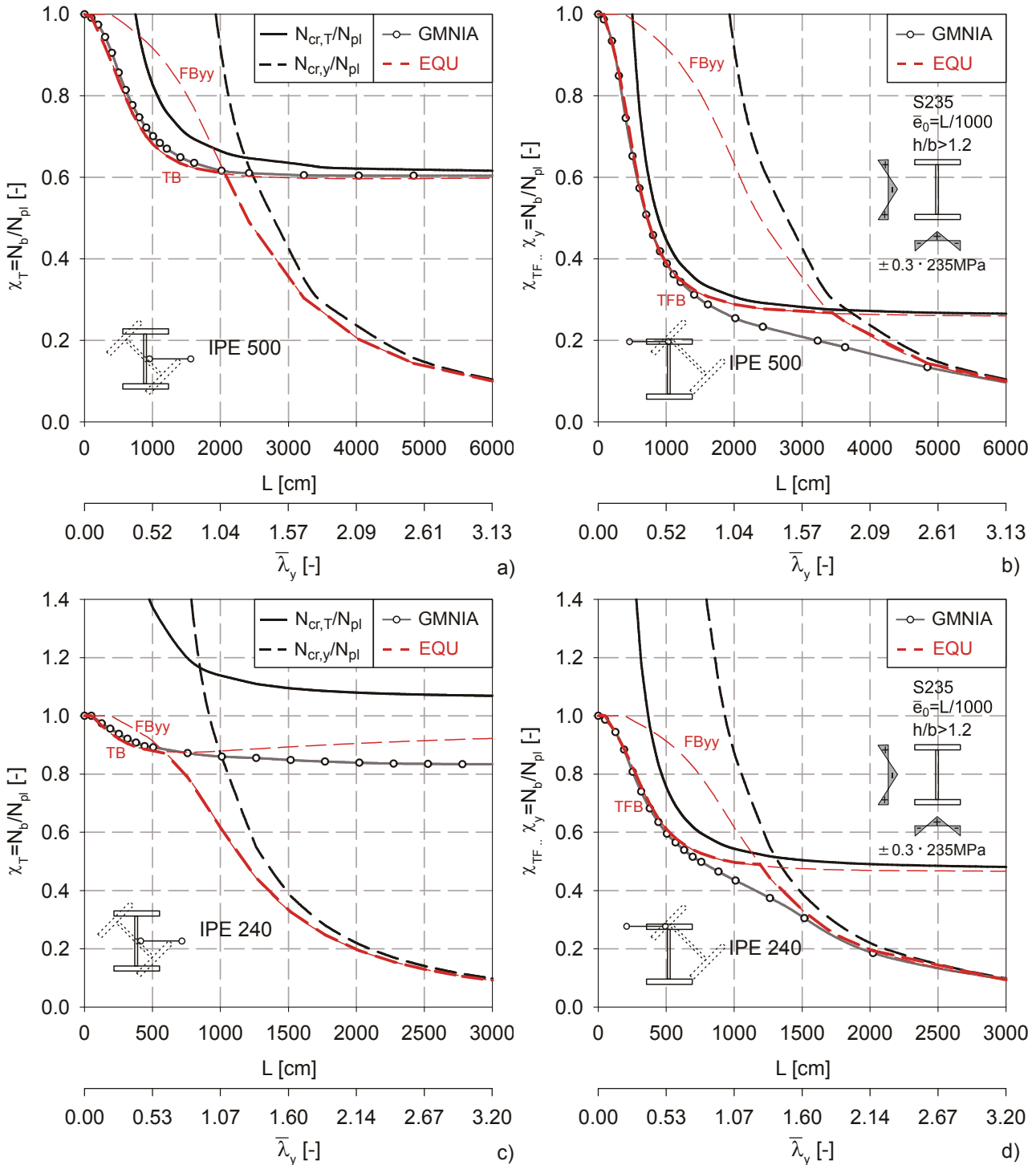
Fig 7-18 *Analytical formulations (EQU) for TB/TFB and FByy (=EC3 curve a) compared with GMNIA buckling curves, IPE 500 (a-b) and IPE 240 (c-d) section.*

The plots confirm the general tendencies shown in Fig 7-17, possibly showing even more clearly how precisely the proposed formulation is able to describe the TB and TFB buckling phenomenon in the (lower) range of length where the phenomenon is entirely independent of the FByy mode.

In the case of TB of the IPE 500 section (Fig 7-18a), the proposed formulation is only slightly "conservative" up the lengths of ca. 20m, when FByy becomes the prevalent buckling mode for the studied column. In the case of TFB with $d=h_s$ (Fig 7-18b), the proposed formulation is very accurate up to lengths of ca. 12m, after which the transitional behaviour between TFB and FByy becomes prevalent. The proposed formulation does not attempt to take this behaviour into account, and therefore yields results that are "unconservative" in the transitional range, with discrepancies that – in relative terms- are rather high (with over-estimations of strength by factors of up to 1.5). In practical applications, this might have to be kept in mind; however, the "unsafe" transitional range only starts at lengths (L/h~20, L/b~50) and buckling reduction factors that approach the lower limits of practical occurrence for the studied boundary condition.

Very similar findings are obtained for the TB and TFB case of the IPE 240 section (Fig 7-18c &d). Again, the TB case appears to be very well described by the proposed formulation. The FByy formula (EC3 buckling curve b) becomes dominant at lengths of approximately 6.0 m. The "upwards" tendency of the TB buckling formulation only occurs beyond this point, confirming that the buckling formulation is accurate throughout the realistic range of application. In the TFB case, the transitional behaviour sets in at lengths corresponding to L/h~22, and causes larger relative discrepancies for members with lengths between 8 and 13m; this is again at –or mostly beyond- the upper-most limit of applicability of this slender section as a laterally not fully restrained column.

For a typical heavy column section like an HEM 400, the results of the evaluation of the new design formula is plotted in Fig 7-19. In the TFB case in Fig 7-19a, this column is not affected by this specific buckling mode, and fails in strong-axis buckling only due to the (small) deformation component parallel to web, which initiates FByy buckling. The Eurocode 3 formula for FByy for this section is more critical throughout all ranges of length for this section, making the TFB mode irrelevant.

The HEM 400 section is affected by TFB only if the eccentricity of the lateral support exceeds half the member depth, see Fig 7-19b, where d=h. In this case, the proposed, new TFB buckling formulation is able to describe the column's behaviour very well up to lengths of ca. 15m, where the dominant failure mode switches to FByy both according to the design formulae (EC3 for FByy with buckling curve a) and the GMNIA calculations.
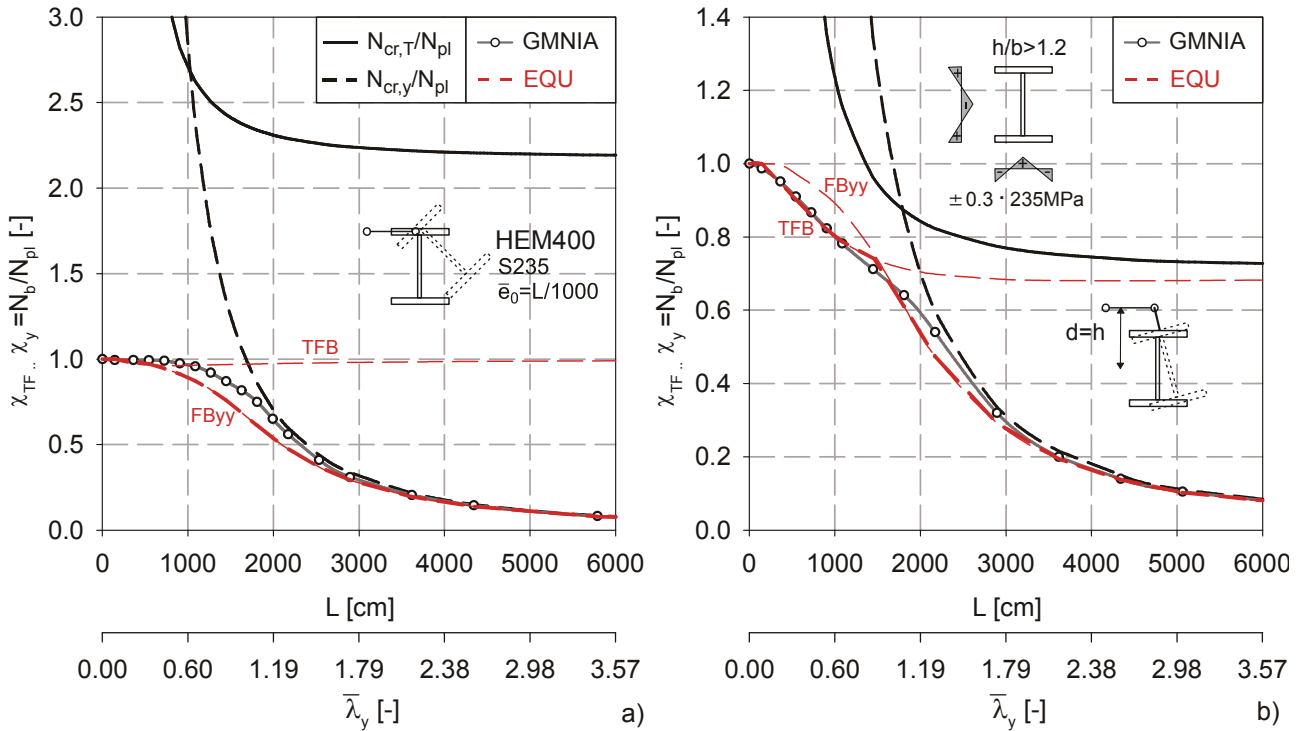
Fig 7-19 *Analytical formulations (EQU) for TFB and FByy (=EC3 curve b) compared with GMNIA buckling curves, HEM 400 section.*

In a final figure, the accuracy of the proposed formulation is investigated for the HEA 360 section, where h/b=1.167<1.2 and the residual stresses are customarily assumed to have higher amplitudes of $0.5 \cdot f_{y,S235}$=117.5 N/mm². As was shown in Fig 7-12, the GMNIA curves for this case again approach the Eurocode buckling curve for weak-axis flexural buckling FBzz with increasing lateral support eccentricity d. If equation (7.35) is to be used appropriately in the proposed Ayrton-Perry formulation, the value of α_z must be set equal to 0.49 in this case. The resulting analytical formulation (EQU) is compared to the GMNIA curves for the HEA 360 in Fig 7-20a in terms of χ_{TF} plotted over $\overline{\lambda}_{TF}$. Again, the figure shows the generally quite good accuracy of the proposed formulation. Quite clearly, the proposed interpolation expression (7.35) between a zero-lateral and a pure lateral weak-axis buckling behaviour is quite well able to describe an arbitrary section's TFB buckling loads. In Fig 7-20b, the results for the specific case of $d=h_s/2$ are plotted over the member length. This specific configuration was chosen for illustration because it's with this positioning of the lateral support that the largest transitional effects between TFB and FByy are observed within the (upper) limits of practical application. As is shown in the figure, the Eurocode FByy buckling curve (curve b for this section) becomes relevant before the transitional behaviour sets in at lengths of ca. 12.5m.
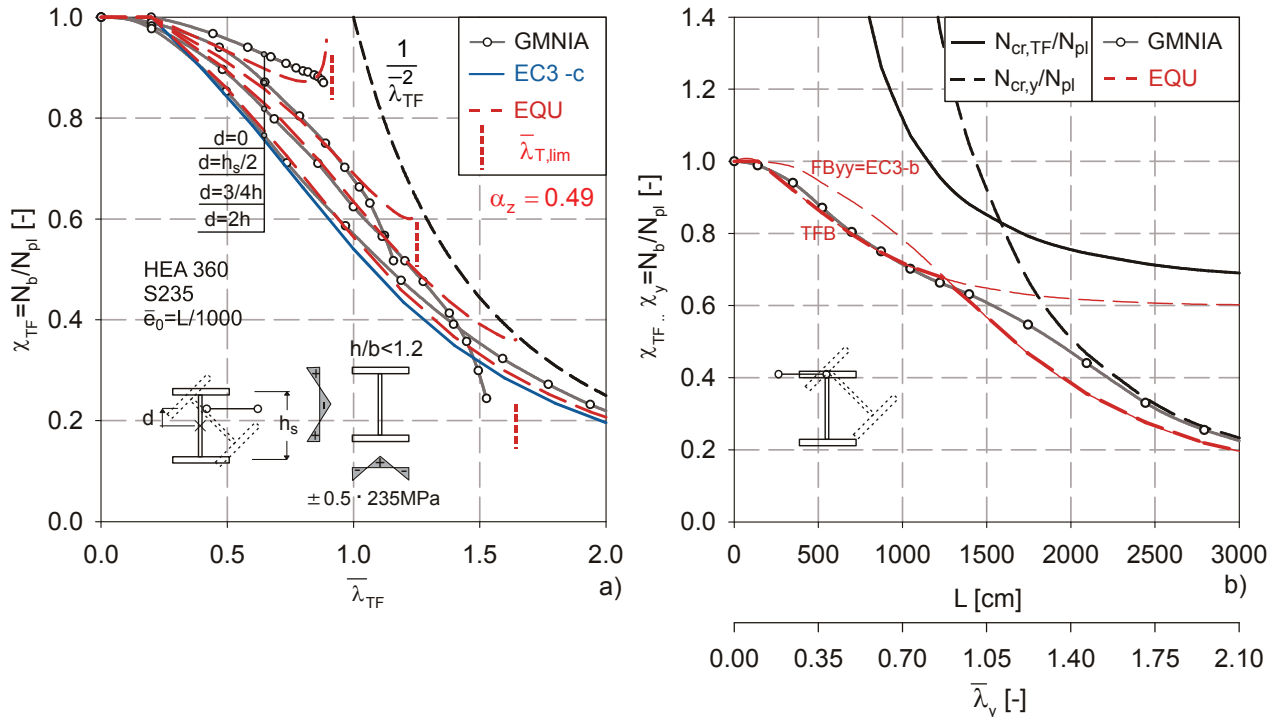
Fig 7-20 *Proposed analytical and GMNIA numerical buckling curves for an HEM 400.*

7.7. Conclusions

In this chapter, the less well-known column buckling mode of torsional- and torsional-flexural buckling (TB / TFB) of laterally restrained I-& H-sections was studied by means of numerical calculations, and compared to a specifically developed and calibrated Ayrton-Perry formulation. The practical relevance of this buckling mode was pointed out and demonstrated by comparing the buckling reduction factors for the TFB mode to the two more commonly treated flexural buckling modes about the main axes of inertia. The developed Ayrton-Perry formulation was shown to represent a huge increase in the accuracy of description of the real behaviour of columns in TFB. The proposed design formulation for this mode, and the corresponding cross-sectional classification for this mode, is therefore summarized in the following table:

Buckling reduction factor χ_{TF}	$\chi_{TF} = \dfrac{1}{\Phi_{TF} + \sqrt{\Phi_{TF}^2 - \overline{\lambda}_{TF}^2}} \leq 1.0$ ... with $\Phi_{TF} = \dfrac{1}{2} \cdot \left(1 + \eta \cdot \dfrac{\overline{\lambda}_{TF}^2}{\overline{\lambda}_z^2} + \overline{\lambda}_{TF}^2 \right)$
Generalized imperfection η	$\eta = \alpha_{TF} \cdot \left(\overline{\lambda}_z - 0.2 \right)$
Generalized imperfection amplitude α_{TF}	$\alpha_{TF} = \alpha_z \cdot \sin\left(\arctan(\overline{\lambda}_{TF,lim} / 2) \right);$ $\alpha_z = \begin{cases} 0.34 .... \text{hot} - \text{rolled I- \& H-sections, h/b>1.2} \\ 0.49 .... \text{hot} - \text{rolled (h/b} \leq 1.2) \ \& \text{ welded I- \& H-sections} \end{cases}$

Table 7-2 *Summary of the design proposal of this chapter*

225

8

Summary of Design Proposals – "Code Clauses"

8.1. Scope

The new design formulations proposed in this thesis for the description of buckling curves for lateral-torsional (LTB) and torsional/torsional flexural buckling (TB/TFB) are summarized in the following pages in a form comparable to "code clauses". Of course, this is not intended to be a complete representation; it is however intended as a conceptual draft for a possible codification.

8.2. "Code clauses"

Design of columns and beams with hot-rolled or welded I- & H-sections against:

(1) The buckling resistance $R_{b,s}$ of hot-rolled or welded, compact or semi-compact I- & H sections, used as columns or beams may be assessed by applying the following formula:

$$R_{b,S} = \frac{R_{ult,k,S}}{\gamma_{M1}} \cdot \chi_S \qquad (8.1)$$

where

$$\chi_S = \frac{\varphi}{\Phi_S + \sqrt{\Phi_S^2 - \varphi \cdot \overline{\lambda}_S^2}} \leq 1.0 \qquad (8.2)$$

and

$$\Phi_S = \frac{1}{2}\left[1 + \varphi \cdot \left(\alpha_{0,S} \cdot \alpha_S \cdot \left(\overline{\lambda}_{imp} - 0.2\right) + \overline{\lambda}_S^2\right)\right] \qquad (8.3)$$

$R_{ult,k,S}$... characteristic plastic section capacity. The following values shall be used:

For columns under axial forces (FB, TB/TFB): $R_{ult,k,S} = N_{R,k} = A \cdot f_y$

For beams in bending (LT-buckling): $R_{ult,k,S} = M_{R,k} = W_{y,pl} \cdot f_y$

χ_S ..... case-specific buckling reduction factor, see Table 8-1

$\overline{\lambda}_S$ ..... normalized slenderness for the specific buckling case, see Table 8-1

$\overline{\lambda}_{e_0}$ ..... slenderness used for the definition of the generalized imperfection, see Table 8-1

α_S .... generalized imperfection amplitude factor of the specific case, see Table 8-1

$\alpha_{0,S}$ ... case-specific second-order stiffness term, see Table 8-2

φ .... load diagram factor to account for variable loads, see Table 8-2

BUCKLING MODE	χ_S	$\bar{\lambda}_S$	$\bar{\lambda}_{e_0}$	α_S (index)	Values of α_S		
					Hot-rolled $h/b > 1.2$	Hot-rolled $h/b \leq 1.2$	Welded
FB_{yy}	χ_y	$\bar{\lambda}_y$	$\bar{\lambda}_y$	α_y	0.21	0.34	0.34
FB_{zz}	χ_z	$\bar{\lambda}_z$	$\bar{\lambda}_z$	α_z	0.34	0.49	0.49
TB/ TFB	χ_{TF}	$\bar{\lambda}_{TF}$	$\bar{\lambda}_z$	α_{TF}	$0.34 \cdot \beta_{TF}$	$0.49 \cdot \beta_{TF}$	$0.49 \cdot \beta_{TF}$
LTB	χ_{LT}	$\bar{\lambda}_{LT}$	$\bar{\lambda}_z$	α_{LT}	$0.12 \cdot \beta_{LT} \leq 0.34$	$0.16 \cdot \beta_{LT} \leq 0.49$	$0.21 \cdot \beta_{LT} \leq 0.64$

Table 8-1 *Generalized imperfection amplitude α_S for hot-rolled and welded I- & H-sections.*

Note 1: the additional coefficients used in Table 8-1 are defined as follows:

$$\beta_{LT} = \sqrt{W_{y,el} / W_{z,el}}$$

$$\beta_{TF} = \sin\left(\arctan(\bar{\lambda}_{TF,lim} / 2)\right)$$

$$\bar{\lambda}_{TF,lim} = \sqrt{\frac{A \cdot f_y \cdot \left(i_p^2 + d^2\right)}{GI_T}}$$

d: eccentricity of lateral support;

$W_{y,el}$ ... $W_{z,el}$: elastic section moduli

Note 2: The numerical values of α_S in Table 8-1 are based on geometrically and materially non-linear numerical (FEM) calculations that considered nominal cross-sectional parameters and imperfection assumptions as shown in Fig 8-1.
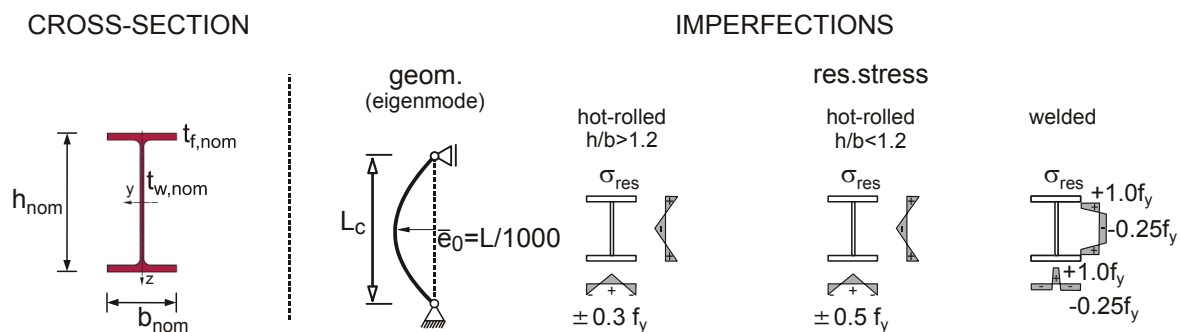
Fig 8-1 *Assumptions used to derive the values of α_S in Table 8-1.*

	BUCKLING MODE	$\alpha_{0,S}$	LOAD CASE	φ
columns	FB$_{yy}$	1.00	N=const.	1.00
columns	FB$_{zz}$	1.00		
columns	TB/TFB	$\left(\dfrac{\overline{\lambda}_{TF}}{\overline{\lambda}_z}\right)^2$		
beams	LTB	$\left(\dfrac{\overline{\lambda}_{LT}}{\overline{\lambda}_z}\right)^2$	M=const.	1.00
beams				0.95
beams				0.90
beams			M — ψ·M	$1.25 - 0.1\cdot\psi - 0.15\cdot\psi^2$

Table 8-2 *Stiffness factor $\alpha_{0,S}$ and bending diagram factor φ*

(2)   The slenderness for single buckling modes may be calculated as follows:

For columns failing in strong-axis flexural buckling FB$_{yy}$: $\overline{\lambda}_y = \sqrt{\dfrac{A\cdot f_y}{N_{cr,y}}}$

For columns failing in weak-axis flexural buckling FB$_{zz}$: $\overline{\lambda}_z = \sqrt{\dfrac{A\cdot f_y}{N_{cr,z}}}$

For columns failing in torsional or torsional-flexural buckling TFB: $\overline{\lambda}_{TF} = \sqrt{\dfrac{A\cdot f_y}{N_{cr,TF}}}$

For beams failing in lateral-torsional buckling LTB: $\overline{\lambda}_{LT} = \sqrt{\dfrac{W_{y,pl}\cdot f_y}{M_{cr}}}$

(3)   In the case of semi-compact class 3 sections, the following condition shall be additionally checked:

$$R_{b,S} = \frac{M_{R,k}}{\gamma_{M1}}\cdot\chi_{LT} \le M_{Rd,class3} \qquad (8.4)$$

Where $M_{Rd,class3}$ is the elastic cross-sectional moment capacity $W_{y,el}\cdot f_y / \gamma_{M1}$

8.3. Comments

The above clauses allow for an accurate determination of the buckling resistance of columns and beams with hot-rolled, compact and semi-compact sections under either constant axial force (flexural, torsional and torsional-flexural buckling) or a variety of bending moment diagrams (lateral-torsional buckling). In terms of practicality, the proposed formulation is thereby absolutely comparable to current formulations found in the Eurocode.

The main differences between the current Eurocode formulation and the new proposal are the following:

i. In the proposal, the generalized imperfection η is defined in terms of a linear relationship between the imperfection and the normalized slenderness for strong- or weak-axis flexural buckling $\bar{\lambda}_y$ or $\bar{\lambda}_z$, -respectively the length-, of the member. In the present Eurocode formulation, η increases linearly with the normalized slenderness $\bar{\lambda}_S$ of the specific buckling case, which is not necessarily proportional to the length. In the case of torsional, torsional-flexural and lateral-torsional buckling, this has been shown to cause problems for the calibration in the specific chapters 5 to 7, due to the fact that the GMNIA numerical curves onto which the analytical curve was calibrated are also largely dominated by the (length-proportional) assumption for the geometric imperfection $\bar{e}_0 = L/1000$; also see section 5.3.2

ii. The consistent definition of the generalized imperfection η as a function of $\bar{\lambda}_z$ allows for a straightforward inclusion of a transitional behaviour between the specific (lateral) buckling case and the limit case of weak-axis flexural buckling; this is observed in Table 8-1 by the delimitation of the value of α_S by the value of α_z valid for weak-axis flexural buckling FB_{zz}. This delimitation is implicit in the formulation of α_{TF}, which "automatically" converges towards the applicable value of α_z, and explicit in the definition of α_{LT}, which needs a specific "check" to see whether or not it has exceeded α_z. The implications of this delimitation have been discussed in detail in section 6.8.6 and 7.5.

iii. The formulation for χ_S, respectively Φ_S, contains a specific stiffness correction term $\alpha_{0,S}$, which takes into account the characteristic sensitivity towards imperfections of the different studied buckling modes. This term stems from second-order, elastic derivations for the single specific cases, see chapters 6 and 7.

iv. Additionally, formulae (4.3) and (8.3) contain a factor φ to account for variable bending moment diagrams in the LT buckling case, developed in section 6.9 of chapter 6 in this thesis. It shall be noticed that this factor is set to 1.0 for the column buckling cases, where only the case with constant axial force was considered in this thesis; as a matter of fact, it is believed that a very similar concept, i.e. a specific factor φ for these column buckling cases, could be developed along the lines of what has been done for the LTB case, with no need for a modification of the formulae (4.3) and (8.3) themselves.

v.   By defining the normalized slenderness $\bar{\lambda}_{LT}$ uniformly as a function of the *plastic* moment capacity for compact *and semi-compact* sections, a definition is used that allows for a homogeneous description of the buckling resistance as observed in GMNIA calculations. On one hand, if the elastic moment capacity had been used in the definition of both χ_{LT} and $\bar{\lambda}_{LT}$ in the case of class 3 sections, these sections would be designed (too) conservatively with the above formulation. This is currently the case in the Eurocode. On the other hand, in order to avoid an *unconservative* regulation in the low LT slenderness range, the proposal needs an additional check against the applicable cross-sectional capacity, see clause (3). The accuracy presented by this clause depends on the formula used to determine $M_{Rd,class3}$. Models for the determination of the cross-sectional capacity of semi-compact sections, which are more refined than the simple elastic capacity, have recently been developed and presented e.g. by Kettler (2008), and could be used to increase the accuracy and consistency of clause (3).

PART III

Design Rules for Beam-Columns, Summary & Conclusions

9

On the Derivation of Design Rules for Beam-Columns

9.1. Introduction and Scope

In this chapter, an outlook is given on some aspects of beam-column design that are currently of interest to the scientific community and at code-committee level. The chapter begins with a discussion of the main concepts for the design of members subjected to combined load cases, the "interaction" and the "generalized slenderness" concept. Then, it proceeds with a brief numerical study of the in-plane buckling behaviour of beam-columns, thereby using types of representation of strength that are not commonly used in the literature. After a discussion of the design rules currently contained in Eurocode 3, which are based on the interaction concept, a new formulation for the in-plane buckling check of beam-columns is developed and presented that is integrated in the "generalized slenderness" concept and makes use of an overall, in-plane buckling reduction factor formulated using an Ayrton-Perry type representation. The accuracy and efficiency of the proposed formulation is demonstrated by means of comparative numerical (GMNIA) calculations, leading to the conclusion that the proposal is fully compatible in terms of safety and mechanical soundness–if not slightly superior- to the design rules currently found in the Eurocode. In a final section of this chapter, some remarks are made with respect to the "general method" in EN 1993-1-1 – clause 6.3.4 for the design of beam-columns against spatial buckling.

9.2. Concepts for Beam-Column Design

Beam-columns are characterized by the presence of compressive axial forces and bending moments. The resistance of a steel member against either one of these two sources of compressive stresses has been dealt with at lengths in part II of this thesis, and can be determined using the methods detailed therein. For a given level of the axial force N and the bending moment M, one can thus calculate the utilization of a steel member for *either* N *or* M by using the design formulae for columns and beams of Eurocode 3, or of part II; these can be written as $n_{FB} = N / \left(\chi \cdot A \cdot f_y / \gamma_{M1} \right)$ for flexural buckling of a member under axial load and $m_{LT} = M / \left(\chi_{LT} \cdot W \cdot f_y / \gamma_{M1} \right)$ for LT-buckling of a member in bending.

Due to the non-linearity of both stresses and deformations with respect to the level of loading, the resistance against the combination of axial forces and bending moments cannot generally be calculated directly from a (linear) superposition of the utilizations for the single loading components. In other words, the total utilization under N+M will often be higher, sometimes smaller, and only by pure chance equal to $n_{FB}+m_{LT}$. This obviously must be –and is- considered by design rules for beam columns.

In this context, two distinct concepts have come to be seen as the most advantageous ways of dealing with the beam-column buckling behaviour, see Fig 9-1:

i.   The first and (currently) most common is the so-called "interaction concept". It directly makes use of the valuable information contained in the utilizations n_{FB} and m_{LT} by adding them together, and accounts for the mentioned effects of the simultaneous presence of N and M by an *interaction factor* k. As described by Lindner (1986) and later Greiner et al. (1998), different uses (multiplier or addend) and positions (before n_{FB} or m_{LT}) of k have been considered. For the Eurocode, a format where k is a multiplier of the bending term was used.
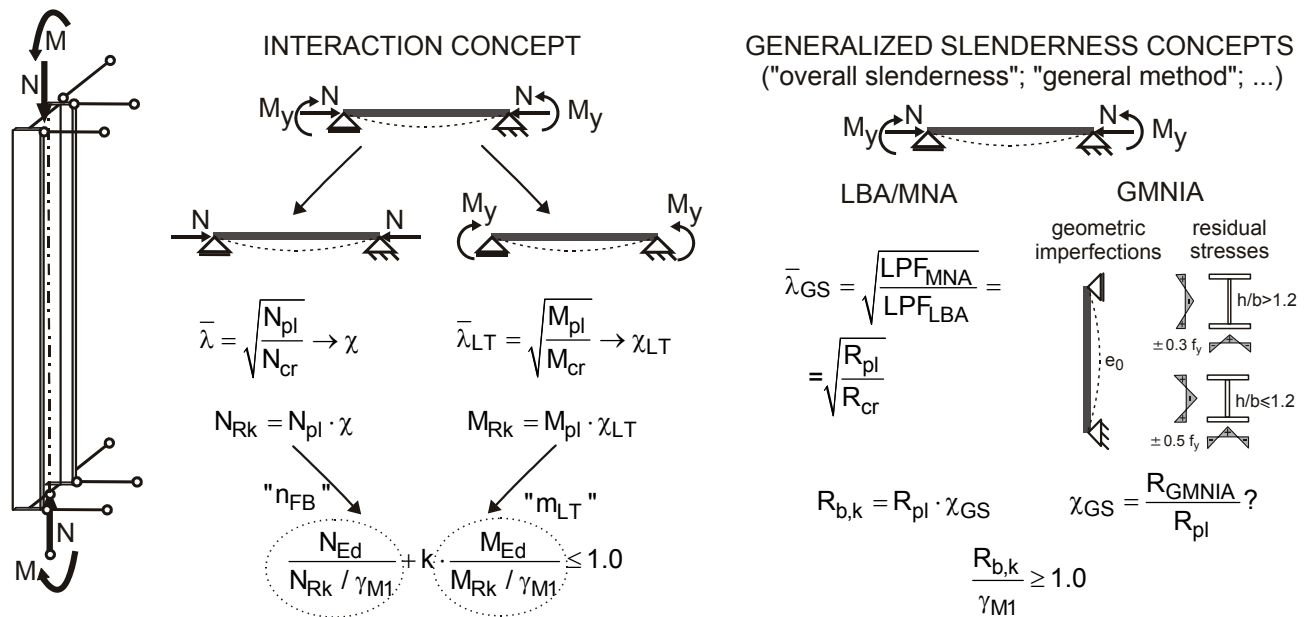
Fig 9-1 *Concepts for beam-column design; interaction concept versus generalized slenderness concepts.*

ii. In the second type of concepts, a generalized definition of the (normalized) slenderness is used; they are therefore called "generalized slenderness concepts" in the following. Specifically, these concepts encompass the "overall method" commonly used for the design of plates and shells (see e.g. Rotter, 2002) and the so-called "general method" for the design of beam-columns of clause 6.3.4 of Eurocode 3 - EN 1993-1-1 (2005). These methods have in common that they do not explicitly consider the utilizations for the single components of a given loading condition, but rather consider total utilizations for the combined case as

basis for design. As is illustrated in Fig 9-1, these methods define the slenderness $\overline{\lambda}_{GS}$ in a generalized form as the square root of total load proportionality factors LPF:

$$\overline{\lambda}_{GS} = \sqrt{\frac{LPF_{MNA}}{LPF_{LBA}}} = \sqrt{\frac{R_{pl}}{R_{cr}}} \qquad (9.1)$$

LPF_{MNA} is the maximum amplifier of a combined load case that can be reached in a (materially non-linear) analysis of the structure *without taking into account the effects of the studied buckling case.* In the "overall method" used for plate and shell buckling analysis, this load proportionality factor is calculated by omitting *all* stability effects, but taking into account the material non-linearity in a materially non-linear analysis. This corresponds to the plastic resistance R_{pl} of the studied structure for a linear amplification of a given load case. In the "general method" of EN 1993-1-1, LPF_{MNA} is replaced by the *in-plane buckling strength*, i.e. the (plastic) resistance $R_{b,ip}$ of the studied member for a linear amplification of (N+M), including the second-order effects of imperfections and deformations in the main plane of bending.

LPF_{LBA} is the maximum amplifier of a combined load case *until bifurcation is reached* for the studied buckling phenomenon. It can also be seen as the resistance R_{cr} against elastic buckling of the studied member for a linear amplification of (N+M).

In the concepts that make use of the "generalized slenderness", the buckling design check has the following format:

$$R_{b,d} = \frac{\chi_{GS} \cdot LPF_{MNA}}{\gamma_{M1}} \geq 1.0 \qquad (9.2)$$

Thereby, $R_{b,d}$ is the design resistance (in terms of a maximum load amplification factor) of the structure against the studied buckling phenomenon for a given load combination.

Equation (9.2) contains a buckling reduction factor χ_{GS}, which is a function of the generalized slenderness $\overline{\lambda}_{GS}$. As is indicated by the question mark in Fig 9-1, the values to be adopted for χ_{GS} are not clear and still up for debate, with a common opinion being that they must be studied and calibrated by means of GMNIA calculations, see e.g. Greiner (2003). This is also the topic of section 9.6 of this chapter.

(It shall be noted that in the "general method" of EC3 for the design of beam-columns the index of both slenderness and reduction factor is "op" for "out-of-plane", instead of the general "GS").

In summary, the "interaction concept" and the "generalized slenderness" concepts ("overall" and "general method") use different formulations for the buckling resistance of members under combined loading. Clearly, the formulation for the buckling design check according to (9.2) can be said to be "consistent" in the sense that it is a generalized formulation that also implicitly contains the buckling checks used for single load cases of only N or only M. (In the case of the general method this is only true for M, since for N it is based in $\chi_y N_{pl}$ instead of on N_{pl} alone). However,

the formulation does not –by itself- contribute to a solution of the design problem of members under combined loading, since the buckling reduction factor χ_{GS} must account for the exact same effects as the interaction factor k. The two concepts are therefore best thought of merely as two different forms of representation of the same information, without attributing an (inexistent) higher degree of mechanical consistence to any of the two concepts. Therefore, both concepts are considered in the remainder of this chapter.

9.3. In-Plane Buckling Behaviour of Beam-Columns

As has been stated in the introductory section 7.1, this chapter focuses on the in-plane buckling behaviour FB_{ip} of beam-columns, and thereby aims at developing a new formulation that better harmonizes the design rules for this buckling mode with the Eurocode rules for the modes associated with single load cases. A preliminary step in this direction is to study the behaviour of beam-columns for FB_{ip} by means of GMNIA calculations, and to compare the results of these calculations to the current Eurocode rules for beam-columns. This is done in this section.

9.3.1. Variable definitions

The variables and forms of representation used in the remainder of this chapter are presented and discussed in the following. The plots in Fig 9-2 thereby serve the purpose of helping to interpret the single variables. Plot (a) in Fig 9-2 shows the strength of a certain beam-column, an IPE 500 with $\bar{\lambda}_y$=1.0, and load case ($N+M_{y,constant}$) as obtained from GMNIA calculations in terms of a N-M_y interaction curve (line with circles indicating the single results). This type of representation indicates the maximum obtainable value of $n=N/N_{pl}$ and $m=M/M_{pl}$, whereby m refers to the maximum applied first order moment, which for this load case is constant over the member length.
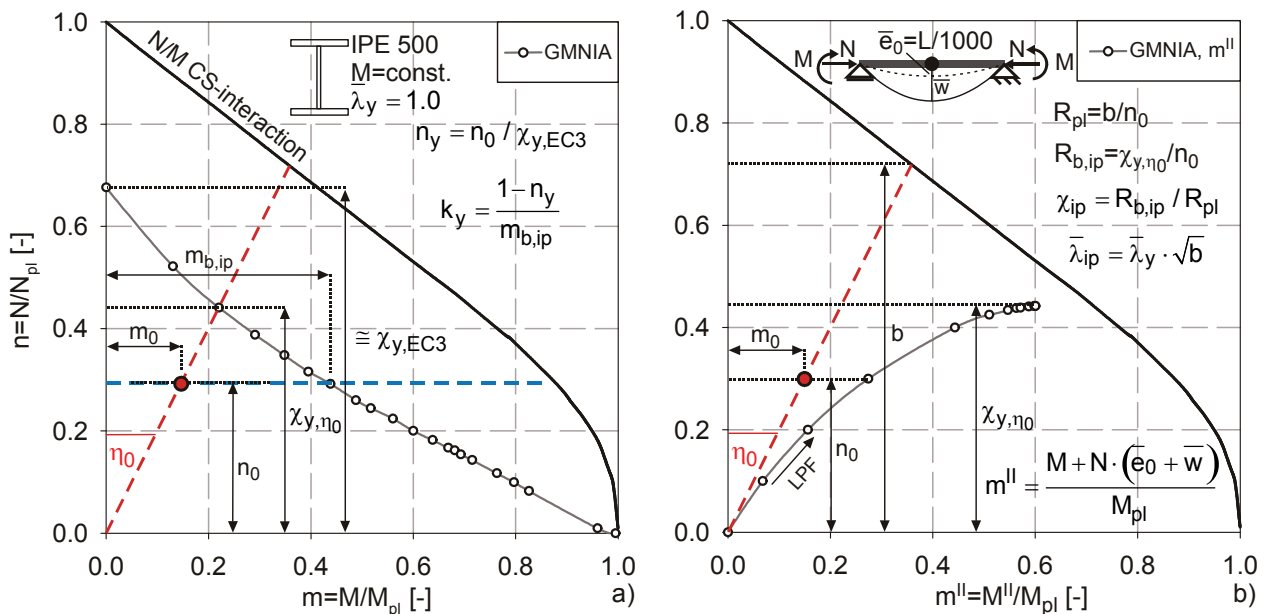
Fig 9-2 *Used variables as they appear in a GMNIA N-My interaction resistance plot (a) and in a N-MyII plot (b).*

The plot also shows the N-M cross-sectional interaction curve, i.e. the plastic limit load for this section. In this plot, the following characteristic values and variables can be identified:

i. At a given (design) load level, a certain ("zero") reference combination of n and m is present. This loading condition is identified by the red circle with coordinates $n=n_0$ and $m=m_0$ in the plot. For the beam-column to be "safe" against in-plane buckling, n_0/m_0 must lie below the GMNIA curve.

ii. The ratio m_0/n_0, which represents the eccentricity of the axial force $N=n_0 \cdot N_{pl}$ that would equivalently lead to m_0, is denominated by the variable η_0 in the following.

$$\eta_0 = \frac{\left(M / M_{pl}\right)}{\left(N / N_{pl}\right)} = \frac{m_0}{n_0} \tag{9.3}$$

iii. The value of the GMNIA N-M_y resistance curve lying on the straight line passing throuh the the plot's origin and the point m_0/n_0 indicates the combination of n and m at which the given beam-column has just reached its GMNIA buckling strength if n_0 and m_0 are both amplified proportionally, i.e. by maintaining the ratio η_0 constant. The value of n reached in this case is denominated as χ_{y,η_0} in the following. It is the buckling reduction factor with regard to the axial force section capacity N_{pl} that can be reached if a N/M pair is proportionally increased until failure.

iv. If no bending moment is present, the value of the GMNIA resistance curve at m=0 is (practically) identical with the buckling reduction factor $\chi_{y,EC3}$ valid for a column failing in in-plane flexural buckling, provided of course that the same imperfections and input data are used in the GMNIA calculations as done by Beer & Schulz (1970) for the original ECCS column buckling curves, see chapter 5.

v. In the interaction design concept for beam-columns of EN 1993-1-1, the variable of n_y is used, which represents the ratio of the acting, normalized axial force n_0 over $\chi_{y,EC3}$.

vi. Instead of through amplification of both n_0 and m_0 at the same pace, the N-M_y resistance curve can also be reached starting from m_0/n_0 by maintaining N constant and increasing only M. The total value of the applied, normalized bending moment at failure is denominated $m_{b,ip}$ for this case. This value isof relevance for the definition of the imteraction factor k_y according to the interaction concept design formulae of EN 1993-1-1, see section 9.3.3.

Fig 9-2b also shows results of a GMNIA calculation, but presented in a different format: the GMNIA curve (with circles) in this case shows the combination of n and m^{II} that is present in the IPE 500 section with $\overline{\lambda}_y=1.0$ if a given load ratio $\eta_0=m_0/n_0$ is maintained throughout a loading path from zero load up to failure, whereby m^{II} is the (normalized) *total, second order* bending moment present in the critical section (at mid-span in this case):

$$m^{II} = \frac{M + N \cdot \left(\overline{e}_0 + \overline{w}\right)}{M_{pl}} \tag{9.4}$$

The dashed red line in Fig 9-2b therefore represents the first-order, load bending moments M throughout the loading path, while the GMNIA curve shows the bending moments that are actually acting on the most critical cross-section, i.e. M plus second order effects. This form of representation is useful in order to understand the steps needed to formulate a "generalized slenderness" approach for the FB_{ip} buckling case:

i. A "generalized slenderness" in the sense of the "overall method" discussed in section 9.2 requires the identification of the maximum load amplification factor R_{pl} up to the plastic limit load for a given, fixed load combination. After calculating the ordinate value b of this amplification factor (by considering the in-plane interaction relationship), R_{pl} can be simply calculated from:

$$R_{pl} = b / n_0 \qquad (9.5)$$

ii. For the in-plane buckling case, the elastic, bifurcation buckling load needed for the calculation of the slenderness is governed solely by the axial force, and is independent of the bending moment. The elastic buckling resistance R_{cr} in terms of load amplification can therefore be written as follows:

$$R_{cr} = \frac{N_{cr}}{n_0 \cdot N_{pl}} = \frac{1}{n_0 \cdot \overline{\lambda}_y^2} \qquad (9.6)$$

iii. The "generalized", in-plane slenderness $\overline{\lambda}_{ip}$ can therefore be written as follows:

$$\overline{\lambda}_{ip} = \sqrt{\frac{R_{pl}}{R_{cr}}} = \overline{\lambda}_y \cdot \sqrt{b} \qquad (9.7)$$

As can easily be seen, the in-plane slenderness $\overline{\lambda}_{ip}$ defined in this way is equal to $\overline{\lambda}_y$ if $m_0=0.0$, and equal to zero if $n_0=0.0$, which is descriptive of the buckling proneness for these cases.

iv. The plot shows the maximum load amplification factor $\chi_{y,\eta0}$ for proportional load case amplification as the ordinate value of the peak of the GMNIA curve.

v. The in-plane buckling strength in terms of load amplification factor $R_{b,ip}$ is thus defined as follows:

$$R_{b,ip} = \frac{\chi_{y,\eta0}}{n_0} \qquad (9.8)$$

vi. Finally, the "generalized" buckling reduction factor χ_{ip} for FB_{ip} can be defined as follows:

$$\chi_{ip} = \frac{R_{b,ip}}{R_{pl}} = \frac{\chi_{y,\eta0}}{b} \qquad (9.9)$$

The forms of representation and variable definitions given above will be used in the following, whereby the first step is to show the GMNIA buckling behaviour for FB_{ip} in the above terms.

9.3.2. Buckling behaviour in numerical (GMNIA) calculations

The figures in this section illustrate the load-carrying and buckling behaviour of laterally restrained beam-columns as shown by GMNIA calculations. Thereby, all calculations refer to single-span members loaded by constant bending moments. The yield stress of the material is $f_y=235$ N/mm² in all shown cases, while the residual stress patterns follow the recommendations given in the ECCS (1984) recommendation. The in-plane geometric imperfection was assumed to be of sinusoidal shape and to have a magnitude of $\bar{e}_0=L/1000$, leading to the EC3 buckling reduction factors χ_y – which are based on calculations that used the same assumptions- for cases where M=0.

The first plots, shown in Fig 9-3, are of the type already presented in Fig 9-2a. The buckling resistance is presented in terms of buckling interaction curves for two different sections and three different values of $\bar{\lambda}_y$.
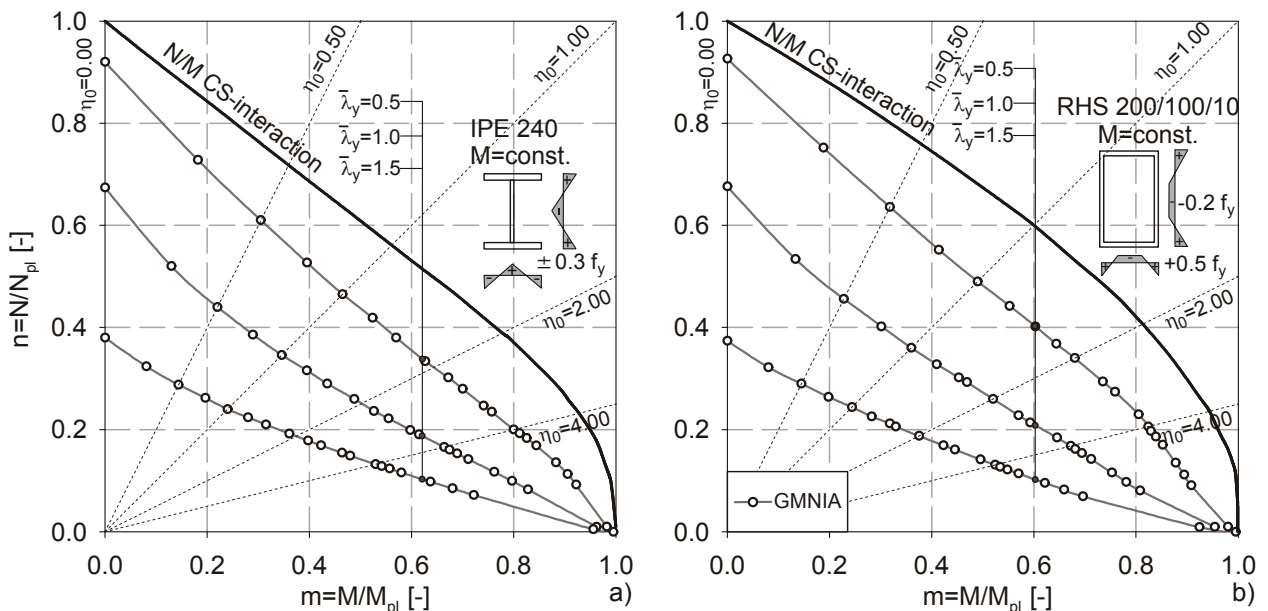
Fig 9-3 *N-M$_y$ interaction resistance curves for an IPE 240 (a) and an RHS 200/100/10 (b) section and various values of $\bar{\lambda}_y$.*

For both sections, the same general behaviour can be observed in these plots:

i.   With increasing slenderness, the buckling $N+M_y$ interaction curves move farther away from the cross-sectional interaction curve. The ordinate value of the curves at m=0 corresponds to the buckling reduction factor for FB_{yy} and m=0, while n=0 at m=1.0, meaning the plastic bending capacity M_{pl} is reached.

ii.   In between these two points, a (visually not very pronounced, but present) non-linear relationship is observed. This is the non-linear interaction effect that needs to be taken into account by either an interaction factor k or a specific definition of the buckling reduction factor χ, as mentioned in section 9.2.
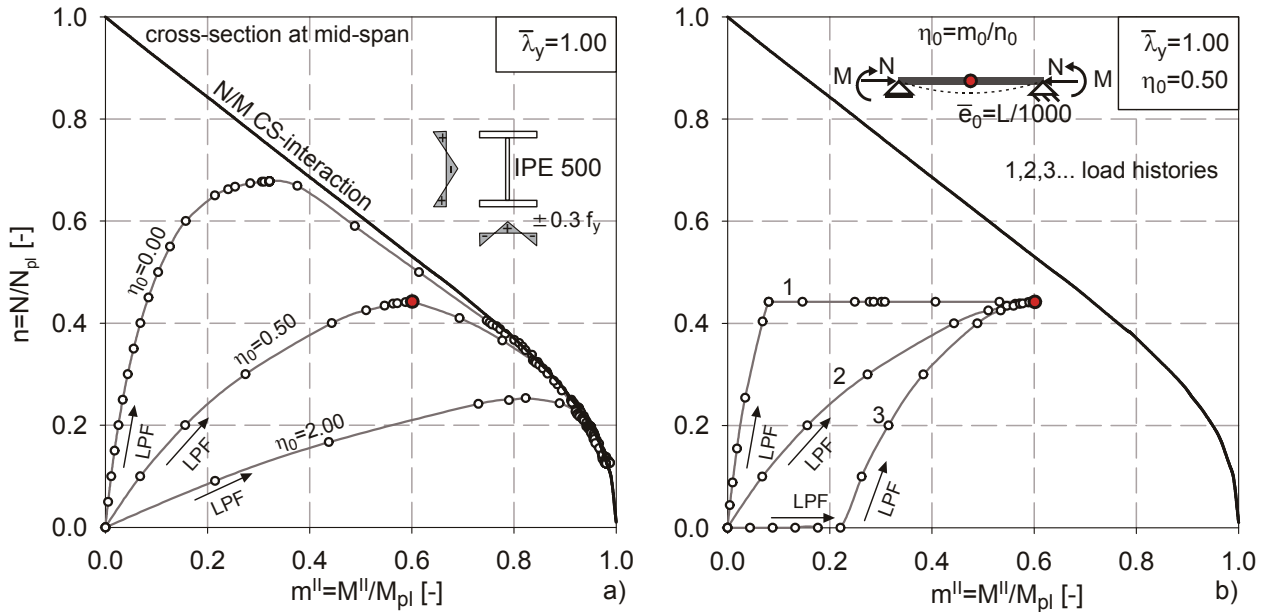
Fig 9-4   *N-M_y^{II} plots for an IPE 500 and different values of η_0 obtained using the Riks algorithm (a); for $\eta_0=0.5$ and three different loading paths up to failure (b).*

The type of representation used in Fig 9-3 only shows the final results –in terms of obtained combinations of n and m- of GMNIA calculations and is therefore not very informative with regard to the actual load-carrying behaviour. In order to better understand what the single GMNIA result points of Fig 9-3 represent, it is convenient to plot the total, second-order bending moments in loading path curves as first presented in Fig 9-2b. This is done in Fig 9-4.

Fig 9-4a shows the loading path curves for three different values of the ratio $m/n=\eta_0$ for an IPE 500 section. The loading paths are thereby calculated using the Riks algorithm in Abaqus, allowing for an analysis of the post-buckling behaviour. Two observations are of relevance:

i. The peak of the loading path curves is reached prior to obtaining the full plastic bending resistance given by the N-M_y cross-sectional interaction curve. This is due to the loss of stiffness caused by yield stresses in the flanges, which are obtained early on through a combination of compressive residual stresses and direct load stresses.

ii. After the peak is passed, the loading path curves descend into the N-M_y interaction curve and follow this curve until the end of the numerical calculation.

Fig 9-4b shows three different loading path curves, with all of them resulting in a final value of the ratio of (first order) bending moment to axial force at failure of $\eta0=m/n=0.22/0.44=0.50$, but each representing a different loading history up to this point:

i. The loading path marked as "2" in the figure is the one also shown in Fig 9-4a, i.e. one where the ratio of $\eta_0=0.5$ is present from the load level zero and kept constant with increasing load up to failure. At failure, the normalized axial force is $n=\chi_{y,\eta0}=0.44$, and the respective normalized bending moment is $m=0.5 \cdot 0.44=0.22$. The total, second order value of

$m=m^{II}$ is much higher than this value, reaching $m^{II}=0.6$, which illustrates the significance of stability effects for this member at the given slenderness of $\bar{\lambda}_y=1.0$.

ii. The curve marked as "1" represents a loading history where an axial force corresponding to $n=0.44$ is applied in a first step, and a first order bending moment corresponding to $m=0.22$ is applied in a second step, keeping n constant. The axial force alone already causes second-order bending moments of ca. $m^{II}=0.08$. Due to the presence of the axial force, these bending moments increase over-proportionally with the increase of m, finally resulting in the same failure point at $n=0.44$ and $m=0.22$, with $m^{II}=0.60$.

iii. The curve marked as "3" in the figure represents the case were a bending moment equivalent to $m=0.22$ is applied first, with no normal force, and a normal force of $n=0.44$ is applied in a second step, keeping m constant. Again, the same failure load is finally reached.

The observations made with regard to Fig 9-4b are quite relevant, as they imply that the ultimate buckling load for a certain total loading state is actually independent of the loading history. Only this fact allows for a definition of buckling rules that is independent of the sequence of loading.

The fact that the non-linear, GMNIA buckling load does not reach the plastic N-M_y interaction curve is quite relevant for the development of an accurate design rule and should therefore be discussed with more detail. Some results of a study concerned with this specific aspect are plotted in Fig 9-5a-d. The figures show N-M^{II} loading path curves for an IPE 500 section failing in in-plane buckling under N+M for different values of the ratio η_0 and for four different values of $\bar{\lambda}_y$.

It would be desirable to be able to include the exact parameters and effects that lead to this "premature" failing of a beam-column in a design formulation. However, this seems to be beyond the scope of the task of developing an accurate but simple buckling rule, as a precise formulaic representation would require an inclusion of effects and stiffness terms that exceeds what is practical in a design rule. However, the plots in Fig 9-5 do help to indentify the key parameters of the problem:

i. The comparison of figures a to d shows that the distance between peak of the loading path curve and the plastic interaction curve increases with slenderness; at $\bar{\lambda}_y=0.5$, the GMNIA curves are fairly close to the plastic N-M_y interaction curve, while at $\bar{\lambda}_y=2.0$ this distance is generally larger.

ii. The load ratio $\eta_0=m_0/n_0$ also appears to be of relevance. This is particularly evident in Fig 9-5c, which shows loading path curves for $\bar{\lambda}_y=1.5$: while for a value of $\eta_0=4.0$ the peak of the curve is close to the plastic interaction curve, for $\eta_0=0.0$ ($m_0=0$) the peak is even *prior to the elastic interaction,* represented by the straight line "1" (see figure d for the definition of the straight interaction lines). This means that the slenderness $\bar{\lambda}_y$ alone is not fully descriptive, and that the level of normal force is also relevant.
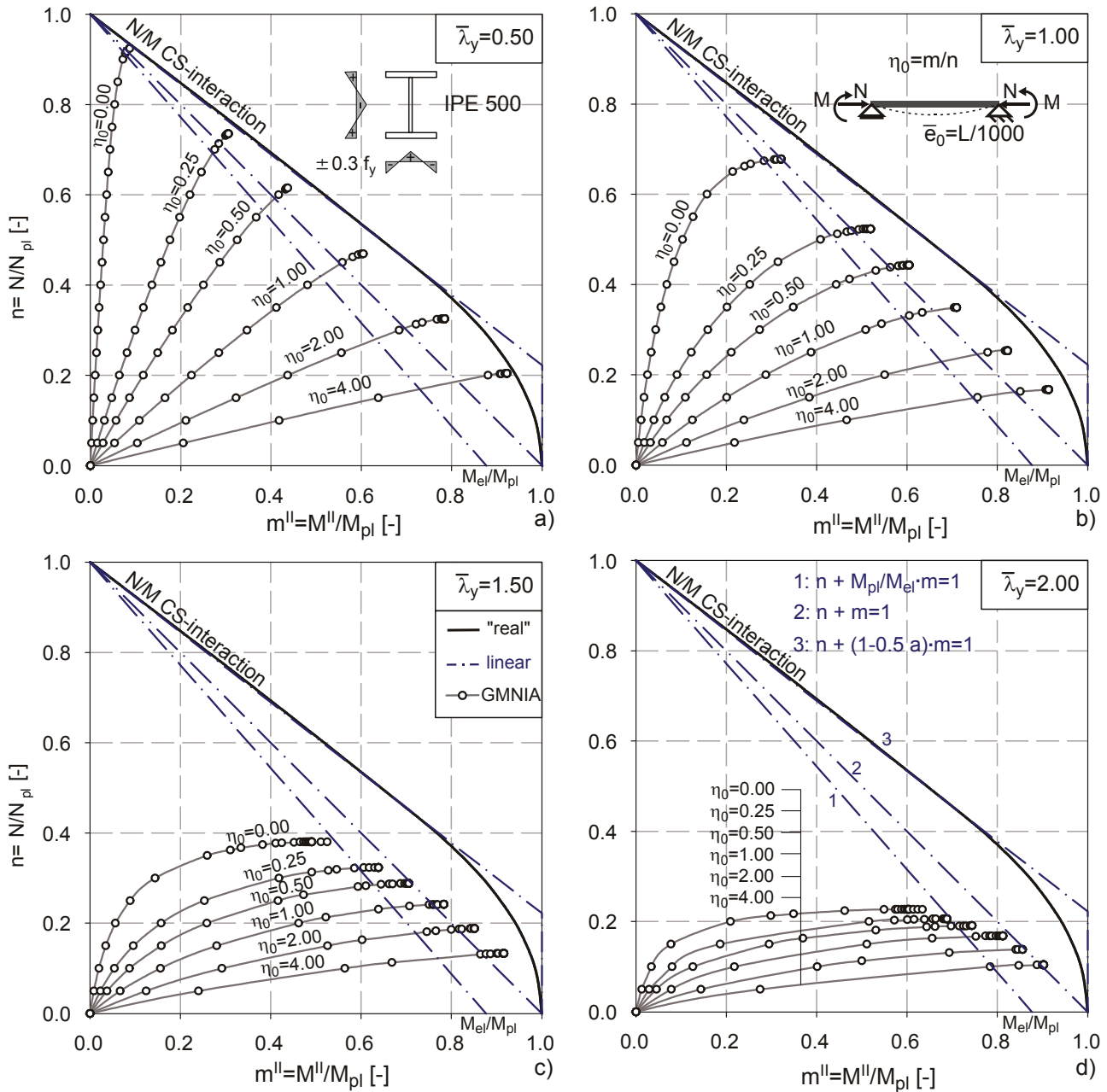
Fig 9-5   *N-M_y^{II} plots for an IPE 500 and different values of η_0 for $\overline{\lambda}_y$ =0.5 (a), 1.0 (b), 1.5 (c) and 2.0 (d).*

As will be shown in section 9.3.3, the effect illustrated in Fig 9-5 is explicitly addressed in the interaction concept buckling formulae of Annex A ("French-Belgian formulae") of EN 1993-1-1, and implicitly in the formulations of Annex B ("Austrian-German formulae") of the same code.

In a final figure dealing with the GMNIA results for the in-plane buckling behaviour of beam-columns, the buckling reduction factors χ_{ip} and $\chi_{y,\eta 0}$ defined in (9.9) and (9.8), and illustrated in Fig 9-2, are plotted over the slenderness values $\overline{\lambda}_{ip}$ -as defined in (9.9)- and $\overline{\lambda}_y$, respectively.
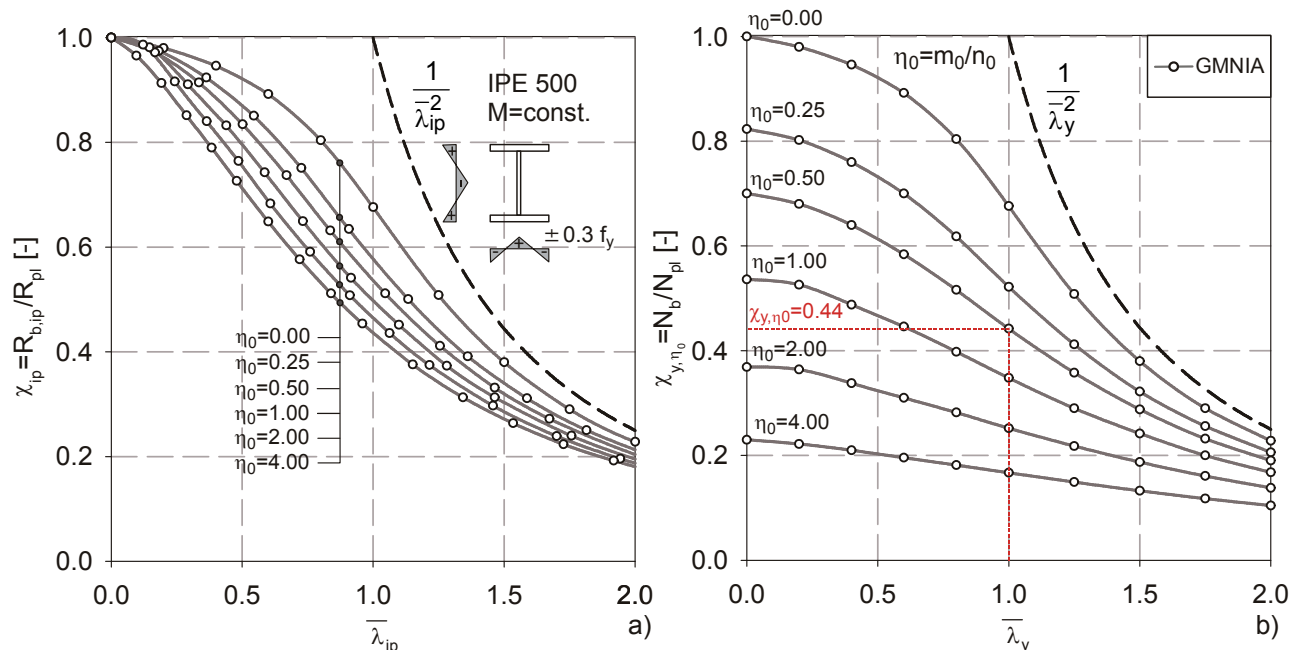
Fig 9-6 *Buckling reduction factor χ_{ip} (a) and $\chi_{y,\eta0}$ (b) for the in-plane buckling of an IPE 500 section under constant bending moment.*

Fig 9-6a shows the buckling reduction factors χ_{ip} for an IPE 500 under axial force and a constant bending moment diagram, calculated for different values of η_0 and plotted over $\overline{\lambda}_{ip}$. The figure shows that each value of the ratio η_0 leads to a distinctly separate, unique buckling curve, with high values of η_0 (i.e. load cases with a large bending component) resulting in lower curves. Thereby, the distance between the single curves increases under-proportionately with rising value of η_0. With increasing η_0, the curves can be shown approach a limit curve representing a lower bound for very high η_0 values.

The plots in Fig 9-6b are a different representation of the same GMNIA results, where the buckling reduction factor $\chi_{y,\eta0}$ is plotted over $\overline{\lambda}_y$. As was discussed in the description of Fig 9-2, $\chi_{y,\eta0}$ is the maximum ratio of $n=N/N_{pl}$ that can be reached for a certain value of η_0 if the two load components N and M are increased proportionately. Thus, the plot for example indicates that at $\overline{\lambda}_y=1.0$ a beam-column loaded with $\eta_0=0.5$ can reach a maximum value of $n=\chi_{y,\eta0}=0.44$, and thus a value of $m=\eta_0 \cdot n=0.22$; this is the same result discussed at length in Fig 9-4.

Both types of representation shown in Fig 9-6 are used extensively in sections 9.4 and 9.5, whereby more detailed descriptions are given there.

9.3.3.   Eurocode design rules – interaction factors k_y and k_z

Clause 6.3.3 of EC3- EN 1993-1-1 (2005) contains interaction concept design formulae for beam-columns. The theoretical and statistical background of these formulae, including the full list of references for single papers and research reports, has been collected and published in the ECCS Document N°119 (Boissonade et al., 2006).

The general form of the design formulae for the special case of pure in-plane buckling without any out-of-plane effects can be written as follows, whereby the partial safety factor γ_{M1} is omitted:

for N+M_y:
$$\frac{N}{\chi_y \cdot N_{pl}} + k_y \frac{M_y}{M_{y,pl}} \leq 1.0 \qquad (9.10)$$

for N+M_z:
$$\frac{N}{\chi_z \cdot N_{pl}} + k_z \frac{M_z}{M_{z,pl}} \leq 1.0 \qquad (9.11)$$

While these formulae (or rather, extended versions of them that account for in- and out-of plane effects) are contained in the main part of EC3 – EN 1993-1-1, the all-important interaction coefficients k are contained in two separate annexes of the code, Annex A and B. Thereby, Annex A contains what came to be known as the "French-Belgian" coefficients, and Annex B contains the "Austrian-German" ones. The reason for this distinction is the following:

i.   Two different research teams, one composed of French and Belgian researchers, the other of Austrian and German ones, were concerned with the revision and improvement of beam-column design curves for ECCS TC8. Thereby, the original intent was to provide two different levels of complexity and validity of the resulting formulae.

ii. While an agreement was found regarding the general formulation of the interaction design equation, two completely different proposals were made for the interaction coefficients. On one hand, the "French-Belgian" proposal was primarily based on a rigorous (elastic) second-order formulation, with some calibration needed only for the inclusion of effects stemming from material non-linearity. The "Austrian-German" proposal, on the other hand, was based primarily on the calibration to GMNIA calculations, with the goal in mind of keeping the resulting formulation as simple as possible without giving up too much accuracy.

iii. Contrary to the original intent of having two formulae that cover different levels of complexity of the structure and loading case, the Annex A and B formulae ended up being valid for the exact same type of member: prismatic members with double-symmetric cross-section.

iv. Thus, the two Annexes are seen in EC3 as two alternative options for the treatment of the same problem, with the selection of either one of the sets of formulae open to national code committees' or even the designers' choice.

For the case treated in this section of in-plane buckling of beam-columns of members with class 1 or 2 cross-sections, the following equations are used to determine the interaction factors k_y or k_z according to Annex A and B:

Annex A:

$$k_y = \frac{C_{mS,y}}{1-\chi_y \cdot N/N_{cr,y}} \cdot \frac{1}{MAX\left\{1+(w_y-1)\cdot\left(2-\frac{1.6 \cdot C_{mS,y}{}^2}{w_y}\cdot\left(\overline{\lambda}_y+\overline{\lambda}_y{}^2\right)\right)\cdot\frac{N}{N_{pl}};\frac{1}{w_y}\right\}} \quad (9.12)$$

$$k_z = \frac{C_{mS,z}}{1-\chi_z \cdot N/N_{cr,z}} \cdot \frac{1}{MAX\left\{1+(w_z-1)\cdot\left(2-\frac{1.6 \cdot C_{mS,z}{}^2}{w_z}\cdot\left(\overline{\lambda}_z+\overline{\lambda}_z{}^2\right)\right)\cdot\frac{N}{N_{pl}};\frac{1}{w_z}\right\}} \quad (9.13)$$

With $w_y = W_{y,pl}/W_{y,el} \le 1.5$

$w_z = W_{z,pl}/W_{z,el} \le 1.5$

$C_{mS,y}$, $C_{mS,z}$... equivalent *sinusoidal* moment factor; $C_{mS,j}=f(N/N_{cr})$

It shall be noted that the two equations (9.12) and (9.13) are identical in all but the indices, indicating that the expression is thought to be valid for arbitrary (double-symmetric) cross-sectional geometries.

Annex B:

$$k_y = C_{mU} \cdot \left[1+\frac{N}{\chi_y \cdot N_{pl}}\cdot MIN\left\{\overline{\lambda}_y-0.2;0.8\right\}\right] \quad (9.14)$$

$$k_z = C_{mU} \cdot \left[1+\frac{N}{\chi_z \cdot N_{pl}}\cdot MIN\left\{2\cdot\overline{\lambda}_z-0.6\;;\;0.8\right\}\right] \quad (9.15)$$

With C_{mU}... equivalent *uniform* moment factor

It is self-evident that the mechanically more rigorous derivation of the formulae in Annex A resulted in a more complex mathematical expression when compared to the approximate, purely calibrated expressions of Annex B. In terms of accuracy of the resulting design equation –when compared to GMNIA results for the "model beams"-, several examples given in the mentioned ECCS background document confirmed the two methods to yield largely comparable results. This is illustrated in the following, beginning with the representation of the resulting N-M buckling interaction curves according to GMNIA calculations and the two Annexes of EC3 shown in Fig 9-7. Thereby, Fig 9-7a shows the curves for a strong-axis in-plane case for an IPE 240, while Fig 9-7b shows the comparison for weak-axis in-plane buckling of an HEA 500.
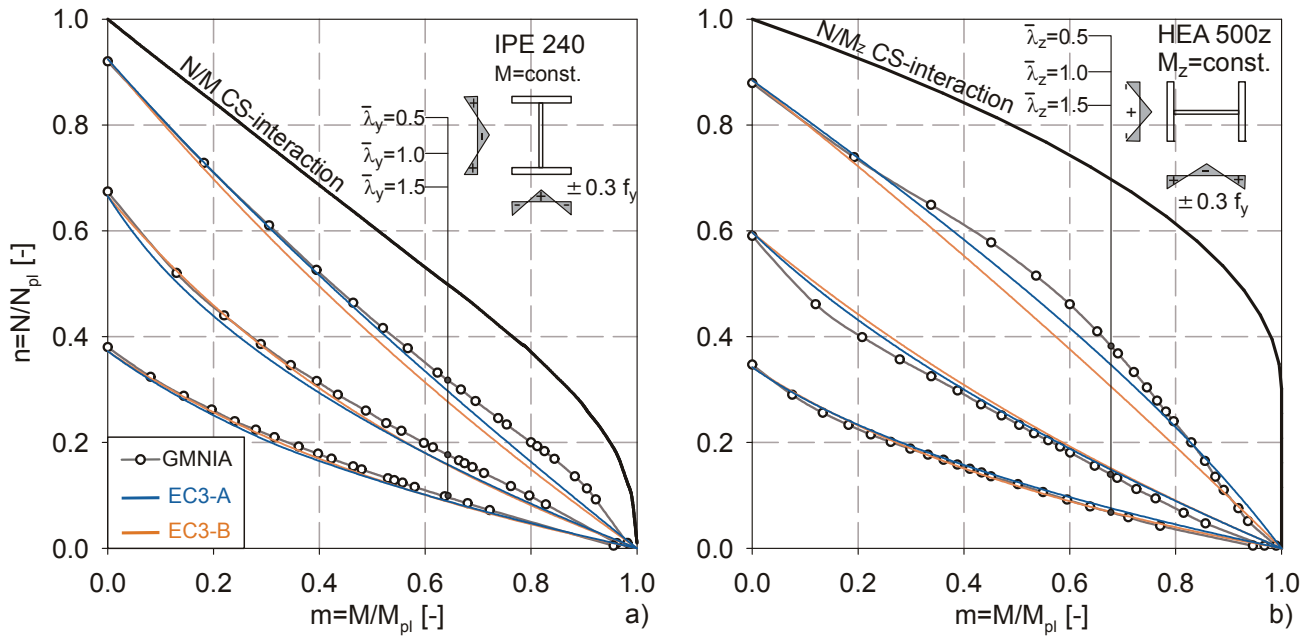
Fig 9-7 *N-M interaction for an IPE 240 subject to N+M_y (a) and an HEA 500 subject to N+M_z (b); comparison of GMNIA results and interaction concept formulae with coefficient of Annex A and B of EC3- EN 1993-1-1.*

The figure shows that for the studied case with constant bending moment diagram the two sets of formulae of Annex A and B result in very similar design curves, which in both cases lie satisfactorily close to the GMNIA curves. As lower slenderness, the Annex A curve appears to be slightly more accurate than the Annex B line. While at higher slenderness the differences between the two methods all but disappear.

One major difference between the two sets of formulae is represented by the consideration of the cross-sectional resistance at zero slenderness. By evaluating equation (9.10) or (9.11) with (9.12) to (9.15), we obtain the following equation for the interaction curve at zero-slenderness:

Annex A

for N+M_y:
$$\frac{N}{N_{pl}} + \frac{1}{MAX\left\{1+2\cdot(w_y-1)\cdot\dfrac{N}{N_{pl}};\dfrac{1}{w_y}\right\}}\cdot\frac{M_y}{M_{y,pl}} = 1.0 \qquad (9.16)$$

for N+M_z:
$$\frac{N}{N_{pl}} + \frac{1}{MAX\left\{1+2\cdot(w_z-1)\cdot\dfrac{N}{N_{pl}};\dfrac{1}{w_z}\right\}}\cdot\frac{M_z}{M_{z,pl}} = 1.0 \qquad (9.17)$$
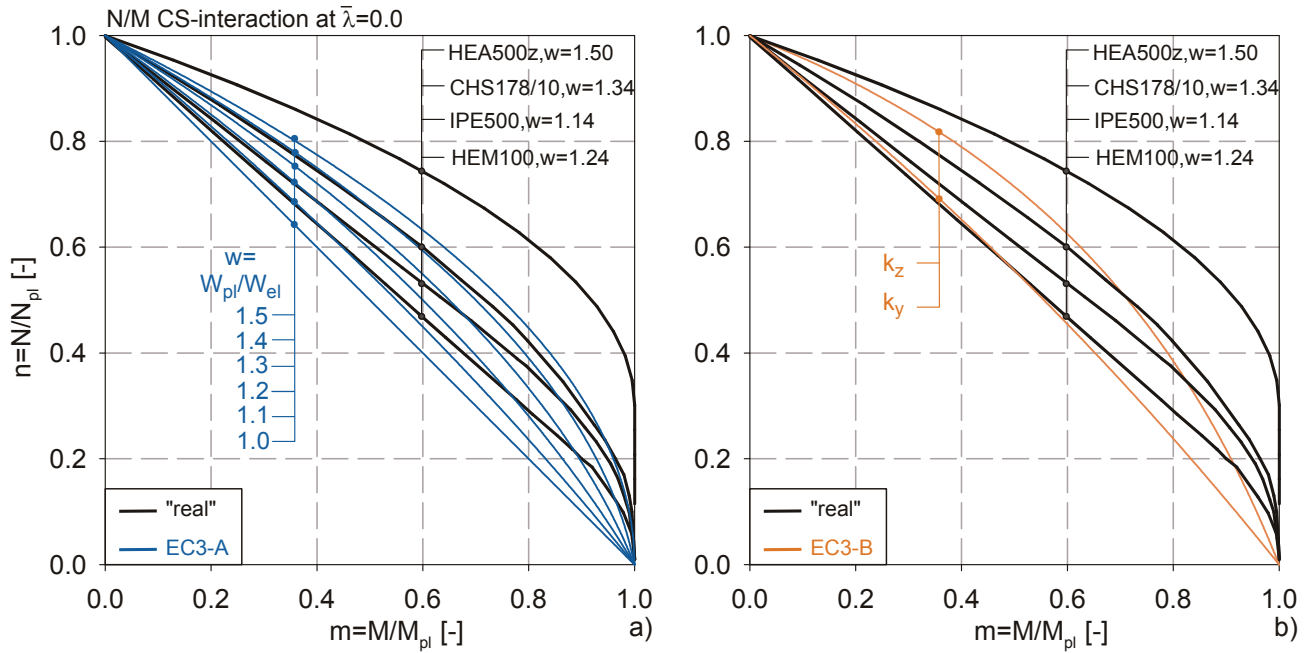
Fig 9-8 *Cross-sectional N-M interaction at zero slenderness for Annex A (a) and B (b) interaction factor formulae of EC3 - EN 1993-1-1. HEA 500z subject to N+M$_z$, all other cases to N+M$_y$.*

Annex B

For N+M$_y$:

$$\frac{N}{N_{pl}} + \left(1 - 0.2 \cdot \frac{N}{N_{pl}}\right) \cdot \frac{M_y}{M_{y,pl}} = 1.0 \qquad (9.18)$$

For N+M$_z$:

$$\frac{N}{N_{pl}} + \left(1 - 0.6 \cdot \frac{N}{N_{pl}}\right) \cdot \frac{M_z}{M_{z,pl}} = 1.0 \qquad (9.19)$$

These functions are plotted in Fig 9-8 and compared to real plastic interaction curves for some selected cross-sections. It shall be noticed that both sets of equations for Annex A and B result in non-linear interaction curves at zero slenderness, with the exception of cases where W$_{pl}$/W$_{el}$=1.0 in the Annex A formulation, where a linear interaction applies. While in the case of the Annex B formulae the distinction between different cross-sectional interaction curves is only very coarsely taken into account by the distinction between weak- and strong-axis buckling, the differentiation between different cross-sections is somewhat more refined in the Annex A formulation, where the shape of the curve is determined by the factor w=W$_{pl}$/W$_{el}$. The cross-sectional interaction formulation of Annex A was proposed by Villette et al. (2000) and is based on the approximation of the relationship valid for *rectangular cross-sections*. The comparison of formulaic and "real" interaction curves in Fig 9-8 shows this assumption to be rather inaccurate, albeit safe-sided, for some sections, particularly for weak-axis flexural buckling cases, where the presence of the web area in the calculation of N$_{pl}$, and the web's negligible significance for the weak-axis bending strength, results in very advantageous cross-sectional interaction curves.
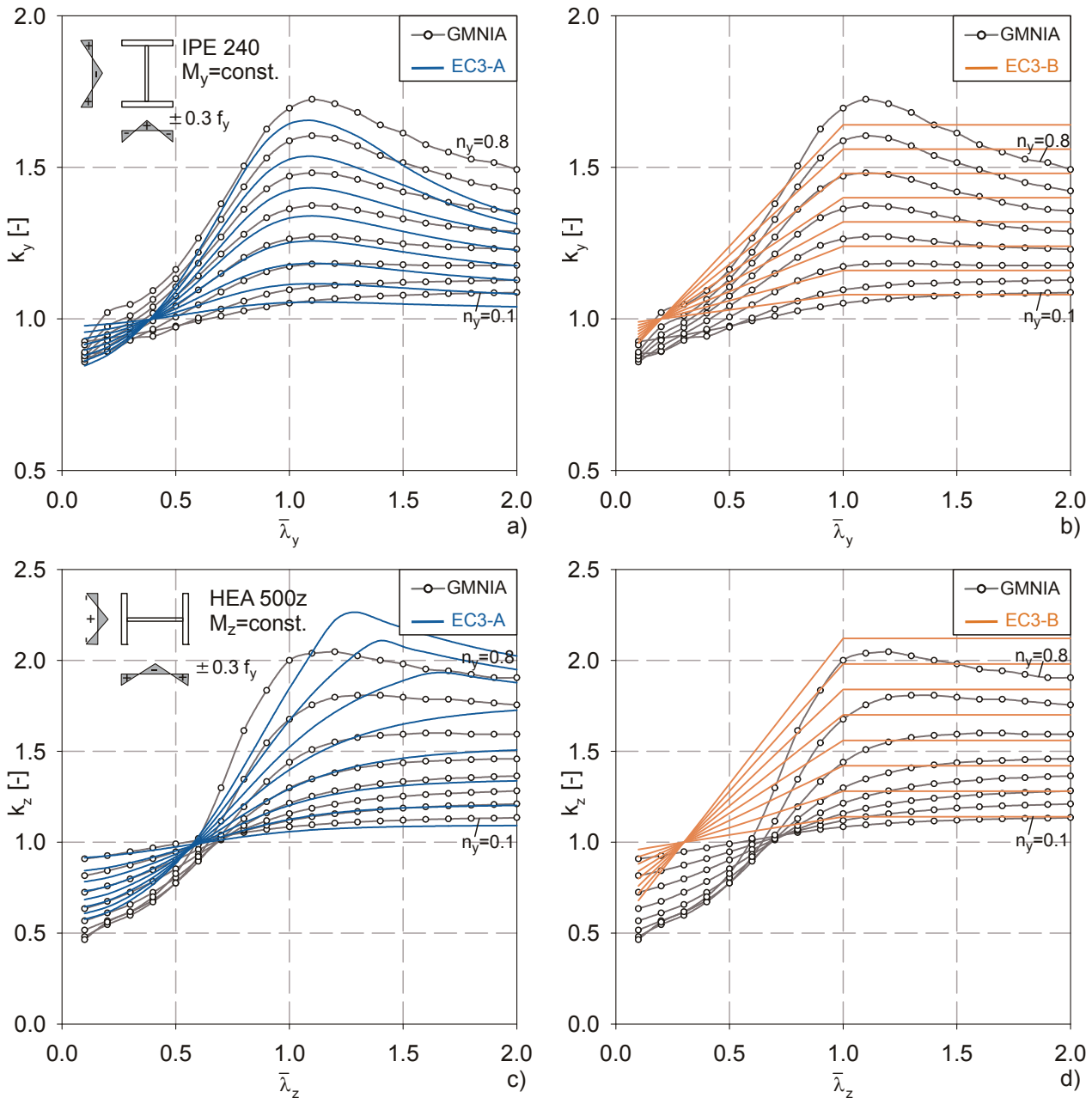
Fig 9-9 *Comparison of k_y and k_z values according to the formulae of Annex A (a,c) and B (b,d) of EC3 - EN 1993-1-1 with GMNIA results.*

At least from a theoretical point of view, the main "advantage" of the more refined formulations of the cross-sectional resistance in equations (9.12) and (9.13) when compared to the Annex B formulae lies in the explicit inclusion of the effects discussed in Fig 9-5, i.e. the increasing distance between the peak of the n-m^{II} curves and the plastic cross-sectional interaction with increasing slenderness and higher values of $N=n_0 \cdot N_{pl}$. Indeed, the expression term C_{yy} contained in the denominator of (9.12) is chosen so that the underlying cross-sectional resistance parabolically approaches the *elastic cross-sectional resistance* with increasing slenderness and axial force.

$$C_{yy} = 1 + (w_y - 1) \cdot \left(2 - \frac{1.6 \cdot C_{mS,y}^2}{w_y} \cdot \left(\overline{\lambda}_y + \overline{\lambda}_y^2 \right) \right) \cdot \frac{N}{N_{pl}} \geq \frac{W_{y,el}}{W_{y,pl}} \qquad (9.20)$$

In a final representation of the two sets of formulae for the interaction coefficient in the Annexes of EC3 – EN 1993-1-1, the values of k_y and k_z are themselves compared to the equivalent values of the interaction factors as obtained from GMNIA calculations. This is done in Fig 9-9. It shall be noted that the GMNIA values where obtained from calculations of the type shown in Fig 9-2a: the axial force was applied in a first step, with a defined value of $n_y = N / (\chi_{y,EC3} \cdot N_{pl})$, and the bending moment was applied in a second step and increased until failure, when the normalized moment $m_{b,ip}$ is acting. By setting the utilization at failure equal to 1.0 and solving (9.10) for k_y, we obtain the formula by which the GMNIA values of k_y were calculated, see also Ofner (1997):

$$k_y = \frac{1.0 - n_y}{m_{b,ip}} \qquad (9.21)$$

The comparison of the interaction factors shown in Fig 9-9 can be commented upon as follows:

i.   The Annex A formulae yield shapes of the curve representing the interaction factors that are qualitatively and quantitatively well comparable with the GMNIA curves. This is particularly true for the IPE 240 section loaded in strong-axis, particularly when the axial force term n_y is small.

ii. The Annex B formulae result in a bilinear curve in the representation chosen in Fig 9-9. This is of course intended, as this type of representation forms the basis of the proposal for the Annex B interaction factors, see Greiner et al. (1998). The extensive set of GMNIA parametric studies that underpin the Annex B formulae led to the conclusion that a constant value of k beyond $\overline{\lambda} = 1.0$ is recommendable in order to describe the behaviour of an as-wide-as possible range of cross-sectional geometries with such a simple formulation for k_y. It shall also be noticed that for lower values of n_y, the GMNIA curves indeed show an almost constant value of k_y at higher slenderness. Only for higher values of n_y a drop of k_y is observed, causing deviations from the design interaction factors both for Annex A and B.

iii. However, not describing this specific shape by a formulaic description is not at all cause of a larger error for higher values of n_y, since for these the total utilization is already taken in by n_y itself, and a (mostly safe-sided) error on the remaining bending component's utilization hardly affects the overall accuracy.

iv. The comparison of the design interaction factors with GMNIA calculations shall not express direct consequences to safety aspects, since the design formulae of both annexes have been statistically calibrated to test results and FE-calculations, see Boissonade et al. (2006).

In summary, the comparison between the two interaction concept formulae discussed in this section has resulted in the conclusion that –at least for the studied in-plane buckling case- both formulations are absolutely comparable in accuracy, even though the Annex A formulation has an advantage

from the point of view of mechanical interpretability. In this context, ideas from the Annex A concept could be taken and adapted to the proposed, Ayrton-Perry type formulation developed in the next section.

9.4. Ayrton-Perry formulation for In-Plane Buckling of Beam-Columns

In this section, the Ayrton-Perry type formulation developed for flexural column buckling under pure axial compression is expanded to include the in-plane beam-column buckling phenomenon. The steps that had to be taken in order to obtain a formulation of this type are detailed in the following, whereby the first step consists of a linearization of the (non-linear) plastic interaction curve.

9.4.1. Linearization of the N-M_y interaction curve

As will be shown in this section, one requirement for the development of an Ayrton-Perry type formulation for an "overall" in-plane buckling reduction factor is that the the cross-sectional N-M plastic interaction curve is linear, at least section-wise. The exact, non-linear interaction curves must therefore be linearized in order to be able to proceed with this type of formulation. The way that this has been done for the purposes of this section is illustrated in Fig 9-10. The figure makes a distinction between strong- and weak axis buckling of I-sections, and treats hollow sections similarly to the strong-axis I-section case:
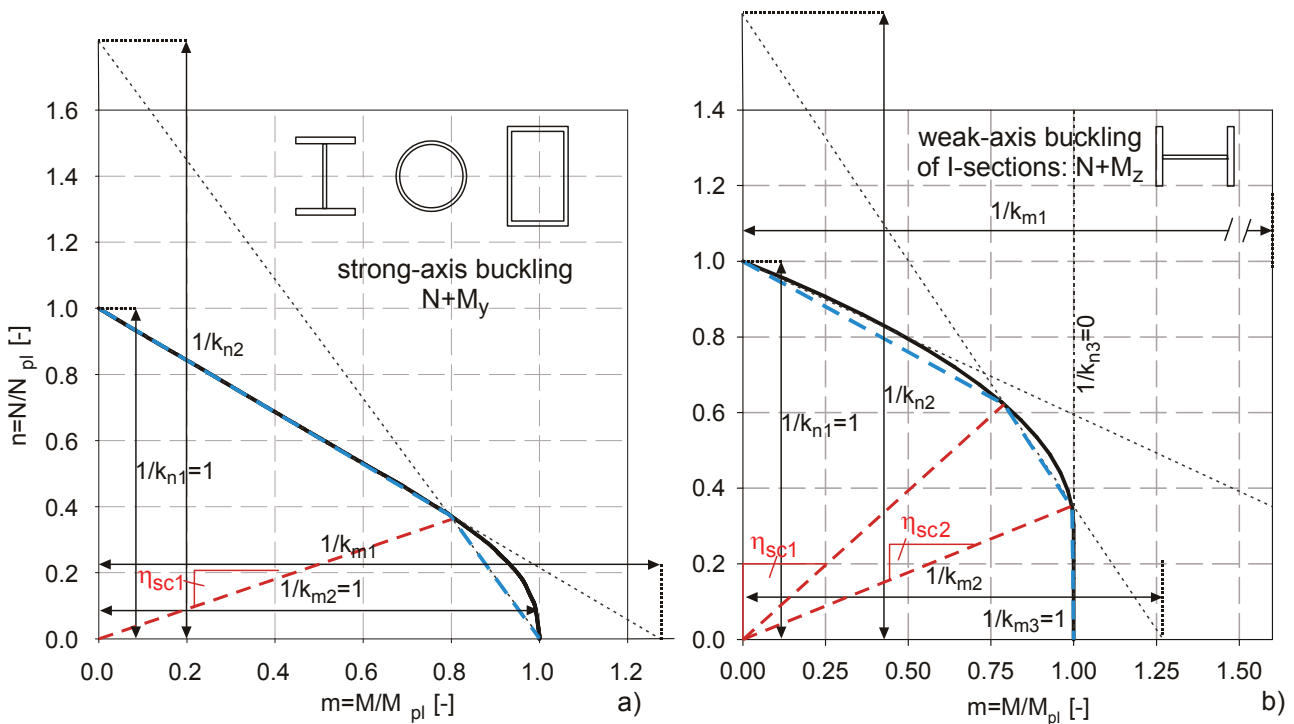
Fig 9-10 *Linearization of the cross-sectional interaction curves, definition of used variables; for hollow sections and strong-axis buckling of I-sections (a); for weak-axis buckling of I-sections.*

i. The interaction curve for circular and rectangular hollow sections, as well as for strong-axis buckling of I-sections (N+M_y) is linearized by two different segments. The slope change occurs at the value of η_{SC1}, chosen to correspond to a abscissa value of m=0.8.

ii. The distinctly non-linear interaction curve for weak-axis flexural buckling of I-sections (N+M_z) is linearized by three segments, with one segment approximating the curve between m=0 and 0.8, and a vertical segment describing the range where the axial force is smaller than $A_w \cdot f_y$ and one segment connecting these two. Two slope changes are present, occurring at values of η_{SC1} and η_{SC2}.

iii. The single straight segments are characterized in their position by their intersection points with the coordinate axes. The following definitions are used:

$1/k_{ni}$ .... ordinate value of the intersection of the segment i of the multi-linear approximation with the vertical n-axis.

$1/k_{mi}$ .... abscissa value of the intersection of the segment i of the multi-linear approximation with the horizontal m-axis.

Within a given segment i, the interaction curve is thus described by the following equation:

$$n_{pl}(m) = \frac{1}{k_{ni}} - m \cdot \left(\frac{k_{mi}}{k_{ni}}\right) = \frac{1 - m \cdot k_{mi}}{k_{ni}} \qquad (9.22)$$

with $n_{pl}(m)$.... normalized plastic capacity for axial loading under consideration of the reduction caused by the simultaneous presence of bending moments.

Appropriate parameters need to be selected in order to make the proposed linearization as accurate and consistent as possible. In this respect, the plastic interaction functions found in clause 6.2.9 of EC3 – EN 1993-1-1 are of help: For the cases of strong-axis bending of I-sections and rectangular hollow sections, this clause already makes use of a linearization of the "exact" plastic interaction curve. Accordingly, this expression is adopted for the first section of the curve in Fig 9-10a for these cases.

The proposed values of k_{ni} and k_{mi} for the different studied cross-sections are summarized in Table 9-1. Thereby, values for I-sections in strong-axis bending and rectangular hollow sections are based on the above-mentioned linearized cross-sectional resistance given in clause 6.2.9 (5) of EC3 – EN 1993-1-1. The proposed values for circular hollow sections are based on the N-M interaction curve valid for thin-walled, circular hollow sections:

$$m_{pl,CHS,exact}(n) = \cos\left(\frac{\pi}{2} \cdot n\right) \qquad (9.23)$$

Considering the slope change at m=0.8, the following values can therefore be calculated:

$$n_{pl,CHS,exact}(m = 0.8) = \frac{2}{\pi} \cdot \arccos(0.8) = 0.41 \qquad (9.24)$$

$$k_{m1} = \frac{1 - 0.41}{0.8} = 0.74 \qquad (9.25)$$

#	Type of section and loading	Parameters of the N-M interaction linearization
1	I-section, strong axis buckling N+M$_y$	$k_{n1}=1.0$; $k_{m1}=1-0.5\cdot a \geq 0.75$; $\eta_{SC1} = \dfrac{0.8}{1-0.8\cdot k_{m1}}$
2	Rectangular hollow section RHS, N+M$_y$	$k_{n2}=\dfrac{0.2}{1-0.8\cdot k_{m1}}$; $k_{m2}=1.0$; $\eta_{SC2}=\infty$
3	Circular Hollow Section CHS, N+M	$k_{n1}=1.0$; $k_{m1}=0.74$; $\eta_{SC1} = \dfrac{0.8}{1-0.8\cdot k_{m1}}=1.95$ $k_{n2}=\dfrac{0.2}{1-0.8\cdot k_{m1}}=0.49$; $k_{m2}=1.0$; $\eta_{SC2}=\infty$
4	I-section, weak axis buckling N+M$_z$	$k_{n1}=1.0$; $k_{m1}=\dfrac{1-a}{1.45}$; $\eta_{SC1} = \dfrac{0.8}{1-0.8\cdot k_{m1}}$ $k_{n2}=\dfrac{0.8}{1.81-a}$; $k_{m2}=\dfrac{1-a}{1-0.55\cdot a}$; $\eta_{SC2}=\dfrac{1}{a}$ $k_{n3}=0.0$; $k_{m3}=1.0$; $\eta_{SC3}=\infty$
$a = \dfrac{A-2\cdot b\cdot t_f}{A}=\dfrac{A_w}{A}$		

Table 9-1   *Parameters of the linearized N-M interaction*

Quite similarly, the proposed value of k_{ni} and k_{mi} for weak-axis flexural buckling under N+M$_z$ of I-sections is based on the a linearization of the following, non-linear "exact" formulation, taken from EN 1993-1-1 clause 6.2.9:

$$n \leq a \rightarrow m_{pl,I-Mz,exact}(n)=1$$
$$n > a \rightarrow m_{pl,I-Mz,exact}(n)=1-\left(\frac{n-a}{1-a}\right)^2 \qquad (9.26)$$

9.4.2. In-plane slenderness

The linearized cross-sectional interaction curve can now be used to calculate the generalized, "overall" slenderness for in-plane buckling $\overline{\lambda}_{ip}$ presented in section 9.3.1. Fig 9-11 is used for reference; it schematically illustrates the underlying concepts for a case where the first section "1" of the linearized cross-sectional interaction curve is applicable.

Since load amplification factors R$_{pl}$ and R$_{cr}$ are used in this concept, the reference load level must be defined. Quite generally, it can be written as a certain combination of m$_0$ and n$_0$, corresponding to a point on the straight line with "slope" η_0. We can write:

$$n = n_0 = \frac{m_0}{\eta_0} \qquad (9.27)$$

Fig 9-11 *Variables used for a formulaic definition of the "overall" in-plane slenderness $\bar{\lambda}_{ip}$ using the linearized cross-sectional interaction curve*

This load combination is always proportionally increased in the following. For example, it can be increased by R_{pl} before it reaches the plastic section capacity. Using the linearized interaction relationship (9.22), R_{pl} can be calculated:

$$R_{pl} \cdot n_0 = R_{pl} \cdot \frac{m_0}{\eta_0} = \frac{1 - R_{pl} \cdot m_0 \cdot k_{mi}}{k_{ni}} \tag{9.28}$$

$$R_{pl} \cdot m_0 \cdot \left(\frac{1}{\eta_0} + \frac{k_{mi}}{k_{ni}} \right) = \frac{1}{k_{ni}} \tag{9.29}$$

$$R_{pl} = \frac{\eta_0}{m_0 \cdot (k_{ni} + \eta_0 \cdot k_{mi})} = \frac{1}{n_0 \cdot (k_{ni} + \eta_0 \cdot k_{mi})} = \frac{1}{n_0 \cdot c_0} \tag{9.30}$$

With $c_0 = (k_{ni} + \eta_0 \cdot k_{mi})$.

For the slenderness definition of equation (9.7), the elastic (bifurcation) buckling amplification factor R_{cr} is also needed. This can be calculated as follows:

$$R_{cr} = \frac{N_{cr}}{N} = \frac{N_{cr}}{n_0 \cdot N_{pl}} = \frac{1}{n_0 \cdot \bar{\lambda}_y^2} \tag{9.31}$$

Finally, the "overall" in-plane slenderness can be calculated:

$$\bar{\lambda}_{ip} = \sqrt{\frac{R_{pl}}{R_{cr}}} = \frac{\bar{\lambda}_y}{\sqrt{c_0}} \tag{9.32}$$

It can be observed that the slenderness $\overline{\lambda}_{ip}$ is a function of the loading ratio η_0, which is kept constant in this definition, and of the parameters governing the cross-sectional interaction curve.

Since $k_{ni}=k_{n1}$ for m_0 and η_0 equal to zero, and k_{n1} is always equal to one, the overall in-plane slenderness is "automatically" equal to $\overline{\lambda}_y$ when no bending moment is present, which is logically consistent.

9.4.3. Plastic-elastic transitional behaviour of the interaction curve

One last preliminary step must be taken before the buckling strength for in-plane buckling can be formulated in terms of an Ayrton-Perry formulation, which is connected with the phenomena discussed in the description of Fig 9-4a and Fig 9-5: in a (realistic) GMNIA calculation, the n-m^{II} curve reaches the peak value before the plastic interaction curve is reached. This fact must be taken into account by a mechanically rational formulation.

In the interaction concept formulations of Annex A of EC3 – EN 1993-1-1, the transitional behaviour of the valid cross-sectional interaction has been shown to be explicitly taken into account in equation (9.20) by formulating the factor C_{yy} so that it converges towards the (linear) elastic cross-sectional interaction curve with increasing values of the normal force ratio n and the slenderness $\overline{\lambda}$. A comparable formulation is proposed in the following, see Fig 9-12, based on the following criteria:

i.   The segmentally linear description of the failure curve should be retained also for the slenderness-dependent transitional case. This is done by expressing the interaction curves that are thought to be valid at failure by straight lines, which are defined by the same type of parameters used in Table 9-1 for the fully plastic interaction curve. These slenderness-dependent parameters are designated as k* (specifically, k_{ni}* and k_{mi}*) in Fig 9-12a and the following, to distinguish them from the parameters k of the fully plastic case.

ii. At zero slenderness and/or axial force component of the load point ($\overline{\lambda}=0$, $\eta_0=\infty$), the full plastic interaction should be maintained, meaning that k* should be equal to the applicable value of k (k_{ni}*=k_{ni}, k_{mi}*=k_{mi}).

iii. At high value of slenderness and axial force components, the elastic cross-sectional interaction line should be valid, i.e. one were the strength is governed by the equation

$$n + w \cdot m = 1.0 \tag{9.33}$$

with w... W_{pl}/W_{el} ; n=N/N_{pl} ; m=M/M_{pl}

iv. The described transitional behaviour is a highly complex phenomenon that can only rather coarsely be described by simple formulations suitable for design. The GMNIA calculations carried out in the context of the study presented in this chapter, partly reproduced in sections 9.3.2 and 9.5, pointed out that the cross-sectional shape, as well as the residual stresses, also play a significant role in determining the "speed" at which the valid cross-sectional

interaction curve moves from the plastic to the linear elastic curve with increasing slenderness. While this cannot be easily included in a comprehensive way, it was found important to include a specific factor that accounts for the differences between section types.
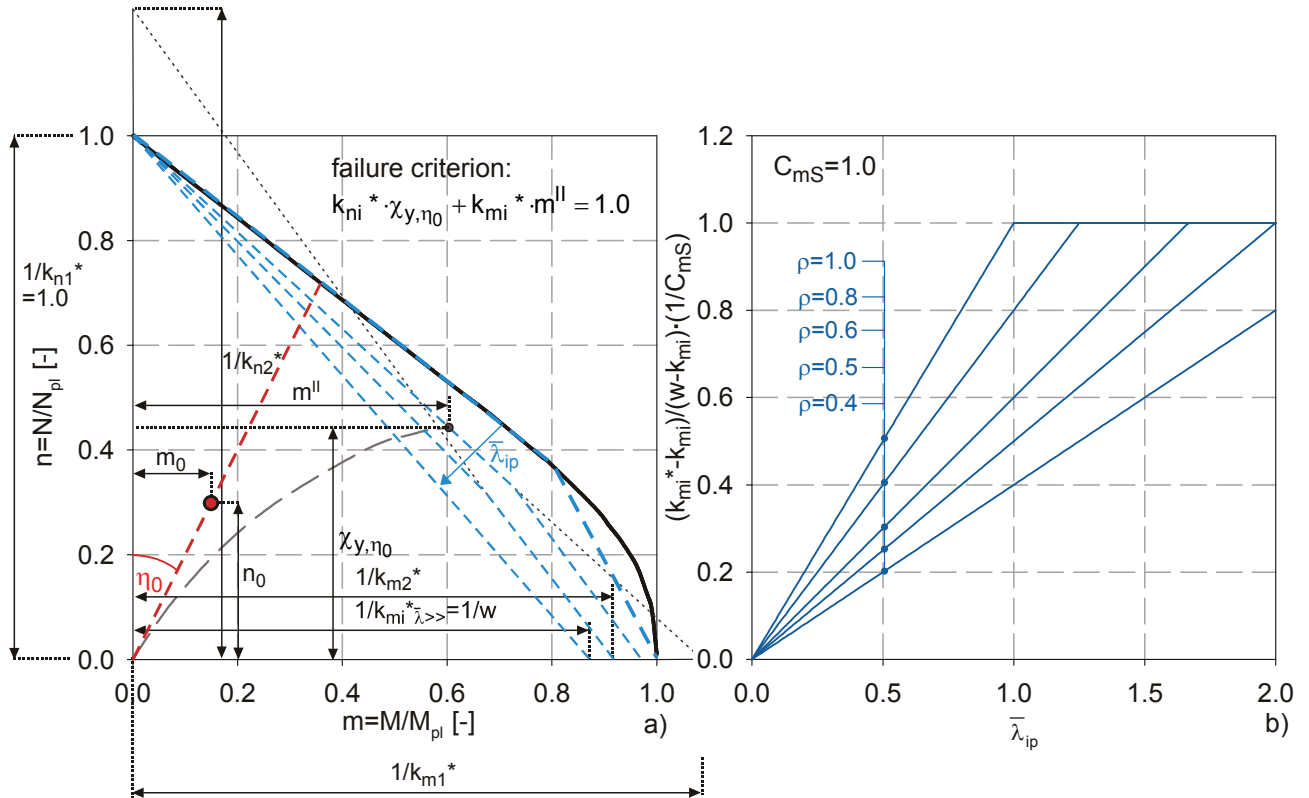
Fig 9-12 *Slenderness-dependent transition of the linearized cross-sectional interaction from the the plastic to the elastic case; representation of the modified values $k_{ni}*$ and $k_{mi}*$ (a); transition expression as formula of the overall in-plane slenderness $\overline{\lambda}_{ip}$ (b).*

v.   The shape of the bending moment diagram, which is shown to be quite generally important for the obtained buckling strength, also has an impact on the plastic-elastic transitional behaviour of the interaction relationship. This effect should therefore also be taken into account.

Finally, the following proposal is made for the definition of the values of $k*$:

$$k_{ni}* = k_{ni} + (1 - k_{ni}) \cdot \rho \cdot \overline{\lambda}_{ip} \cdot C_{mS} \leq 1 \tag{9.34}$$

$$k_{mi}* = k_{mi} + (w - k_{mi}) \cdot \rho \cdot \overline{\lambda}_{ip} \cdot C_{mS} \leq w \tag{9.35}$$

Whereby $\overline{\lambda}_{ip}$ ...   overall, in-plane slenderness as given by equation (9.32)

ρ .....   factor accounting for the specific transitional behaviour of a certain cross-section type.

C_{mS} ....   equivalent moment factor for sinusoidal moment diagram.

The general meaning of equation (9.35) is illustrated in Fig 9-12b for different values of ρ and for a value of C_{mS}=1.0. This form of representation shows the transition with increasing values of $\overline{\lambda}_{ip}$; the ordinate variable is thereby equal to 1.0 when the elastic, and 0.0 when the plastic N-M interaction curve is applicable.

The figure illustrates the very simple shape of the the proposed transition function, with the ordinate value being a linear function of $\overline{\lambda}_{ip}$. Thereby, the overall in-plane slenderness $\overline{\lambda}_{ip}$ is a very convenient and descriptive parameter, as it includes both the "pure" effects of slenderness and instability ($\overline{\lambda}_y$) and of the level of normal force to be expected at failure, accounted for by the cross-sectional parameters k_{ni} and k_{mi} and the load ratio η_0 in the definition of $\overline{\lambda}_{ip}$.

The factor ρ is quite relevant, as it allows for a consideration of the specific behaviour of different types of cross-sections. GMNIA calculations can be used to investigate the behaviour of different types of sections, and ρ can be used to as a perhaps coarse, yet effective tool for calibration. The large series of GMNIA calculations conducted in the context of the study presented in this chapter led to the conclusion that the values of ρ given in Table 9-2 are well suited for being used in conjunction with expressions (9.34) and (9.35) and with the formulation developed in the following section 9.4.4.

Type of section and loading	Residual stress distribution	ρ
I-section, strong axis buckling N+M$_y$	± 0.3-$0.5\,f_y$	0.8
Rectangular hollow section RHS, N+M$_y$	$-0.2\,f_y$ $+0.5\,f_y$	0.4
Circular Hollow Section CHS, N+M	$\pm 0.15\,f_y$	0.6
I-section, weak axis buckling N+M$_z$	± 0.3-$0.5\,f_y$	0.6
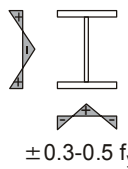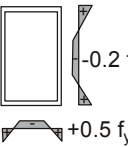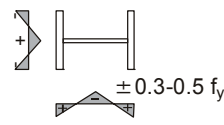
Table 9-2   *Recommended values for ρ to be used in expressions (9.34) and (9.35)*

It shall be noticed that a lower value of ρ is an indicator of a more lenient behaviour from the point of view of the plastic-elastic transition of the applicable cross-sectional N+M interaction curve in inelastic buckling. Since residual stresses play a significant role in this context, the values assumed in GMNIA calculations are also included in Table 9-2. They are believed to be responsible for much of the differences in the applicable value ρ, specifically for the large difference between the I-section and the rectangular hollow section, both under N+M_y.

9.4.4. Ayrton-Perry formulation of the buckling reduction factors $\chi_{y,\eta0}$ and χ_{ip}

The ground has been prepared now for the development of Ayrton-Perry type formulation for generalized buckling reduction factors for the overall N+M load case $\chi_{y,\eta0}$ and χ_{ip}. The variables shown in Fig 9-12 will thereby be used in the following. The necessary, missing steps that lead up to the desired formulation are listed in the following. For reasons of better readability, the equations are written down for the strong-axis in-plane buckling case (indices "y"); the weak-axis in-plane case would lead to the same results, with only a change of index to "z".

i. The first step consists of formulating the failure equation that describes the maximum combination of $n=N/N_{pl}$ and the second order value of $m^{II}=M_y^{II}/M_{y,pl}$ under consideration of the transitional, linearized cross-sectional interaction described in the previous section:

$$n = \frac{1}{k_{ni}*} - \frac{m^{II}}{1/k_{mi}*} \cdot \frac{1}{k_{ni}*} \longrightarrow k_{ni}* \cdot \frac{N}{N_{pl}} + k_{mi}* \cdot \frac{M_y^{II}}{M_{y,pl}} = 1.0 \qquad (9.36)$$

Notice that this is a *linear cross-sectional interaction equation.* This is essential to the present derivation. In a beam-column with imperfections and loaded by axial forces N and first-order bending moments M_y, the total bending moment at failure contains second-order moments and is therefore written as M_y^{II} in (9.36).

It shall be noted that the index "i" of the factors k* is to be determined by the value of the loading ratio $\eta_0=m_0/n_0$; if, for example, η_0 is smaller than η_{SC1} in Table 9-1 for the studied section, the index "1" applies for the rest of the calculation.

ii. In the case of a simply supported beam-column with sinusoidal geometric imperfections of amplitude $\bar{e}_0$ and a sinusoidal bending moment diagram with maximum value M_S, M^{II} is calculated as follows, using the well-known elastic amplification factor.

$$M_y^{II} = \left(M_{y,S} + N \cdot \bar{e}_0\right) \cdot \frac{1}{1 - N/N_{cr,y}} \qquad (9.37)$$

Since the first-order bending moment diagram will only rarely be sinusoidal, it is customary to make use of "equivalent moment factors" C_{mS} as corrective multipliers of M_y, thus yielding:

$$M_y^{II} = \left(C_{mS} \cdot M_y + N \cdot \bar{e}_0 \right) \cdot \frac{1}{1 - N / N_{cr,y}} \tag{9.38}$$

iii.   The buckling failure equation can now be written in the following form by combining (9.36) and (9.38):

$$k_{ni} \ast \cdot \frac{N}{N_{pl}} + k_{mi} \ast \cdot \frac{\left(C_{mS} \cdot M_y + N \cdot \bar{e}_0 \right)}{M_{y,pl}} \cdot \frac{1}{1 - N / N_{cr,y}} = 1.0 \tag{9.39}$$

iv.   In order to account for the effects of the geometric imperfections in a consistent way, with a smooth transition to the pure column buckling case when η_0 and M are zero, it is convenient to recall the derivation of the formulae that describe the ECCS (now EC3) column buckling curves in chapter 5, section 5.3. For $M_y=0.0$, equation (9.39) is written as follows:

$$k_{ni} \ast \frac{N}{N_{pl}} + k_{mi} \ast \cdot \frac{N \cdot \bar{e}_0}{M_{y,pl}} \cdot \frac{1}{1 - N / N_{cr,y}} = 1.0 \tag{9.40}$$

By expanding the second summand by N_{pl}/N_{pl}, we obtain

$$k_{ni} \ast \frac{N}{N_{pl}} + k_{mi} \ast \cdot \frac{N_{pl} \cdot \bar{e}_0}{M_{y,pl}} \cdot \frac{N}{N_{pl}} \cdot \frac{1}{1 - N / N_{cr,y}} = 1.0 \tag{9.41}$$

Other than the factors $k_{n1}\ast$ and $k_{m1}\ast$, this equation is identical with (5.1) and can be rewritten in normalized form by introducing $\chi_y = N/N_{pl}$ $\bar{\lambda}_y = \sqrt{N_{pl} / N_{cr,y}}$:

$$k_{ni} \ast \cdot \chi_y + k_{mi} \ast \cdot \frac{N_{pl} \cdot \bar{e}_0}{M_{y,pl}} \cdot \frac{\chi_y}{1 - \chi_y \cdot \bar{\lambda}_y^2} = 1.0 \tag{9.42}$$

According to section 5.3.1, the next step leading to an explicit formulation for χ_y consists of introducing the Ayrton-Perry generalized imperfection η_{imp} (9.43) and replacing this term with the generalized imperfection definition for column buckling of Eurocode 3, (9.44).

$$\eta_{imp} = k_{mi} \ast \cdot \frac{N_{pl} \cdot \bar{e}_0}{M_{y,pl}} \tag{9.43}$$

$$\eta_{imp} = \eta_{imp,EC3} = \alpha \cdot \left(\bar{\lambda}_y - 0.2 \right) \tag{9.44}$$

By using (9.44) and (9.43) in (9.42), and considering that for M=0, $\eta_0=0.0<\eta_{SC1} \longrightarrow$ $k_{ni}\ast=1.0$, it is easily shown that (9.42) leads to the Eurocode design curve for column buckling. The important aspect here is to note that, in order to be consistent with the Eurocode regulations for columns under pure axial compression, the imperfection amplitude $\bar{e}_0$ must be replaced as follows:

$$\overline{e}_0 = \frac{M_{y,pl}}{N_{pl} \cdot k_{mi}{}^*} \cdot \eta_{imp,EC3} \tag{9.45}$$

v. Equation (9.45) can now be used in (9.39) to obtain (9.46):

$$k_{ni}{}^* \cdot \frac{N}{N_{pl}} + k_{mi}{}^* \cdot \frac{\left(C_{mS} \cdot M_y + N \cdot \dfrac{M_{y,pl}}{N_{pl} \cdot k_{mi}{}^*} \cdot \eta_{imp,EC3} \right)}{M_{y,pl}} \cdot \frac{1}{1 - N/N_{cr,y}} = 1.0 \tag{9.46}$$

which can be simplified as follows:

$$k_{ni}{}^* \cdot \frac{N}{N_{pl}} + \left(k_{mi}{}^* \cdot C_{mS} \cdot \frac{M_y \cdot N_{pl}}{M_{y,pl} \cdot N} + \eta_{imp,EC3} \right) \cdot \frac{N}{N_{pl}} \cdot \frac{1}{1 - N/N_{cr,y}} = 1.0 \tag{9.47}$$

vi. It can now be observed that the term $(M_y \cdot N_{pl})/(M_{y,pl} \cdot N)$ in (9.47) is identical to the definition of the ratio $\eta_0 = m_0/n_0$ used e.g. for the definition of the overall in-plane slenderness in (9.27) and the following. Additionally, at failure the ratio N/N_{pl} is identical to the sought-for reduction factor $\chi_{y,\eta0}$, see Fig 9-12. By introducing η_0, as well as the normalized variables $\chi_{y,\eta0} = N/N_{pl}$ and $\overline{\lambda}_y = \sqrt{N_{pl}/N_{cr,y}}$, we obtain:

$$k_{ni}{}^* \cdot \chi_{y,\eta0} + \left(k_{mi}{}^* \cdot C_{mS} \cdot \eta_0 + \eta_{imp,EC3} \right) \cdot \frac{\chi_{y,\eta0}}{1 - \chi_{y,\eta0} \cdot \overline{\lambda}_y{}^2} = 1.0 \tag{9.48}$$

The term $\left(k_{mi}{}^* \cdot C_{mS} \cdot \eta_0 + \eta_{imp,EC3} \right)$ is designated η_{tot} in the following:

$$\eta_{tot} = k_{mi}{}^* \cdot C_{mS} \cdot \eta_0 + \eta_{imp,EC3} \tag{9.49}$$

This leads to: $$k_{ni}{}^* \cdot \chi_{y,\eta0} + \eta_{tot} \cdot \frac{\chi_{y,\eta0}}{1 - \chi_{y,\eta0} \cdot \overline{\lambda}_y{}^2} = 1.0 \tag{9.50}$$

vii. Equation (9.50) is once again a quadratic equation in $\chi_{y,\eta0}$ that can now be solved and progressively simplified, as was shown for the original Ayrton-Perry derivation in chapter 2, section 2.5:

$$\chi_{y,\eta0} = \frac{-0.5\sqrt{\overline{\lambda}_y{}^4 - 2 \cdot (k_{ni}{}^* - \eta_{tot}) \cdot \overline{\lambda}_y{}^2 + (k_{ni}{}^* + \eta_{tot})^2} - \left(\overline{\lambda}_y{}^2 + k_{ni}{}^* + \eta_{tot} \right)}{k_{ni}{}^* \cdot \overline{\lambda}_y{}^2} \tag{9.51}$$

$$\chi_{y,\eta0} = \frac{-0.5\sqrt{\left(\overline{\lambda}_y{}^2 + k_{ni}{}^* + \eta_{tot} \right)^2 - 4 \cdot k_{ni}{}^* \cdot \overline{\lambda}_y{}^2} - \left(\overline{\lambda}_y{}^2 + k_{ni}{}^* + \eta_{tot} \right)}{k_{ni}{}^* \cdot \overline{\lambda}_y{}^2} \tag{9.52}$$

$$\left(\overline{\lambda}_y{}^2 + k_{ni}{}^* + \eta_{tot} \right) = 2 \cdot \Phi_{ip} \tag{9.53}$$

$$\chi_{y,\eta 0} = \frac{-0.5\sqrt{4 \cdot \Phi_{ip}{}^2 - 4 \cdot k_{ni} * \cdot \overline{\lambda}_y{}^2} - 2 \cdot \Phi_{ip}}{k_{ni} * \cdot \overline{\lambda}_y{}^2} \tag{9.54}$$

The following step includes an expansion by the complementary term.

$$\chi_{y,\eta 0} = \frac{\Phi_{ip} - \sqrt{\Phi_{ip}{}^2 - k_{ni} * \cdot \overline{\lambda}_y{}^2}}{k_{ni} * \cdot \overline{\lambda}_y{}^2} \cdot \left(\frac{\Phi_{ip} + \sqrt{\Phi_{ip}{}^2 - k_{ni} * \cdot \overline{\lambda}_y{}^2}}{\Phi_{ip} + \sqrt{\Phi_{ip}{}^2 - k_{ni} * \cdot \overline{\lambda}_y{}^2}} \right) \tag{9.55}$$

viii. By further simplifying and reducing terms in the fraction, the following, Ayrton-Perry type equation is finally obtained:

$$\chi_{y,\eta 0} = \frac{1}{\Phi_{ip} + \sqrt{\Phi_{ip}{}^2 - k_{ni} * \cdot \overline{\lambda}_y{}^2}} \tag{9.56}$$

Equation (9.56) is almost identical to the Ayrton-Perry design formula for flexural column buckling found in the Eurocode, with the main differences lying in the presence of the transitional cross-sectional interaction parameters k*, as well as in the presence of the first-order bending moment in the ratio η_0 and thus in η_{tot}, as well as the appropriate value of the equivalent, sinusoidal bending moment factor C_{mS}. The latter factor will be specifically addressed in the following section 9.4.5.

Expression (9.56) is referred to the maximum load amplification factor for a combination of N+M_y, but applied as a buckling reduction factor to the axial force resistance N_{pl}. This is the form of representation of the buckling strength discussed in section 9.3.1 and first applied in Fig 9-6b. In order to write the buckling factor in terms of a factor χ_{ip} as function of the "overall" in-plane slenderness $\overline{\lambda}_{ip}$, equations (9.30) and (9.32) have to be used, leading to the following relationships

$$\chi_{ip} = \frac{R_{b,ip}}{R_{pl}} = \frac{\chi_{y,\eta 0}/n_o}{1/(n_0 \cdot c_0)} = \chi_{y,\eta 0} \cdot c_0 \tag{9.57}$$

$$\chi_{ip} = \frac{c_0}{\Phi_{ip} + \sqrt{\Phi_{ip}{}^2 - k_{ni} * \cdot \overline{\lambda}_{ip}{}^2 \cdot c_0}} \leq 1.0 \tag{9.58}$$

With

$$\Phi_{ip} = \frac{1}{2} \cdot \left(k_{ni} * + \eta_{tot} + \overline{\lambda}_{ip}{}^2 \cdot c_0 \right) \tag{9.59}$$

Or if η_{tot} is written out:

$$\Phi_{ip} = \frac{1}{2} \cdot \left(k_{ni} * + \left(k_{mi} * \cdot C_{mS} \cdot \eta_0 + \eta_{imp,EC3} \right) + \overline{\lambda}_{ip}{}^2 \cdot c_0 \right) \tag{9.60}$$

Thereby, the fully plastic, cross-sectional interaction factor c_0 is equal to $\left(k_{ni} + \eta_0 \cdot k_{mi} \right)$. The differences between k_{ni} / k_{mi}, which refer to the full plastic cross-sectional interaction curve, and k_{ni} */ k_{mi}*, which refer to the transitional interaction, must of course be kept in mind here.

9.4.5. Sinusoidal equivalent moment factors C_{mS}

The derivation of section 9.4.4 requires the use of equivalent *sinusoidal* moment factors C_{mS} whenever a bending moment diagram is present that is not sinusoidal. As Gonçalves & Camotim (2004) noted, the importance of a correct distinction between equivalent moment factors for *uniform* and *sinusoidal* bending moments is often not fully appreciated. Furthermore, the equivalent uniform bending moment coefficients (C_{mU}) have usually been formulated in the literature in a way that omits the effects of the axial force level N/N_{cr}, while the sinusoidal coefficients C_{mS} usually include this effect, adding to the confusion in the application of the two formulations. One typical example for the omission of the axial load effects in the C_{mU} factors is the often-used formula proposed by Austin (1961) for constant moment-gradient diagrams: $C_{mU}=0.6+0.4\Psi$.

In the above derivation of an Ayrton-Perry type formula for in-plane buckling of beam-columns, the tacit assumption was also made that the sinusoidal, equivalent moment factor is *independent of the level of axial force*. The developed, explicit formulation of $\chi_{y,\eta0}$ or χ_{ip} as a function of the slenderness and plastic strength is only rigorous if no additional terms containing N are present. In reality, however, the equivalent sinusoidal bending moments are dependent on the ratio $N/N_{cr,y}$ for all but the basic case of a sinusoidal moment diagram. For many basic cases, functions for C_{mS} are found in the literature, see e.g. Petersen (1993) or Chen (2007):

i. parabolic bending moment diagram: $C_{mS} = 1 + 0.03 \cdot \dfrac{N}{N_{cr,y}}$ (9.61)

ii. constant bending moment diagram: $C_{mS} = 1 + 0.27 \cdot \dfrac{N}{N_{cr,y}}$ (9.62)

iii. triangular bending moment diagram: $C_{mS} = 1 - 0.18 \cdot \dfrac{N}{N_{cr,y}}$ (9.63)

The ratio $N/N_{cr,y}$ can be re-written as follows:

$$\frac{N}{N_{cr,y}} = \frac{N}{N_{pl}} \cdot \frac{N_{pl}}{N_{cr,y}} = \chi_{y,\eta0} \cdot \bar{\lambda}_y{}^2 = \frac{\chi_{ip}}{c_0} \cdot \bar{\lambda}_y{}^2 \tag{9.64}$$

It can be seen that (9.64) contains the (unknown) variable $\chi_{y,\eta0}$, respectively χ_{ip}. The presence (within C_{mS} and thus η_{tot}) of this additional term $\chi_{y,\eta0}$ was not considered when solving expression (9.50), and would have prevented the explicit solution for $\chi_{y,\eta0}$ or χ_{ip} of (9.56) or (9.58). This term must therefore be replaced by an accurate-enough, "pre-emptive" estimation of $\chi_{y,\eta0}$ or χ_{ip}. For this purpose, the following expression is proposed, based on a simple Merchant-Rankine formulation for $\chi_{ip}=f(\bar{\lambda}_{ip})$, see section 2.4 of chapter 2, equation (2.19):

$$\chi_{ip} \approx \frac{1}{1+\bar{\lambda}_{ip}{}^2} = \frac{1}{1+\bar{\lambda}_y{}^2 / c_0} \tag{9.65}$$

By using (9.65) in (9.64), we obtain the following expression for the approximation n_{ce} of N/N_{cr}:

$$\frac{N}{N_{cr,y}} \cong n_{ce} = \frac{\bar{\lambda}_y^{\,2}}{\left(c_0 + \bar{\lambda}_y^{\,2}\right)} \tag{9.66}$$

It can be seen that this expression is independent of the load level N, making its application in the context of the derivation of section 9.4.5 possible. It is therefore proposed to calculate the equivalent moment factors C_{mS} by replacing terms with $N/N_{cr,y}$ with n_{ce}.

One might ask whether (9.66) is accurate enough, and why one should need the Ayrton-Perry formula (9.58) if (9.65) were accurate. The following can be said with respect to this:

i.   Obviously, the expression (9.65) is not very accurate in describing χ_{ip} as a function of $\bar{\lambda}_{ip}$. As the comparative calculations in section 9.5 show, the buckling curves in terms of $\chi_{ip}=f(\bar{\lambda}_{ip})$ have a wider scatter band and depend on a variety of factors that are not at all accounted for by (9.65). The differences between (9.65) and the "actual" values can be in the range of ca. 20-30% in some cases. A more accurate formulation like the one proposed in (9.58) is therefore definitely needed if the value of χ_{ip} is to be accurately determined.

ii. However, (9.65) is only (implicitly) contained in (9.66), with the intent of using it in the calculation of C_{mS} and η_{tot} of equation (9.59), and not to calculate χ_{ip} itself. It is thus only related to the bending component of the load, which will be of negligible importance at higher values of N/N_{cr}, i.e. when the influence of the axial force on C_{mS} is the greatest.

iii. Furthermore, it can be shown that (9.65) and thus (9.66) result in rather high, conservative estimates of N/N_{cr} whenever the bending component is dominant, i.e. when the beam-column is subjected to high "imperfections" in the sense of first-order deflections, see the discussion of Fig 2-9 in chapter 2. A certain, minor degree of additional conservatism in the bending term can be thought of as being acceptable in this context.

The use of (9.66) therefore appears to be fully justified in the context of the calculation of C_{mS} values, thus allowing for an accurate application of the Ayrton-Perry formulations (9.56) and (9.58) also for cases where the bending moment diagram is not sinusoidal.

9.4.6. Summary of the proposed formulation

Several different aspects had to be discussed in section 9.4 in order to explain the background of the newly proposed Ayrton-Perry formulations (9.56) and (9.58). In order to facilitate understanding of the proposal, it is summarized in the following in a more compact form resembling code clauses.

(1) The in-plane buckling resistance of beam-columns subjected to $N+M_j$, with j being the axis (y or z) about which the bending moment acts, may be determined using the following formulae:

$$R_d = R_{b,ip} = \frac{\chi_{ip} \cdot R_{pl}}{\gamma_{M1}} \overset{!}{\geq} 1.0 \qquad (9.67)$$

with $R_{b,ip}$:   amplification factor of the design load combination $N_d+M_{j,d}$ that results in the achievement of the ultimate, in-plane buckling condition.

R_{pl}:   amplification factor of the design load combination $N_d+M_{j,d}$ that results in the achievement of the plastic section capacity.

χ_{ip}:   overall, in-plane buckling reduction factor.

(2) The plastic amplification factor may be determined using the following set of formulae:

$$R_{pl} = \frac{\eta_0}{m_0 \cdot c_0} = \frac{1}{n_0 \cdot c_0} \qquad (9.68)$$

with m_0, n_0: ratios between the design levels of the load components N_d and $M_{j,d}$ to the respective plastic section capacities: $m_0=M_d/M_{pl}$; $n_0=N_d/N_{pl}$

η_0:   ratio of m_0/n_0

c_0:   plastic cross-sectional capacity factor; $c_0=\left(k_{ni} + \eta_0 \cdot k_{mi}\right)$

The cross-sectional capacity factor c_0 may be calculated with the specific values of k_{ni} and k_{mi} valid for the studied cross-sectional type, taken from Table 9-3. Thereby, the index of the applicable factors k_{ni} is decided by the following case distinction:

-   If $\eta_0 < \eta_{SC1}$: $k_{ni}=k_{n1}$; $k_{mi}=k_{m1}$

-   If $\eta_{SC1} \leq \eta_0 < \eta_{SC2}$: $k_{ni}=k_{n2}$; $k_{mi}=k_{m2}$

-   If $\eta_{SC2} \leq \eta_0 < \eta_{SC3}$: $k_{ni}=k_{n3}$; $k_{mi}=k_{m3}$

#	Type of section, loading, underlying residual stress distributions	Parameters of the N-M interaction linearization	ρ
1	I-section, strong axis buckling N+M_y ±0.3-0.5 f_y	$k_{n1}=1.0$; $k_{m1}=1-0.5\cdot a\geq0.75$; $\eta_{SC1}=\dfrac{0.8}{1-0.8\cdot k_{m1}}$	0.8
2	Rectangular hollow section RHS, N+M_y -0.2 f_y +0.5 f_y	$k_{n2}=\dfrac{0.2}{1-0.8\cdot k_{m1}}$; $k_{m2}=1.0$; $\eta_{SC2}=\infty$	0.4
3	Circular Hollow Section CHS, N+M ±0.15 f_y	$k_{n1}=1.0$; $k_{m1}=0.74$; $\eta_{SC1}=\dfrac{0.8}{1-0.8\cdot k_{m1}}=1.95$ $k_{n2}=\dfrac{0.2}{1-0.8\cdot k_{m1}}=0.49$; $k_{m2}=1.0$; $\eta_{SC2}=\infty$	0.6
4	I-section, weak axis buckling N+M_z ±0.3-0.5 f_y	$k_{n1}=1.0$; $k_{m1}=\dfrac{1-a}{1.45}$; $\eta_{SC1}=\dfrac{0.8}{1-0.8\cdot k_{m1}}$ $k_{n2}=\dfrac{0.8}{1.81-a}$; $k_{m2}=\dfrac{1-a}{1-0.55\cdot a}$; $\eta_{SC2}=\dfrac{1}{a}$ $k_{n3}=0.0$; $k_{m3}=1.0$; $\eta_{SC3}=\infty$	0.6
$a=\dfrac{A-2\cdot b\cdot t_f}{A}=\dfrac{A_w}{A}$			
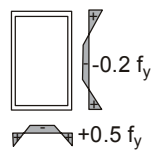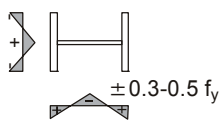
Table 9-3 *Summary of the coefficients used for the description of the cross-sectional N+M interaction behaviour.*

(3) The overall, in-plane buckling reduction factor can be calculated by using the following equation:

$$\chi_{ip}=\frac{c_0}{\Phi_{ip}+\sqrt{\Phi_{ip}^2-k_{ni}*\cdot\overline{\lambda}_{ip}^2\cdot c_0}}\leq1.0 \qquad (9.69)$$

with

$$\Phi_{ip}=\frac{1}{2}\cdot\left(k_{ni}*+\eta_{tot}+\overline{\lambda}_{ip}^2\cdot c_0\right) \qquad (9.70)$$

and $\overline{\lambda}_{ip}$:   overall, in-plane normalized slenderness, calculated as follows: $\overline{\lambda}_{ip}=\overline{\lambda}_j/\sqrt{c_0}$.

η_{tot}:   total value of the generalized Ayrton-Perry imperfection:

$\eta_{tot}=k_{mi}*\cdot C_{mS}\cdot\eta_0+\eta_{imp,EC3}$, with

$\eta_{imp,EC3} = \alpha \cdot \left(\overline{\lambda}_j - 0.2\right)$; generalized imperfection for column buckling according to clause 6.3.1.2 of EC3 – EN 1993-1-1.

C_{mS}: equivalent sinusoidal moment factor, calculated with the formulae given in Fig 9-4.

k_{ni}^*, k_{mi}^*: slenderness-dependent, transitional cross-sectional capacity coefficients, see (4)

#	Moment diagram	C_{mS} [-]
1		$C_{mS} = 1 + 0.27 \cdot n_{ce}$
2		$C_{mS} = 1 + 0.03 \cdot n_{ce}$
3		$C_{mS} = 1 - 0.18 \cdot n_{ce}$
4	M ⬜ ψ·M	$0.79 + 0.21 \cdot \psi + 0.36 \cdot \left(\psi - 0.33\right) \cdot n_{ce}$ *
$n_{ce} = \dfrac{\overline{\lambda}_j^{\,2}}{\left(c_0 + \overline{\lambda}_j^{\,2}\right)}$ * formula due to Villette et al. (2000); notice that case #4 with Ψ=1.0 is not identical to case #1. A discussion of this formula is given in section 9.5.		
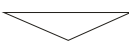
Table 9-4 *Proposed values for the equivalent sinusoidal bending moment factors C_{mS}.*

(4) The factors k_{ni}^* and k_{mi}^* are calculated from a modification of the applicable values of k_{ni} and k_{mi} (with the applicable index i) using the following formulae:

$$k_{ni}^* = k_{ni} + (1 - k_{ni}) \cdot \rho \cdot \overline{\lambda}_{ip} \cdot C_{mS} \leq 1 \tag{9.71}$$

$$k_{mi}^* = k_{mi} + (w - k_{mi}) \cdot \rho \cdot \overline{\lambda}_{ip} \cdot C_{mS} \leq w \tag{9.72}$$

w: ratio of plastic to elastic section moduli: $w = W_{j,pl}/W_{j,el}$.

ρ: factor accounting for the specific transitional behaviour of a certain cross-section type, taken from Table 9-3.

(5) As an equivalent alternative to clause (1), the in-plane buckling resistance may also be formulated in terms of the maximum obtainable axial force $N_{Rd,\eta 0}$ that can be achieved if the design load combination of $N_d + M_{j,d}$ is proportionally increased up to failure:

$$\frac{N_d}{N_{Rd,\eta 0}} = \frac{N_d}{\chi_{j,\eta 0} \cdot N_{pl}} \overset{!}{\leq} 1.0 \tag{9.73}$$

with
$$\chi_{j,\eta 0} = \frac{1}{\Phi_{ip} + \sqrt{\Phi_{ip}^2 - k_{ni} * \cdot \bar{\lambda}_j^2}} \leq \frac{1}{c_0}$$
(9.74)

and the variables in (9.73) taken from clauses (1) to (4).

9.5. Comparison with GMNIA Calculations and EC3 Rules

In this section, the Ayrton-Perry type formulation developed in section 9.4 for the description of the in-plane buckling strength of beam-columns under N+M is compared to the results of GMNIA calculations, carried out mostly using beam element models as outlined in chapter 3. The comparison will be carried out using three different forms of representation:

i. In terms of buckling reduction factors χ_{ip} and $\chi_{y,\eta 0}$
ii. As buckling resistance N+M interaction curves
iii. In terms of the applicable factor k in the terminology of the interaction factor concept

All calculations in this section were carried out for steel grade S235. The residual stress amplitudes used for the GMNIA calculations and shown in the single figures are referred to the yield stress of S235, f_y=235 N/mm². The geometric imperfection was always assumed to have a sinusoidal distribution and to have an amplitude of $\bar{e}_0$=L/1000.

Most calculations refer to the basic case of a constant bending moment diagram. Other cases have also been considered and specifically marked in the figures.

9.5.1. Buckling reduction factors

In the first type of comparison of analytical and GMNIA results, the buckling reduction factors χ_{ip} and $\chi_{j,\eta 0}$ are calculated using equations (9.69) and (9.74), and are plotted together with the equivalent values obtained from GMNIA calculations.

The first group of these plots is shown in Fig 9-13, where results for an IPE 240 and an HEA 300 section, both loaded by strong-axis bending moments plus axial force are shown. Five different ratios of M to N, expressed by the value $\eta_0 = (M \cdot N_{pl})/(N \cdot M_{pl})$, were considered.

The plots in Fig 9-13 show that equations (9.69) and (9.74) are very accurate in describing the calculated resistance of the GMNIA model beam-column with fixed imperfections. Thereby, the analytical line for η_0=0.0 is identical to the Eurocode / ECCS column buckling curve a in both types of representation. This is inherent to the proposed formulation, which makes explicit use of the Eurocode generalized imperfection $\alpha \cdot (\bar{\lambda}_y - 0.2)$, with α=0.21 for the IPE 240 and α=0.34 for the HEA 300 section. It can be observed that the biggest differences –themselves rather small- between the proposed analytical and the GMNIA curve are actually present in the case of the HEA 300 section at η_0=0.0, i.e. when the proposed formulation is identical to the EC3 column buckling curve for this section.
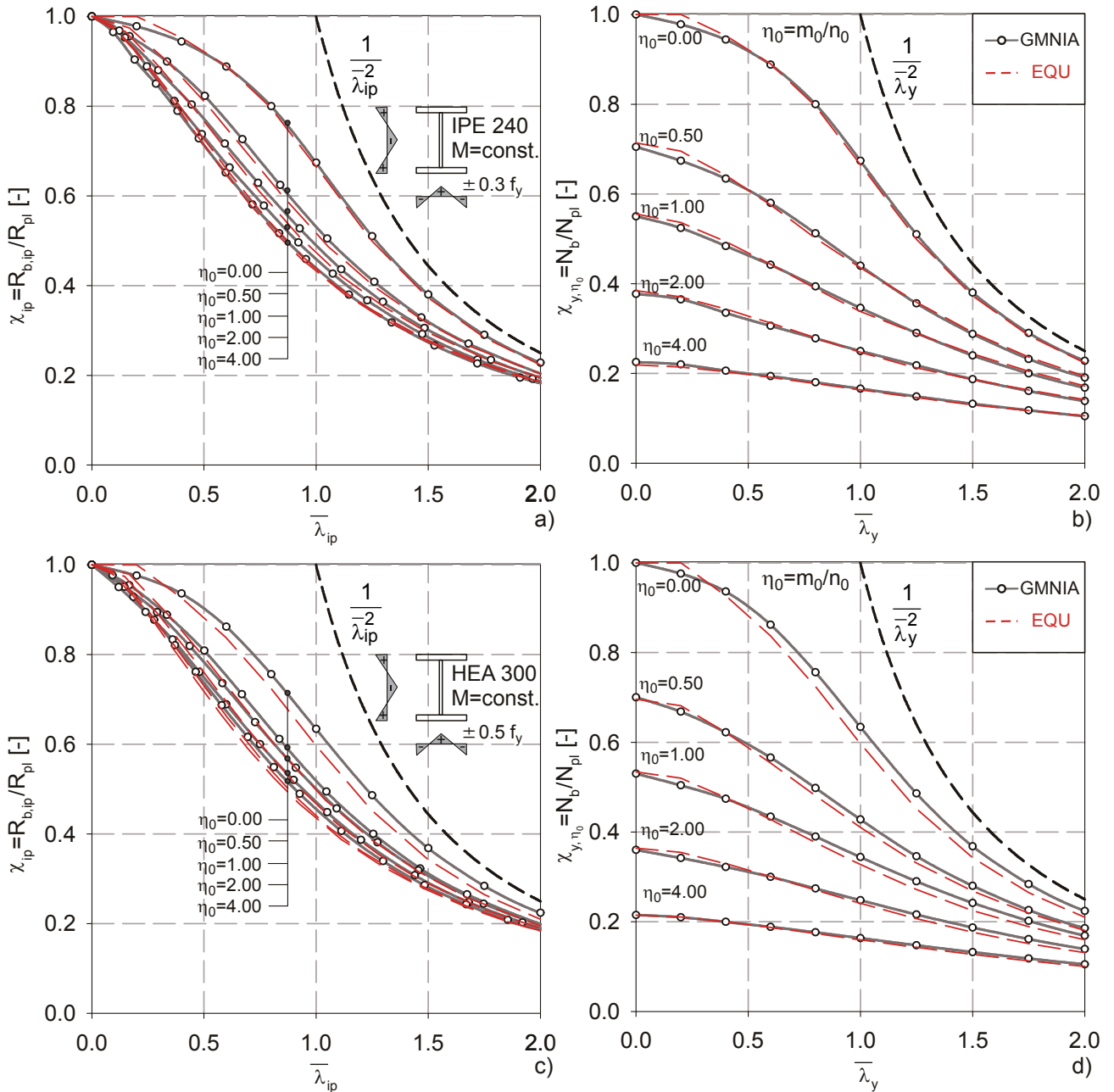
Fig 9-13 *Comparison of buckling reduction factors according to GMNIA calculations and equation (9.69) and (9.74); for an IPE 240 (a-b) and HEA 300 (c-d) section, both under constant bending moment.*

The lines of most interest here, i.e. those where $\eta_0 > 0.0$, which describe cases where the studied beam-column behaviour is present, appear to be very well able to describe the GMNIA buckling loads. Some minor differences in the (apparent) accuracy of the representation in terms of χ_{ip} and $\chi_{y,\eta0}$ are observed; these are due to the fact that different reference values of R_{pl} are used in the case of the $\chi_{ip}=f(\overline{\lambda}_{ip})$ curves, as these are calculated "correctly" in the case of the GMNIA curves by calculating the numerical value of $R_{pl,MNA}$ in a preceding, materially non-linear analysis (MNA); this value is of course not 100% identical to the value of $R_{pl,linearization}$ obtained by applying (9.68), which is based on a linearization of the non-linear plastic N+M interaction curve. However, the

differences between $R_{pl,MNA}$ and $R_{pl,linearization}$ were small in all cases. In the case of the representation in terms of the obtainable axial force, i.e. of $\chi_{y,\eta 0}$, the reference value is $N_{pl}=A \cdot f_y$ in both cases. For an estimation of the "safety" of the proposed formulation, the representation in terms of $\chi_{y,\eta 0}$ is actually more purposeful, as it directly compares obtained strength based on the same basic variable: whenever the analytical line lies below the GMNIA line, the equation is "safe".

Fig 9-14 shows the same type of representation, for the same load case of constant bending moment plus axial force, for two hollow sections, one with circular and one with rectangular section.
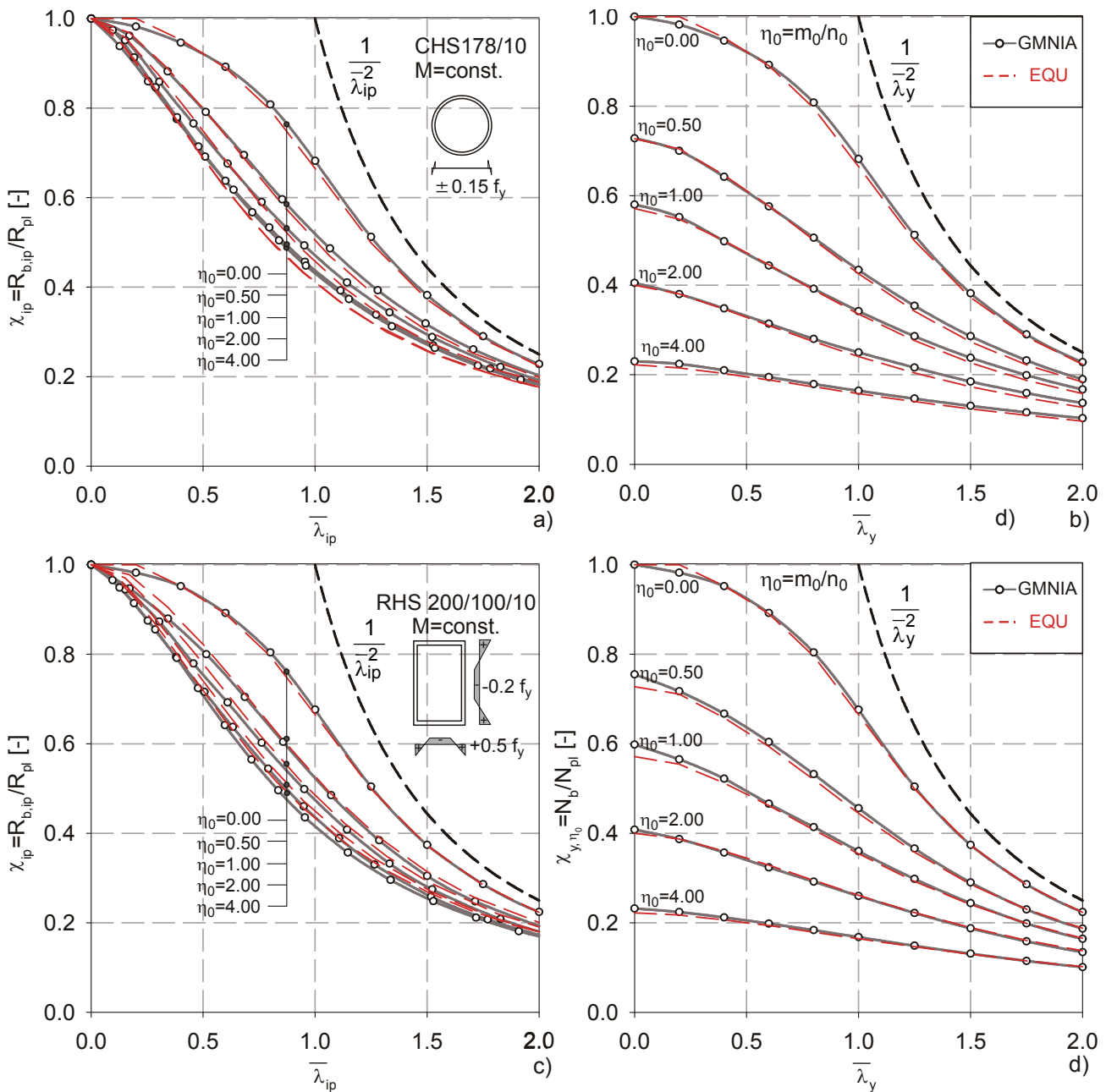
Fig 9-14 *Comparison of buckling reduction factors according to GMNIA calculations and equation (9.69) and (9.74); for a CHS 178/10 (a-b) and RHS 200/100/10 section (c-d), both under constant bending moment.*

The distinctly different residual stress patterns valid for these sections are plotted in the figure. The accuracy of the proposed description is again very satisfactory. As Fig 9-14b and d, the proposed formulation is always slightly safe-sided in terms of $\chi_{y,\eta0}$. In terms of χ_{ip}, the analytical curve appears to be slightly less accurate, but once again this (minimal) inaccuracy is to attributed more on the conservative, linearized approximation of the plastic N+M interaction than on the formulation itself.

As a final type of cross-sectional shape, an HEA 500 section is studied in Fig 9-15 that is loaded by a combination of axial force and constant weak-axis bending moment M_z. For this type of section and loading, a linearization of the cross-sectional plastic interaction curve was proposed in Fig 9-10 that consist of three different (linear) segments. Due to the more distinctly non-linear cross-sectional interaction curve for weak-axis bending, the cross-sectional capacity at $\overline{\lambda}_z = 0.0$ is slightly underestimated by the proposed linearization. This is visible in the small, safe-sided differences between the analytical and GMNIA values of $\chi_{y,\eta0}$ at $\overline{\lambda}_z = 0.0$ for the cases where $\eta_0 = 0.5$, 1.0 and 2.00. At $\eta_0 = 4.00$, the "exact" interaction curve is reached by the linearized one, since for this value of η_0 the vertical portion of the interaction curve (see Fig 9-10b) is valid for this section, meaning that M_{pl} can be reached at $\overline{\lambda}_z = 0.0$ in spite of the presence of some axial force. This fact is included in the proposed formulation.

After having established the high accuracy of the proposed formulation for the most basic case of constant bending moment, it is now interesting to study this accuracy for other load cases. This is done in Fig 9-16 and Fig 9-17 for an IPE 240 subjected to a load combination of N+M_y with different, variable bending moment diagrams.
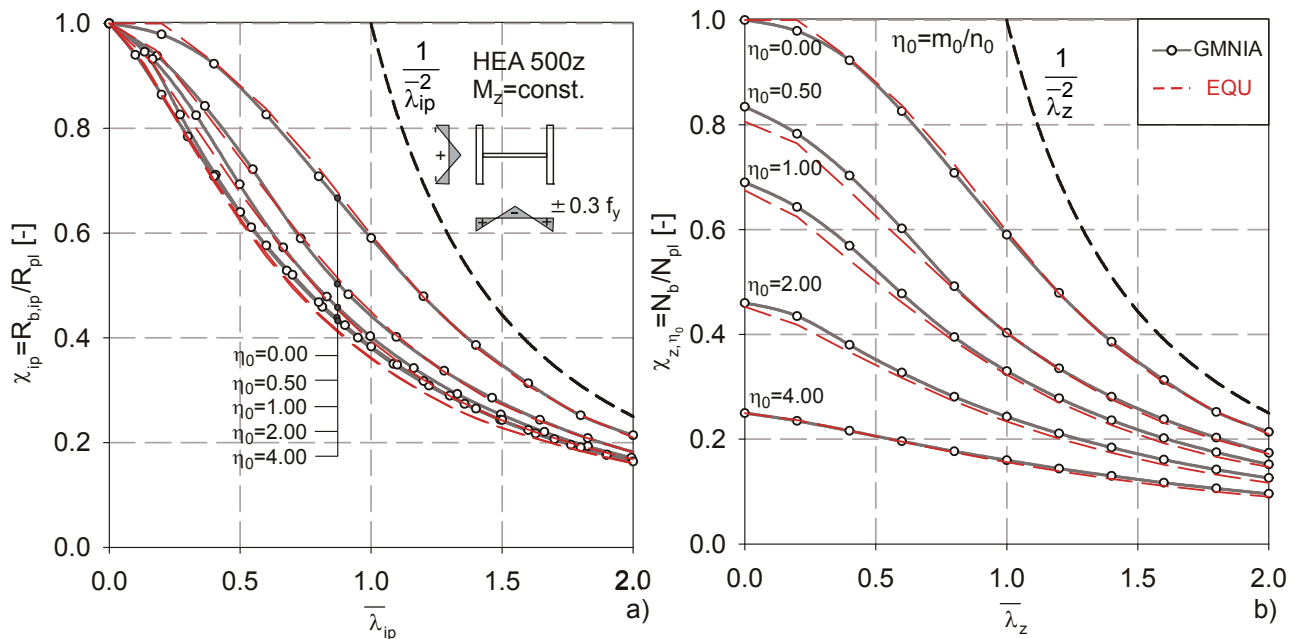
Fig 9-15 *Comparison of buckling reduction factors according to GMNIA calculations and equation (9.69) and (9.74) for a HEA 500 section loaded by N+M_z.*
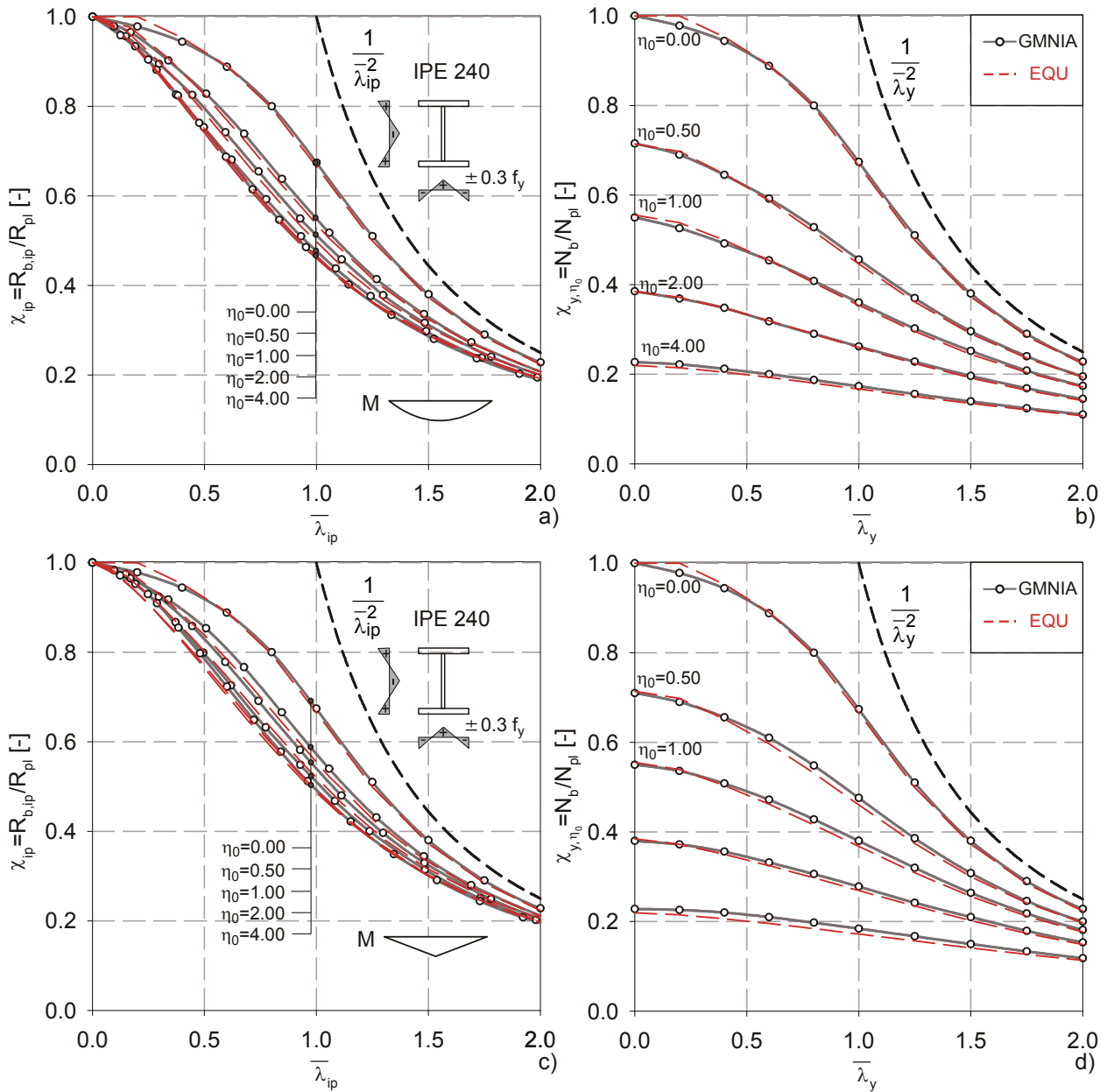
Fig 9-16 *Comparison of GMNIA and analytical buckling reduction factors for an IPE 240 and different load cases, with N+M_y; parabolic (a-b) and triangular moment diagram (c-d).*

Fig 9-16 shows the comparison of proposed analytical and GMNIA curves for the simple cases of parabolic and triangular bending moment with maximum at mid-span. The accuracy in the case of the parabolic bending moment diagram (Fig 9-16a-b) is remarkably high and is probably to be attributed to the high accuracy of the C_{mS} values for this case, which most closely resembles the actual sinusoidal moment diagram that underlies the analytical formulation.

In Fig 9-17, the analytical and GMNIA curves are compared for cases with constant moment gradient, again for an IPE 240 section. Thereby, the formula developed by Villette et al. (2000) is used for the calculation of the equivalent sinusoidal moment factor C_{mS}, see Table 9-4.
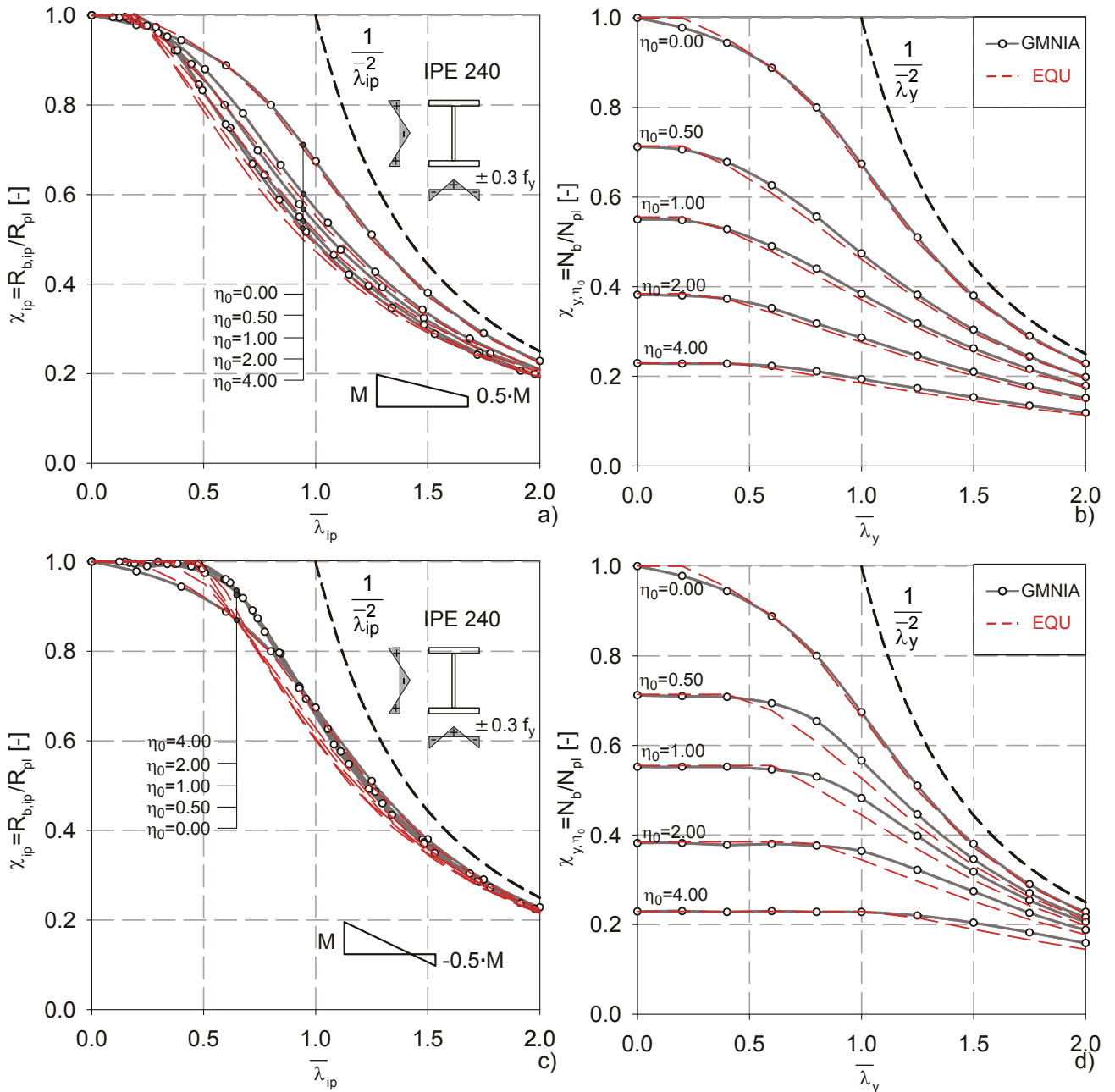
Fig 9-17 *Comparison of GMNIA and analytical buckling reduction factors for an IPE 240 and moment diagrams with constant moment gradients; for Ψ=0.5 (a-b) and Ψ=-0.5 (c-d).*

The following aspects are of interest here, which are particularly well observable in Fig 9-17c and d, which deal with a moment diagram with sign change and Ψ=-0.5:

i.   The sign change of the moment gradient leads to a buckling/ultimate strength behaviour that is largely dominated by the cross-sectional capacity at the beam-column's extremity, i.e. where the highest first-order bending moment is acting, for all but very high slenderness values. This becomes increasingly true with higher values of η_0, i.e. with an increasing bending moment component of the load. This is observed in the wide extension of the

"plateau" in both types of representation, particularly in the plot in terms of $\chi_{y,\eta 0}$, in the case of $\Psi=-0.5$.

ii. The proposed analytical expression is very well able to reproduce this behaviour as observed in GMNIA calculations. Both the formulation for χ_{ip} and for $\chi_{y,\eta 0}$ are explicitly limited by the plastic cross-sectional capacity of the section, which leads to the observed plastic plateau. Through the selection of a more appropriate value of C_{mS} for the given load case, the extension of the plateau value would be reached.

iii. For the particular case of constant moment gradients, the formula contained in Table 9-4, as well as in Annex A of EC3- EN 1993-1-1, appears to be a somewhat conservative, yet acceptable approximation. The conservativeness is most likely to be attributed to the fact that the formula is based purely on the elastic second-order moment amplification, while the GMNIA curves of course include effects of plasticity. As Kaim (2004) pointed out, other formulae, particularly the already mentioned formula by Austin (1961), can actually be shown to be more accurate for the description of the beam-column buckling strength in the elasto-plastic case.

9.5.2. N-M buckling interaction diagrams

In Fig 9-18, a different type of representation is used to compare the results of the analytical formulation of equation (9.69) with results of GMNIA calculations. The plots in this figure show the predicted ultimate buckling strength in terms of maximum obtainable pairs of N+M for different sections and different slenderness values. All calculations were carried out for the most basic load case of constant bending moment plus axial force.

The plots once again confirm the high accuracy obtained by the application of the proposed analytical formulation. The analytical description closely follows the GMNIA curves throughout all values of η_0 for all four shown sections, and gives minimally "conservative" results for almost all points.

A characteristic feature of the analytical interaction curves is the fact that a certain, minor slope discontinuity is present at certain values. In the plots, this is perhaps best appreciated for the case of weak-axis buckling of the HEA 500 section (Fig 9-18b). The discontinuity (primarily of slope) is a direct reflection of the underlying shape of the cross-sectional interaction curve. Since this curve was segmentally linearized, and this linearization is maintained (with the same points of slope change at $\eta_0=\eta_{SCi}$) also for the transitional, slenderness-dependent interaction discussed in section 9.4.3, it is clear that the change of the underlying segment of the interaction linearization also causes a certain discontinuity of the resulting buckling strength interaction plots. However, this does not present any practical disadvantages for the user of the proposed design formulae, who will generally be interested in a discrete strength prediction.
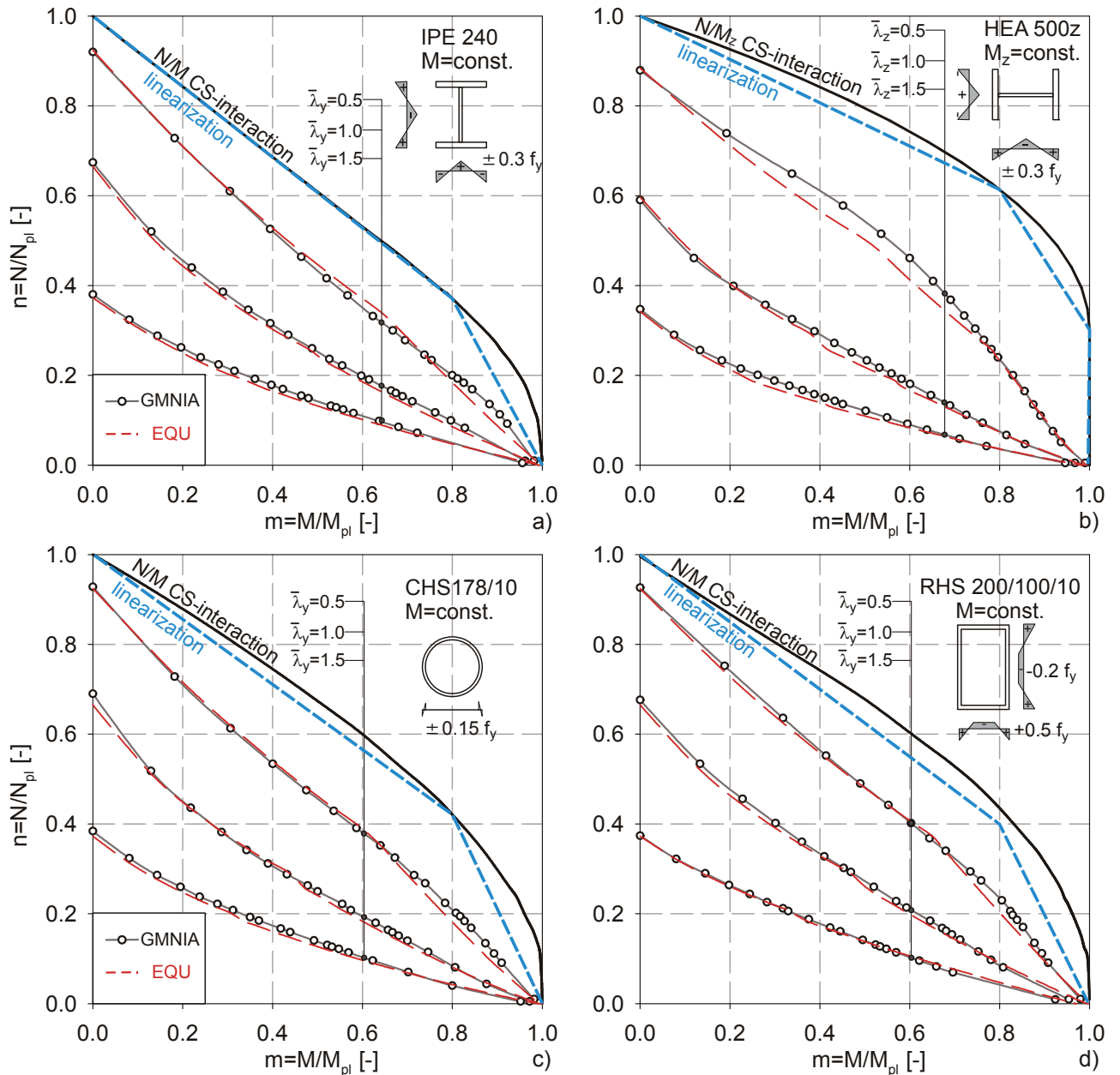
Fig 9-18 *Comparison of GMNIA and analytical results in terms of N+M interaction curves for different sections and values of $\overline{\lambda}$; constant bending moment diagram.*

One advantage of the proposed formulation, when compared with the current Eurocode design rules based on the interaction concept described in section 9.3.3, is the fact that the transition of cross-sectional check to buckling check is explicitly included and very accurate. This is due to the fact that, unlike the interaction concept curves, the proposed formulae are based on a very accurate, linearized approximation of the *actual* cross-sectional N+M interaction curve of the studied section; a comparison between the underlying cross-sectional interaction curves of Fig 9-8 and the linearization of the actual curves in Fig 9-18 clearly illustrates this. This fact is particularly felt in the case of in-plane buckling checks with N+M where the bending moment diagram has a rather steep gradient, see Fig 9-19.
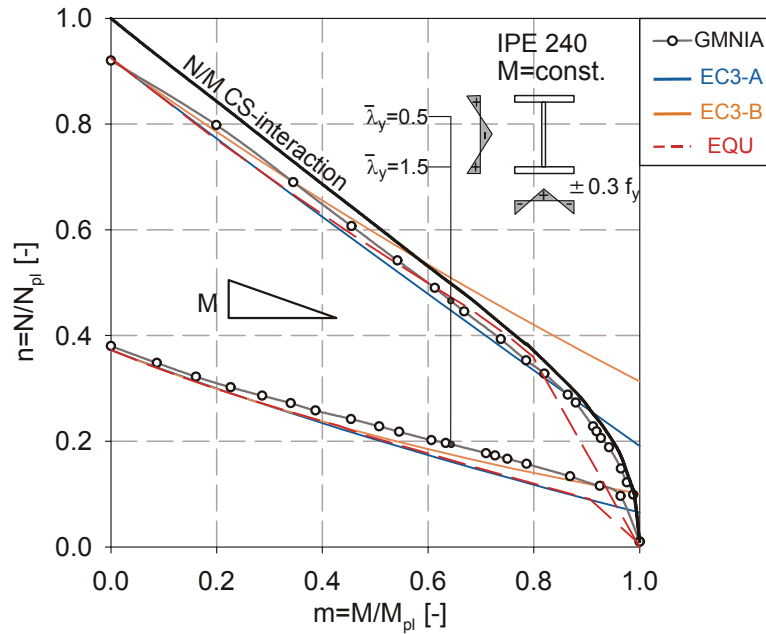
Fig 9-19 *Comparison of GMNIA and analytical results in terms of N+M interaction curves; analytical resistance calculated with the interaction coefficients of Annex A & B of EC3, as well as the proposed formulation for χ_{ip}; moment diagram with constant gradient, $\Psi=0.0$.*

In these cases, especially in cases where the bending moment is dominant, the buckling checks using the interaction concept in EC3 can result in a prediction of the buckling strength that exceeds the cross-sectional interaction curve. This is due to the fact that the buckling check using the interaction concept is referred –through the equivalent moment coefficient C_m- to a point in the member where the largest stability effects are present. In the case of the bending moment diagram in Fig 9-19, this point might not be the critical, strength-determining point in the member when stability effects are not too significant. In these cases, the strength will be dominated by the cross-sectional N+M interaction at the beam-column's extremity. Since the proposed formulation is based on a precise representation of this exact strength, and the buckling reduction factor χ_{ip} according to (9.69) has an upper limit value of 1.0, cross-sectional and buckling check are covered by the same design formula in the proposed formulation. This is not the case for the interaction concept formulae, as can be seen in Fig 9-19, where for $\bar{\lambda}_y=0.5$ both the interaction lines calculated by using the coefficients of EC3 Annex A and (even more so) B exceed the cross-sectional capacity beyond certain values of m. This is the reason why the EC3 design formulae explicitly require checks of the cross-sectional capacity at the member ends in addition to the buckling check.

As far as the accuracy of the proposed formulation is concerned for the case studied in Fig 9-19, it can be said that the proposal again shows a high accuracy, comparable to the one obtained by using the EC3 interaction concepts. When compared to the cases with constant bending moment diagram of Fig 9-18, the proposed formulation appears to be somewhat more conservative, particularly for higher slenderness, where it follows the EC3 Annex A curve very closely. This is to be attributed to the use of the same C_{mS} value for this loading case. As was already mentioned in the context of Fig

9-17, the equivalent sinusoidal moment equation in Table 9-4for this load case is rather conservative at higher slenderness. The Annex B interaction curves make use of the Austin formula, which is slightly more accurate –and less conservative- in describing the inelastic buckling behaviour of beam-column. This is reflected in Fig 9-19, where the Annex B curves lie slightly higher than the other two analytical curves.

9.5.3. Interaction factor k_{yy}

One additional form of comparison is used in this section in order to illustrate the differences between the proposed formulation, GMNIA results and the existing rules found in the Eurocode. The results are thereby compared in terms of *interaction coefficients* k, as presented in section 9.2 and defined in 9.3.1.

The methodology used to obtain the GMNIA results for these coefficients has already been described in the context of Fig 9-9. The Eurocode coefficients are explicit formulations for the interaction coefficients and are therefore fairly easily calculated with the formulae of section 9.3.3. In the case of the proposed Ayrton-Perry type formulation, however, the factors k_y or k_z cannot be directly calculated, at least not in a form that is fully compatible with the interaction concept design expression of clause 6.3.3 of EC3- EN 1993-1-1. This is due to the fact that the proposed Ayrton-Perry formulation entails a *total load amplification*, where the ratio of M to N is considered to be fixed and the design resistance is expressed in terms of a load amplification factor R_d for the combined load case, see (9.67). This factor corresponds to the inverse of the utilization of the beam-column under the design load. In the case of the interaction coefficients, however, not the ratio of M/N, but the utilization of the pure flexural column buckling case $n_j = N / (\chi_j \cdot N_{pl})$ is fixed; see equations (9.10) and (9.11), which are written in general form for a bending axis "j" in (9.75):

$$\frac{N}{\chi_j \cdot N_{pl}} + k_j \frac{M_j}{M_{j,pl}} \leq 1.0 \qquad (9.75)$$

It shall be noted that, due to the fact that the factor k_j is a function of n_j, the result of the sum in (9.75) is actually *not a utilization* in the commonly understood sense of the inverse of the still-possible amplification of a given load case before failure. It is a utilization ratio for a fixed axial force plus an arbitrary bending moment, which could be increased alone until the sum is equal to one. If one desires to know the utilization for the *combined* load case, (9.75) would have to be solved iteratively.

Just as (9.75) would have to be solved iteratively in order to calculate a utilization for the combined load case of N+M, the proposed Ayrton-Perry formulation of section 9.4 must be solved by iteration to obtain values of k_j *as a function of a fixed value of n_j*. Thereby, the most efficient way is to perform the iteration by using the factor $\chi_{j,\eta 0}$ of equation (9.74) as reference, and making the following considerations:

i. As has been shown in Fig 9-4b, a certain point on the failure curve in an N-M interaction diagram is reached independently of the loading history. Therefore, the utilization of 1.0 is reached in both the interaction concept as given by (9.75) and with the Ayrton-Perry formula (9.74). We can therefore write:

$$\frac{N}{\chi_j \cdot N_{pl}} + k_j \frac{M_j}{M_{j,pl}} = 1.0 = \frac{N}{\chi_{j,\eta 0} \cdot N_{pl}} \tag{9.76}$$

ii. This equation can be solved for k_j:

$$k_j = \frac{M_{j,pl}}{M_j} \cdot \left(\frac{N}{\chi_{j,\eta 0} \cdot N_{pl}} - \frac{N}{\chi_j \cdot N_{pl}} \right) = \frac{M_{j,pl}}{M_j} \cdot \frac{N}{N_{pl}} \cdot \left(\frac{1}{\chi_{j,\eta 0}} - \frac{1}{\chi_j} \right) = \frac{1}{\eta_0} \cdot \left(\frac{1}{\chi_{j,\eta 0}} - \frac{1}{\chi_j} \right) \tag{9.77}$$

iii. Equation (9.76) can now be re-written as follows:

$$n_j + \frac{1}{\eta_0} \cdot \left(\frac{1}{\chi_{j,\eta 0}} - \frac{1}{\chi_j} \right) \cdot m = \frac{n}{\chi_{j,\eta 0}} \tag{9.78}$$

iv. Equation (9.77) contains both η_0 and n_j, which are both functions of n. χ_j is a constant for a certain value of $\overline{\lambda}_j$. For a fixed value of n_j, a solution for (9.78) can be found through iterative variation of the possible combinations of n and m, i.e. of η_0. Once this is achieved, the factor k_j can be calculated from (9.77) for this numerical value of η_0.

The above procedure has been adopted to calculate factors k_j that are "inherently" contained in the proposed Ayrton-Perry formulation of section 9.4. These are compared to the GMNIA calculations and the factor k_j according to Annex A and B of EC3 – EN 1993-1-1 in Fig 9-20. Three different sections are studied, an IPE 240 in strong-axis bending, a circular hollow section CHS 178/10, and a HEA 500 in weak-axis bending, all loaded by a constant moment diagram plus axial force.

The three diagrams in the top row of Fig 9-20 show the interaction factors according to the Eurocode, while the bottom row shows the ones retrieved from the proposed Ayrton-Perry formulation. The following observations can be made:

i. The proposed formulation seems to follow the GMNIA values of k_j quite well, particularly from a qualitative point of view, but also quantitatively. Thereby, the Ayrton-Perry curves appear to have a similar course as the ones of the EC3- Annex A formulae, but with some advantages in accuracy particularly in the case of the circular cross-section, for which the cross-sectional interaction is poorly represented by the Annex A formulae.

ii. The discontinuities of the interaction curve addressed in section 9.5.2 that result from the linearized, segmental representation of the actually curved N+M cross-sectional interaction relationship also result in discontinuities of the k_j values for the Ayrton-Perry formulation, see in particular the "jump" of k_y in Fig 9-20b, $\eta_y = 0.4$ a $\overline{\lambda}_y > 1.0$. Again, this is inherent to the formulation, but not necessarily to be seen as a disadvantage to the user.
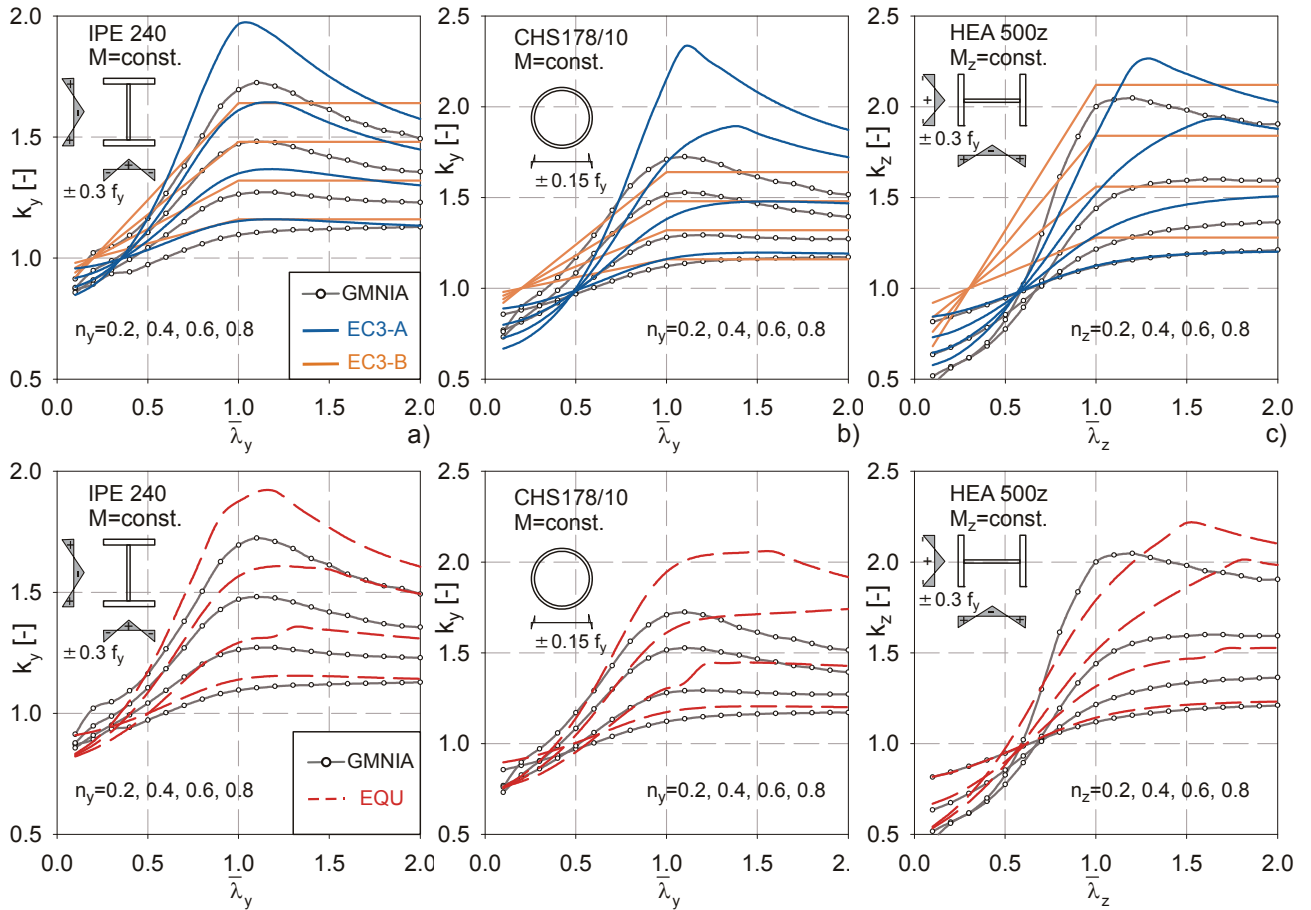
Fig 9-20 *Comparison of interaction coefficients k_y and k_z for different cross-sections.*

iii.   It should again be noted that the accuracy of the k_y values gives a rather misleading representation of the accuracy of the formulation itself, particularly for higher values of n_y or n_z. Even errors of some 20-30% in terms of k_j only lead to total errors of only a few percentage points at values of n_j beyond 0.5. In this sense, it is a welcome observation that the accuracy of the proposed formulation in terms of k_j is highest for low values of n_j, and mostly conservative in all other cases.

iv.   The comparison of the proposed formulation and the Eurocode coefficients leads to the conclusion that the new proposal has a very similar, inherent safety level. An adoption of the proposal for practical design as an alternative method based on the "overall" slenderness concept would therefore appear to be consistent with the safety level of current rules.

9.6. Some comments on the "general method" for out-of-plane beam-column buckling

In section 9.2, the so-called "general method" contained in clause 6.3.4 of EC3 – EN 1993-1-1 was conceptually introduced as a proposal for a general methodology for the design of members (or indeed whole structures) against spatial instability, based on a "generalized slenderness" concept.

Using the general variable naming adopted in this chapter, the method's basic design equation can be written as follows

$$R_{b,op} = \frac{\chi_{op} \cdot R_{b,ip}}{\gamma_{M1}} \overset{!}{\geq} 1.0 \tag{9.79}$$

With $R_{b,op}$ ...   design resistance (in terms of a maximum load amplification factor) of the structural element against out-of-plane instability.

       $R_{b,ip}$ ...   design resistance of the structure against in-plane instability, i.e. the same resistance determined in sections 9.3 to 9.5 of this chapter, as defined e.g. in (9.8).

       χ_{op}...   buckling reduction factor for out-of-plane buckling.

Thereby, the buckling reduction factor χ_{op} is stated to be a function of $\overline{\lambda}_{op}$, defined as follows:

$$\overline{\lambda}_{op} = \sqrt{\frac{R_{b,op}}{R_{cr,op}}} = \frac{\chi_{op} \cdot R_{b,ip}}{\gamma_{M1}} \geq 1.0 \tag{9.80}$$

With $R_{cr,op}$ ...   maximum load amplification factor (for a given load combination) until the first out-of-plane bifurcation mode is reached.

The Eurocode gives two options for the assessment of the value χ_{op}:

1) In a first method, the value of χ_{op} is determined by taking the minimum of χ_z and χ_{LT}, both taken from the current clauses 6.3.1 and 6.3.2 of EC3 – EN 1993-1-1.

2) In second method, an interpolation between χ_z and χ_{LT} is recommended, "based on the cross-sectional interaction". Simões da Silva et al. (2010) gave an interpretation of this as entailing the combination of $N/N_{pl} + M/M_{pl} = \chi_{op}$ and $N/(\chi_z N_{pl}) + M/(\chi_{LT} M_{pl}) = 1.0$. This can be shown to result in the following interpolation function for χ_{op}, with $\eta_0 = m/n$ as used in the previous sections of this chapter:

$$\chi_{op} = \frac{(1+\eta_0) \cdot \chi_z \cdot \chi_{LT}}{\chi_{LT} + \eta_0 \cdot \chi_z} \tag{9.81}$$

In both interpolation methods, the values of χ_z and χ_{LT} are to be evaluated for the slenderness $\overline{\lambda}_{op}$, and not for $\overline{\lambda}_z$ or $\overline{\lambda}_{LT}$.

As has also been already mentioned in section 9.2, the main problem of the "generalized slenderness" methods, of which the "general method" is one example, is the determination of the

appropriate values of the buckling reduction factor, i.e. in this case of χ_{op}. Indeed, the whole point of the development of an Ayrton-Perry derivation for the in-plane buckling case in section 9.4 was to determine the appropriate values of the buckling reduction factor χ_{ip}, which is a reduction factor that is also based on a "generalized slenderness" concept, albeit for the in-plane case. It was shown that very accurate results can be achieved for such a buckling reduction factor if the specific effects of the cross-sectional capacity and of the non-linear load-deformation behaviour are taken into account by an in-depth analysis of the realistic load-carrying behaviour, primarily by means of complementary GMNIA calculations.

For the proposal for χ_{op} currently contained in EC3- EN 1993-1-1 clause 6.3.4., no such studies appear to have been performed prior to the inclusion of the method in the code. In the PhD thesis by Müller (2003), the adoption of the method is advocated, and statistical evaluations are carried out on the basis of specific test data. Some first calculations have been performed by Greiner & Ofner (2007). Simões da Silva et al. (2010) also noticed the lack of a comprehensive parametric study for the assessment of the accuracy of the proposed formulae, and provided a number of new calculations for prismatic beam-columns. The considerations made in the following paragraphs are to be seen in the context of the on-going discussion of the accuracy and of the mechanical soundness of the "general method". Thereby, all comments are related to the simplest imaginable application of the method: simply supported, laterally unrestrained I-sections with double symmetric cross-section, loaded by axial force and a constant bending moment diagram.

One observation that should be discussed is the fact that the "general method" is inherently not consistent with the column buckling case for weak-axis buckling. This can be appreciated when this special case is entered in the design equation (9.79). For one, the in-plane buckling resistance can be written as the product of an in-plane buckling reduction factor (e.g. calculated with the formulae developed in this chapter) and the plastic resistance R_{pl}. Thus, the out-of-plane buckling resistance according to the "general method" becomes:

$$R_{b,op} = \frac{\chi_{op} \cdot R_{b,ip}}{\gamma_{M1}} = \frac{\chi_{op} \cdot \chi_{ip} \cdot R_{pl}}{\gamma_{M1}} \geq 1.0 \tag{9.82}$$

In the case of a column (M=0), this term becomes:

$$R_{b,op} = \frac{\chi_z(\overline{\lambda}_{op}) \cdot \chi_y \cdot R_{pl}}{\gamma_{M1}} \geq 1.0 \tag{9.83}$$

$$\overline{\lambda}_{op} = \sqrt{\frac{\chi_y \cdot N_{pl}}{N_{cr,z}}} \tag{9.84}$$

The value of $R_{b,op}$ calculated in this way will generally be lower than $(\chi_z \cdot N_{pl}) / (N \cdot \gamma_{M1})$, which is the correct value –written in terms of a possible load amplification- according to the column buckling curves of the Eurocode – clause 6.3.1. This will be particularly felt when the effects of χ_y

are relatively high in relation to χ_z, meaning cases where χ_y is not much larger than χ_z. In the case of I-sections, this applies to stocky sections with wide flanges.

One could argue that this additional "safety" is really to be attributed to the fact that imperfections of the full magnitude (e.g. $\overline{e}_0 = L/1000$ in GMNIA calculations) in *both* main directions are thereby account for even for the simple column buckling case. Indeed, this assumption was made in the paper by Simões da Silva et al. (2010), and leads to smaller –yet still present- differences between the results of GMNIA calculations and (9.82) for columns. However, one should be aware of the fact that this changes the safety level of precisely the one stability case which is universally regarded as the benchmark case for member buckling and which is most firmly substantiated by test results Due to this observation, geometric imperfections affine to the first eigenmode with amplitudes of $\overline{e}_0 = L/1000$ have commonly been considered to be the appropriate choice for GMNIA calculations for "model members".

More importantly than the implications for the pure column buckling case (which will perhaps not be a field of application of the "general method"), it is interesting to check the effects of the above-mentioned "bi-directional strength reduction" on combined load cases with N+M. For these cases too, the prescription of the "general method" implies that the in-plane buckling load be further reduced to account for out-of-plane effects.

While, of course, there indeed are effects of in-plane second-order deformations on the out-of-plane ultimate buckling load in such cases, these are likely over-estimated by the procedure of the "general method", once again particularly in cases where the bending stiffness of the member about the strong axis is not hugely larger than the one about the weak axis.
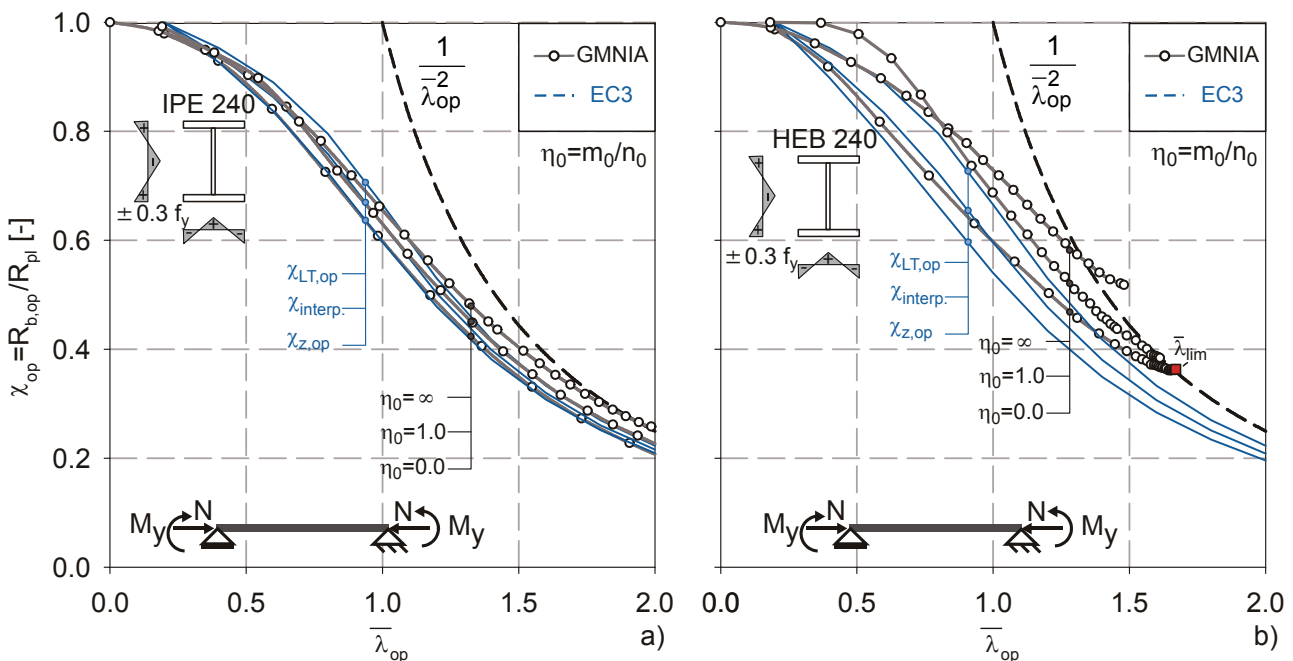
Fig 9-21 *Comparison of GMNIA buckling curves and EC3 proposals for the "general method"; IPE 240 (a) and HEB 240 (b) sections.*

The above comments are now reinforced by numerical examples. Two sections are studied within the context of the "general method", one slender (for lateral deformation) IPE 240, and a stockier HEB 240 section. Both are loaded by an axial force plus a constant bending moment diagram.

The GMNIA results were obtained with separate calculations for the in-plane and out-of-plane buckling strength, whereby the in-plane strength was needed to calculate the applicable value of $\bar{\lambda}_{op}$ according to (9.80). In both types of GMNIA calculation, eigenmode-affine imperfections were assumed, with amplitude $\bar{e}_0 = L/1000$.

The plots in Fig 9-21 show the comparison between the behaviour of the two studied sections, and compare the obtained GMNIA curves with the different proposals for the reduction factor χ_{op} found in the Eurocode. The following comments can be made:

i. In the case of the slender IPE 240 section, where the in-plane bending stiffness (and buckling strength) is much higher than the out-of-plane stiffness, the buckling curves obtained from GMNIA calculations for different values of $\eta_0 = (M/M_{pl})/(N/N_{pl})$ lie in a fairly narrow scatter band, which also happens to be well described by the EC3 curves that apply for column buckling ($\chi_{z,op}$) and LT-buckling ($\chi_{LT,op}$) when plotted over $\bar{\lambda}_{op}$. Furthermore, the interpolated curve, obtained from an application of equation (9.81) for the studied case of $\eta_0 = 1.0$, seems to be very well able to describe the behaviour of this particular beam-column loaded in N+M.

This is the desired scenario for the application of the "general method". The accuracy of the description of the "real" buckling strength is clearly very high for this case.

ii. However, the case of the stockier HEB 240 section gives a completely different picture. In this case, already the curve that applies for pure column buckling ($\eta_0 = 0.0$) lies distinctly above the EC3 curve for $\chi_{z,op}$, and furthermore has a remarkable feature: it stops at certain slenderness $\bar{\lambda}_{lim}$. This is actually quite easily explained by forming a limit value at infinite length of equation (9.84):

iii.
$$\bar{\lambda}_{op,lim} = \lim_{L\to\infty} \sqrt{\frac{\chi_y \cdot N_{pl}}{N_{cr,z}}} = \lim_{L\to\infty} \sqrt{\chi_y} \cdot \bar{\lambda}_z = \sqrt{\frac{1}{\bar{\lambda}_y^2}} \cdot \bar{\lambda}_y \cdot \frac{\bar{\lambda}_z}{\bar{\lambda}_y} = \frac{\bar{\lambda}_z}{\bar{\lambda}_y} = \frac{i_y}{i_z} \qquad (9.85)$$

Thereby, the limit value of χ_y was determined to be the Euler buckling load, which is what results from the Ayrton-Perry type formulation for the EC3 column buckling curves at infinite length. Thus, the limit slenderness $\bar{\lambda}_{op,lim}$ is equal to the ratios of the two radii of gyration, respectively of the slenderness $\bar{\lambda}_z$ to $\bar{\lambda}_y$. In the case of the HEB 240 section, this value is equal to 1.694 and thus lies within the shown section of the χ-$\bar{\lambda}$ plane. In the case of the IPE 240 section, this value is 3.704 and far beyond what is shown in the plot.

The GMNIA buckling curve is clearly influenced by the presence of this limit value of slenderness, and has a shape that appears to be "drawn away" from the curve for $\chi_{z,op}$ towards the value $1/(\bar{\lambda}_{op,lim})^2$.

iv. The case where only bending moments are present ($\eta_0 = \infty$) represents the pure LT-buckling case. Since no normal forces are present, the plastic bending strength determines $R_{b,ip}$ in (9.79) and thus there are no differences between $\overline{\lambda}_{op}$ and $\overline{\lambda}_{LT}$. For this case, the "general method" would be very conservative for the HEB 240 section if indeed one were to use the first recommendation for the determination of χ_{op}, which would lead to the use of the very low-lying column buckling curve c for this section. As the figure shows, for this case also the general-case LT buckling curve lies a bit low. A better curve would of course be found by using the formulations developed in chapter 6 of this thesis for the pure LT buckling case.

v. The most remarkable behaviour, however, is shown by the GMNIA curve in terms of χ_{op} for the HEB 240 section and $\eta_0 = 1.0$. This curve comes to lie above the curve for $\eta_0 = \infty$ for a certain portion of its length, then drops below it. It can be shown to converge towards the same point as the curve for $\eta_0 = 0.0$, reaching the same limit value of slenderness.

This behaviour of the GMNIA curve for $\eta_0 = 1.0$ for the stocky HEB 240 section matches the comments made above, and can be explained accordingly:

v. The "general method" uses the convention that the reference value of the buckling strength be given by the in-plane buckling limit load. This is a departure from most other stability rules, which implicitly use a cross-sectional capacity as the reference value for both slenderness and buckling reduction factor, and not a quantity related to the load carrying capacity of the whole member.

vi. The buckling behaviour of beam-columns is actually dominated by the first (spatial) eigenmode, with only comparatively secondary effects from the in-plane deformations.

vii. This causes the GMNIA curve -in terms of this definition of slenderness- to have a shape similar to the one observed for $\eta_0 = 1.0$ whenever the in-plane and out-of-plane modes are not too far apart. This is not in itself a problem, since the χ_{op} is just a form of representation of results. However, very conservative results will be achieved in design for these cases if one applies another "full" reduction of the load-carrying capacity by $\chi_{z,op}$ or $\chi_{LT,op}$ to the in-plane strength in this range.

These findings are further corroborated by the calculation results illustrated in Fig 9-22. This figure shows the same type of GMNIA results plotted as values χ_{op} over $\overline{\lambda}_{op}$, but with the difference that the results are plotted separately for single *members of a certain length* (identified by values of $\overline{\lambda}_z$) and varying factors of η_0. This type of representation has the advantage of showing how the buckling reduction factor for a certain member is affected by the load case in the "general method" type of representation. The lower-right point of the GMNIA curves always represents the "column buckling" case, where $\eta_0 = 0.0$. The arrows in the figure indicate the direction of increase of η_0. The other extremity of the single curves is given by the case of $\eta_0 = \infty$, where only bending moments are present. The following comments can be made about these plots:
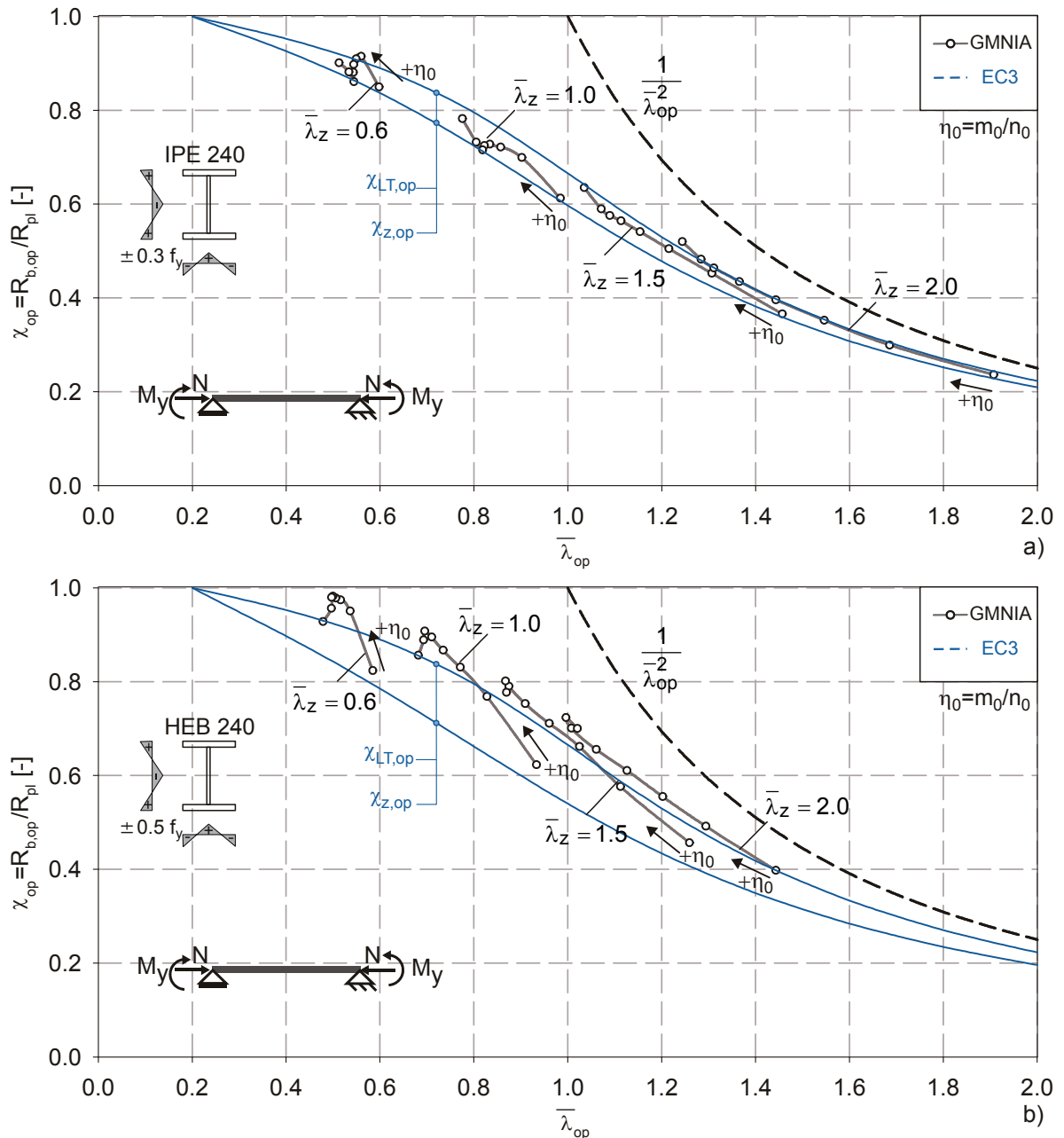
Fig 9-22 *Comparison of GMNIA results (plotted for single sections and progressively increasing values of η_0) and EC3 proposals for the "general method"; IPE 240 (a) and HEB 240 (b).*

i. This type of representation illustrates fairly well the dependency between the buckling reduction factor χ_{op} and the load case as given by η_0. One fact that is particularly well represented by this type of plotting is that an interpolation between the curves for $\chi_{z,op}$ and $\chi_{LT,op}$ might not be as straightforward as envisaged by equation (9.81). In this sense, the fact that the interpolation was thought to be fairly accurate in the description of the case with $\eta_0=1.0$ for the IPE 240 section in Fig 9-21 must be thought to be rather fortuitous. An interpolation of this type would require the GMNIA curves in Fig 9-22 to show a smooth transition from the "column curve" $\chi_{z,op}$ to the "beam curve" $\chi_{LT,op}$. This is clearly not generally the case for the two studied sections. Particularly at lower lengths of the members,

the GMNIA values of χ_{op} "jump" quite unpredictably with changing η_0 in the chosen type of representation. It is important to recall here that this is not due to a numerical problem in the GMNIA calculations, which indeed give smooth transitions of the *actual* load carrying capacity with changing values of η_0. The shown shape of the curves is entirely due to the form of representation itself.

ii.   The fact that none of the results fall below the lower of the two EC3 curves, which in these cases was always the "column curve" $\chi_{z,op}$, is certainly a welcome observation, particularly if the lowest χ_{op}-curve is used for design. However, the conservatism that this method entails can be very large; compare e.g. the results for $\overline{\lambda}_z = 1.0$ and upper-intermediate values of η_0 with the $\chi_{z,op}$ curve for the HEB 240 section. Differences of this magnitude are generally not considered to be adequate.

To conclude this section, it can be stated that the "general method", albeit being fairly simple in its application and inviting for designers due to its putatively unlimited scope of application, seems to require a thorough and comprehensive reconsideration from the point of view of its accuracy and theoretical background in order to meet the standards set by the other buckling design rules present in the Eurocode.

Only the simplest imaginable cases were considered in this section, yet some major inconsistencies were discovered. Further discrepancies were also noticed by the mentioned other authors who have studied the accuracy of this method. The fact that the method implicitly considers imperfections at their maximum extent to be present in both directions of a beam-column, and more importantly that it over-estimates the impact of this double-curvature in many practical cases, is certainly one point of inconsistency with other rules.

From a theoretical point of view, the method provides little insight in the mechanisms that actually dominate a spatial failure mode: an in-plane failure mode is first declared as the upper limit value of a spatial buckling phenomenon that has its bifurcation load far before this in-plane mode can be activated, and a rather arbitrary choice of buckling curve is then used to reduce this in-plane strength to estimate the spatial, out-of-plane strength. For practical purposes, this might be accurate enough in those particular cases where specific design rules are presently missing, e.g. for tapered beams, castellated or cellular beams, and similar cases that are not explicitly covered by the current Eurocode design rules but may be considered to behave at least qualitatively similarly to standard cases. However, it does not appear to be a generally appropriate procedure for as wide a spectrum of application as stated in the code, which would include all types of sections and whole spatial frame structures. In this sense, attributing a "general validity" to the "general method" would seem to be a rather far-fetched conclusion.

9.7. Conclusions

This chapter gave an overview of the issues involved with the development of design rules for (class 1 & 2) beam-columns. Thereby, a new proposal for the design of such members against in-plane buckling was made that is fully compatible with the increasingly popular trend in the scientific community of using "generalized" slenderness definitions for "overall" load cases for the design of structures.

It is believed that the proposed formulation is the first such expression for steel members that integrates a consistent mechanical derivation and all relevant mechanical effects in an "overall" (in-plane) buckling reduction factor. The proposal makes once again use of the Ayrton-Perry format, making the expression fully compatible with the other Eurocode member design rules. The plastic cross-sectional capacity of the members is fully taken into account in the formulation, having the welcome side effect that the check of the critical cross-section is "automatically" included in the stability design check, which is something that is not the case in the current rules.

As a further result of this derivation and of the pertinent numerical study, it could also be illustrated how the given design formulae for in-plane buckling under N+M in Eurocode 3 - EN 1993-1-1 cope with this more complex buckling behaviour. In this context, both design formulations of Annex A and B of the Eurocode were shown to appropriately cover the main effects with good accuracy as far as practical applications are concerned.

In order to further emphasize the significance of an adequate derivation of buckling design rules that takes into account the idiosyncrasies of the studied instability case, a brief discussion was given in the final section of the chapter of the strengths and weaknesses of the so-called "general method" for the design of steel members and structures against spatial instability. This method is essentially based on an inventive way of expressing the buckling design condition. Besides pointing out some general inconsistencies, the need was stressed for a consistent and accurate formulation of the buckling reduction factor for this method in order to meet the standards of accuracy and mechanical soundness inherent to other Eurocode design rules. It is believed that the methodology employed in this chapter for the development of a formulation for the in-plane case could serve as a blueprint for any such effort of formulating buckling reduction factors for more complex cases.

10

Summary and Conclusions

10.1. Summary

This thesis is concerned with the improvement of the consistency, in terms of safety level and mechanical soundness, of buckling design rules for steel members. It discusses a number of different topics, with the aim of increasing the understanding of the studied engineering problems and of providing designers with simpler, safer and better understandable formulae for certain, very common design tasks. More specifically, the following summary can be given of the topics treated in this thesis, listed in the order of appearance in the main body of the text:

I. In the 1st, introductory chapter, the identified inconsistencies and problems in current buckling design rules are presented in a general form. The scope and limitations of the studied cases are stated, and the thesis' organization in parts is introduced and explained.

II. In chapter 2, comprehensive background information is given regarding the source, the derivation, the mechanical soundness and the strengths and weaknesses of the most common buckling design formulae found in international design codes and the technical literature. Many of these design formulae have been codified and used –in one or the other form- for several decades by structural engineers in different countries. Nevertheless, or perhaps precisely *because* of their long-established use, the mechanical background of some of them is not always readily available. The comparison of the different backgrounds given in this chapter is therefore intended to shed some light on the often controversial matter of what type of design formulation is most appropriately used as a format for buckling checks. Two very different types of formulation could be identified:

1) Formulations that are based on pure curve-fitting of an essentially arbitrary mathematical expression (polynomials, exponential functions, etc.) to previously established numerical and/or experimental data points.

2) Formulations based on a more-or-less mechanically sound, rational formulation.

The most important formulation of the second type is the one that is most present in the Eurocode, i.e. the so-called Ayton-Perry formula, which in its simplest manifestation takes on the following form:

$$\chi = \frac{1}{\Phi + \sqrt{\Phi^2 - \bar{\lambda}^2}} \tag{10.1}$$

with
$$\Phi = \frac{1}{2} \cdot \left(1 + \eta + \bar{\lambda}^2\right) \tag{10.2}$$

and η being the so-called "generalized imperfection coefficient".

III.   In chapter 3, the used methodology is explained. In this thesis, state-of-the-art numerical, analytical and probabilistic methods have been used and combined. While the employed numerical modelling techniques, as well as the fundamental equations used as starting point for the single derivations of new design formulae, can be considered to be part of the accepted standard methodology in buckling analysis and design, the probabilistic concepts involving Monte Carlo simulations and random number generation are perhaps more rarely used in these contexts and are described accordingly.

IV.   In chapter 4, the main inconsistencies in current buckling design rules for steel members subjected to simple load cases (columns or beams) are listed, and common strategies for the overcoming of these inconsistencies are introduced. Specifically, the following points were seen as the source of inaccuracies and as worth of a reassessment:

-   The classification of cross-sections with respect to their geometrical parameter h/b are noticed not to be consistent for the single, basic buckling design rules. Different classification criteria exist for the flexural (column) and the lateral-torsional (beam) buckling case. This is an indicator for the lack of descriptiveness of at least one of these rules, which was also confirmed by numerical calculations in the specific chapters 5 to 7.

-   The underlying equivalent geometric imperfections for the single basic member buckling checks are shown to not only be very different for each case in absolute terms, but also to have a completely different length-dependency. While for the column buckling case the underlying, equivalent geometric imperfection is essentially linearly dependent on the member's length, a highly non-linear relationship was found to apply for the design rules for lateral-torsional and torsional buckling according to the Eurocode.

-   The reliability level of the single basic buckling design rules, expressed in terms of required partial safety factor γ_M^*, is shown to be non-constant throughout slenderness ranges.

The chapter proceeds with a discussion –in general terms- of how these inconsistencies can be removed. Particularly the non-constant reliability level for different ranges of slenderness is addressed in chapter 4 itself, where two different statistical methods based on First Order Reliability Methods (FORM) are proposed and discussed. If based on a representative range

of statistical input data for the most dominant structural parameters governing the studied buckling case, these methods can be used to obtain true "constant reliability curves".

V.   The first part of chapter 5 discusses the background of the European column buckling curves developed by ECCS (1978) and currently found in the Eurocode. Thereby, particular emphasis is put on the experimental program underpinning these curves, which also includes an early application of Monte Carlo simulations in the study of buckling phenomena, as well as on the numerical studies and their underlying assumptions that led to the final shape of the ECCS curves. These numerical buckling curves were obtained on the basis of "model columns", i.e. members with fixed (non-random) imperfection amplitudes and geometrical input data, whereby the assumptions regarding the imperfections were calibrated to match the experimental data points obtained from large-scale tests.

For the purposes of this thesis, it was important to clarify that these numerical curves based on "model columns", and hence the assumptions for the "model column" calculations, are essentially the main theoretical foundation of the current safety and reliability level of the European design rules for columns. In this sense, it was also important to place the background of the calibration (performed by Maquoi and Rondal, 1978), of an Ayrton-Perry formula to these numerical curves in the correct conceptual context. Due to the very comprehensive background given in the case of the development of the column buckling curves now found in the Eurocode, this buckling case and its derivation were regarded as the "benchmark" case for member stability cases in the context of this thesis.

The chapter then proceeds with the treatment of a current problem in the application of these long-established column buckling curves: the changes in the specification of permissible out-of-straightness of compression members brought about by the introduction of a new, Europe-wide standard for the fabrication and erection of structural steelwork, EN 1090-2:2008. Monte Carlo simulations are used to evaluate a series of plausible scenarios, which could develop as a consequence of the introduction of the new standard, in order to answer the question of the impact of "relaxed" curvature tolerances on the safety of commonly used buckling checks. Thereby, such a probabilistic approach is shown to be the only consistent approach to quantify the impact of such a change in production habits in a meaningful way.

Finally, the FORM methods described in chapter four to obtain "constant reliability curves" are applied to the column buckling curve, illustrating the possibility of moving away from "semi-deterministic" buckling design rules based on "model columns" on to truly probabilistic curves in the future, provided that agreement is found with respect to the scatter-band of basic input variables to be used in such calculations.

VI.   In chapter 6, a new design formulation for lateral-torsional buckling of beams is systematically developed, calibrated and statistically justified. Thereby, a new Ayrton-Perry type formulation is obtained that is based on a specific second-order derivation for the case at hand. The significance of accurately -and mechanically sensibly- formulating the

expression for the generalized imperfection coefficient η, and of calibrating this expression to match a comprehensive series of numerical GMNIA buckling curves is highlighted. By doing so, a formulation is finally obtained that very accurately describes the course of numerical buckling curves, which themselves were calculated using the same ("model beam") assumptions for imperfections and geometry as for the benchmark column buckling case. This assures that a comparable level of inherent safety is present in the proposed formulation as in the column buckling case. This is further emphasized by specific assessments of the reliability level through probabilistic means at the end of the chapter. By resulting in a separate buckling curve for each single studied cross-section, the formulation specifically takes the torsional characteristics of each cross-section into account in a very precise way. Thereby, the categorization with respect to cross-sectional geometries no longer needs an arbitrarily set limit at h/b=2.0, but categorizes the cross-sections in accordance with the underlying imperfection assumptions made during the development of the curves, which is consistent with the situation found for column buckling. This highlights the mechanical soundness of the newly proposed formulae.

VII.   The case of laterally supported columns with I- & H-shaped cross-sections failing in torsional and torsional-flexural buckling is treated in chapter 7 both numerically and analytically. After a comprehensive numerical study and description of the peculiarities and the practical significance of this buckling phenomenon, and of the high conservatism of current code provisions dealing with this buckling case, the chapter proceeds with the development of a new, Ayrton-Perry type formulation for torsional and torsional-flexural buckling. Thereby, analogous steps are followed as in chapter 6 for the LT buckling case. In this way, a formulation could again be found that very well describes the shape of numerical buckling curves obtained from calculations with the "model column" assumptions, and that is thereby consistent both in the type of formulation and in descriptive accuracy with the benchmark column buckling case.

VIII.   In order to better illustrate the high degree of consistency between the different basic member buckling cases obtained by the newly proposed formulations for lateral-torsional and torsional-flexural buckling, these proposals were combined with the long-established column buckling case in a common design formula and table, contained in chapter 8 of the thesis. The common Ayrton-Perry type formulation is thereby convenient for a generalized formulation of the buckling reduction factors. The peculiarities of the single buckling cases are then easily implemented through separate coefficients, tabulated in the mentioned design table.

IX.   Some important aspects of the derivation of design rules for beam-columns, i.e. members subjected to the combined action of axial and transversal loads, are treated in chapter 9. Thereby, the two main concepts currently implemented in design codes for the design of

such elements are first discussed: the interaction concept and the "generalized slenderness" concept. As far as the consistency of the design rules is concerned, it is noted that the "generalized slenderness" concept, particularly in its manifestation as the so-called "general method" in Eurocode 3- clause 6.3.4, is *formally* more consistent with the other buckling design rules in the code, because it makes use of the same concept of applying a buckling reduction factor to an ultimate strength criteria that is not affected by the studied stability phenomenon. However, it is shown in this chapter that the interaction concept as it is included in the Eurocode – clause 6.3.3 is *mechanically* much more coherent and consistent with the mechanical soundness and safety of the benchmark column buckling case.

Recognizing these two different levels of consistency, a new proposal is made in chapter 9 for a formulation (again resulting in an Ayrton-Perry formula) for beam-column design that is both *formally and mechanically* consistent with the basic benchmark cases. This is done for the in-plane beam-column buckling case. Through a very accurate, yet simple linearization of the plastic, cross-sectional N+M interaction relationship for a variety of practical cross-sections, the "exact" cross-section capacity of specific sections was placed at the centre of the new proposal, thereby consistently integrating cross-sectional and buckling check in one design task. The more complex effects of the buckling phenomenon as observed in numerical GMNIA calculations, e.g. the detrimental effects of flange yielding on the obtainable buckling loads at high slenderness, or the effects of residual stresses, are taken into account through simple, yet efficient coefficients. A comparative study of calculated buckling strengths with GMNIA calculations using the "model column" assumptions, as well as with the mechanically sound interaction formulae of Eurocode 3, confirm the consistency of the proposed formulation in terms of safety and accuracy.

10.2. Original Contributions

The original contributions to engineering knowledge made in this thesis include the points listed in the following:

- The development of *new, far more accurate formulations* to describe the buckling strength of beams and columns for lateral-torsional and torsional-flexural buckling. They are obtained by deriving specific second-order, first-yield ("Ayrton-Perry") failure expressions and systematically calibrating the imperfection amplitudes to the numerical curves. By doing so, full methodological consistency with the long-established flexural column buckling case is obtained (Chapters 6 & 7).
- Using these new expressions, a *consistent classification* of structural sections with regard to their buckling behaviour was obtained. Contrary to what is currently the case, assumptions made in the development of numerical buckling curves (regarding geometry, strength and imperfections) are thus fully reflected in the classification for all studied basic buckling cases (Chapter 8).

- The known inconsistencies in terms of reliability level of current member buckling rules are *shown to be mechanically/statistically explicable*. Methods suitable for the removal of these inconsistencies are presented and applied. These include Monte Carlo random number generation methods and "First Order Reliability Methods" (FORM) combined with non-linear, GMNIA Finite Element calculations (Chapters 4, 5, 6).

- Again using Monte Carlo and FORM methods, a way of answering questions regarding the impact of changes to production tolerances or habits of curvature-control is presented. Specifically, the possible *impact* of modifications of straightness tolerances for compression members is *quantified* (Chapter 5).

- An *expansion* of the column buckling design formula to the *in-plane beam-column case* with combined axial and bending loading is developed and calibrated to obtain very high accuracy when compared to numerical results. Thereby, a linearization of the cross-sectional N-M interaction curve is shown to be essential. The new formulation is conceptually integrated in the two existing design concepts for beam-columns (Chapter 9). Full formal and mechanical consistence is thereby obtained with the benchmark column buckling case.

Contributions to the consolidation of existing engineering knowledge include:

i. A comprehensive discussion of the origins, underlying assumptions, strengths and limitations of the most common buckling design formulae (Chapter 2).

ii. The description of the applicability of numerical, analytical and statistical tools for the development of buckling rules (Chapter 3).

iii. An outline of the development of the ECCS European Column Buckling Curves (Chapter 5).

iv. A discussion of the viability of the application of the "general method" as the standard design tool for out-of-plane stability checks of beam-columns (Chapter 9).

10.3. Conclusions

In addition to the more specific implications of the numerical parametric studies and of the new design proposals presented in this thesis, which are discussed in detail in the pertinent chapters, the findings of this work allow one to draw the following general conclusions:

I. The different rules and formulae currently used by designers to determine the structural safety of steel members against the various modes of global instability do not have a consistent level of mechanical justification and were not developed following a unified procedure. While the design rules for the "benchmark" flexural column buckling case are based on a large and concerted experimental and numerical research effort and statistical evaluation, and are expressed in terms of a simple but mechanically coherent second-order (Ayrton-Perry) formula, the rules for other global member buckling rules are often based on mechanically not fully coherent adaptations of the buckling curves for the benchmark case.

This applies to the current EC3- EN 1993-1-1 rules for lateral-torsional buckling of beams (clause 6.3.2) and for torsional-flexural buckling of (laterally restrained) columns (clause 6.3.1.4), as well as for the so-called "general method" for the design of beam-columns (clause 6.3.4). In contrast to this, rules that are based on a firm mechanical background, such as the formulae for beam-columns according to clause 6.3.3 of the Eurocode, are not presented in a mathematical format that is consistent with other buckling rules, since they use an additive "interaction concept" formula instead of a single buckling reduction factor.

II. A number of recent studies (e.g. Müller, 2003; Naumes et al., 2009) have already noticed the above-mentioned difficulties and inconsistencies and have tried to overcome them, thereby focusing primarily on aspects of consistency of formulaic representation and of reliability. Through the evaluation of existing physical test results, the safety and reliability level of some current or proposed design rules could thereby be shown to be acceptable and similar for different studied cases and, in this sense, "consistent" for the evaluated scope of test data. Accordingly, there is an increasing tendency of *primarily* using statistical tools as provided by the Eurocode (2002) - EN 1990 to determine the acceptability of a certain design rule. By adopting such a procedure, the assessment of the accuracy of the design formulation is often lost (or rather "blurred") into the statistics. Although this is not necessarily very important to safety (as long as the safety level is "proven" by the statistical evaluation), the tendency of drawing broad conclusions from statistical evaluations alone, including for fields of application not covered by the considered tests, is nevertheless rather problematic. An example for this is the application of the "general method" for the design of beam-columns: as was shown in section 9.6, the mechanical background of this method is – at the current stage- not clear, and results can significantly diverge from numerical calculations that are commonly used to verify buckling rules. It is therefore concluded that a methodology for the development of buckling rules that omits (numerical) accuracy studies is not conclusive and should not be regarded as a general foundation for buckling design.

III. This thesis set out to overcome the inconsistencies mentioned above for some of the most relevant member buckling cases, thereby using a methodology that very closely follows the steps taken during the development of the "benchmark" rules for member buckling design, i.e. the (flexural) column buckling rules. Thereby, both aspects of safety *and* of accuracy could be covered systematically. Expressed in a more generalized form, the used procedure is schematically represented in Fig 10-1, and the conclusions to be drawn from this procedure are discussed in the following.

   i. The methodology used in this thesis for the development of new design rules for lateral-torsional, torsional-flexural and in-plane beam-column buckling achieved full consistency with the benchmark case of column buckling in terms of formal presentation of the design equation, mechanical accuracy and reliability level. It did so by focusing on *accuracy and safety* simultaneously.
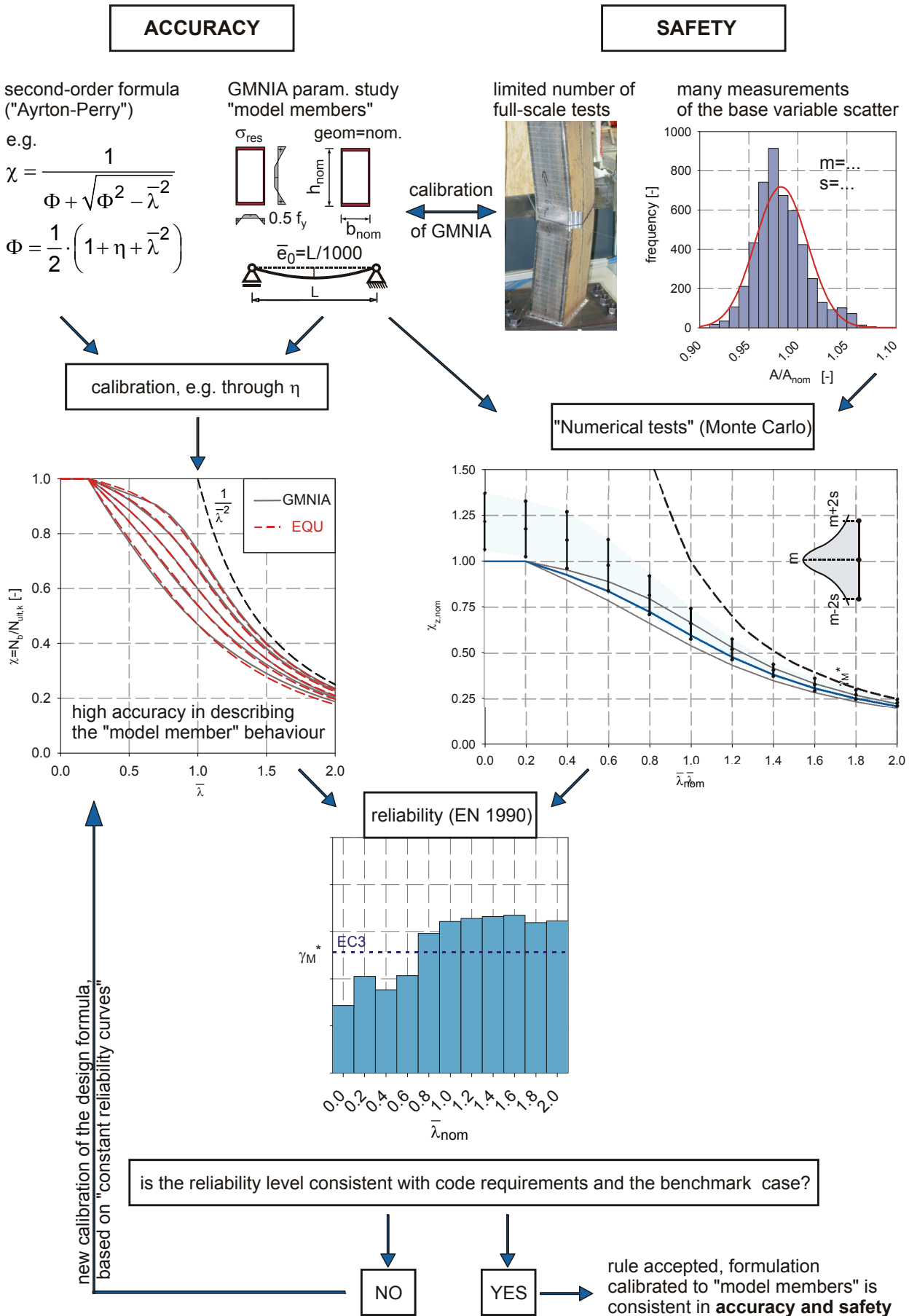
Fig 10-1 *Schematical representation of the proposed methodology*

ii. The *accuracy* of a proposed formulation is assured first of all through the development of specific formulations of a buckling failure condition that are based on second-order internal forces and on elastic (or linearized plastic) cross-sectional interaction conditions. This results in equations for the buckling reduction factor that take on the form of the classical Ayrton-Perry formula, with mechanically coherent modifications to account for the specific effects of the studied buckling case.

Specifically, the *modifications* must not only include case-specific stiffness terms that stem from the second-order derivation itself, but must also account for effects that are otherwise omitted in such a simple design equation. The latter stem from the complex behaviour shown by the inelastic buckling of steel members with geometric and structural imperfections. In the basic cases of flexural, lateral-torsional and torsional-flexural buckling, these effects can conveniently be included in the definition of the "generalized imperfection" η. This is what was done by Maquoi & Rondal (1978) for the benchmark case of flexural column buckling, and was successfully expanded in this thesis for lateral-torsional and torsional-flexural buckling. For the more complex, combined load-cases found in beam-columns, additional effects must specifically be taken into account. In particular, these refer to the transition from the fully plastic cross-sectional N+M interaction valid at low slenderness to a purely elastic, "first-yield" buckling condition valid for very slender elements. Considerations of this type were made in chapter 9 for the in-plane beam-column buckling phenomenon and also resulted in very high accuracy.

Of course, a measure of comparison is needed in order to determine the *accuracy* of a formulation. In this sense, the state of the art currently consists of regarding a formulation as accurate when it manages to describe the studied buckling strength as shown in realistic GMNIA calculations for a wide range of parameter variations. These calculations must thereby make use of modelling techniques that are widely accepted as realistic reflections of the actual behaviour, and/or are validated by comparison with specific test results whenever possible and necessary. As far as the input parameters of these calculations are concerned, the commonly accepted methodology is to determine the behaviour of so-called "model members", i.e. members with deterministic, fixed input parameters representing rather safe-sided, lower strength fractiles. The benchmark for this type of calculations is represented by the assumptions made by Beer & Schulz (1970) in the large parametric study that directly led to the ECCS column buckling curves. These assumptions lead over to considerations of safety, as they were explicitly linked to the target reliability level for member buckling checks.

iii. The *safety* or reliability of a buckling design rule is usually determined on the basis of methods contained in the Eurocode – EN 1990. These are essentially First Order Reliability Methods (FORM) that allow one to determine the required value of the partial

safety factors γ_M to be used in combination with a certain design rule in a semi-probabilistic design philosophy.

In the past, the test data used as basis for a reliability assessment were usually provided by large-scale physical ("real") tests. Nowadays, simulated tests obtained from GMNIA calculations with random input variables ("Monte Carlo method") are increasingly being used instead. Thereby, the evaluation of a data set obtained by "numerical tests" can be thought to be fully representative of the real scatter of tests, *provided that the real scatter bands of the single input parameters,* as well as the way these parameters correlate, are known. Very valuable studies of these scatter bands and correlations have been published in the literature (Alpsten, 1972; ECCS, 1978; Melcher, 2004). In an application that made use of the data given in these publications, Monte Carlo simulations could be carried out in this thesis that allowed for a *quantification of the reliability impact* of the changes of geometric tolerances for compression members currently being brought about by the introduction of the new fabrication standard for constructional steelwork EN 1090-2. Deterministic methods alone would not be able to produce results of this type.

It is believed that a coordinated, international effort (by steel producers) in order to obtain a fully comprehensive and reliable data pool on the variability of properties of structural steel members would be very valuable to the steel construction industry. This would ensure that safety assessments based on Monte Carlo simulations or other reliability methods are routinely accepted by members of the research, design and building authority communities.

In this context, the possibility was also addressed in this thesis to move away from "semi-deterministic" buckling rules calibrated onto "model member" GMNIA calculations, and to directly base the calibration of buckling rules on "constant reliability curves". As was shown in chapters 4 and 5 of this thesis, such curves can be obtained from a combination of numerical GMNIA calculations and probabilistic FORM methods. They once again require information regarding the scatter band and correlation of the properties of steel members. The computation effort needed to obtain buckling curves of this type is larger than the one needed for "model member" curves, but can still be contained within a reasonable time-frame.

iv. The last step consists of assessing the final acceptability of a certain buckling design rule. According to the philosophy pursued in this thesis, the acceptance should depend on the *combination of mechanical coherence, accuracy, safety and practicality*. In this sense, it is believed that the way in which specific member buckling cases were treated in this thesis can serve as guidance and starting point for future developments.

10.4. Publications

The following publications have so far resulted from the work presented in this thesis:

Journals

(1) Taras, A., Greiner, R. (2008), *Torsional and flexural torsional buckling— A study on laterally restrained I-sections*, Journal of Constructional Steel Research, 64, pp. 725-731

(2) Taras, A., Greiner, R. (2008), *Development of Consistent Buckling Curves for Torsional and Lateral-Torsional Buckling*, Steel Construction, 1, pp. 42-50.

(3) Taras, A., Greiner, R. (2010), *New Design Curves for Lateral-Torsional Buckling –Proposal Based on a Consistent Derivation*, Journal of Constructional Steel Research, 66, pp. 648-663

Conference Proceedings

(4) Taras, A., Greiner, R. (2006), *Torsional and flexural torsional buckling— A study on laterally restrained I-sections*, Proceedings of the Conference "Stability and Ductility of Steel Structures", Lisbon (PT), 09/06/2006 – 09/09/2006, pp. 259-266.

(5) Taras, A., Greiner, R. (2008), *Use of Ayrton-Perry type formulae to represent buckling curves for torsional and lateral-torsional buckling modes*, Proceedings of the Conference "Eurosteel 2008", Graz (AUT), 09/03/2008 – 09/05/2008, pp. 1551-1556.

(6) Taras, A., Greiner, R. (2009), *Consistent Analytical Description of Buckling Curves for Lateral-Torsional Buckling of Steel Members*, Proceedings of the "7th EUROMECH Solid Mechanics Conference", Lisbon (PT), 09/07/2009 – 09/11/2009, 20 pp. (CD proceedings).

ANNEX

A

NOTATION

It was attempted to describe all used variables in the text at their first appearance. The following pages therefore only list the most important symbols used in this thesis. Specific sub-indices are not always included, but are explained in the text and can be easily inferred.

General acronyms

CHS   Circular hollow section

FByy   Flexural buckling about the y-axis

FBzz   Flexural buckling about the z-axis

LPF   Load Proportionality Factor

LTB   Lateral-torsional buckling

QHS   Quadratic hollow section

RHS   Rectangular hollow section

TB/TFB   Torsional and Torsional-flexural buckling

Methods of analysis

GMNIA   Geometrically, materially nonlinear analysis with imperfections

LBA   Linear Buckling Analysis

MNA   Materially nonlinear analysis

Geometrical parameters

b   Section width

D   External diameter of circular hollow sections

h   Section depth

L   Length

r   Fillet radius for H-shaped sections

t	Thickness
t_{act}, A_{act}...	Actual values of e.g. a thickness or area, as measured.
t_f	Flange thickness
t_{nom}, A_{nom}...	Nominal values of e.g. a thickness or area.
t_w	Web thickness

Deformations and imperfections

u, $\bar{u}$	Displacement in longitudinal x-axis direction and its maximum amplitude
v, $\bar{v}$	Displacement in (lateral) y-axis direction and its maximum amplitude
w, $\bar{w}$	Displacement in (in-plane) z-axis direction and its maximum amplitude
θ, $\bar{\theta}$	Rotation about the longitudinal axis and its maximum amplitude
e_0, $\bar{e}_0$	Values of the initial geometric imperfection and its maximum amplitude
$\bar{v}_0$	Amplitude of a trasnversal initial geometric imperfection
$\bar{w}_0$	Amplitude of an in-plane initial geometric imperfection
$\bar{\theta}_0$	Amplitude of a rotational initial geometric imperfection

Section properties

I_T	Torsional constant
I_y	Moment of inertia, related to strong axis bending
I_z	Moment of inertia, related to weak axis bending
I_ω	Warping constant
W_j, $W_{j,el}$	Elastic section modulus, related to the axis "j" (j=y or z)
W_{pl}, $W_{j,pl}$	Plastic section modulus, related to the axis "j" (j=y or z)

Material parameters

ν	Poisson's ratio
E	Young's modulus of elasticity
f_u	Ultimate tensile strength, mean
f_y	Yield strength
G	Shear modulus
ε_y	Strain at yielding
ε	Strain

Forces, resistances and load amplification factors

m, m^{II} Normalized bending moment acc. to first or second order theory, equal to M/M_{pl}

M_{Ed} Design value of the acting bending moment

M_{el} Elastic cross-section resistance for pure bending moment

M_{pl} Plastic cross-section resistance for pure bending moment

M_T Torsional moment

M_y Bending moment about the strong axis (y)

M_z Bending moment about the weak axis (z)

M_ω Warping moment

N Axial Force

n Normalized axial force, equal to N/N_{pl}

N_b Axial force at the ultimate limit state (buckling resistance)

N_{cr} Axial force at the first bifurcation, "Euler load"

N_{Ed} Design value of the acting axial force

N_{pl} Plastic cross-section resistance for pure axial force

N_R *see N_b*

$N_{ult,k}$ *see N_{pl}*

R_b Buckling resistance in terms of maximum load amplification factor

R_{cr} Load amplification factor at (first) bifurcation

R_{pl} Plastic resistance in terms of load amplification factor

R_{ult} *see R_{pl}*

Statistical parameters

γ_M^* Partial safety factor related to nominal values

γ_{M1} Partial safety factor for member resistance (buckling strength)

b Least squares estimator

cdf   Cumulative distribution function

pdf   Probability density function

r_d Design resistance

$r_{e,i}$ Resistance values (from tests)

$r_{t,i}$	Theoretical values of the resistance (from a model function)
V_δ	Coefficient of variations of the error terms
V_r	Total coefficient of variations of the model
V_{rt}	Coefficient of variations of the model function

Slenderness

λ	geometric slenderness, equal to L/i
λ_1	"normalization slenderness", equal to $\pi \cdot \sqrt{E/f_y}$
$\bar{\lambda}$	Normalized slenderness
$\bar{\lambda}_0,\ \bar{\lambda}_{LT,0}$	Plateau value of the buckling curve, e.g. for LT buckling
$\bar{\lambda}_{act}$	Normalized slenderness calculated with actual (measured) values of geometry and f_y
$\bar{\lambda}_{GS}$	"Generalized slenderness", equal to $\sqrt{R_{pl}/R_{cr}}$
$\bar{\lambda}_{nom}$	Normalized slenderness calculated with nominal values of geometry and f_y
$\bar{\lambda}_{ip}$	Normalized "overall" slenderness for in-plane buckling
$\bar{\lambda}_{LT}$	Normalized slenderness for lateral-torsional buckling
$\bar{\lambda}_{op}$	Normalized "overall" slenderness for out-of-plane buckling
$\bar{\lambda}_T$	Normalized slenderness for torsional buckling
$\bar{\lambda}_{TF}$	Normalized slenderness for torsional-flexural buckling
$\bar{\lambda}_y$	Normalized slenderness for in-plane flexural column buckling
$\bar{\lambda}_z$	Normalized slenderness for out-of-plane flexural column buckling

Coefficients used in buckling check

χ	buckling reduction factor
χ_j	... for flexural buckling about the axis "j" (j=y or z)
χ_S	... for the specific, studied buckling case
χ_{LT}	... for lateral-torsional buckling
χ_T, χ_{TF}	... for torsional or torsional-flexural buckling
χ_{ip}	... for in-plane flexural buckling under N+M
$\chi_{y,\eta0}$	... for in-plane flexural buckling under N+M, referred to the axial force alone.
χ_{op}	... for out-of-plane buckling under N+M
k, k_j	interaction factor, related to buckling about the axis "j" (j=y or z)

B

REFERENCES

1. ABAQUS, v. 6.7 (2007), Dassault Systems/Simulia, Providence, RI, USA.

2. AISC (2001), *Load and Resistance Factor Design (LRFD) Manual of Steel Construction, 3rd Edition*, American Institute of Steel Construction, Chicago, IL.

3. AISC (2005), *Code of Standard Practice for Steel Buildings and Bridges*, American Institute of Steel Construction, Chicago, IL.

4. Allen, D. (1978), *Merchant-Rankine Approach to Member Stability*, Journal of the Structural Division, ASCE **104**/12, pp. 1909-1914

5. Alpsten, G. (1967), *Residual Stresses in Hot-Rolled Steel Profiles,* PhD thesis, Inst. Of Structural Engineering and Bridge Building, Royal Inst. Of Technology, Stockholm.

6. Alpsten, G. (1972), *Variations in mechanical and cross-sectional properties of steel*, State of Art Report, Proceedings of the International Conference on the Planning and Design of Tall Buildings, ASCE-IABSE, Lehigh University, August 1972.

7. Alpsten, G. (2002), *On the use of reliability assessment methods for structural design*, Proceedings of "Euro-SiBRAM'2002" Prague, Czech Republic, June 24 to 26, 2002.

8. Andrade, A., Camotim, D., Providencia e Costa, P. (2007), *On the evaluation of elastic critical moments in doubly and singly symmetric I-section cantilevers*, J. Constr. Steel Res., **63**, pp.894-908.

9. Ayrton, W. E., Perry, J. (1886), *On Struts*, The Engineer, **62**, London, pp.464-465, 513-515

10. Austin, W. J. (1961), *Strength and design of metal beam-columns*. ASCE J. Struct. Div.; **87**(4): pp.1–32.

11. Ballio, G., Mazzolani, F.M. (1983), *Theory and Design of Steel Structures,* Chapmann and Hall, London.

12. Beer, H., Schulz, G. (1969), *Die Traglast des planmäßig mittig gedrückten Stabes mit Imperfektionen,* VDI-Zeitschrift, **21**, pp.1537-1541, 1683-1687, 1767-1772.

13. Beer, H., Schulz, G. (1970), *Bases Théoriques des Courbes Européennes de Flambement,* Construction Métallique, No. 3, pp.37-57.

14. Beier-Tertel, J. (2009), *geometrische Ersatzimperfektionen für Tragfähigkeitsnachweise zum Biegedrillknicken von Trägern aus Walzprofilen*, PhD thesis, Ruhr-Universität Bochum, Schriftenreihe des Instituts für Konstruktiven Ingenieurbau, Heft 2009-2.

15. Bjorhovde, R. (1972), *Deterministic and Probabilistic Approaches to the Strength of Steel Columns,* PhD thesis, Lehigh University, Bethlehem, PA.

16. Bjorhovde, R. (1992), *Compression Members*, in "Constructional Steel Design: An International Guide", ed. P.J. Dowling, J.E. Harding, R. Bjorhovde, Elsevier Applied Science, London

17. Bleich, F. (1952), *Buckling Strength of Metal Structures*, Engineering Societies Monographs, McGraw-Hill Book Company Inc., New York - Toronto - London.

18. Boissonade, N., Greiner, R., Jaspart, J.P., Lindner, J. (2006), *Rules for Member Stability in EN 1993-1-1, Background documentation and design guidelines*, ECCS Technical Committee 8 – Stability, European Convention for Constructional Steelwork, Brussels.

19. BS 449-2 (1969): *Specification for the use of structural steel in building. Metric units*, British Standards Institute, London

20. BS 5950-1 (2000), *Structural use of steelwork in building – Part 1: Code of practice for design – rolled and welded sections*, British Standards Institute, London.

21. BS 5950-2 (2001), *Structural use of steelwork in building – Part 2: Specification for materials, fabrication and erection — Rolled and welded sections*, British Standards Institute, London.

22. Brozzetti, J., Alpsten, G., Tall, L. (1971), *Welding Parameters, Thick Plates, and Column Strength,* Supplement to The Welding Journal, August 1971, pp. 331-342.

23. Byfield, M.P., Nethercot, D.A. (1997): *Material and geometric properties of structural steel for use in design*, The Structural Engineer, **75**, pp. 363-367.

24. Byfield, M.P., Nethercot, D.A. (1998), *An analysis of the true bending strength of steel beams*, Proc. Inst. Civ. Engrs. Structs & Bldgs., **128**, pp. 188-197.

25. Camotim D, Gonçalves R. (2001), *Comparison between Level 1/Level 2 interaction formulae and FEM results for beam-columns with general support conditions,* Report TC8-2001-020, European Convention for Constructional Steelwork - ECCS Technical Committee 8.

26. Carpena, A. (1967), *Calcul probabiliste des structures métalliques*, Construction Métallique, No. 1.

27. Carpena, A. (1970), *Détermination des limites élastiques pour l'analyse du flambement*, Construction Métallique, No. 3. *Also published in*:

    Carpena, A. (1972), *Determination of the Elastic Limits for Buckling Analysis*, in "International Colloquium on Column Strength", Proceedings, Paris, Nov. 23-24, pp. 292-300.

28. Chan, T.M., Gardner, L. (2009), *Flexural Buckling of Elliptical Hollow Section Columns,* Journal of Structural Engineering, 05/2009, ASCE, pp. 546-557.

29. Chen, W., Atsuta, T. (2007), *Theory of Beam-Columns,* J. Ross Publishing Classics, Fort Lauderdale. (Reprint of a McGraw-Hill (NY) edition of 1976).

30. CEC (1988), *ENV background doc. 5.03,* Commission of the European Community, Brussels.

31. Dassault Systemes (2007), *ABAQUS 6.7 User's Manual,* Pawtucket, R.I.

32. DIN 4114 (1952), *Stahlbau – Stabilitätsfälle (Knickung, Kippung, Beulung),* DIN - Deutscher Normenausschuss, Berlin.

33. DIN 18800-2 (1990), *Stahlbauten – Teil 2: Stabilitätsfälle- Knicken von Stäben und Stabwerken*, DIN – Deutsches Institut für Normung, Berlin.

34. DIN 18800-7 (2002), *Stahlbauten – Teil 7: Ausführung und Herstellerqualifikation*, DIN – Deutsches Institut für Normung, Berlin.

35. Dwight, J.B.. (1972), *Use of Perry-Robertson Formula to Represent the New European Strut Curves,* in "International Colloquium on Column Strength", Proceedings, Paris, Nov. 23-24, pp. 399-411.

36. ECCS (1978), *European Recommendations for Steel Construction*, European Convention for Constructional Steelwork, Brussels.

37. ECCS (1984), *Ultimate Limit State Calculation of Sway Frames with Rigid Joints,* Editor: Vogel, U., European Convention for Constructional Steelwork- TC 8, Brussels.

38. EEC (1988), *Council Directive 89/106/EEC of 21 December 1988 on the approximation of laws, regulations and administrative provisions of the Member States relating to construction products,* Council of European Communities, Brussels.

39. EN 1090-2 (2008), *Execution of Steel Structures and Aluminium Structures – Part 2: Technical Requirements for Steel Structures,* CEN – European Committee for Standardization, Brussels.

40. EN 10034 (1993), *Structural Steel I- & H-sections – Tolerances on Shape and Dimension,* CEN – European Committee for Standardization, Brussels.

41. EN 10210-2 (2006), *Hot finished structural hollow sections of non-alloyed and fine grain steels – Part 2: Tolerances, dimensions and sectional properties–,* CEN – European Committee for Standardization, Brussels.

42. Engesser, F. (1891), *Die Knickfestigkeit gerader Stäbe,* Zentralblatt der Bauverwaltung, Vol. 11, pp. 483-486.

43. ERP (2003) - European Research Project 7210-PR-249: *Probabilistic quantification of safety of a steel structure highlighting the potential of steel versus other materials*, Final Report, 01/07/00 – 31/12/03.

44. Ersvik, O., Alpsten, G. (1970), *Experimental Investigation of the Column Strength of Wide-Flange Shapes ME 200 A, Roller Straightened in Different Ways,* Report 19.3, Swedish Institute of Steel Construction, Stockholm.

45. Euler, L. (1759), *Sur la force des colonnes,* in "Histoire de l'Academie royale des sciences, annee 1757", Berlin, p. 252

46. Eurocode (2002) – EN 1990, *Eurocode – Basis of structural design,* CEN, Brussels.

47. Eurocode 3 (1992) – ENV 1993-1-1:1992, *Eurocode 3. Design of steel structures. General rules and rules for buildings*, CEN, Brussels.

48. Eurocode 3 (2005) - EN 1993-1-1, *Eurocode 3. Design of steel structures. General rules and rules for buildings*, CEN, Brussels.

49. Feder, D., Lee, G.C. (1959), *Residual Stress and the Strength of Members of High Strength Steel,* Fritz Laboratory Report 269.2, Lehigh University, Bethlehem, PA.

50. Fukumoto, Y., Kubo, M. (1977), *An Experimental Review of Lateral Buckling of Beams and Girders,* Stability of Structures under Static and Dynamic Load, pp. 541-555, Washington D.C.

51. Fukumoto, Y. (1982), *Numerical Data Bank for the Ultimate Strength of Steel Structures,* Stahlbau, **51**, pp. 21-27, Ernst & Sohn, Berlin.

52. Fukumoto, Y., Itoh, Y. (1983), *Evaluation of Multiple Column Curves using the Experimental Data-Base Approach*, J. of Const. Steel Res., **3**, Nr.3, pp. 2-19.

53. Galambos (1998), *Stability Design Criteria for Metal Structures,* Wiley & Sons, NY.

54. Glassermann, P. (2004), *Monte Carlo Methods in Financial Engineering,* Springer, NY.

55. Greiner R, Ofner R, Salzgeber G. (1998), *Flexural buckling of beam-columns*, ECCS TC8 - Validation group, Working item 8, Review of rules for members in bending and axial compression, Report Nr. 3, European Convention for Constructional Steelwork, Brussels.

56. Greiner R, Ofner R, Salzgeber G. (1999), *Lateral torsional buckling of beam–columns: Theoretical background*, ECCS TC8 -Validation group, Report Nr.5, European Convention for Constructional Steelwork, Brussels.

57. Greiner, R., Salzgeber, G., Ofner, R. (2000), *New lateral-torsional buckling curves – numerical simulations and design formulae,* ECCS TC8 – Report No. TC8-2000-014, European Convention for Constructional Steelwork, Brussels.

58. Greiner, R., Kaim, P. (2001), *Comparison of LT-buckling design curves with test results,* ECCS TC8 – Report, April 23-2001, European Convention for Constructional Steelwork, Brussels.

59. Greiner, R., (2003), *Concepts for the Numerically-based Buckling Check of Steel Structures*, Proc. of "Steel Structures and Bridges 2003", Prague, Sept. 17-20, pp.511-516.

60. Greiner, R., Ofner, R. (2005), *Buckling Design of Steel Structures Based on Overall Load Cases According to Eurocode 3,* Proc. of "Eurosteel 2005", Maastricht (NL), June 8-10, Vol. A, pp.1.4-1 – 1.4-8.

61. Greiner, R., Lindner, J. (2006), *Interaction formulae for members subjected to bending and axialcompression in EUROCODE 3—the Method 2 approach*, Journal of Constructional Steel Research, **62**, Elsevier, pp. 757-770.

62. Greiner, R., Taras, A. (2006), *On the variety of buckling curves,* Proc. of "Stability and Ductility of Steel Structures", Lisbon (PT), Sept. 6-9, pp. 1101-1108.

63. Greiner, R., Ofner, R. (2007), *Comparison of General Method with traditional methods Example of a sway frame with lateral restraints*, ECCS TC8 Stability, TC8-2007-006, European Convention for Constructional Steelwork, Brussels.

64. Gonçalves, R., Camotim, D. (2004), *On the application of beam-column interaction formulae to steel members with arbitrary loading and support conditions,* Journal of Constructional Steel Research, **60**, Elsevier, pp.433-450

65. Horne, M.R. (1963) *Elastic-Plastic Failure Loads of Plane Frames*. Proc. Roy. Soc. London, Series A, **274**, pp. 343-364.

66. Horne, M.R., Merchant, W. (1965), *The Stability of Frames*, Pergamon Press Ltd., London

67. Horne M.R., Ajmani J.L. (1971), *Design of columns restrained by side-rails*, The Structural Engineer, **49**, 8/1971, pp.339-345.

68. Horne M.R., Ajmani J.L. (1971), *The post-buckling behaviour of laterally restrained columns*, The Structural Engineer, **49**, 8/1971, pp.346-352

69. Itoh, Y., Usami, T., Fukumoto, Y. (1996), *Experimental and numerical analysis database on structural stability*, Engineering Structures, **18**, No. 10, pp. 812-820, Elsevier, London.

70. Jacquet, J. (1970), *Essais de Flambement et Exploitation Statistique,* Construction Métallique, No. 3, pp. 13-36.

71. Kaim, P. (2004), *Spatial buckling behaviour of steel members under bending and compression,* PhD thesis, Graz University of Technology, Institute for Steel Structures and Shell Structures.

72. Karman, T. von, (1910), *Untersuchungen über Knickfestigkeit*, Mitteilungen über Forschungsarbeiten auf dem Gebiete des Ingenieurwesens, Volume 81, Springer, Berlin.

73. Kettler, M. (2008), *Elastic-Plastic Cross-Sectional Resistance of Semi-Compact H- and Hollow Sections*, PhD thesis, Graz University of Technology, Institute for Steel Structures and Shell Structures.

74. King, C.M., The Steel Construction Institute (2001), *Design moment resistance at $\bar{\lambda}_{LT} = 0.4$*, ECCS TC8 paper No. 2001-18, European Commission for Constructional Steelwork, Brussels.

75. King, C.M. (2005), *Member stability at plastic hinges,* Eurosteel 2005 conference proceedings, Volume B, pp.3/25-3/32.

76. King, C.M., The Steel Construction Institute (2008), *LTB calibration to EN 1990,* ECCS TC8 – Report No. TC8-2008-017, European Convention for Constructional Steelwork, Brussels.

77. King, C.M. (2009), *correspondence within ECCS TC8.*

78. Kurrer, K. (2008), *The History of the Theory of Structures,* Ernst & Sohn, Berlin.

79. Ligtenberg, F.K. (1965), *Stability and Plastic Design*. Heron, **3**, pp.1 - 12.

80. Lindner, J. (1978), *Näherungen für die Europäischen Knickspannungskurven*, die Bautechnik, **10**, pp. 344-347

81. Lindner, J., Gregull, T. (1986), *Biaxial loaded beam-columns, Comparison of design equations and ultimate load calculations by Matthey*, Technische Universität Berlin, Institut für Baukonstruktionen und Festigkeit, Report No. VR 2075, 1986

82. Lindner, J., Scheer, J., Schmidt, H. (1994), *Stahlbauten – Erläuterungen zu DIN 18800 Teil 1 bis 4*, Beuth Kommentare, Beuth Verlag GmbH, Berlin.

83. Lindner, K. (2000)*, Lateral torsional buckling consideration of different moment distributions by factor f,* ECCS TC 8 Report No. 2000-019, European Convention for Constructional Steelwork, Brussels.

84. Maquoi, R., Rondal, J. (1978), *Mise en Équation des Nouvelles Courbes Européenned de Flambement,* Construction Métallique, No. 1, pp. 17-30

85. Maquoi, R., Jaspart, J.P. (2001), *Merchant-Rankine Approach for the Design of Steel and Composite Sway Building Frames*, Festschrift Prof. Greiner, Graz

86. Marek, P, Brozzetti, J., Gustar, M. (2001), *Probabilistic assessment of structures using Monte Carlo simulation. Background, exercises and software*, ITAM, Academy of Sciences of the Czech Republic, Prague.

87. Melcher, J., Kala, Z., Holicky, M., Fajkus, M., Rozlívka, L. (2004), *Design characteristics of structural steel based on statistical analysis of metallurgical products,* J. of Const. Steel Res., **60**, pp. 795-808.

88. Merchant, W. (1954), *The Failure Load of Rigidly Jointed Frameworks as Influenced by Stability*, Structural Engineer, **32**, pp.185-190

89. Müller, C. (2003), *Zum Nachweis ebener Tragwerke aus Stahl gegen seitliches Ausweichen*, PhD thesis, RWTH Aachen – Shaker Verlag.

90. Murzewski, J. (1977), *Joint probability of elastic and plastic instability modes*, Proc. of the Regional Coll. on Stability of Steel Structures, Budapest, pp. 249-268

91. Naumes, J., Strohmann, I., Ungermann, D., Sedlacek, G. (2008), *Die neuen Stabilitätsnachweise im Stahlbau nach Eurocode 3,* Stahlbau, **77**, pp.748-761, Ernst&Sohn, Berlin.

92. NSSS (2007), *National Structural Steelwork Specification for Building Construction – 5th Edition*, BCSA - British Constructional Steelwork Association, London.

93. Ofner, R. (1997), *Traglasten von Stäben aus Stahl bei Druck und Biegung,* PhD thesis, Institut für Stahlbau, Holzbau und Flächentragwerke, TU Graz, Heft 9.

94. Osgood, W.R. (1946), *Column Formulas,* Transactions of the American Society of Civil Engineers, Paper No. 2269, p.165-214

95. ÖNORM B 4700 (1994), *Stahlbau - Ausführung der Stahltragwerke*, ÖN – Österreichisches Normungsinstitut, Wien.

96. Petersen, C. (1993), *Stahlbau*, Vieweg Verlag, Wiesbaden.

97. Plum, C. (2008), *Comments to a part of CEN Document N1639E (Sedlacek et alt. 2008)* – Correspondence within the CEN Eurocode SC3 group.

98. Popov, E.P. (1952), *Mechanics of Materials*, Prentice-Hall Inc., New York

99. Preussische Ministerialbestimmung (1910), *regulations of the Prussian Regional Building Department*, Berlin.

100. Rankine, W.J.M. (1866), *Useful Rules and Tables Relating to Mensuration, Engineering, Structures, and Machines*, London.

101. Rankine, W.J.M. (1898), *A Manual of Civil Engineering*, 20th edition, London, Griffin.

102. Rebelo, C., Lopes, N. et al. (2008), *Statistical Evaluation of the Lateral-Torsional Buckling Resistance of Steel I-beams, Part 1: Variability of the Eurocode 3 resistance model,* J. of Const. Steel Res., **64**, pp. 818-831.

103. Reichsbahn (1925), *Vorschriften für Eisenbauwerke, Grundlagen für das Entwerfen und Berechnung eiserner Eisenbahnbrücken (BE),* Deutsche Reichsbahn-Gesellschaft / Ernst & Sohn, Berlin

104. Robertson, A. (1925), *The Strength of Struts*, The Institution of Civil Engineers − Selected Engineering Papers, **28**, London

105. Roik, K. (1978), *Vorlesungen über Stahlbau,* Ernst & Sohn, Berlin.

106. Rondal, J., Maquoi, R. (1979), *Formulations d'Ayrton-Perry pour le Flambement des Barres Métalliques,* Construction Metallique, No. 4, pp.41-53

107. Rondal, J., Maquoi, R. (1979b), *Single Equation for SSRC Column-Strength Curves,* J. of the Struct. Div., ASCE, **105**, pp.247-250.

108. Ross, S.M. (2009), *Introduction to Probability and Statistics for Engineers and Scientists,* Elsevier, Amsterdam.

109. Rotter, J.M. (1982), *Multiple Column Curves by Modifying Factor,* ASCE J. Struct. Div., **108**, pp.1665-1669.

110. Rotter, J.M. (2002), *Shell Buckling and Collapse Analysis for Structural Design: The New Framework of the European Standard*, Festschrift for Prof. Calladine, Cambridge

111. Salvadory M.G. (1955), *Lateral buckling of I-beams*. ASCE Transaction, **120**, pp.1165−1177

112. Schleich, J.B., Sedlacek, G., Kraus, O. (2002), *Realistic Safety Approach for Steel Structures,* Proceedings of Eurosteel, 3th European Conference on Steel Structures, Coimbra, 19-20 September.

113. Schulz, G. (1968), *Traglastermittlung von planmäßig mittig belasteten Druckstäben aus Baustahl unter Berücksichtigung von geometrischen und strukturellen Imperfektionen*, PhD thesis, Graz University of Technology.

114. Schulz, G., Alpsten, G., Daussy, R. et alt. (1977), *The ECCS Column Curves,* in "Second International Colloquium on Stability", Proceedings, International Association of Bridge and Structural Engineers, Tokyo-Liege-Washington, pp. 55-67.

115. Sedlacek, G., Müller, C. (2006), *The European Standard Family and its Basis,* Journal of Constructional Steel Research, **62**, pp. 1047-1059.

116. Sedlacek, G., Naumes, J., Bijlaard, F., Maquoi, R., Mueller, Ch. (2008), *CEN Document: N1639E - Excerpt from the Background Document to EN 1993-1-1 Flexural buckling and lateral buckling on a common basis: Stability assessments according to Eurocode 3*, CEN − European Committee for Standardization − Eurocode Sub-Committee SC3, Brussels.

117. Serna, M.A., López, A., Puente, I., Yong, D.J. (2006), *Equivalent uniform moment factors for lateral–torsional buckling of steel members*, Journal of Constructional Steel Research, **62**, pp. 566-580.

118. Sfintesco, D. (1970), *Fondement Expérimental des Courbes Européennes de Flambement*, Construction Métallique, No. 3, pp. 5-12.

119. Sfintesco, D., Carpena, A., Dauphin, P. et alt. (1966), *Flambement Simple – Diagramme expérimental des contraintes d'affaissement pour les pièce pleines bi-articulées en acier doux à section constante, sollicitèes en compression axiale,* Construction Métallique, No. 2, pp. 48-49.

120. Sfintesco, D., Carpena, A. (1977), *Experimental Bases of the ECCS Column Curves,* in "Second International Colloquium on Stability", Proceedings, International Association of Bridge and Structural Engineers, Tokyo-Liege-Washington, pp. 68-75.

121. Shanley, F.R. (1947), *Inelastic Column Theory,* Journal of the Aeronautical Sciences

122. Simões da Silva, L., Rebelo C., Nethercot D. et al. (2008), *Statistical Evaluation of the Lateral-Torsional Buckling Resistance of Steel I-beams, Part 2: Variability of steel properties,* J. of Const. Steel Res., **64**, pp. 832-849.

123. Simões da Silva, L., Marques, L., Rebelo, C. (2010), *Numerical validation of the general method in EC3-1-1 for prismatic members,* J. of Const. Steel Res., **66**, pp. 575-590.

124. Singer, J., Arbocz, J., Weller, T. (1998), *Buckling Experiments – Experimental Methods in Buckling of Thin-Walled Structures, Volume 1 – Basic Concepts, Columns, Beams and Plates*, Wiley & Sons, Chichester.

125. Snijder, H.H., Hoenderkamp, M.C.M. et (2008), *Buckling Curves for Lateral-Torsional Buckling of Unrestrained Beams,* Festschrift for René Maquoi, pp.239-248, Liege.

126. Stangenberg, H. (2007), *Zum Bauteilnachweis offener, stabilitätsgefährdeter Stahlbauprofile unter Einbeziehung seitlicher Beanspruchungen und Torsion*, PhD thesis, RWTH Aachen, Heft 61, Shaker Verlag.

127. Strating, J., Vos, H. (1972), *Computer Simulation of the E.C.C.S. Buckling Curve using a Monte-Carlo Method,* in "International Colloquium on Column Strength", Proceedings, Paris, Nov. 23-24, pp. 334-355.

128. Taras, A., Greiner, R. (2008a), *Torsional and flexural torsional buckling— A study on laterally restrained I-sections*, Journal of Constructional Steel Research, **64**, pp. 725-731

129. Taras, A., Greiner, R. (2008b), *Development of Consistent Buckling Curves for Torsional and Lateral-Torsional Buckling*, Steel Construction, **1**, pp. 42-50.

130. Taras, A., Greiner, R. (2010), *New Design Curves for Lateral-Torsional Buckling –Proposal Based on a Consistent Derivation*, Journal of Constructional Steel Research, **66**, pp. 648-663

131. Tebedge, N., Chen, W., Tall, L. (1972), *Experimental Studies on column Strength of European Heavy Shapes,* in "International Colloquium on Column Strength", Proceedings, Paris, Nov. 23-24, pp. 334-355.

132. Tetmajer, L. von (1890), *Methoden und Resultate der Prüfung der Festigkeitsverhältnisse des Eisens und anderer Metalle,* Mitteilungen der Anstalt zur Prüfung von Baumaterialien in Zürich, **4**, p. 50.

133. Tide, R.H.R. (1985), *Reasonable Column Design Equations,* Proc. SSRC Annu. Tech. Session, Cleveland (OH), Apr. 1S17

134. Timoshenko, S.P. (1910), *Einige Stabilitätsprobleme der Elastizitätstheorie,* Zeitschrift für Angewandte Mathematik und Physik, **28,** pp. 357–385.

135. Timoshenko, S.P., Lessells, I.M. (1928), *Festigkeitslehre*, Springer, Berlin

136. Timoshenko, S.P. (1964), *Theory of Elastic Stability* Engineering Societies Monographs, McGraw-Hill Book Company Inc., New York - Toronto - London

137. Timoshenko, S.P. (1983), *History of Strength of Materials*, Dover Publications, New York

138. Trahair (1993), *Flexural-Torsional Buckling of Structures,* E&FN Spon, London

139. Unger, B. (1977), *Ein Konzept zur Berechnung der Traglast von biegedrillknickgefährdeten Stäben unter Berücksichtigung des Einflusses geometrischer und werkstofflicher Imperfektionen*, der Stahlbau 11, Berlin, pp.329-338

140. Villette, M. (1997), *Considérations sur le flambement, proposition de révision de l'Eurocode 3*, Construction Métallique, No. 2, pp. 15-38.

141. Villette, M., Boissonade, N., Muzeau J.P., Jaspart, J.P. (2000), *Development of a comprehensive formula for the design of beam-columns,* Internal report, Baudin-Chateauneuf, LERMES-CUST, University of Liege.

142. Villette, M. (2004), *Analyse critique du traitement de la barre comprimée et fléchie et propositions de nouvelles formulations,* PhD thesis, Facultè des Sciences Appliquées, Universitè de Liège.

143. Wolf, C. (2006), *Tragfähigkeit von Stäben aus Baustahl*, PhD thesis, Ruhr-Universität Bochum, Schriftenreihe des Instituts für Konstruktiven Ingenieurbau, Heft 2006-2.

144. Young, B.W. (1971), *Steel Column Design,* PhD thesis, Cambridge.

145. Young, B.W., Dwight, J.B. (1971), *Residual Stresses and their Effect on Moment Curvature Properties of Structural Steel Sections,* CIRIA Tech. Note 32, Cambridge/London.

146. Young, B.W. (1972), *Residual Stresses in Hot-rolled Members,* in "International Colloquium on Column Strength", Proceedings, Paris, Nov. 23-24, pp. 25-38.

147. Young, B.W., Schulz, G., (1977), Mechanical Properties and Residual Stresses, in "Second International Colloquium on Stability", Proceedings, International Association of Bridge and Structural Engineers, Tokyo-Liege-Washington, pp. 31-45.